

A11102 953152

NAT'L INST OF STANDARDS & TECH R.I.C.



A11102953152

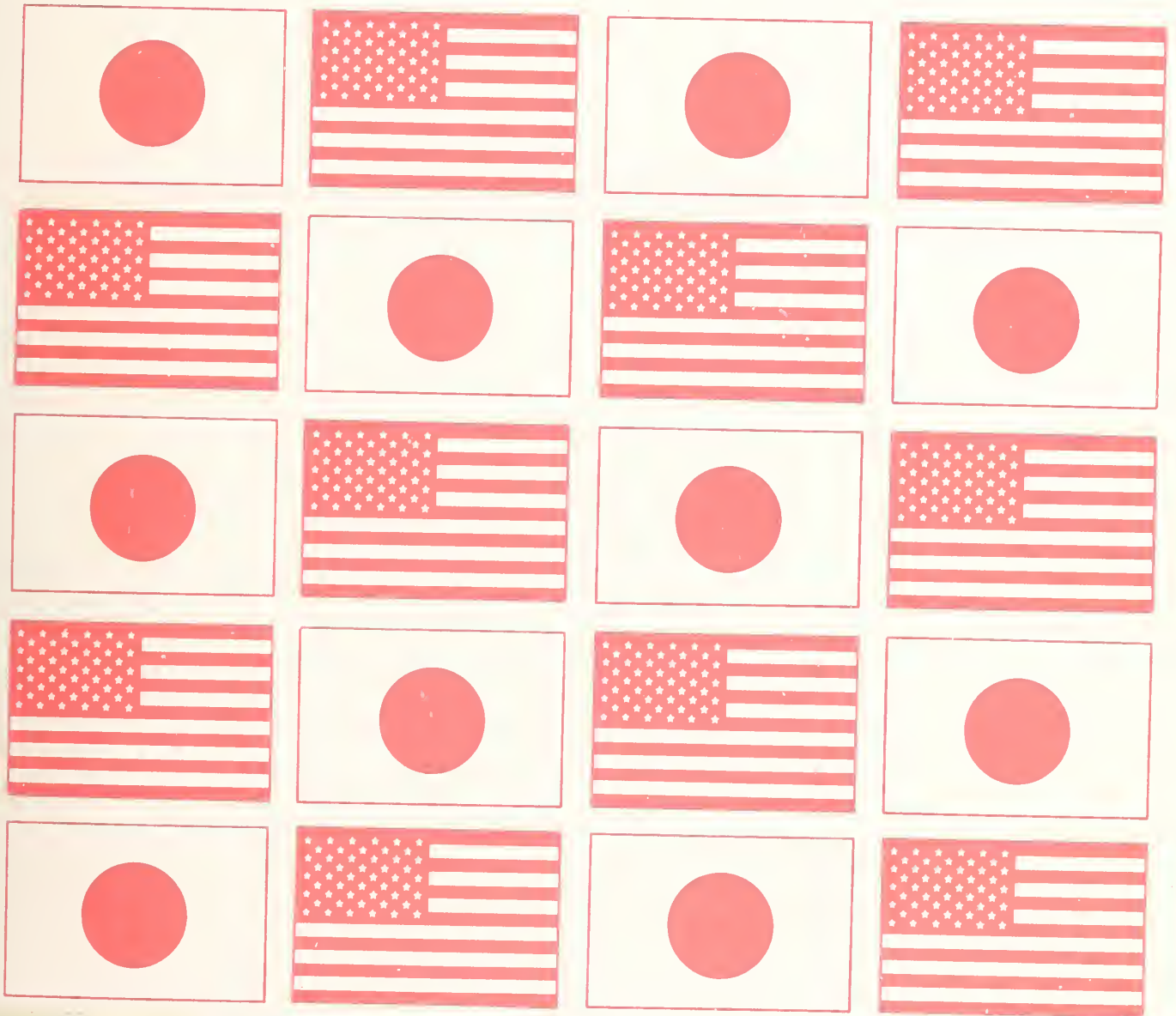
Raufaste, Noel J/Wind and seismic effect  
QC100 .U57 NO.760 1989 V1989 C.1 NIST-PU

# and Seismic Effects

## Proceedings of the 20th Joint Meeting

NIST SP 760

NIST  
PUBLICATIONS



QC  
100  
U57  
#760  
1989  
C.2

DEPARTMENT OF COMMERCE  
Institute of Standards and Technology

# **NIST** *Technical Publications*

## *Periodical*

---

**Journal of Research of the National Institute of Standards and Technology**—Reports NIST research and development in those disciplines of the physical and engineering sciences in which the Institute is active. These include physics, chemistry, engineering, mathematics, and computer sciences. Papers cover a broad range of subjects, with major emphasis on measurement methodology and the basic technology underlying standardization. Also included from time to time are survey articles on topics closely related to the Institute's technical and scientific programs. Issued six times a year.

## *Nonperiodicals*

---

**Monographs**—Major contributions to the technical literature on various subjects related to the Institute's scientific and technical activities.

**Handbooks**—Recommended codes of engineering and industrial practice (including safety codes) developed in cooperation with interested industries, professional organizations, and regulatory bodies.

**Special Publications**—Include proceedings of conferences sponsored by NIST, NIST annual reports, and other special publications appropriate to this grouping such as wall charts, pocket cards, and bibliographies.

**Applied Mathematics Series**—Mathematical tables, manuals, and studies of special interest to physicists, engineers, chemists, biologists, mathematicians, computer programmers, and others engaged in scientific and technical work.

**National Standard Reference Data Series**—Provides quantitative data on the physical and chemical properties of materials, compiled from the world's literature and critically evaluated. Developed under a worldwide program coordinated by NIST under the authority of the National Standard Data Act (Public Law 90-396). NOTE: The Journal of Physical and Chemical Reference Data (JPCRD) is published quarterly for NIST by the American Chemical Society (ACS) and the American Institute of Physics (AIP). Subscriptions, reprints, and supplements are available from ACS, 1155 Sixteenth St., NW., Washington, DC 20056.

**Building Science Series**—Disseminates technical information developed at the Institute on building materials, components, systems, and whole structures. The series presents research results, test methods, and performance criteria related to the structural and environmental functions and the durability and safety characteristics of building elements and systems.

**Technical Notes**—Studies or reports which are complete in themselves but restrictive in their treatment of a subject. Analogous to monographs but not so comprehensive in scope or definitive in treatment of the subject area. Often serve as a vehicle for final reports of work performed at NIST under the sponsorship of other government agencies.

**Voluntary Product Standards**—Developed under procedures published by the Department of Commerce in Part 10, Title 15, of the Code of Federal Regulations. The standards establish nationally recognized requirements for products, and provide all concerned interests with a basis for common understanding of the characteristics of the products. NIST administers this program as a supplement to the activities of the private sector standardizing organizations.

**Consumer Information Series**—Practical information, based on NIST research and experience, covering areas of interest to the consumer. Easily understandable language and illustrations provide useful background knowledge for shopping in today's technological marketplace.

*Order the above NIST publications from: Superintendent of Documents, Government Printing Office, Washington, DC 20402.*

*Order the following NIST publications—FIPS and NISTIRs—from the National Technical Information Service, Springfield, VA 22161.*

**Federal Information Processing Standards Publications (FIPS PUB)**—Publications in this series collectively constitute the Federal Information Processing Standards Register. The Register serves as the official source of information in the Federal Government regarding standards issued by NIST pursuant to the Federal Property and Administrative Services Act of 1949 as amended, Public Law 89-306 (79 Stat. 1127), and as implemented by Executive Order 11717 (38 FR 12315, dated May 11, 1973) and Part 6 of Title 15 CFR (Code of Federal Regulations).

**NIST Interagency Reports (NISTIR)**—A special series of interim or final reports on work performed by NIST for outside sponsors (both government and non-government). In general, initial distribution is handled by the sponsor; public distribution is by the National Technical Information Service, Springfield, VA 22161, in paper copy or microfiche form.

# Wind and Seismic Effects

NIST SP 760

---

PROCEEDINGS OF  
THE 20TH JOINT  
MEETING OF  
THE U.S.-JAPAN  
COOPERATIVE PROGRAM  
IN NATURAL RESOURCES  
PANEL ON WIND AND  
SEISMIC EFFECTS

Issued January 1989

Noel J. Raufaste,  
EDITOR

Center for Building Technology  
National Engineering Laboratory  
National Institute of Standards and Technology  
Gaithersburg, MD 20899

NOTE: As of 23 August 1988, the National Bureau of Standards (NBS) became the National Institute of Standards and Technology (NIST) when President Reagan signed into law the Omnibus Trade and Competitiveness Act.

U.S. DEPARTMENT OF COMMERCE  
C. William Verity, Secretary

Ernest Ambler, Acting Undersecretary  
for Technology

National Institute of Standards and Technology  
Raymond G. Kammer, Acting Director



Research Information Center  
National Institute of Standards  
and Technology  
Gaithersburg, Maryland 20899

Library of Congress Catalog Card Number: 88-600610

National Institute of Standards and Technology Special Publication 760  
Natl. Inst. Stand. Technol., Spec. Publ. 760, 482 pages (Jan. 1989)  
CODEN: NSPUE2

U.S. GOVERNMENT PRINTING OFFICE  
WASHINGTON: 1989

---

For sale by the Superintendent of Documents, U.S. Government Printing Office, Washington, DC 20402-9325

## PREFACE

The UNITED STATES and JAPAN, in 1961, created the US-JAPAN Cooperative Science Program. The US-JAPAN Natural Resources Development Program (UJNR), one of three collateral programs making up the Cooperative Service Program, was created in January 1964. The objective of UJNR is to exchange information on research results and exchange scientists and engineers in the area of natural resources for the benefit of both countries. UJNR is composed of 17 Panels each responsible for specific technical subjects.

The Panel on Wind and Seismic Effects was established in 1968 to provide technologies, for US and Japanese governments, to reduce damages from high winds, earthquakes, storm surge, and tsunamis. The Panel provides for cooperative activities of fifteen US and six JAPANESE agencies with participating representatives of private sector organizations. Annual meetings alternate between JAPAN and the US (odd numbered years in JAPAN; even numbered years in the US). The Panel provides the vehicle to exchange technical data and information on design and construction of buildings, bridges, dams, and lifeline and waterfront structures, and to exchange high wind and seismic measurement records. Results from this Panel's efforts have impacted engineering practices and improved codes and standards in both countries.

The Twentieth Joint Meeting was held at the National Bureau of Standards, Gaithersburg, Maryland, May 17-20, 1988. The Panel featured six themes: 30 technical papers were presented out of the 36 authored manuscripts. The Panel's ten task committees held their meetings during this period to review joint research projects and planned for future activities.

These proceedings include the program of the Twentieth Joint Meeting, the Panel resolutions, all technical papers, and the task committee reports.

Partial support to maintain the US Panel was provided by the Federal Highway Administration, National Science Foundation, Department of State, Federal Emergency Management Administration, Department of Army, Bureau of Reclamation, and the National Bureau of Standards.

Noel J. Raufaste, Secretary  
US-Side, Panel on Wind and Seismic Effects

## ABSTRACT

The 20th Joint Meeting of the U.S.-JAPAN Panel on Wind and Seismic Effects was held at the National Bureau of Standards, Gaithersburg, MD, from May 17-20, 1988. This publication, the proceedings of the Joint Meeting, includes the program, list of members, panel resolutions, task committee reports, and technical papers.

Papers were presented under five themes:

- Theme I - Wind Engineering
- Theme II - Earthquake Engineering
- Theme III - Storm Surge and Tsunamis
- Theme IV - Summary of U.S.-Japan Cooperative Research Program
- Theme V - Two Decades of Accomplishments and Challenges for the Future

Subjects covered in the papers presented include:

- (1) modeling aerodynamic wind forces
- (2) wind loads on structures and design criteria
- (3) earthquake ground motions
- (4) soil liquefaction studies and methods to improve liquefaction resistance
- (5) seismic loads on structures and design criteria
- (6) stress analyses of pipelines during earthquakes
- (7) full-scale seismic experiments
- (8) earthquake hazard reduction program
- (9) Mexico City earthquakes
- (10) seismic hazards and risk assessment
- (11) coordinated masonry building research
- (12) bridge design to resist seismic loads
- (13) tsunami research projects
- (14) storm waves and surge
- (15) two decades of Panel accomplishments

KEYWORDS: accelerograph; bridges; codes; concrete; design criteria; disaster; earthquakes; earthquake hazards; earthworks; geotechnical engineering; ground failures; liquefaction; masonry; pipeline; repair and retrofit; risk assessment; seismicity; standards; storm surge; structural engineering; tsunami; and wind loads.

## CONTENTS

	PAGE
<b>PREFACE</b> .....	iii
<b>ABSTRACT</b> .....	iv
<b>AGENDA FOR 20th JOINT UJNR MEETING</b> .....	ix
<b>LIST OF PANEL MEMBERS</b> .....	xv
<b>LIST OF TASK COMMITTEE MEMBERS</b> .....	xxv
<b>RESOLUTIONS</b> .....	xxvii
<b>THEMES AND TECHNICAL PAPERS</b> .....	1
 <b>THEME I: Wind Engineering</b>	
<b>Modeling the Effect of Spanwise Coherence of Aerodynamic Forces on Full-Bridge Response</b> .....	3
Fazl Ehsan and Harold R. Bosch	
<b>Studies on Wind-Resistant Design of Highway Bridges and New Design Codes in Japan</b> .....	18
Nobuyuki Narita, Koichi Yokoyama, and Hiroshi Sato	
<b>Anchorage and Foundations for Wind Resistance of Manufactured Homes</b> .....	31
G. Robert Fuller	
<b>Present State of Wind Engineering Research Related to Building Design in Japan</b> .....	59
Tatsuo Murota and Hisashi Okada	
 <b>THEME II: Earthquake Engineering</b>	
<b>Outline on Research Results of Wind and Seismic Effects During 2 Decades at the National Research Center for Disaster Prevention</b> .....	63
Keiichi Ohtani and Hiroshi Takahashi	
<b>Development of Design Criteria for Mitigating Earthquake Damage—The Program of the Federal Emergency Management Agency</b> .....	86
Richard W. Krimm	
<b>State-of-the-Art on Earthquake Engineering to Port and Harbour in Japan</b> .....	88
Setsuo Noda and Hajime Tsuchida	

## CONTENTS

	PAGE
<b>Overburden Correction for Blowcounts in Gravels</b> .....	100
Mary Ellen Hynes-Griffin and A. G. Franklin	
<b>Sand Liquefaction Tests Using a Geotechnical Dynamic Centrifuge</b> .....	110
Yasuyuki Koga, Eiichi Taniguchi, Jun-ichi Koseki, and Tadashi Morishita	
<b>In Situ Measurement of Pore Pressure Build-Up During Liquefaction</b> .....	118
Thomas L. Holzer, T. Leslie Youd, and Michael J. Bennett	
<b>Two Directional Loading Test for Partially Concrete Filled Steel Columns</b> .....	131
Shoichi Saeki, Minoru Fujiwara, Koichi Minosaku, and Jun Hikino	
<b>Similitude Studies of Prototype and 1/6-Scale Model Bridge Columns Under Reversed Cyclic Loading</b> .....	143
William C. Stone, Geraldine S. Cheok, and H. S. Lew	
<b>Study on the Development of the Mixed Structural System Composed of Reinforced Concrete Column and Structural Steel Girder</b> .....	168
Hiroyuki Yamanouchi and Isao Nishiyama	
<b>Effects of Soil and Rock on Ground Motion and Potential Damage in an Earthquake</b> .....	177
Walter W. Hays	
<b>Seismic Performance of Reinforced Concrete High-Rise Frame Structure with Wall Columns—Part 1: Deformation Capacity of Critical Structural Elements such as Wall Columns, Beams and Shear Walls</b> .....	197
Masaya Hirose, Hisahiro Hiraishi, Masashi Fujisawa, and Manabu Yoshimura	
<b>Vibration Studies of Richard B. Russell Concrete Gravity Dam</b> .....	208
Robert Hall, Tommy Bevins, and Stephen Wright	
<b>Base Isolated Building Structures in Japan</b> .....	226
Yoshikazu Kitagawa and Masaya Hirose	
<b>Shaking Table Test on the Ridge Response During Earthquake</b> .....	238
Yasushi Sasaki, Tetsuro Kuwabara, and Seitaro Yoshimi	
<b>Investigation of Two Buildings Shaken During the 19 September 1985 Mexico Earthquake</b> .....	251
Douglas A. Foutch, Keith D. Hjelmstad, and Enrique Del Valle Calderon	

## CONTENTS

	PAGE
<b>Recorded Behavior of Structures—Whittier Narrows Earthquake, 1 October 1987</b> .....	258
A. Gerald Brady	
<b>Field Experiments on Pipelines in the Parkfield Earthquake Zone</b> .....	266
J. Isenberg and E. Richardson	
<b>The Drawing Image of Earthquake Hazard</b> .....	278
Keiichi Ohtani and Hiroshi Takahashi	
 <b>THEME III: Storm Surge and Tsunamis</b>	
<b>Combined Effect of Storm Waves and Surge</b> .....	287
Paul D. Farrar and H. Lee Butler	
<b>Stability of Submerged Dike at the Opening Section of Tsunami Protection Breakwaters</b> .....	291
Katsutosi Tanimoto and Katsutoshi Kimura	
<b>Marine Applications of Geographic Information System</b> .....	300
Celso S. Barrientos	
 <b>THEME IV: Summary of U.S.-Japan Cooperative Research Program</b>	
<b>U.S.-Japan Coordinated Earthquake Research Program on Masonry Buildings—Seismic Test of the Five Story Full-Scale Reinforced Masonry Buildings</b> .....	307
Shin Okamoto, Yutaka Yamazaki, Takashi Kaminosono, and Masaomi Teshigawara	
<b>Current Status of the U.S. Coordinated Program for Masonry Building Research</b> .....	321
James L. Noland	
<b>Dynamic Strength and Ductility of Reinforced Concrete Bridge Piers</b> .....	335
Toshio Iwasaki, Osamu Ueda, Kazuhiko Kawashima, Kinji Hasegawa, and Takeshi Yoshida	
 <b>THEME V: Two Decades of Accomplishments and Challenges for the Future</b>	
<b>U.S. Side: Accomplishments and Challenges—Panel on Wind and Seismic Effects</b> .....	351
Noel J. Raufaste and Richard N. Wright	
<b>Two Decades of Accomplishments and Challenges for the Future</b> .....	365
Nobuyuki Narita	

## CONTENTS

	PAGE
<b>MANUSCRIPTS AUTHORED FOR PANEL MEETING BUT NOT PRESENTED ORALLY</b>	
<b>Seismic Loading Test of 15 Story Frame-Wall Reinforced Concrete Building</b> .....	389
Masaya Hirosawa, Shinsuke Nakata, Hisahiro Hiraishi, Tetsuro Goto, and Manabu Yoshimura	
<b>Safety Analysis on the Vertical Bearing Capacity of Piles</b> .....	398
Hiroshi Shinohara, Michio Okahara, Shouichi Nakatani, and Keiji Taguchi	
<b>Model Shaking Table Tests on Seismic Resistance of Reinforced Embankment (Part 2)</b> .....	405
Yasuyuki Koga, Yoshihiro Ito, Shuzo Washida, and Takao Shimazu	
<b>Seismic and Tsunami Disaster Prevention Surveys and Preparing Geographical Information in Geographical Survey Institute, Japan</b> .....	412
Masatoshi Nagaoka	
<b>Dynamic Shear Moduli of Rockfill Materials</b> .....	427
Norihsa Matsumoto, Nario Yasuda, and Masahiko Ohkubo	
<b>APPENDIX: Task Committees A-J Reports</b> .....	435

## AGENDA FOR 20th JOINT UJNR MEETING

17 - 20 May 1988

17 May Tu 1000

### OPENING CEREMONIES

(Lecture Room A, Administration Building)

Call to order by Noel RAUFASTE,  
Secretary-General US Side, UJNR Panel  
Opening remarks by Samuel KRAMER, Deputy  
Director, National Engineering  
Laboratory, NBS

Remarks by Kaname IKEDA, Counsellor for  
Science and Technology, Embassy of  
JAPAN

Remarks by Richard N. WRIGHT, Chairman  
US Side, UJNR Panel

Remarks by Nobuyuki NARITA, Chairman JAPAN  
Side, UJNR Panel

Introduction of US Members by US Panel  
Chairman

Introduction of JAPAN Members by JAPAN  
Panel Chairman

Elect Joint Meeting Chairman

Adopt Agenda

Remarks by Edward O. PFRANG, Past Chairman  
US Side, UJNR Panel; Executive  
Director, ASCE

Adjourn

Group Photograph

1200 Lunch: Hosted by Ernest AMBLER, Director NBS

### TECHNICAL SESSIONS

1300-1640 Technical Session - Wind Engineering  
Chairman: R N WRIGHT

1300 Modeling the Effect of Spanwise Coherence  
of Aerodynamic Forces on Full Bridge  
Response; F. EHSAN and H. BOSCH\*, FHWA

1320 Studies on Wind-resistant Design of Highway  
Bridges and New Design Codes in JAPAN;  
Nobuyuki NARITA, Koichi YOKOYAMA\*,  
Hiroshi SATO, PWRI

- 1340 Foundation and Anchorages for Manufactured Housing Against High Winds; Robert FULLER\*, HUD
- 1400 Present State of Wind Engineering Research Related to Building Design in JAPAN; H. OKADA, Tatsuo MUROTA\*, BRI
- 1420 Discussions
- 1440 Break
- 1500-1640 **Technical Session - Earthquake Engineering**  
Chairman: R N WRIGHT
- 1500 Outline--Research Results of Wind and Seismic Effects During Two Decades at the National Research Center for Disaster Prevention; Hiroshi TAKAHASHI, Keiichi OHTANI\*, NRCDP
- 1520 Development of Design Criteria for Mitigating Earthquake Damage - The Program of the Federal Emergency Management Agency; Richard KRIMM, FEMA (Presented by K. THIRUMALAI)
- 1540 State-of-the-Art of Earthquake Engineering at Port and Harbours in JAPAN; Setsuo NODA\*, Hajime TSUCHIDA, PHRI
- 1600 Overburden Correction for Blowcounts in Gravelly Soils: Mary Ellen HYNES-GRIFFIN, Gus FRANKLIN\*, WES
- 1620 Discussion
- 1640 Conclusion of Day 1

18 May We 0900-1200 **Technical Session - Earthquake Engineering**  
Chairman: N. NARITA

- 0900 Sand Liquefaction Tests Using a Geotechnical Dynamic Centrifuge; Yasuyuki KOGA, Eiichi TANIGUCHI, Jun-ichi KOSEKI, Tadashi MORISHITA, PWRI (Presented by O. MATSUO)
- 0920 In-Situ Measurement of Pore Pressure Build-up During Liquefaction; Thomas HOLZER\*, T. Leslie YOUD, Michael J. BENNETT, USGS
- 0940 Two Directional Loading Test for Partially Filled Concrete in Steel Columns; Shoichi SAEKI, Minoru FUJIWARA, Koichi MINOSAKU, Jun HIKINO, PWRI (Presented by K. YOKOYAMA)
- 1000 Discussions
- 1020 Break
- 1040 Seismic Behavior of Full-Scale Bridge Columns; William STONE\*, Geraldine CHEOK, NBS
- 1100 Study on the Development of the Mixed Structural System Composed of Reinforced Concrete Column and Structural Steel Girder; Hiroyuki YAMANOUCHI, Isao NISHIYAMA, BRI (Presented by T. MUROTA)
- 1120 Effects of Soil and Rock on Ground Motion and Potential Damage in an Earthquake; Walter HAYS\*, USGS
- 1140 Discussions
- 1200 **Lunch:** Hosted by Samuel KRAMER, Deputy Director, NEL
- 1300 Seismic Performance of Reinforced Walled-Frame Structure -- Part 1: Deformation Capacity of Main Structural Elements such as Walled Columns, Beams, and Shear Walls; Masaya HIROSAWA, H. HIRAISHI, M. YOSHIMURA, Minoru FUGISAWA, BRI (Presented by T. MUROTA)

- 1320           Vibration Studies of Richard B. Russell  
Concrete Gravity Dam; Robert HALL, Tommy  
BEVINS\*, Stephen WRIGHT, CORPS
- 1340           Base Isolated Building Structure in JAPAN;  
Y. KITAGAWA, Masaya HIROSAWA, BRI  
                  (Presented by Y. YAMAZAKI)
- 1400           Discussions
- 1430           Task Committee Meetings  
T/C "A", Employees Lounge  
T/C "B", Lecture Room A  
T/C "C", Lecture Room B  
T/C "H", Lecture Room C  
T/C "J", Room B111
- 1700           Conclusion of Day 2

**19 May Th 0900-1140 Technical Session - Earthquake Engineering**  
Chairman: R N WRIGHT

- 9000           Shaking Table Test on the Ridge Response  
During Earthquakes; Yasushi SASAKI\*,  
Tetsuro KUWABARA, Seitaro YOSHIMI, PWRI
- 0920           New Initiatives in Seismic Hazards and  
Risk Assessment; Ted ALGERMISSEN\*, USGS
- 0940           Investigation of Two Buildings Shaken  
During the 19 September 1985 Mexico  
Earthquake; Douglas A. FOUTCH\*, Keith D.  
HJELMSTAD, Enrique Del Valle CALDERON, U  
of IL
- 1000           Discussions
- 1020           Recorded Behavior of Structures, Whittier  
1 Oct 87; Gerald BRADY, USGS  
                  (Presented by Thomas HOLZER)
- 1040           Field Experiments on Pipelines in the  
Parkfield Earthquake Zone; J. ISENBERG\*,  
E. RICHARDSON, Weidlinger Assoc.
- 1100           The Drawing Image of Earthquake Hazard;  
Keiichi OHTANI\*, Hiroshi TAKAHASHI, NRCDF
- 1120           Discussions

1000	Discussions
1020-1135	<u>Summary of T/C Workshops</u>
1020	T/C "A" Strong-Motion Instrumentation Arrays and Data (Presented by H. MEYERS)
1035	T/C "H" Soil Behavior and Stability During Earthquakes (Presented by Y. SASAKI)
1050	T/C "J" Wind and Earthquake Engineering for Transportation Systems (Presented by C. GALAMBOS)
1105	Discussions
1120-1200	<u>Two Decades of Accomplishments and Challenges for the Future</u>
1120	US paper - Two Decades of Accomplishments and Challenges for the Future (Presented by R. WRIGHT)
1140	JAPAN paper - Two Decades of Accomplishments and Challenges for the Future (Presented by N. NARITA)
1200	Discussions
1215	<b>Lunch:</b> Hosted by US Chairman Richard WRIGHT

- 1315           **Task Committee Reports & Resolutions**
- T/C A Strong Motion Instrumentation Arrays and Data  
T/C B Large-scale Testing Program  
T/C C Repair and Retrofit of Existing Structures  
T/C D Evaluation of Performance of Structures  
T/C E Natural Hazard Assessment and Mitigation  
          through Land-use Programs  
T/C F Disaster Prevention Methods for Lifeline  
          Systems  
T/C G Wind Characteristics and Structural Response  
T/C H Soil Behavior and Stability During Earthquakes  
T/C I Storm Surge and Tsunamis  
T/C J Wind and Earthquake Engineering for  
          Transportation Systems
- 1500           Adoption of Final Resolutions
- 1530           Break
- 1600           **CLOSING CEREMONIES**
- Call to Order by N.J. RAUFASTE, Secretary-  
                                  General US Panel
- Closing Remarks by N. NARITA, Chairman  
                                  JAPAN Panel
- Closing Remarks by R.N. WRIGHT, Chairman  
                                  US Panel
- 1620           Adjourn

(\* identifies oral presenters)

## LIST OF PANEL MEMBERS

### UNITED STATES PANEL ON WIND AND SEISMIC EFFECTS MEMBERSHIP LIST 1988

Dr. Richard N. Wright  
Chairman  
Director, Center for Building Technology  
National Bureau of Standards  
Gaithersburg, MD 20899  
(301) 975-5900

Mr. Noel J. Raufaste  
Secretary-General  
Head, Cooperative Research Programs  
Center for Building Technology  
National Bureau of Standards  
Gaithersburg, MD 20899  
(301) 975-5905

Dr. S. T. Algermissen  
Office of Earthquake Studies  
Branch of Earthquake Tactonics  
US Geological Survey  
Denver, CO 80225  
(303) 236-1611 FTS 776-1611

Dr. Celso S. Barrientos  
Supervisory Physical Scientist  
National Oceanic and Atmospheric Administration  
1825 Connecticut Ave., N.W.  
Universal Bldg., Rm. 518, E/AI3  
Washington, DC 20009  
(202) 673-5400

Dr. Eddie N. Bernard  
Director, Pacific Marine Environmental Laboratory  
National Oceanic and Atmospheric Administration  
7600 San Point Way, NE  
Seattle, WA 98115  
(206) 526-6239 FTS 392-6800

Dr. Roger D. Borcherdt  
Chief, Branch of Engineering  
Seismology and Geology  
Office of Earthquake Studies  
US Geological Survey  
345 Middlefield Road  
Menlo Park, CA 94025  
(415) 323-8111 X2755

Dr. A. Gerald Brady  
Physical Scientist  
Office of Earthquake Studies  
US Geological Survey  
345 Middlefield Road  
Menlo Park, CA 94025  
(415) 329-5664

Mr. Lee Butler  
Chief, Research Division  
Coastal Engineering Research Center  
US Army Engineer Waterways Experiment Station  
Office CEWES-CR  
P.O. Box 631  
Vicksburg, MS 39180  
(601) 634-2405

Dr. Charles G. Culver  
Chief, Structures Division  
Center for Building Technology  
National Bureau of Standards  
Gaithersburg, MD 20899  
(301) 975-6048

Dr. Robert H. Falk  
Research Engineer  
Engineered Wood Products and Structures Group  
Forest Products Laboratory  
One Gifford Pinchot Drive  
Madison, WI 53705-2398  
(608) 264-5626 FTS 364-5626

Dr. A. G. Franklin  
Chief, Earthquake Engineering & Geophysics Division  
CEWES-GH Geotechnical Laboratory  
US Army Engineer Waterways Experiment Station  
Vicksburg, MS 39180  
(601) 634-2658

Mr. G. Robert Fuller  
Chief, Compliance Branch  
Manufactured Housing and Construction Standards  
Division  
Dept. of Housing and Urban Development  
Washington, DC 20410-8000  
(202) 755-6920

Mr. Charles F. Galambos  
Chief, Structures Division  
Office of Engineering & Highway Operations R & D  
Federal Highway Administration  
Department of Transportation  
6300 Georgetown Pike  
McLean, VA 22101  
(703) 285-2087

Mr. James H. Gates  
Office of Structures Design  
Department of Transportation  
State of California  
1120 N Street  
Sacramento, CA 95807  
(916) 445-1439

Dr. Michael P. Gaus  
Director, Division of Critical Engineering Systems  
National Science Foundation  
1800 G Street, N.W.  
Washington, DC 20550  
(202) 357-9500

Mr. Peter E. Gurvin  
A/FBO, SA-6  
Department of State  
Washington, DC 20520  
(202) 235-3689

Dr. Walter W. Hays  
Deputy for Research Application  
Office of Earthquake Survey  
US Geological Survey  
905 National Center  
Reston, VA 22043  
(703) 648-6711

Dr. William B. Joyner  
Office of Earthquake Studies  
Branch of Ground Motion & Faulting  
US Geological Survey  
345 Middlefield Road  
Menlo Park, CA 94025  
(415) 323-8111

Mr. Roger Kenneally  
Structural and Seismic Engineering Branch  
Seismic Section  
Office of Nuclear Regulatory Research  
U.S. Nuclear Regulatory Commission  
Washington, DC 20555  
(301) 492-3934

Mr. Richard W. Kramer  
Technical Review Staff, D-3210  
Bureau of Reclamation  
Department of Interior  
P.O. Box 25007  
Denver, CO 80225  
(303) 236-8539 FTS 776-8539

Mr. Richard Krimm  
Office of Natural & Technological Hazards  
Federal Emergency Management Agency  
Washington, DC 20472  
(202) 646-2871

Mr. Paul K. Krumpe  
Office of Foreign Disaster Assistance  
Agency for International Development  
Department of State  
Washington, DC 20523  
(202) 647-9758

Dr. H.S. Lew  
Leader, Structural Evaluation Group  
Structures Division  
Center for Building Technology  
National Bureau of Standards  
Gaithersburg, MD 20899  
(301) 975-6061

Dr. Shih-Chi Liu  
Earthquake Hazards Mitigation Program  
National Science Foundation  
1800 G Street, N.W.  
Washington, DC 20550  
(202) 357-9780

Mr. Robert MacDonald  
Geologic Service Branch, Code D  
Bureau of Reclamation  
Department of the Interior  
Building 67, Denver Federal Center  
Denver, CO 80225  
(303) 236-4195 FTS 776-4195

Dr. Richard D. Marshall  
Earthquake Engineering Group  
Structures Division  
Center for Building Technology  
National Bureau of Standards  
Gaithersburg, MD 20899  
(301) 975-6071

Dr. Richard D. McConnell  
Office of Construction  
Veterans Administration  
811 Vermont Avenue, N.W.  
Washington, DC 20420  
(202) 233-3103

Dr. Francis G. McLean  
Chief, Division of Research & Laboratory Services,  
D-1500  
Bureau of Reclamation  
P.O. Box 25007  
Denver, CO 80225  
(303) 234-3303 FTS 776-5981

Mr. John F. Meehan  
Principal Structural Engineer  
Research Director  
Structural Safety Section  
Office of the State Architect  
Department of General Services  
Sacramento, CA 95805  
(916) 445-8730

Mr. Herbert Meyers  
Chief, Earth Geophysics  
National Oceanic & Atmospheric Administration  
325 Broadway  
Boulder, CO 80303  
(303) 497-6215 FTS 320-6215

Dr. William E. Roper  
Assistant Director  
Research and Development (Civil Works)  
US Army Corps of Engineers  
20 Massachusetts Avenue, N.W.  
Washington, DC 20314-1000  
(202) 272-0257

Dr. John B. Scalzi  
Program Director, Systems Engineering for Large  
Structures  
National Science Foundation  
1800 G Street, N.W.  
Washington, DC 20550  
(202) 357-7710

Dr. Joseph T. Schaefer  
Chief, Techniques Development Unit  
National Severe Storm Forecast Center  
National Weather Service, NOAA  
601 E. 12th Street  
Kansas City, MO 64106  
(816) 374-5672

Mr. Robert J. Smith  
Office of the Chief of Engineers  
Department of the Army  
HQUSACE (CEEC-ED)  
Washington, DC 20314-1000  
(202) 272-0220

Mr. Joseph Tyrrell  
Deputy Chief Engineer  
Naval Facilities Engineering Command  
Department of the Navy  
200 Stovall Street  
Alexandria, VA 22332  
(703) 325-0047

Mr. Dominic Zigant  
Head, Structural Branch, Western Division  
Naval Facilities Engineering Command  
Department of the Navy  
P.O. Box 727, Code 402  
San Bruno, CA 94066  
(415) 877-7340

ALTERNATE MEMBERS

Dr. Clifford Astill  
Division of Critical Engineering Systems  
National Science Foundation  
1800 G Street, N.W.  
Washington, DC 20550  
(202) 357-9500

Mr. Michael Changery  
National Climatic Center  
Federal Building  
Asheville, NC 28801  
(704) 259-0765 FTS 672-0765

Dr. James Costello  
Structural and Seismic Engineering Branch  
Structural Section  
Office of Nuclear Regulatory Research  
US Nuclear Regulatory Commission  
Mail Stop 007NL  
Washington, DC 20555  
(301) 443-7709

Dr. A. J. Eggenberger  
Division of Critical Engineering Systems  
National Science Foundation  
1800 G Street, N.W.  
Washington, DC 20550  
(202) 357-9500

Mr. Lucian G. Guthrie  
Structural Engineer  
Office of Chief of Engineers  
HQUSACE (CEEC-ED)  
Department of the Army  
Washington, DC 20314-1000  
(202) 272-8673

Dr. James Houston  
Chief, Coastal Engineering Research Center  
US Army Engineer Waterways Experiment Station  
P.O. Box 631  
Vicksburg, MS 39180-0631  
(601) 634-2000

Mr. Robert R. Ledzian  
Senior Staff Assistant for Research, WO-220  
Bureau of Reclamation  
Department of the Interior  
18th & C Streets, N.W.  
Washington, DC 20240  
(202) 343-6703

Dr. T. K. Lew  
Naval Civil Engineering Laboratory  
L51  
Port Huenene, CA 93043  
(805) 982-5785

Ms. Janina Mirski  
Chief, Structures Division  
Office of Facility (088C12)  
Veterans Administration  
811 Vermont Avenue, N.W.  
Washington, DC 20420  
(202) 233-2394

Mr. Ronald J. Morony  
Director, Innovative Technology and Special  
Projects Division  
Room 8232  
Dept. of Housing and Urban Development  
Washington, DC 20410-6000  
(202) 755-0640

JAPAN PANEL ON WIND AND SEISMIC EFFECTS

MEMBERSHIP LIST

1988

Dr. Nobuyuki Narita  
Chairman  
Director-General  
Public Works Research Institute  
Ministry of Construction  
1, Asahi, Tsukuba-shi,  
Ibaraki-ken 305  
Tel. 0298-64-2211

Dr. Katsuyoshi Ishizaki  
Secretary-General  
Director, Planning and Research  
Administration Department  
Public Works Research Institute  
Ministry of Construction  
1, Asahi, Tsukuba-shi,  
Ibaraki-ken 305  
Tel. 0298-64-2211

Mr. Tokunosuke Fujitani  
Chief, The Second Research  
Laboratory  
Applied Meteorology Research  
Division  
Meteorological Research Institute  
Meteorological Agency  
1-1 Nagamine, Tsukuba-shi,  
Ibaraki-ken 305  
Tel. 0298-51-7111

Mr. Miroru Fujiwara  
Head, Bridge Division  
Structure and Bridge Department  
Public Works Research Institute  
Ministry of Construction  
1, Asahi, Tsukuba-shi,  
Ibaraki-ken 305  
Tel. 0298-64-2211

Dr. Sadaiku Hattori  
Special Senior Scientist  
Building Research Institute  
Ministry of Construction  
1, Tatehara, Tsukuba-shi,  
Ibaraki-ken 305  
Tel. 0298-64-2151

Dr. Masaya Hiroswa  
Director, International Institute  
of Seismology and Earthquake  
Engineering Department  
Building Research Institute  
Ministry of Construction  
1, Tatehara, Tsukuba-shi,  
Ibaraki-ken 305  
Tel. 0298-64-2151

Dr. Yuji Ishiyama  
Head, Planning and Investigation  
Division  
Research Planning and Information  
Department  
Building Research Institute  
Ministry of Construction  
1, Tatehara, Tsukuba-shi,  
Ibaraki-ken 305  
Tel. 0298-64-2151

Dr. Toshio Iwasaki  
Assistant Director-General  
Public Works Research Institute  
Ministry of Construction  
1, Asahi, Tsukuba-shi,  
Ibaraki-ken 305  
Tel. 0298-64-2211

Dr. Mamoru Katsumata  
Head, Seismological and  
Volcanology Division  
Meteorological Research Institute  
Meteorological Agency  
1-1, Nagamine, Tsukuba-shi,  
Ibaraki-ken 305  
Tel. 0298-51-7111

Dr. Kazuhiko Kawashima  
Head, Earthquake Engineering  
Division  
Earthquake Disaster Prevention  
Department  
Public Works Research Institute  
Ministry of Construction  
1, Asahi, Tsukuba-shi,  
Ibaraki-ken 305  
Tel. 0298-64-2211

Mr. Yasuyuki Koga  
Head, Soil Dynamics Division  
Construction Method and Equipment  
Department  
Public Works Research Institute  
Ministry of Construction  
1, Asahi, Tsukuba-shi,  
Ibaraki-ken 305  
Tel. 0298-64-2211

Mr. Kiyoshi Kurashige  
Head, Typhoon Research Division  
Meteorological Research  
Institute  
Meteorological Agency  
1-1, Nagamine, Tsukuba-shi,  
Ibaraki-ken 305  
Tel. 0298-51-7111

Dr. Norihisa Matsumoto  
Head, Fill Type Dam Division  
Dam Department  
Public Works Research Institute  
Ministry of Construction  
1, Asahi, Tsukuba-shi,  
Ibaraki-ken 305  
Tel. 0298-64-2211

Mr. Tatsuo Murota  
Director, Structural  
Engineering Department  
Building Research Institute  
Ministry of Construction  
1, Tatehara, Tsukuba-shi,  
Ibaraki-ken 305  
Tel. 0298-64-2151

Mr. Masatoshi Nagaoka  
Head, Second Geographic Division  
Geographical Survey Institute  
Ministry of Construction  
Kitasato-1, Tsukuba-shi,  
Ibaraki-ken 305  
Tel. 0298-64-1111

Dr. Setsuo Noda  
Chief, Geotechnical Earthquake  
Engineering Laboratory  
Structure Division  
Port and Harbour Research  
Institute  
Ministry of Transport  
3-1-1, Nagase, Yokohama-shi,  
Kanagawa-ken 239  
Tel. 0468-41-5410

Mr. Keiichi Ohtani  
Head, Earthquake Engineering  
Laboratory  
Third Research Division  
National Research Center for  
Disaster Prevention  
Science and Technology Agency  
3-1, Tennodai, Tsukuba-shi,  
Ibaraki-ken 305  
Tel. 0298-51-1611

Mr. Michio Okahara  
Head, Foundation Engineering  
Division  
Structure and Bridge Department  
Public Works Research Institute  
Ministry of Construction  
1, Asahi, Tsukuba-shi,  
Ibaraki-ken 305  
Tel. 0298-64-2211

Dr. Shin Okamoto  
Director, Research Planning  
and Information Department  
Building Research Institute  
Ministry of Construction  
1, Tatehara, Tsukuba-shi,  
Ibaraki-ken 305  
Tel. 0298-64-2151

Mr. Shoichi Saeki  
Director, Structure and Bridge  
Department  
Public Works Research Institute  
Ministry of Construction  
1, Asahi, Tsukuba-shi,  
Ibaraki-ken 305  
Tel. 0298-64-2211

\* Dr. Yasushi Sasaki  
Head, Ground Vibration Division  
Earthquake Disaster Prevention  
Department  
Public Works Research Institute  
Ministry of Construction  
1, Asahi, Tsukuba-shi,  
Ibaraki-ken 305  
Tel. 0298-64-2211

Dr. Hiroshi Takahashi  
Director-General  
National Research Center for  
Disaster Prevention  
Science and Technology Agency  
3-1, Tennodai, Tsukuba-shi,  
Ibaraki-ken 305  
Tel. 0298-51-1611

Dr. Katsutoshi Tanimoto  
Director, Hydraulic  
Engineering Division  
Port and Harbour Research  
Institute  
Ministry of Transport  
3-1-1, Nagase, Yokohama-shi,  
Kanagawa-ken 239  
Tel. 0468-41-5410

Dr. Hajime Tsuchida  
Director-General  
Port and Harbour Research  
Institute  
Ministry of Transport  
3-1-1, Nagase, Yokohama-shi,  
Kanagawa-ken 239  
Tel. 0468-41-5410

Dr. Takaaki Uda  
Head, Coastal Engineering  
Division  
River Department  
Public Works Research Institute  
Ministry of Construction  
1, Asahi, Tsukuba-shi,  
Ibaraki-ken 305  
Tel. 0298-64-2211

Mr. Osamu Ueda  
Director, Earthquake Disaster  
Prevention Department  
Public Works Research Institute  
Ministry of Construction  
1, Asahi, Tsukuba-shi,  
Ibaraki-ken 305  
Tel. 0298-64-2211

Dr. Hiroyuki Yamanouchi  
Head, Structural Dynamics  
Division  
Structural Engineering Department  
Building Research Institute  
Ministry of Construction  
1, Tatehara, Tsukuba-shi,  
Ibaraki-ken 305  
Tel. 0298-64-2151

Dr. Yutaka Yamazaki  
Head, Large-Scale Structure  
Testing Division  
Production Department  
Building Research Institute  
Ministry of Construction  
1, Tatehara, Tsukuba-shi,  
Ibaraki-ken 305  
Tel. 0298-64-2151

\* Mr. Koichi Yokoyama  
Head, Structure Division  
Structure and Bridge Department  
Public Works Research Institute  
Ministry of Construction  
1, Asahi, Tsukuba-shi,  
Ibaraki-ken 305  
Tel. 0298-64-2211

\* Secretary

## LIST OF TASK COMMITTEE MEMBERS

<u>Task Committee</u>	<u>US SIDE</u>	<u>Japanese Side</u>
A. Strong-Motion Instrumentation Arrays and Data	*A.G. Brady A.F. Franklin W.B. Joyner F.G. McLean H. Meyers	*H. Tsuchida S. Hattori M. Ichikawa Y. Ishiyama K. Ohtani Y. Sasaki H. Yamanouchi
B. Large-Scale Testing Programs	*H.S. Lew J.B. Scalzi R.J. Smith	*K. Ohtani Y. Koga S. Noda S. Okamoto K. Yokoyama H. Yamanouchi
C. Repair and Retrofit of Existing Structures	*J.B. Scalzi C.F. Galambos P.E. Gurvin H.S. Lew R.D. McConnell R.J. Morony	*M. Hirose T. Iwasaki S. Okamoto H. Shinohara
D. Evaluation of Performance of Structures	*G.R. Fuller R.D. McConnell J.F. Meehan J.B. Scalzi R.J. Smith	*S. Okamoto Y. Ishiyama M. Okahara H. Shinohara H. Yamanouchi
E. Natural Hazard Assessment and Mitigation Through Land Use Programs	*S.T. Algermissen A.G. Brady G.R. Fuller R.D. Marshall	*K. Kawashima S. Hattori T. Iwasaki M. Nagaoka Y. Sugimura
F. Disaster Prevention Methods for Lifeline Systems	*S.C. Liu J.B. Scalzi	*T. Iwasaki K. Kawashima T. Murota S. Noda K. Ohtani Y. Sasaki
G. Wind Characteristics and Structural Response	*R.D. Marshall C.S. Barrientos C.F. Galambos M.P. Gaus	*K. Masamura T. Hanafusa T. Murota N. Narita K. Yokoyama

Task Committee-continued

US Side

Japanese Side

H. Soil Behavior and Stability  
During Earthquakes

\*A.G. Franklin  
F.G. McLean  
R.J. Smith

\*Y. Sasaki  
Y. Koga  
N. Matsumoto  
M. Okahara  
Y. Sugimura  
H. Tsuchida

I. Storm Surge and Tsunamis

\*C.S. Barrientos  
E.N. Bernard  
L. Butler  
M.P. Gaus  
H. Meyers

\*T. Uda  
M. Ichikawa  
K. Masamura  
H. Takahashi  
K. Tanimoto

J. Wind and Earthquake Engineering  
for Transportation Systems

\*C.F. Galambos  
C.G. Culver  
A.G. Franklin  
J.B. Scalzi

\*H. Shinohara  
M. Fujiwara  
T. Iwasaki  
K. Kawashima  
N. Narita  
M. Okahara  
Y. Sasaki  
K. Yokoyama

---

\*Chairman

## RESOLUTIONS

### RESOLUTIONS OF THE TWENTIETH JOINT MEETING U.S.-JAPAN PANEL ON WIND AND SEISMIC EFFECTS (UJNR)

National Bureau of Standards  
Gaithersburg, Maryland

May 17-20, 1988

The following resolutions are hereby adopted:

1. The Twentieth Joint Panel Meeting provided an opportunity to exchange valuable technical information which was beneficial to both countries. In view of the importance of cooperative programs on the subject of wind and seismic effects, the continuation of Joint Panel Meetings is considered essential.
2. The following activities have been conducted since the Nineteenth Joint Meeting:
  - a. Guest researchers from both countries performed joint research that advanced the state of wind and earthquake engineering.
  - b. Technical documents and research reports were exchanged; information from the Whittier Narrows, Superstition Hills, Mexico City, and Eastern Chiba Earthquakes; proceedings from workshops; and information on application of base isolation and active damping systems.
  - c. The Japanese MOC document, "Manual for Repair Methods of Civil Engineering Structures Damaged by Earthquakes" was translated into English and soon will be disseminated to the US engineering profession.
  - d. Phase I of the Joint Masonry Program was completed. Phase II of the Program, initiated in October 1987, includes large subassemblage evaluation and a 5-story full-scale experimental test. Research is coordinated by the Joint Technical Coordinating Committee on Masonry Research (JTCCMAR).
  - e. Workshops were held:
    - a) Strong-Motion Earthquake Observation, Task Committee (A), Menlo Park, CA, August 3-6, 1987.
    - b) Remedial Treatment of Liquefiable Soils, Task Committee (H) Jackson Hole, WY, May 11-14, 1988.
    - c) Fourth Bridge Workshop, Task Committee (J), San Diego, CA May 11-14, 1988.

These findings promoted improved knowledge for wind and seismic disaster mitigation.

3. Recognizing the common interests in improved technology for better design and construction practices for structures to resist extreme wind and seismic loads; the Task Committees on Evaluation of Structural Performance (T/C "D") and on Wind Characteristics and Structural Response (T/C "G") proposed combining their work into a single Task Committee on Evaluation of Structural Performance. The Panel recommends that each side consider the combination of T/C's "D" and "G" and that both chairmen inform each other with their approval by August 1988.
4. Recognizing that the 20th Joint Meeting signifies a major milestone in the history of the Panel on Wind and Seismic Effects, both sides developed and presented papers on their many accomplishments and proposed future directions.
5. The Panel recognizes the importance of the following items:
  - a. Both sides are planning the Program on Large-scale Testing of Precast Seismic Structural Systems. Information about the Program will be exchanged prior to the 21st Joint Meeting.
  - b. Continue to exchange data and information on application of active and passive control of buildings and other structures and encourage the appropriate Task Committees to advance these technologies.
  - c. Collect strong motion data on the performance of buried pipeline systems.
  - d. Obtain experimental verification of the effectiveness of retrofiting and strengthening methods for structures and soils.
6. The Panel endorses the following workshops and planning meeting proposed by the Task Committees:
  - a. Fifth Workshop on Repair and Retrofit, Task Committee (C), to be held in Southern CA prior to the 21st UJNR Joint Meeting.
  - b. Workshop on Sensor Technology Applied to Large Engineering Systems, Task Committee (D), to be held in Boulder, CO.
  - c. Workshop on Earthquake Hazard and Risk Assessment -- Research and Progress, Task Committee (E) to be held in Tsukuba in conjunction with the 21st UJNR Joint Meeting.
  - d. Workshop on Disaster Prevention for Lifeline Systems, Task Committee (F), to be held in Tsukuba in conjunction with the 21st UJNR Joint Meeting.
  - e. Planning Meeting on cooperative research in Remedial Treatment of Liquefiable Soils, Task Committee (H), to be held in conjunction with the 21st UJNR Joint Meeting.

- f. Fifth Bridge Workshop, Task Committee (J), to be held in Tsukuba in conjunction with the 21st UJNR Joint Meeting.

Scheduling for the workshops and planning meeting shall be performed by the chairmen of each Task Committee with concurrence of the Joint Panel chairmen. Results of each activity shall be presented at the next Joint Panel Meeting.

7. The Panel recognizes the importance of continued exchange of personnel, technical information, research results and recorded data that lead to mitigating losses from earthquakes and strong winds. The Panel also recognizes the importance of using available large-scale testing facilities in both countries. Thus, these activities should continue to be strengthened and expanded and, as appropriate, share Task Committee work at other meetings having similar task committee objectives. To facilitate these exchanges, the Panel will provide official sponsorship.
8. The Panel requests Task Committee chairmen to clearly define their respective T/C objective(s), their current and proposed scope-of-work, and their expected short - and mid-term accomplishments for discussion and approval at the 21st UJNR Joint Meeting. Task Committee Chairmen should furnish copies of Task Committee objective(s), scope-of work, accomplishments, and other appropriate correspondence to the Secretariats of both sides.
9. Recognizing that wind and seismic disaster mitigation plans benefit disaster-prone countries worldwide, that many developing countries suffer from natural disasters such as extreme winds, storm surges, earthquakes, and tsunamis, and that both the U.S. and Japan have been involved in international technical cooperative programs, the Panel recommends development of a policy for discussion and approval at the 21st Joint Meeting about the best methods for Panel contribution, through appropriate Task Committee(s), to the International Decade of Natural Disaster Reduction (IDNDR). In addition, the Panel will continue efforts to develop and coordinate projects that provide aid and training to developing countries and that maintain the exchange of technical information.
10. The Twenty-first Joint Meeting of the UJNR Panel on Wind and Seismic Effects will be held at Tsukuba, Japan, May 1989. Specific dates, program, and itinerary will be proposed by the Japan Panel with concurrence of the US Panel.



**Theme I**

---

**Wind Engineering**



# Modeling the Effect of Spanwise Coherence of Aerodynamic Forces on Full-Bridge Response

BY

Fazl Ehsan<sup>1</sup> and Harold R. Bosch<sup>2</sup>

## ABSTRACT

A method for modeling the effect of the loss of spanwise coherence of aerodynamic forces on the vortex-shedding response of long-span flexible bridges is described. The method is based on a semi-empirical non-linear vortex-shedding model and results of wind-tunnel tests on bridge deck section models. Curves describing the variation of the spanwise coherence of wind pressure fluctuations with distance from a fixed reference point downstream of a rigid, elastically mounted model undergoing locked-in oscillations are obtained from wind-tunnel tests. These are used to obtain a shape function for the loss of spanwise coherence for long-span flexible bridges. This function is incorporated into the vortex-shedding model to obtain modified values for the response. An example for the application of the method is provided.

**KEYWORDS:** Aerodynamics; Long-Span Bridges; Spanwise Coherence; Vortex Shedding.

## 1. INTRODUCTION

A study is currently being undertaken at the Turner-Fairbank Highway Research Center of the Federal Highway Administration at McLean, VA., to develop a model for predicting the vortex-induced response of long-span flexible bridges, together with an implementation scheme for direct use in design.

The study consists of two main parts. The first part deals with methods to identify the parameters of a semi-empirical non-linear mathematical model for the vortex-induced response of rigid, elastically mounted bridge-deck section models. The second part of the study involves developing methods to extend the two-dimensional model to long-span flexible bridges, taking into account the three-dimensional nature of vortex shedding as manifested in the loss of spanwise correlation of aerodynamic forces.

This paper concerns the second part of the study. The two-dimensional mathematical model is briefly described, its extension to flexible bridges discussed and a method is presented that attempts to account for the loss of spanwise correlation of forces due to both natural turbulent loss at constant oscillation amplitudes and de-

creasing deflection of a bridge vibration mode away from its highest point.

## 2. MATHEMATICAL MODEL FOR RIGID BODY

A rigid, elastically mounted bluff body free to oscillate in the across-wind direction will be driven periodically under the action of vortices shed in its wake when subjected to a uniform flow. When the frequency of vortex-shedding approaches the natural across-flow frequency of the body, a phenomenon known as 'lock-in' occurs, the main characteristics of which are large, self-limiting amplitudes of oscillation and entrainment of the vortex-shedding frequency by the body natural frequency over a range of wind speeds.

Various mathematical models that reflect the main aspects of the phenomenon described above have been proposed (e.g [1],[2]). The mathematical model used in this study is an empirical non-linear model in which aerodynamic excitation, non-linear aerodynamic damping and aerodynamic stiffness are provided to a linear mechanical oscillator [5]. The model takes the following form:

$$m \left[ \ddot{y} + 2\zeta\omega_1\dot{y} + \omega_1^2 y \right] = \frac{1}{2}\rho U^2 (2D) \left[ Y_1(K) \left( 1 - \epsilon \frac{y^2}{D^2} \right) \frac{\dot{y}}{U} + Y_2(K) \frac{y}{D} + \frac{1}{2} C_L(K) \sin(\omega t + \phi) \right] \quad (1)$$

where  $m$ ,  $\zeta$  and  $\omega_1$  are the model mass per unit length, damping ratio and circular frequency of the model,  $K$  is the reduced frequency ( $K = D\omega/U$ ),  $D$  is the depth of the section,  $U$  is the mean wind speed, and  $\omega$  is the frequency of vortex shedding which satisfies the Strouhal relation  $\frac{\omega D}{U} = 2\pi S$  where  $S$  is the Strouhal number.  $Y_1$ ,  $Y_2$ ,  $\epsilon$  and  $C_L$  are the model parameters to be determined experimentally.

<sup>1</sup>FHWA Graduate Research Fellow  
The Johns Hopkins University  
Baltimore, MD 21218

<sup>2</sup>Research Structural Engineer  
Federal Highway Administration, HNR-10  
6300 Georgetown Pike  
McLean, VA 22101

At lock-in ( $\omega \approx \omega_1$ ) the term reflecting aerodynamic damping effects predominates and it can be assumed that  $Y_2 \approx 0$  and  $C_L \approx 0$ . Equation (1) simplifies to:

$$m \left[ \ddot{y} + 2\zeta\omega_1\dot{y} + \omega_1^2 y \right] = \frac{1}{2}\rho U^2 (2D)Y_1 \left( 1 - \varepsilon \frac{y^2}{D^2} \right) \frac{\dot{y}}{U} \quad (2)$$

Parameters  $Y_1$  and  $\varepsilon$  can be estimated using a method described in [5]. In the following discussion it will be assumed that estimates of the parameters are available.

### 3. EXTENSION TO PROTOTYPE RESPONSE

The phenomenon of lock-in picks a particular mode for 'resonance'. Assuming that the natural frequencies of a given bridge are not too close together, it may be reasonable to suppose that the vortex-induced response of the bridge will take place at the natural frequency of a single mode. The vertical motion  $y$  at the spanwise location  $x$  of the deck coordinate at any time  $t$  may then be expressed as:

$$y(x, t) = \Phi(x)\xi(t)D \quad (3)$$

where  $\Phi(x)$  is the non-dimensional mode shape,  $\xi(t)$  is its generalized coordinate and  $D$  is included for dimensional compatibility.

The generalized coordinate is required to satisfy the following equation obtained by inserting (3) into (2), multiplying both sides by  $\Phi(x)$  and integrating over the span  $L$  of the deck:

$$M \left[ \ddot{\xi}(t) + 2\zeta\omega_1\dot{\xi}(t) + \omega_1^2 \xi(t) \right] = \rho U D L Y_1 (K) \left[ \Phi_2 - \varepsilon \Phi_4 \xi^2(t) \right] \dot{\xi}(t) \quad (4)$$

where  $M$  (the generalized mass),  $\Phi_2$  and  $\Phi_4$  are defined as

$$M = \int_0^L m \Phi^2(x) dx \quad (5)$$

$$\Phi_2 = \int_0^L \Phi^2(x) \frac{dx}{L} \quad (6)$$

$$\Phi_4 = \int_0^L \Phi^4(x) \frac{dx}{L} \quad (7)$$

In equation (4) the aerodynamic forces are assumed to be completely spanwise coherent as is evident from the definitions (6) and (7).

The criterion that the net energy loss per cycle is zero in the limit cycle of oscillation (at lock-in) can be stated mathematically as:

$$\int_0^T F_d \dot{\xi}(t) dt = 0 \quad (8)$$

where  $F_d$  is the total damping force:

$$F_d = \left[ 2M\zeta\omega_1 - \rho U D L Y_1 (K) (\Phi_2 - \varepsilon \Phi_4 \xi^2) \right] \dot{\xi}(t) \quad (9)$$

from (4),  $T = \frac{2\pi}{\omega}$  and  $\omega \approx \omega_1$ . For an approximate response form of:

$$\xi(t) = \xi_0 \cos(\omega t) \quad (10)$$

equations (8) and (9) yield the following expression for the amplitude of the generalized coordinate  $\xi_0$ :

$$\xi_0 = \frac{2}{\sqrt{\varepsilon}} \left[ \frac{\Phi_2}{\Phi_4} - \frac{2M\zeta K}{\rho D^2 L Y_1 \Phi_4} \right]^{\frac{1}{2}} \quad (11)$$

where  $Y_1$  and  $\varepsilon$  are the values of the parameters at the reduced frequency  $K$ . In order to obtain the maximum amplitude of the generalized coordinate, the parameters should be evaluated at that value of  $K$  ( $=K_1$ , say) at which the maximum lock-in response of the model is observed, since lock-in persists over a range of wind speeds and thus of reduced frequencies. In addition, if the mass distribution of the deck is constant along the length of the span, then:

$$M = \int_0^L m \Phi^2(x) dx = mL\Phi_2 \quad (12)$$

The maximum amplitude of the generalized coordinate can then be expressed as:

$$\xi_0 = \frac{2}{\sqrt{\varepsilon}} \left[ \frac{\Phi_2}{\Phi_4} - \frac{2m\Phi_2\zeta K_1}{\rho D^2 Y_1 \Phi_4} \right]^{\frac{1}{2}} \quad (13)$$

where  $Y_1$  and  $\varepsilon$  are estimated at the reduced frequency  $K_1$ . The spanwise distribution of the maximum displacement is then given from (3) as:

$$y(x) = \xi_{0max} \Phi(x) D \quad (14)$$

### 4. CORRECTION FOR LOSS OF SPANWISE COHERENCE

The assumption of the previous section that the aerodynamic forces are fully coherent along the length of the bridge deck is conservative. Various experiments on rigid circular sections (e.g. [3],[6]), square sections [7] and D-sections [3] have shown that the correlation of forces falls off as the distance from a given reference point is increased, the fall-off being more rapid if the incoming flow is turbulent [7]. However, the phenomenon of lock-in acts as a controller of these effects and the rate of fall-off decreases as the oscillation amplitude increases. In this section a method is described which attempts to account for this inevitable loss of spanwise coherence, both due to natural turbulent loss at constant oscillation amplitude and due to decreasing deflection of the mode away from its highest point.

#### 4.1 Modified Equations

A simple modification that may be introduced in order to account for the loss of spanwise coherence is as follows. Let the definitions of the functions  $\Phi_2$  and  $\Phi_4$  be modified to:

$$\Phi_2^m = \sum_{i=1}^m \left[ \int_{-bL_i}^0 g_{1i}(x_i) \Phi^2(x_i) \frac{dx_i}{L} + \int_0^{aL_i} g_{2i}(x_i) \Phi^2(x_i) \frac{dx_i}{L} \right] \quad (15)$$

and

$$\Phi_4^m = \sum_{i=1}^m \left[ \int_{-bL_i}^0 g_{1i}(x_i) \Phi^4(x_i) \frac{dx_i}{L} + \int_0^{aL_i} g_{2i}(x_i) \Phi^4(x_i) \frac{dx_i}{L} \right] \quad (16)$$

where  $m = n + 1$  and  $n$  is the number of nodes of  $\Phi(x)$ , and  $x_i$  is the coordinate corresponding to the  $i^{th}$  segment between successive nodes centered at the point where the maximum amplitude occurs in that segment.  $g_{1i}(x_i)$  and  $g_{2i}(x_i)$  are shape functions that define the fall-off characteristics of spanwise coherence for the  $i^{th}$  segment of the bridge to the left and the right of the origin of  $x_i$  respectively. This is shown in Figure 1 at the end of the paper. Equations (15) and (16) are general expressions applicable to any arbitrary mode shape  $\Phi(x)$ . The expressions simplify considerably if the mode can be approximated by a sine wave. In such a case  $g_{1i}(x_i) = g_{2i}(x_i) = g(x_i)$  say. In addition  $a = b = \frac{1}{2}$  and equations (15) and (16) reduce to :

$$\Phi_2^m = \sum_{i=1}^m \left[ 2 \int_0^{\frac{L_i}{2}} g(x_i) \Phi^2(x_i) \frac{dx_i}{L} \right] \quad (17)$$

$$\Phi_4^m = \sum_{i=1}^m \left[ 2 \int_0^{\frac{L_i}{2}} g(x_i) \Phi^4(x_i) \frac{dx_i}{L} \right] \quad (18)$$

It may be noted that the case discussed in Section 1 is a special case of the above, with  $g_{ji}(x_i) = 1$  for  $j = 1, 2$  and  $i = 1, 2, \dots, m$ , and the origin of the  $x$ -coordinate is at the end of the span.

The amplitude of the generalized coordinate can be written as:

$$\xi_0 = 2 \sqrt{\frac{\Phi_2^m}{\varepsilon \Phi_4^m}} \left[ 1 - \frac{2m \Phi_2 \zeta K_1}{\rho D^2 Y_1 \Phi_2^m} \right]^{\frac{1}{2}} \quad (19)$$

It may be noted from (19) that the condition of zero response is defined by:

$$\frac{2m \Phi_2 \zeta K_1}{\rho D^2 Y_1 \Phi_2^m} \geq 1.0 \quad (20)$$

A method for obtaining the shape functions  $g(x)$  from experiments is described in the next section. A prelim-

inary study was conducted using four assumed shape functions to evaluate the effect of the loss of spanwise coherence of aerodynamic forces on the amplitude of the generalized coordinate using the above approach. A sine wave with  $m$  nodes was assumed for the mode shape of the bridge, i.e:

$$\Phi(x) = \sin \frac{(m+1)\pi x}{L} \quad (21)$$

#### 4.2 Results of Preliminary Study

The shape functions used in the study were a rectangular function (i.e  $g(x) = 1$ ), a triangular or linear decay function, a cosine-tapered function and an exponential decay function with variable decay parameter  $n$  (i.e  $e^{-n\bar{x}}$  where  $\bar{x}$  is a normalized distance). These are illustrated in Figure 2. In addition to the above, the length of the bridge over which vortex-shedding occurs was also varied, so that the effect of coherent shedding over portions of the bridge could be assessed. In this context, the 'coherent fraction' was defined as the length over which non-zero vortex shedding is assumed divided by the length of the span (Figure 2). The shape functions were then used in equations (17), (18) and (19) along with experimentally determined values of  $Y_1$  and  $\varepsilon$  for an H-section ( $Y_1 = 18.0$ ,  $\varepsilon = 110.0$ ) to calculate  $\xi_{0max}$  for a bridge 2,800 ft (853.44 m) long, 8 ft (2.438 m) deep, 32 ft (9.754 m) wide and weighing 4,800 lbs/ft (70,047.24 m). The bridge was assumed to have the same cross-sectional shape as the model. The results of the analysis are shown in graphical form in Figure 3. The values of  $\xi_0$  for the four cases calculated for a coherent fraction (CF) of 1.0 and 0.70 are shown in Table 1 for comparison.

The percent reduction of the amplitude of the generalized coordinate calculated using the cosine-tapered and triangular shape functions from that obtained using the rectangular shape function (fully coherent shedding) is approximately 15 % for shedding assumed to occur over the full span (coherent fraction = 1.0). The percent reduction for the exponential shape function with  $n = 1$  is about 12 %. Comparing results at a coherent fraction value of 0.70 indicates that the percent reduction from the rectangular case increases to almost 25 % for the cosine-tapered and triangular functions. It may be observed that the amplitude of the generalized coordinate drops off very sharply for values of coherent fraction less than 0.5 in the cases of the linear and cosine-tapered fall-off.

To gain further insight into the actual behavior of the coherence fall-off and its possible incorporation into the design process, the following experiment is proposed and the application of its results discussed.

## 5. SHAPE FUNCTION FOR FLEXIBLE BRIDGES

A method to determine a suitable shape function  $g_f(x)$  describing the fall-off characteristics of aerodynamic forces for the case of a flexible bridge, given its mode shape, is discussed in this section. The method requires wind-tunnel tests on the bridge-deck section model as well as certain numerical computations. The proposed method is outlined below.

### 5.1 Model Correlation Curves

The first step is to experimentally obtain force correlation curves which describe the variation of spanwise coherence of aerodynamic forces with distance from a reference point, for a rigid, elastically mounted section model. Pressure measurements can be taken along the span of the model and a set of curves obtained by varying the amplitude ratio  $\frac{y}{D}$  where  $y$  is the amplitude of oscillation and  $D$  is the section depth. Such curves are available for rigid circular sections (e.g [3],[6]) but not for bluff sections representative of bridge decks.

An examination of such curves obtained by previous investigators show that the correlation between forces at any two points depends on the distance between the points as well as the amplitude of oscillation. Let  $\hat{x} = \frac{x}{D}$  be the normalized distance between sensors where  $D$  is the depth of the section. The correlation coefficient at a given normalized amplitude of oscillation  $\left(\frac{y}{D}\right)_i$  may then be approximated by an expression of the form:

$$C_i(\hat{x}) = \exp^{-\alpha_i \hat{x}^p} \quad (22)$$

where  $\alpha_i$  is a decay parameter and  $C_i(\hat{x})$  is the cross correlation coefficient at zero lag for a separation  $\hat{x}$  between sensors.

Using experimental data for correlation at  $n$  values of the normalized amplitude  $\left(\frac{y}{D}\right)_i$ ,  $i = 1, 2, \dots, n$ , the corresponding values of  $\alpha_i$  may be estimated. The decay parameter can then be expressed as a function of normalized amplitude:

$$\alpha = f\left(\frac{y}{D}\right) \quad (23)$$

From (22) and (23) the general expression for correlation is thus obtained in the form:

$$C(\hat{x}, y/D) = \exp^{-f\left(\frac{y}{D}\right)\hat{x}^p} \quad (24)$$

### 5.2 Bridge Correlation Curve

The curves obtained from tests and relations of the form (24) correspond to rigid section models. Actual

bridges, however, are flexible and  $\frac{y}{D}$  at any section  $x$  will be a function of  $x$  so that any single curve obtained from experiment will not be strictly applicable. Let the shape of a given mode be  $\Phi(x)$ , such that  $\Phi\left(\frac{L}{2}\right) = 1$ . In addition, assume that the maximum amplitude of the model at lock-in  $\left(\frac{y}{D}\right)_{max}$  is known from experiment.

For the purpose of estimating the shape of  $g_f(x)$  it may be assumed, without great loss of accuracy [4] that  $\left(\frac{y}{D}\right)_{max}$  of the model is approximately equal to the maximum amplitude ratio of the prototype at its midspan. The spanwise distribution  $\left(\frac{y}{D}\right)_{prot}$  is thus approximated by:

$$\left(\frac{y}{D}\right)_{prot} = \Phi(x) \left(\frac{y}{D}\right)_{max(model)} \quad (25)$$

Using representative points along the span of the bridge and computed values of  $\left(\frac{y}{D}\right)_{prot}$  at those points, values of  $C(\hat{x}, y/D)$  may be calculated from (24). The shape function  $g_f(x)$  is thus defined by these points. As before, it is assumed that the highest value of correlation occurs at the midpoint of any section of the flexible bridge between successive nodes. The integrals  $\Phi_2^m$  and  $\Phi_4^m$  are then evaluated according to (15) and (16) for the prototype bridge and the amplitude of the generalized coordinate calculated from (19).

In order to extend the results obtained from rigid models to flexible bridge decks, it has been implicitly assumed that each section of the bridge is part of a rigid body extending on both sides from the points of maximum amplitude of any section of the bridge between successive nodes. The known mode shape of the bridge controls the phasing between each small segment. The effects of varying amplitudes of each section of the bridge as well as their variable distances from the points of maximum amplitude are taken into account. The assumption that  $\left(\frac{y}{D}\right)_{max}$  of the model is equivalent to  $\left(\frac{y}{D}\right)_{prot}$  at midspan may be replaced by actual prototype amplitudes calculated from the assumption of fully coherent vortex shedding for greater accuracy.

## 6. THE EXPERIMENT

The experiments were conducted at the G. S. Vincent Wind Tunnel located at the Turner-Fairbank Highway Research Center, McLean, VA. The wind tunnel is of the open-circuit design with a nozzle measuring 6 ft.  $\times$  6 ft. Several stainless steel screens and an expansion and contraction are used to create a very smooth flow with turbulence intensities less than 0.5 %. The mean air exhaust velocity is continuously adjustable from 0 to 40 ft/sec. A sketch of the tunnel is shown in Figure 4.

## 6.1 Experimental Setup

The section model tested in the first set of experiments was an H-section representative, in a general sense, of such bridges as the Deer Isle-Sedgwick bridge and the original Tacoma Narrows bridge. The 4 ft (1.219 m) long wood model was 3.75 inches (9.525 cm) deep and 15 inches (38.1 cm) wide resulting in a depth-to-width ratio of 0.25. Circular aluminum plates, aligned streamwise, were attached to each end of the model to reduce edge and three-dimensional flow effects. Aluminum trusses were used to attach the model-endplate assembly to the model support system. The complete model assembly was mounted on four flexible coil springs, two at each end. Each spring connects the model to a thin copper-beryllium strain link for model displacement measurements. The model was allowed to have essentially two degrees of freedom, vertical and torsional, using a system of guy-wires. Rocking motion could not be explicitly prevented but was not observed during tests. The mass of the model assembly was dynamically measured to be 0.6842 slugs (9.983 kg.).

As mentioned previously, the function  $g(x)$  defines the fall-off characteristics of the spanwise coherence of forces on an oscillating rigid body. Assuming that the spanwise correlation of fluctuating wind pressures immediately downstream of the bluff body has identical fall-off characteristics, the function  $g(x)$  can be obtained from wind pressure correlation measurements. The main advantage of adopting this approach is that special purpose models are not required for the tests and any of the existing models can be used.

Two pitot tubes, having practically identical frequency response characteristics, connected to two Setra Systems electronic manometers were used to measure the wind pressure fluctuations directly. The signals output from the electronic manometers were low-pass filtered using Precision Filters' System 616-02-LP1 Multi-Channel Filter System. The system, which is capable of processing up to 16 analog signal channels, is a 6-pole, 6-zero elliptic low-pass filter. A total of 60 discrete cutoff frequencies are available in the range of 1 Hz to 15 kHz. Signal gains of 1,2,5 and 10 are available. A gain of 10 was used in these tests.

The pressure fluctuation signals were further amplified 3 times using the IFA-100 Intelligent Flow Analyzer. This further amplification was provided to utilize the full  $\pm 5V$  pk-pk input range of the data acquisition system. (Note: raw data was not recorded for this set of experiments.) The filtered and amplified signals were input to the Ono-Sokki Dual Channel FFT Analyzer for on-line processing. Displacement signals were am-

plified and filtered using a Vishay Instruments 2310 Signal Conditioning Amplifier. The model setup is sketched in Figure 5.

## 6.2 Experimental Procedure

Correlation measurements were made during locked-in vertical and torsional oscillations of the model at four different values of the normalized amplitude by varying the wind speed. These ranged from the lowest locked-in response amplitude to the largest response that could be obtained without endangering the experimental setup. Data could not be obtained at the largest attainable response amplitudes because measurements at each amplitude required oscillations to be sustained for up to five hours which would be damaging to the system.

Correlations were calculated between signals recorded by a reference sensor located in the plane of the midspan of the model and a sampling sensor placed successively at intervals of  $0.5D$  on either side of the reference sensor, where  $D$  is the depth of the model. The sampling sensor was mounted on a traverse system which allowed it to be moved in the direction of the wind, across the wake and along the span of the model with ease. In order to locate the exact position of the sensors for tests at each wind speed, the sampling sensor was placed at a certain distance downstream of the model at its midspan and spectra of the wind pressure fluctuations obtained for different locations across the wake. The position of the sensor for which the spectral peak had the largest magnitude was identified as the reference point. The procedure was initially rather time-consuming and tedious, but a pattern for the location of this point gradually emerged as tests were continued. The procedure was necessary however since an arbitrary location of the sensors led to very low correlation values at all wind speeds. Due to physical limitations of the setup, the two sensors could not be placed any closer than  $1D$ . No attempt was made to modify the setup since a closer spacing may have resulted in mutual flow interference by the sensors in any case.

## 6.3 Data Processing

The data was processed on-line using an Ono-Sokki Dual Channel FFT Analyzer. Cross-correlations were obtained from the finite inverse Fourier transform of the cross-spectral density of the two fluctuating wind pressure signals. A minimum of 8704 and a maximum of 16896 data points (i.e 16 to 32 spectral averages using 50 % overlap processing) were used to obtain each correlation value depending on whether the value

was sufficiently stable. A flat top window was used in the spectral estimation.

No attempt was made to filter out the sub- and superharmonics of the fundamental vortex-shedding frequency from the wind pressure signals prior to correlation calculations as was done in [3]. It was found that the correlation values increase significantly when the harmonics are filtered out. However, since the selection of the width of the band-pass filter is rather arbitrary, the correlations obtained from such a filtered signal could be misleading.

## 7. RESULTS OF THE EXPERIMENT

### 7.1 Vertical Oscillation Tests

The natural frequency of vertical oscillation of the model was 5.275 Hz and the damping ratio to critical was measured to be  $\zeta = 0.00444$ . The corresponding torsional frequency was 7.950 Hz.

The cross-correlation coefficient between wind pressure fluctuations at zero time lag is shown in Figure 6 for separation  $\hat{x}$  between sensors ranging from 1 to 5 to the left and right of the reference point, where  $\hat{x} = \frac{x}{D}$ . End effects appear to affect the correlation values at  $\hat{x} = 5$  (i.e. 5.25 inches from ends), perhaps even at  $\hat{x} = 4.5$ . The average values of the correlation to the left and right of the reference point were computed and curves of the form:

$$C_{vi}(\hat{x}) = e^{-\alpha_i \hat{x}^p} \quad (26)$$

were fitted. Subscript  $v$  denotes correlations for the vertical case. It was observed that  $p = 0.5$  gave the best fit, i.e. the curves have the form

$$C_{vi}(\hat{x}) = e^{-\alpha_i \sqrt{\hat{x}}} \quad (27)$$

The best fit curves and the average correlation values are shown in Figure 7. The values of the normalized amplitudes  $\left(\frac{y}{D}\right)_i$  are shown in Table 2. A relation between  $\alpha$  and  $\frac{y}{D}$  was sought in the form:

$$\alpha = \frac{a_1}{b_1 + \frac{y}{D}} \quad (28)$$

which satisfies the two conditions: (i)  $\alpha$  approaches a finite value as  $\frac{y}{D}$  approaches 0, which may be used to infer a correlation curve for the stationary case; (ii)  $\alpha$  approaches zero for large  $\frac{y}{D}$ , implying fully coherent vortex-shedding along the full span.

The parameter values were identified to be  $a_1 = 0.01578$  and  $b_1 = 0.02694$  from which a value of  $\alpha_s = 0.58575$  may be inferred for the stationary case. The corresponding curve is shown in Figure 7 in dotted lines.

The decay parameters  $\alpha_i$  and the curve fitted according to (23) are shown in Figure 10 a. The final expression for the H-section model in vertical oscillation was:

$$C_v \left( \hat{x}, \frac{y}{D} \right) = e^{-0.01578\sqrt{\hat{x}} / (0.02694 + \frac{y}{D})} \quad (29)$$

### 7.2 Torsional Oscillation Tests

Correlations of downstream wind pressure fluctuations were also obtained for the same model in torsional oscillation. The frequency was adjusted so that very high wind speeds would not be required for lock-in. The torsional frequency for this test was 4.550 Hz and the corresponding vertical frequency was 1.830 Hz.

The correlation values are shown in Figure 8 while the averaged data and best-fit curves are shown in Figure 9. To be consistent with the method used for vertical oscillations, the curves were assumed to have the same general form:

$$C_{ti}(\hat{x}) = e^{-\beta_i \sqrt{\hat{x}}} \quad (30)$$

where the subscript  $t$  refers to torsional motion. The values of the normalized angle of rotation  $\frac{\theta B}{2D}$  ( $B$ =deckwidth) and the corresponding values of  $\beta$  are shown in Table 3. The relation between  $\beta$  and  $\frac{\theta B}{2D}$  expressed in the same form as (28) was found to be (Figure 10 b):

$$\beta = \frac{0.01102}{0.02116 + \frac{\theta B}{2D}} \quad (31)$$

yielding an estimated value of  $\beta_s = 0.520794$  for the stationary case. The inferred curve is shown in Figure 9. The final expression for the torsional case is:

$$C_t \left( \hat{x}, \frac{\theta B}{2D} \right) = e^{-0.01102\sqrt{\hat{x}} / (0.02116 + \frac{\theta B}{2D})} \quad (32)$$

These results may be incorporated into a modified form of (2) to obtain the torsional response.

## 8. APPLICATION OF THE METHOD

The method was applied to the hypothetical bridge described in Section 4.2. The effect of the loss of spanwise coherence on the amplitude of the bridge was computed as follows.

The bridge was assumed to be oscillating in the first vertical mode approximated by a half sine-wave, i.e.  $\Phi(x) = \sin \frac{\pi x}{L}$  where  $L$  is the length of the main span. It was also assumed that the maximum normalized amplitude of the model was  $\left(\frac{y}{D}\right)_{\max(model)} = 0.15$ . The spanwise distribution of  $\left(\frac{y}{D}\right)_{prot}$  was thus approximated by

$$\left(\frac{y}{D}\right)_{prot} = \left(\frac{y}{D}\right)_{\max(model)} \times \Phi(x) = 0.15 \sin \frac{\pi x}{L} \quad (33)$$

The shape function  $g_f(x)$  was then obtained from equations (29) and (33):

$$g_f(x) = e^{-0.01578\sqrt{x}/(0.02694+0.15\sin \frac{\pi x}{L})} \quad (34)$$

The mode shape and corresponding shape function are plotted in Figure 11. The integrals  $\Phi_2^m$  and  $\Phi_4^m$  were calculated by numerical integration. The amplitude of the generalized coordinate was computed from (19) to be 0.12787. This value can be compared to the case of fully coherent vortex-shedding over the full span ( $g_f(x) = 1.0$ ) computed from (13) which was found to be 0.18163. This indicates a reduction of almost 30 % from the original value when the loss of spanwise coherence is accounted for. The spanwise distribution of maximum amplitude of response for the two cases is shown in Figure 12.

## 9. DISCUSSION

All wind pressure fluctuation data was taken downstream of the model undergoing locked-in vertical and torsional oscillations. This made it difficult to select the exact amplitudes of motion. The alternative of using forced vibrations was rejected, however, due to the possibility of altering the energy exchange between the oscillating model and the flow at lock-in.

At low vibration amplitudes, a beating phenomenon was observed in the response for both vertical and torsional cases. The corresponding normalized amplitudes quoted are thus average values. The beating phenomenon was not observed at high amplitudes of response (Figure 13 a,b).

The sub- and first superharmonic of the fundamental vortex-shedding frequency were retained in the signal to take into account their effect on the response. Typical spectra of wind pressure fluctuations (Figure 14 a,b) indicate the contributions of the harmonics may be significant.

Since both vertical and torsional tests were performed on the same section model, the decay parameters  $\alpha_s$  and  $\beta_s$  inferred for the stationary case should be identical. The value of  $\alpha_s$  was however about 11 % higher than that of  $\beta_s$ . This discrepancy may be the result of frequency modifications to the system for the torsional tests as well as experimental error. In addition, the assumption that the fall-off behavior is identical for the two modes of oscillation may not reflect the actual case.

The method for estimation of a shape function describing the fall-off characteristics of vortex-induced forces for a long-span flexible bridge described in this paper is

not dependent on the particular vortex-shedding model used. The results may be incorporated into other models.

All tests were performed in laminar wind flow. The effect of upstream turbulence on the correlation values will be studied at a later stage.

## CONCLUSION

The method described in this paper uses an empirical vortex-shedding model and experimental results to attempt to account for the effect of the loss of spanwise coherence of vortex-shedding forces on the amplitudes of prototype response. It does not presume to take the detailed aspects of the fluid-structure interaction into account except in a general way. The main advantage of the proposed method may be that relatively simple experimental and numerical techniques are utilized to obtain an approximate solution to a problem that is extremely complex by nature.

## REFERENCES

1. Hartlen, R.T and Currie, I.G., "Lift-Oscillator Model of Vortex-Induced Vibration," *J. Eng. Mech. Div.*, ASCE, **96** (1970)
2. Iwan, W.D., and Blevins, R.D., "A Model for the Vortex-Induced Oscillation of Structures," *J. Appl. Mech.*, ASME, **41** (1974)
3. Feng, C.C., *The Measurement of Vortex-Induced Effects in Flow Past Stationary and Oscillating Circular and D-Section Cylinders*, M. A. Sc. Thesis, The University of British Columbia (Oct. 1968)
4. Scanlan, R.H., "On the State-of-the-Art Methods for Calculations of Flutter, Vortex-Induced and Buffeting Response of Bridge Structures," FHWA Report, **FHWA/RD-80/050**, Washington D.C (1981)
5. Simiu, E., and Scanlan, R.H., *Wind Effects on Structures*, 2<sup>nd</sup> ed., John Wiley and Sons (1986)
6. Toebes, G.H., "Fluidelastic Features of Flow Around Cylinders," *Proc. Int'l. Research Seminar on Wind Effects on Bldgs. and Structures, Ottawa, Canada, 1967*, V. 2, University of Toronto Press, Toronto (1968)
7. Vickery, B.J., "Fluctuating Lift and Drag on a Long Cylinder of Square Cross-Section in a Smooth and in a Turbulent Flow," *Journal of Fluid Mechanics*, **25** (1966), Cambridge University Press, New York

Table 1: Amplitude of Generalized Coordinate

Shape Function	$\xi_0$		Percent Reduction From Rectangular	
	CL=1.0	CL=0.70	CL=1.0	CL=0.70
Rectangular	0.1762	0.1645	0.00	0.00
Triangular	0.1469	0.1259	16.63	23.46
Cosine-tapered	0.1507	0.1242	14.47	24.50
Exponential (n=1)	0.1548	n.a	12.15	n.a

Table 2: Decay Parameter  $\alpha$   
(Vertical Oscillation)

Wind Speed (ft/sec)	$y/D$	$\alpha$
10.69	0.0304	0.24858
11.01	0.0708	0.17073
11.44	0.0894	0.14193
11.83	0.1235	0.10189

Table 3: Decay Parameter  $\beta$   
(Torsional Oscillation)

Wind Speed (ft/sec)	$\theta B/2D$	$\beta$
10.25	0.009595	0.40314
10.69	0.023562	0.22234
11.01	0.032392	0.14503
11.83	0.082312	0.10804

FIGURE 1. DEFINITION DIAGRAM FOR MODIFIED EQUATIONS

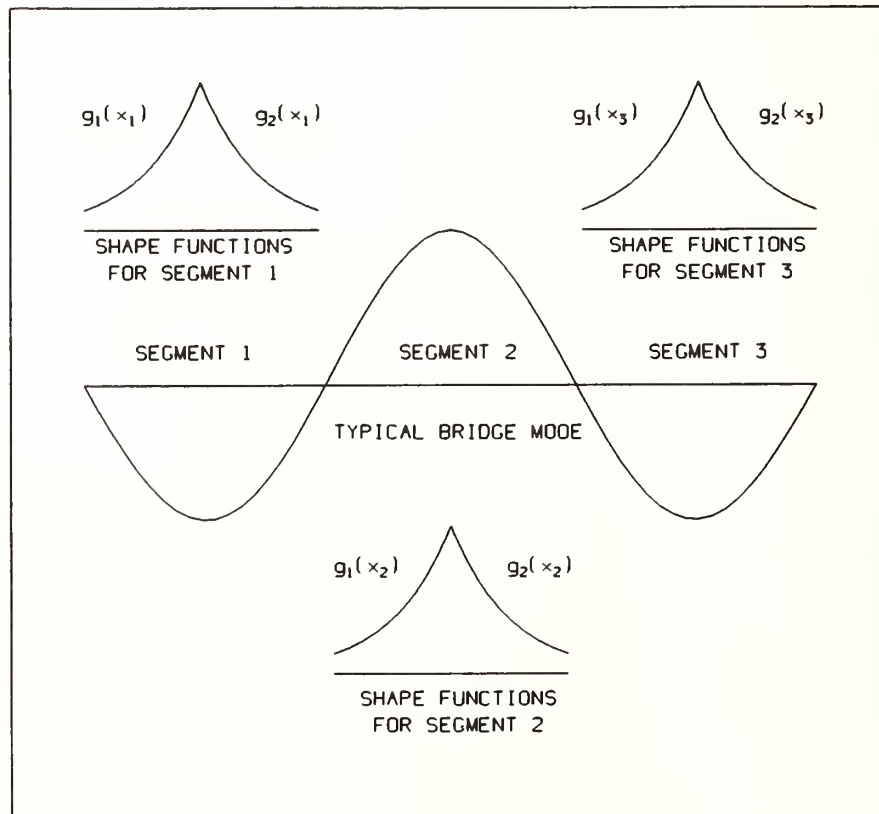


FIGURE 2. SHAPE FUNCTIONS FOR PRELIMINARY STUDY  
(COHERENT FRACTION = 1-2C)

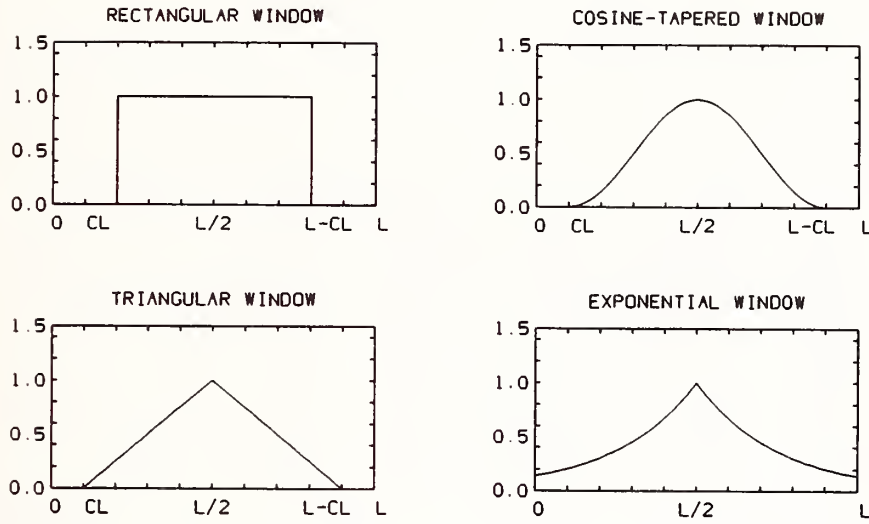


FIGURE 3. COMPARISON OF THE EFFECT OF ASSUMED SPANWISE COHERENCE FUNCTIONS ON MAXIMUM GENERALIZED AMPLITUDE OF A BRIDGE.

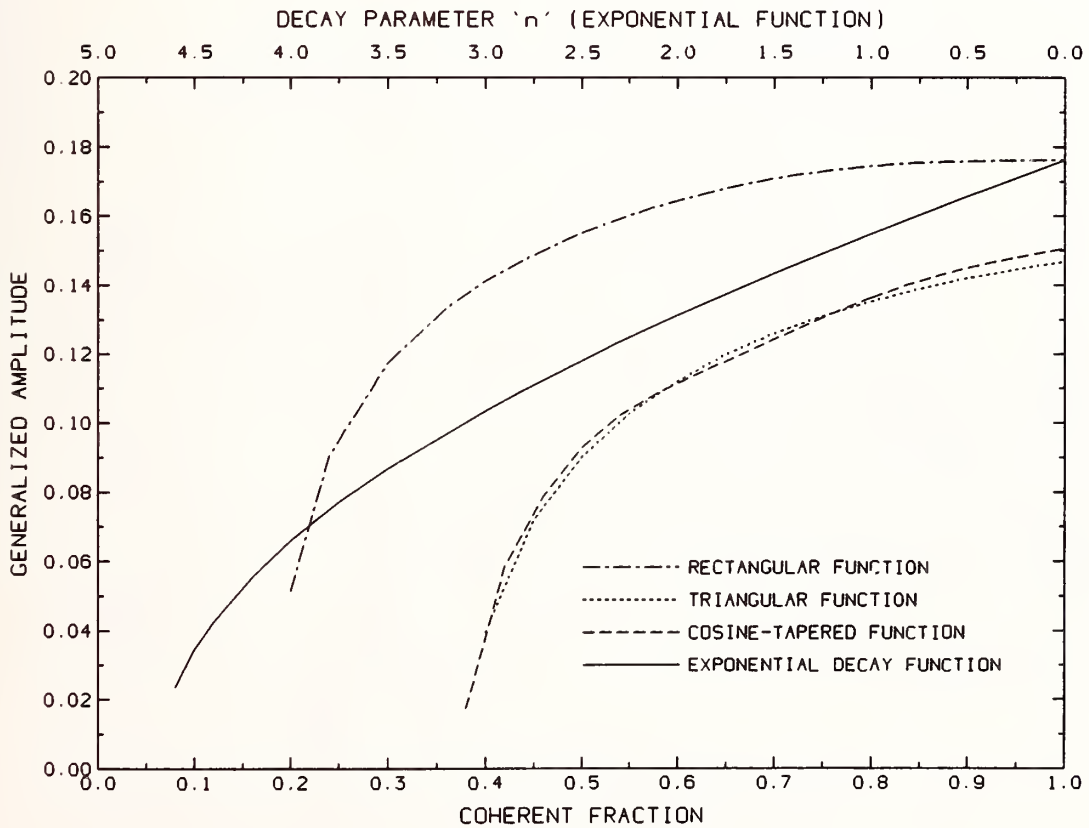


FIGURE 4. LINE DRAWING OF WIND TUNNEL

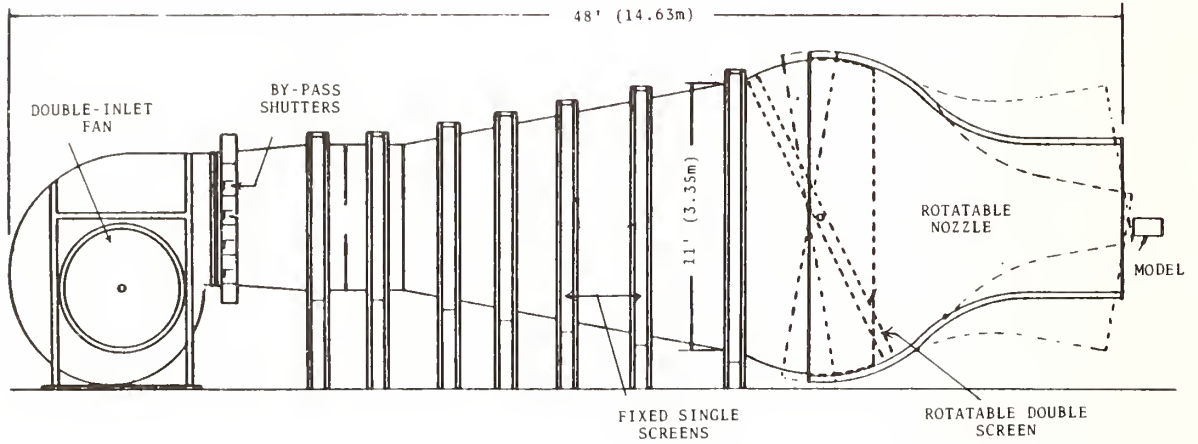


FIGURE 5. SKETCH OF EXPERIMENTAL SETUP

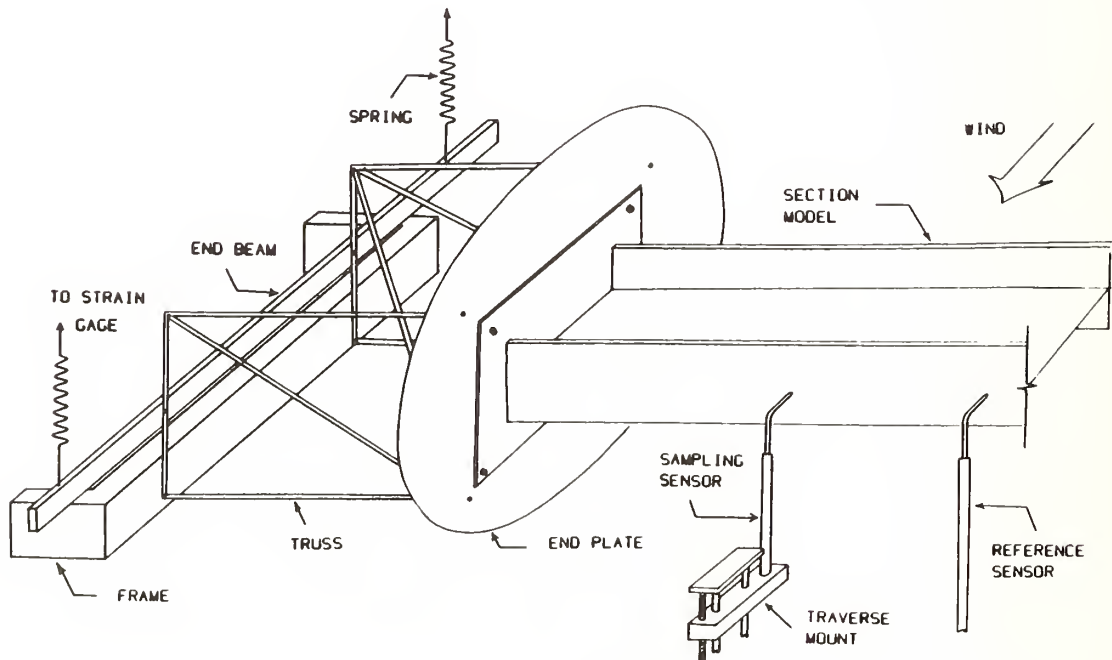


FIGURE 6.  
SPANWISE CORRELATION OF WIND PRESSURE FLUCTUATIONS DOWNSTREAM  
OF AN H-SECTION UNDERGOING LOCKED-IN VERTICAL OSCILLATION

\*:  $y/D = 0.0304$      $\Delta$ :  $y/D = 0.0708$   
+:  $y/D = 0.0894$      $\circ$ :  $y/D = 0.1235$

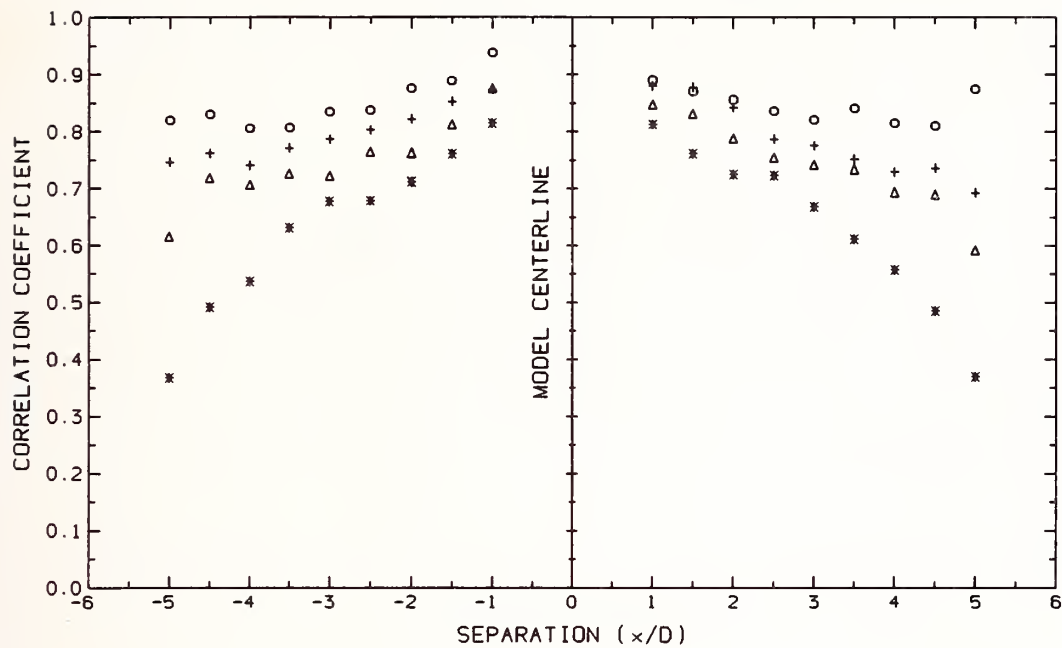


FIGURE 7.  
SPANWISE CORRELATION OF WIND PRESSURE FLUCTUATIONS DOWNSTREAM  
OF AN H-SECTION UNDERGOING LOCKED-IN VERTICAL MOTION

———— BEST FIT CURVES  
- - - - - STATIONARY CASE (INFERRED)

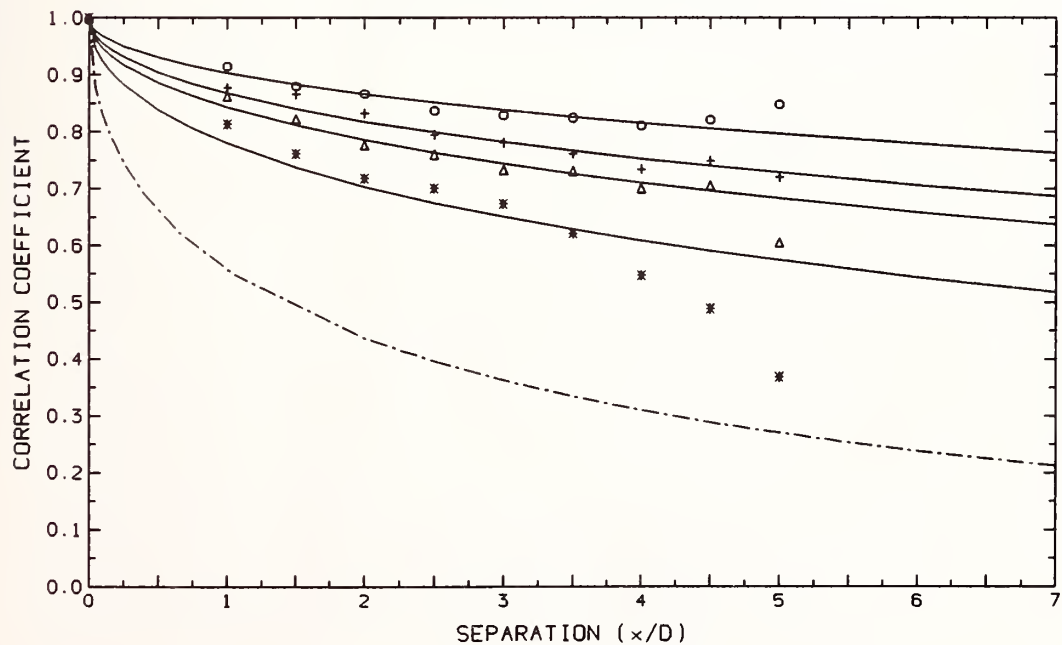


FIGURE 8.  
 SPANWISE CORRELATION OF WIND PRESSURE FLUCTUATIONS DOWNSTREAM  
 OF AN H-SECTION UNDERGOING LOCKED-IN TORSIONAL OSCILLATION  
 \*:  $\theta B/2D = 0.009595$      $\Delta$ :  $\theta B/2D = 0.023562$   
 +:  $\theta B/2D = 0.032392$      $\circ$ :  $\theta B/2D = 0.082312$

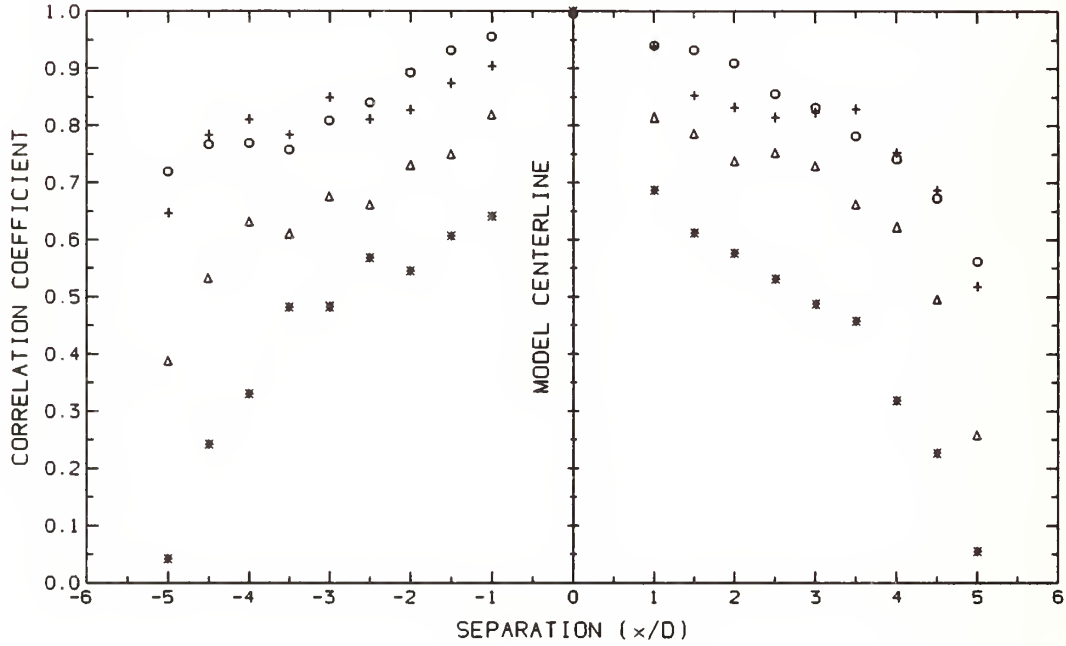


FIGURE 9.  
 SPANWISE CORRELATION OF WIND PRESSURE FLUCTUATIONS DOWNSTREAM  
 OF AN H-SECTION UNDERGOING LOCKED-IN TORSIONAL MOTION

————— BEST FIT CURVES  
 - - - - - STATIONARY CASE (INFERRED)

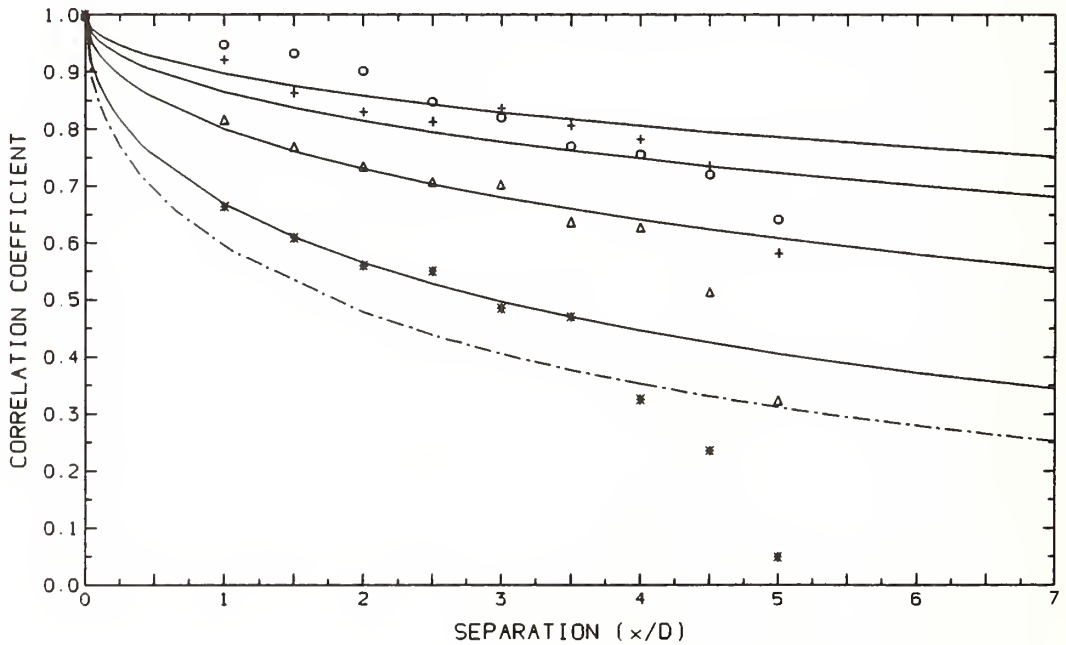


FIGURE 10 (a). RELATION BETWEEN DECAY PARAMETER  $\alpha$   
AND NORMALIZED AMPLITUDE  $\gamma/D$  : (VERTICAL OSCILLATION)

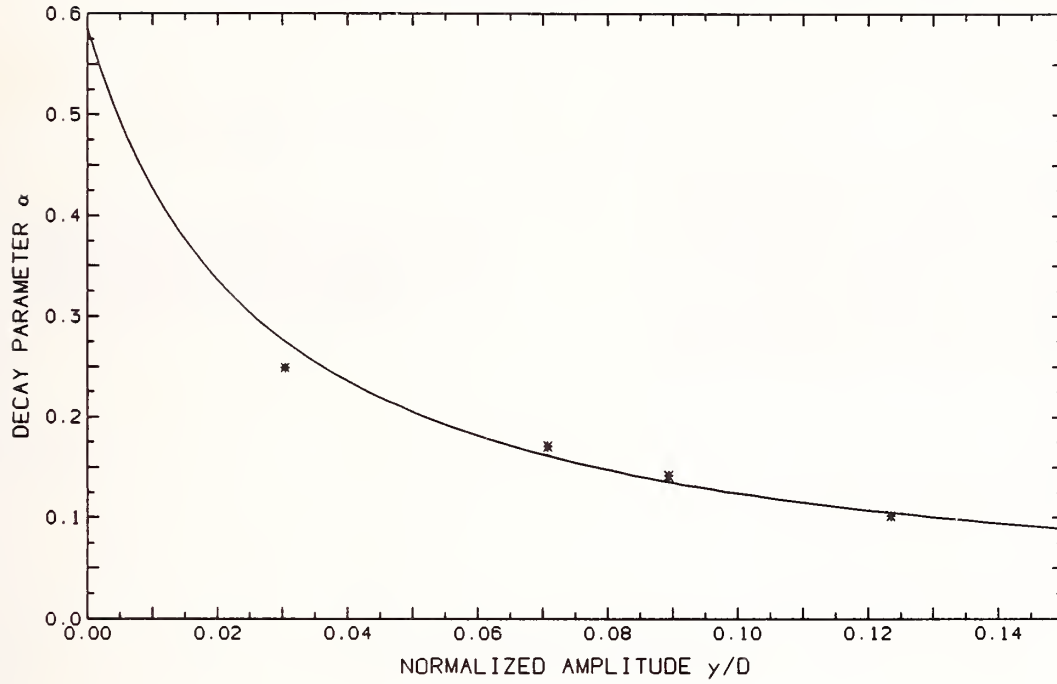


FIGURE 10 (b). RELATION BETWEEN DECAY PARAMETER  $\beta$   
AND NORMALIZED ROTATION  $\theta B/2D$  : (TORSIONAL OSCILLATION)

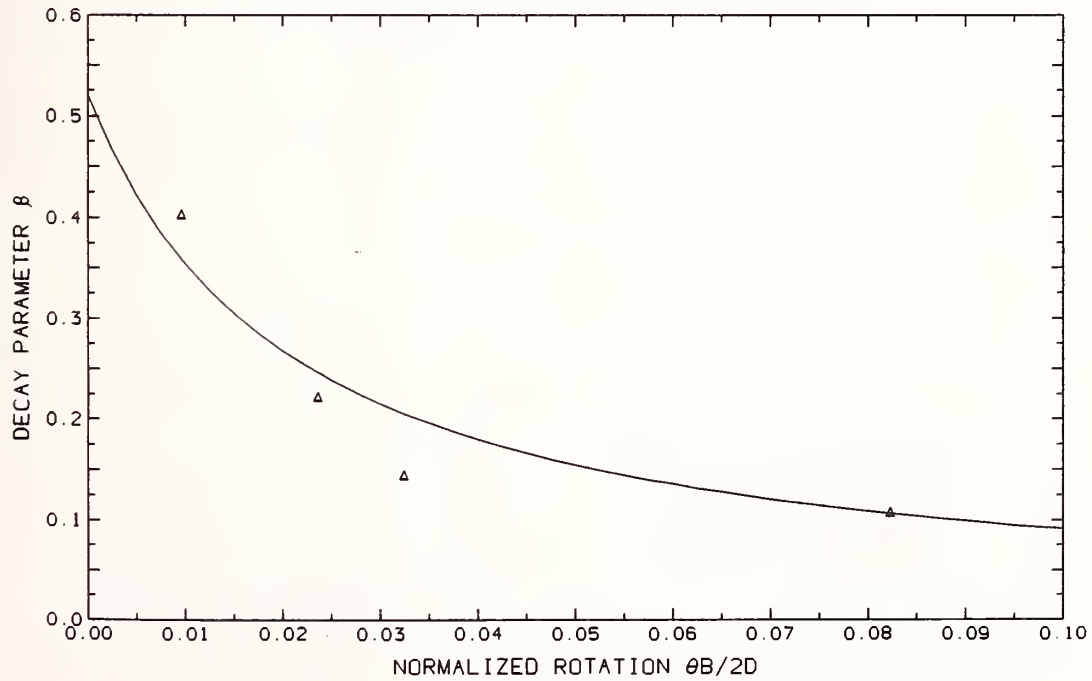


FIGURE 11. MODE SHAPE  $\phi(x)$  AND CORRELATION (SHAPE) FUNCTION  $g_r(x)$  FOR FLEXIBLE BRIDGE

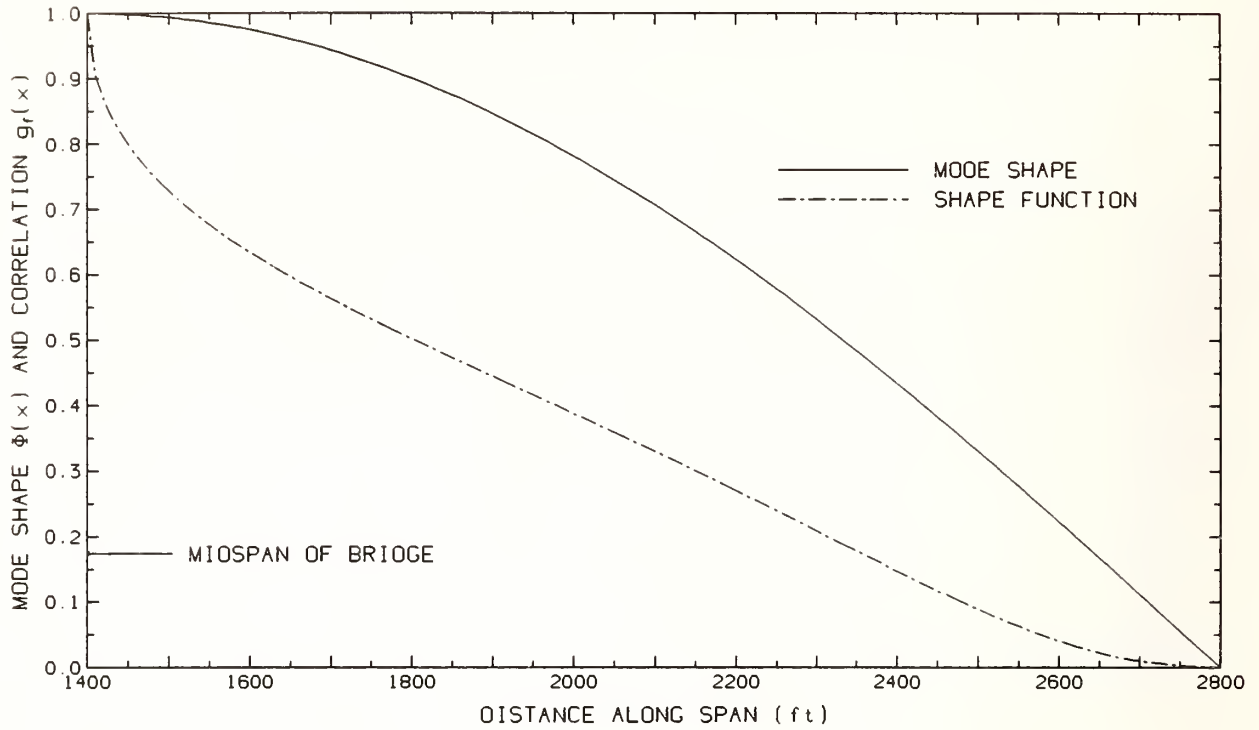


FIGURE 12. SPANWISE DISTRIBUTION OF MAXIMUM VORTEX-SHEEDING RESPONSE

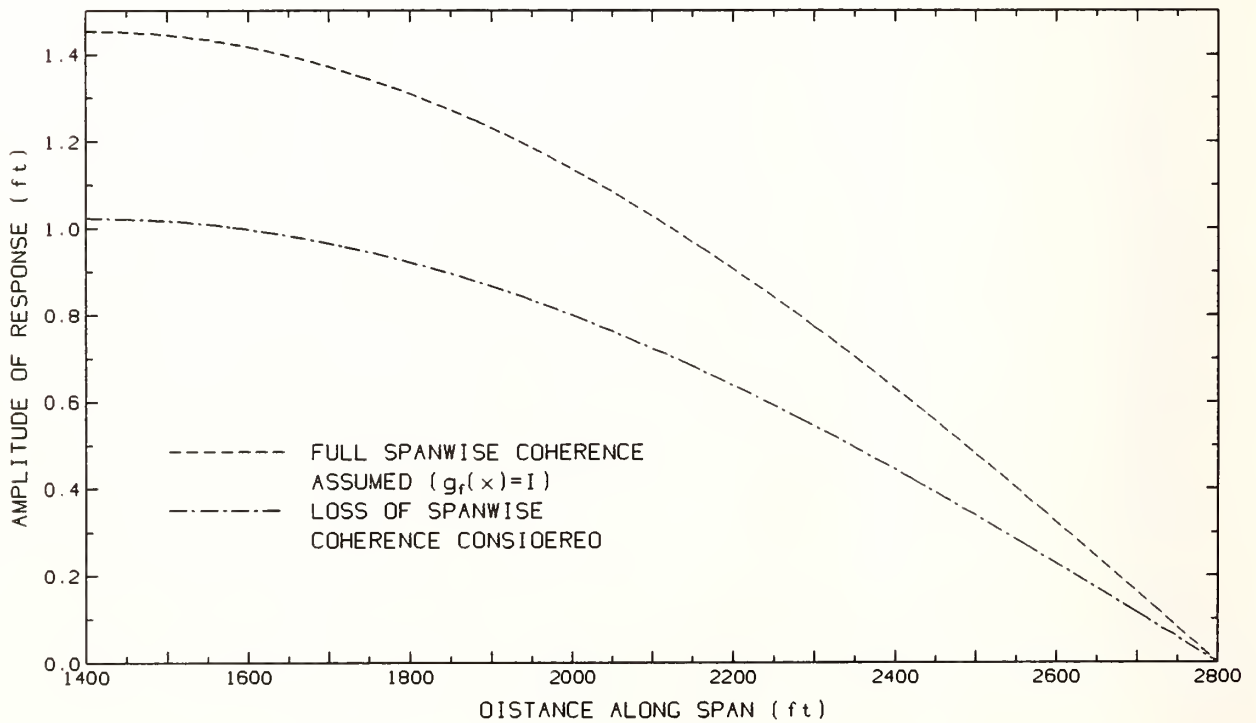
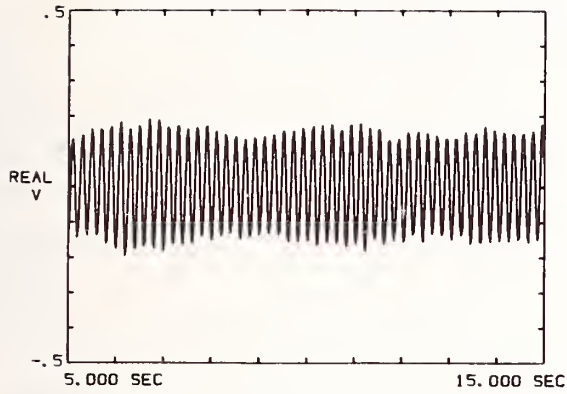
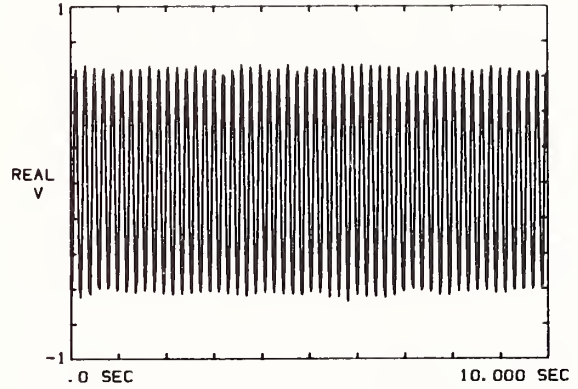


FIGURE 13. SAMPLES OF VERTICAL RESPONSE AT LOCK-IN

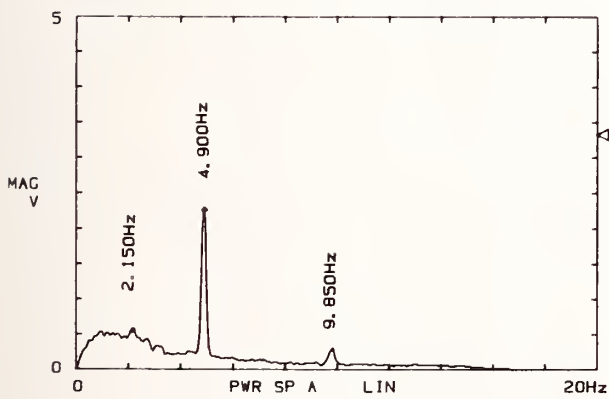


(a) BEATING AT LOW AMPLITUDE OF OSCILLATION ( $\gamma/D = 0.0304$ )

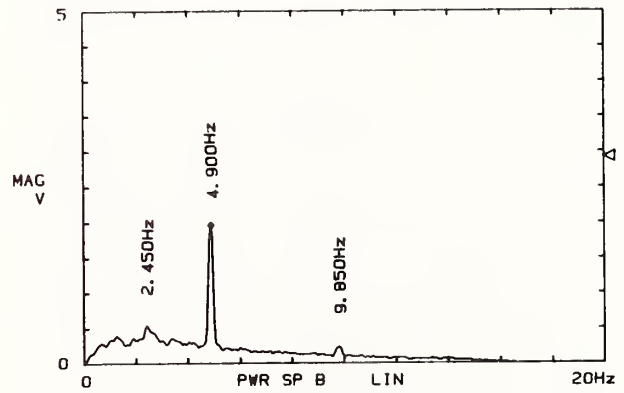


(b) BEATING REDUCED AT HIGHER AMPLITUDE ( $\gamma/D = 0.1235$ )

FIGURE 14. SPECTRA OF DOWNSTREAM WIND PRESSURE FLUCTUATION AT  $U=10.69$  ft/sec SHOWING SUB- AND SUPERHARMONIC OF FUNDAMENTAL VORTEX-SHEDDING FREQUENCY



(a) SPECTRUM OF SIGNALS MEASURED BY REFERENCE SENSOR



(b) SPECTRUM OF SIGNALS MEASURED BY SAMPLING SENSOR (LOCATED AT 3D FROM REF)

# Studies on Wind-Resistant Design of Highway Bridges and New Design Codes in Japan

by

Nobuyuki Narita\*1

Koichi Yokoyama\*2

Hiroshi Sato\*3

## Abstract

Not a few bridges have been damaged by wind loading and wind-induced vibrations, and Japan is located in the area where severe typhoons attack every year. Therefore, it is important to confirm sufficient wind-resistant safety in design of bridges.

After the World War II, road improvement program was promoted and lots of bridges including suspension bridges and cable-stayed bridges have been planned and constructed in Japan. Relating to the bridge construction, wind-resistance of bridges has been studied actively. On the basis of the results of the researches, wind-resistant design codes were published and wind-resistant design methods based on wind tunnel tests are established.

In this paper, described are trends of construction of highway bridges after World War II in Japan and the related studies on bridge aerodynamics. Finally new wind-resistant design codes are introduced.

## 1. Introduction

Many incidents of bridges damaged by strong wind have been reported. In 1879, 13 spans of the Tay Bridge in Scotland, which had bridge length of 3km and was 85 span lattice truss bridge, fell down into the sea with trains in windstorm, and seventy-five passengers were killed. Maximum wind speed in that day was reported about 36m/s. It is famous that this accident was caused by lack of proper assessment of static wind loading.

In 1940, the Tacoma-Narrows Bridge in the U.S.A., which had 853m center span length and was the third longest bridge in the world at that time, collapsed due to violent vibration caused by wind of 19m/s four months after its completion. Flutter of the bridge deck caused the collapse, and the importance of dynamic effects of wind has been recognized since that time.

Studies of wind effects on bridges in Japan started after the World War II. In 1950s, highway improvement program was promoted and construction of long span bridges including the Honshu-Shikoku Bridges were planned. The Honshu-Shikoku Bridge Project is to link between the Honshu Island (Main Island) and the Shikoku Island by highway and railway bridges, and ad hoc committee was organized in the Japan Society of Civil Engineers in early 1960s

to start research work related to the Project. Studies on bridge aerodynamics in Japan has been deeply related to the Honshu-Shikoku Bridge Project.

In this paper, described are trends of construction of highway bridges after World War II in Japan first and the related studies on bridge aerodynamics. Finally new wind resistant design codes are introduced.

## 2. Development of highway bridges in Japan

Construction of comprehensive road network started in the end of 1950s in Japan. After this, the number of bridge construction increased and maximum span length of bridge was extended gradually. Here, development of suspension bridge and cable-stayed bridge which are closely connected with wind-resistant design are reviewed.

In Japan, the first large-scale suspension bridge is the Wakato Bridge completed in 1962. It has the main span length of 367m and truss stiffening girder. After construction of the Wakato Bridge, the Kanmon Bridge (main span length: 770m, completed in 1983), the Ohnaruto Bridge (main span length: 876m, completed in 1985) and the Minami-Bisan Seto Bridge (main span length: 1100m, completed in 1988) were constructed and the span length of suspension bridge has been extended year by year. These suspension bridges adopted truss as stiffening girder, and the Ohnaruto Bridge and the Minami-Bisan Seto Bridge are highway and railway bridges.

With regard to suspension bridge stiffened by box-girder, the Ohshima Bridge (main span length: 560m) was constructed first, and the Hakucho Bridge (main span length: 720m) is under construction. Furthermore, the Akashi Kaikyo Bridge which will be the longest suspension bridge in the world is under construction, then main span length of suspension bridge will reach about 2000m in near future.

On the other hand, cable-stayed bridge is a new type bridge which suit for medium span bridge and the number of construction of cable-stayed bridges has been increasing

\*1 Dr. of Eng. Director-General, Public Works Research Institute, Ministry of Construction

\*2 Head, Structure Division, Structure and Bridge Department, PWRI

\*3 Senior Researcher, Structure Division, Structure and Bridge Dept. PWRI

recently. Up to now, the Hitsuishu-Jima Bridge and the Iwaguro-Jima Bridge (main span length:420m, completed in 1988), the Meiko-Nishi Bridge (main span length:405m, completed in 1985), the Yamatogawa Bridge (main span length:355m, completed in 1982) and the Suehiro Bridge (main span length:250m, completed in 1875) have been constructed and several bridges, ie the Meiko-Chuo Bridge, the Tsurumi-Koro Bridge, the Higashi Kobe Bridge, the Yokohama Bay Bridge are under construction as shown in Table-2. The span length of cable-stayed bridge has been gradually extended as well.

The Higashi Kobe Bridge and the Yokohama Bay Bridge have double deck. As the Meiko-Nishi Bridge and the Tsurumi-Koro Bridge are planned to have two bridges parallel to each other, it is expected that new aerodynamic problems should be studied. The Katsushika Harp Bridge (S-shape bridge) completed in 1987 is a curved cable-stayed bridge which has main span length of 220m and takes pride in esthetics.

### 3. Wind effects on bridges

Taking convenience of bridge design, limited states of bridge due to wind effects are classified as follows;

- (1) Static effects
  - a) Deformation and stress due to steady wind loads
  - b) Static instability
    - Lateral buckling
    - Divergence
- (2) Dynamic effects
  - a) Restricted oscillation
    - Buffeting (gust response)
    - Vortex-induced oscillation
  - b) Catastrophic oscillation
    - Self-excited oscillation (galloping and flutter)

These wind effects are illustrated in Fig.-2. Most primitive effect among wind effects is wind loading. As fluctuation of wind speed in time and space causes gust response of structure, design wind load is defined taking account of gust response. Other important wind effects are wind-induced vibrations. Especially, it is well-known that free-standing tower of suspension bridge has vibrated due to vortex-induced oscillation under construction. Vortex-induced oscillation have been observed in main girder of cable-stayed bridge and hanger of Langer bridge as well. As a matter of fact, catastrophic oscillation must be confirmed not to occur in design of suspension bridges, cable-stayed bridges and long span box-girder bridges.

In addition, much attention should be paid to new topics which are rain vibration of cables of cable-stayed bridges and

aerodynamic interaction of structures constructed parallel to each other.

### 4. Studies on wind resistant design of highway bridges in Japan

#### 4.1 Wind tunnel test

##### (1) Wind tunnel test method

Wind resistant safety of a long-span bridge should be confirmed at planning and design stage. As cross-section of bridge is usually not streamlined, theoretical approach is not sufficient to predict the behavior of the bridge due to strong wind. Therefore, at present wind tunnel test are the most effective methods which provide estimation of wind-induced vibrations caused by strong wind.

A great amount of wind tunnel tests have been conducted in relation to construction of suspension bridges and cable-stayed bridges. About twenty years ago, only a few research laboratories such as Public Works Research Institute, MOC, universities and private firms conducted wind tunnel tests with regard to bridge aerodynamics. Many wind tunnels, however, were constructed last two decades and a lot of laboratories as shown in Table-3 carry out wind tunnel tests at present. Dr. R. D. Marshall, NBS, visited Japan as part of the UJNR personal exchange program to study present state of wind tunnel facilities in Japan and published a report. [1]

Sectional model test in smooth flow is usually adopted to observe the behavior of structure in strong wind. A sectional model, a geometrical copy of a structure, is supported in wind tunnel by coil springs. Mass and damping are adjusted in accordance with required similarity law, and relation between wind speed and response of the model is investigated. In comparison with full model test, sectional model test has a few merits, that is, it is easy to make a sectional model and details of structure can be replicated precisely because of large scale. Additionally, it is considered that the response of the full structure can be predicted from the response of sectional model in case of a slender structure like bridge on the basis of strip theory. A sectional model is also used to measure unsteady aerodynamic forces using pressure valve or unsteady aerodynamic force balance. [2, 3] In unsteady aerodynamic force tests, aerodynamic forces which generate vibration can be measured directly, compared with sectional model tests in which response is observed.

On the other hand, wind tunnel test in turbulent flow is conducted as well. It is necessary to make use of turbulent flow which is simulated to natural wind in order to study the effects of turbulence. As wind forces in turbulent flow fluctuate in space, an elastic full model or a taut-strip model [4] are suitable for a study of

turbulent effects. Steel beam and wires provide required stiffness to an elastic model and a taut-strip model, respectively.

## (2) Aerodynamic characteristics of suspension bridge

Main girder of suspension bridge has been usually stiffened by truss. In this case, torsional flutter of stiffening truss is a main subject in wind-resistant design. To obtain safe design against strong wind, several attention are paid in design of main girder, that is, open grating arranged in bridge deck, sufficient rigidity of stiffening truss girder and careful arrangement of structural members which do not lessen aerodynamic characteristics. Typical design of stiffening truss of the Honshu-Shikoku Bridges is shown in Fig. 4. Vertical stabilizer was invented and installed under central barrier in the Ohnaruto Bridge to improve safety against flutter.

On the other hand, suspension bridges with box-girder have also been designed. The suspension bridge with box-girder whose main span length is less than 1000m has as usual enough safety against flutter, but it suffers from vortex-induced oscillation which occurs at low wind speed range. Fig. -5 shows the test results of comparative wind tunnel tests of box-girder suspension bridges. It is clarified that the vortex-induced oscillations can be suppressed if an adequate cross-section of girder is selected. [5].

## (3) Aerodynamic characteristics of Cable-stayed Bridge

Investigation on wind resistant design of cable-stayed bridges started after 1965. [6] The Ishikari-Kako Bridge, which is a cable-stayed bridge completed in 1972, has main span length of 160m. The original cross-section of its girder was rectangular and semicircular fairings were attached to both sides of the girder. At the construction stage, this bridge vibrated at wind speed of 10-12m/s and the maximum amplitude reached 9cm. Therefore, the arrangements of fairing were modified as shown in Fig.-6, that is, one block every two blocks was dismantled.

The Suehiro Bridge adopts trapezoidal shape as cross-section of the girder, after several series of wind tunnel tests. Flap was invented and installed on the handrail as a means to suppress vortex-induced oscillations. The flap is quite effective and has been adopted to several cable-stayed bridges. [7] (Fig. -7)

Wind-induced vibrations of cables of cable-stayed bridge are reported. [8] So-called rain vibration was observed on the Meiko-Nishi Bridge first. This vibration occurs only during rainfall. It is estimated that rivulet run along a cable changes the shape of cross-section of the cable and this causes aerodynamic instability. Furthermore, vibrations of

parallel cables were observed on the Hitsuishi-Jima Bridge and the Iwaguro-Jima Bridge. This vibration is called wake galloping which is derived from aerodynamic interaction of two cables arranged in the clearance of 4-6 D (D: diameter of the cable). At design stage, connection of two cables by a spacer was studied. As the vibrations at higher modes occurred and rain vibrations were also observed in the site, all cables were connected each other by additional wires and this vibration was suppressed. It is required to develop urgently effective and esthetical countermeasures. The number of construction of bridges parallel to each other as well as parallel cables is increasing, so there are not a few cases of researches on aerodynamic characteristics of parallel structures.

Wind resistant safety of suspension bridges and cable-stayed bridges under construction should be confirmed as well as after completion, because rigidity of the structure often lessens at construction stage. Especially, it is well-known that free-standing tower of suspension bridge has vibrated due to vortex-induced oscillation under construction. Several wind tunnel tests have been conducted to study relation between wind conditions and response, and sliding block method, which is able to increase damping, is often adopted in the site and has been confirmed to be effective as a means. Also safety against static deformation and flutter of main girder should be examined during erection of main girder. [9]

## (4) Other bridges

Generally speaking, wind effects on the bridges except suspension bridges and cable-stayed bridges are not so severe, but wind resistance of long-span box-girder bridges [10, 11] and hangers of Langer bridges [12] have been studied. Tozaki Viaduct is a box-girder bridge which has main span length of 190m. Because this bridge is located near steep cape and angle of attack of approaching wind was estimated to be large, wind tunnel tests were conducted. According to the test results, plate and double flap as shown in Fig. -8 were installed to the girder to cope with galloping and vortex-induced oscillations

Hanger of Langer bridge is a structural member which resists tensile force, and H-shape or circular cross-section are usually adopted. These hangers were damaged by vibrations due to wind. Several kinds of measures were studied, namely strake wire in case of circular cross-section and connection of all hangers by wire in case of H-shape cross-section.

## (5) Effects of turbulence

Turbulence of wind causes gust response of bridge and affects wind induced vibrations such as vortex-induced oscillations and so on.

In wind-resistant design of bridge, static wind loads are modified taking account of gust response of horizontal bending mode, that is to say, design wind load  $P_d$  is calculated by the following formula.

$$P_d = 1/2 \rho U_d^2 C_d A G$$

where,  $\rho$  : air density

$U_d$ : design wind speed

$C_d$ : coefficient of drag force

$A$  : projected area

$G$  : gust modification factor

Gust modification factor  $G$  is provided according to turbulence intensity and span length of bridges. Though wind-resistant design of bridges does not take account of both vertical and torsional gust response, conducted are studies on prediction method by means of experiments and theoretical calculations.

It is well-known that flow conditions around structure in turbulent flow is different from those in smooth flow. Especially, amplitudes of vortex-induced vibration are different between in smooth flow and in turbulent flow, then wind tunnel tests in turbulence is quite important with regard to vortex-induced oscillation. [13] The method of wind tunnel tests in turbulent flow has not been established, then it is required to study the method of generation of turbulent flow in wind tunnel which simulates natural winds, the required similitude of turbulent flow and model, and the evaluation of accuracy of the tests results. At present, wind tunnel tests in smooth flow is often conducted combined with wind tunnel tests in turbulent flow.

#### 4.2 Wind resistant design codes

The design of highway bridge in Japan has been made according to The Specification for Highway Bridges. With regard to wind resistant design, the Specification prescribes design wind load of bridges and provides the limitation of dimensions of pipe structure to prevent from wind-induced vibrations, however, there is no sufficient provision on wind-induced vibrations in the Specifications.

The wind resistant design of long-span bridges in Japan has been mostly based on the Wind Resistant Design Criteria for the Honshu-Shikoku Bridges. The Criteria was originally formulated in 1967 [14] and revised in 1976 [15] by ad hoc committee in the Japan Society of Civil Engineers.

Compared with the preceding design codes, the Criteria (1967) is characterized in the following points;

(1) The design wind speed shall be assessed according to the topography of construction site, and the altitude and scale of the structure.

(2) Drag coefficient for each structural composition are given for reference to make static design of the structure.

(3) Wind tunnel test should be conducted in order to confirm the drag coefficient used in the static design and to predict the critical wind speed for the self-excited oscillation of the structure.

(4) A design standard for the critical wind speed of elastic instability and self-excited oscillation is prescribed so that the sufficient safety shall be kept for the structure.

(5) Enough care of wind stability should be taken not only after completion but also on each stage of construction.

Though the Wind Resistant Criteria (1967) includes the remarkable progress compared with the preceding design criteria, and it has been effective for designers to recognize the importance of wind stability problems, it is confined to give general regulation for the wind resistant design of long span suspension bridges.

The Criteria (1976) was made, revising the Criteria (1967) on the basis of the fruits of the researches which had been performed since the Criteria (1967) was formulated. The main features of the revised Criteria (1976) are shown in Table-3, and the significant points which have been revised are as follows;

(1) To clarify the design procedure and the structure of articles in the criteria.

(2) To reexamine the basic wind speed in due consideration of the recent wind data recorded in the Seto Inland Sea, and to set the basic wind speed for the respective zone or route.

(3) To determine the modification factors for converting a basic wind speed into the the design wind speed, where analytical method of gust response is tentatively adopted.

(4) To revise the concrete values of drag coefficients, structural damping, wind inclination by using the recent data of observation.

In addition, the Guideline of the Wind Tunnel Tests for the Honshu-Shikoku Bridges (1980) which prescribes standard method of wind tunnel test defined in the Criteria (1976) was formulated in 1980.

Besides the design code of the Honshu-Shikoku Bridges, Hanshin Expressway Public Corporation proposed the Draft of the New Manual of Examination for Wind Resistant Design of Highway Bridges in 1984. This New Manual provides prediction formulae and evaluation method related to both onset wind speed and amplitude of wind-induced vibrations such as vortex-induced oscillation, flutter and galloping. This is the first manual in Japan which provides the prediction method other than wind tunnel tests.

In 1977, Public Works Research Institute and Japan Meteorology Association provided the map of basic wind speed in Japan, processing statistically wind data

obtained in the meteorological observatory stations. [16] This map has been utilized for later wind resistant design.

#### 4.3 Field observation

To increase accuracy of wind resistant design, vibration tests and field observation of bridge response in strong wind have been conducted after bridges were completed.

The amplitude of vibration due to strong wind is closely connected with damping of bridge. It is usually difficult to study damping theoretically. At present design damping value is decided on the basis of results of tests conducted in the site. Vibration tests have been conducted by the use of excitor in Japan. Main results are shown in Table-4. Honshu-shikoku Bridge Authority manufactured the gigantic excitor for vibration tests of long span suspension bridges and cable-stayed bridges in 1985. The Wind Resistant Design Criteria for the Honshu-Shikoku Bridges(1976) prescribes that

- (a)  $\delta=0.03$ , for suspension bridges and cable-stayed bridges with truss girder
- (b)  $\delta=0.02$ , for cable-stayed bridges with box-girder
- (c)  $\delta=0.01$ , for free-standing tower

According to the recent vibration tests results[17], these damping values have been confirmed to be appropriate.

Anemometers and accelerometers have been installed at many suspension bridges and cable-stayed bridges after their completion to measure wind and response of the bridge. [18, 19] As a lot of assumptions are involved in the procedure of wind resistant design, it is required to confirm the safety of the bridge in site. Response of the bridge observed in site can be compared with design. [20, 21]

### 5. New design codes

#### 5.1 The Wind Resistant Design Manual for the Akashi Kaikyo Bridge

The main span length of the Akashi Kaikyo Bridge will be as twice as the other Honshu-Shikoku Bridges, so that the effects of strong wind on the Bridge would be remarkable. From this point of view, the Wind Resistant Design Manual for the Akashi Kaikyo Bridge was formulated by ad hoc committee of the Japan Society of Civil Engineers in 1988.

The features of the Manual are as follows;

(1) With regard to gust response of suspended structure, theoretical analysis on three components of vibrations such as horizontal, vertical and torsional vibrations should be conducted for the examination.

(2) Self-excited oscillations and vortex-induced oscillations are to be examined basically by means of sectional model tests in smooth flow. If necessary, comprehensive

examinations should be conducted by means of wind tunnel tests in turbulent flow, elastic model test and so on.

(3) Based on the results of field observation of wind, this Manual prescribes detailed property of wind turbulence such as intensity of turbulence, power spectral density function and so on.

(4) This Manual provides provisions related to suspension bridges with box-girder as well as truss-stiffened suspension bridge.

#### 5.2 Wind Resistant Design Manual for Highway Bridges

Since the revision of the Criteria, wind engineering has made a remarkable progress and a considerable amount of aerodynamic data of bridge have been acquired. The wind resistant design for limited kinds of bridges can be made without wind tunnel testing if reliable formulae for the estimation are provided. The prediction of wind-induced vibration will become more reasonable and reliable if the effect of turbulence is incorporated appropriately in the design.

From these reasons, the new wind resistant design manual for highway bridges has been required recent years. The working group was organized in the Japan Road Association in 1984 to prepare the manual. The working group was reformed into the ad hoc committee in 1986, and the draft of The Proposed Wind Resistant Design Manual For Highway Bridges was completed.

Table-5 shows main contents of the Manual and the main features of the Manual are as follows.

- (a) The basic wind speeds of the whole country are provided.
- (b) The design wind speed and the properties of wind turbulence can be estimated considering the altitude of structure and the terrain around the structure.
- (c) The critical wind speed for flutter and galloping can be obtained by simple formulae as well as by wind tunnel testing.
- (d) The amplitude of vortex-induced vibrations can be estimated by simple formulae as well as by wind tunnel testing. The effect of turbulence on vortex-induced vibrations are incorporated.
- (e) The method of verification of flutter, galloping and vortex-induced vibrations are provided.
- (f) The guideline of wind resistant design for bridge members and for bridges at their erection stages are described.
- (g) The standard wind tunnel testing methods are described.

### 6. Concluding remarks

- (1) A lot of long-span bridges including

suspension bridges and cable-stayed bridges have been planned and constructed in conjunction with promotion of road improvement program after the World War II in Japan. Researches on bridge aerodynamics have been conducted in laboratories of the Ministry of Construction, universities and private firms in relation to construction of the bridges.

(2) Especially, the researches related to the Honshu-Shikoku Bridge Project have produced a great deal of excellent results. In 1976, the Wind-resistant Design Criteria for the Honshu-Shikoku Bridges was formulated. This Criteria has been used not only for the design of the Honshu-Shikoku Bridges but also for the other long-span bridges.

(3) Sectional model test in smooth flow has been usually adopted to wind resistant design of bridge. This test seems to be simple and to provide safer results. But, in order to take account of the effects of turbulence of wind, the wind tunnel tests in turbulent flow are often carried out using an elastic full model or a taut-strip model. It is considered that the wind tunnel test in turbulent flow will be adopted as a means of wind resistant design in near future.

(4) To improve characteristics of truss stiffened suspension bridges against flutter, open-grating is arranged in bridge deck. In addition, sufficient rigidity of stiffening truss girder should be provided and structural members should be arranged carefully not to lessen aerodynamic characteristics. Furthermore, vertical stabilizer was invented to improve aerodynamic characteristics of truss-stiffened suspension bridge.

(5) Suspension bridges and cable-stayed bridges with box-girder are mostly quite safe against flutter, but they suffer from vortex-induced oscillation which occurs at low wind speed. Flap was invented to suppress this vibration, and modification of cross-section including fairings has been studied.

(6) Wind-induced vibrations were observed and countermeasures were studied in case of free-standing tower of suspension bridge under construction, cable of cable-stayed bridge and hanger of Langer bridge.

(7) The draft of The Proposed Wind Resistant Design Manual for Highway Bridges was prepared this year. This Manual provides formulae for prediction of wind-induced vibration based on a considerable amount of aerodynamic data of bridge.

(8) New subjects, which attracted the attention recently, are galloping and vortex-induced oscillation of long-span box-girder bridge, rain vibration of cable of cable-stayed bridge and aerodynamic interaction of line-like structures constructed close to each other.

(9) Suspension bridge and cable-stayed

bridge have extended their maximum span lengths, as represented by the Akashi Kaikyo Bridge (main span length: 1980m) and the Meiko-Chuo Bridge (main span length: 590m). As this trends seem to bring new subjects in the wind-resistant design, further researches are needed.

#### Reference

1. R. D. Marshall; Wind Tunnel Applied to Wind Engineering in Japan, J. Structural Engineering Vol. 110, No. 6, June, 1984
2. T. Okubo, N. Narita, K. Yamamoto and H. Sato; Unsteady Aerodynamic Forces for a Suspended Structure with Stiffening Trusses, Proc. 13th Joint Meeting, U. S. - Japan Panel on Wind and Seismic Effects, UJNR, Tsukuba, May, 1981
3. T. Okubo, N. Narita, K. Yamamoto and H. Sato; Effect of Solidity on Unsteady Aerodynamic Forces for Stiffening Trusses, Proc. 14th Joint Meeting, U. S. - Japan Panel on Wind and Seismic Effects, UJNR, Washington D. C., May, 1982
4. N. Narita, H. Tada, K. Yokoyama, H. Sato, K. Kanzaki and M. Fukuda; The response of Taut-Strip Models: Comparisons of Theoretical and Experimental Results, Proc. 18th Joint Meeting, U. S. - Japan Panel on Wind and Seismic Effects, UJNR, Washington D. C., May, 1986
5. N. Narita, K. Yamamoto, H. Sato, S. Yuzawa, K. Kanzaki and K. Nishikawa; Wind Resistant Design of a Long-Span Suspension Bridge with a Stiffening Box Girder, Proc. 16th Joint Meeting, U. S. - Japan Panel on Wind and Seismic Effects, UJNR, Washington D. C., May, 1984
6. T. Okubo, N. Narita and K. Yokoyama; Cable-Stayed Bridges and Wind Resistant Design, Proc. 5th Joint Meeting, U. S. - Japan Panel on Wind and Seismic Effects, UJNR, Tokyo, May, 1973
7. T. Okubo, N. Narita and K. Yokoyama; Some Approaches for Improving Wind Stability of Cable-Stayed Girder Bridges, Proc. 4th Int. Conf. on Wind Effects on Bldgs. and Sts., Heathrow, 1975
8. Y. Hikami and N. Shiraishi; Rain-Wind Induced Vibration of Cable-Stayed Bridges, Proc. 7th Int. Conf. Wind Engineering, Vol. 4, pp293-311, Aachen, West Germany, July, 1987
9. T. Kunihiro, N. Narita and K. Yokoyama; Wind-Resistant Safety of Long Span Suspension Bridge under Construction, Proc. 9th Joint Meeting, U. S. - Japan Panel on Wind and Seismic Effects, UJNR, Tokyo, May, 1977
10. N. Narita, K. Yamamoto and H. Sato; A Study of Aerodynamic Responses of a Multi- and Long-Span Road Bridge with Steel Box Girder, Proc. 15th Joint Meeting, U. S. - Japan Panel on Wind and Seismic Effects, UJNR, Tsukuba, May, 1983
11. N. Narita, K. Yokoyama, H. Sato and Y. Nakagami; Aerodynamic Characteristics of Continuous Box Girder Bridges

- Relevant to Their Vibrations in Wind, Proc. 19th Joint Meeting, U. S. -Japan Panel on Wind and Seismic Effects, UJNR, Tsukuba, May, 1987
12. T. Okubo and N. Narita; Wind-Induced Vibrations of Hangers of Langer Bridges, Proc. 3rd Joint Meeting, U. S. - Japan Panel on Wind and Seismic Effects, UJNR, Tokyo, May, 1971
  13. N. Narita, H. Tada, K. Yokoyama and H. Sato; Characteristics of Aerodynamic Forces on Bridge Decks in Smooth Flow and in Turbulent Flow, Proc. 17th Joint Meeting, U. S. -Japan Panel on Wind and Seismic Effects, UJNR, Tsukuba, May, 1985
  14. T. Okubo and N. Narita; On the Revised Wind Resistant Design Criteria for the Proposed Honshu-Shikoku Bridges, Proc. 4th Joint Meeting, U. S. -Japan Panel on Wind and Seismic Effects, UJNR, Washington D. C., May, 1972
  15. T. Okubo and N. Narita; On the Wind Resistant Design Specifications for the Proposed Honshu-Shikoku Bridges (1975), Proc. 8th Joint Meeting, U. S. -Japan Panel on Wind and Seismic Effects, UJNR, Washington D. C., May, 1976
  16. T. Okubo and N. Narita; On the Distribution of Expected Strong Wind in Japan Proc. 10th Joint Meeting, U. S. -Japan Panel on Wind and Seismic Effects, UJNR, Washington D. C., May, 1978.
  17. K. Yamada, N. Yamamoto and H. Akiyama; Full-Scale Dynamic Testing of Long-Span Bridges, 4th U. S. -Japan Bridge Workshop, San Diego May 1988.
  18. N. Narita and K. Yokoyama; On the Gust Response of Long-Span suspension Bridges, Proc. 6th Joint Meeting, U. S. - Japan Panel on Wind and Seismic Effects, UJNR, Washington D. C., May, 1974
  19. T. Okubo, N. Narita and K. Yokoyama; On the Aerodynamic Characteristics of the Kanmon Bridge, Proc. 7th Joint Meeting, U. S. -Japan Panel on Wind and Seismic Effects, UJNR, Tokyo, May, 1975
  20. N. Narita and H. Sato; Calculation of the Gust Responses of Long-Span Bridges, Proc. 11th Joint Meeting, U. S. - Japan Panel on Wind and Seismic Effects, UJNR, Tsukuba, September, 1979
  21. N. Narita and H. Sato; Calculation of the Gust Responses of Long-Span Bridges (II), Proc. 12th Joint Meeting, U. S. - Japan Panel on Wind and Seismic Effects, UJNR, Washington D. C., May, 1980

Table-1 Long Span Suspension Bridges in the world

Rank	Name of bridge	Main span (m)	Country	Completion year
1	Akashi Kaikyo Br.	1,990	Japan	under construction
2	Humber Br.	1,410	U. K.	1981
3	Verrazano Narrows Br.	1,298	U. S. A.	1964
4	Golden Gate Br.	1,280	U. S. A.	1937
5	Mackinac Straits Br.	1,158	U. S. A.	1957
6	Minami Bisan-Seto Br.	1,100	Japan	1988
7	2nd. Bosphorus Br.	1,090	Turkey	1988
8	Bosphorus Br.	1,074	Turkey	1973
9	George Washington Br.	1,067	U. S. A.	1931
10	April 25th Br.	1,013	Portugal	1966
11	Forth Road Br.	1,006	U. K.	1964
12	Kita Bisan-Seto Br.	990	Japan	1988
13	Severn Br.	988	U. K.	1966
14	Shimotsui-Seto Br.	940	Japan	1988
15	Ohnaruto Br.	876	Japan	1985
16	New Tacoma Narrows Br.	853	U. S. A.	1950
17	Innoshima Br.	770	Japan	1983

Table-2 Long-span cable-stayed bridges in the world

Rank	Name of bridge	Main span(m)	Country	Completion year
1	Meiko-Chuo Br.	590	Japan	Under Construction
2	Tsurumi-Koro Br.	510	Japan	Under Construction
3	Ikuchi Br.	490	Japan	Under Construction
4	Higashi Kobe Br.	485	Japan	Under Construction
5	Annacis Br.	465	Canada	1987
6	Yokohama Bay Br.	460	Japan	Under Construction
7	The 2nd Hooghly Br.	457	India	1987
8	Chao-Phya Br.	450	Thailand	1987
9	Barrios de Luna Br.	440	Spain	1983
10	Hitsuishi Jima Br.	420	Japan	1988
10	Iwaguro Jima Br.	420	Japan	1988
12	Meiko-Nishi Br.	405	Japan	1985

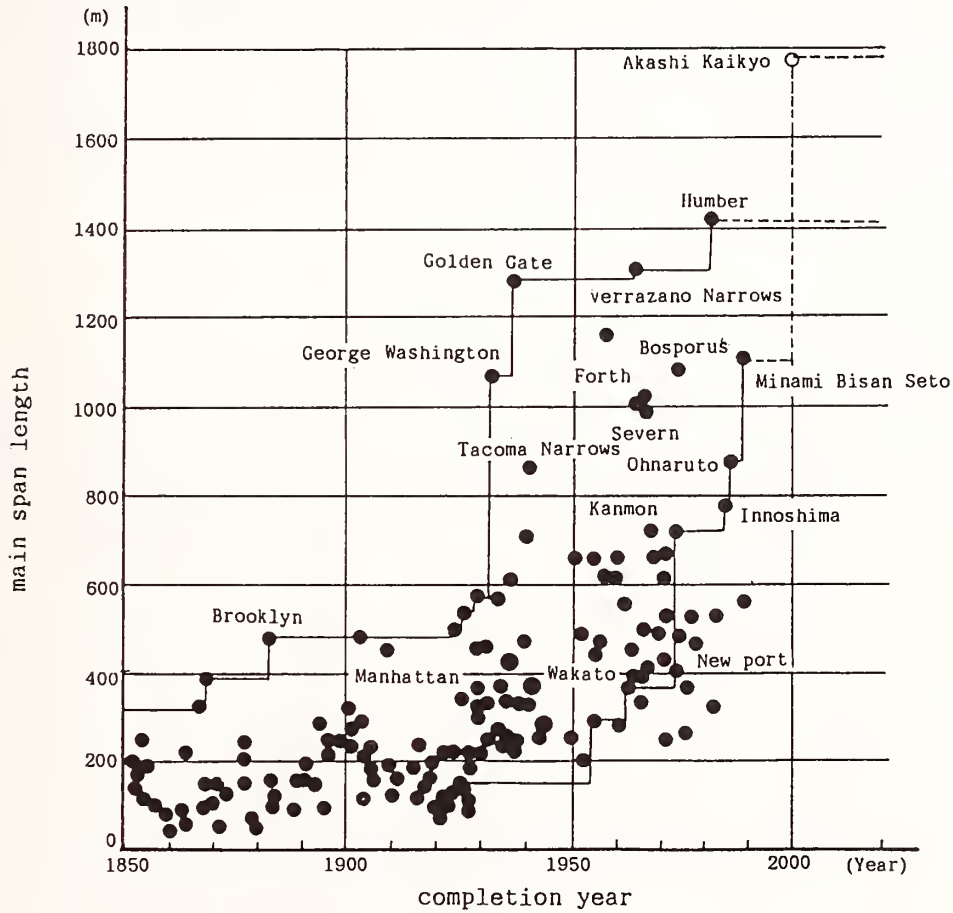


Fig. -1 Advance of maximum span length of suspension bridge

Table-3 Contents of the Wind-Resistant Design Criteria for the Honshu-Shikoku Bridges (1976)

- 1 General
- 2 Static Design
  - 2.1 Basic wind speed
  - 2.2 Design wind speed
  - 2.3 Design wind load
  - 2.4 Way of loading
  - 2.5 Combination of wind loads with other loads and allowable stress
  - 2.6 Proofing of lateral buckling
- 3 Dynamic Analysis
  - 3.1 Outlines
  - 3.2 Structural damping
  - 3.3 Vertical inclination of wind
  - 3.4 Critical wind speed for self-excited oscillation
  - 3.5 Restricted oscillation
- 4 Examination to be taken during construction

Table-4(1) Structural Damping of Suspension Bridges

Name of bridge		Minami-Bisan Seto Br.		Ohnaruto Br.		Kanmon Br.		Ohshima Br.	
Span		274+1100+274		(93)+330+876+330		178+712+178		140+560+140	
Vibration mode		natural frequency (Hz)	logarithmic decrement						
bending	As 1st	0.151	0.095	0.164	0.109	0.180	0.062	0.189	0.122~0.228
	s 1st	0.168	0.035	0.165	0.112	0.212	0.037	0.232	0.011~0.034
	s 2nd	0.228	0.097	0.284	0.080	0.298	0.028	0.323	0.014~0.049
torsional	s 1st	0.329	0.025	0.328	0.033	0.384	0.016	0.550~0.553	0.012~0.031
	As 1st	0.457	0.041	0.506	0.057	0.472	0.025	0.744~0.774	0.040~0.084

Table-4(2) Structural Damping of Cable-Stayed Bridges.

Name of bridge		Onomichi Br.		Toyosato Br.		Arakawa Br.		Kamome Br.	
Completion Year		1967		1970		1970		1975	
Span (m)		85+215+85		80.5+216+80.5		60.3+160+60.3		100+240+100	
Vibration mode		natural frequency (Hz)	logarithmic decrement						
bending	1st	0.58	0.05	0.52		0.75	0.024	0.47	0.076
	2nd	0.92	0.045	1.22		1.25	0.034		
	3rd	1.38		1.92	0.051	1.91	0.051	0.99	0.083
torsional	1st	1.66	0.035	1.43	0.071	1.45			
	2nd	2.94	0.03	3.25	0.083	2.80			
	3rd			4.08		4.24			
Name of bridge		Suehiro Br.		Rokko Br.		Yamatogawa Br.			
Completion Year		1975		1977		1982			
Span (m)		110+250+110		89.35+220+89.35		149+355+149			
Vibration mode		natural frequency (Hz)	logarithmic decrement	natural frequency (Hz)	logarithmic decrement	natural frequency (Hz)	logarithmic decrement		
bending	1st	0.47	0.031	0.94		0.34	0.023		
	2nd	0.71	0.018	1.76	0.206	0.42	0.031		
	3rd	1.07	0.018	2.42	0.066	0.63			
torsional	1st	1.45	0.016	2.05	0.067	0.87	0.012		
	2nd	2.69	0.056	3.92		1.67			
	3rd	4.44		4.97	0.084				

NATIONAL GOVERNMENT

1. Public Works Research Institute, MoC

UNIVERSITIES

2. Tokyo University
3. Yokohama National University
4. Kyoto University
5. Osaka University
6. Ritsumeikan University
7. Tokushima University
8. Kyushu University
9. Kyushu Institute of Technology
10. Kyushu Sangyo University

PRIVATE INDUSTRY

11. Nippon Kokan K. K.
12. Ishikawajima-Harima Heavy Industries, Ltd
13. Kawasaki Heavy Industries, Ltd
14. Mitsubishi Heavy Industries, Ltd
15. Mitsui Engineering & Shipbuilding, Ltd
16. Hitachi Shipbuilding & Engineering, Ltd
17. Sumitomo Heavy Industries, Ltd

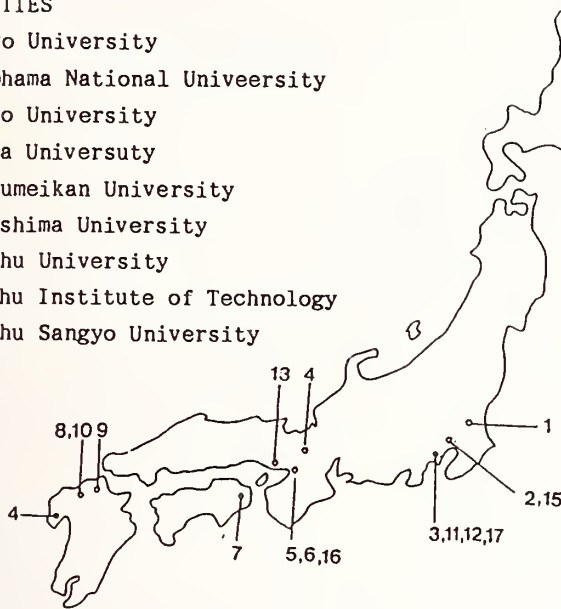


Fig. -3 Research organizations on bridge aerodynamics

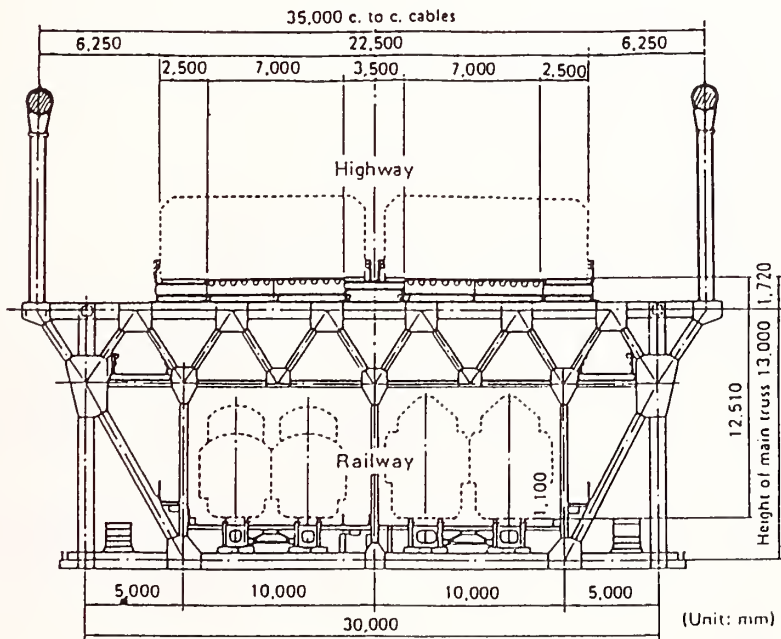


Fig. -4 Typical cross section of suspension bridges on Kojima-Sakaide route

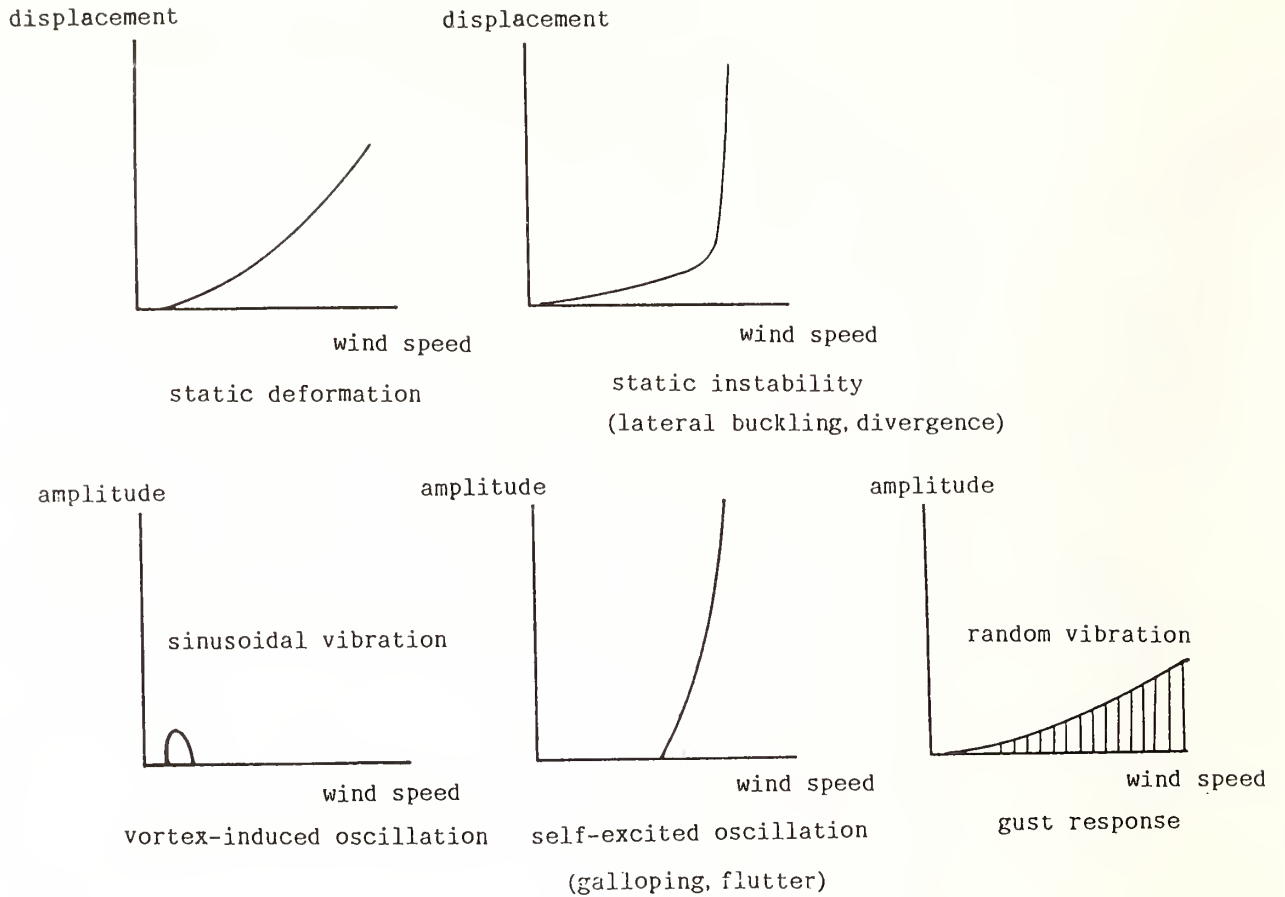


Fig. -2 Illustrated diagram of wind effects

Table-5 Contents of The Proposed Wind Resistant Design Manual for Highway Bridges

- |   |  |
|---|--|
| <ol style="list-style-type: none"> <li>1. GENERAL REMARKS</li> <li>2. GUIDELINE OF WIND RESISTANT DESIGN</li> <li>3. WIND PROPERTIES USED IN DESIGN <ul style="list-style-type: none"> <li>···Basic Wind Speed, Design Wind Speed, Intensity of Turbulence etc.</li> </ul> </li> <li>4. DESIGN WIND LOAD</li> </ol> | <ol style="list-style-type: none"> <li>5. WIND-INDUCED VIBRATIONS OF BRIDGE DECK <ul style="list-style-type: none"> <li>···Estimation, Evaluation, Method of Alleviation Flutter, Galloping, Vortex-Induced Vibrations, Buffeting</li> </ul> </li> <li>6. WIND-INDUCED VIBRATIONS OF TOWERS AND BRIDGE MEMBERS</li> <li>7. WIND RESISTANT DESIGN AT ERECTION STAGES</li> <li>8. WIND TUNNEL TESTING METHODS</li> </ol> |
|---|--|

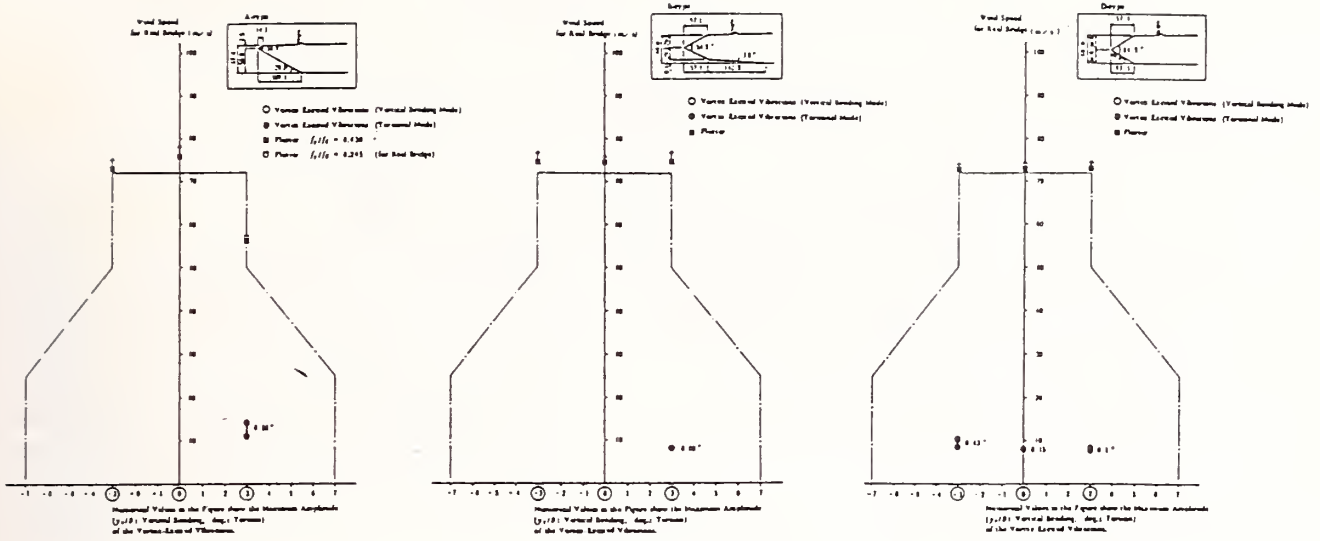


Fig. -5 Comparison of aerodynamic characteristics of suspension bridges stiffened with box girder

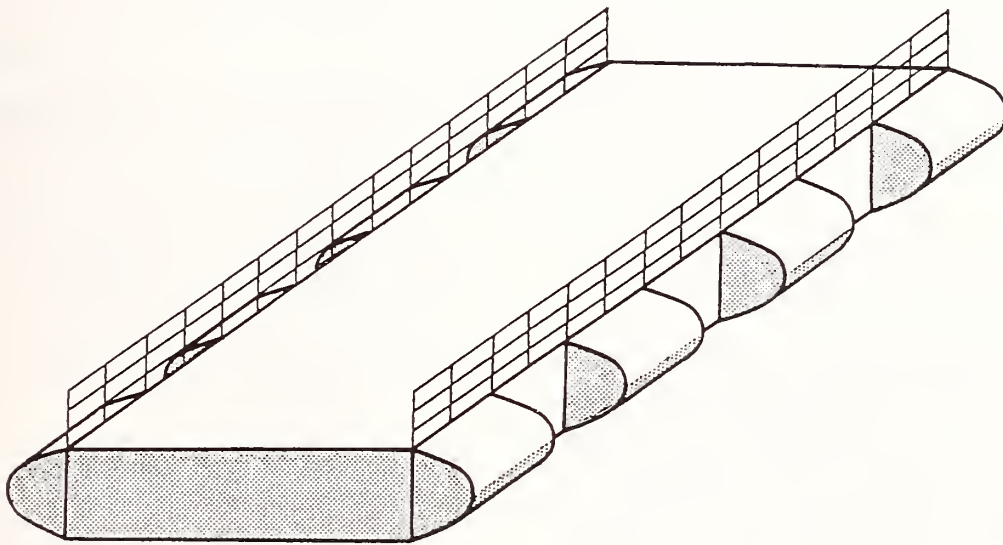


Fig. -6 Ishikari-kako bridge

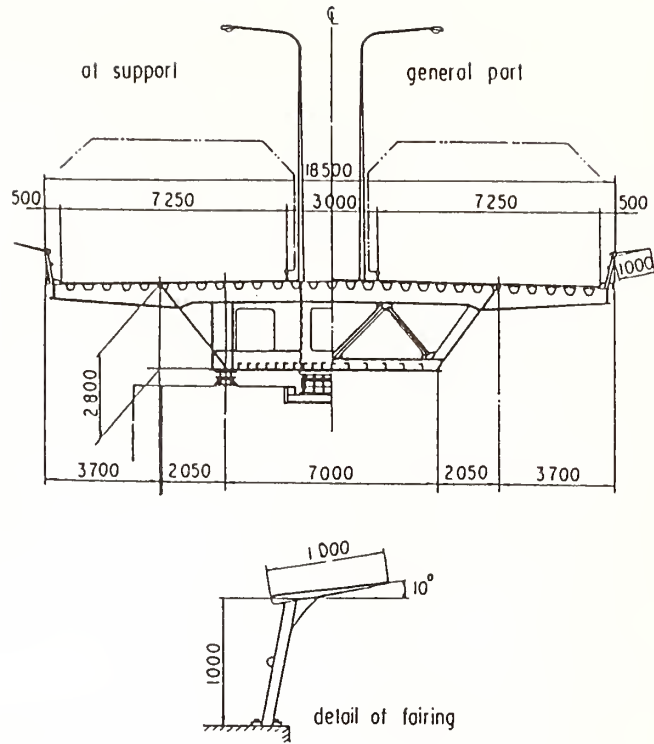


Fig. -7 Suehiro bridge (cross-section)

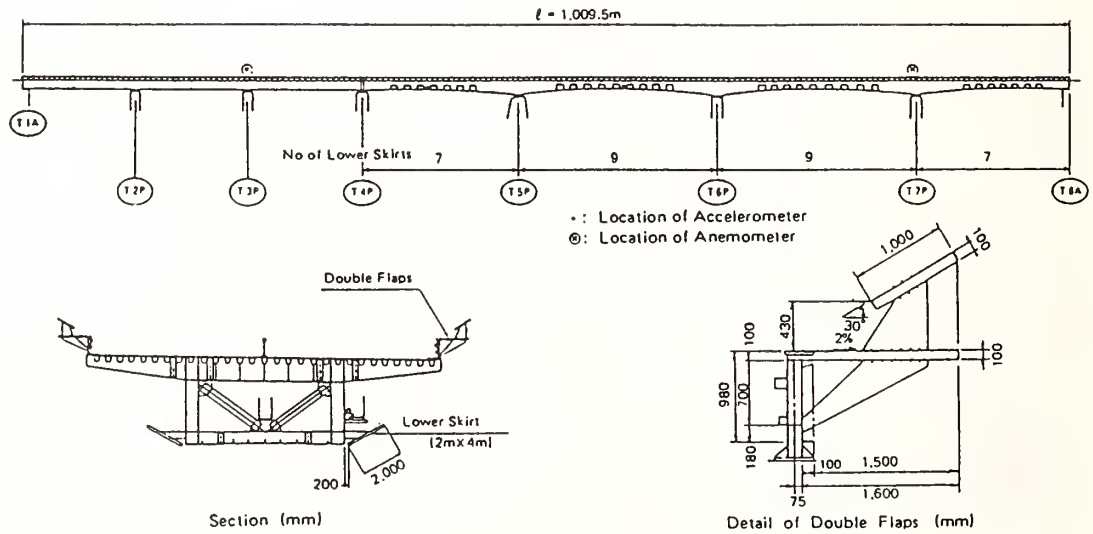


Fig. -8 Arrangement of attachment

# Anchorage and Foundations for Wind Resistance of Manufactured Homes

BY

G. ROBERT FULLER, P.E.<sup>1</sup>

## ABSTRACT

Each year significant damage to manufactured (mobile) housing is caused by winds, hurricanes and tornadoes. Damage is primarily in the form of roof failures and tiedown/anchorage failures. These failures sometimes consist of sudden and total destruction of the housing units. Wind load standards, design criteria, and construction practices are reviewed in this paper. In addition, recommended foundation design criteria and details are presented.

**KEYWORDS:** Anchorages; Foundations; Manufactured Housing; Wind Resistance.

## 1. INTRODUCTION

Manufactured (mobile) homes are regulated by the U.S. Department of Housing and Urban Development (HUD) under the Federal Manufactured Housing Program authorized by the U.S. Congress in 1974. Under this program, HUD developed Manufactured Home Construction and Safety Standards (MHCSS) for all manufactured housing units produced after June 15, 1976. [1]

These Standards govern the design and construction of each transportable section of manufactured homes, either single wide or multi-wide, intended for residential use in the United States. Another aspect of the MHCSS is that they are Federal preemptive standards for the construction of the structure. Therefore, no state or local jurisdiction can impose higher or more restrictive building code requirements or standards on the construction of the units.

However, the foundations and anchorages are left to local municipalities and states to regulate. Enforcement and inspection of the installation and foundation supports are also under the jurisdiction of the local government. The Federal Standards only require that one acceptable, approved, and designed system of support be provided by the manufacturer.

The only other Federal requirements are those of the Farmers Home Administration, U.S. Department

of Agriculture, and HUD for inclusion under mortgage insurance or grant programs. These have requirements for permanent foundations that comply with major national building codes. These programs only cover a small percentage of manufactured homes constructed, although the number appears to be increasing each year.

Almost one third of all new single-family homes sold in America are manufactured housing; a total of about 250,000 homes per year. Most manufactured homes are single-wides (60%) which are produced in over 300 factories.

Most single wide units are 12' or 14' wide, and are 50' to 72' long, constructed on two 8" or 10" steel chassis beams, with 2" x 8" transverse wood joists at 16", 19.2" or 24" on center for the floor system. The steel chassis beams are then typically supported on concrete block piers, spaced at 8'0" to 12'0" on centers.

Anchorage to resist overturning and sliding from wind forces is generally provided by diagonal galvanized steel straps from the chassis beams to screw-in anchors into the ground. Many designs also specify over the roof steel straps connected to the same ground anchors.

## 2. WIND DESIGN STANDARDS

### 2.1 Federal Manufactured Home Construction and Safety Standards: [1]

Wind design criteria in the MHCSS subdivides the U.S. into two wind zones: (1) Standard and (2) Hurricane (see Figure 1.). The Hurricane Wind Zone roughly parallels the contours shown in American National Standard Institute (ANSI) Standard A58.1-1982 [2] for wind velocities of 80 mph or above, along the East Coast and Gulf of Mexico

---

1 Chief, Manufactured Housing Compliance Branch, U.S. Department of Housing and Urban Development, Washington, D.C. 20410-8000

Design wind pressures for the two zones are as follows:

	<u>Horizontal</u>	<u>Net Uplift</u>
Standard Zone I	15 psf	9 psf
Hurricane Zone II	25 psf	15 psf

Most other provisions of the Federal Standards are performance standards. Each manufactured home shall be designed and constructed as a completely integrated structure, capable of sustaining design load requirements and shall be capable of transmitting these loads to stabilizing devices without exceeding allowable load stresses or deflections. Roof framing shall be securely fastened to wall framing, walls to floor structure, and floor structure to chassis, so as to resist wind overturning and sliding as imposed by design loads.

Each home shall also have provisions for support and anchoring systems, which, when properly designed and installed, will resist overturning and lateral movement (sliding). The design wind loads to be utilized for calculating resistance to overturning and lateral movement shall be increased by a factor of safety of 1.5.

Manufacturers shall provide for the support and anchoring systems. They shall furnish printed instructions with each home specifying the location and required capacity of stabilizing devices on which the design is based. The manufacturer shall also provide drawings and specifications certified by a registered professional engineer indicating at least one acceptable system of anchorage needed to transfer the wind loads from the manufactured home to ground anchors.

Anchoring equipment shall be capable of resisting an allowable working load of 3150 pounds (1429 kg), and shall be capable of withstanding a 50% overload (4725 pounds (2143 kg)) without failure of either the anchoring equipment or the attachment point on the manufactured home.

## 2.2 American National Standard Institute (ANSI) A225.1: [3]

ANSI A225.1-1982 "Manufactured Home Installations" provides the identical wind zone map as the MHCSS. There are also requirements for manufactured home foundations, stabilizing systems, piers, anchoring ties, and ground anchors.

However, the ANSI A225.1 Standard is designed to be adopted by jurisdictions responsible for the safety and health of manufactured home users, and for establishing regulations applicable to manufactured home communities. It is not a mandatory building code or standard unless so adopted and enforced by local or state building officials. Contained in Appendix C of ANSI A225.1 are typical designs of piers and load-bearing supports used by several producers of manufactured homes. These are not requirements of the Standard, and are only included for informational purposes.

The typical designs presented do not provide for lateral wind resistance, and they are not designed for earthquake forces. In addition, they allow construction of pier supports that have questionable structural adequacy. For example, piers less than 36" (91.5 cm) high can be 8" x 16", constructed of ungrouted concrete blocks, and supported on a 16" x 16" x 4" solid concrete base just below ground level. Soil should have a minimum loadbearing capacity of 2000 psf, but there is no requirement for footings to be below frost level.

For piers of 36" (91.5 cm) to 80" (203.2 cm) high, ungrouted double concrete blocks (16" x 16") may be used; supported on a 16" x 16" x 4" solid concrete base on undisturbed soil or controlled backfill compacted to a minimum capacity of 2000 psf. Again, there is no requirement to be below frost level. Only if piers are to be over 80" (2.0 m) in height, is reinforcement recommended.

## 2.3 ANSI Standard A58.1 "Minimum Design Loads for Buildings and Other Structures" [2]

This Standard, which is adopted by several nationally acceptable model building codes in the United States, contains specific design criteria for design of most buildings, structures, components and appurtenances. Contained in the Standard is a Basic Wind Speed Map (See Figure 2) which contains contours of fastest-mile per hour wind speeds at 33' (10 m) above ground for Exposure Category C (Open Country), with a 50 year mean recurrence interval.

Mc Donald and Mehnert [4] compared the wind load design criteria, including the wind zone and contour maps, in ANSI A58.1 with the MHCSS, even though the wind zones do not exactly match the

expected wind speeds. Calculations were made to relate the MHCSS, design wind pressures to equivalent wind speeds. Procedures and criteria in ANSI A58.1-1982 were used to obtain these wind speeds.

Table 1 summarizes the calculated results, which include adjustments for reducing the height from 33' (10M) to 15' (4.6M) above ground.

As shown in this comparison of standards, manufactured housing designed, constructed and supported to resist wind load pressures in the MHCSS would only be adequate to resist a maximum of 80 mph winds. Conclusions reached by McDonald and Mehnert [4] are that, unless manufacturers provide additional strength and support, manufactured homes in Hurricane Zone II would not be able to resist design wind speeds in ANSI A58.1.

### 3. WIND DAMAGE TO MANUFACTURED HOUSING

#### 3.1 General

In the United States, each year there are significant losses in terms of injuries, deaths, and property damage associated with manufactured (mobile) homes exposed to windstorms [4]. Consequently, the Aerospace Division of the American Society of Civil Engineers (ASCE) "Task Committee on Mitigation of Damages Due to High Winds" in 1985 included in its "Purpose" the following:

"Tornadoes, hurricanes and other high winds cause billions of dollars of damage in the U.S. each year. The toll is especially high for mobile homes and non-engineered buildings...It is the purpose of this committee to apply recent advancements in building aerodynamics to study this problem."

A session on "Mitigation of Hurricane Wind Damage" was then organized for the ASCE Structures Congress, held in New Orleans in September 1986. At this session, a paper on "Hurricane Damage to Mobile Homes" was presented by James R. Mc Donald, Texas Tech University [5].

#### 3.2 Damage Caused by Hurricane Elena (1985)

The study reported by Mc Donald was supported by

the Manufactured Housing Institute and the Institute for Disaster Research at Texas Tech. It consisted of an investigation of the performance of manufactured homes in several communities in Mississippi and Alabama hit by Hurricane Elena, on September 2, 1985 [5].

A survey was conducted that included a systematic collection of statistical data as well as details of performance of the individual units. The objectives of the survey were also to determine the hurricane path relative to location of manufactured home communities, and to obtain records of wind speeds.

3.2.1. Wind Speeds: Measurements of wind speeds were collected and analyzed by Perry and Sparks (1985). Table 2 shows wind speeds for four different locations near the path of the storm. The values give a general indication of intensity of the hurricane. It was relatively weak with wind speeds (fastest-mile) less than those prescribed for design in ANSI A58.1-1982 (approximately 114 mph) [2]. Damage to structures other than manufactured homes also showed correlation to wind speeds of 80 to 90 mph.

3.2.2 Damage Statistics: A method was developed by Vann and Mc Donald to estimate the extent of damage, which categorizes damage of manufactured homes into five classes (see Table 3). These classes range from 0 to 4 (Class 0, 1 and 2 are for units that are still inhabitable) Class 3 is judged uninhabitable, but repairable; and Class 4 indicates units not repairable. No attempt was made to prescribe dollar amounts to classes of damage.

Table 4 gives overall statistics of damage observed in the ten manufactured housing communities surveyed. Of the 740 units surveyed, 517 (70%) were undamaged or had only minor damage (Damage Class 0); 150 Units (20%) had minor to moderate damage (Class 1 or 2); while 73 (10%) were severely damaged or destroyed (Classes 3 or 4).

Also shown in Table 4 is that for four communities: Trade Winds, Old Fort Village, Isle of Pines-North, and Isle of Pines-South; 79 out of 305 total units had major damage (Class 2 to 4); 17% had Class 4 damage. A tremendous amount of damage resulted from a relatively moderate hurricane.

Primary types of major damage were then evaluated for Hurricane Elena. Table 5 summarizes damage in Class 2 through Class 4 for three of the

four communities that had a detailed survey. Trav. Park, West Shore is not included, because there were only 12 units, and they either had no damage or very minor damage. Categories of damage causes were collapsing trees, roof failures, tie down failures, impact and other.

Where detailed surveys were conducted, only Isle of Pines-North had damage caused by trees, the other communities had few trees.

The major cause of damage for the 59 homes with major damage was from tie-down failures (26 homes, 44%). "Roof failures" was the next most common category with 17 homes (29%). Generally, it was concluded by Mc Donald that if a unit's structure and tie-down system held, only minor damage occurred, if either system failed, extensive damage or complete destruction resulted.

**3.2.3 Tiedown Failures:** Table 6 shows tie down information for four communities for which detailed surveys were made. Performance is expressed in terms of how well tiedowns held the unit in place. Three categories are considered according to whether the unit stayed on the concrete block piers, shifted off the piers (shift more than one foot), or had significant tie down failure (unit shifted far to one side or rolled over). In addition, it was determined if there were no tiedowns, or whether the tiedowns were adequate or not, based on ANSI A225.1 [3].

As shown in Table 6, only 17 of 231 units (7%) had no tiedowns. However, despite compliance with the tiedown and anchorage requirements, less than half of the units (104; 45%) in those four communities remained on their block piers. Also, most of the systems that appeared to be adequate failed because soil anchors pulled out of the ground or moved laterally which allowed units to shift off pier foundations.

**3.2.4 Conclusions:** As stated by Mc Donald [5], roof construction and tiedown systems need improvement to resist windstorms: "The use of helical-type ground anchors does not appear to be an optimum solution for anchoring single wide manufactured homes. The problem is not so much the fault of present criteria, but the inability of the anchors to achieve the needed pull-out resistance."

Because single wide units are lightweight and have relatively large surface areas exposed to wind, they

offer little resistance to overturning and sliding. Therefore, particularly in Hurricane Wind Zones, more substantial foundations need to be designed and constructed.

Single-wide manufactured homes are normally supported on concrete block piers with no mortar. The units are anchored by metal frame ties of galvanized steel straps, 0.35" thick by 1.25" wide with specified minimum strength. The number and spacing of ties is specified by the home manufacturer and designed to resist forces specified by the MHCSS. [1]

Tiedown/foundation failures range from a sliding off the piers to a complete pullout of ground anchors allowing a unit to roll over (Yann and Mc Donald, 1978).

Manufactured housing units are usually four to six times longer than they are wide, with shear walls spaced at over 20' on center. This often requires a very stiff roof diaphragm to transfer wind forces to end shear walls. Actual construction of the roof/ceiling diaphragms is relatively flexible, thus leading to abnormal loads on ground anchors from high wind forces. This was reported by Mc Donald and Mehnert [4], as evident in several destroyed units exposed to Hurricane Elena in Alabama.

## 4. FOUNDATION AND ANCHORAGE DESIGNS

### 4.1 Soil and Rock Anchors

One of the most common forms of manufactured home anchor is the helix or multi-helix which is turned under load and forced into the ground to a specified depth [8]. Torque is applied by either hand or power tools, in accordance with anchor manufacturer's instructions. Pull-out capacity in pounds is then approximately 10 times the installation torque in foot-pounds. However, pull-out force is usually considered as in line with the anchor shaft (see Figure 4). In fact, some anchor details show straps from the steel chassis beam to the anchor at a specified angle which would require installation of the anchor prior to set-up of the home (see Figure 5).

ANSI A225.1-1982 requires compliance with anchor manufacturer's installation instructions. In addition, values are provided which correlate Blow Counts for certain types of soil (ASTM D 1586) to a "Test Probe Torque Value." Unfortunately, soil values can vary considerably, and observations of

actual installations show that anchors are often not installed properly. Resistance to hurricane winds, therefore, is difficult to predict.

The conclusion of Mc Donald and Mehnert [4] is that it would be very difficult to install a tiedown-foundation system using straps and ground anchors that will resist pressures equivalent to 100 mph winds. "Improvements or changes must be made in the construction practice and in the tiedown/foundation system. "

Their conclusion is also that: "Even if the most creative approaches to redundancy and ductility are developed, without a permanent foundation system, the goal of wind damage mitigation could not be achieved. Stated simply, ground anchors and concrete masonry piers do not work."

## 4.2 Permanent Foundations:

### 4.2.1 General:

HUD requires permanent foundations for manufactured homes to be acceptable under Title II Mortgage Insurance (usually 30 year Federal Housing Administration Mortgage Insurance financing). Permanent foundations are required for valuation as real estate, and to improve reliability, safety, and durability. Screw-in ground anchors are prohibited.

Permanent foundations will improve wind and earthquake resistance by improving stiffness of the overall structure. Connections to permanent foundations provide anchorages that will not yield excessively when homes are subjected to high wind forces.

Building codes for single-family home construction in the U.S., generally provide minimum requirements and details for permanent foundations for onsite housing construction. Because manufactured homes must be transported to a site and erected on previously constructed foundations, HUD decided to develop a handbook guide for use by HUD-FHA field offices to determine acceptability of permanent foundations. This HUD Handbook 4930.3, "Permanent Foundations Guide for Manufactured Housing" is in final draft stage, and should be published in another month. It was prepared, under contract with HUD by the Small Homes Council of the University of Illinois [9].

Main parts of the Manual are:

- a. Design Concepts,
- b. ANSI A58.1-1982 Criteria,
- c. Design Load Tables, and
- d. Foundation Capacity Tables.

4.2.2 Design Concepts: Three types of foundation systems are presented: 1. C-Chassis supported, 2. E-Exterior supported and 3. I-Interior supported. The systems contained in the Handbook were selected from over 40 actual designs used by the manufactured housing industry. Several examples and details are shown in Appendix [9].

Design loads used were taken from ANSI A58.1 [2]. In all cases selected, magnitude wind loads govern over seismic loads for the design. This is due to the fact that units are generally very light, but have relatively large vertical surfaces.

4.2.3 Design Load Tables: These foundation design tables in the Handbook provide design values for the three design concepts, and for the following three conditions:

- a. Required anchorage to prevent uplift and overturning ( $A_v$ ),
- b. Required anchorage to prevent sliding ( $A_h$ ), and
- c. Required footing area based on allowable bearing capacity of soil under full gravity loading.

Examples of Tables to provide the required anchorages are shown in the Appendix. These tables show wind speeds for Inland and Coastal Hurricane Zones, pier spacings and required anchorage for Type C Foundations. Required anchorage loads in pound per lineal foot are shown for wall footings used for Type E Foundations [9].

4.2.4 Capacity Tables: These tables provide foundation design capacities and dimensions for three foundation design conditions:

- a. Withdrawal Resistance: Ability of foundation wall or pier to resist uplift and overturning.
- b. Vertical Anchor Capacity: Required size and spacing of anchors to meet required

- c. Horizontal Anchor Capacity: Required size and spacing of anchors to resist sliding.

Examples of these tables are also shown in the Appendix [9].

#### 4.3 Conclusions:

Permanent foundation systems recommended by Small Homes Council [9] must have reinforced masonry piers or reinforced walls on footings carried below frost level, to resist high wind forces (over 80 mph winds). Foundations are designed to resist uplift, sliding and overturning. Footings are also designed so that soil bearing capacity is not exceeded.

Wind damage mitigation can be achieved without adding tremendous costs to manufactured housing. However, to adequately resist high winds, specific attention needs to be paid to the anchorages and foundations.

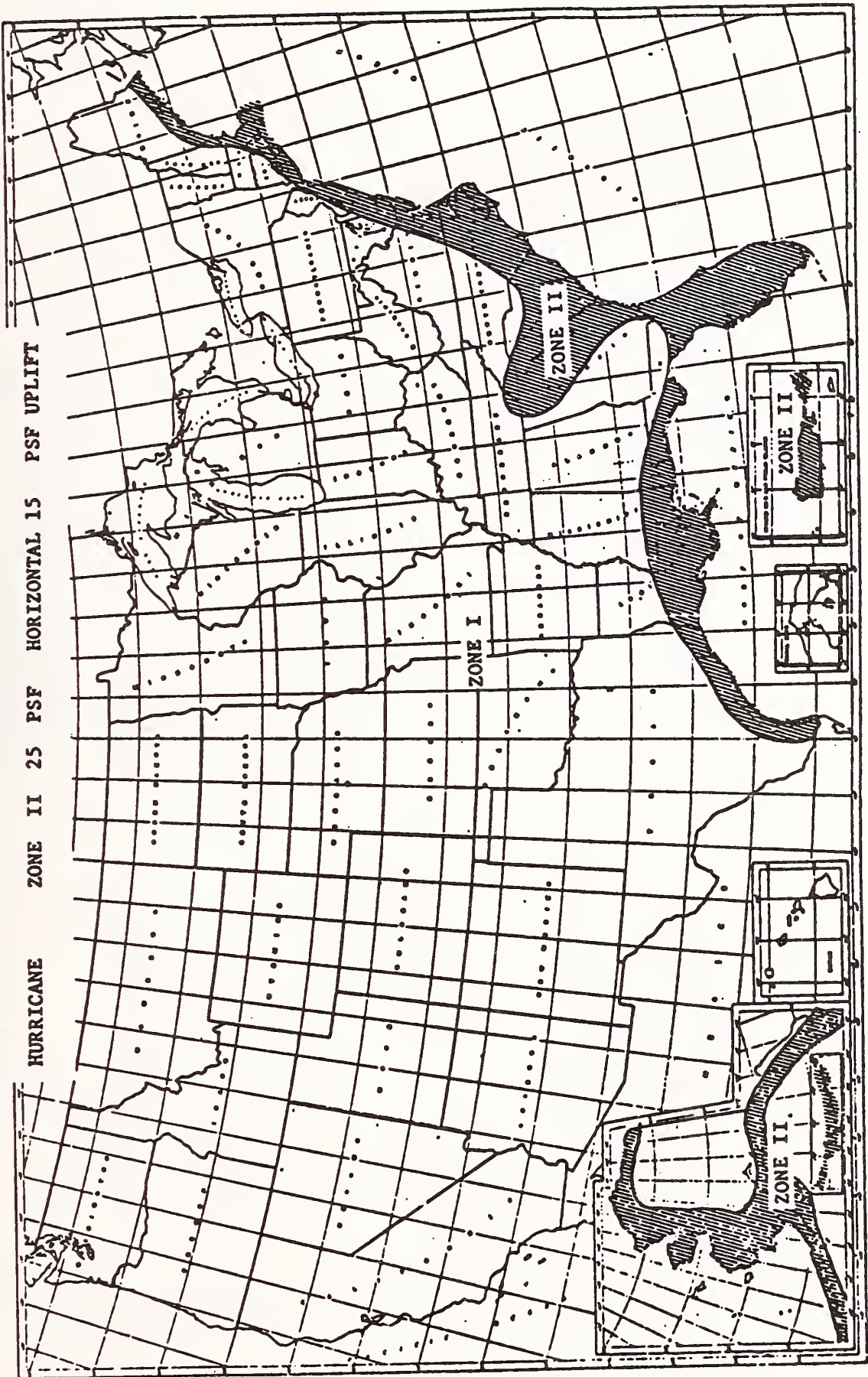
Since foundations and anchorages for manufactured homes are under jurisdiction of local or state building officials, those officials in hurricane and tornado prone areas need to be more cognizant of these requirements and their enforcement and inspection programs need to be strengthened.

---

#### REFERENCES

- [1] U.S. Department of Housing and Urban Development, 1976: "Federal Manufactured Home Construction and Safety Standards," 24 CFR 3280, HUD, Washington, D.C.
- [2] American National Standards Institute, 1982: "Minimum Design Loads for Buildings and Other Structures," ANSI A58.1-1982; New York, N.Y.
- [3] American National Standards Institute, 1982: "Manufactured Home Installations," ANSI A225.1 and NFPA 501 A-1982; NFPA, Quincy, MA.
- [4] Mc Donald, J.R. and Mehnert, J.F., 1987: "A Review of Standards of Practice for Wind Resistant Manufactured Housing," HUD Region VI, Kansas City, MO.
- [5] Mc Donald, James, R. 1986: "Hurricane Damage to Mobile Homes," ASCE Structures Congress, Session on Mitigation of Hurricane Wind Damage, New Orleans, Sept. 1986, Institute for Disaster Research, Texas Tech Univ., Lubbock, TX.
- [6] Perry, D.C. and Sparks, P., 1985: "The Effects of Hurricane Elena," Institute for Disaster Research, Texas Tech, Lubbock, TX.
- [7] Vann, W.P. and Mc Donald, J.R., 1978: "An Engineering Analysis: Mobile Homes in Windstorms," Doc. 32D, Institute for Disaster Research, Texas Tech Univ., Lubbock, TX.
- [8] Kovacs, W.D. and YokeI, F.Y., 1979: "Soil and Rock Anchors for Mobile Homes - A State-of-the-Art Report," NBS-BSS 107, National Bureau of Standards, Department of Commerce, Gaithersburg, MD.
- [9] U.S. Department of Housing and Urban Development, 1988: (Draft Handbook), "Permanent Foundations Guide for Manufactured Housing," Handbook 4930.3, Small Homes Council, Univ. of Illinois, HUD, Washington, D.C.

**FIGURE 1 - WIND ZONE MAP**  
STANDARD WIND ZONE I 15 PSF HORIZONTAL 9 PSF UPLIFT  
HURRICANE ZONE II 25 PSF HORIZONTAL 15 PSF UPLIFT



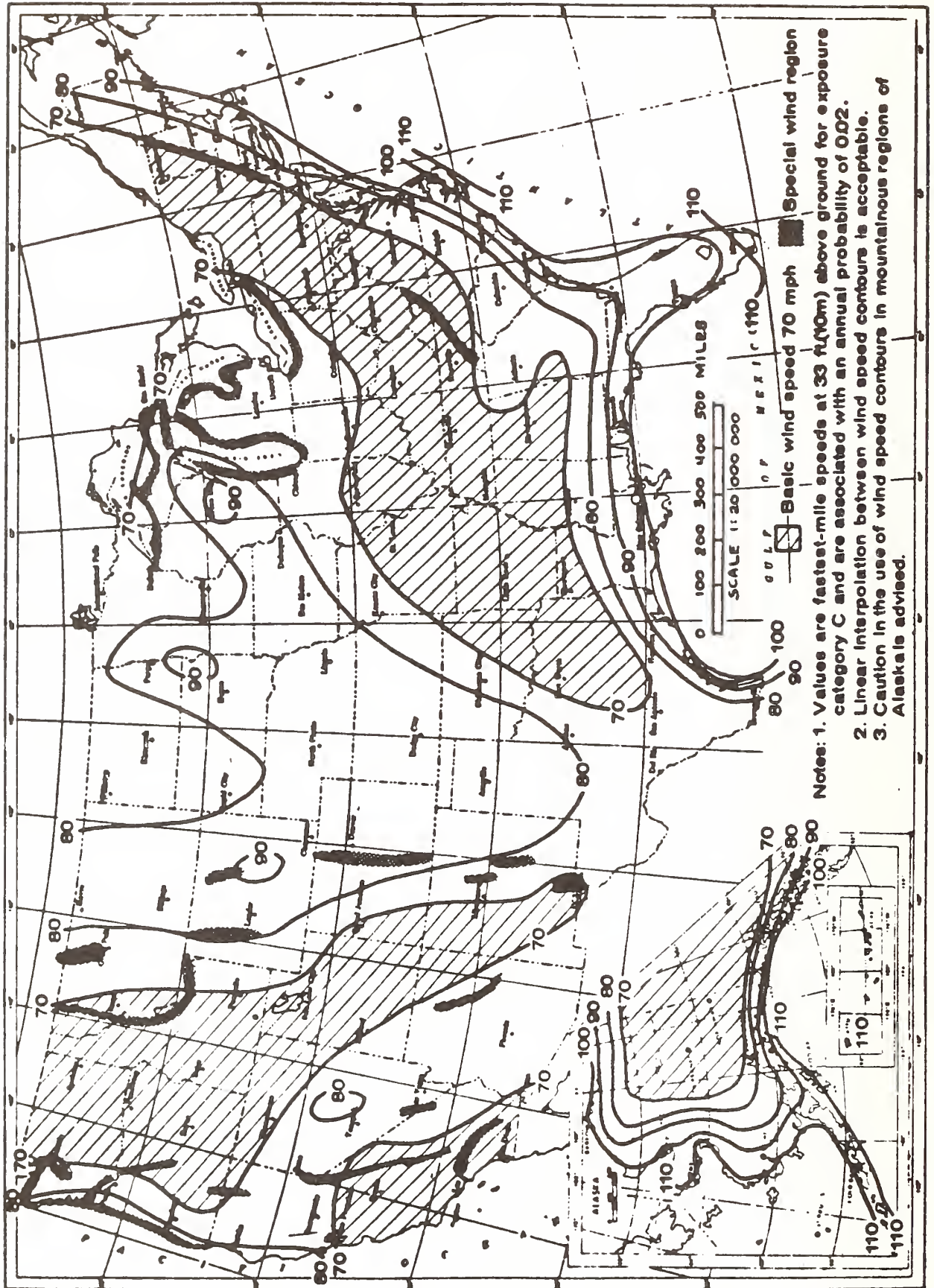
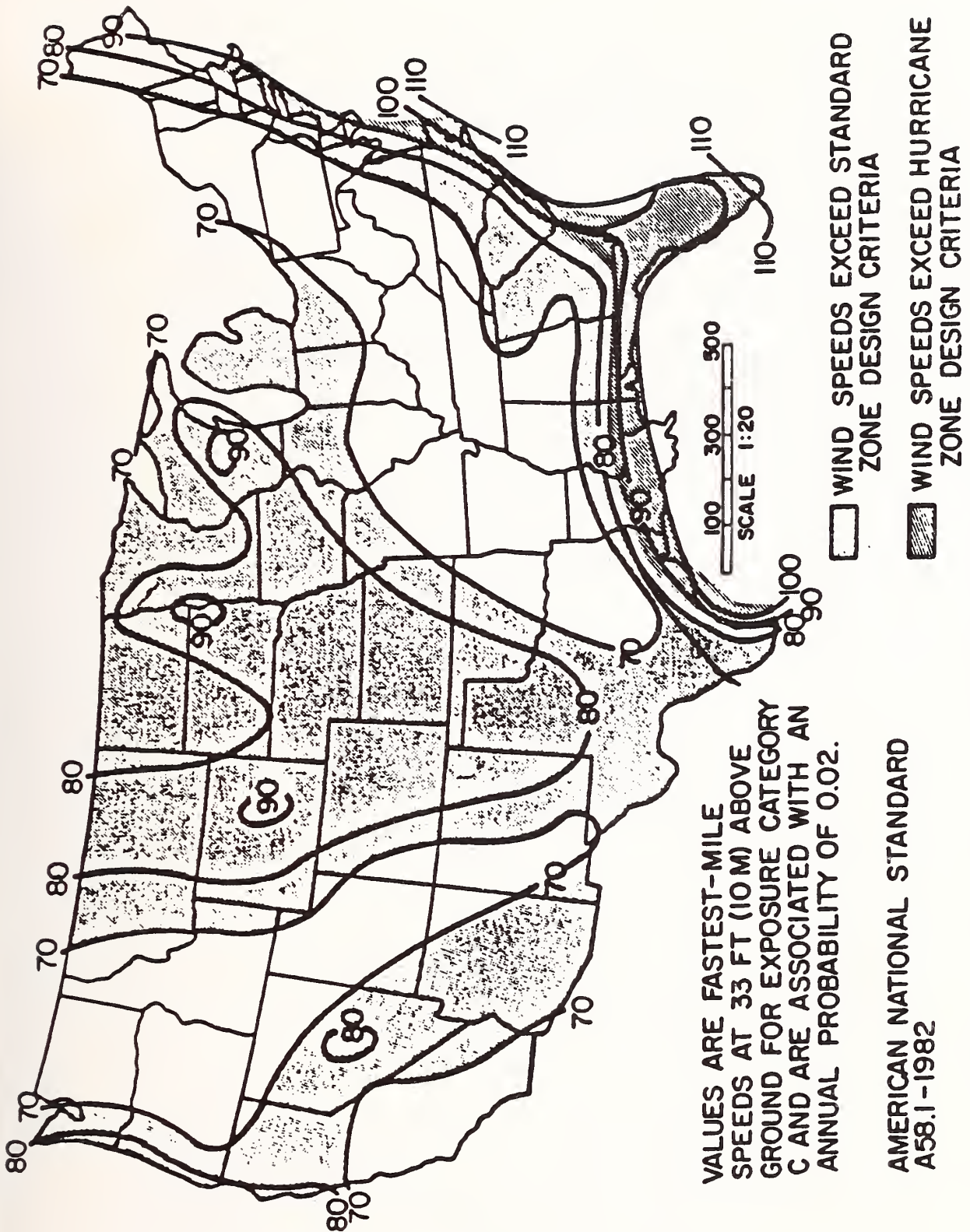


Fig. 2  
Basic Wind Speed



VALUES ARE FASTEST-MILE SPEEDS AT 33 FT (10 M) ABOVE GROUND FOR EXPOSURE CATEGORY C AND ARE ASSOCIATED WITH AN ANNUAL PROBABILITY OF 0.02.

AMERICAN NATIONAL STANDARD A58.1-1982

FIGURE 3. AREAS IN STANDARD AND HURRICANE ZONES WHERE WIND SPEEDS EXCEED DESIGN CRITERIA

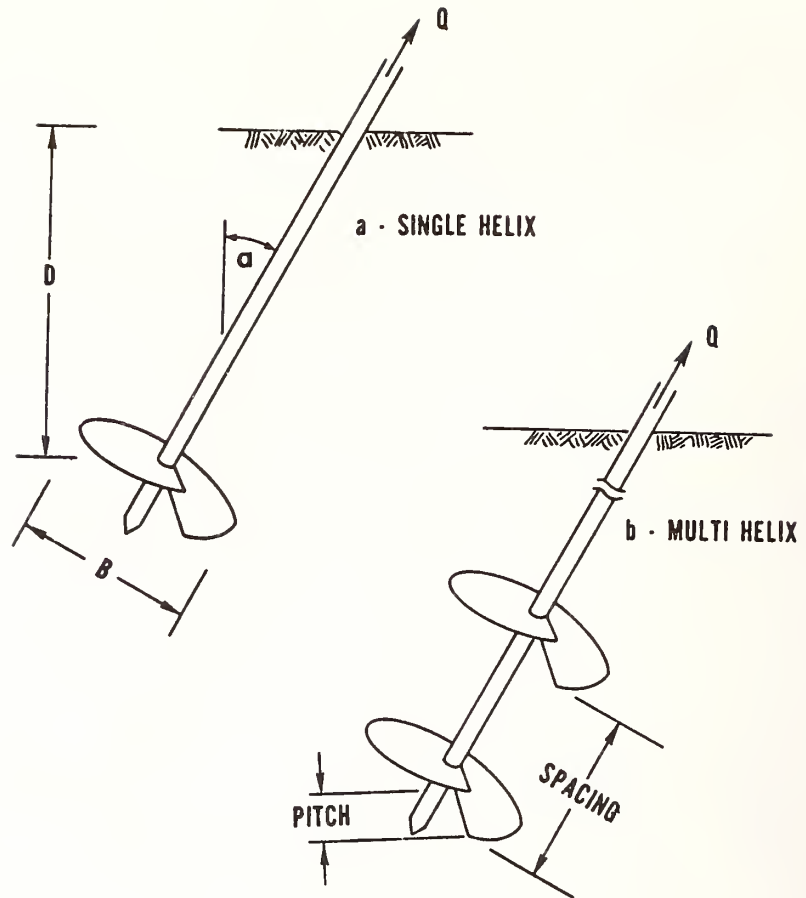
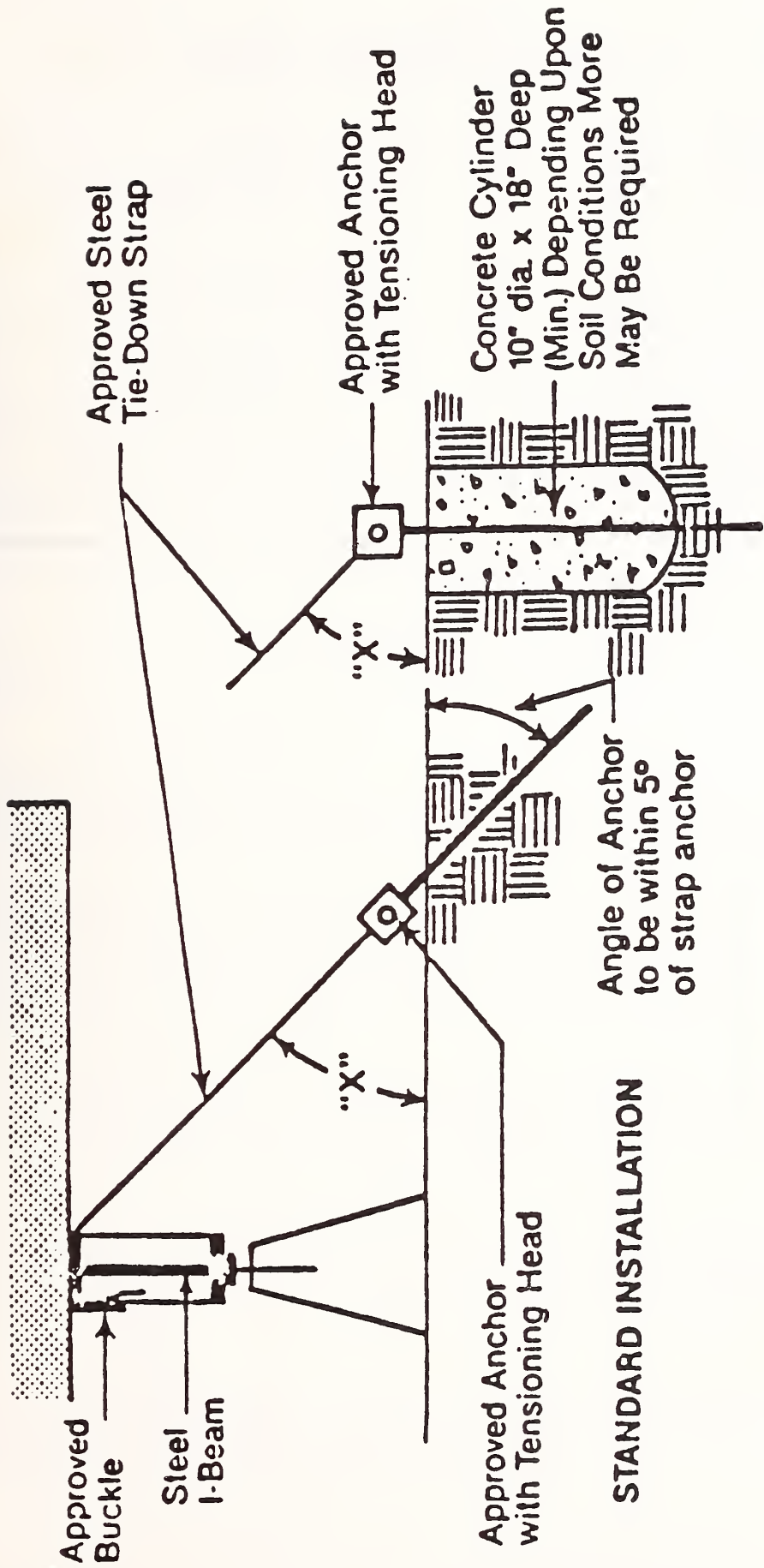


Figure 4 Helix and Multi-helix Anchors



STANDARD INSTALLATION

ALTERNATE INSTALLATION

FIGURE 5

TABLE 1  
WIND SPEEDS FOR MHCSS WIND PRESSURES

Standard Wind Zone						
	p (1)	K <sub>h</sub> (2)	I (3)	G <sub>h</sub> (2)	C <sub>p</sub> (3)	V
Horizontal	15	0.80	1.0	1.32	1.3	65
Uplift	9	0.80	1.0	1.32	0.7	69
Hurricane Wind Zone						
	p (1)	K <sub>h</sub> (2)	I (3)	G <sub>h</sub> (2)	C <sub>p</sub> (3)	V
Horizontal	25	0.80	1.05	1.32	1.3	80
Uplift	15	0.80	1.05	1.32	0.7	85

(1) Wind Pressure (psf) from MHCSS

(2) K<sub>h</sub> and G<sub>h</sub> based on open terrain exposure at 15 ft above ground

(3) Factors from ANSI A58.1-1982

Table 2  
 MAXIMUM FASTEST-MILE WIND SPEEDS MEASURED IN HURRICANE ELENA  
 Perry and Sparks, 1985

Location	Fastest-Mile Wind (mph)
1. University of Alabama, Sealab Dauphin Island, Alabama	83 (Mean)
2. National Weather Service Office Bates Field, Mobile, Alabama	52 (Mean)
3. Gulf Coast Research Laboratory Biloxi Point, Mississippi	96 (Peak)
4. Civil Defense Council Gulfport, Mississippi	79 (Peak)

Corrected to 10 meters and flat, open terrain exposure.

Table 3  
 DESCRIPTION OF WIND DAMAGE CLASSES FOR MANUFACTURED HOUSES  
 (Yann and Mc Donald, 1978)

Damage Class	Description of Damage
0	No Damage or Very Minor Damage Little or no visible damage from the outside. Slight shifting on the blocks that would suggest releveing, but not off the blocks. Some cracked windows, but no resulting water damage.
1	Minor Damage Shifting off the blocks or so that blocks press up on the floor; releveing required. Walls, doors, etc. buckled slightly, but able to be corrected by releveing. Minor eave and upper wall damage, with slight water damage, but roof not pulled all the way back. Minor pulling away of siding, with slight water damage. Minor missile and/or tree damage. Slight window breakage and attendant water damage.
2	Moderate Damage (Still Livable) Severe shifting off blocks with some attendant floor and superstructure damage (punching, racking, etc.) Roof removed over a portion of all of the home, but joists intact, walls not collapsed. Missile and/or tree damage to a section of the wall or roof, including deep dents or punctures. Serious water damage from holes in the roof, walls, windows, doors or floors.
3	Severe Damage (Not Livable but Repairable) Unit rolled onto side but frame intact. Extreme shifting causing severe racking and separations in the superstructure. Roof off, joists damaged or removed, walls damaged from lack of lateral support at top. Severe tree damage, including crushing of one wall or roof section. Superstructure partially separated from underframe.
4	Destruction (Not Repairable) Unit rolled onto top or rolled several times. Unit tossed or vaulted through the air. Superstructure separated from underframe or collapsed to side on the underframe. Roof off, joists removed and walls collapsed. Destruction of a major section by a falling tree.

TABLE 4

STATISTICS OF OBSERVED DAMAGE TO  
MANUFACTURED HOMES IN HURRICANE ELENA

Manufactured Housing Community, Location	Total Number of Units	Number of Units in Damage Class				
		0	1	2	3	4
<b>A. Detailed Survey</b>						
Trade Winds, Dauphin Island, Alabama	20	1	7	4	0	8
Trav Park, West Shore of Mobile Bay, Alabama	12	9	3	0	0	0
Isle of Pines - North Gautier, Mississippi	102	49	24	6	4	19
Subtotal	231	100	72	14	7	38
<b>B. Summary Survey</b>						
Isle of Pines-South, Gautier, Mississippi	86	47	19	4	2	14
Imperial Estates, North Biloxi, Mississippi	87	77	3	1	3	3
Rolling Hills, North Biloxi, Mississippi	175	153	18	1	2	1
Anchor Gaitoer, Mississippi	70	53	13	1	0	3
Subtotal	418	330	53	7	7	21
<b>C. Cursory Surveys</b>						
Starlight, Gautier, Mississippi	60	59	0	1	0	0
Pine Grove, North Biloxi, Mississippi	31	28	3	0	0	0
Totals	740	517	128	22	14	59
Percentage	100	70	17	3	2	8
				! 30% !		

TABLE 5  
MAJOR DAMAGE CATEGORY ANALYSIS

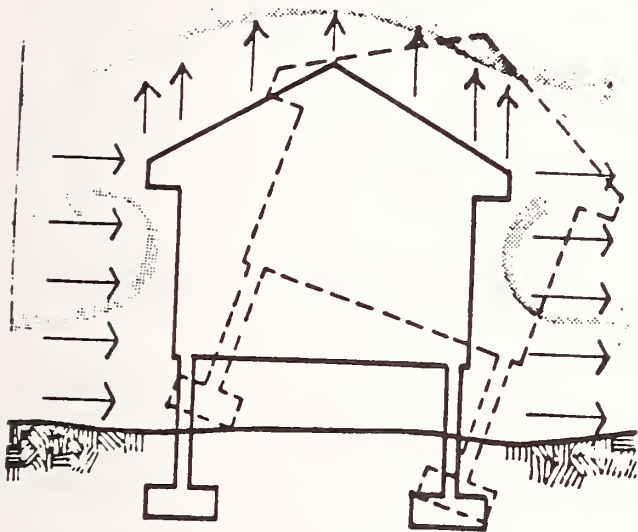
Community	No of Units	Damage Class	Tree	Roof	Ties	Impact	Other	Total
Trade Winds	20	2	0	0	3	1	0	4
		3	0	0	0	0	0	0
		4	0	5	3	0	0	8
		Total	0	5	6	1	0	12
Old Fort Village	97	2	0	0	3	0	1	4
		3	0	2	1	0	0	3
		4	0	3	8	0	0	11
		Total	0	5	12	0	1	18
Isle of Pines North	102	2	3	1	1	0	1	6
		3	2	1	0	0	1	4
		4	7	5	7	0	0	19
		Total	12	7	8	0	2	29
Four Combined	219	2	3	1	7	1	2	14
		3	2	3	1	0	1	7
		4	7	13	18	0	0	38
		Total	12	17	26	1	3	59
Percent of Major Damage			20	29	44	2	5	100

TABLE 6  
ANALYSIS OF TIEDOWN PERFORMANCE

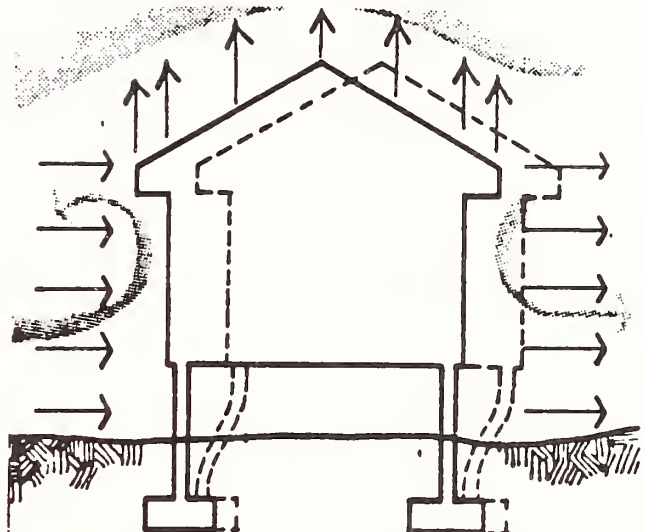
Community	Number of Units	Apparent Adequacy	Performance			Total
			On Blocks	Off Blocks	Major Shift	
Trade Winds	20	No tiedowns	0	5	1	6
		Inadequate	0	2	4	6
		Adequate	2	3	3	8
		Total	<u>2</u>	<u>10</u>	<u>8</u>	<u>20</u>
Trav Park	12	No tiedowns	0	0	0	0
		Inadequate	4	1	0	5
		Adequate	5	2	0	7
		Total	<u>9</u>	<u>3</u>	<u>0</u>	<u>12</u>
Old Fort Village	97	No tiedowns	0	0	0	0
		Inadequate	2	6	4	12
		Adequate	40	31	14	85
		Total	<u>42</u>	<u>37</u>	<u>18</u>	<u>97</u>
Isle of Pines-North	10	No tiedowns	1	1	9	11
		Inadequate	11	14	6	31
		Adequate	39	9	12	60
		Total	<u>51</u>	<u>24</u>	<u>27</u>	<u>102</u>
Four Combined	231	No tiedowns	1	6	10	17
		Inadequate	17	23	14	54 }71 (1/3)
		Adequate	86	45	29	160
		Total	<u>104</u>	<u>74</u>	<u>53</u>	<u>231</u>

## APPENDIX A-1

4-4. WIND EFFECT ON FOUNDATIONS. Wind exerts pressures on a structure and parts thereof. Horizontal pressure on the front (windward) wall combined with a horizontal suction on the rear (leeward) wall will cause overturning, as shown in Figure A. These wind pressures can also slide the structure off its foundation as shown in Figure B.



Wind Overturning Forces  
Figure A



Wind Sliding and Bending Forces  
Figure B

High wind forces tend to stress the connections between structural members, such as those connecting floor beam girders and those connecting them to vertical supports. Such stresses may cause a progressive weakening of these connections to the point where failure is possible.

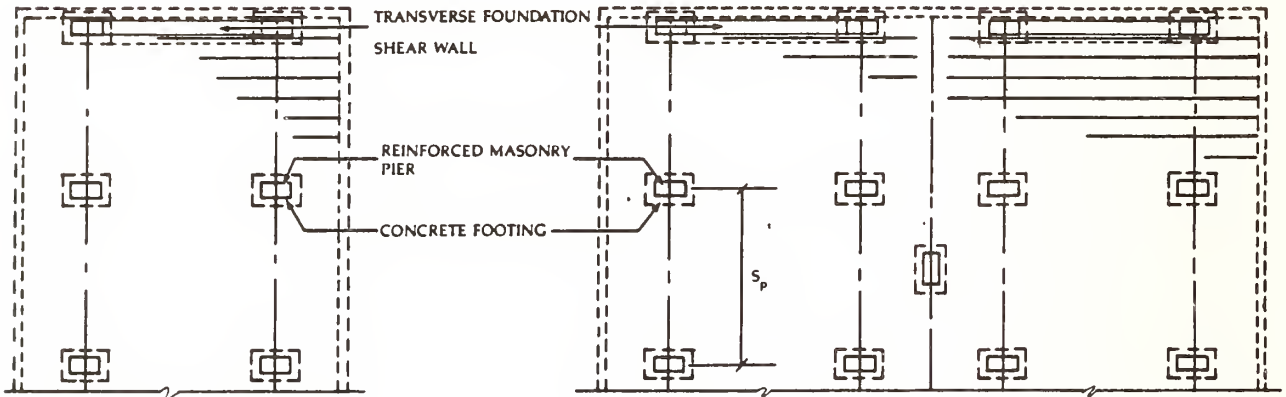
It cannot be overemphasized that attention to connection details is a most important requirement.

# APPENDIX A-2

FOUNDATION TYPE <b>Reinforced masonry or concrete piers</b>	SYSTEM NUMBER <b>C2</b>
SUPERSTRUCTURE TYPE <b>Chassis supported single and multi-wide</b>	

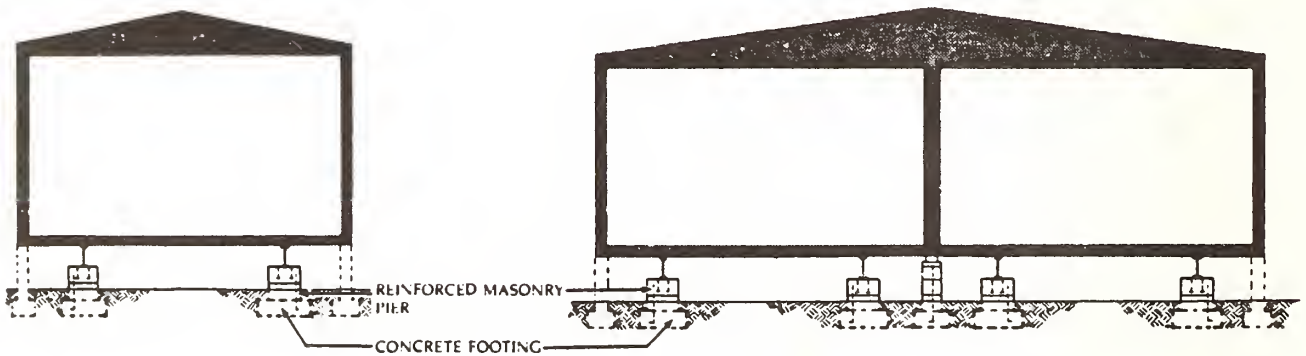
## SINGLE-WIDE

## MULTI-WIDE



**FOUNDATION PLAN**

**FOUNDATION PLAN**

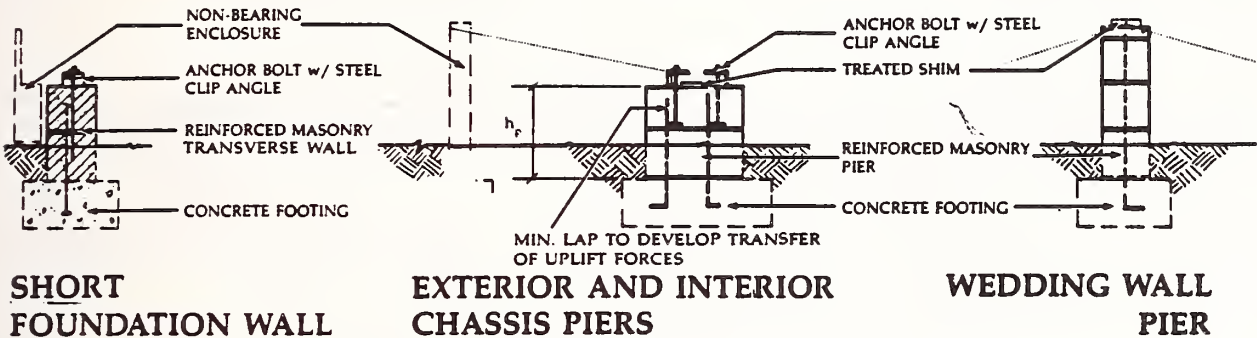


**BUILDING SECTION**

**BUILDING SECTION**

# APPENDIX A-3

FOUNDATION TYPE Reinforced masonry or concrete piers	SYSTEM NUMBER C2
SUPERSTRUCTURE TYPE Chassis supported single and multi-wide	



C 2

## TABLES

Use C tables for vertical anchorage ( $A_v$ ) and horizontal anchorage ( $A_h$ ). For Required Effective Footing Area ( $A_{ftg}$ ) for multi-wide units, use C tables if there is a wedding wall pier. Use Cnw if there is no wedding wall pier.

## REGIONAL APPLICATIONS:

1. Suitable in all seismic zones with proper footing size and depth.
2. Suitable in all wind regions with proper footing size and depth.
3. Suitable in areas with high frost penetration with proper footing depth.

## ACCEPTABLE ALTERNATIVES:

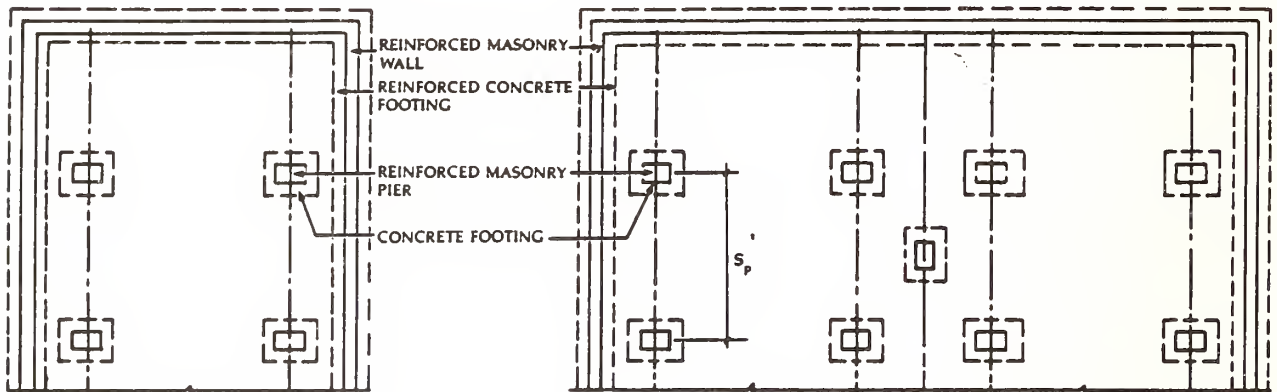
1. Chassis may be anchored either with anchor bolt with clamps, as pictured, or weld plates as shown in system C3.
2. If transverse foundation shear walls are not used, designed by a registered engineer.

# APPENDIX A-4

FOUNDATION TYPE <b>Reinforced masonry or concrete perimeter walls and piers</b>	SYSTEM NUMBER <b>E3</b>
SUPERSTRUCTURE TYPE <b>Exterior and chassis anchored single or multi-wide</b>	

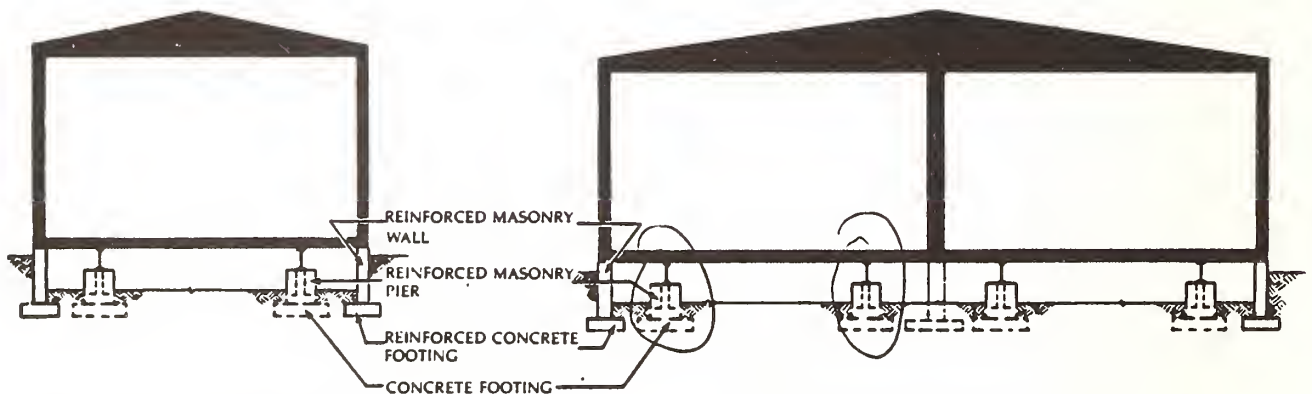
## SINGLE-WIDE

## MULTI-WIDE



**FOUNDATION PLAN**

**FOUNDATION PLAN**

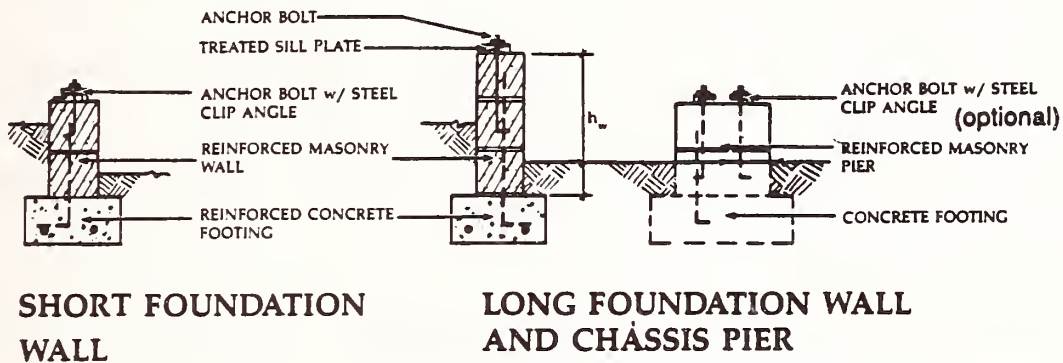


**BUILDING SECTION**

**BUILDING SECTION**

# APPENDIX A-5

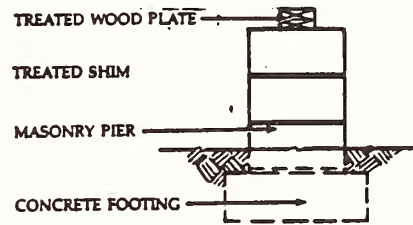
FOUNDATION TYPE Reinforced masonry or concrete perimeter walls and piers	SYSTEM NUMBER
SUPERSTRUCTURE TYPE Exterior and chassis anchored single or multi-wide	<b>E3</b>



**E3**

### TABLES

For single-wide units, use single-wide Type E tables for Vertical Anchorage ( $A_v$ ), Horizontal Anchorage ( $A_h$ ) and Required Effective Footing Area ( $A_{ftg}$ ). For vertical anchorage of exterior piers, use Type C tables.



**WEDDING WALL PIER**

### REGIONAL APPLICATIONS:

1. Suitable in all wind and seismic regions under "normal" soil conditions. Reinforced piers required for seismic zones 3 and 4.
2. Suitable in areas with high frost penetration.

### NOTES

1. Anchor bolt and clip angle at interior pier only--optional at exterior pier. If a clip angle is used on the exterior pier to provide an additional safety factor, use  $A_v/2$  to determine the footing size and reinforcing for withdrawal capacity.

### ACCEPTABLE ALTERNATIVES:

1. Weld plate at pier instead of block pier. Metal pier must be welded to chassis, and its legs must be welded to a base anchored to the footing.

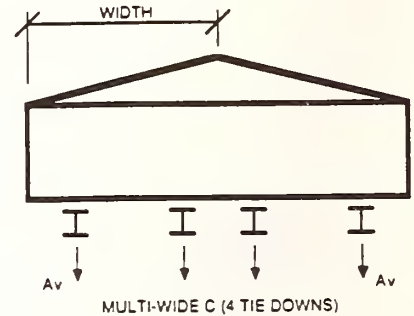
# APPENDIX A-6

## Multi-wide C, I

Required Vertical Anchorage (lbs)

**Multi-wide C, I**  
Width: 12.0 feet  
(4 tiedowns)

A <sub>v</sub>	Wind (mph)	Pier Spacing (ft.)				
		4	5	6	7	8
Inland	70	*	*	*	*	*
	80	30	40	40	50	60
	90	170	210	250	290	340
Coastal	70	30	40	40	50	60
	80	260	320	390	450	520
	90	460	570	690	800	920
	100	680	850	1020	1190	1360
	110	930	1160	1390	1630	1860

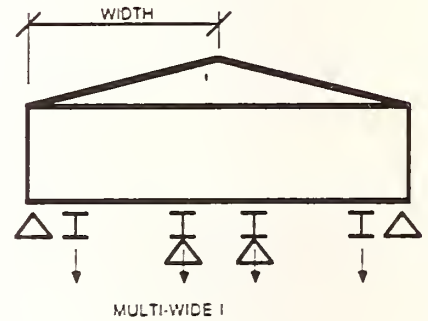


\* Use code-specified minimum anchorage, based on Foundation Capacity Tables

Required Vertical Anchorage (lbs)

**Multi-wide C, I**  
Width: 14.0 feet  
(4 tiedowns)

A <sub>v</sub>	Wind (mph)	Pier Spacing (ft.)				
		4	5	6	7	8
Inland	70	*	*	*	*	*
	80	60	70	80	100	110
	90	220	270	330	380	430
Coastal	70	60	70	80	100	110
	80	320	400	480	560	640
	90	550	690	830	970	1100
	100	810	1010	1210	1420	1620
	110	1100	1370	1640	1920	2190



\* Use code-specified minimum anchorage, based on Foundation Capacity Tables

Required Vertical Anchorage (lbs)

**Multi-wide C, I**  
Width: 16.0 feet  
(4 tiedowns)

A <sub>v</sub>	Wind (mph)	Pier Spacing (ft.)				
		4	5	6	7	8
Inland	70	*	*	*	*	*
	80	80	100	120	140	160
	90	260	330	400	460	530
Coastal	70	80	100	120	140	160
	80	380	480	570	670	760
	90	640	800	960	1120	1280
	100	930	1170	1400	1630	1860
	110	1260	1570	1880	2200	2510

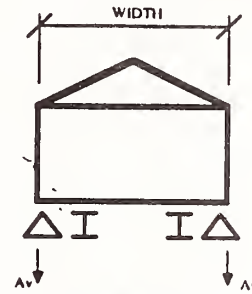
\* Use code-specified minimum anchorage, based on Foundation Capacity Tables

# APPENDIX A-7

## Single-wide E

Required Vertical Anchorage (lbs./ft.) Single-wide E  
Width: 12.0 feet

A <sub>v</sub>	Wind (mph)	Lbs./ft.
Inland	70	30
	80	80
	90	140
Coastal	70	80
	80	170
	90	250
	100	340
	110	440



SINGLE WIDE E

Required Vertical Anchorage (lbs./ft.) Single-wide E  
Width: 14.0 feet

A <sub>v</sub>	Wind (mph)	Lbs./ft.
Inland	70	20
	80	70
	90	130
Coastal	70	70
	80	170
	90	250
	100	340
	110	450

Required Vertical Anchorage (lbs/ft) Single-wide E  
Width: 16.0 feet

A <sub>v</sub>	Wind (mph)	Lbs./ft.
Inland	70	20
	80	70
	90	130
Coastal	70	70
	80	170
	90	250
	100	350
	110	460

\* Use code-specified minimum anchorage, based on Foundation Capacity Tables

## APPENDIX B - I PART 2

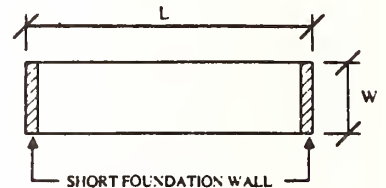
### REQUIRED HORIZONTAL ANCHORAGE-Ah

#### Single-wide C, E, & I

Required Horizontal Anchorage (lbs./ft.)  
Two (2) Short Walls

Single-wide C, E, I  
Width: 12.0 feet

Ah	Wind (mph)	Location	Length				
			40	50	60	70	80
Inland	70	end	250	320	380	440	510
	80	end	380	480	580	670	770
	90	end	530	670	800	930	1070
Coastal	70	end	380	480	580	670	770
	80	end	630	790	950	1100	1260
	90	end	830	1040	1250	1460	1660
	100	end	1030	1280	1540	1800	2050
	110	end	1240	1550	1870	2180	2490



Required Horizontal Anchorage (lbs./ft.)  
Two (2) Short Walls

Single-wide C, E, I  
Width: 14.0 feet

Ah	Wind (mph)	Location	Length				
			40	50	60	70	80
Inland	70	end	210	270	320	370	430
	80	end	330	410	500	580	660
	90	end	460	580	700	810	930
Coastal	70	end	330	410	500	580	660
	80	end	550	690	830	960	1100
	90	end	720	900	1080	1260	1440
	100	end	890	1110	1330	1550	1780
	110	end	1080	1350	1610	1880	2150

Required Horizontal Anchorage (lbs./ft.)  
Two (2) Short Walls

Single-wide C, E, I  
Width: 16.0 feet

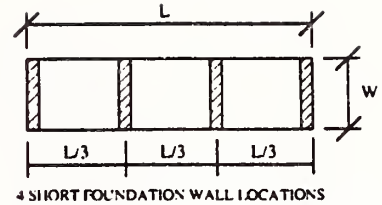
Ah	Wind (mph)	Location	Length				
			40	50	60	70	80
Inland	70	end	190	230	280	320	370
	80	end	290	370	440	510	580
	90	end	410	520	620	720	830
Coastal	70	end	290	370	440	510	580
	80	end	490	610	740	860	980
	90	end	640	800	960	1120	1280
	100	end	790	980	1180	1380	1580
	110	end	950	1190	1430	1670	1910

## APPENDIX B-2

Required Horizontal Anchorage (lbs./ft.)  
Four (4) Short Walls

Single-wide C. E. J  
Width: 12.0 feet

Ah	Wind (mph)	Location	Length				
			40	50	60	70	80
Inland	70	end	80	110	130	150	170
		int	170	210	250	290	340
	80	end	130	160	190	220	260
		int	260	320	380	450	510
	90	end	180	220	270	310	360
		int	360	450	530	620	710
Coastal	70	end	130	160	190	220	260
		int	260	320	380	450	510
	80	end	210	260	320	370	420
		int	420	530	630	740	840
	90	end	280	350	420	490	550
		int	550	690	830	970	1110
	100	end	340	430	510	600	680
		int	680	860	1030	1200	1370
	110	end	410	520	620	730	830
		int	830	1040	1240	1450	1660



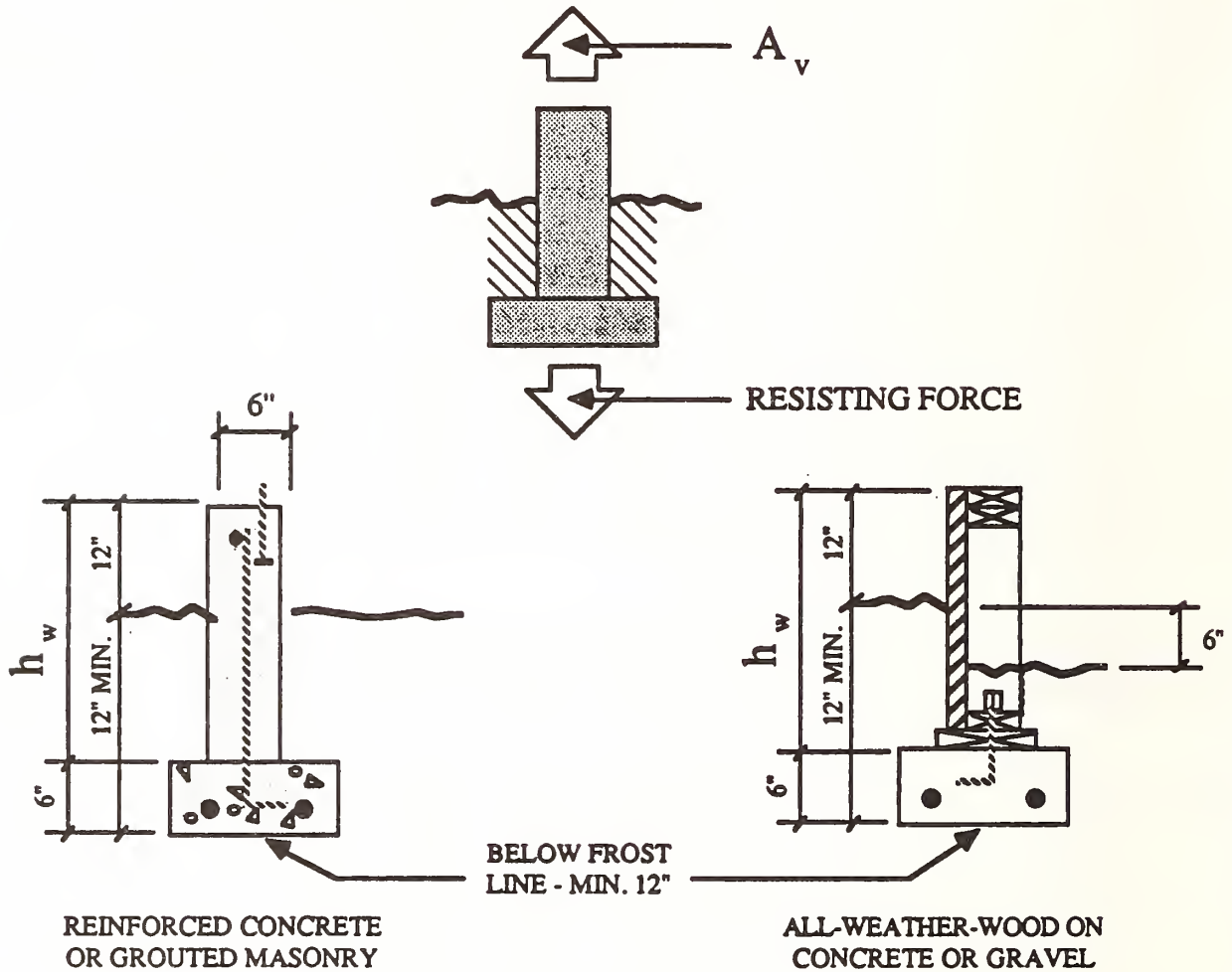
Required Horizontal Anchorage (lbs./ft.)  
Four (4) Short Walls

Single-wide C. E. J  
Width: 14.0 feet

Ah	Wind (mph)	Location	Length				
			40	50	60	70	80
Inland	70	end	70	90	110	120	140
		int	140	180	210	250	280
	80	end	110	140	170	190	220
		int	220	280	330	390	440
	90	end	150	190	230	270	310
		int	310	390	460	540	620
Coastal	70	end	110	140	170	190	220
		int	220	280	330	390	440
	80	end	180	230	280	320	370
		int	370	460	550	640	730
	90	end	240	300	360	420	480
		int	480	600	720	840	960
	100	end	300	370	440	520	590
		int	590	740	890	1040	1180
	110	end	360	450	540	630	720
		int	720	900	1080	1260	1430

# APPENDIX B-3

TABLE 1  
WITHDRAWAL RESISTANCE\*  
LONG FOUNDATION WALL -TYPE E<sup>1,2</sup>  
(In pounds per linear foot of wall)



$h_w$	Reinforced Concrete		Masonry-Fully Grouted		Masonry-Grouted @ 48" o.c.		All-Weather Wood w/ Conc. Footing		All-Weather Wood w/ Gravel Base
	12"	16"	12"	16"	12"	16"	12"	16"	
2'	285	350	245	310	220	285	170	225	35
3'	420	525	360	465	320	425	290	385	75
4'	555	700	475	620	420	565	340	475	120

\* Potential resistance to withdrawal is the maximum uplift resistance which can be provided by the foundations shown. It is computed by adding the weights of building materials and soil over the top of the footing. To fully develop this potential, adequate connections to the footing and superstructure must be provided.

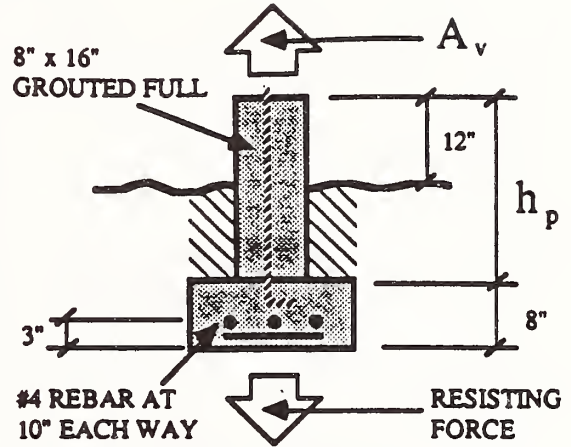
<sup>1</sup> Foundations must be designed for bearing pressure, gravity loads, and uplift loads in addition to meeting the anchorage requirements tabulated in the Foundation Design Tables.

<sup>2</sup> Values shown in this table could be increased by widening the footing, provided the system is designed for the increased load, or by a more detailed analysis of the shearing strength of the soil overburden.

## APPENDIX B-4

**TABLE 2**  
**WITHDRAWAL\* RESISTANCE FOR PIERS<sup>1,2</sup>**  
**TYPES C, I, and E (interior)**  
**(In pounds per pier)**

h <sub>p</sub> Depth	Width of Square Footing			
	1' - 0"	2' - 0"	3' - 0"	4' - 0"
2' - 0"	260	990	2065	3560
2' - 8"	340	1325	2780	4785
3' - 4"	410	1655	3485	5990
4' - 0"	490	1990	4200	7220
4' - 8"	565	2320	4910	8445



\* Potential withdrawal resistance is the maximum uplift resistance which can be provided by the foundations shown. It is computed by adding the weights of building materials and soil over the top of the footing. To fully develop this potential, adequate connections to the footing and superstructure must be provided.

<sup>1</sup> Foundations must be designed for lateral soil pressure, bearing pressure, gravity loads, and uplift loads, in addition to meeting the anchorage requirements tabulated in the Foundation Design Tables. The bottom of the footing must also be below the maximum depth of frost penetration.

<sup>2</sup> Values shown in this table could be increased by widening the footing, providing the wall system is designed for the increased load, or by a more detailed analysis of the shear strength of the soil overburden.

**TABLE 3**  
**VERTICAL ANCHOR CAPACITY FOR PIERS\***  
**TYPES C, I AND E (INTERIOR)**  
**(In pounds)**

Anchor bolt dia	Capacity per number of bolts	
	1	2
1/2"	3930	7860
5/8"	6140	12280

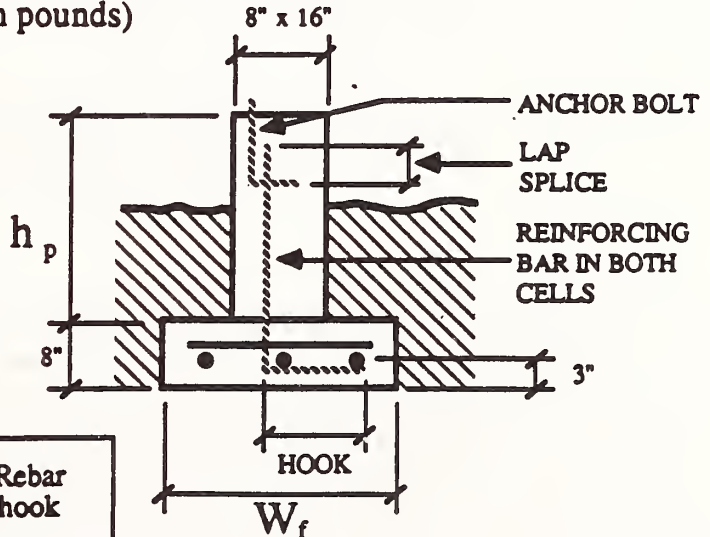


**TABLE 3A**

Anchor bolt dia.	Vertical rebar	Minimum lap splice	Rebar hook
1/2"	# 4	20"	6"
5/8"	# 5	25"	7"

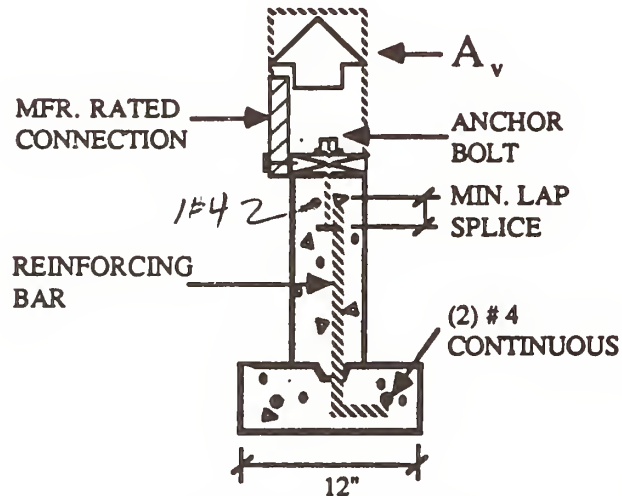
\* The vertical anchor capacity is based upon the working capacity of ASTM A - 307 anchor bolts in 2500 psi concrete or grout. To fully develop this capacity, anchor bolts must be properly connected to the foundation and superstructure.

<sup>1</sup> The capacity is based on  $F_c = 2500$  psi;  $f_y = 40,000$  psi

## APPENDIX B-5

### TABLE 4A - CONCRETE OR MASONRY WALL VERTICAL ANCHOR CAPACITY FOR LONG FOUNDATION WALL\* TYPE E

( $A_v$  in pounds per linear foot of wall.)



CONCRETE OR MASONRY WALL

$A_v$ lbs./ft.	Required Anchorage <sup>1</sup>		
	Anchor Bolt <sup>4</sup>	Rebar	Spacing <sup>5</sup>
650	1/2"	#4	72"
785	1/2"	#4	60"
See Table 3A For Rebar Details			

\* Anchor capacity is based on the capacity of ASTM A-307 anchor bolts properly embedded, enclosed, and spaced. The foundation wall must be adequate to develop the full capacity of the bolts.

<sup>1</sup> Values are based on horizontal load per foot of wall.

<sup>2</sup> Assuming 1 1/2" thick sill plate, 3/4" edge distance for wood or composite nailer plates or 20 diameter end distance for plywood sheathing; C-C exterior, properly seasoned wood, 33% increase for wind loads; Group III woods, not permanently loaded, and a 10% reduction for fasteners in treated wood.

<sup>3</sup> Nailing scheduled in this table is intended to secure the wood foundation wall to the footing only, and not to provide required edge fastening for plywood siding or sheathing

<sup>4</sup> It is assumed that a reinforcing bar of the same diameter as the anchor is adequately embedded in the footing and lapped with the anchor. In the case of a treated wood foundation wall, the wood wall and its connections must be designed to transfer the anchor load to a concrete footing. This table does not apply to treated wood foundation walls on gravel bases.

<sup>5</sup> Spacing based on capacity of anchor bolt in grout / concrete. (see also #4.)

<sup>6</sup> Spacing based on allowable compression of wood perpendicular to grain for  $F_c = 565$  psi and washer with total diameter equal to bolt diameter plus 1/2".

# Present State of Wind Engineering Research Related to Building Design in Japan

Tatsuo Murota<sup>1</sup> by  
and Hisashi Okada<sup>2</sup>

## ABSTRACT

This paper describes present state of wind engineering research related to building design in Japan. More accurate estimation of gust response, estimation of response in a direction perpendicular to wind, characteristics of wind pressure on exterior and interior of buildings, etc. are major research topics, some of which have been brought into focus relating to the development of some leading technologies in the field of wind engineering.

**KEY WORDS** : building design, wind engineering, controlled damping system, wind around buildings, natural ventilation, internal pressure

## 1. INTRODUCTION

In the design of buildings it is important to take a certain extent of safety for structural frames, substructural elements and non-structural elements against winds into consideration. In Japan the minimum requirements for design wind loads in every local districts has been specified by the Building Standard Law Enforcement Order (hereinafter referred as Cabinet Order).

Values of the minimum requirements for seismic forces specified by Cabinet Order are in many cases far greater than those for wind loads. Therefore, cases are limited that values of calculated wind loads are greater than or comparatively equal to seismic forces. Such cases are seen in the design of buildings or building elements as follows:

- (1) timber construction buildings
- (2) one-or two-storied steel buildings
- (3) steel towers
- (4) membrane structures
- (5) roofs
- (6) claddings

Those buildings or building elements concerned, structural engineers want to use wind-resistant design methodologies which give engineers wind load more accurate and reasonable than those specified by Cabinet Order.

In the period of recent several years in Japan research and development of new technologies have been increasing. One of the technologies is the base-isolation system using multi-layer rubber bearing and another is the controlled damping system. Development of controlled damping system has come to a step of practical use and a few types of controlled damping devices have been used to decrease the vibration of towers. At the front of controlled damping system development, there exists a research need of an advanced method for the estimation of structural response in winds.

In the design of higher or large-scale buildings, it is necessary to estimate the existence and location of windy environment at ground level around the buildings, because the windy environment, which has been known in Japan since 1960's, may cause troubles to pedestrians and nearby habitants. In some cities the building official requests building owners to make assessment on this problem prior to the application for confirmation of construction of the building concerned. Assessment of windy environment around buildings has been made based on data obtained by the

wind tunnel model test, which costs much money and time. With the increase of capacity of business computers, there arose a request for the numerical simulation as alternative technique for the assessment and the development of simulation technique is being conducted.

Another problem relating to wind which shall be taken into account in the design of large scale buildings is that of estimation of interior air flow and internal pressure caused by wind. Technical information about this problem is not enough at present and therefore have to be investigated.

The natural ventilation system is effective to save energy and it has drawn attention of ventilation engineers. Need of such ventilation systems exists in southwest district of Japan, for example in Okinawa, and also in ventilation system design of depositories for calorific radioactive waste produced in nuclear power plants.

In the following sections are described present state and technical topics in wind engineering related to building design in Japan.

## 2. WIND-RESISTANT DESIGN OF STRUCTURAL FRAMES

It is pointed out by structural engineers that the wind load for building design specified by Cabinet Order is not a good estimate of wind loading because the number of parameters which should relate wind loading is too small, and it gives an over-estimate. Wind loads provided in Recommendation of Loads and External Forces for Building Design proposed by Architectural Institute of Japan are based upon the theoretical estimation of gust response of line-like structures. The wind load in this recommendation can be calculated by assuming several parameters concerned and is considered very reasonable compared with the wind load specified by Cabinet Order. However, wind load in recommendation also give an over-estimate for low-rise buildings.

Revision of wind load in Cabinet Order is one of the urgent topics to be concluded by the Ministry of Construction.

## 3. WIND-RESISTANT DESIGN OF MEMBRANE STRUCTURES

Buildings of membrane structure had been dealt as temporary buildings by the Building Standard Law, but however in 1987 the Minister of Construction has come to deem that buildings of membrane structure are equal to permanent buildings, if the structural and fire-related performance of them meets the technical standards specified by the Minister of Construction. The largest permanent building of membrane structure at present is Tokyo Dome, which is an air-supported membrane dome of 45570m<sup>2</sup> roof area. Basic technical ideas of this dome system was imported from U.S.A. and it was revised based upon the data obtained from the great amount of research works concerned.

Wind load in the design of membrane structures is the same one as is adopted for rigid buildings that is

1. Director, Structural Engineering Department, Building Research Institute, Ministry of Construction, Japan
2. Dr. of Eng., Senior Research Officer, Aerodynamics Section, Structural Engineering Department, ditto.

specified by Cabinet Order. It is considered that the current wind load for membrane structure should be modified reasonably by carrying out researches on the following items:

- (1) pressure fluctuation acting on curved roof
- (2) Characteristics and spatial distribution of wind surfaces expanded in horizontal direction
- (3) Response of membrane and boundary cables in winds
- (4) Interaction between wind pressure and response

According to these research needs, the Japan Membrane Structure Association has started to collect the wind pressure data obtained in wind tunnel tests.

#### 4. CONTROLLED DAMPING SYSTEM

In 1975, a dynamic damper was equipped to Sydney Tower of 325m high in Sydney, Australia to decrease the wind response. And in 1977, a tuned-mass damper system was equipped to a 59-storied office building in New York, U.S.A. with the same objectives as above.

In Japan, Chiba Port Tower (125m high, Chiba City) and Higashiyama Garden Watch Tower (134m, Nagoya City) were equipped with dynamic damper systems in 1986 and 1988, respectively. And Gold Tower (136m Utatsu-Cho, Kagawa Prefecture) was equipped with "throshing dampers" on its top. The damper is a tank which contains water in it. If the tank is subjected to vibration, water moves in the tank under a special movement control. The objectives of those devices used in Japan are to decrease the vibration caused by both winds and earthquakes.

Data of tower response observed at the events of winds and earthquakes show an enough effect of these devices, and it is considered that the research and development of these technologies will be carried out energetically in the future.

The most important research topics in this technology is to estimate the effect of damping systems quantitatively. In order to investigate the effects of controlled damping devices, it is necessary to estimate the response of buildings or towers in winds at a satisfactory level of accuracy. This leads to research needs for increasing the accuracy of gust response estimation described in section 2 and for development of methods for estimation of structural response perpendicular to wind direction. A practical method for the estimation of structural response normal to wind direction is proposed in the prescribed recommendation of AIJ. It is necessary to examine the availability of this method.

#### 5. ESTIMATION OF FLOW AROUND TALL BUILDINGS

In case that the assessment of windy environment around tall buildings is carried out based upon the wind tunnel test data, the accuracy or reliability of the data depends on the similarity of boundary layer produced on wind tunnel floor. According to a series of research on the similarity of wind tunnel tests of flow around tall buildings in Japan, buildings and structures around the tall building concerned should be realized as scaled models of buildings and structures if they are located at a distance (measured from the surface of the tall building concerned) less than twenty times of the average height of buildings in the city area. It is not easy to use such a model for wind tunnel test, because it costs much money. Research works are expected to be carried out with emphasis on the simplification of urban models.

Computer simulation for flow in urban area by solving three-dimensional Navier-Stokes equation is far more expensive than the wind tunnel tests. And therefore, investigation of simplified computer

simulation methods has been carried out in recent years and many computer simulation programs have been sold in the market. At present they are available only for an extremely simple case that does not exist in real urban areas.

#### 6. WIND-RESISTANT DESIGN OF CLADDINGS

In the design of cladding, wind load is usually the predominant design force. However the wind load for cladding design calculated in accordance with Cabinet Order does not always give a good estimation of wind load. In addition, a considerably large number of buildings are designed to have large void space extending vertically, which may affect greatly on the estimation of internal pressure. We don't have enough information about the problem and therefore it will be encouraged to carry out research on the internal pressure.

#### 7. NATURAL VENTILATION SYSTEM

A unique requirement given to designers who entered the design competition of a city hall building held by Nago City, Okinawa in 1979 was the adoption of natural ventilation system for air-conditioning. Based on the first prize design proposal of this competition, Nago City Hall was constructed and after that the ventilation system has been showing the effectiveness.

In the design of such a system it is necessary to get information on the pressure distribution on exterior walls and roofs of the building in daily and stormy conditions and in addition to this the air-flow in the building. The basic studies about this problem are being carried out at some universities and private companies.

**Theme II**

---

**Earthquake Engineering**



# Present State of Wind Engineering Research Related to Building Design in Japan

By

Keiichi OHTANI<sup>1</sup>, Hiroshi TAKAHASHI<sup>2</sup>

## ABSTRACT

The National Research Center for Disaster Prevention (NRCDP) celebrated its 25th anniversary on April 1, 1988. NRCDP is active in step to the activities of UJNR Panel on Wind and Seismic Effects in the last 2 decades of this 25 years. It may fairly to said that the mostly research activities at NRCDP goes round with UJNR. NRCDP was presented the 37 Papers to the past 19 joint meetings. This paper is turned round the outline of research results on wind and earthquake engineering at the NRCDP, and is search the research direction in future. This paper is described that the outline of research results of continuous meteorological observation at the observation tower on the ocean, application of the remote sensing technology to the research of disaster prevention, seismic microzoning using the urban ground information, propelling of work on strong-motion earthquake observation, practice of the array observation of strong-motion earthquake, experimental research of seismicities of structures using large-scale earthquake simulator and multi-input excitation system and renewal plan of large-scale earthquake simulator, etc., and is considered the developed direction of research in future.

**KEYWORDS:** Observation of sea wind, Application of remote sensing technology, Seismic microzoning, strong-motion earthquake observation, Array observation, aseismic Test, Experimental device.

## 1. INTRODUCTION

The scope of disaster prevention consists of the elucidation of the process by which a natural hazard develops into a disaster, and the prevention of its development. This is thus an essential responsibility of a modern country. In Japan, duties of this kind have been dispersed among various governmental organizations, and consequently, some defects have been found. It can still be freshly recalled that 6,000 inhabitants were drowned by the flood and the storm surge induced by Typhoon 5915 which attacked Nagoya and the coastal area of Ise Bay in September 1959. In order to remedy the defects, the need was urgently felt to establish

a new organization which would manage intensively the coordination of existing organizations and effectively promote research in the field of disaster prevention from the viewpoints of science and technology. As a result, the National Research Center for Disaster Prevention (NRCDP) was founded in 1963.

According to the governmental ordinance of the Science and Technology Agency, NRCDP is to perform the following roles:

- (a) To establish facilities which are necessary for tests and research, but which are so expensive as to make it impossible to install at each of the various organizations concerned, and to place these facilities at the common disposal of all of them,
- (b) To conduct basic research and make tests of synthetic nature which necessitate the cooperation of various fields of study, and to conduct basic research and make tests common to various branches of research,
- (c) To collect, arrange and distribute internal and external data,
- (d) To carry out other activities related to the science and technology of disaster prevention.

Now, a wide range of subjects, which include the prediction and forecast of extraordinary natural phenomena, the control of natural phenomena by making various kinds of structures, evacuation and elusion from high risk areas, rehabilitation and establishment of an anti-disaster social system, are tackled within the areas of the following NRCDP targets:

- (a) To carry out a wide range of research, from basic to applied research,
- (b) To conduct research through the mutual cooperation of the concerned institutes, specially making use of the large-scale common-use facilities,
- (c) To disseminate general knowledge of disaster prevention and preparedness;
  - (1) To collect, arrange and

---

1) Head, Earthquake Engineering Laboratory, National Research Center for Disaster Prevention, Science and Technology Agency

2) Dr. of Sci. Director-general, NRCDP, STA

distribute internal and external data,

(2) To make proposals for various kinds of countermeasures against disasters,

(3) To train and educate various levels of personnel.

(d) To cooperate with various kinds of foreign organizations.

## 2. CHARACTERISTICS OF HIGH WINDS MEASURED AT AN OBSERVATION TOWER ABOVE THE OCEAN

The core of research related to the wind engineering at NRCDP is the continuous observation of wind velocity, air temperature, wave height and other marine phenomena at the observation tower 20 m in height above the sea surface which is installed in the Sagami Bay faced the Pacific Ocean.

The location of the tower is about 1km off the shore of Hiratsuka coast (see Fig.1). The Hiratsuka district is situated in an open field, but general hills extend towards the west. Therefore, land winds measured at the tower can be analyzed as the air flow over the simple terrain. Presently, we mainly studied winds in the open sea. As shown in Fig. 1, southern winds can have the infinite fetch. The tower is based on the sea bed about 20 m deep. Since the water surface somewhat varies due to the tide, the top level also varies and is about 20 m high above the sea surface. Fig. 2 shows the illustration of the tower. The upper large part is an observation room where the data from various sensors of instruments are amplified, recorded and digitized to be transmitted to the data processing system on land. The electric power is sufficient for the demand of instruments, because of the supply from the land by the cable buried in the sea bed. Transmitted data are gathered to a computer by an on-line system and are statistically proceeded using various available techniques.

Continuous data of wind direction and speed for a long period were obtained by a aero-vane anemometer mounted on the top of the tower. While fluctuating velocities were measured by a couple of 3-dimensional sonic anemometers. The aero-vane anemometer is fixed at the 23 m height above the mean sea level. Two sonic anemometers are usually set in the vertical or horizontal array for the purpose of the space correlation experiment. We made the effort to avoid the error produced by the tower under the condition of expected wind direction, but measurements were restricted to only the atmospheric layer

from 8 m in height to the sea surface, because of the shape of the tower and the difficulty of mounting sensors.

The interface between waves and air flow is a very important factor to clarify the structure of the boundary layer above the ocean. In several experiments, the capacitance-type wave gauge is arranged at the same position of a sonic anemometer, and ocean waves were simultaneously measured with wind velocity in order to estimate this interface. Air and sea surface temperatures were always obtained using platinum-wire resistance thermometers to evaluate the atmospheric stability. The stability scarcely contributes characteristics of the atmospheric turbulence under the condition of high winds, but was always remarked during experiments.

Fluctuating wind vectors usually sampled every 0.1 sec but for every 0.04 sec in the special case that spectral behaviours were estimated in high frequency regions. The duration of one run was 1,600 sec, and in many observations several runs could be successively acquired.

We obtained the seasonal variation of wind velocity in the coastal region from the data measured by the aero-vane anemometer at the 23 m height. Analyzed data were obtained for a year from October 1979 to September 1980. From the previous and afterwards data, we can also show the similar feature of wind to the present results. Fig. 3 shows the monthly relative frequency distribution of wind direction for every season and the monthly azimuth pattern of wind speed, or the magnitude distribution of wind vector for every direction. A mean wind direction and speed were given from a 10 m minute-record every one hour. These diagrams are the features in October, January, April and August. We then can see the intermediate tendency between the two months shown in the figure for the unshown months. Here the northern wind is land breeze and the southern wind sea breeze. Remarkable results of wind vector for a year are:

(1) The wind vector is almost restricted to northern or southern direction, and is rarely eastern or western along the sea-shore line. Therefore, we should consider that their exists the deep interchange of air flow between the ocean and the land.

(2) Northern wind blows very often. While southern wind is averagely stronger than northern one. Consequently the amount of flow

towards northern direction is little different from that towards southern direction.

(3) The land and sea breeze clearly arises from April to August. This feature is caused by the strong solar radiation in those months.

(4) High winds frequently appear from January to April, and have the direction between south and south-west. The typical case arises under the condition that cyclone moves north-eastward with developing in the Japan Sea after the winter pressure pattern was distorted. We have open experience of such a severe storm as the mean wind speed exceeds 20 m/s at the 10 m height.

The statistical quantities in October shown in Fig. 3 are somewhat different from those for an ordinary year and show relatively high winds, because the large typhoon 7920 passed over the Honshu Island at the end of October, 1979. Generally, we carried out experiments of studying characteristics of high winds, mainly in winter, expecting to measure the sea wind by means of sonic anemometers.

### 3. APPLICATION OF THE REMOTE SENSING TECHNOLOGY TO THE RESEARCH OF DISASTER PREVENTION

The characteristics of the information obtained from remote sensing are in its wideness, simultaneity and periodicity. Techniques for synthetic information processing are being developed, combining in the geographic coordinate system, the remotely sensed data collected mainly by Landsat and the surveys data collected by usual method for disaster or disaster prevention.

As for the application of the study to the detection of natural disasters, there are several examples such as the detection of volcanic ash-fall areas, the detection of landslides, the detection of damaged rice-fields affected by flood and etc..

As for the application of the study to the prediction of damage done by disasters, there are the production of up-to-date land use maps of the areas around volcanoes for volcanic disaster prevention and the estimation of the potential for earthquake disasters in urban areas made by overlying the land use and the under-ground information which is independent of remote sensing.

An examination to discriminate the flooded areas macroscopically from vegetation changes appearing in satellite images was made on the tsunami

of the Nihonkai-Chibu earthquake in 1983.

Fig. 4 shows the detection result of flooded area of the coast of Minehama village, Akita prefecture. Two scenes of satellite data were used for analysis of the examination.

One is Scene No. 108-32 of LANDSAT-4 observed on July 12, 1983, one month and a half after the tsunami. Another one is Scene No. 116-32 of LANDSAT-3, on July 8, 1982, just one year before the former was observed, which was selected for the comparison assuming that seasonal conditions of vegetation was almost equivalent except for the stricken areas. Each scene covers the areas required for analysis. Data of each scene consist of 4 spectral images of Band 4 through Band 7, respectively. In present analysis, however, images of Band 5 and Band 7 were used. Because these two bands are very important in relevant to vegetation changes: Band 5 (0.6 - 0.7 micron) involves an absorption band and Band 7 (0.8 - 1.1 micron) a reflection band of chlorophyll in green plants, while other two are less important. The ground resolution of each image is 80 m. (a) in Fig. 4 is the analytical result for Band 5, and (b) is one for Band 7. It is found that almost all the SDPs (significant difference pixel) in two figures of Fig. 4 lie within the flooded areas.

Fig. 5 is a halftone picture in the grade of 10 meters which shows the distribution of thickness of soft ground, gained from the database of urban ground information, overlying the boundaries of land and water areas gained from Landsat data in place of the map. Similarly, it is possible to overlay the map with information about the urban area such as the density of houses extracted from Landsat data.

### 4. SEISMIC MICROZONING USING URBAN GROUND INFORMATION

We were conducted the construction of database from bore-hole record, and the development of the application methods for the prediction of earthquake disaster. The data of depth of layer, soil name, N-value, etc. on the bore-hole records mainly produced at the fundamental survey for construction of various structures are stored in the database. The mnemonic code tables for non-numerical data, such as soil name and soil colour, were designed in order to make the input work easier. A part of soil code is shown in Fig. 6. And the other hand, the location of boring is given by the mesh with one side about 100 meter long. This mesh size is equal to the size of dividing side and length

of the 1:25,000 topographic map, published by Geographical Survey Institute of Japan, into 100 equal parts, i.e. 4.5" in longitude and 3.0" in latitude, and is convenient in practical use.

A method of prediction of the regional distribution of vibrational characteristics of ground from database is performed. Here we define the layer with N-value more than 50 as an engineering bedrock and presume the upper layer, i.e. surface grounds a single layer of which elastic property is determined from the average of N-value. Fig. 7 shows the contours on the topographic map. The microtremor measurements were carried out in this studied area. The most noiseless part for 10 seconds in the record were input to the spectrum analyser and a period which showed a maximum response was read as the predominant period of the ground.

This predominant periods are shown in the same figure. Solid line and broken line show the contours of the predominant periods obtained from the measurement and estimated from the database, respectively. Black dots show the measurement points of microtremors with calculated predominant periods (sec). In Fig. 7, outline of contours of measured and estimated predominant periods coincide with each other. While the contours of 1 sec coincide well, the contour of measured period of 0.5 sec is seemed to lie on the contour of estimated period of 0.75 sec.. On the other hand, the boring data are densely distributed than the measuring points of microtremors and therefore discordance between both contours are seen in the region where could not be interpolated by the measured data.

Seismic microzonation is to evaluate the characteristics of the earthquake motions in each mesh in the objective region as large as a municipality, considering the difference of earthquake motions due to the locality of the ground condition, and to apply the result to make the various kinds of maps predicting the seismic damage.

In this study we divide a whole ground structure into seismic basement and sedimentary layer. The seismic basement is the Pre-Tertiary layer and the sedimentary layer is a general term for Tertiary and Quaternary layer. Moreover we divide the sedimentary layer into engineering bedrock and surface ground. The surface ground is the alluvial layer with N-value less than 50 and the engineering bedrock is equivalent to Tokyo-gravel-layer with N-value more

than 50. The characteristics of the seismic basement and the average amplification characteristics of the sedimentary layer and the engineering bedrock were expressed the estimation equation by the observation results of deep bore-hole and ground surface. And we made the seismic microzoning maps. Fig.8 shows an example of the distribution of the spectral intensity of earthquake motions in the study area estimated though this method. Magnitude and hypocentral distance of the assumed earthquake is respectively 7.0 and 100 km. Estimated spectral intensity is displayed in each mesh with the number corresponding to each rank of the intensity. Contours are drawn by band for the intensity 200 and 240 ( $\text{galxsec}^2$ ).

Looking wholly at the figure a tendency is found that the spectral intensities become larger from northern region (the upper part) to southern reclaimed land (the lower part). The tendency appears similarity in the distribution of the predominant period of the surface ground in Fig. 7, and generally speaking the tendency corresponds to the distribution of the thickness of soft ground.

The values of the spectral intensities displayed in Fig. 8 shows not only the regional relation on the surface, but also the result of amplification of earthquake motions from the basement to the surface in the absolute scale. In this connection, comparing that the spectral intensity distributed on the surface are about 200, that of the engineering bedrock was about 82 and that of the Pre-Tertiary basement was about 17. Namely, the spectral intensity of the earthquake motion has been amplified 4 times between the Pre-Tertiary basement and the engineering bedrock, 2.5 times between the engineering bedrock and the ground surface, and 10 times between the Pre-Tertiary basement and the ground surface.

#### 5. PROPELLING OF THE PROJECT OF STRONG-MOTION EARTHQUAKE OBSERVATION

In March 1953, a prototype of seismograph for measuring the acceleration of strong-motion earthquakes was completed, and it was named "SMAC type" after the initial letters in the name of the "Committee for the Standard Strong-Motion Accelerograph". This accelerograph No. I was installed at the Earthquake Research Institute of the University of Tokyo, and the observation was started on June 29, 1953. Based on the experiences of the use of SMAC type in

the subsequent period, improvement upon this were put one after another. The SMAC type has now 14 variations. The installation of accelerographs has been developed, and as of March 1988, Japan has about 1,450 SMAC type accelerographs and 420 observation sites in total.

On June 21, 1967, the Strong-Motion earthquake Observation Council was established in the NRCDP, and this council was now able to promote the project of strong-motion earthquake observation. This council as a liaison organization has been preparing a plan of distribution of accelerographs all over the country and making an effort to secure the budget corresponding to the increase in the number of accelerographs and records. The representative publication is the series of entitled "Strong-Motion earthquake Records in Japan". This publication was started in March 1960, and 31 volumes have already issued. According to the latest number Volume 31, the accelerographs of which the records were the objects of collection are 1,360 apparatus. And the council was published the other series of entitled "Prompt Report on Strong-Motion Accelerograms". This publication is issued at the case of observation of earthquake when the Seismic Intensity of JMA scale is greater than 5, and the case of the collection of valuable records when Seismic Intensity less than 5. This report was published 37 volumes already, and was described the maximum acceleration of each component at the each observation site.

It comes to wish for realization of new strong-motion seismometers, which has high performance and is easy to analyse using the electronic computer, by the diversification of the observation purposes and the complexity of the observation objects. Against this situation, the council was published the specifications of the digital strong-motion accelerograph in 1983 (see Table 2), and was made an effort of realization of this new seismograph. Now, the plural number of companies are manufactured and sold the seismographs which is satisfied to the above mentioned specifications.

NRCDP serve the secretariat of the council, in addition to carry out the strong-motion earthquake observation using SMAC type accelerographs and other type of seismographs. We have 52 observation sites in total (this number include the site of next mentioned array observation). The greater part of this sites were arranged in the Tokyo

metropolitan area. Fig. 9 shows the observation sites in the Chiba prefecture, and Fig. 10 shows the frequency characteristics of seismograph (SAMTAC-17 (made by Tokyo Sokushin Co.)). The acceleration waves obtained at Chiba prefecture, shown in Fig. 9, at the Chibaken-Toho-Okai earthquake occurred on December 17, 1987. (a), (b) and (c) of Fig. 11 are illustrated the records of NS component, EW component and UD component, respectively. The origin of the horizontal axis is expressed the origin time of the earthquake reported by Japan Meteorological Agency, and the position of each record is adjusted by the recorded absolute time. The vertical scales of each record are not same, and justify to easy to see the records.

#### 6. PRACTICE OF THE ARRAY OBSERVATION OF STRONG-MOTION EARTHQUAKES

In order to investigate the earthquake response of thick sedimentary layers in the metropolitan area, the NRCDP has been successively performing the strong motion observation. For that purpose, two types of observations, i.e., the vertical (down-hole) array by three-components acceleration meters and the horizontal array by three-components velocity meters, have been established.

##### 1) The vertical array

The earthquake data were obtained at three observation sites in the metropolitan area. These sites are IWT (Iwatsuki, Saitama prefecture), SHM (Shimohsa, Chiba prefecture) and FCH (Fuchu, Tokyo) where are shown in Fig. 12. This arrays are consisted the acceleration meters at the deep bore-hole reached to the Pre-Tertiary basement, shallow bore-hole of the depth of 100 - 200 m and the ground surface. FCH has a additional 500 m bore-hole.

The NRCDP has three deep bore-hole for the study of earthquake prediction, this study is performing by using this facilities. The acceleration meters for each site aeration at,

IWT	G.L., G.L.-108 m, G.L.-3.51 km
SHM	G.L., G.L.-200 m, G.L.-2.30 km
FCH	G.L., G.L.-200 m, G.L.-500 m G.L.-2.75 km

The bottom of deep bore-hole is several hundred meters below the upper boundary of the Pre-Tertiary basement, where S-wave velocity was about 2.5 km/s. The triaxial force-balanced type accelerometer is installed at the bottom of each well and the ground surface. The available frequency range of over-all observation system is almost flats from 0.1 to 30 Hz.

## 2) The horizontal array

In the Tokyo metropolitan area, the thick sedimentary layers with thickness of several kilometers on the Pre-Tertiary basement, is one of the most important factors for earthquake disasters. The purpose of observation is to investigate the earthquake response of the thick sedimentary layers, NRCDP was developed two type of horizontal array observation.

The observation sites of the first horizontal array are located at the Fuchu area in the west of Tokyo (see Fig. 13). This array consists of the Center site FCH (Fuchu (same site of the vertical array) and five satellite sites: ING, KFC, TMA, HFC and CHF. A triaxial velocity type seismograph is installed at the ground surface at all sites. By January 1983, all instruments were in place. The seismic waves with period of from 7 to 10 seconds are predominant, because of the modulation effects by the thick sedimentary layers.

In such period range, the velocity waves are emphasized as compared with the acceleration waves. Also, the velocity type strong-motion seismographs are now accurate enough for practical usage. Therefore, the array observation by the velocity type strong-motion seismograph has been constructed at the Fuchu area.

The second horizontal array is spreading out at the downtown of Tokyo. This area is a typical soft ground area in Tokyo, and is constructed the old town of the excessive crowded housing lots and newly reclaimed area. We were selected the limited area of nearly 10 km X 10 km, and are installed 20 seismometer in this area (see Fig. 14). The purpose of this observation is the prediction of earthquake motion which will be occurred in near future. 16 seismographs were installed already before March 1983, and 4 seismographs will be installed until the end of this year.

Fig.15 is an illustration of recorded waveforms across the whole array at Fuchu area. This record demonstrate clearly the process in which a direct shear wave is modulated by the thick sedimentary layers. The record was obtained during the earthquake which had origin at the Eastern Yamanashi Prefecture. This figure shows the NS component records of the earthquake of February 14, 1984 (M5.2). The NS component is almost identical to SH component of earthquake. The wave train shows in Fig. 15 has five parts: P-wave and its coda, direct S-wave ( $S_0$ ), two total reflected pulses of  $S_0$  ( $S_1$ , and

$S_2$ ), Later large amplitude wave packets and final coda wave. It is care to be taken that the waves  $S_0$ ,  $S_1$ ,  $S_2$  and later packets appear to be necessary to explain the shear wave modulated by the sedimentary layers. These pulses corresponding to  $S_0$ ,  $S_1$  and  $S_2$  in the wave trains recorded by velocity-meters installed on the ground surface are clearly seen in the records by bore-hole observation. Two pulses  $S_1$  and  $S_2$  are phase modulated waves of  $S_0$ , propagating between the surface of basement and the ground surface. This is a kind of multiple reflections. Phase velocities of  $S_0$ ,  $S_1$  and  $S_2$  in Fig. 15 are 3.9 km/s, 2.1 km/s and 1.7 km/s, respectively. These values are shown that these pulses are propagating in down-dip direction.

## 7. ASEISMIC TESTS USING LARGE-SCALE EARTHQUAKE SIMULATOR

For the purposes of shaking table tests for prototype and large-scale models of various structures, such as bridges, earth embankments, underground tunnels, buildings, industrial equipment, power plants, etc., and investigations into the aseismicity of structures, the large-scale earthquake simulator was installed. Planning of this equipment was started in 1965 with the aid of the elite of learning and of some corresponding research institutions, and it was decided that the shaking table should be utilized by national research institutions, universities and private research centers. A part of the construction of this equipment was commences by the Mitsubishi Heavy Industrial Co. at Nagoya in October 1967, and the construction of the concrete foundation was started in October 1968. The whole equipment was completed in June 1970 by the construction expenses of about 950 million Yen. The large-scale earthquake simulator facility which is counted as the largest facility of this kind in the world at that time, consists of shaking table (15 m X 15 m), actuators, pumping units, measuring equipments and controlling devices. This facility was used for the shaking table test of many kinds of structures till February, 1988.

During seventeen and half years from the opening of operation to the launching of renewal works, the research themes using this facility were counted to 110 cases. Table 3. shows the result of the clarification and the total in these 110 research themes. The research forms are divided the three patterns. Own researches by the NRCDP were counted 36, about 1/3 of total. Joint researches with other governmental research

institutions were 24 cases, and the entrusted researches with the private companies were 50 ones.

the researches on soil structures were 23 cases, ground were 7, submerged tunnels were 4, foundations of bridge were 5, therefore the researches related to soil and ground were reached to 39 cases, a little over 1/3. But, most part of these researches were conducted before 1980. The researches on building structures and industrial equipments were 17 cases, the ones on water tanks and nuclear power plants were 16 cases, respectively. The request of tests related nuclear power plants is increased recently.

#### 8. EXPERIMENTAL RESEARCH USING MULTI-INPUT TESTING METHOD

The structures which arranged complex shapes, such as piping systems, are installed at the several floors of building or connected to many equipments and support structures. Therefore, these structures are received different earthquake motions from many points. It is the very important question to make clear failure mechanism and seismic safety margin for these complex structures during earthquakes. We were developed the multi-input testing method for the research of seismic behaviour of these structures, and were conducted the dynamic test of piping systems.

Fig. 16 shows the general view of this testing apparatus. The multi-input vibration system was installed in a large framed structure of 40 tons weight. Main parts of the system are on four small shaking tables (0.8 m X 2.5 m) on which a model piping and support structures can be set up. Each shaking table is connected to a hydraulic actuator and mechanical guide system. The motion of each actuator-table system can be controlled by electrical servo control unit independently, and the multi-input signal is generated by a computer system.

Fig. 17 shows the outline of piping model. A test part, which is L-shaped 4 inch piping shown in Fig. 16, is replaced by a new specimen after the leak or breaking in each failure test. The whole model was designed considering a typical shape of feedwater piping systems and the ease of layout in the multi-input testing systems. Total length of the model is about 20 m. Piping model was supported by structural restraint at 3 portions, one is vertical restraint and the others are horizontal and vertical ones. Teflon sheets were used at contact surface of pipe and

restraint to make as small effect of friction as possible, and gap clearance was adjusted to be about zero. In normal conditions, the maximum stress of L-shaped pipe element would occur at the elbow, but the analysis of experimental results would be more difficult in the initially cracked elbow than the straight part. Thus, the pipe section near the restraint was selected as a crack position though it is secondary. The crack condition of five element pipes are specified as following ( see Fig. 18).

- A. Normally conditioned pipe (1 piece)
- B. Locally cracked pipes in circumference (2 pieces)
- C. Wholly cracked pipes in circumference (2 pieces)

The results of dynamic response test have confirmed the adequacy of multi input response analysis method of time history and spectra. Dynamic pipe failure test has shown that cracked pipes have high toughness against a severe earthquake. However, repeated loadings by the most severe earthquake may cause the penetration of a crack and also break in 50 % depth into a wholly circumferential crack condition. Piping without any defect have shown to have very high toughness against the severe earthquake, as much as ten times until its ratchet-fatigue failure. In order to demonstrate more clearly the failure process and the stability of the defective pipings, more detailed studies would be necessary.

#### 9. RESEARCH AND DEVELOPMENT OF THREE-DIMENSIONAL SHAKING TABLE

Many researchers and engineers were demanded to develop the three-dimensional shaking table which is possible to reappearance the actual motion of earthquake by reason that the actual earthquake motion is the cubic motion (three-dimensional motion). Since 1978, the NRCDP have consistently studied to develop the high-accuracy medium-size three-dimensional shaking table which has a sufficient accuracy of acceleration wave form and sympathize motion and high responsibility.

The technical problems and the targets of development are as follows;

- 1) To develop the mechanism of three-dimensional motion (joint).  
Development of the mechanism to completely free mutual interference at three independent motions activating on X, Y and Z axes and to stabilized set the floor at the time of except for the operation.
- 2) To maintain the high accuracy of the limit performance.

Development of the system to maintain high characteristics of the performance for the large-flow servo valve.

3) To maintain the accuracy of the wave form.

Improvement the total accuracy to add the accuracy of mechanical elements such as actuator, joint, servo valve and etc., to the control technique.

4) To improve the sympathize motion control of the multiple actuators.

Adoption of the acceleration control (feedback) system in which directly controlled the acceleration of the table motion to mixed with the parallel sympathize control by using the signals of amplitude, velocity and acceleration of the table.

5) To betterment the response characteristics in the region of medium and small amplitude.

Improvement the servo valve characteristics in the region near by zero.

6) To secure the safety supporting system of dead load, the protection system for the safety and the maintainability.

7) To rapid measure and treat the enormous data.

By the arrangement of these many technical problems, we were manufactured the full-scale joint and large-flow servo valves as prototypes and completed the performance tests on them to clarify the control of three-dimensional motions. And, we were confirmed a degree of accomplishment of the target of the development by the performance tests of actuating system (system constructed by a actuator, joint and servo valves).

The joint is united with actuator and table mechanically, its job is the mechanism to communicate effectively the activating force to the table, to free the orthogonal in-plane motion for the activating motion, and to prevent the mechanical gap to the utmost. In this plan, we were adopted the hydro-static bearing joint, which is not generated the geometrical cross-talk. The general view of the hydraulic actuator with hydro-static joint is shown in Fig. 19, and the section of joint is shown in Fig. 20. This hydro-static joint is the mechanism to communicate the activating force by the thin oil films among up and down sides of slide bar and spherical bearing, to smoothly slide by almost ignore of friction between this oil films to the orthogonal in-plane motions. The section of the joint is shown in Fig. 21.

To control the large output force by the

small input force, we use the electro-hydro servo valve. The many types of servo valve are made in the world. We were selected to the force motor and moving coil type (see Fig. 22), and were manufactured the prototype of the servo valve, tested the performance of the valve.

Through this development include the manufacturing of prototype, we were considered to break off the technical problems at the development of three-dimensional shaking table. We made the construction plan of this table, and make an effort to secure the construction budget. Unfortunately, the budget does not be approved at present time. Nevertheless, the developed techniques were recognized to the practical use at the some research institutions. Nowadays, the several three-dimensional shaking tables were completed in Japan.

#### 10. RENEWAL OF THE LARGE-SCALE EARTHQUAKE SIMULATOR

The deterioration of the performance of the large-scale earthquake simulator was realized by the results from the aging of the constitute parts, the wearing of sliding parts and the increasing of gaps. Therefore, we are wrestle with the renewal of the simulator from 1986 fiscal year by the 3 years plan. Table 4 shows the main features between the original plan and renewal plan, and Fig.22 shows the limit performances.

The fundamental principles of the renewal plan are summarized as follows;

1) The usable existing elements are used again to the utmost in the overall this plan.

To reuse the shaking table, the most of piping system, the electric motors of the pumping units and etc..

2) To investigate the maximum amplitude which is fitted into between the foundation and the table.

Maximum amplitude is determined to  $\pm 220$  mm by the result of the trial designs.

3) Maximum acceleration of the simulator is maintained the present condition, but the maximum velocity is changed to 75 cm/sec from 37 cm/sec. For this change, the pumping units are increase.

4) By the rearrangement of the oil pressure systems, the oil pressure for main pressure system and subsidiary oil system are unify  $210 \text{ kg/cm}^2$ , and  $140 \text{ kg/cm}^2$ , respectively.

The place work is conducting from March, 1988, and will be completed at the end of this year. By this renewal work, the

large-scale earthquake simulator has the performance of the confirming the dynamic behaviour at the large deformation or near the failure of the structures. We consider that the simulator is able to use for considerable long duration.

### 11. CONCLUSION

A part of the wind and earthquake engineering research at the NRCDP is introduced in this paper. We will continue the propelling of the accumulation of observed data by the steady practice of observation, the secure of seismic safety of each structure by the conducting of aseismic

testing and the improvement of the awareness of disaster prevention through the cooperation of municipal corporation. We seem to not easily obtained the remarkable results immediately by the limited members operation, however, we will be accumulated the results little by little in the future.

This paper is summing up the research results which were conducted by many members of the NRCDP. these research are share with the second, third, and fourth research divisions and Hiratsuka branch for ocean engineering research.

Table 2. Major Specifications of the Digital Strong-motion Accelerograph  
Recommended by the Strong-Motion Earthquake Observation Council

Item	Specification	Reference
Total	Recording range: $\pm$ (0.1 - 2,000) gals	
Characteristics	Frequency range: 0.05 - 25 Hz	Option: 0.05 - 50 Hz
	Dynamic range: more than 86 dB	
Sensor	Acceleration type (3 components)	To be able to install at separate site
	Ability of resolution: $10^{-5}$ (for example, force-balanced type $f_0 > 30$ Hz, $h = 0.6 - 0.7$ )	
Amplifier	Binary gain amplifier ( $2^n$ , $n = 0, 1, 2, 3$ ) Filter: $> 30$ Hz, 18 dB/oct.	Option: 16 bits A/D converter
A/D Converter	Number of bits: 12 bits Sampling frequency: 100 Hz	Option: 200 Hz
Recording Information	Recording number, Signal of sensitivity, Tape number, Station number, Instrumentation number, etc.	
Absolute Time	Accuracy: 1/100 sec (always)	Automatic correction
Delay of Signal	5 sec	Option: 10 sec
Start and Stop	To start and to stop by trigger of acceleration level	Level will be variable
Connection Use	Record of sampling frequency and same time signal	
Recorder	Seismic motion: 3 components, Time signal: 1 component, Recording duration: more than 30 min.	
Calibration	To be able to calibrate a total characteristics involved a sensor.	
Power Source	AC. 100V, 50/60 Hz Battery capacity: more than 30 min.	
Body	Air-tite and water-proof structure, To have the Properties of aseismic, durable and dampproof capacity.	
Maintenance	Technical check: one time per year	
Durable years	More than 10 years	
Cost	Less than 3 million Yen	

Table 1. Presented Papers to the Joint Meetings

No <sup>*1</sup>	Title	Authors
1	"The Status of Strong-Motion Earthquakes in Japan"	S. Ariga
3	"Human Behaviour and Inelastic Response of Structures for the Maximum Acceleration during Earthquakes"	Y. Ohsaki, M Watabe
	"The Outline of Recent Research of Wind and Earthquake Engineering in Japan"	K. Sawada
		S. Ariga
4	"The State of Research Activities of Wind and Earthquake"	K. Sawada
5	"The Status of Research of Wind and Earthquake Engineering in Japan"	S. Inaba
	"Investigation Report of Disasters at Managua Earthquake, 1972"	T. Ohkubo, S.Okamoto
		S. Inaba
6	"Aseismic Test using by Large-Scale Earthquake Simulator"	S. Inaba
7	"Dynamic Test of Structures for Oil Tanks and Nuclear Power Plants"	S. Inaba
8	"Study of Seismic Performance for Electric Power Supply Units"	S. Inaba, S. Kinoshita
		S. Kinoshita
9	"Present Situation of Earthquake Prediction Research in Japan"	K. Hamada, H. Takahashi
	"Vertical Distribution of the Seismic S-wave Velocities at the Site of The Iwatsuki Deep Borehole Observatory of Crustal Activities"	H. Sato, A. Suwa
		F. Yamamizu, Y. Ohta
		H. Takahashi, N. Gotoh
	"On a Method for Synthesizing the Artificial Earthquake Waves by Using the Prediction Error Filter"	K. Shiono
	"Studies on the Aseismic Properties of Under-ground Pipes"	K. Ohtani, S Kinoshita
	"Earthquake Resistant Design of High-Rise Building in Japan"	K. Ohtani, N. Ogawa
		C. Minowa
		K. Ohtani
10	"Dynamic Behaviour of Rectangular Water Tank Assembled with Panels"	K. Ohtani, C. Minowa
11	"Dynamic Behaviour of Reinforced Concrete Frame Structures"	K. Ohtani, C. Minowa
	"Orientation of Tsunami's Research in Japan"	Y. Fujinawa,
		H. Takahashi
12	"Dynamic Test of 3-story Reinforced Concrete Structure"	K. Ohtani
13	"Strong Motion Earthquake Observation by Velocity Type Seismometer"	K. Ohtani, S. Kinoshita
	"High Tide and Wind Waves Generated by Typhoon 7920"	Y. Tsuji, H. Takahashi
14	"Reconsideration of the Input Waves for Dynamic Analysis"	K. Ohtani
15	"Characteristics of High Winds Measured at an Observation Tower above the Ocean"	G. Naito, I. Watabe
	"Earthquake Engineering Research at National Research Center for Disaster Prevention"	M. Tokuda, H. Takahashi
		K. Ohtani, H. Takahashi
	"Research and DEvelopment of 3-Dimensional Shaking Table"	K. Ohtani, H. Takahashi
		G. Fujiwara
	"Tidal Anomalies Induced by the Typhoons 8210 and 8218"	Y. Tsuji, A. Takeda,
		T. Konishi, H. Takahashi
16	"Development of Strong Earthquake Alarm System for Tokai Earthquake"	K. Ohtani, H. Takahashi
	"Distribution of Inundation Height of the Nihonkai-Chubu Earthquake Tsunami along the Coasts of Japan and Korea"	Y. Tsuji, H. Takahashi,
		T. Konishi, T. Kinoshita
		U. S. Peak, K. S. Chu,
		H. S. An
17	"Features of Ocean Wind Fluctuations During Typhoon Passages"	G. Naito, H. Takahashi
	"Array Observation of Strong-Motion Earthquakes in the Fuchu Area"	K. Ohtani, S. Kinoshita,
		T. Mikoshiba
	"Tsunamis in the Japan Sea with Numerical Calculation"	Y. Tsuji, T. Konishi,
		H. Takahashi
	"Studies on Storm Surges in Tidal Estuaries"	T. Konishi, T. Kinoshita
		H. Takahashi
	"Rock Avalanche and Slope Failures Induced by the Nagano-Seibu Earthquake, 1984"	K. Tanaka, N. Ohyagi,
		T. Inokuchi, S. Uehara,
		H. Takahashi
18	"Spectral Characteristics of Ground Motion in the Tokyo Metropolitan Area"	K. Ohtani, S. Kinoshita
	"Discrimination of Flood Areas Caused by Tsunami or Storm Surge using Satellite Data"	A. Takeda, Y. Tsuji,
		H. Takahashi
19	"Dynamic Behaviour of Rock Filled Dam"	K. Ohtani, K. Baba,
		T. Nakai
	"Seismic Microzonation using Ground Information"	S. Kishi, T. Moroboshi,
		K. Ohtani, H. Takahashi
	"An Estimation of Tsunami Generated by Submarine Landslide"	S. Iwasaki, H. Takahashi

\*1; No. of the Joint Meeting of Wind and Seismic Effects, UJNR

Table 3. Research Projects using the  
Large-Scale Earthquake Simulator

Research Form	Own Research by NRDCP	36
	Joint Research	24
	Entrusted Research	50
Research Object	Building Structure	17
	Soil Structure	23
	Ground	7
	Submerged Tunnel	4
	Foundation of Bridge	5
	Industrial Equipment	17
	Water Tank	16
	Nuclear Power Plant	16
	Piping System	5
<b>Total</b>		<b>110</b>

Table 4. Main Features of Large-Scale Earthquake Simulator

ITEMS	ORIGINAL PLAN	RENEWAL PLAN
Shaking Table	15m X 15m	15m x 14.5m
Driving System	Electro-hydraulic System	The same as the left
Actuators	360 tons (90 tons X 4)	ditto
Max. Model Weight	500 tons	ditto
Max. Amplitude	30 mm	220 mm
Max. Velocity	37 cm/sec	75 cm/sec
Max. Acceleration	0.55 G (with 500 tons model)	The same as the left
	0.75 G (with 300 tons model)	ditto
	1.0 G (with 200 tons model)	ditto
	2.2 G (with table only)	ditto
Frequency Range	0.1 - 50 Hz	ditto
Wave Forms	Sinusoidal wave, Random wave,	ditto
	Earthquake wave, etc	
Servovalves	MOOG 72-103	MOOG J079-200
	(4.valves for each actuator)	(2 valves for each actuator)
Main Pump Units	13 units of 156 KW electric	15 units
	motor	(11 units of 156 KW electric motor + 4 units of 356 KW electric motor)
Subsidiary Pump	Oil pressure of 210 kg/cm <sup>2</sup>	The same as the left
	Oil flow 3,900 l/min	Oil flow of 7,160 l/min
	4 units	2 units
	Oil pressure of 70 kg/cm <sup>2</sup> and 140 kg/cm <sup>2</sup>	Oil pressure of 140 kg/cm <sup>2</sup>
	Oil flow of 1,200 l/min	Oil flow of 800 l/min

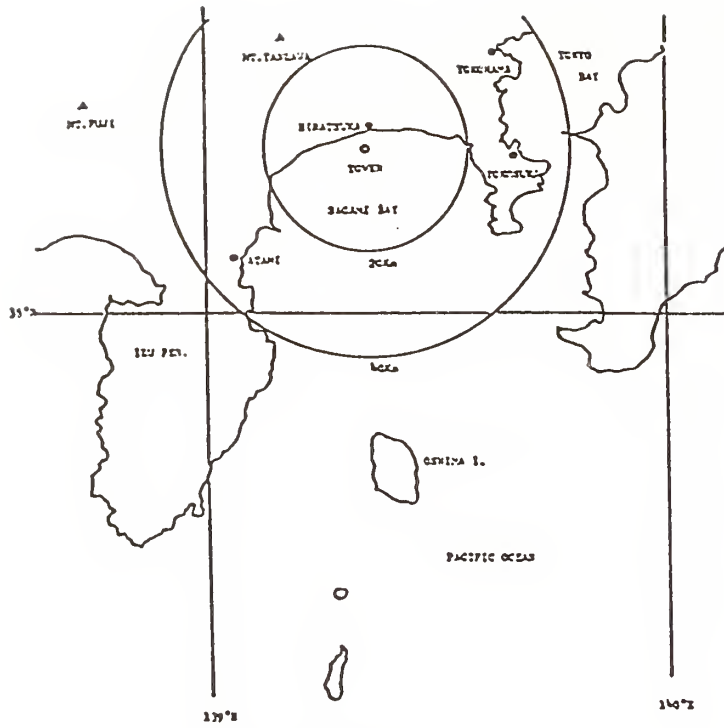


Fig. 1. Observational site

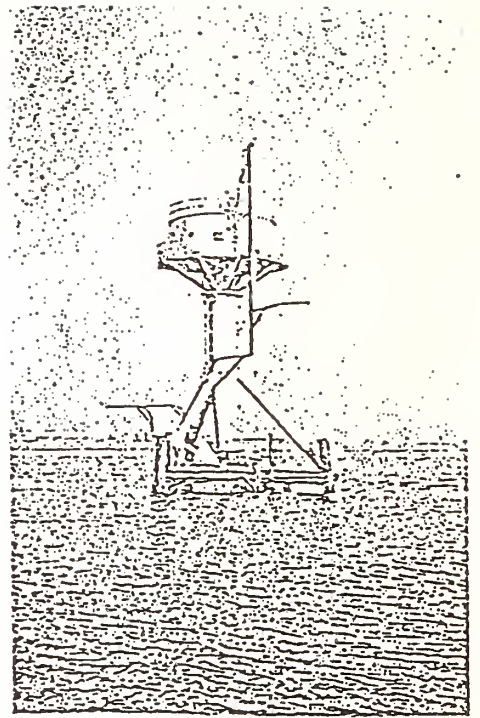


Fig. 2. Marine observation tower off Hiratsuka

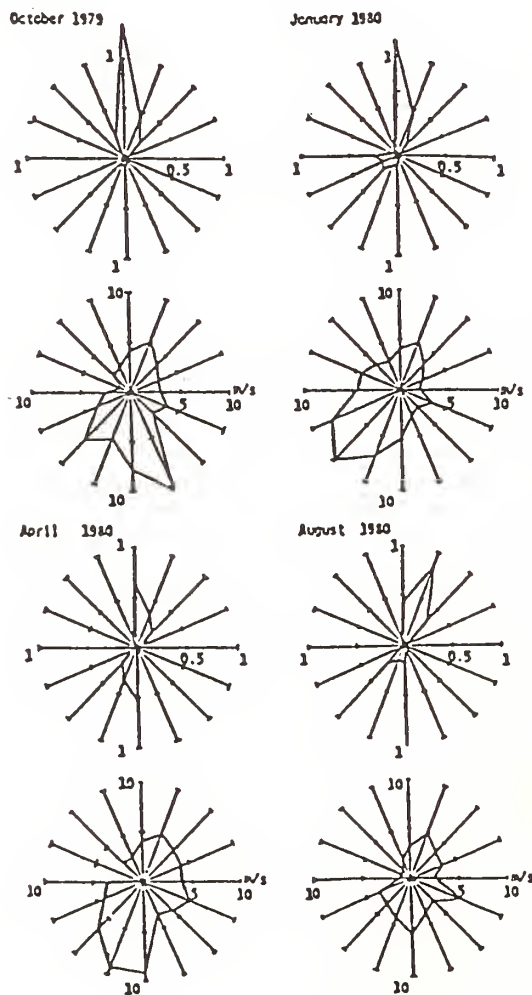


Fig. 3. Monthly relative frequency distribution of wind direction (upper) and azimuth pattern of wind speed (lower)

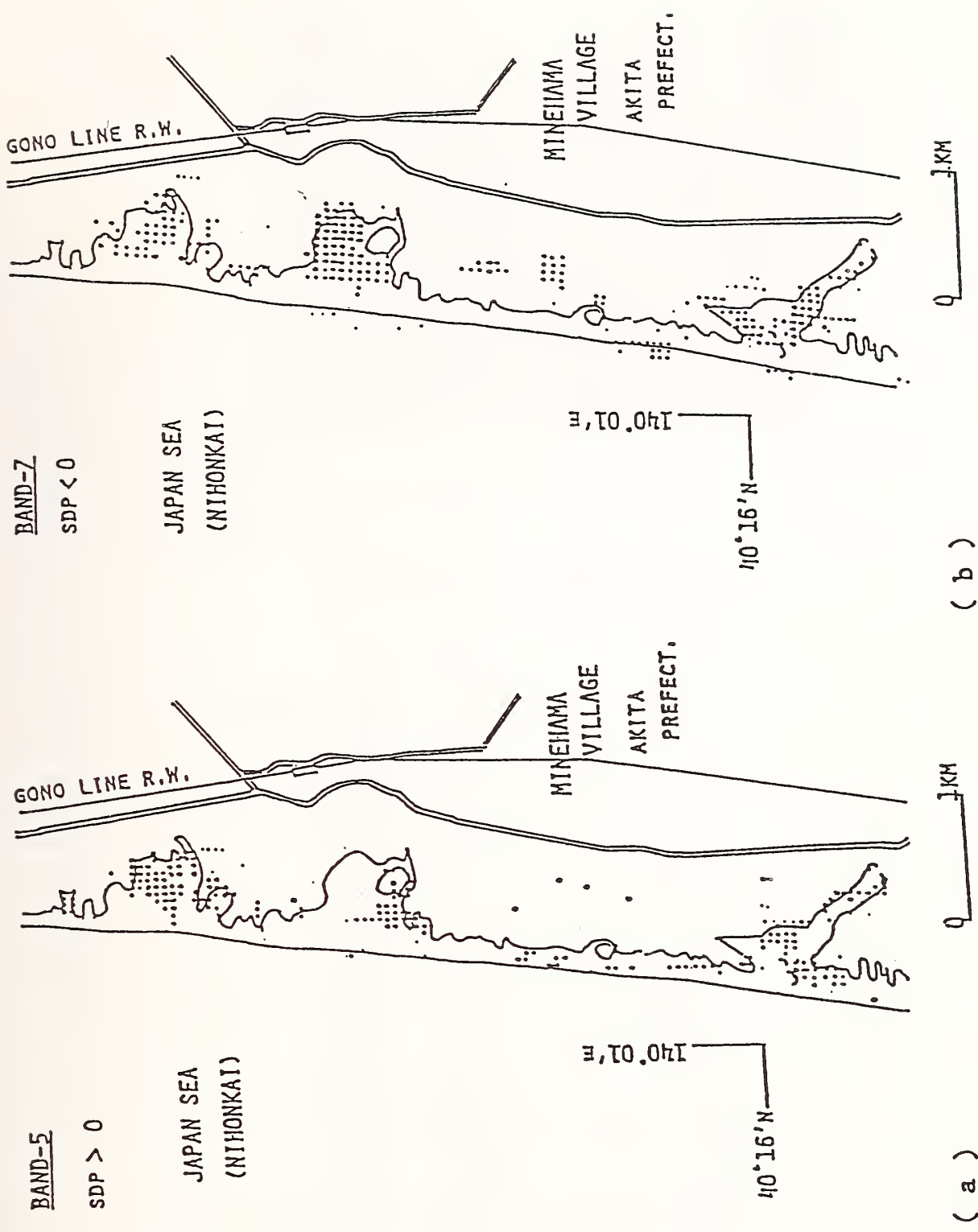


Fig. 4. Distribution Map of SDP, (a) Band 5 and (b) Band 7



Fig. 5. Distribution of Thickness of Soft Ground According to the Database of Urban Ground Data

Soil Name	Card	MT	LP	CRT
Surface	SUR	0		
Humus	Y	1	Y	Y
Shell	Q	2	Q	⊙
Pumice	P	3	P	△
Boulder	B	4	B	○
Gravel	G	5	O	o
Sand gravel	DG	6	O.	⋮
Sand	D	7	.	⋮
Fine sand	F	8	.	⋮
Medium sand	M	9	:	⋮
Silt	T	10	-	⋮
Clay	C	11	=	⋮
Sandstone	DN	12	I.	
Siltstone	TN	13	I-	
Mudstone	MN	14	I=	

MT : Magnetic Tape

LP : Line Printer

CRT: Cathode Ray Tube

Fig. 6. Table of Soil Code

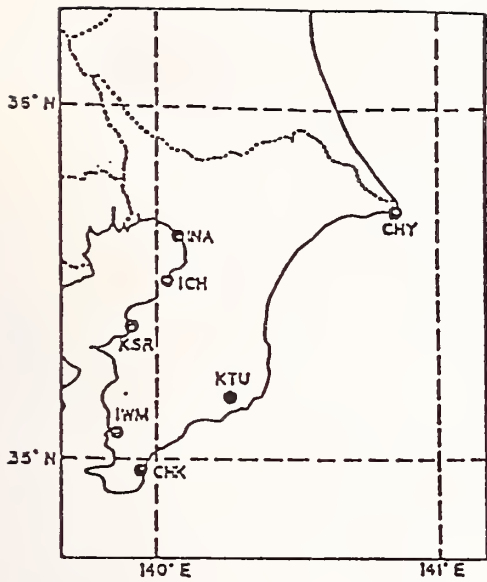


Fig. 9. Observation Site in the Chiba Pref.

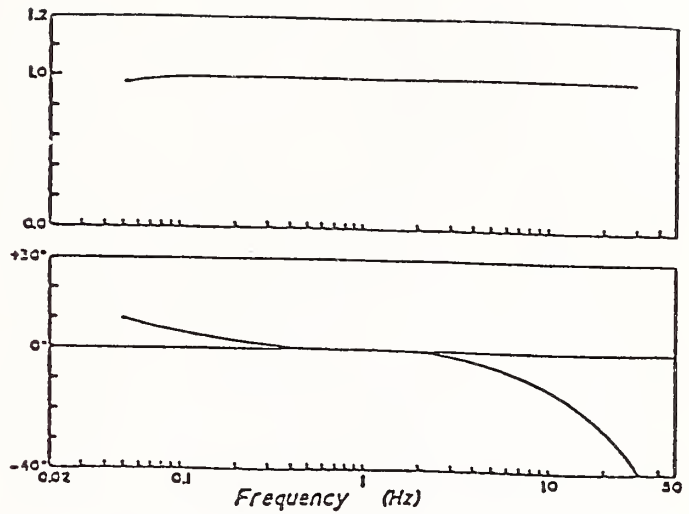


Fig. 10. Frequency Characteristics of Seismometer

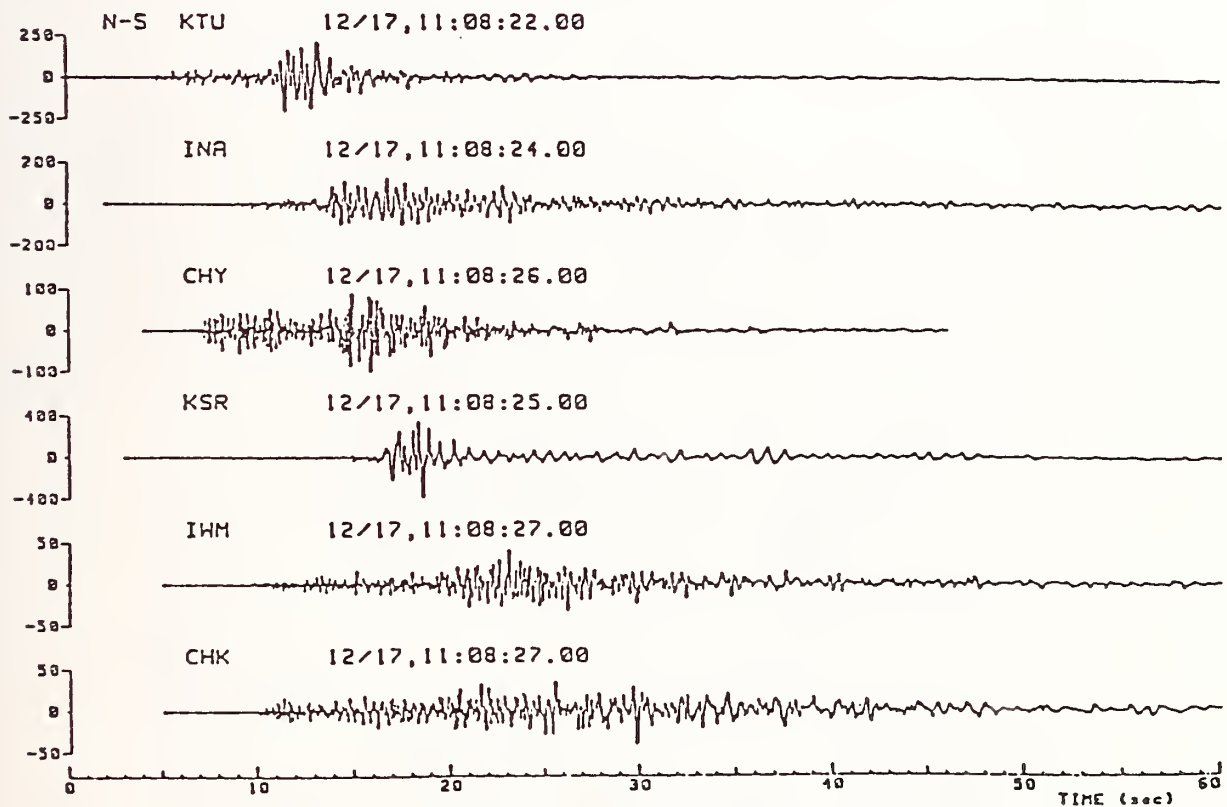


Fig. 11. (a) Acceleration Waves obtained at Chiba Pref. (NS Comp.)

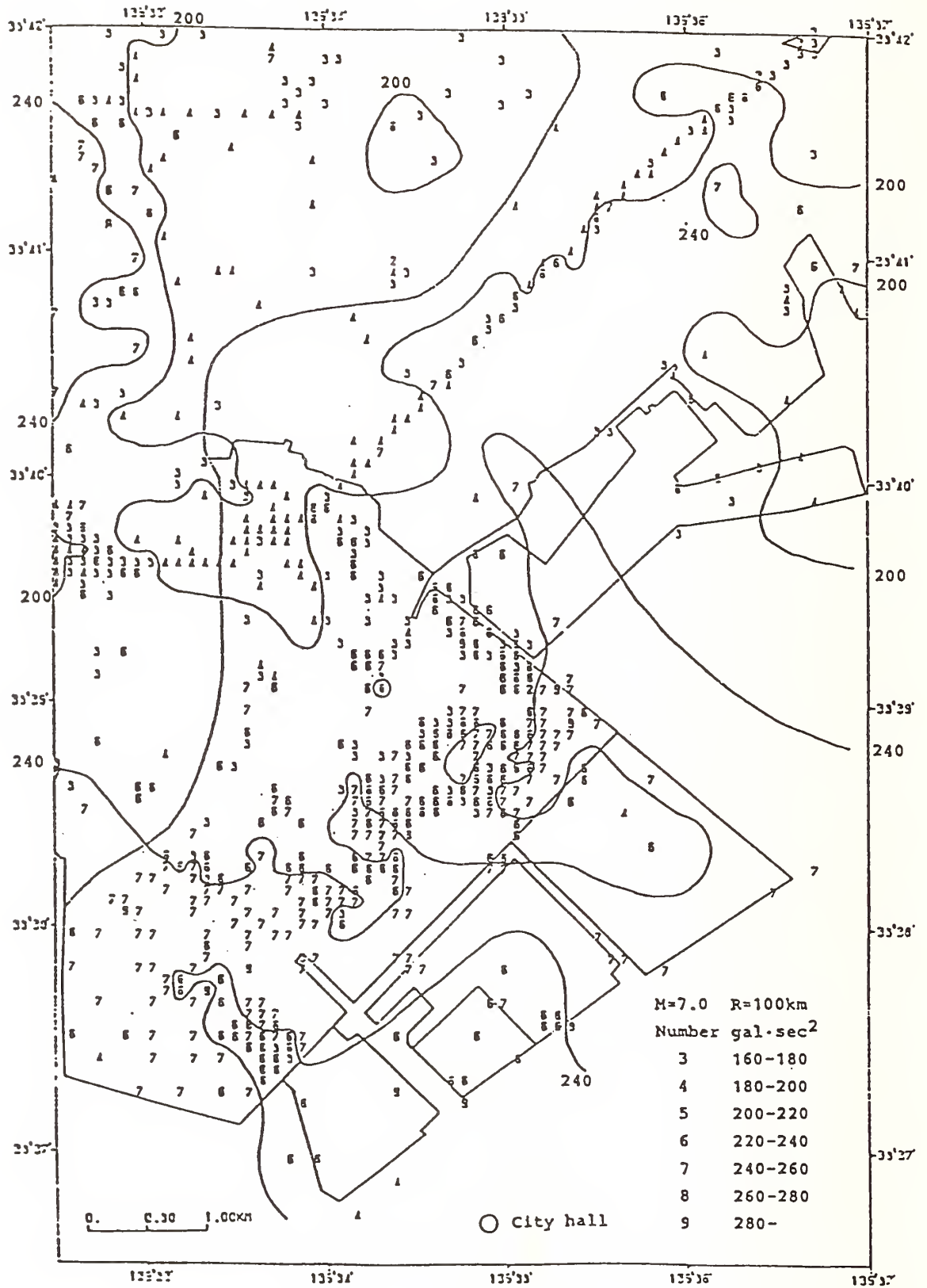


Fig. 8. Regional Distribution of Spectral Intensity

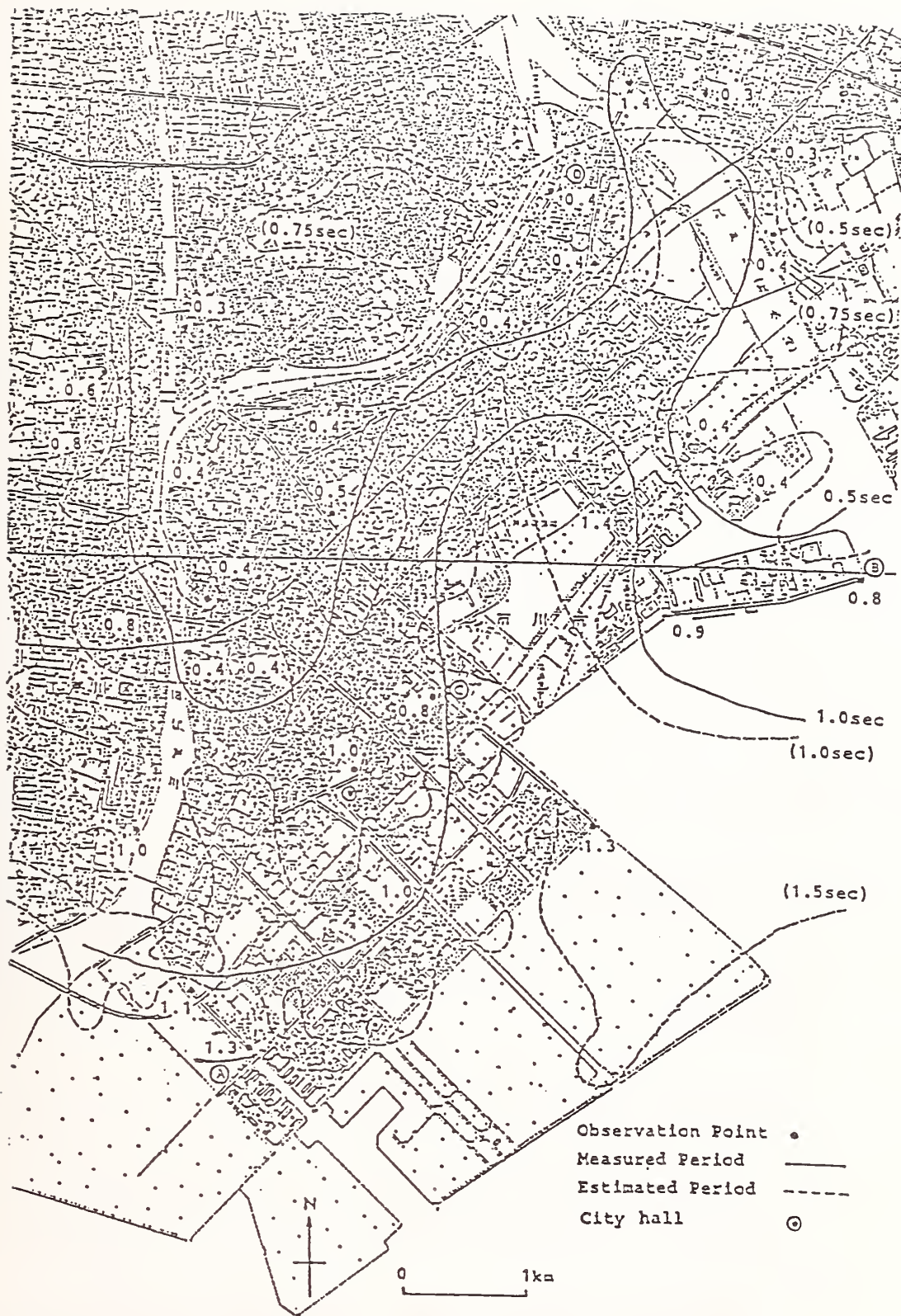


Fig. 7. Predominant Period of Surface Layer and Observation Point of Microtremors (Eastern Neighbour of Tokyo)

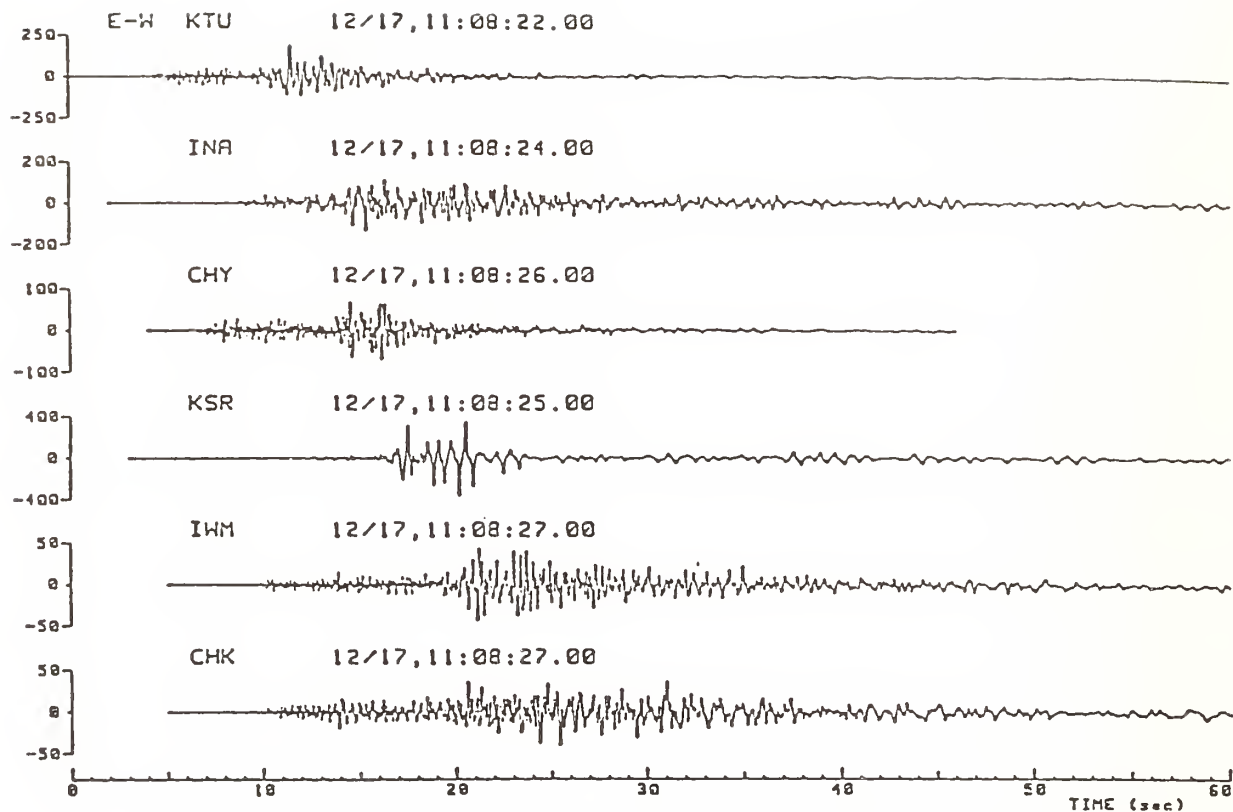


Fig. 11. (b) Acceleration Waves obtained at Chiba Pref.  
(EW Comp.)

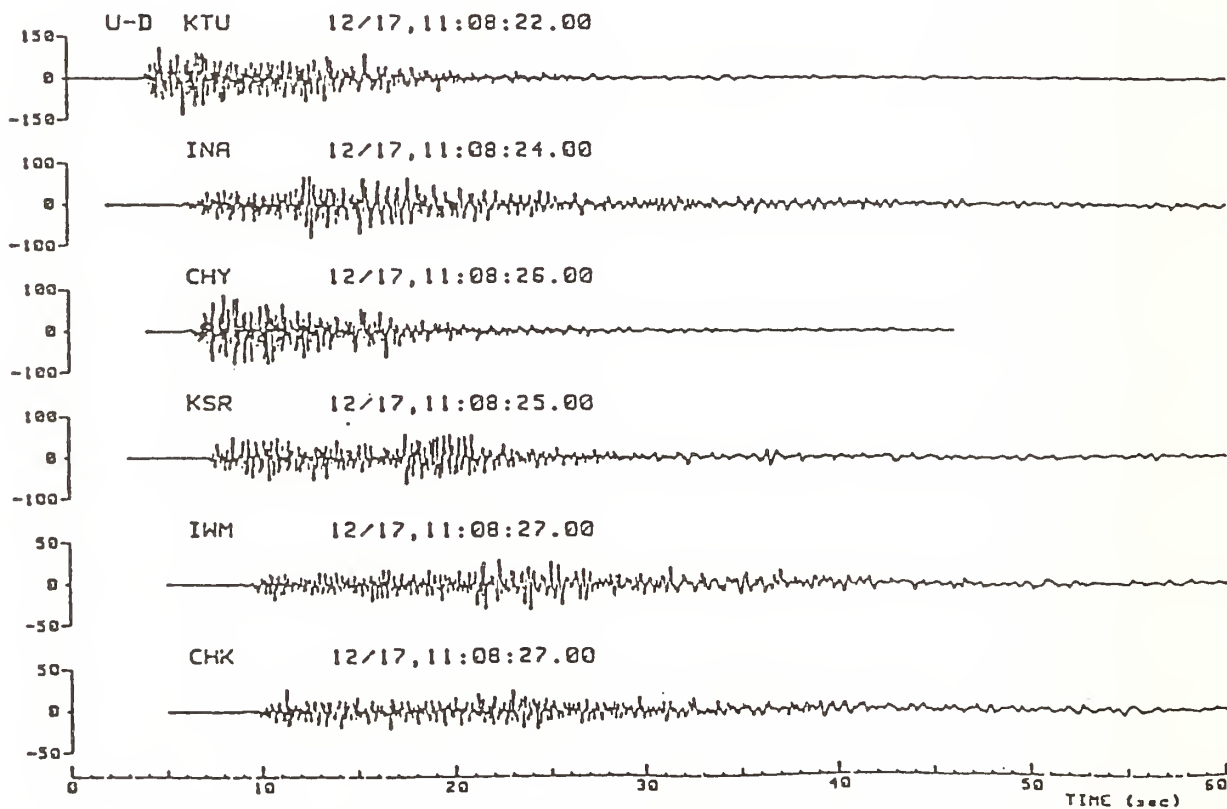


Fig. 11. (b) Acceleration Waves obtained at Chiba Pref.  
(UD Comp.)

IWT: 35°55'33"N, 139°44'17"E  
 SHM: 35°47'36"N, 140°01'26"E  
 FCH: 35°39'02"N, 139°28'25"E

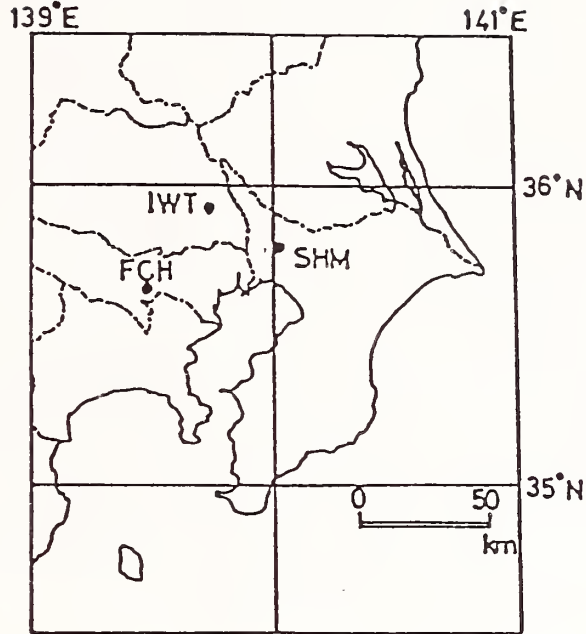


Fig. 12. Location of Vertical Array Observation Sites

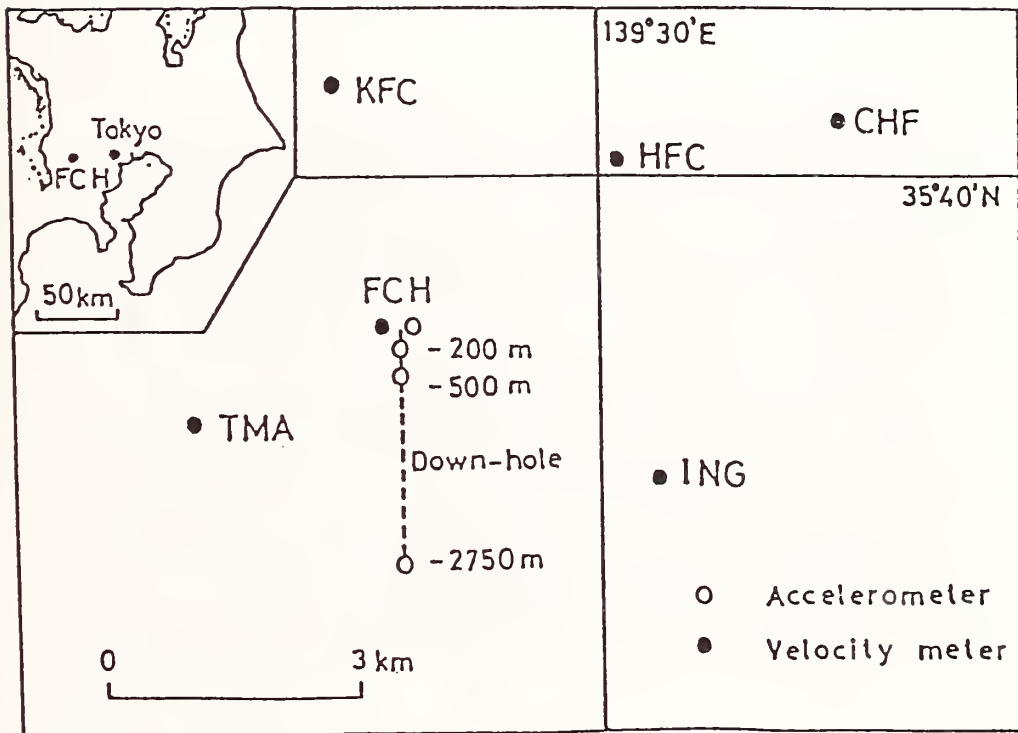


Fig. 13. Layout of Seismographs at the Fuchu Area



Fig. 14. Dense Array Observation Sites at Downtown of Tokyo

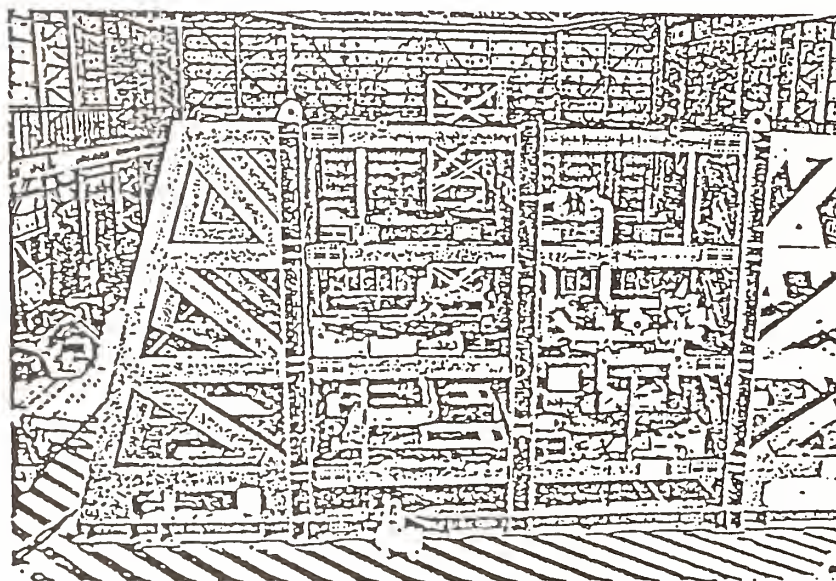


Fig. 16. General View of the Testing Apparatus

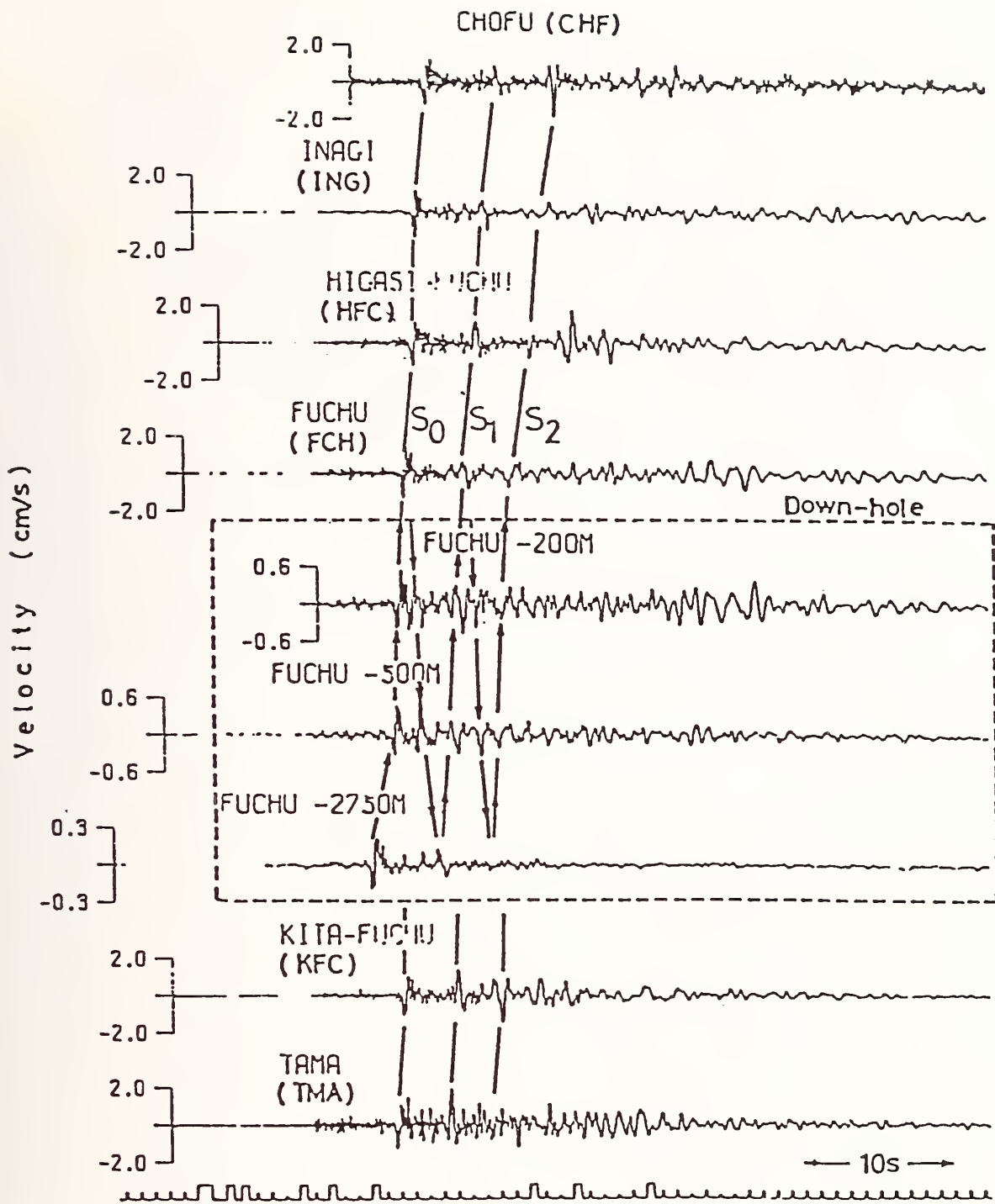


Fig. 15. Velocity Waves obtained by Array Observation shown in Fig. 13

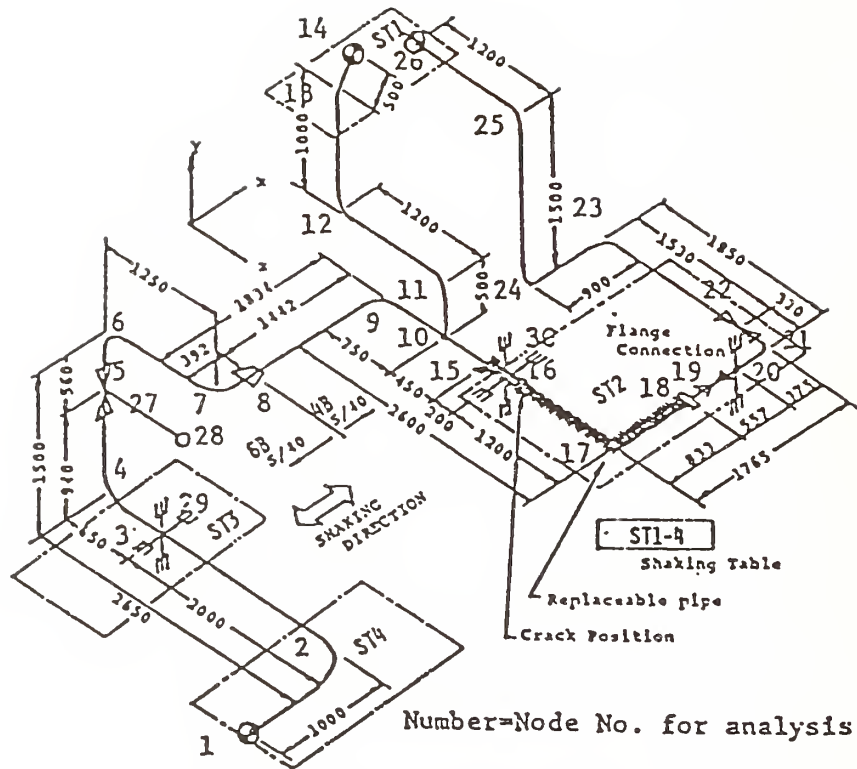


Fig. 17. Test Piping Model

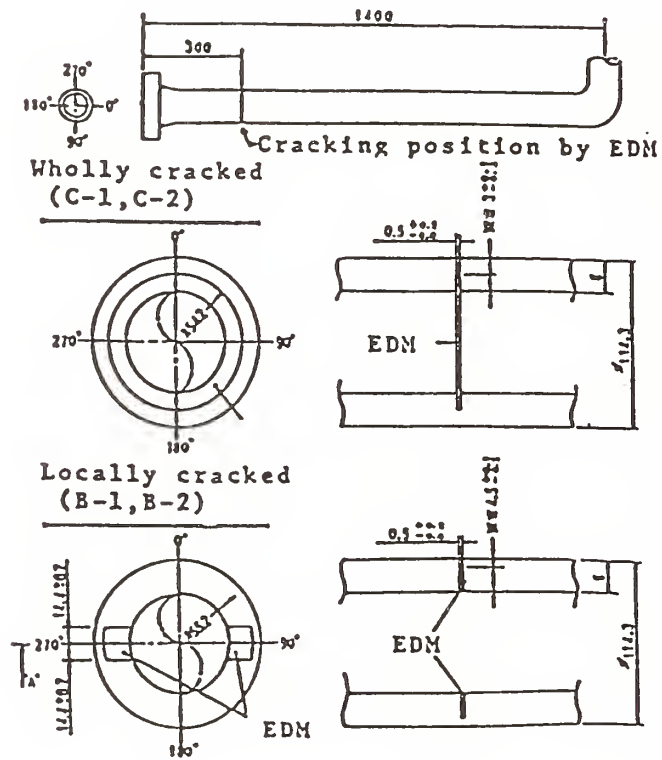


Fig. 18. Drawing of Pipe Cracks

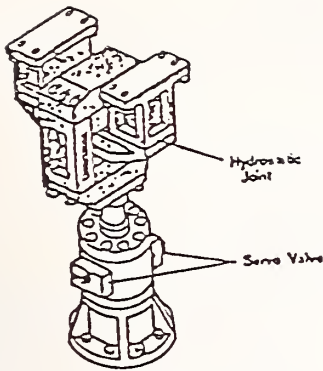


Fig. 19. Hydraulic Actuator with Joint

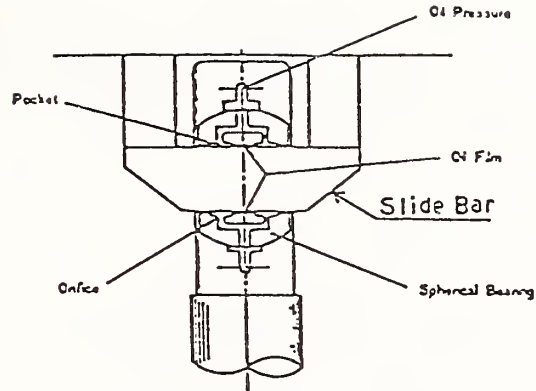


Fig. 20. Hydrostatic Bearing Joint

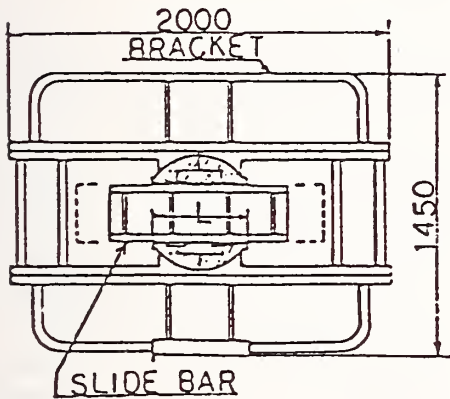


Fig. 21. Hydrostatic Joint

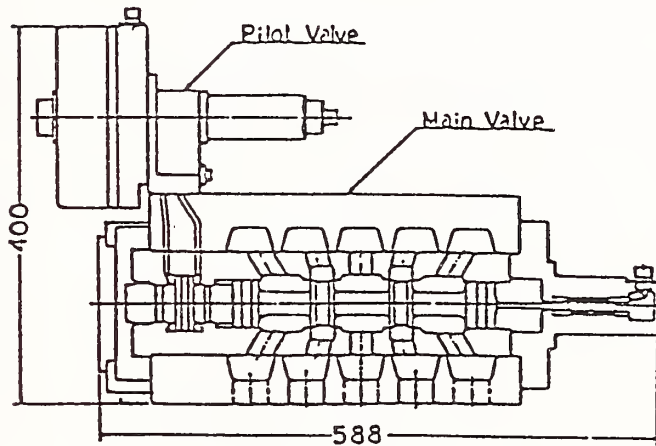


Fig. 22. Section of Servo Valve

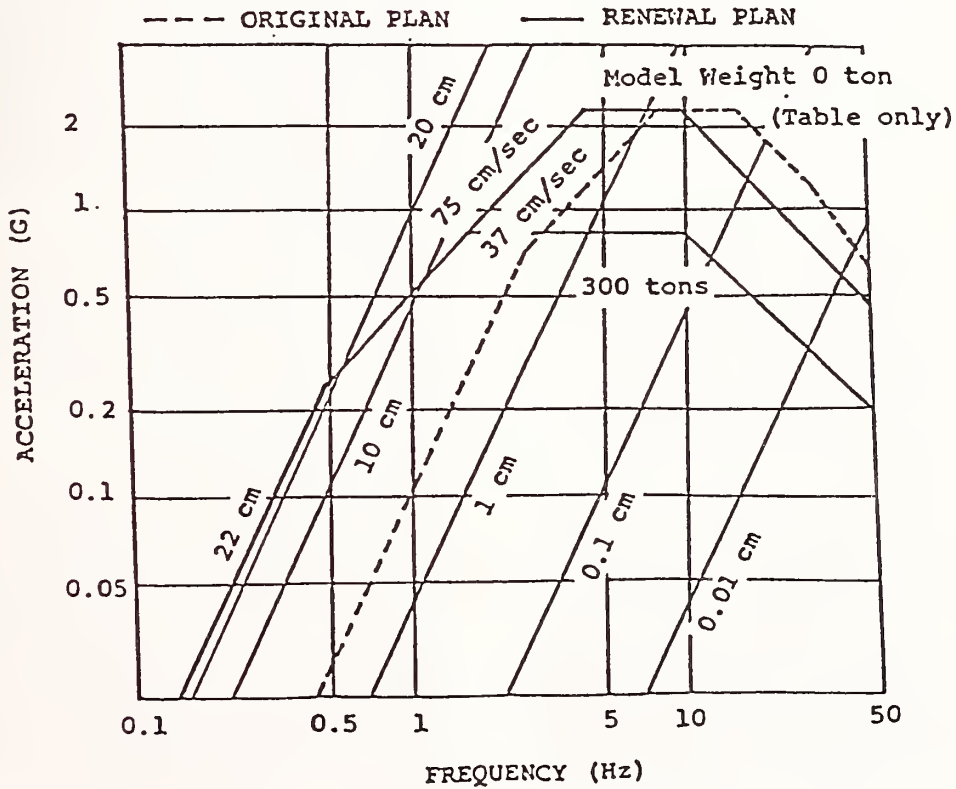


Fig. 23. Limit Performance of Large-Scale Earthquake Simulator

# Development of Design Criteria for Mitigating Earthquake Damage—The Program of the Federal Emergency Management Agency

BY  
Richard W. Krimm

## ABSTRACT

The Federal Emergency Management Agency has developed a strategy to reduce the effects of earthquakes on buildings. This strategy begins with addressing what can be done with new buildings, existing buildings and lifelines. The overall plan is divided into two categories - Federal and non-federal buildings and lifelines.

### 1. INTRODUCTION

When the Congress passed the Earthquake Hazards Reduction Act of 1977 and made amendments in 1980, their purpose was to reduce the risk to life and property from future earthquakes in the United States. This purpose is incorporated in the National Earthquake Hazards Reduction Program (NEHRP).

Each of the four principal agencies in the NEHRP which are the Federal Emergency Management Agency (FEMA), the United States Geological Survey (USGS), the National Science Foundation (NSF), and the National Bureau of Standards (NBS), have hazard reduction as a goal. FEMA, as the lead agency, works with and provides the data to State and local governments to prepare for, mitigate and respond to earthquakes. This is done through hazard delineation and assessment; seismic design and engineering; and preparedness planning and hazard awareness.

### 2. THE ROLE OF FEMA

The role of FEMA's work in seismic design practices through the funding of applied research is the publication of manuals and guides for the use of practitioners such as State and local governments. At the FEMA, we believe significant earthquake hazard reduction can be achieved in time, and by time we mean decades, through the development and implementation of seismic design and construction standards.

Because the actions of buildings and lifelines pose the greatest threat to life and property during and after an earthquake, we believe that measures taken to reduce the threat can best meet the intent of the Congress to reduce the risks of life and property from future earthquakes. The strategy which we have developed at FEMA addresses New Buildings - Federal and non-federal, existing buildings - Federal and non-federal, and Lifelines - Federal and non-federal.

### 3. FEDERAL BUILDINGS

The problem of Federal buildings is being addressed by the Interagency Committee on Seismic Safety in Construction (ICSSC). This is a subcommittee of the Interagency Coordinating Committee of NEHRP, which is composed of the four principal agencies. The ICSSC is made up of 25 Federal agencies that are involved in construction.

Using consensus procedures, the ICSSC recommends earthquake hazard reduction practices for use by Federal Agencies in their ongoing programs.

Federal guidelines for new Federal buildings were published in 1987. The ICSSC is working on working on guidelines for existing Federal buildings which we plan to publish in 1988. A significant accomplishment of the ICSSC was the development of a Federal Executive Order on Seismic Safety of Federal and federally-assisted or Regulated Construction. The proposed Executive Order would require that federal preparedness and mitigation activities are to include development and promulgation of specifications, building standards, design criteria and construction practices to achieve appropriate earthquake resistance for new and existing structures and an examination of alternative provisions and requirements for reducing earthquake hazards through Federal and Federally-financed construction, loans, loan guarantees, and licenses. The proposed Executive Order is now under consideration by the President's staff.

The ICSSC has developed model administrative procedures for Federal agencies to use. At the Federal level, we believe that Federal buildings have to set an example if we expect State and local governments and the private sector to mitigate their seismic risk through better design and construction standards.

### 4. NON-FEDERAL BUILDINGS

In 1985, we published the NEHRP Recommended Provisions for the Development of Seismic Regulations for New Buildings. These provisions are to be used on a voluntary basis by design professions, the construction industry, building regulatory personnel and researchers. In addition, a series of technical assistance publications were developed to encourage the use of the NEHRP provisions. These provisions

are not a Federal building code, but are techniques that can be used in constructing seismic resistant buildings.

In 1988, an update of the provisions will be published to include the results of new research and the lessons learned from the Mexico City Earthquake. There is an active dissemination of these provisions through the use of a toll free number, a speaker's bureau set up by the Building Seismic Safety Council, which is an independent voluntary group established by the National Institute of Building Sciences. Demonstration of the use of the NEHRP provisions will be performed in various cities throughout the United States.

A very difficult area is the seismic design and construction standards for non-federal existing buildings. In 1986, the FEMA published an action plan for reducing earthquake hazards in existing buildings. This plan, which was developed by the three leading groups in earthquake engineering; the Applied Technology Council (ATC); the Building Seismic Safety Council (BSSC), and the Earthquake Engineering Research Institute (EERI), calls for actions by the four principal agencies costing \$40 million over the next five years.

FEMA has started a study of typical costs of seismic rehabilitation which will result in a report for the use of design professionals, building regulatory personnel, elected and appointed officials and model code groups. This report will be available in 1988.

As a follow-up to the typical cost study, there will be a rapid visual survey handbook, a seismic evaluation methodology handbook, a rehabilitation priorities handbook, a seismic strengthening handbook with a cost estimation methodology and financial incentives for seismic rehabilitations. There is a logic to what the FEMA is doing which is as follows:

First, identify hazardous buildings in the community that appear susceptible to damage from earthquakes.

Second, identify what about the building is hazardous.

Third, provide techniques to strengthen buildings to reduce the damage that may occur from an earthquake.

Lastly, develop a cost methodology to strengthen the building.

##### 5. LIFELINES

A plan of action for the seismic design and construction standards for non-federal lifelines was prepared in 1987 by experts under the auspices of the BSSC. The plan identifies about \$28 million of high priority tasks that

should be undertaken. FEMA has an engineer on the staff who will analyze the report and is going to recommend how to proceed with a study. The lifelines which the FEMA is studying are:

1. Gas and liquid fuel
2. Transportation
3. Power
4. Communication
5. Water and sewer

##### CONCLUSION

The results of all these projects will lead to the mitigation of the earthquake hazard in many areas of the United States, provided there is the support of design professionals, building regulators, financial institutions, the insurance industry, and State and local officials. However, with a small budget it will take a long time to achieve the goals.

# State-of-the-Art on Earthquake Engineering to Port and Harbour in Japan

by  
Setsuo NODA\* and Hajime TSUCHIDA\*\*

## ABSTRACT

This paper presents the present condition of earthquake engineering in port and harbour in Japan.

This paper includes damages of port structures by the recent great earthquakes, outline of earthquake resistant design procedure, results of research activities by Port and Harbour Research Institute on strong motion observation, liquefaction of sandy soil, aseismicities of breakwater, gravity quaywall, steel piled pier, steel plate cellular bulkhead and improved ground by Deep Mixing Method.

KEY WORDS: Port Structure, Earthquake Damage, Earthquake Resistant Design, Strong Motion Observation, Liquefaction

## 1. DAMAGE BY PAST EARTHQUAKES

Port and harbour structures in Japan have often suffered severe damage by the past earthquakes. Followings are some of the characteristic features of damage by the recent great earthquakes.

Most facilities in Niigata port suffered seriously by the Niigata Earthquake in 1964.<sup>1)</sup> Some of quaywalls sank completely under the water. We got valuable lessons from the earthquake that the major cause of damage was the liquefaction of foundation soil.

At the time of the Tokachi-oki Earthquake in 1968, accelerations of ground motions were perfectly recorded at various ports. The present design method for earthquake resistance on quaywalls has been re-examined in the light of the damage to the structures and observed ground motion records.<sup>2)</sup>

Steel sheetpile quaywalls in Ishinomaki port were damaged by the 1978 Miyagi-ken-oki earthquake.<sup>3)</sup> Steel sheetpile quaywalls and gravity quaywalls in Akita port were also severely damaged by the 1983 Nipponkai-chubu earthquake.<sup>4)</sup> It was concluded by the field investigation that liquefaction of the backfilling sand mainly caused damage in both ports.

Damage costs due to earthquakes are listed in Table 1. It is clear from the table that damage costs of the ports where liquefaction took place are fairly large, even if other conditions were similar.

### 1.2 Damage of Akita Port by the 1983 Nipponkai-chubu Earthquake 4)

#### 1) Outline of Damage

On May 26, 1983 an earthquake of magnitude 7.7 hit northern Japan. The epicenter located at about 100 km west of

Akita city. The seismic disturbance and the tsunami of this earthquake brought serious damage to coastal area along the Japan sea.

The public port facilities of 14 ports were damaged by this earthquake. The total cost of damage was about 8100 million yen. Akita port which locates at estuary of Omono river proper was damaged most seriously. Most of quaywalls in the port were tilted and concrete aprons were crushed. The function of the port was lost for a time. 6400 million yen of damage cost in this port corresponds to about 79 % of total cost by this earthquake.

#### 2) Strong Motion Records

Strong motion records were obtained in several stations and maximum ground accelerations of major records are included in Fig.1. The largest peak acceleration in the port area was 205 Gals at Akita port and its wave forms are shown in Fig.2.

#### 3) Damage of Port Facilities at Akita Port

Followings are major damage in this port.

Concrete caisson type quaywalls as shown in Fig.3 were tilted and moved towards sea by the earthquake, but the foundation soil was not destroyed. Aprons of 9 m wide and 270 m long settled about 1.5 m. A person who was in the site during the earthquake testified that concrete aprons sank with sound just after the earthquake and dark colored water boiled out 1 m high into air. Foundation piles, beams and slabs of the transit shed were broken.

As shown in Fig.4, the steel sheetpile walls with pipe pile anchor were damaged most seriously and their function were completely lost. For instance, coping of 185 m long moved towards sea 170 cm in maximum and especially a part of 40 m long sank under water. The sheetpiles were bent seriously and some of them were broken. At boundary between the reclaimed ground and the old revetment, difference of ground level of 70 cm occurred. Person testified that concrete aprons vibrated like waves with sound during the earthquake.

As shown in Fig.5, concrete cellular block walls of 55 m long collapsed and completely sank under water. Aprons settled over 50 cm and some of concrete piles for foundation of transit sheds were broken. An unloader on aprons derailed.

---

\*\* Dr. Eng., Director General, PHRI, MOT

\* Dr. Eng., Chief, Geotechnical Earthquake Engineering Laboratory, Structures Division, PHRI, MOT

#### 4) Liquefaction

In Table 2 main facilities are classified in terms of liquefaction and degree of damage. Judging from the table damage of facilities are very closely related with liquefaction of ground at Akita port.

In port area the liquefaction potential of ground is estimated by the Port and Harbour method in which grain size distributions and the SPT N-value are used. It was examined that estimating method agrees or not with cases of liquefaction at Akita port. Examination includes not only the sites of liquefaction but also the sites of non-liquefaction. As the results the Port and Harbour method agreed well with actual cases of liquefaction.

#### 5) Restoration Works

In order to strengthen against liquefaction, compaction of the backfilling sand by the vibrating rods was adopted to the restoration works at Akita port. Preceding the compaction gravel piles were also set up just behind walls. The gravel drain piles discharged the excess pore water pressure due to compaction.

### 2. EARTHQUAKE RESISTANT DESIGN PROCEDURE

#### 2.1 History of Design Standard

The first design standard for the port structures was published by the Japan Port and Harbour Association in 1950. In the manual inertia force, earthpressure and dynamic water pressure were considered. For the estimation of the earthpressure during earthquakes, a formula proposed by Matsuo based on his experimental study was adopted. However, Mononobe-Okabe's formula was also explained as an applicable formula.

The second design standard was published by the Japan Port and Harbour Association in 1959. In this manual Japan was divided into three regions and a seismic coefficient was specified for each region. The formula to estimate earthpressure during earthquake consisted of Monobe-Okabe's formula.

The third design standard was published also by the Japan Port and Harbour association in 1967. This design standard has various unique characteristics, in comparison to the previous two design standards. This design standard presented to the design of the structures, such that even a less experienced engineers could design the structures without any other textbook, and it also presented the background information on the procedure.

In 1973 the Port and Harbour Law was revised. Because of social demands on the safety of facilities in port and harbour, the ministry established engineering requirements on port facilities. The engineering requirements specifies only important points. Therefore, the third design standard was used as a supplement to the requirement. The basic

consideration of earthquake resistant design to port structures is the seismic coefficient method; however, earthquake resistant design based on the dynamic analysis was also acceptable.

#### 2.2 Basic Consideration of the Engineering Requirement 5)

##### 1) Design Earthquake Load

###### a) Earthquake Load

The earthquake loads acting on port structures should be calculated by the following formula, where the most sever condition should be chosen.

Earthquake load = Dead load x Seismic coefficient

Earthquake load = (Dead load + Surcharge) x Seismic coefficient

###### b) Seismic coefficient

The seismic coefficient should be calculated by the following formula.

Seismic coefficient = Regional seismic coefficient x Factor for subsoil condition x Importance factor

In general the earthquake load is applied horizontally at the center of gravity of the structure. The earthquake load in the vertical direction is not considered, except for those special structures which are influenced by a vertical load.

###### c) Regional seismic coefficient

Standard values of the regional seismic coefficient are shown in Fig.6.

###### d) Factor for subsoil condition

The standard value of the factor for subsoil condition should be determined as shown in Table 3. The classification of the subsoil condition should be assigned as shown Table 4, considering the thickness of the quaternary deposit and the kind of subsoil.

###### e) Factor depending on importance of structure

The standard value of the factor relative to the importance of the structure should be determined as 1.5 for special class, 1.2, 1.0, 0.5 for A,B,C class, respectively.

##### 2) Earthpressure during Earthquake

###### a) Calculation of Earthpressure

Lateral earthpressure of sandy soil in earthquake is computed by Mononobe-Okabe's formula which is derived from Coulomb's formula by statically applying the earthquake load to the soil mass in question.

###### b) Apparent seismic coefficient

The apparent seismic coefficient is introduced to compensate the influence of buoyant force in water. The apparent seismic coefficient is given by the following equation.

$$k' = \frac{r}{r-1} k$$

where; k': apparent seismic coefficient  
k: seismic coefficient in air  
r: unit weight of saturated soil (t/m<sup>3</sup>)

### 3) Dynamic Water Pressure

Rigid wall- and column-like structures facing the water designed by taking the dynamic water pressure into consideration. However, if the structure is retaining soil and the earthpressure is calculated by Mononobe-Okabe's formula with the apparent seismic coefficient, the dynamic water pressure is not considered in the design calculation.

### 4) Allowable Stress

Allowable stresses of steel and concrete, for short period load such as earthquake load, may be equal to or smaller than 1.5 times of the allowable stresses in normal condition.

### 5) Earthquake Resistant Design based on Special Study

When the seismic coefficient is determined from the special studies on regional seismicity, earthquake motion and earthquake response of the ground, the requirement described in 1) need not to be applied to design. It is also advised that in case of necessity the earthquake resistant design is confirmed by the consideration of the dynamic characteristics of the structure and the ground.

## 3. STRONG MOTION RECORDS

### 3.1 Strong Motion Observation

The strong motion earthquake observation in port areas in Japan was started in 1962 by PHRI in cooperation with the several organizations related to the harbour construction work. At the present the network consists of 80 strong motion accelerograph stations at 54 ports as shown in Fig.7.<sup>67</sup> Two kinds of accelerograph are being used in the network; the SMAC-B2 accelerograph and the ERS accelerograph which was developed by PHRI. By the end of 1987 about 3400 accelerograms were obtained in the network. They were published as the annual reports every year, in which the digitized records and their computer plots, the response spectra and the Fourier spectra with large acceleration amplitude were included. The records of the major earthquakes such as the 1968 Tokachi-oki earthquake and the 1983 Nipponkai-chubu earthquake published separately, but in the same format. The site conditions of the observation stations were published in details as the separate reports. The procedures of the data processing are consisting of base line corrections, instrument corrections and integration of acceleration time histories.

### 3.2 Dense Instrument Array Observation

#### 1) Types of Array System

Increasing the large-scale and complicated structures in ports, it becomes significantly important to make clear the behavior of soft alluvial layers in coastal areas during earthquakes. From this point of view, PHRI has also been conducting the following three types of dense instrument array systems consisting of several accelerometers installed on and in grounds.<sup>7)</sup>

#### a) Vertical Instrument Arrays

Earthquake response characteristics of surface layers are very important factor to the seismic design of structures constructed on the layers. For example, the characteristics are taken into consideration as factors of subsoil conditions for determining the seismic coefficient and as response spectra of various subsoil conditions.

PHRI has established the vertical instrument arrays since 1967. Observations have been continued at 3 stations around Tokyo bay.

#### b) Horizontal and Vertical Instrument Arrays

An aseismicity of long extending structures such as subaqueous tunnels and pipelines are significantly dependent not only on accelerations but also on deformations of ground along structures. The horizontal and vertical instrument array has been established in Tokyo airport at Haneda in 1974. The array consists of 6 sets of accelerometers on the ground in every 500 m along the runway of 2500 m and of 2 sets in the bedrock. Horizontal and vertical configurations of accelerometers are shown in Fig.8. In 1988 the larger scale system have newly been established along the No.A runway at the extended area of Haneda airport. The array consists of 16 sets of accelerometers on the ground along the runway of 2500 m, and 24 sets of accelerometers and 24 sets of pore water pressure gauges in the ground.

#### c) Three Dimensional Instrument Array

In order to investigate the behavior of surface layers more accurate, the PHRI has established the three dimensional observation system. This system was equipped at Daikoku island in Yokohama port in 1980. Observation points in plane locate at apexes of a triangle with sides of about 150 m. The vertical configuration of the array consists of 9 seismometers in the three different levels; the ground surface, the intermediate clay layer and the mudstone.

### 3.3 Utilization of Strong Motion Records

Strong motion records must give useful information to many subjects in the earthquake engineering. The followings are some examples of results achieved by PHRI.

#### 1) Average Response Spectra

Response spectra of 122 horizontal components of 61 earthquakes ground acceleration records were calculated, and effects of subsoil conditions to the shapes of response spectrum curves were studied. The

relationships between the shapes of response spectrum curves and the earthquake magnitude, microtremor spectra and spectrum intensities were also examined.<sup>8)</sup>

The spectra were classified into 3 groups by their shapes, and the average response spectra of the groups were given as shown in Fig.9. These average response spectra with generalized subsoil conditions give an instructive information to us for deciding the seismic coefficient.

## 2) Characteristics of Vertical Components

Characteristics of vertical components of the 574 strong motion accelerograms were studied in order to know effects of vertical ground motions to dynamic stability of structures.<sup>9)</sup>The followings were made clear;

a) According to accelerograms with the maximum acceleration of over 50 Gals, the ratio of the maximum acceleration of the vertical component to that of the horizontal component was less than 1/2.

b) The occurrence time of the maximum acceleration of the horizontal component was different from that of the vertical component. At the time when the safety factors against sliding and overturning were the smallest, the ratio of the vertical acceleration to the horizontal acceleration was less than 1/3.

c) The stability analysis of the gravity type quaywalls by the current design method to port facilities were performed on consideration of the vertical seismic coefficient. Consequently, the vertical seismic coefficient had little influence on the safety factors for gravity type quaywalls.

## 3) Propagation of seismic waves

Earthquake ground motion records obtained by the two dimensional seismometer array at Tokyo airport were analysed.<sup>10)</sup> From the analysis of the results the followings are found;

a) Travel times of shear wave in the surface layer were estimated from the shear wave velocities obtained by the in-situ measurement and it was compared with the observed travel times. Both coincided very well.

b) From the findings above, it may be deduced that the shear wave velocities by the in-situ measurement are applicable to the simulation of seismic ground motions, if the shearing strain in the ground is not large. Also, it may be deduced that the shear waves traveled vertically in the surface layer.

c) The results of analysis are supporting the multiple reflection theory which is widely used in practice of engineering seismology.

## 4. LIQUEFACTION OF SANDY SOIL

### 4.1 Assessment of Liquefaction Potential

### 1) The 1970 Criterion

By the Niigata earthquake of 1964 the extensive damage due to the liquefaction of subsoil was caused in the area of new alluvial sand deposits and the engineers began to consider the liquefaction as one of the important problems in earthquake resistant design.

In PHRI a lot of shaking table tests to the saturated sand layers have been carried out and in 1970 the results together with the field experiences on the liquefaction in the past earthquakes were interpreted into the critical SPT N-value for liquefaction and the grain size distributions of soils which are in danger of liquefying during an earthquake.<sup>11)</sup> This criterion for assessing liquefaction potential was adopted in the third design standard for port structures mentioned in Chapter 2 and it was also widely referred in design manuals for other facilities as well as port structures.

### 2) The 1985 Criterion

Since the proposal of the criterion in 1970, Several great earthquakes have occurred in Japan and caused liquefactions. The liquefaction case records by these great earthquakes have not been contradictory of the 1970 Criterion. However, a minor aspect of the 1970 Criterion has come out; i.e. the 1970 Criterion has a lack of ability to predict the depth of liquefiable layers because it uses N-values of subsoils located around the ground water level. It has been sometimes difficult to decide how deeply the liquefiable site should be improved. Therefore, in 1985 the 1970 Criterion is extended to include the ability to predict the depth of liquefiable layers.<sup>12)</sup>

In the new criterion some items such as the relation between N-value and the effective vertical pressure, the relation between the maximum ground acceleration and the shear stress ratio, and the influence of fines contents of soil were considered.

The new criterion is summarized as follows;

a) Soils are classified by Fig.10.

b) Equivalent N-value is converted by the relation between N-value and effective vertical pressure.

c) Equivalent acceleration is converted by the maximum shear stress which is computed by the ground response analysis.

d) Critical N-value is reduced depending on the fines content.

e) Judgment whether liquefaction take place or not are obtained from Fig.11.

Extensive study on the applicability of the new criterion has been carried out by using liquefaction case records in Japan. The result of the study has confirmed the applicability of the new criterion.

### 4.2 Remedial Measures against Liquefaction

## 1) Area of Compacted Ground

Compaction of a loosely deposited sandy ground is one of the remedial measures against liquefaction. The compaction of the ground needs a reliable design in the degree of the compaction and the extent of the compacted area. In order to make clear these items shaking table tests were conducted to partly loose and partly dense saturated sands in a container of 5 m long, 1.5 m high and wide.<sup>13)</sup> The results of the tests indicated several factors which should be considered for designing the compaction of the ground. The followings are major results;

a) When the ground is compacted enough, it is probably said that the ground does not liquefy due to the liquefaction of uncompact ground. The standard value of the compaction is about 80 % of relative density and 16 of equivalent N-value ( corresponding to 0.66 kgf/cm<sup>2</sup> of effective vertical pressure) against usual design seismic conditions.

b) Even if the ground is compacted well, the excess pore water pressure is raised in the adjacent uncompact ground due to the seepage flow. Therefore, it must be considered that  $\nabla$ ACD of the compacted ground in Fig.12 is unstable part.

c) At CD of the boundary between the compacted and the uncompact grounds in Fig.12, the hydraulic pressures act. These are the static pressure with 1.0 of coefficient of earthpressure, and the dynamic pressure expected by the Westergaad's formula.

d) In order to decrease the compacted area, it may be effective to shut out the excess pore water pressure due to seepage flow. However, if gravel drains are applied, the capacity of drainage and other items must be properly designed.

## 5. ASEISMICITY OF BREAKWATER

In order to prevent damages by tsunami a large composite breakwater is under construction in deep sea of -60 m at the bay mouth of Kamaishi in Tohoku district. For the purpose of examining the aseismicity of the breakwater the coupled hydrodynamic response characteristics and water pressures of the breakwater were examined by shaking table model tests and the earthquake response calculations by Finite Element Method.<sup>14)</sup>

When caissons of the composite type breakwater did not resonate, the model tests showed that the hydrodynamic pressures acting on caissons are calculated by the Westergaad's formula.

In order to use earthquake response calculation for practical application, it is essential to investigate whether the modeling and material property values simulate adequately or not. Fig.13 shows the comparison of the dynamic water pressures by the Westergaad's formula and the Finite Element Method(program:BEAD).It was concluded that the FEM analysis on structures-water

systems was appropriate for simulating the dynamic response and hydrodynamic pressures of the fill type breakwater.

The strong motion accelerograms were obtained at the Ofunado fill type breakwater which was constructed against tsunami in water depth of -38 m. The accelerograms at the base, the top of rubble mound and the top of caisson were compared with those by the FEM(BEAD program).<sup>15)</sup> It was concluded that results showed relatively good agreement, and the estimated strain-depended characteristics of materials of mound were almost same to the cyclic triaxial test results of the gravel.

## 6. ASEISMICITY OF GRAVITY QUAYWALL

As mentioned in Chapter 2 the present earthquake resistant design to port structures is based on the static theory, so called as the seismic coefficient method. As the seismic effect acting on the structures varies complicated with time, the stability of the structure depends usually on such factors as the predominant period, amplitude and duration of the earthquake motion. Therefore, the dynamic design is becoming an effective method for the port structures with advance of the computation procedure. On the other hand, the seismic coefficient method is still often accepted to the common structures because this method is based on many experience and requires simple calculation on the stability analysis.

In order to improve the reliance of the seismic coefficient method, damaged gravity quaywalls were reconsidered under the light of knowledge of present earthquake engineering.<sup>16)</sup> 123 gravity quaywalls at 49 ports damaged by 12 past earthquakes were analyzed by the present design procedure, and the seismic coefficients corresponding to the severity of the seismic effect were obtained. The maximum ground accelerations in the ports were also estimated by calculating the ground response during the earthquake. The results were investigated from the aforementioned point of view. The followings were major outcomes;

a) Judging from the stability analysis on the gravity quaywalls by the current design standard, 0.25 was the maximum value of the seismic coefficient corresponding to the severity of the ground motions in the ports during the past great earthquakes.

b) The maximum ground accelerations  $a$  in the ports were estimated by calculating the ground response during earthquakes with reference to the attenuation curves of the base rock accelerations based on the accelerograms in port area. The upper limit of the relation between  $e_A$  and  $\alpha$  is expressed by the following equation.

$$e_A = \frac{1}{3} \left( \frac{\alpha}{g} \right)^{\frac{1}{3}}$$

where,  $e_A$ : seismic coefficient

$\alpha$ : maximum ground acceleration(Gal)

$g$ : gravitational acceleration(Gal)

## 7. ASEISMICITY OF STEEL PILED PIER

A steel piled pier, unlike other type of quaywalls, has high flexibility and carrying out earthquake resistant design of this type of pier by the seismic coefficient method has been subject to question. By using the prototype model with 4 piles of 508 mm in diameter and 10.45 m high above the sea bottom, the characteristics of a pier both in its elastic and plastic range were investigated experimentally.<sup>17)</sup> The results were summarized into following two items;

- a) Dynamic properties of a pier can be described by that of a one degree-of-freedom system.
- b) Restoring force can be approximated by the family of smooth hysteretic curves proposed by P.C.Jennings.

Then, the earthquake responses of above-mentioned model were computed for 9 strong motion records with over 100 Gals observed in ports. Final results are arranged into a chart as shown in Fig.14.

By using this method the earthquake response of piled piers such as maximum response acceleration and ductility factor can be easily evaluated for its natural frequency.

## 8. ASEISMICITY OF STEEL PLATE CELLULAR BULKHEAD

In recent years the quaywalls and the revetments in port areas tend to be constructed in poor seabeds and deep sites. The steel plate cellular bulkhead with embedment may be useful in these circumstances.

Then, the earthquake resistance of this new type of structure was investigated by the shaking table tests to large models.<sup>18)</sup> The dynamic behavior of cells, the distribution of earthpressure, the residual displacement of cells, and the effective mass of cell fill were investigated. Major results are as follows;

- a) The cells behave like rigid body, and the predominant mode is rocking. The installation of embedment significantly affects the stability of cellular bulkheads.
- b) The current design method overestimates the earthpressure acting on back face of cells and underestimates that on front face of embedded part.
- c) When the ground acceleration increases, the mass of cell fill which contributes to the inertia force decreases apparently.
- d) The analytical method using spring-solid cell model as shown in Fig.15 gives good agreement with experimental results. Therefore, this method is useful for evaluation of earthquake stability of steel plate cellular bulkheads.

## 9. ASEISMICITY OF IMPROVED GROUND

In Japan, Deep Mixing Method (D.M.M) was recently developed and have been applied as a new soil improvement technique to soft clay

ground. Fig.16 shows the idea of improvement by D.M.M. By this method, the stabilizing agent such as a cement slurry is forced into soft clay ground and mixed with soft soil to change it into hard treated soil at a construction site. Shear strength and Young's modulus of the treated soil are extremely higher than those of the untreated soil. In the present earthquake resistant design procedure, the improved ground is considered to be rigid buried structure. However, dynamic behavior of this special type of the ground is not always made clear. In order to rationalize the earthquake resistant design procedure, the shaking table tests, the computer simulations and the earthquake observation at the prototype ground have been carried out.

A series of model tests using the shaking table were carried out to the wall type improved ground.<sup>19)</sup> The experimental results and the calculated results by the present design procedure are summarized as follows;

- a) Vibration characteristics of the untreated soil between the treated walls are the same as those of the treated walls.
- b) Improved ground behaves like a rigid body. Distribution of vertical dynamic pressure beneath the improved ground indicates a rocking vibration of the improved ground.
- c) The experimental results were analyzed using the acceleration and the lateral earthpressure observed in the vibration tests. It was found that the stability of the wall type improved ground touched directly on rigid layer was able to be estimated by the present design procedure.

Results of earthquake observation, which has been carried out at Daikoku island in Yokohama port, were analyzed.<sup>20)</sup> The dimension of improved ground is 57 m wide and 37 m deep. The base ground of improved ground is soft clay from -49 m to -73m. As the bottom of improved ground dose not touch to rigid layer, this is called Floating type. The dynamic behavior of this improved ground was studied by using records from 33 earthquake events. The results of observation are summarized as follows;

- a) When the acceleration of improved ground indicates maximum value, vibration mode of original soft ground was the second or third mode. Its phenomenon affects to restrain vibration of improved ground.
- b) Dynamic behavior of the floating type improved ground was the same as that of original ground in low frequency range, but in high frequency range behavior of improved ground was different from that of original ground.
- c) The horizontal translation motion at the gravity center of improved ground was dominant in horizontal acceleration of improved ground.
- d) FEM analysis using equivalent linear method can explain results of observation.

## CONCLUDING REMARKS

The present state of the earthquake engineering to port and harbour in Japan was introduced. It is expected still more that port structures will become large-sized, and will be constructed in poor grounds and deep sea sites, for responding to social demands. In the present design procedures it is assumed that port structures do not take displacement at all. However, in order to overcome above-mentioned circumstances, it is necessary to be introduced in the design that some amount of displacement are allowed, as far as structures are stable and fulfill its function.

## REFERENCES

- 1) S.Hayashi, K.Kubo and A.Nakase: Damage to Harbour Structures by the Niigata Earthquake, Soils and Foundations, Vol.6, NO.1, Jan.1966.
- 2) S.Hayashi and T.Katayama: Damage to Harbour Structures by the Tokachi-oki Earthquake, Soils and Foundations, Vol.10, No.2, June 1970.
- 3) H.Tsuchida and S.Noda: Damage to Port Structures by the 1978 Miyagi-ken-oki Earthquake, 11th Joint Meeting, U.S.-Japan Panel on Wind and Seismic Effects, UJNR, Sept.1979.
- 4) S.Noda, T.Inatomi and H.Tsuchida: Damage to Port Facilities due to Liquefaction during the Nihonkai-chubu Earthquake, 1983, 16th Joint Meeting, PWSE, UJNR, May, 1984.
- 5) S.Hayashi, H.Tsuchida and S.Noda: Recent Revision of Design Standards on Seismic Effects for Port and Harbour Structures, 7th Joint Meeting, PWSE, UJNR, May 1975.
- 6) E.Kurata, S.Iai and S.Noda: Annual Report on Strong-Motion Earthquake Records in Japanese Ports (1986), Technical Note of PHRI, No.588, June 1987.
- 7) S.Noda, E.Kurata and H.Tsuchida: Dense Instrument Arrays of the Port and Harbour Research Institute for Observing Earthquake Motion, 13th Joint Meeting, PWSE, UJNR, May 1981.
- 8) S.Hayashi, H.Tsuchida and E.Kurata: Average Response Spectra for Various Subsoil Conditions, 3rd Joint Meeting, PWSE, UJNR, May 1971.
- 9) T.Uwabe, S.Noda, E.Kurata and S.Hayashi: Characteristics of Vertical Components of Strong Motion Accelerograms, 9th Joint Meeting, PWSE, UJNR, May 1977.
- 10) H.Tsuchida, S.Noda, S.Iai and E.Kurata: Analysis of Earthquake Ground Motion Records from Two Dimensional Seismometer Array, 15th Joint Meeting, PWSE, UJNR, May 1983.
- 11) H.Tsuchida and S.Hayashi: Estimation of Liquefaction Potential of Sandy Soils, 3rd Joint Meeting, PWSE, UJNR, May 1971.
- 12) S.Iai, H.Tsuchida and S.Noda: A New Criterion for Assessing Liquefaction Potential, 18th Joint Meeting, PWSE, UJNR, May 1986.
- 13) S.Iai, K.Koizumi and E.Kurata: Basic Consideration for Designing the Area of the Ground Compaction as a Remedial Measure against Liquefaction, Technical Note of PHRI, No.590, June 1987.
- 14) T.Uwabe, S.Noda and H.Tsuchida: Coupled Hydrodynamic Response Characteristics and Water Pressures of Large Composite Breakwaters, 14th Joint Meeting, PWSE, UJNR, May 1982.
- 15) T.Uwabe and H.Tsuchida: Hydrodynamic Response Analysis based on Strong-Motion Earthquake Records of Fill Type Breakwater, Ocean Space Utilization '85, June 1985.
- 16) S.Hayashi, S.Noda and H.Tsuchida: Relation between Seismic Coefficient and Ground acceleration for Gravity Quaywall, 8th Joint Meeting, PWSE, UJNR, May 1976.
- 17) S.Hayashi, H.Tsuchida and T.Inatomi: Inelastic Response of Steel Pile Structure and its Seismic Stability, 4th Joint Meeting, PWSE, UJNR, May 1972.
- 18) S.Noda, S.Kitazawa, T.Iida, N.Mori and H.Tabuchi: An Experimental Study on the Earthquake Resistance of Steel Plate Cellular Bulkheads with Embedment, 8th WCEE, July 1984.
- 19) T.Inatomi, H.Tsuchida and S.Noda: An Experimental Study on the Earthquake Resistance of Wall Type Improved Ground by Deep Mixing Method: 16th Joint Meeting, PWSE, UJNR, May 1984.
- 20) T.Inatomi, M.Kazama and K.Ohtsuka: Observation and Analysis of Seismic Response of Floating Type Improved Ground by Deep Mixing Method, Report of PHRI, Vol.25, No.4, Dec.1986.

Earthquake	Magnitude	Port	Epicentral Distance (km)	Ground	Maximum Acceleration (Gal)	Duration (20.05G) (second)	Liquefaction	Damage Cost (million yen)
1964 Niigata	7.5	Niigata	50	Sand	159	(26)	Occur	21,800(49,700)*
1968 Tokachi-Oki	7.9	Hachinohe	68	Sand	233	59	Not occur	890(1,980)*
1973 Nemurohanto-Oki	7.4	Kushiro	129	Sand	164	38	Not occur	10(20)*
		Hanasaki	46	Sand	280(Estimated)		Not occur	420(720)*
1978 Miyagiken-Oki	7.4	Shiogama	100	Clay	273	21	Not occur	160
		Ishinomaki	84	Sand	196-313(Estimated)		Occur	3,008
1982 Urakawa-Oki	7.3	Urakawa	20	Rock			Not occur	240
		Muroran	136	Sand	164	16	Not occur	120
1983 Nipponkai-Chubu	7.7	Akita	105	Sand	205	50	Occur	6,400
		Noshiro	111	Sand	218-249(Estimated)		Occur	670

(\*) : Converted cost in 1980

Table 1 Damage Cost and Liquefaction in Past Earthquakes

Liquefaction	Damage	
	Not Damaged or Slightly Damaged	Severely Damaged
Certainly Liquefied		Gaiko -13m, Ohama No.2, Nakajima No.1 Nakajima No.2, Kita A, Minami D, Minami -4m, Mukaihama No.3
Probably Liquefied		Ohama No.3, Nakajima No.3, Mukaihama No.1, Mukaihama No.2
Partly Liquefied	Mukaihama No.1, Mukaihama No.2, Terauchi	
Not Liquefied	Ohama No.1	

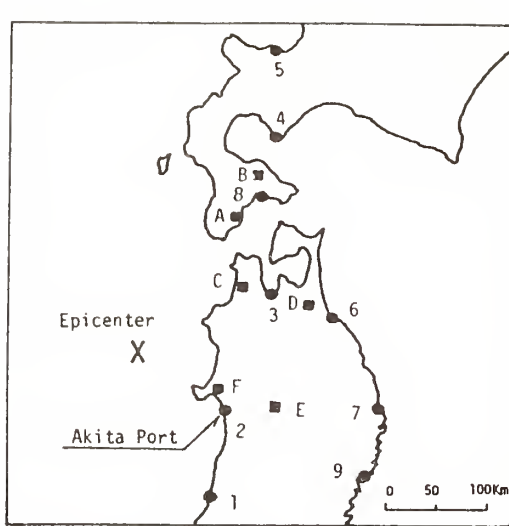
Table 2 Damage of Facilities and Case of Liquefaction (Akita Port)

Classification	1st kind	2nd kind	3rd kind
Factor	0.8	1.0	1.2

Table 3 Factor for Subsoil Condition

Thickness of quaternary deposit	Gravel	Sand or clay	Soft ground
Less than 5 m	1st kind	1st kind	2nd kind
5~25 m	1st kind	2nd kind	3rd kind
More than 25 m	2nd kind	3rd kind	3rd kind

Table 4 Classification of Subsoil



Stations of PHRI	Max. Acceleration (Gal)		
	NS	EW	UD
1. Sakata-S	36	45	15
2. Akita-S	190	205	41
3. Aomori-S	95	118	--
4. Muroran-S	26	21	11
5. Otaru-S	6	6	5
6. Hachinohe-S	20	22	14
7. Miyako-S	8	8	3
B. Hakodate-M	59	59	44
9. Ofunato-Bochi-S	6	6	4
Stations of Other Organizations.			
A. Nanamine Bridge *	260	275	88
B. Kantorizaki Bridge*	125	128	50
C. Tsugaru Bridge*	270	245	180
D. Anegasaki**	119	110	63
E. Takarakaze Bridge*	90	100	30
F. Hachirogata*	138	168	100
*PWRI Ministry of Construction			
**RTRI, Japanese National Railways			

Fig.1 Max. Ground Acc. at Observation Stations (Nihonkai-chubu Earthquake)

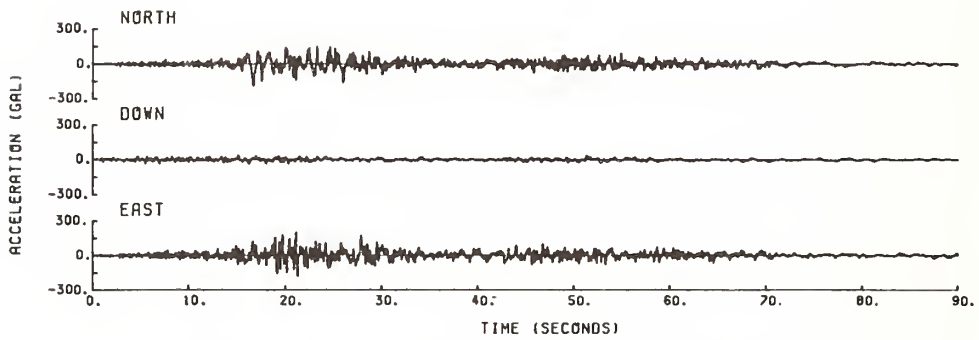


Fig.2 Accelerograms of Nihonkai-chubu Earthquake (Akita Port)

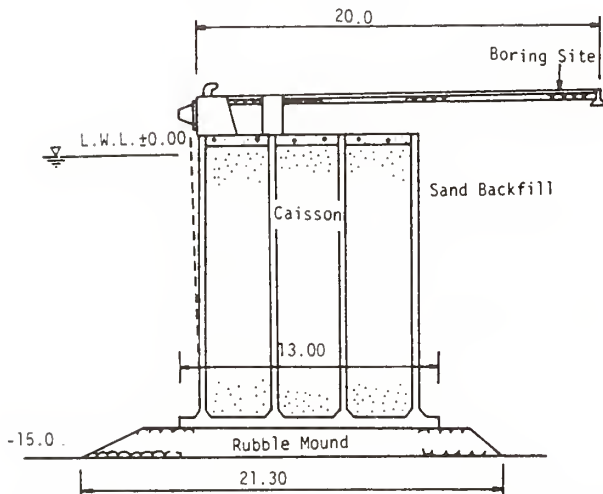


Fig.3 Cross Section of Caisson Type Quaywall (Akita Port)

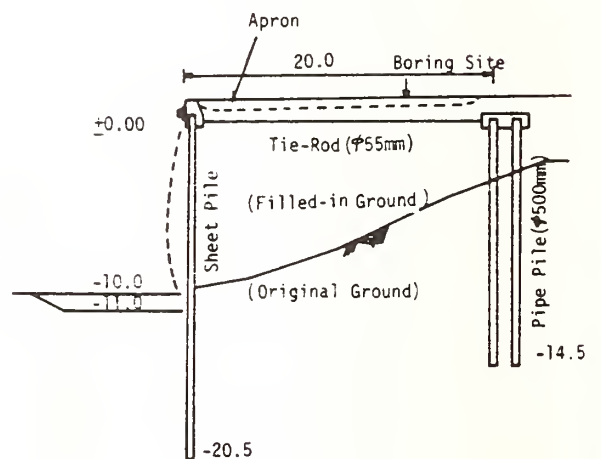


Fig.4 Cross Section of Sheetpile Quaywall (Akita Port)

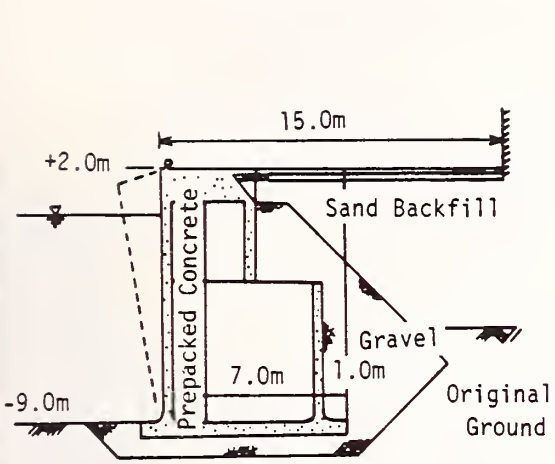


Fig.5 Cross Section of Cellular block Quaywall (Akita Port)

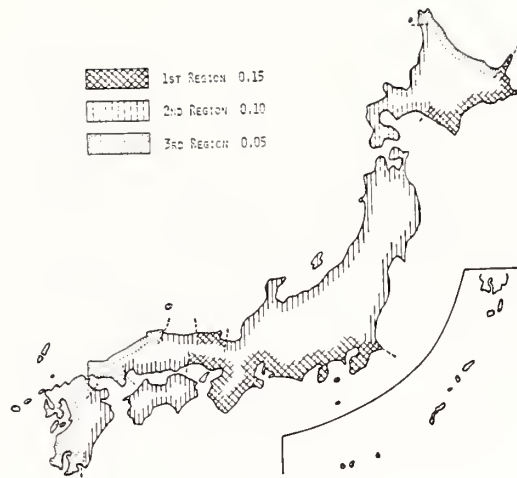


Fig.6 Seismic Zoning Map for Port Structures



Fig.7 Strong Motion Observation Stations

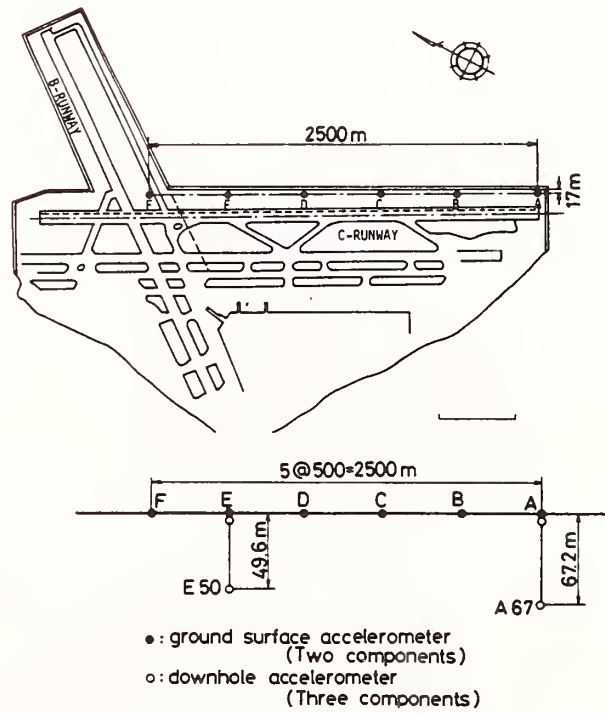


Fig.8 Deployment of Seismometers (Haneda Airport)

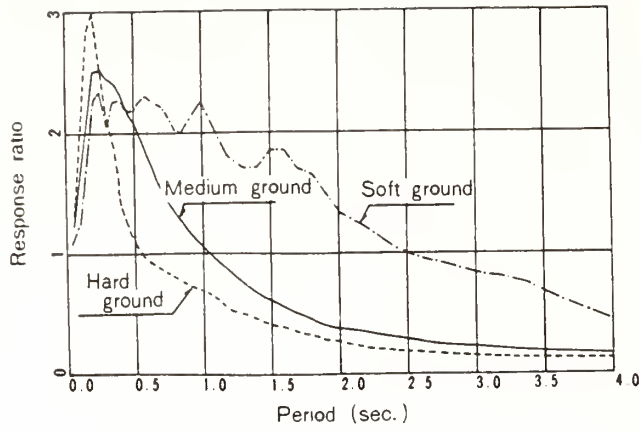


Fig.9 Average Response Spectra ( $h=0.05$ )

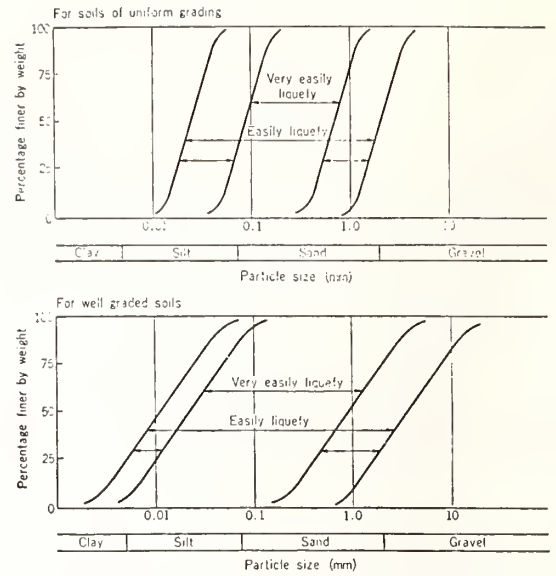
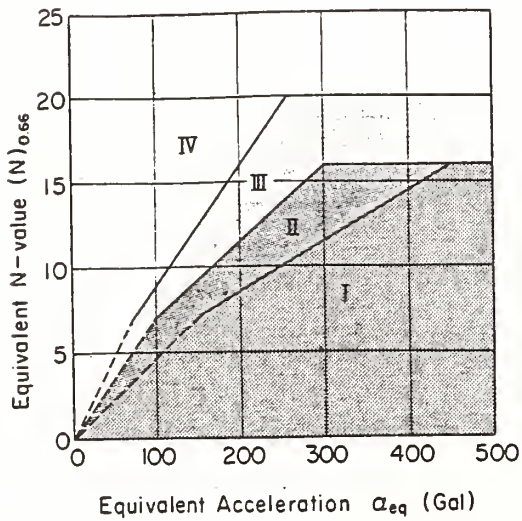


Fig.10 Ranges of Grain Size Distribution Curves of Liquefiable Soils



Region I: Liquefaction takes place  
 Region II: Liquefaction likely takes place  
 Region III: Liquefaction does not likely take place  
 Region IV: Liquefaction does not take place

Fig.11 Chart for Assessing Liquefaction Potential (the 1985 Criterion)

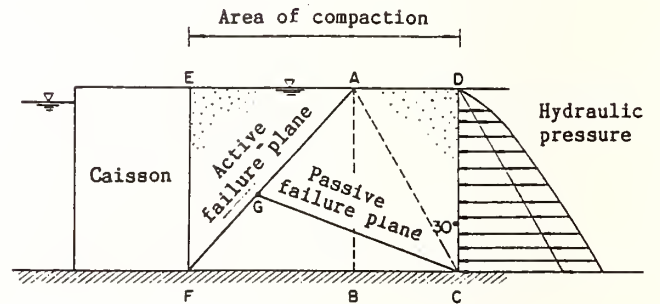


Fig.12 Area of Ground Compaction against Liquefaction

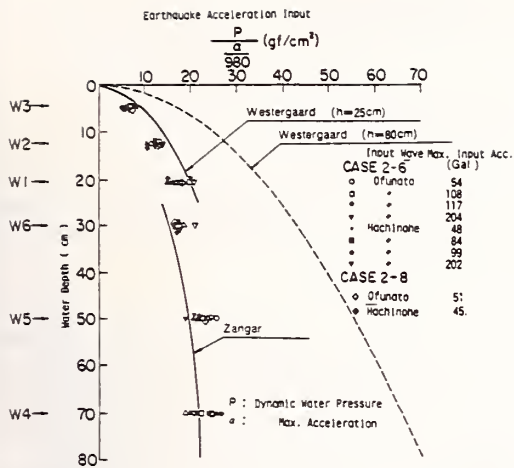


Fig.13 Dynamic Water Pressures on Wall of Breakwater

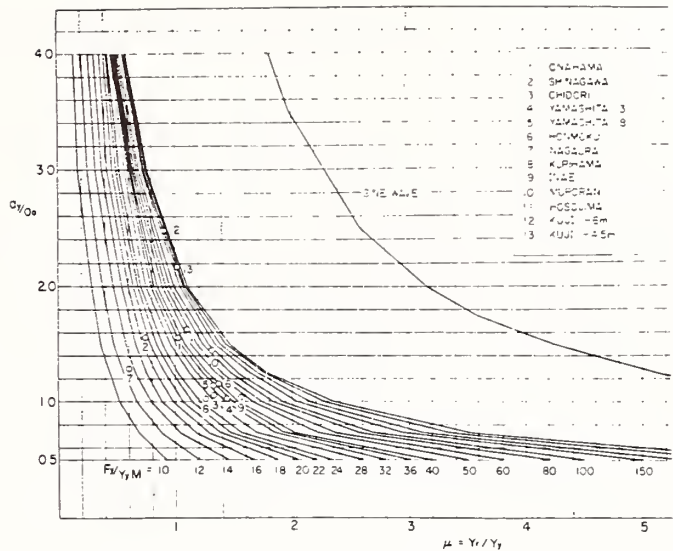


Fig.14 Generalized Curves for Ductility Factor of Steel Piled Pier

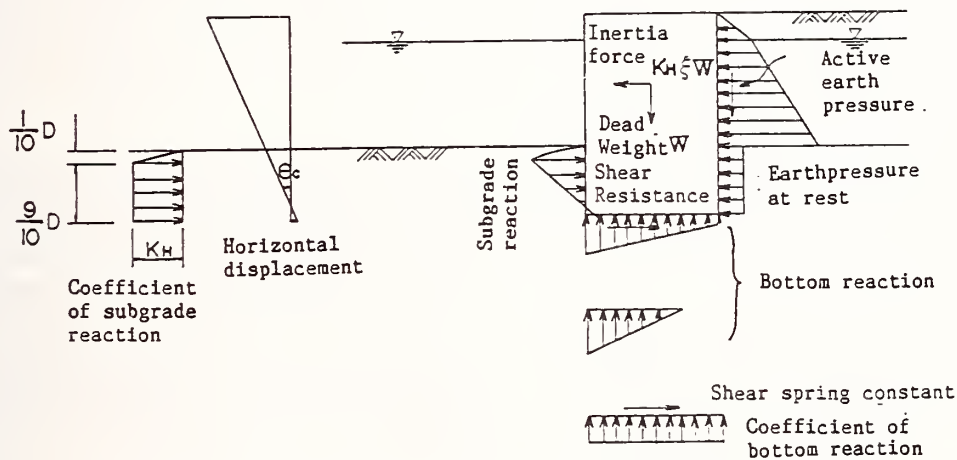


Fig.15 Calculation Model of Steel Plate Cellular Bulkhead

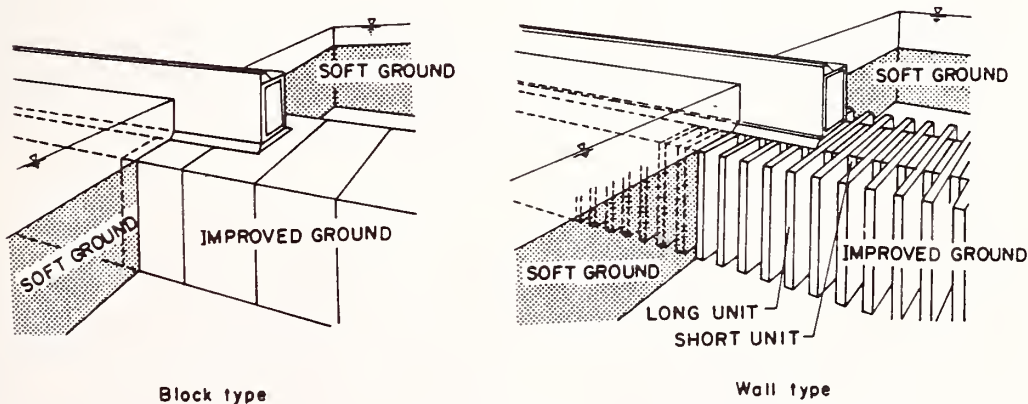


Fig.16 Improved Ground by Deep Mixing Method

# Overburden Correction for Blowcounts in Gravels

by

Mary Ellen Hynes-Griffin<sup>1</sup> and A. G. Franklin<sup>1</sup>

## 1. INTRODUCTION

Concern for liquefaction in gravelly soils is a fairly recent development in geotechnical earthquake engineering, as it had been long assumed that such soils could not develop high excess pore pressures because of their permeability. Recent laboratory studies, re-examination of past field occurrences of ground instability, and new occurrences of liquefaction in gravelly soils have all contributed to an awareness that these soils may be vulnerable under unfavorable circumstances (low density, sufficiently strong ground motions, impeded drainage.)

Early laboratory testing of the cyclic strength of gravelly soils (e.g. Lee and Fitton, 1968; Wong, et al., 1974) tended to show that liquefaction resistance increased with increasing grain size. These results were erroneous because of the effects of membrane compliance in the cyclic triaxial test, which permitted partially drained conditions to occur during the test (Martin, et al., 1978; Finn, 1981; Hynes-Griffin, 1988). When these effects are accounted for, the liquefaction resistance of gravels under undrained conditions appears to be not greatly different from that of sands.

Notable field occurrences of liquefaction-related ground instability in gravels or gravelly soils include liquefaction and surface boils in gravelly sands of an alluvial fan deposit during the 1948 Fukuï earthquake (Ishihara, 1971, 1985); the flow slide in gravelly sand and sandy gravel zones at Valdez, Alaska, during the 1964 Good Friday earthquake (Coulter and Migliaccio, 1966); the liquefaction-induced flow slide in the upstream sand-and-gravel shell of Baihe Dam during the Tangshan earthquake of 1976 (Liu, et al., 1980; Wang, 1984); and most recently, surface boils, lateral spreading, and flow sliding in gravelly alluvial fan deposits during the 1984 Mount Borah, Idaho earthquake (Andrus, et al., 1986; Youd, et al., 1985).

Because of the great difficulties in sampling gravelly soils and testing them in the laboratory, an in situ test analogous to the SPT test for liquefaction resistance evaluation in sands is highly desirable; and it has recently become available with the development of the Becker Hammer Test (Harder and Seed, 1986). Corrected values of the Becker Hammer blow count can be used to obtain equivalent Standard Penetration Test (SPT) blow count values, and it is assumed that these values can be used in the same way as conventional SPT blow counts to evaluate liquefaction susceptibility, with the procedure described by Seed, et al. (1984). This procedure

requires that the penetration resistance be corrected for the effect of overburden pressure.

## 2. THE BECKER HAMMER TEST

The Becker Hammer Drill, shown in Figure 1, uses a double-acting diesel hammer to drive a double-walled casing into the ground. The number of blows required to achieve each foot of penetration is recorded as the uncorrected blow count, thus producing a continuous log of penetration resistance versus depth. Samples of the soil can be obtained if the test is performed with an open-ended bit at the end of the casing. Compressed air is circulated down the annulus of the double casing and up the inner casing to carry soil particles entering the casing to the surface. For liquefaction evaluations, it is considered preferable to use a closed-end bit, because the open-end bit yields more erratic blow counts. This, of course, precludes the recovery of samples.

Corrections to the raw blow counts can be made to account for variations in drive energy due to throttle settings, atmospheric pressure, equipment differences, and other variables; these are described in detail by Harder and Seed (1986). The blow counts thus obtained have been correlated with  $N_{60}$  values obtained from the SPT in soils where both methods could be used (sands and slightly gravelly sands). In this manner, values of equivalent  $N_{60}$  can be obtained for liquefaction evaluations in soils which cannot be tested with the SPT.

Studies to determine energy and overburden correction have focused mainly on sands and silty sands. Overburden correction procedures for the equivalent SPT N-values in gravels have not been thoroughly researched, but trends can be observed from the work that has been performed on sands. These trends will be examined in this paper and recommended curves for overburden correction of translated blowcounts in gravels will be presented.

## 3. OVERBURDEN CORRECTIONS

### Trends from SPT and CPT Data

The empirically based procedures to evaluate liquefaction resistance and residual strength developed by Professor H. B. Seed and his colleagues at the University of California, Berkeley (Seed, et al., 1984) relate liquefaction resistance and residual strength to energy and

1. U. S. Army Engineer Waterways Experiment Station Vicksburg, Mississippi

overburden corrected blowcounts,  $(N_1)_{60}$ . That is, SPT blow counts corrected to the values that would presumably have been obtained in the same soil under an overburden pressure of 1 ton per square foot (1 kilogram per square centimeter), and with a hammer/drive assembly that delivered 60% of the theoretical free-fall energy to the top of the drill rod string. The overburden correction can be made by the relation

$$(N_1)_{60} = C_N \times N_{60} \quad (1)$$

where  $N_{60}$  is the blow count for 60% energy efficiency and  $C_N$  is the overburden correction factor, which is obtained from an empirically derived plot of  $C_N$  versus overburden pressure.

Laboratory test results on the SPT indicate that the overburden correction is a function of relative density and grain size distribution of the soil. Figure 2 shows the  $C_N$  versus overburden pressure curves recommended by Seed et al. (1983) for sands; these are derived from laboratory tests by Marcuson and Bieganousky (1977). The mean of the two curves can be described well by the equation

$$C_N = (\sigma'_v)^{-n} \quad (2)$$

where  $\sigma'_v$  is the effective overburden pressure, in tons per square foot or kilograms per square centimeter, and  $n = 0.5$ . The loose sand curve, for relative density in the range of 40 to 60 percent, corresponds approximately to  $n = 0.55$  and the dense sand curve, for relative density of 60 to 80 per cent, to  $n = 0.45$ .

Recently published work by Skempton (1986) illustrates the trend of lower  $n$  with increasing density and larger grain size. Skempton's curves, shown in Figure 3, can be described well by Equation 2, with  $n$  approximately equal to 0.45 for the dashed curve, representing "dense coarse sands," and 0.55 for the solid curve, representing "fine sands of medium relative density."

In the interpretation of Cone Penetration Test (CPT) data, the use of the relationship shown in Equation 2 to describe the dependence of the cone tip resistance on effective overburden pressure has been shown by Olsen (1988) to be a powerful tool for the estimation of soil characteristics. Olsen's Soil Characterization Chart, shown in Figure 4, is organized around contours of  $n$ , which are the basis for determination of soil classification<sup>2</sup>. These contours show a trend of values of the exponent  $n$  that decrease from about unity at the silt-clay boundary to less than 0.6 in soils coarser than sand. Values of  $n$  are higher, however, for the CPT than for the SPT in similar soils; which is to say that the penetration resistance of the cone penetrometer is more strongly affected by overburden pressure than that of the SPT. One should also note that the exponent  $n$  used with the SPT is a function of relative density, while that used with the CPT is not. Thus the two are not entirely equivalent.

Data for a liquefaction evaluation were obtained in gravelly alluvium of an ancient channel of the American River, in California. These gold-bearing alluvial deposits were widely worked during the late 19th and early 20th centuries to extract their gold content, and subsequently re-deposited in the channels. Dredging was generally confined to the deeper parts of the channels. Typically, the gravels now present in the shallow parts of the channels are ancient (Pleistocene) alluvial deposits, and in the deeper parts, eighty-year-old dredge tailings, placed by dumping and by conveyer belt in and around the dredge pond. Becker Hammer Tests were performed at several locations in the dredge tailings and in the undisturbed alluvium at a site in the American River Valley. Samples from test pits indicated that the mean particle size,  $D_{50}$ , of the dredge tailings was typically in the range of 30 to 50 mm, and averaged about 40 mm. The  $D_{50}$  of the gravels in the undisturbed alluvium was in the range of 25 to 35 mm and averaged about 30 mm. The relative density of the dredge tailings is typically 35 to 40 percent. From indirect evidence, the relative density of the undisturbed alluvium is estimated to exceed 75 percent.

The laboratory test data of Marcuson and Bieganousky (1977) included tests on three sands with  $D_{50}$  varying from 0.2 mm to 2 mm. An example is shown in Figure 5, which gives  $C_N$  versus  $D_{50}$  data for the three sands at a relative density of 50 percent and under an effective overburden pressure of 3 tons per square foot (shown in the figure as 6 kips per square foot). Extrapolation of the trend of those data to a  $D_{50}$  of 40 mm suggests a  $C_N$  value of about 0.7. This, in turn, implies a value of approximately 0.34 for  $n$ .

These and other data from Marcuson and Bieganousky are replotted in Figure 6 in the form of  $n$  versus  $D_{50}$  for relative densities between 30 and 90 percent. Also shown is the trend observed in Olsen's CPT chart, using mean grain size values estimated from the soil classifications associated with the contours of  $n$ ; and points from the data of Skempton (1986) and Peck and Bazaraa (1969). The trends shown by these data, extrapolated to gravel sizes, imply two things: that  $n$  decreases with increasing grain size, and that the influence of relative density on  $n$  becomes relatively smaller in the extremely coarse soils. Around a  $D_{50}$  of 40 mm, the mean grain size in the dredge tailings,  $n$  is in the range of about 0.25 to 0.40 for loose to medium dense materials. A curve of  $C_N$  versus effective overburden pressure based on  $n=0.34$  was chosen for use with the American River dredge tailings. This curve is

2. Points are plotted on this chart iteratively, beginning with known values of cone tip resistance, sleeve friction, and effective overburden pressure, and an initial guessed value for  $n$ .

shown in Figure 7. The curves recommended by Seed, et al. (1983) for sands are also shown for comparison.

Figure 8 shows an assemblage of several Becker Hammer soundings, made with a closed-end bit, at various locations in the American River dredge tailings. All corrections have been applied to obtain equivalent  $(N_1)_{60}$  values, including overburden corrections using  $n = 0.34$ . For comparison, Becker Hammer soundings made in the undisturbed alluvium are shown in Figure 9, with the same corrections. The upper 10 feet of soil above the gravelly alluvium is clay; this interval shows relatively low blow counts. Below 25 feet depth, the soundings are in the bedrock, a weathered schist.

#### Discussion

In an originally homogeneous deposit of granular soil, there are two conceptually distinct effects that will act to increase the penetration resistance with depth. One of these is the overburden pressure. The other is the structural changes produced by the overburden pressure, acting over time; i.e. consolidation, cementation, and so on. These may be referred to, loosely, as diagenetic effects. The overburden pressure effect and the diagenetic effects, however distinct in principle, are very difficult to separate in data from field tests. The best opportunities to do this would be to test new deposits in which diagenetic effects have not had time to develop, or to do field tests in an ancient deposit under varied conditions of effective overburden pressure, such as would be caused by variations in the elevation of the ground water table.

The sounding curves in Figure 8 show a very slight systematic increase with depth. These eighty-year-old dredge tailing deposits presumably do not have strongly developed diagenetic effects. The weak dependence of the corrected penetration resistance on depth suggests that the depth effects are rather well accounted for by the  $C_N$  correction, which uses  $n = 0.34$ . If there were large diagenetic effects, the corrected curves should show a greater increase in penetration resistance with depth. We may infer either that there are slight diagenetic effects and we have applied about the right correction; or that there are no significant diagenetic effects and we have undercorrected slightly. In terms of the exponent  $n$ , the implication is that the best value for  $n$  in the dredge tailings is about 0.34 or possibly slightly higher.

The soundings in the undisturbed alluvium, shown in Figure 9, show a strong dependence of penetration resistance with depth below the surficial clay layer, even after application of a  $C_N$  correction with  $n = 0.34$ . On the basis of the curves presented in Figure 6, and the estimated relative density of these deposits, a value of 0.34 is probably too high for  $n$ . With a correction using a lower value of  $n$ , the apparent

depth dependence in these soundings would be even more pronounced. The prominent and systematic increase in corrected blow counts with depth suggests that diagenetic effects dominate the penetration resistance in these ancient soils. Unfortunately, there has been no opportunity to test them under conditions of varied ground water level.

#### 4. CONCLUSIONS

Data from several sources have been examined to infer overburden correction curves for penetration resistance in gravelly soils. On the basis of a rather large extrapolation from the overburden corrections for sand sizes, supported by data from several Becker Hammer soundings in gravel-size dredge tailings at one site in California, it is concluded that correction curves of the form of Equation 2 are appropriate, with values of  $n$  in the range of 0.25 to 0.40, for loose to medium dense gravels with  $D_{50}$  of about 40 mm, as shown in Figure 6. Confirmatory research is needed to investigate the extension of observed trends of overburden correction in sands to gravel-size soils. The trend curves for the exponent  $n$  shown in Figure 6 are recommended for provisional use, and as a hypothesis to be tested with new data.

#### 5. ACKNOWLEDGEMENT

The tests described and the resulting data presented herein were obtained from research conducted by the United States Army Corps of Engineers. Permission was granted by the Chief of Engineers to publish this information.

#### 6. REFERENCES

- Andrus, K. D., Youd, T. L., and Carter, R. R. 1986. "Geotechnical Evaluation of a Liquefaction Induced Lateral Spread, Thousand Springs Valley Idaho," Proceedings of the Twenty-Second Annual Symposium on Engineering Geology and Soils Engineering, Boise, Idaho, February 24-26, 1984.
- Coulter, H. W. and Migliaccio, R. R. 1966. "Effects of the Earthquake of March 27, 1964 at Valdez, Alaska," U.S. Geological Survey Professional Paper 542-C.
- Finn, W. D. L. 1981. "Liquefaction Potential: Developments Since 1976," Proceedings, International Conference on Recent Advances in Geotechnical Earthquake Engineering and Soil Dynamics, St. Louis, Vol. II, pp. 655-682.
- Harder, L. F., Jr., and Seed, H.B. 1986. "Determination of Penetration Resistance for Coarse-Grained Soils Using the Becker Hammer Drill," Report No. UCB/EERC-86-08, University of California, Berkeley, California.
- Hynes-Griffin, Mary E. 1988. Pore Water Pressure Generation Characteristics of Gravels under Undrained Cyclic Loading," Research Report (in

preparation), U. S. Army Engineer Waterways Experiment Station, Vicksburg, Mississippi.

Ishihara, K. 1971. "Liquefaction of Subsurface Soil During Earthquakes," Technocrat, Fuji Marketing Research Company, Ltd., Tokyo.

Ishihara, K. 1985. "Stability of Natural Deposits During Earthquakes," Proceedings of the Eleventh International Conference on Soil Mechanics and Foundation Engineering, San Francisco.

Lee, K. L. and Fitton, J. A. 1968. "Factors Affecting the Dynamic Strength of Soil," American Society for Testing and Materials, STP 450, Vibration Effects on Soils and Foundations.

Liu, L., Li, K., and Bing, D. 1980. "Earthquake Damage of Baihe Earth Dam and Liquefaction Characteristics of Sand and Gravel Materials," Proceedings, Seventh World Conference on Earthquake Engineering, Istanbul, Vol. 3, pp. 171-178.

Marcuson, W. F., III, and Bieganousky, W. A. 1977. "Laboratory Standard Penetration Tests on Fine Sands," Journal of the Geotechnical Engineering Division, ASCE, Vol 103, No. GT6, pp. 565-588.

Martin, R. M., Finn, W. D. L., and Seed, H. B. 1978. "Effects of System Compliance on Liquefaction Tests," Journal of the Geotechnical Engineering Division, ASCE, Vol. 104, No. GT4, pp. 463-479.

Olsen, R. S. 1988. "Using the Cone Penetrometer Test (CPT) for Site Characterization by Prediction of SPT Blowcount, Liquefaction, Post-Earthquake Strength, and Maximum Shear Modulus," Proceedings Second ASCE Specialty Conference on Earthquake Engineering and Soil Dynamics, June 27-30, Park City, Utah.

Peck, Ralph B., and Bazaraa, A. R. S. 1969. Discussion on Settlement of Spread Footings on Sand, Journal of the Soil Mechanics and Foundations Division, ASCE, Vol. 95, No. SM3, pp. 905-909.

Seed, H. B., Idriss, I. M., and Arango, I. 1983. "Evaluation of Liquefaction Potential Using Field Performance Data," Journal of the Geotechnical Engineering Division, ASCE, Vol. 109, No. 3, pp. 458-482.

Seed, H. B., Tokimatsu, K., Harder, L. F., and Chung, R. M., 1984. "The Influence of SPT Procedures in Soil Liquefaction Resistance Evaluations," Report No. UCB/EERC-84/15, University of California, Berkeley.

Skempton, A. W. 1986. "Standard Penetration Test Procedures and the Effects in Sands of Overburden Pressure, Relative Density, Particle Size, Ageing, and Overconsolidation," Geotechnique, Vol. XXXVI, No. 3, pp. 425-447.

Wang, Wenshao 1984. "Earthquake Damages to Earth Dams and Levees in Relation to Soil Liquefaction," Proceedings of the International Conference on Case Histories in Geotechnical Engineering, St. Louis.

Wong, R. T., Seed, H. B., and Chan, C. K. 1974. "Liquefaction of Gravelly Soils under Cyclic Loading Conditions," Report No. EERC-74-11, University of California, Berkeley, California.

Youd, T. L., Harp, E. L., Keefer, D. K., and Wilson, R. C. 1985. "The Borah Peak, Idaho Earthquake of October 28, 1983 -- Liquefaction," Earthquake Spectra, Earthquake Engineering Research Institute, Vol. 2, No. 1.

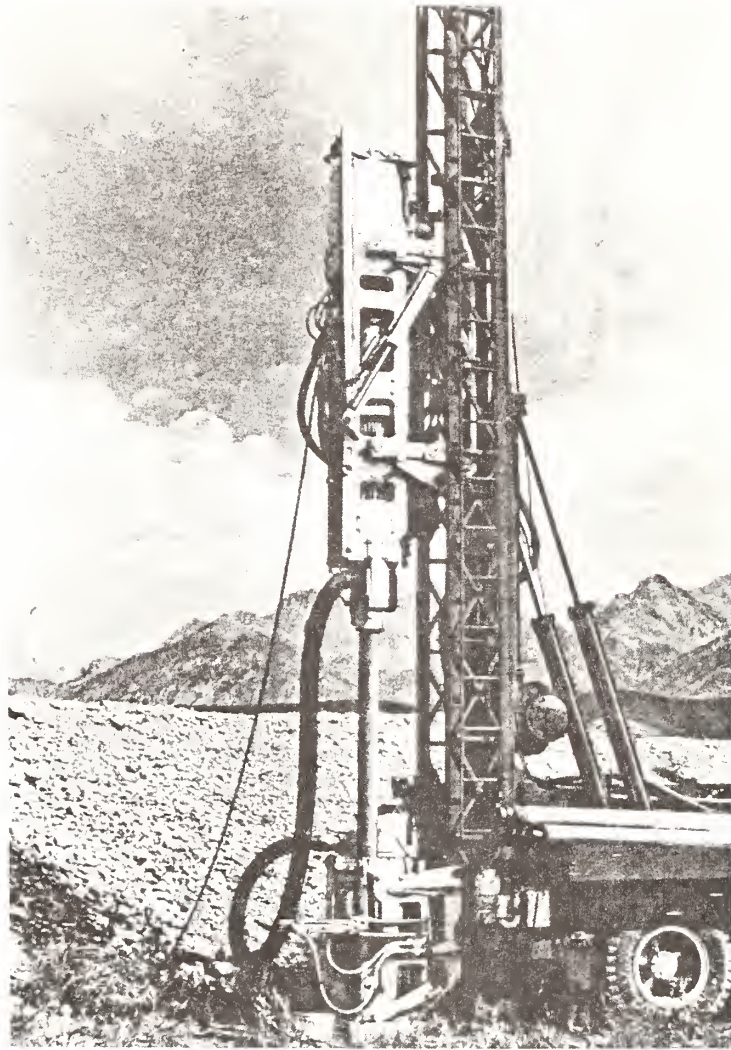


Figure 1. Photograph of Becker Hammer Drill Rig  
(From Harder and Seed, 1986)

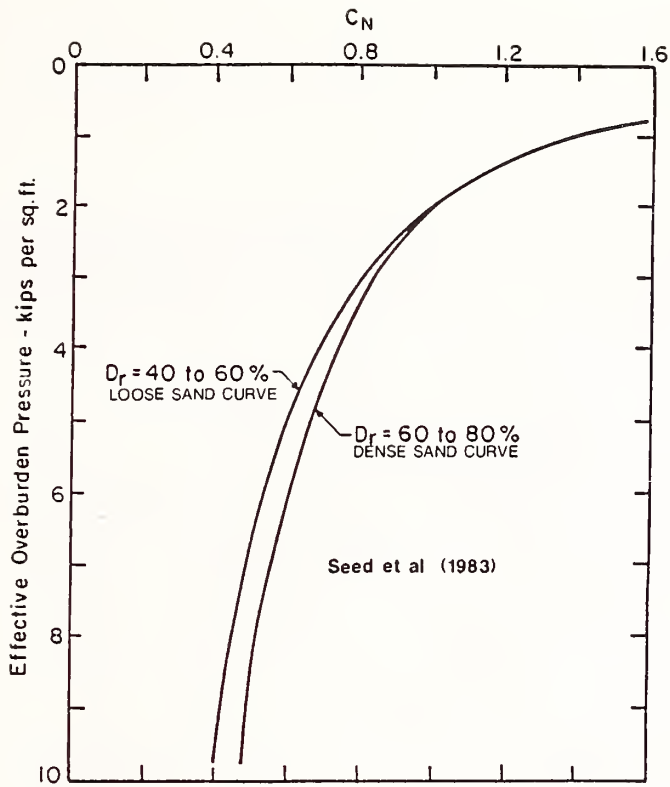


Figure 2. Overburden correction curves for loose and dense sands (from Seed, et al. 1983)

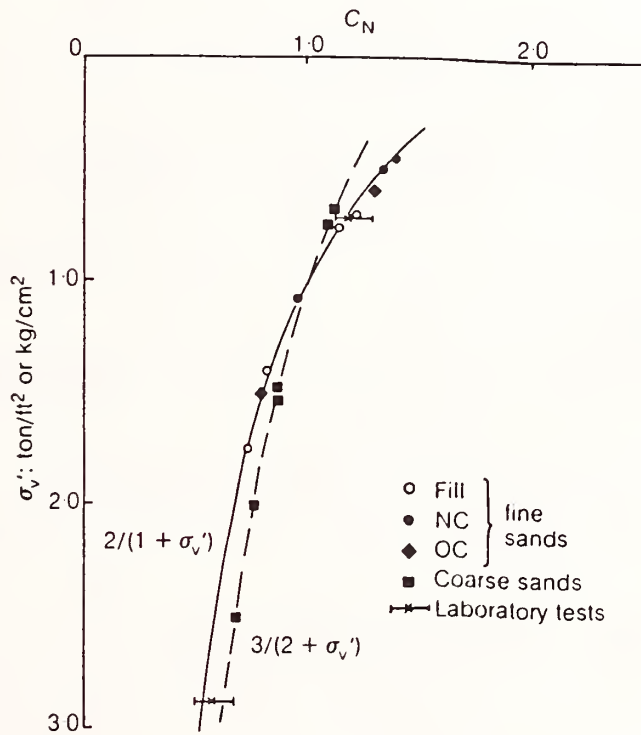
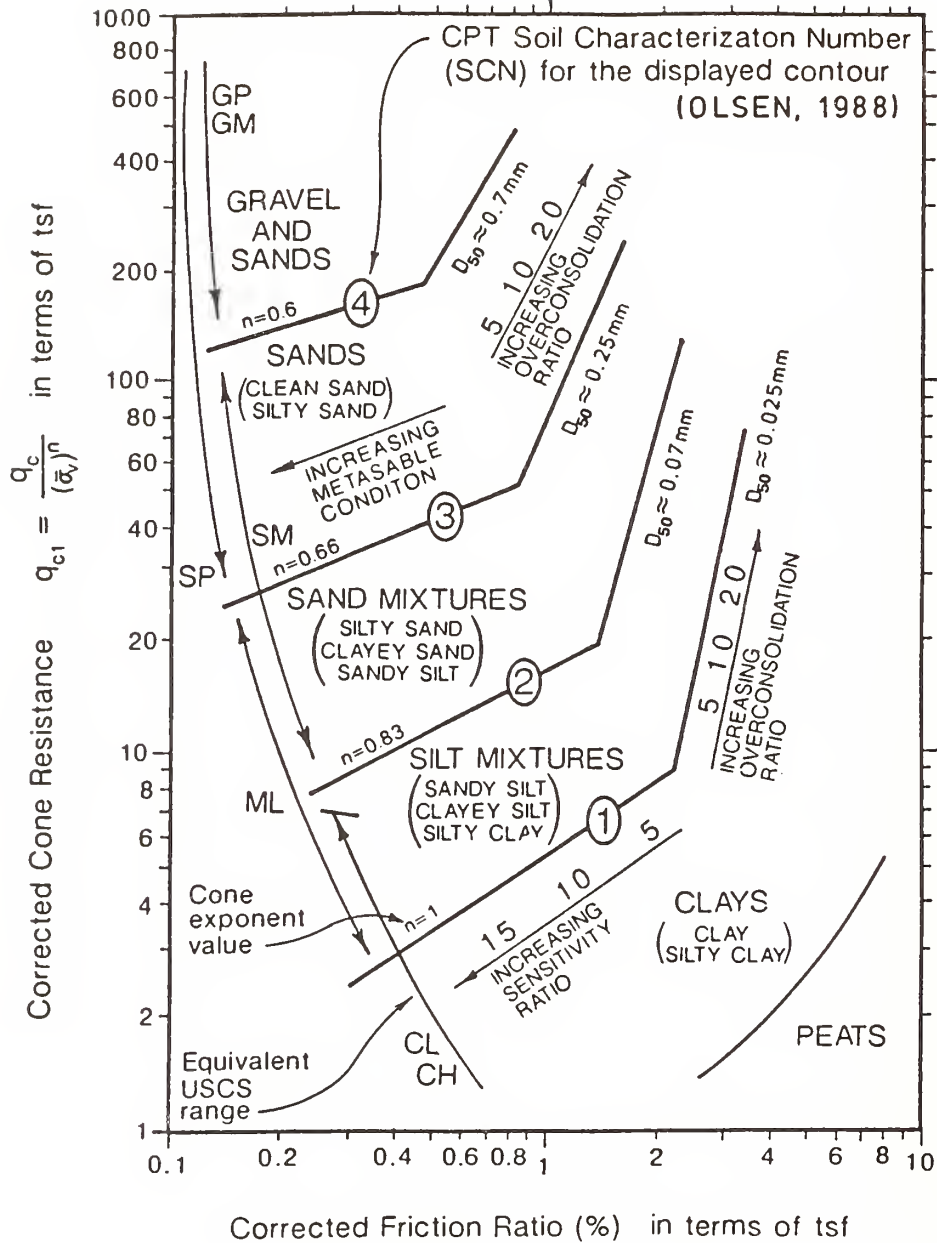


Figure 3. Overburden correction curves for fine and coarse sands (from Skempton, 1986)



$$FR_1 = \frac{f_{s1}}{q_{c1}} 100 = \frac{f_s / \bar{\sigma}_v}{q_c / (\bar{\sigma}_v)^n} 100 = \frac{f_s}{q_c} \frac{1}{(\bar{\sigma}_v)^{(1-n)}} 100$$

Figure 4. Soil Characterization Chart for CPT (from Olsen, 1988)

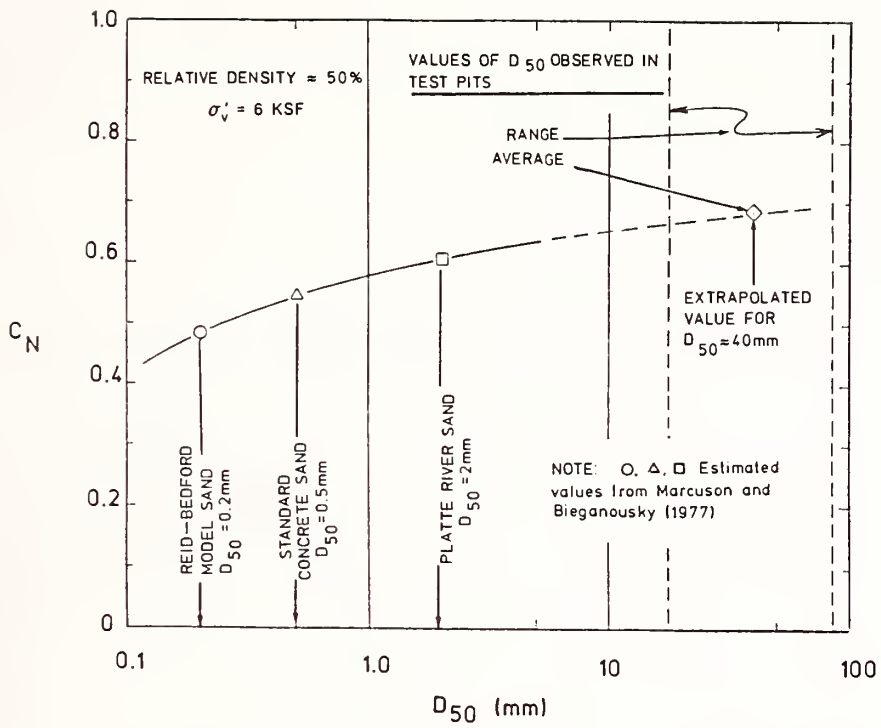


Figure 5. Relationship between  $C_N$  and  $D_{50}$  for an overburden pressure of 6 ksf, based on data from Marcuson and Bieganousky (1977)

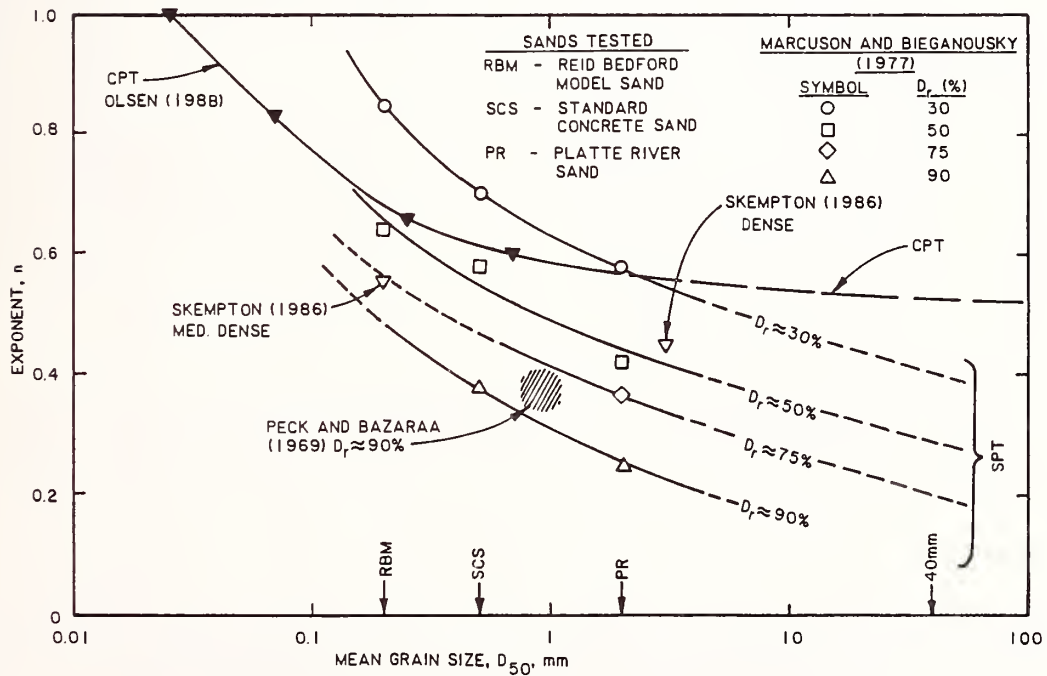


Figure 6. Relationships between "n," mean grain size, and relative density

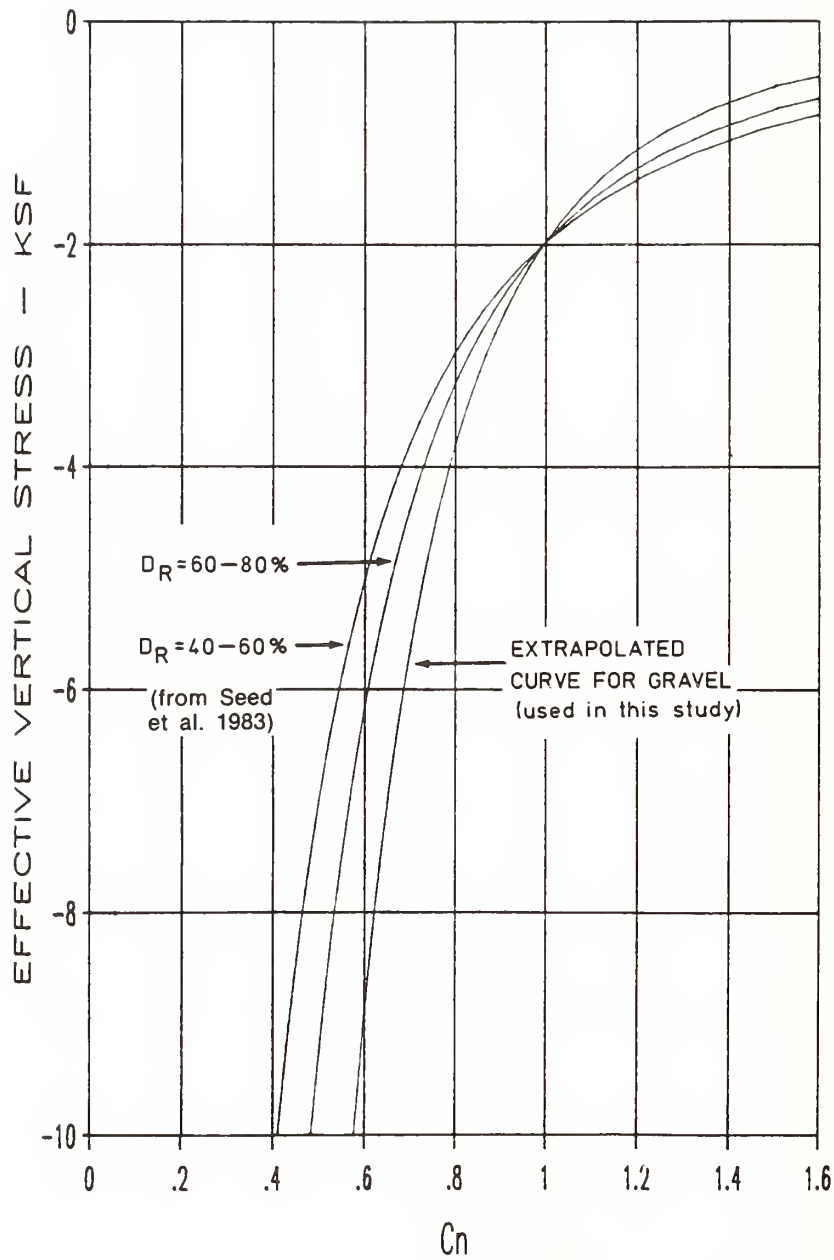


Figure 7. Curve of  $C_N$  vs. effective overburden pressure adopted for dredge tailings, compared with curves recommended for sands by Seed, et al. (1983)

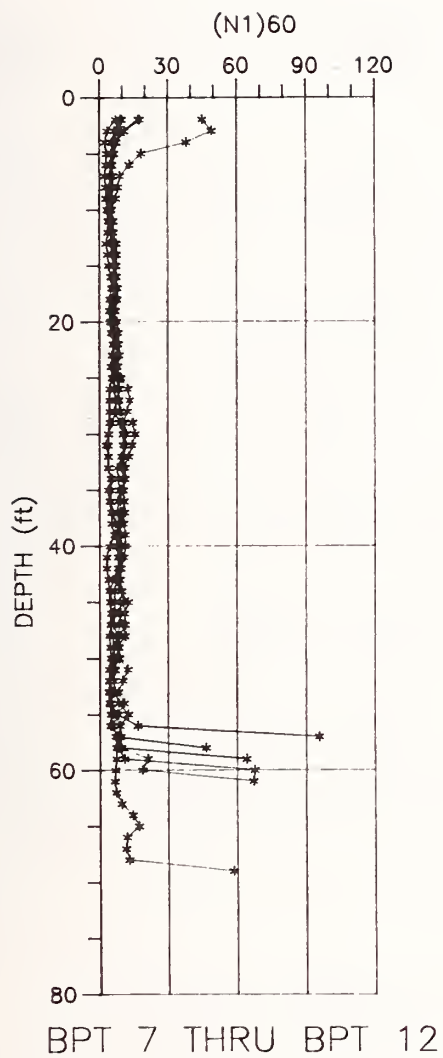


Figure 8. Becker Hammer soundings in dredge tailings of the American River valley

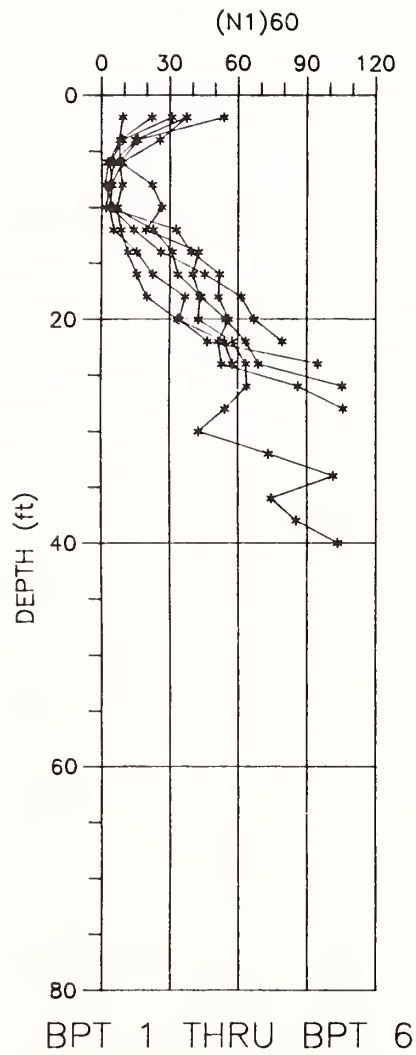


Figure 9. Becker Hammer soundings in undisturbed alluvium of the American River valley

# Sand Liquefaction Tests Using a Geotechnical Dynamic Centrifuge

BY

Yasuyuki Koga<sup>1</sup>, Eiichi Taniguchi<sup>2</sup>,  
Jun-ichi Koseki<sup>3</sup> and Tadashi Morishita<sup>4</sup>

## ABSTRACT

A new geotechnical dynamic centrifuge was constructed at the Public Works Research Institute (PWRI) in 1987. This paper presents the specification of the centrifuge and the results so far obtained using the equipment.

The results of the shaking tests showed that it is important to adjust the apparent permeability by changing the viscosity of the pore fluid when sand liquefaction tests are conducted. They also showed that the amount of excess pore pressure generated by the excitation is affected by the restraint of end walls of the container when a rigid box is used.

KEY WORDS: Geotechnical Centrifuge, Liquefaction

## 1. INTRODUCTION

The mechanical property of soil is significantly affected by the confining pressure arising from the self-weight of soil itself. But it is difficult in scaled model tests under normal gravity to simulate the same stress condition as in the actual ground.

The geotechnical centrifuge which generates a centrifugal acceleration in the model ground has been known as a useful experimental technique to obtain such stress condition, and many centrifuges are now in operation. Some of them have devices to simulate earthquake motions<sup>1)2)3)</sup> although it is difficult to accelerate the model ground dynamically with a high frequency. Tests using a geotechnical dynamic centrifuge have the advantage in time and labor over shaking table tests in addition to the similarity in the stress condition mentioned above.

A new geotechnical dynamic centrifuge was constructed at the Public Works Research Institute (PWRI) in 1987. This paper presents the specifications of the centrifuge, and the results so far obtained using this equipment are also shown.

## 2. SCALING RELATIONS IN CENTRIFUGAL MODELING

If a model ground is built using the same material as that of an actual ground by a scale factor  $1/N$ , a centrifugal acceleration in the model must be  $N$  times  $g$  for the stress condition due to the self-weight of the model to be the same as that of the prototype, where  $g$  is the gravitational acceleration. When the model is accelerated dynamically, the dynamic acceleration must be also  $N$  times as much as the one applied to the prototype.

Table 1 is a summary of the scaling relations<sup>4)</sup> for geotechnical dynamic centrifuge model tests when the above-mentioned condition is achieved. Since the ratio of model to prototype is 1 for both a stress and a strain, the stress-strain relations in the model and the prototype are the same at all equivalent points.

As for time scalings, there is a difference between the one in dynamic terms and the one in diffusion cases, because the former is governed by the equation of motion and the latter by the equation of diffusion. The importance to adjust the difference in time scalings is mentioned in section 4.1.

## 3. EQUIPMENT AND INSTRUMENTATION

A general view of the geotechnical dynamic centrifuge in PWRI is shown in Fig. 1, and its specification is shown in Table 2.

The maximum centrifugal acceleration is 200g in static tests without shaking system. In case of dynamic tests with shaking system, a centrifugal acceleration of 50g is the maximum.

---

<sup>1</sup>Head, Soil Dynamics Division, Construction Equipment and Method Department, Public Works Research Institute, Ministry of Construction

<sup>2</sup>Head, Planning Division, Planning and Research Administration Department, do.

Formerly, Senior Researcher, Soil Dynamics Division, Construction Equipment and Method Department, do.

<sup>3</sup>Researcher, Soil Dynamics Division, Construction Equipment and Method Department, do.

<sup>4</sup>Assistant, Soil Dynamics Division, do.

### 3.1 Radius of the rotor arm

When the rotor arm is rotating with a constant angular velocity, the centrifugal acceleration in the model ground does not have a uniform distribution in the radial direction<sup>5)</sup>. If the height of the container is the same, the error in the centrifugal acceleration decreases as the radius of the rotor increases.

But an enlargement of the equipment is needed to make the radius larger, which will bring disadvantage in the cost of construction and maintenance. The operation of large equipment will take much time and labor.

Taking these aspects into account, a rotor arm with an effective radius of 2m was chosen, where an effective radius is defined as a distance between the axis of the rotation and the middle height of the container.

### 3.2 Hydraulic shaking system

Several shaking systems for a geotechnical centrifuge have been in practical use such as a spring-actuated shaker, a piezoelectric shaker, an explosive shaker and a bumpy road system<sup>1)</sup>.

A hydraulic shaking system was chosen in this centrifuge, because a desired dynamic acceleration and displacement were available with a small actuator, and the frequency of shaking could be controlled easily.

A schematic diagram of the hydraulic shaking system is shown in Fig.2. A hydraulic cylinder actuates the container supported by leaf springs, and the flow of oil to the cylinder is controlled by electro-magnetic servo valve. The pressurized input flow is supplied by an accumulator on the rotor arm, and the exhaust flow is stored in another accumulator. The volume of these accumulator is 6.3 liters, and the maximum shaking duration is about 0.5 seconds per one accumulation with oil pressure of 280 kgf/cm<sup>2</sup>. The other accumulator is connected to the input line to absorb the shock wave in the input flow which occurs when the electro-magnetic valve opens to start shaking.

The direction of shaking corresponds to the horizontal direction in the prototype, and the maximum dynamic acceleration is  $\pm 20g$  when the total weight of the container and the model ground is 100kgf. When a centrifugal acceleration is 50g, a dynamic acceleration of 20g corresponds to that of 0.4g in the prototype.

Both a sinusoidal wave and an irregular wave can be used as an input dynamic acceleration. The frequency of shaking is 50~400 Hz, which

corresponds to 1~8 Hz in the prototype when experiments are conducted with a centrifugal acceleration of 50g.

A performance curve of the shaking system in a sinusoidal shaking is shown in Fig.3. The maximum dynamic acceleration of 20g is available with a shaking frequency of about 140 Hz. Typical records of accelerations measured at the bottom of the container are shown in Fig.4. With a shaking frequency from 100 Hz to 300 Hz sinusoidal waves of good form are available.

In an irregular shaking, a correction of input wave based on a preliminary shaking is needed, because the response characteristics of the shaking system are frequency-dependent. An example of the correction is shown in Fig.5. Fig.5(a) is the result of a preliminary shaking, and Fig.5(b) is the result using a corrected input wave. A desired wave is also shown in both figures.

### 3.3 Data measurement system

A schematic diagram of data measurement system is shown in Fig.6, and the specification of a pore pressure transducer and an accelerometer used in the model ground is shown in Table 3.

In dynamic tests the electric signal outputs of the transducers are transmitted to the control room through slip-rings on the rotating axis. They are recorded temporarily in signal memories as digital data. 16 channels can be used at the same time, and 64,000 points of data can be stored in each channel. The minimum sampling interval is 10  $\mu$  second. A micro-computer is used to analyse the data, and 5-inch floppy disks are used to keep the data.

A high-speed camera can be set on the rotor arm to record the deformation of the model ground visually in dynamic tests. The photographing speed is 3,000 photos per one second at the maximum, and 1,500 photos can be taken continuously at one time. The action of the camera is synchronized with that of the shaking system.

## 4. Experimental Studies

### 4.1 Effect of the viscosity of pore fluid

When dynamic tests using 1/N scaled model are conducted with a centrifugal acceleration of Ng, the time scale factor in dynamic terms is 1/N, and the one in diffusion cases is 1/N<sup>2</sup> as can be seen in Table 1. These two scalings must correspond with each other when combined effects of these phenomena are concerned.

For example, when liquefaction of saturated sand

is studied, the time scaling in diffusion cases is controlled to agree with the one in dynamic terms by means of decreasing the apparent permeability of the model ground. If it is decreased by a scale factor of  $1/N$ , then a diffusional phenomenon proceeds by the time scale factor of  $1/N$  which equals to the one in dynamic terms. The apparent permeability is nearly in inverse proportion to the viscosity of pore fluid, therefore the pore fluid in the model should be  $N$  times as viscous as that of water in the prototype.

Shaking tests using two models of horizontal sand layer were conducted to examine the effect of the viscosity of pore fluid. Model 1-A was saturated with water, and model 1-B with silicone oil.

In both models Toyoura sand was pluviated through the fluid. The relative density of the sand layer of model 1-A was 24%, and that of model 1-B was 42%. The difference in the density may be caused by the difference in the falling speed of the sand particles in the pore fluid which depends on the viscosity of the fluid. After pluviation the pore fluid level was adjusted to the surface of the sand layer and a centrifugal acceleration was increased up to 30g. Then an excitation was conducted with a sinusoidal wave input of 25 cycles. The frequency of the wave was 100Hz, and an average dynamic acceleration was about 5g in both models.

The silicone oil used in model 1-B was 30 times as viscous as water, therefore the time scalings in model 1-B were  $1/30$  in both dynamic terms and diffusion cases. In model 1-A the time scalings did not correspond with each other, and a diffusional phenomenon proceeded 30 times as fast as a dynamic phenomenon did.

The excess pore pressure measured at the depth of 12cm is shown in Fig.7 with the initial effective vertical stress calculated from the unit weight of the sand and the pore fluid. The dynamic acceleration measured at the bottom of the container is also shown. The result of model 1-A is shown in Fig.7(a), and that of model 1-B is shown in Fig.7 (b). In Fig.7(c) the time axis is shortened to show the dissipation of the excess pore pressure in model 1-B.

Obvious difference can be seen in Fig.7 between model 1-A and model 1-B. In model 1-B the state of initial liquefaction is achieved when the excess pore pressure equals to the initial effective vertical stress. The sand layer is much looser in model 1-A than in model 1-B, but the excess pore pressure in model 1-A never reaches the initial

vertical stress. The excess pore pressure dissipates much faster in model 1-A than in model 1-B. The reason for such a difference is that a diffusional phenomenon proceeds much faster in model 1-A than in model 1-B.

Thus, it is important to adjust the apparent permeability of the model ground by changing the viscosity of pore fluid when liquefaction of saturated sand is studied using a geotechnical dynamic centrifuge. The characteristics of the generation and dissipation of the excess pore water pressure in an actual ground may be similar to those obtained in model 1-B. The model ground used in this study was 20cm thick, and the centrifugal acceleration was 30g. Therefore it corresponds to the prototype ground of 6.0m in thickness.

#### 4.2 Effect of the restraint of end walls

When a rigid box is used as a container, shearing deformation of the model ground is restrained by the end walls of the container. The effect of the restraint of end walls on liquefaction of saturated sand is investigated here.

A horizontal sand layer was prepared by pouring Toyoura sand through water in a rigid box of 50cm in length, 30cm in height and 10cm in width. In model 2-B spongy rubbers of 1cm in thickness were put on the end walls of the box to reduce the restraint, and in model 2-A no treatment was made. Water was used as pore fluid, therefore time scalings in dynamic terms and in diffusion cases are different from each other as mentioned in 4.1. Only a qualitative comparison between the two models can be made.

After pluviation the water level was adjusted to the surface of the sand layer, and a centrifugal acceleration was increased up to 50g. Then an excitation was conducted four times with a sinusoidal wave input of 25 cycles. The frequency of the wave was 100Hz. An average dynamic acceleration was about 4g at the first excitation and about 6g at the second excitation in both models.

The excess pore pressure at the second excitation measured at the depth of 12cm is shown in Fig.8 with the initial effective vertical stress calculated from the unit weight of the sand and water. The dynamic acceleration measured at the bottom of the container is also shown. The relative density of the sand layer before the first excitation was almost the same ( 24% ) for the two models. Before the second excitation, it

was 31% in model 2-A and 38% in model 2-B owing to the difference in the amount of the settlement of the sand surface caused by the first excitation.

The result of model 2-A is shown in Fig.8(a), and that of model 2-B is shown in Fig.8(b). The maximum excess pore pressure is higher in model 2-B than in model 2-A although the sand layer is denser in model 2-B. In every case of the four excitations similar results are obtained.

The reason for such difference can be explained as follows. The effect of the restraint of end walls was smaller in model 2-B with spongy rubbers than in model 2-A without them. As a consequence shearing deformation could easily be made in model 2-B than in model 2-A, and that resulted in the difference of the amount of the excess pore pressure between the two models.

Thus, the characteristics of liquefaction of saturated sand are significantly affected by the restraint of end walls of the container when a rigid box is used. To reduce the restraint an enlargement of the box toward the direction of the shaking should be made, or appropriate boundary materials should be placed on the end walls. Stacked ring apparatus<sup>6)</sup> may be effective in simulating a simple shear deformation of a horizontal ground, but the cross section of the ground can not be seen through the front wall of the apparatus.

## 5 CONCLUSIONS

The effects of the viscosity of pore fluid and of the restraint of end walls on the characteristics of liquefaction of saturated sand were studied using a new geotechnical dynamic centrifuge. The result is as follows.

- 1) Correction of the apparent permeability of the model ground by changing the viscosity of pore fluid is necessary to have the same time scalings in dynamic terms and in diffusion cases.
- 2) When a rigid box is used as a container, the restraint of end walls significantly affects the amount of excess pore pressure. Further improvement of the container is needed.

## 6 FUTURE PROBLEM

Fundamental tests are needed to validate the geotechnical dynamic centrifuge in simulating an actual ground during earthquakes. For example, the applicability of scaling laws and the effects of Coriolis force should be studied. And the performance of the miniature transducers used in

the model ground should be tested or improved if necessary.

Furthermore following studies will be made using the equipment.

- 1) Liquefaction of sandy grounds
- 2) Failure and deformation of embankments caused by earthquakes
- 3) Dynamic earth pressure acting on the retaining structures
- 4) Dynamic behavior of foundations

## REFERENCES

- 1) Whitmann, R.V. : Experiments with Earthquake Ground Motion Simulation, Proc. of a Symposium on the Application of Centrifuge Modelling to Geotechnical Design, 1984.
- 2) Saitoh, K. et al. : An Electrohydraulic Device for Shaking Tests in Centrifuge, Proc. of 22th JCSMFE, 1987 (in Japanese).
- 3) Inatomi, T. et al. : Development of a Device for Shaking Tests in Centrifuge, 19th Symposium of Earthquake Engineering, JSCE, 1987 (in Japanese).
- 4) Scott, R.F. : Summary Specialty Session 7, Proc. of Geotechnical Eng. Div. Specialty Conference Earthquake Engineering and Soil Dynamics, 1978.
- 5) Schofield, A.N. : Cambridge Geotechnical Centrifuge Operations, Geotechnique, Vol.30 No.3, 1980.
- 6) Whitmann, R.V. and Lambe, P.C. : Effects of Boundary Conditions upon Centrifuge Experiments Using Ground Motion Simulation, Geotechnical Testing Journal, Vol.9 No.2, 1986.

Table 2. Specification of the Equipment

Effective Rotor Radius	2 m
Maximum Centrifugal Acceleration	200 g ( 50 g in dynamic tests )
Maximum Angular Velocity	300 rpm ( 150 rpm in dynamic tests )
Power of Direct Current Motor	75 kW
Maximum Power of Excitation	$\pm 2,000$ kgf
Maximum Dynamic Acceleration	$\pm 20$ g ( with a total weight of 100 kgf )
Maximum Dynamic Displacement	$\pm 1$ mm
Frequency of Excitation	50 ~ 400 Hz
Wave Form of Excitation	Sinusoidal, Irregular
Inner Size of Container ( length x height x width ) or ( diameter x height )	① 500 x 300 x 100 mm ② 800 x 300 x 100 mm ③ $\phi 300$ x 300 mm
Self Weight of Container	① 83 kgf ② 125 kgf ③ 190 kgf
Maximum Weight of Model Ground	① 30 kgf ② 48 kgf ③ 42 kgf
Slip-rings for Measurement	64 elements
Hydraulic Rotary Joints	4 channels

Table 1. Scaling Relations in Centrifugal Modeling

Quantity	Prototype	Centrifugal Model
Density	1	1
Length	1	1/N
Acceleration (in centrifugal terms)	1	N
(in dynamic terms)	1	N
Mass	1	1/N <sup>3</sup>
Force	1	1/N <sup>2</sup>
Stress	1	1
Strain	1	1
Time (in dynamic terms)	1	1/N
(in diffusion cases)	1	1/N <sup>2</sup>

Table 3. Specification of Transducers Used in the Model Ground

	Pore Pressure Transducer	Accelerometer
Transduction Type	Strain gage type	Piezoelectric type with charge amplifier
Measurement Range	0 ~ 3 kgf/cm <sup>2</sup> ( DC ~ 2,000 Hz )	$\pm 500$ g ( 4 ~ 15,000 Hz )
Output Voltage	15 mV/V F.S.	10 mV/g
Shape and Size of the Transducer	Cylinder $\phi 6.4 \times 11.9$ mm	Cylinder $\phi 5.8 \times 3.8$ mm
Weight	30 gf (including cable of 5m in length)	0.3 gf ( without cable )

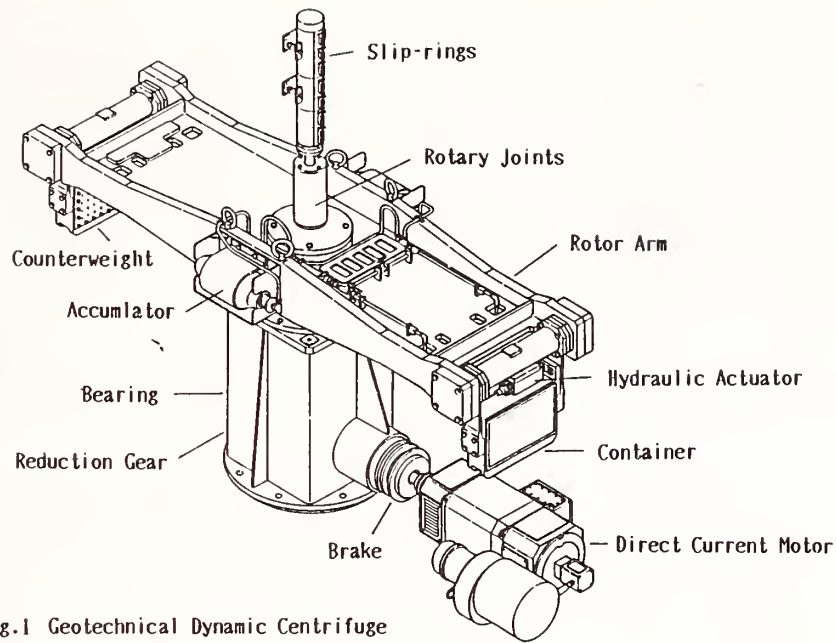


Fig.1 Geotechnical Dynamic Centrifuge

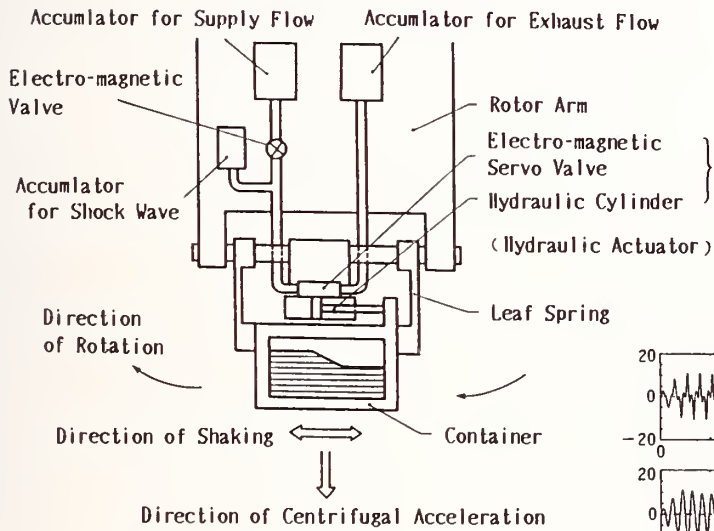


Fig.2 Hydraulic Shaking System

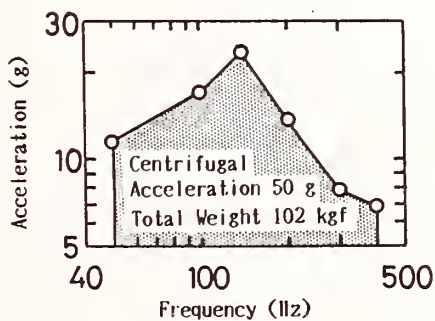


Fig.3 Performance Curve in Sinusoidal Shaking

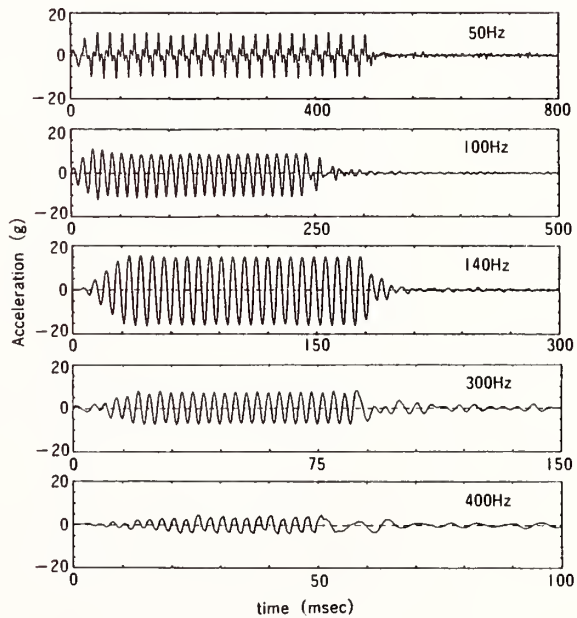
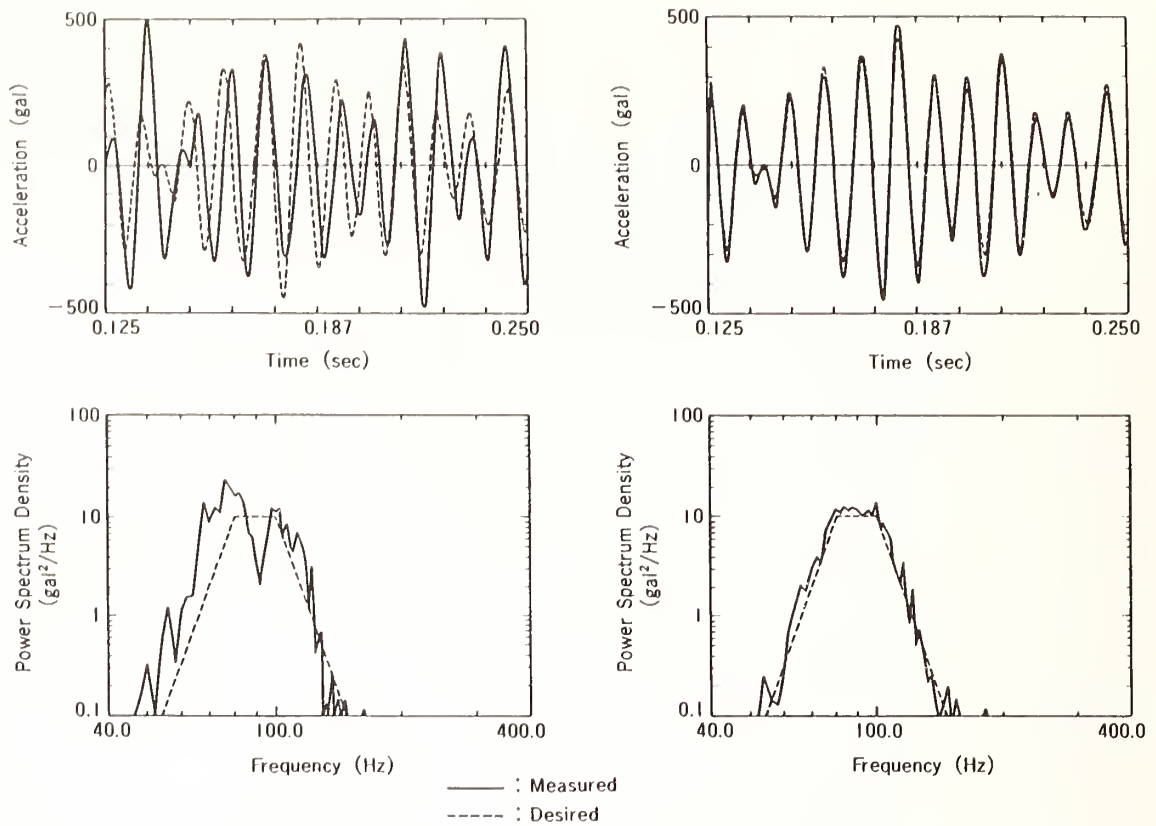


Fig.4 Typical Records of Accelerations in Sinusoidal Shaking



(a) Before Correction

(b) After Correction

Fig.5 Typical Records of Accelerations in Irregular Shaking

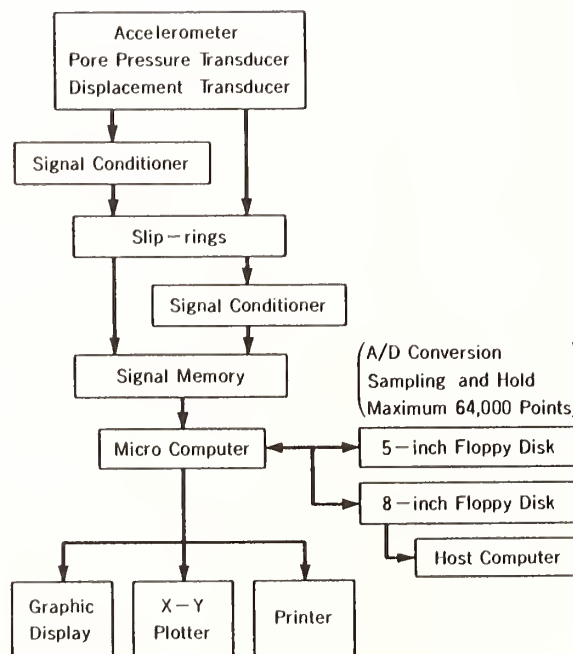


Fig.6 Schematic of Data Measurement System

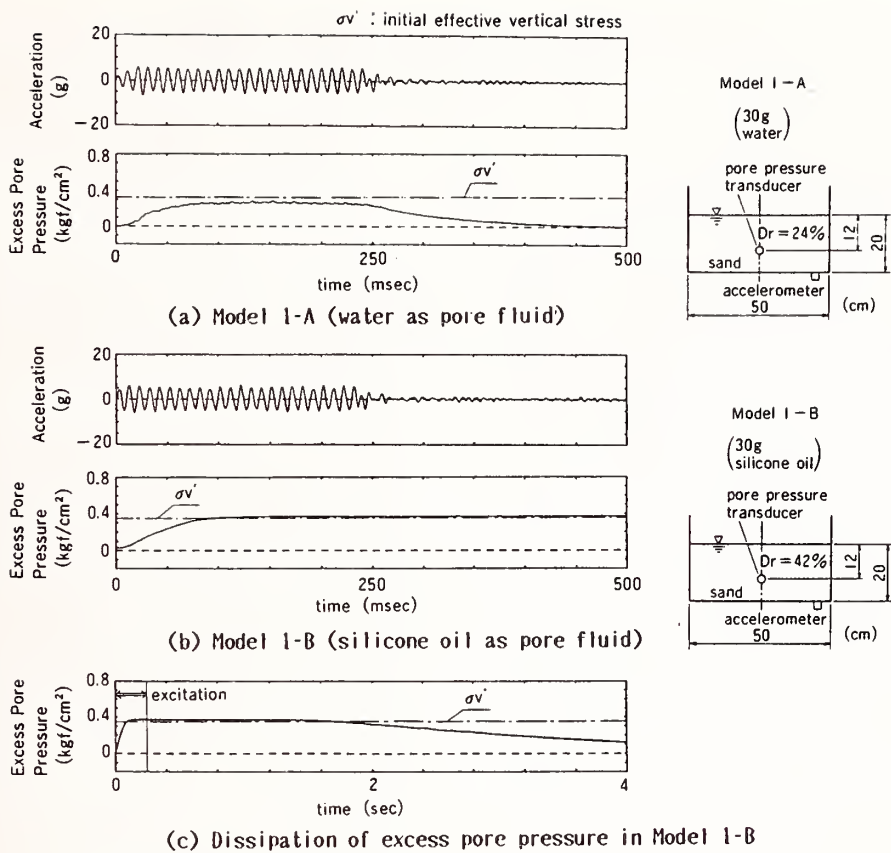


Fig.7 Effect of the Viscosity of Pore Fluid

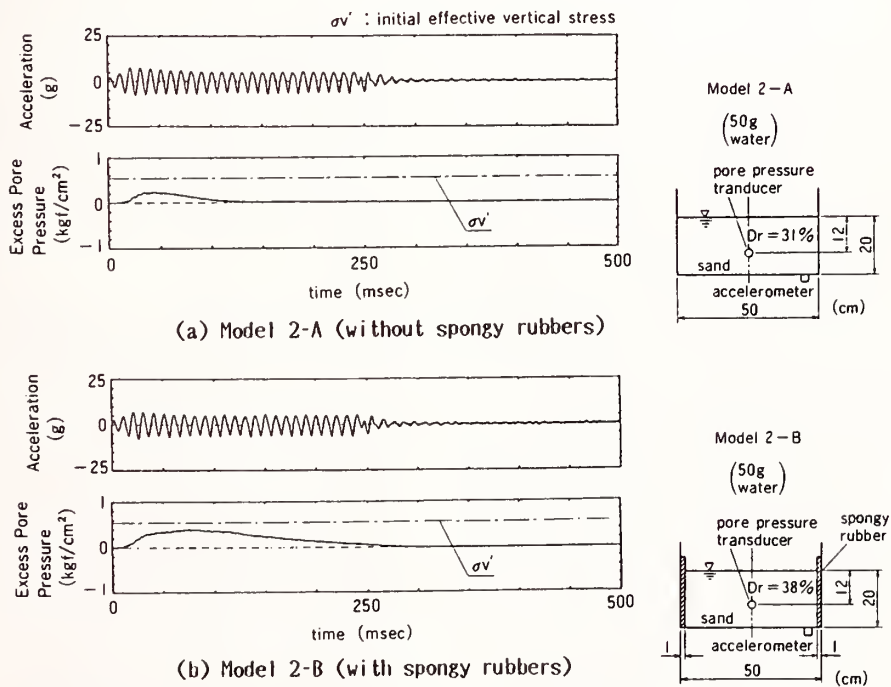


Fig.8 Effect of the Restraint of End Walls

# In Situ Measurement of Pore Pressure Build-Up During Liquefaction

BY

Thomas L. Holzer<sup>1</sup>, T. Leslie Youd<sup>2</sup>, and Michael J. Bennett<sup>1</sup>

## ABSTRACT

The first record of pore-pressure build-up associated with liquefaction in which vertical effective stresses equaled zero was produced by the Wildlife liquefaction array in the Imperial Valley of southern California. The array was triggered by the  $M_s 6.6$  Superstition Hills earthquake on November 24, 1987. Pore pressures built up to overburden pressures and caused sand boils and lateral spreading at the array. The array, which is a special purpose strong-motion station, includes five pore-pressure transducers in a loose- to medium-dense sand, one in dense silt, and surface and downhole accelerometers above and below the sand. Comparison of the pore-pressure and strong-motion records permits an estimate of the threshold shear strain at which excess pore pressures began to develop. Excess pore pressures were generated when peak horizontal accelerations ranged from 0.17 to 0.21g which indicates a minimum value of threshold shear strain of  $5 \times 10^{-2}$  per cent. Horizontal strong motion at the land surface decreased both in amplitude and high-frequency content following liquefaction.

KEYWORDS: Earthquake; liquefaction; pore pressure.

## 1. INTRODUCTION

The Superstition Hills ( $M_s 6.6$ ) earthquake of November 24, 1987, produced the first recording of pore-pressure build-up during liquefaction in which vertical effective stress became equal to zero. The earthquake, which occurred in the Imperial Valley of southern California, triggered a special instrumentation array that was installed in 1982 specifically to monitor earthquake-induced pore pressures in a cohesionless deposit (Youd and Wieczorek, 1984). The array, herein referred to as the Wildlife array, consists of pore-pressure transducers and surface and downhole accelerometers. The array is one of at least eight permanent arrays that have been established world-wide by different investigators to monitor earthquake-induced pore pressures. These arrays include two in Japan (Ishihara and others, 1981), one each in the People's Republic of China and Taiwan (C. K. Shen, personal communication, 1986), and four in the United States. In addition, a temporary array was established near Mammoth Lakes, California, in 1980 as part of an earthquake aftershock investigation (Harp and others, 1984). To date, only the Wildlife array in the Imperial Valley has been triggered by an earthquake large and close enough to cause

liquefaction. Previously reported measurements only have documented increases of pore pressure that were insufficient to reduce effective stresses to zero.

The array is located on level ground and in flood-plain deposits of the Alamo River about 34 km north of El Centro, California, in the Imperial Valley (Fig. 1). It is about 24 km from surface rupture along the Superstition Hills fault that accompanied the 1987 earthquake. The array was installed in 1982 following the 1981 Westmorland earthquake ( $M_s 6.0$ ) which caused widespread liquefaction in the flood plain of the Alamo River near the array (Youd and Wieczorek, 1984). Until the earthquake sequence of November 23-24, 1987, the array had been triggered only once; a  $M_L 3.2$  on April 27, 1987, generated a peak horizontal acceleration of about 0.05g. Only the earthquake of November 24, 1987, which caused a peak horizontal acceleration of 0.21g at the land surface, has caused pore-pressure build-up at the array.

Sand boils and lateral spreading, accompanied the pore-pressure build-up and liquefaction at the array site (Fig. 2). Cumulative horizontal displacement across lateral spreading cracks at the array was at least 126 mm. Cumulative horizontal displacements across other lateral spreads near the array were greater than 210 mm. Heavy vegetation precluded a complete reconnaissance of the Alamo River flood plain, but at least 33 hectares showed evidence of liquefaction that included sand boils and ground cracks.

This manuscript is a preliminary interpretation of the recordings from the Wildlife array. Digitized records, in the process of being made, will facilitate more rigorous analyses of the results. In particular, there is some question about the time response of the pore-pressure transducers. Disturbance of the soil around the transducers during their installation may have created a bulb of soil with greater liquefaction resistance that delayed the detection of pore-pressure build-up in the surrounding undisturbed soil.

<sup>1</sup> U.S. Geological Survey, Menlo Park, California 94025

<sup>2</sup> Dept. of Civil Engineering, Brigham Young University, Provo, Utah 84602

Analysis of the strong motion record and the degradation of the seismic waves as they passed through the liquefied layer may permit resolution of this uncertainty. Digitized records, however, are necessary to facilitate this analysis.

## 2. SITE GEOLOGY AND GEOTECHNICAL PROPERTIES

Subsurface conditions and geotechnical properties of sediment at the Wildlife liquefaction array were described by Bennett and others (1984). The site is underlain by saturated Holocene flood-plain sediments that were deposited in an incised channel of the Alamo River (Fig. 3). The flood-plain sediments are less than 7 m thick at the array and overlie denser and more regionally extensive sedimentary deposits. The flood-plain sequence consists of a 2.5-m-thick silt which is underlain by a 4.3-m-thick silty sand (Table 1). The sequence is very young. A wood fragment from a depth of 6 m in the flood-plain sequence yielded a radiocarbon date of only 230 years B.P.. The water table is maintained within about 1.2 m of the land surface by the Alamo River, which is 23 m east of the center of the array.

Table 1. Grain-size distribution of deposit for samples from hole 3Ag near CPT3 (See Fig. 3)

Depth m	sand/silt/clay per cent	median grain size mm	
.40	13/69/18	.020	
.91	11/89		
1.07	3/75/22	.016	
1.37	2/78/20	.020	silt
1.77	44/44/12	.056	
2.23	4/78/18	.025	---
2.74	37/53/10	.056	
2.90	44/46/10	.057	
3.47	69/26/5	.086	
4.11	78/19/3	.095	silty
4.57	74/23/3	.088	sand
5.49	69/26/5	.086	
5.94	51/43/6	.063	
6.40	79/18/3	.109	

The upper silt is very soft with natural water contents ranging from 27 to 43 per cent and a saturated density of 1.94 g/cm<sup>3</sup>. Its average liquidity index is about 1.6. The average silt and clay content is 90 per cent. Field blow counts from standard penetration tests (SPT) ranged from 1 to 5 blows per foot and averaged around 2; the average tip resistance from cone penetration testing (CPT) was 6 kg/cm<sup>2</sup>. The average in-situ shear-wave velocity of the silt layer is 99 m/sec (Bierschwale, 1984). Although the upper silt layer is predominantly fine grained, approximately 20 per cent of the layer is liquefiable according to the criteria of Seed and others (1981): a natural water content

greater than 90 per cent of the liquid limit, a liquid limit less than 35 per cent, and a clay fraction (<5 $\mu$ ) less than 15 per cent.

The relative density of the 4.3-m-thick silty sand underlying the silt layer is medium to loose on the basis of SPT blow counts. Field blow counts ranged from 3 to 23 and averaged 8.7 blows per foot (standard deviation=4.7). CPT tip resistances averaged 50 kg/cm<sup>2</sup>. The average void ratio and saturated density of undisturbed samples were 0.74 and 1.97 gm/cm<sup>3</sup>, respectively (Vucetic and Dobry, 1986). The average in-situ shear-wave velocity was 116 m/sec (Bierschwale, 1984). The average median grain size increases with depth from 55 to 102 $\mu$ . The average fines content (<75 $\mu$ ) is 33 per cent and ranges from 16 to 60 per cent.

The liquefaction resistance of the silty sand is low. On the basis of the empirical method of Seed and others (1985), most of the layer should liquefy under the loading conditions imposed by the Superstition Hills earthquake (Fig. 4). The top and bottom of the deposit are the most susceptible.

## 3. INSTRUMENTATION

Six pore-pressure transducers and two 3-component accelerometers were installed at the site in 1982. Five pore-pressure transducers were set in the silty sand layer at depths ranging from 2.9 to 6.2 m. The sixth transducer was set at a depth of 12 m in a 1-m-thick dense silt layer beneath the flood-plain sequence. The locations of the transducers are shown in both map view and cross section in figure 3. Transducers were installed in equally spaced holes drilled on the circumference of a 9.2-m-diameter circle. They were Data Instruments<sup>3</sup> model AB transducers, which are bonded-strain-gage type pressure sensors. Each transducer was embedded in a 3.8-cm-diameter cylindrical Delrin housing with a conical tip. Housings were emplaced in the soil by drilling with a hollow-stem auger to the emplacement depth and then pushing the housing approximately 15 cm into the sediment. Bentonite-cement grout was pumped into the hole as the auger was withdrawn. The two accelerometers include surface and downhole types made by Kinometrics. The downhole accelerometer was set at a depth of 7.5 m which is beneath the silty sand. It is wedged in the bottom of a PVC casing installed in a drill hole located in the center of the circular area defined by the transducers. The surface accelerometer is on the concrete foundation of the instrument house.

Records were obtained with a 12-channel Kinometrics CRA-1 analog recorder.

<sup>3</sup> Any use of trade names is for descriptive purposes only and does not imply endorsement by the U.S. Geological Survey.

The recorder triggers at a horizontal acceleration of 0.01g and continues recording for 60 seconds after the last acceleration pulse greater than 0.01g.

#### 4. RECORDINGS

##### 4.1 Earthquakes

The Wildlife liquefaction array was triggered four times during the Superstition Hills earthquake sequence of November 23-24, 1987 (Table 2). Only the  $M_s$  6.2 foreshock and  $M_s$  6.6 main shock caused accelerations greater than 0.05g. Peak horizontal accelerations at the land surface were 0.13 and 0.21g, respectively. Peak horizontal accelerations recorded by the down-hole accelerometer were 0.08 and 0.16g, respectively. The time code on the record for event 4 was incomplete. Only the date and hour could be read; they indicated that event 4 occurred in the same hour as the main shock. Thus, it is known only that the site was triggered by event 4 no later than 45 minutes after the main shock. The largest event during this time period was a  $M_L$  4.8 at 0534 PST. Its epicentral distance was 27 km. Epicentral distances of the other aftershocks ranged from 26 to 34 km.

Table 2. Earthquakes that triggered the Wildlife liquefaction array, November 23-24, 1987, and peak horizontal acceleration at the array.

Event	Magnitude	Date	Time (PST)	Peak Hor. Acc. Surface (g)	7.5m (g)
1	6.2( $M_s$ )	23-Nov	1754	0.13	0.08
2	4.0( $M_L$ )	23-Nov	2223	<0.05	<0.05
3	6.6( $M_s$ )	24-Nov	0515	0.21	0.16
4	4.8( $M_L$ )?	24-Nov	0534	0.05	<0.05

Note: Only local magnitudes,  $M_L$ , have been determined for events 2 and 4 (K. Hutton, written communication, 1987); surface-wave magnitudes,  $M_s$ , are from National Earthquake Information Service.

##### 4.2 Pore-pressure Build-up

Excess pore pressures were generated only by event 3, the  $M_s$  6.6 main shock. Excess pore pressures were not induced by the  $M_s$  6.2 earthquake that preceded the main shock. The first 30 seconds of the records of strong motion and pore-pressure build-up caused by the main shock are shown in figure 5. Note that this is the original record and piezometer outputs are in millivolts. A conversion factor to kPa is indicated for each piezometer on the record. The complete record is 97 seconds long. Pore pressures are relative to static pore pressures at the beginning of the earthquake. Records were obtained from five of the six transducers. Piezometer P-4, which is at a depth of 4 m apparently did not function properly. It had

a large transient signal when the recording system was triggered and showed no increase of excess pore pressure despite increases in pore pressure recorded by transducers at depths of 3 and 5 m.

Excess pore pressures began to increase gradually after the peak horizontal acceleration at both the surface and at a depth of 7.5 m. Excess pore pressures did not develop in the stiff silt layer at 12 m. The low gains of the recording system required to ensure that pore pressure readings did not go off scale largely masked the dynamic fluctuations of pore pressure caused by the earthquake. Thus, it is not possible to examine the waveform details as the transition from elastic to permanent deformation of the soil skeleton took place during liquefaction. Dynamic fluctuations of pore pressure, however, are conspicuous in the record from the stiffer silt layer beneath the liquefied stratum.

##### 4.3 Pore-pressure Dissipation

The time required for the excess pore pressures in the silty sand to dissipate is unknown. That pore pressures did not dissipate immediately is indicated by pore pressures that were still elevated when the site was triggered by event 4 (Table 1). If event 4 does indeed correspond to the largest aftershock in the 45 minutes following the main shock, then pore pressures had not significantly dissipated 19 minutes after the  $M_s$  6.6 event. The earliest large aftershock was a  $M_L$  4.1 event that occurred about three minutes after the main shock; the last large aftershock in the 45-minute window was 38 minutes later. Pore pressures were completely dissipated 29 hours after the main shock when the records were retrieved. In addition, no water was discharging from sand boils 10 hours (1530 PST) after the main shock, when the site was visited for the first time.

#### 5. ANALYSIS

##### 5.1 Liquefaction

The entire silty sand layer was at zero effective stress by the end of the record which was 60 seconds after the last 0.01g acceleration pulse at the surface. Total pore pressures at the top, middle, and bottom of the layer were approximately equal to the total overburden pressure (Fig. 6). Total pore pressures were estimated by adding measured excess pore pressure and the pre-earthquake static pore pressure computed from the depth of the transducer below the water table. The water table was measured in a hand-augered hole eight days after the earthquake. The post-earthquake water level probably is representative of pre-earthquake conditions because the water table is controlled by the Alamo River. The total overburden pressure in figure 6 is based on total soil densities for above and below the water table of

1.60 and 2.00 gm/cm<sup>3</sup>, respectively.

The build-up of excess pore pressure recorded by the transducers continued after the input strong motion ceased. Comparison of excess pore pressures with input strong motions indicates that pore pressures had built up to only approximately 50 per cent of their ultimate value by the time most of the strong motion had ended (Fig. 7). In other words, about half of the excess pore pressure accumulated after the earthquake was over. The normalized pore pressure values shown in figure 7 were computed by dividing pore pressure values for each transducer by their value at the end of the record, 90 seconds. The four normalized curves of pore-pressure build-up are very similar.

The beginning of the build-up of excess pore pressure coincides with the peak horizontal acceleration measured at both the surface and downhole accelerometers. Surface horizontal accelerations as great as 0.17g were observed before the 0.21g pulse, but they did not generate excess pore pressures. Thus, the threshold acceleration required to cause liquefaction was between 0.17 and 0.21g. Recall that excess pore pressures were not generated by the M<sub>s</sub>6.2 foreshock which had a peak horizontal acceleration of 0.13g.

## 5.2 Site Response

The build-up of excess pore pressure appears to have affected the propagation of shear waves through the silty sand layer (Fig. 5). Before the generation of excess pore pressure started, shear waves propagated through the silty sand layer to the land surface without as much degradation as occurred after the build-up of pore-water pressure. After about 2 seconds following the 0.21g pulse, many shear-wave phases that are conspicuous in the recording from the downhole accelerometer at 7.5 m cannot be identified at the land surface. After the development of excess pore pressures, the high-frequency oscillations of the surface accelerations also decreased. By contrast, vertical accelerations, which are caused primarily by P-waves, were not as degraded as they propagated through the silty sand after the excess pore pressures were generated. These generalizations are preliminary and will require spectral analysis of the digitized records to confirm them.

## 6. DISCUSSION

The continued increase of excess pore pressure after the earthquake ended is one of the most striking aspects of the Wildlife recording. The delay in the increase could be caused by several mechanisms. Two that we have seriously considered to date include: (1) migration of pore pressures to the transducers from elsewhere in the deposit and (2) the presence of a nonliquefied bulb of soil around the transducer which was caused by soil disturbance during emplacement.

Migration of pore pressures from elsewhere in the deposit cannot be precluded. If loose pockets of soil are widely distributed throughout the silty sand, local migration of pore pressure within the silty sand could be significant. By this mechanism, liquefaction occurred some distance from each transducer in loose pockets of soil. Excess pore pressures measured by the transducers were caused by propagation of pressures from these liquefied zones. These zones could be either horizontally or vertically separated from the transducers. Horizontal migration is unlikely because sand boils were concentrated near the array. At least on the basis of surface manifestations of liquefaction, it is difficult to identify an alternative source area. Vertical migration also appears to be unlikely since transducers were emplaced in the top, middle, and bottom of the silty sand layer. The similarity of the normalized pore-pressure curves for each transducer (Fig. 7) would require pockets of loose soil equally spaced from each transducer. Cone penetration testing (Fig. 3) near the array did not indicate that the deposit is very heterogeneous on such a scale. SPT values are quite scattered however.

A bulb of disturbed soil that is more resistant to liquefaction than the surrounding undisturbed soil probably is present around each pore-pressure transducer. Transducers were installed by pushing them into place from the bottom of a drill hole. This technique should cause a volumetric decrease in the soil around the transducer which should make the soil more resistant to liquefaction. A simple theoretical model was used to evaluate the potential effect of this disturbed zone on the pore pressure response of the transducer. The model consists of an infinite homogeneous soil body that initially has no excess pore pressures. Consider now a spherical zone of soil in this infinite body that has the same coefficient of consolidation as the surrounding soil. At time,  $t$ , equal to zero, the pore pressure is instantaneously elevated to  $U_0$  throughout the body outside of the sphere, but is not elevated within the sphere. By solving Terzaghi's consolidation equation in three dimensions, the pore-pressure build-up at the center of the sphere,  $U_c$ , can be computed. The problem is similar to that of the thermal cooling of a sphere in an infinite body for which a solution has been published by Ingersoll and others (1954). The normalized pore pressure build-up,  $U_c/U_0$ , is given by:

$$U_c/U_0 = \Phi\left(\frac{1}{2T^{1/2}}\right) - \frac{1}{(\pi T)^{1/2}} e^{-\frac{1}{4T}}$$

where

$r$  = radius of sphere;

$c_v$  = coefficient of consolidation;

$T = c_v t / r^2$ ; and

$\Phi(x) = \text{probability integral, } \frac{2}{\pi^{1/2}} \int_0^x e^{-\beta^2} d\beta$

Good agreement is found between the data and model results if one assumes that the spherical bulb of soil has a radius of 10 cm and a coefficient of consolidation of 2.0 cm<sup>2</sup>/sec

(Fig. 7). The 10-cm radius is based on the assumption that the zone of disturbed soil around a cylindrical cone pushed into a soil mass has a radius approximately equal to 5 times the radius of the cylinder (Acar and Farrag, 1988). The coefficient of consolidation of the silty sand at Wildlife is more uncertain. Coefficients of consolidation are rarely measured for sands because excess pore pressures dissipate so rapidly. The coefficient of clean sands can be estimated from laboratory data by dividing soil permeability by the product of the specific weight of water and the coefficient of volume change. Coefficients of consolidation estimated by this method range from about 60 to 60,000  $\text{cm}^2/\text{sec}$  (Lambe and Whitman, 1969). Coefficients of silt can be measured directly and values typically are less than  $0.5 \text{ cm}^2/\text{sec}$  (Lambe and Whitman, 1969). The effect of silt content is the major uncertainty in estimating the coefficient of consolidation at Wildlife. Vucetic (personal communication, 1987) estimated that the  $c_v$  of undisturbed silty sand from Wildlife ranged from  $0.01$  to  $0.1 \text{ cm}^2/\text{sec}$ . The estimates were based on laboratory tests which were not conducted for the purpose of measuring coefficients of consolidation. They agree within an order of magnitude, however, with  $c_v$ 's determined for silty sands from the Northern Bering Sea (Hampton and Winters, 1983), which ranged from  $0.003$  to  $0.020 \text{ cm}^2/\text{sec}$ . Thus, a value of  $c_v$  of  $2.0 \text{ cm}^2/\text{sec}$  may not be too low a value for the silty sand at Wildlife. In fact, it may even be too high. The point of this discussion is that if the  $c_v$  of the soil at Wildlife is less than  $2.0 \text{ cm}^2/\text{sec}$ , soil disturbance caused by the method of transducer emplacement could affect the response time of the transducer. On this basis, it is difficult to preclude the possibility that the post-earthquake pore-pressure build-up was at least partially caused by migration of pore pressure from undisturbed soil that liquefied into a bulb of disturbed soil around the transducer that did not liquefy.

Analysis of the degradation of seismic waves as they propagated through the silty sand after excess pore pressures started to build-up should help to test the hypothesis that the transducers did not respond instantaneously. Digitized records now being made will facilitate this type of analysis.

Even with the possibility that the delayed response was caused by soil disturbance from the installation procedure, the records permit an estimate of the threshold shear strain required to generate excess pore pressures. On the basis of the procedure proposed by Tokimatsu and Seed (1987) and a shear modulus of 23.9 MPa (Vucetic and Dobry, 1986), the peak horizontal acceleration of  $0.17g$  that preceded the  $0.21g$  pulse yields a minimum value for threshold strain of  $5 \times 10^{-2}$  per cent. This value compares favorably with laboratory-based estimates published by Dobry and others (1981).

## 7. CONCLUSIONS

The  $M_s 6.6$  Superstition Hills earthquake of November 24, 1987, produced the first record of pore-pressure build-up in a natural deposit undergoing liquefaction in which vertical effective stress equaled zero. Pore pressures equaled the overburden pressure throughout the instrumented silty-sand deposit following the earthquake which indicated the entire deposit liquefied. Pore pressures recorded by the transducers continued to build up after earthquake-induced strong motion ceased. The post-earthquake increase may be partly explained by soil disturbance during transducer emplacement. By this explanation, the delay of the response of the transducers is caused by the time required for pore pressures to propagate from undisturbed liquefied soil through the disturbed nonliquefied soil around the transducer. Excess pore pressures were generated when a threshold level of shear strain of about  $5 \times 10^{-2}$  per cent was exceeded.

## 8. ACKNOWLEDGMENTS

We are indebted to John S. Sarmiento, Sam Shaler, Philip V. McLaughlin, and Ronald L. Porcella for their assistance in constructing the liquefaction array. Edward L. Harp and Homa J. Lee reviewed the manuscript and made many helpful comments.

## 9. REFERENCES

1. Acar, Y.B., and Farrag, K., 1988, Discussion of "Consolidation after undrained piezocone penetration. I: Prediction:" by M.M. Baligh and J-N Levadoux: *Journal of Geotechnical Engineering*, v. 114, no. 1, p. 125-126.
2. Bennett, M.J., McLaughlin, P.V., Sarmiento, J.S., and Youd, T.L., 1984, Geotechnical investigation of liquefaction sites, Imperial Valley, California: U.S. Geological Survey Open-File Report 84-252, 103 p.
3. Bierschwale, J.G., 1984, Analytical evaluation of liquefaction potential of sands subjected to the 1981 Westmorland earthquake: University of Texas Geotechnical Engineering Report GR-84-15, 231 p.
4. Dobry, R., Stokoe, K.H. II, Ladd, R.S., and Youd, T.L., 1981, Liquefaction susceptibility from S-wave velocity: Preprint 81-544, American Society of Civil Engineers National Convention, St. Louis, Missouri, October, 1981.
5. Hampton, M.A., and Winters, W.J., 1983, Geotechnical framework study of the Northern Bering Sea, Alaska: U.S. Geological Survey Open-File Report 83-404, 382 p.
6. Harp, E.L., Sarmiento, J., and Cranswick, E., 1984, Seismic induced pore-water pressure records from the Mammoth Lakes, California, earthquake sequence of 25 to 27 May 1980: *Seismological Society of America Bulletin*, v. 74, no. 4, p. 1381-1393.

7. Ingersoll, L.R., Zobel, O.J., and Ingersoll, A.C., 1954, Heat conduction: University of Wisconsin Press, Madison, 325 p.
8. Ishihara, K., Shimizu, K., and Yamada, Y., 1981, Pore water pressure measured in sand deposits during an earthquake: Soils and Foundations, v. 21, no. 4, p. 85-100.
9. Lambe, T.W., and Whitman, R.V., 1969, Soil Mechanics: John Wiley and Sons, New York, 553 p.
10. Seed, H.B., Idriss, I.M., and Arango, I., 1981, Evaluation of liquefaction potential using field performance data: Journal of Geotechnical Engineering, v. 107, no. 3, p. 458-482.
11. Seed, H.B., Tokimatsu, K., Harder, L.F., and Chung, R.M., 1985, Influence of SPT procedures in soil liquefaction resistance evaluations: v. 111, no. 12, p. 1425-1445.
12. Tokimatsu, K., and Seed, H.B., 1987, Evaluation of settlements in sands due to earthquake shaking: Journal of Geotechnical Engineering, v. 113, no. 8, p. 861-878.
13. Vucetic, M., and Dobry, R., 1986, Pore pressure buildup and liquefaction at level sandy sites during earthquakes: Rensselaer Polytechnic Institute Research Report no. CE-86-3, 615 p.
14. Youd, T.L., and Wieczorek, G.F., 1984, Liquefaction during the 1981 and previous earthquakes near Westmorland, California: U.S. Geological Survey Open-File Report 84-680, 36 p.

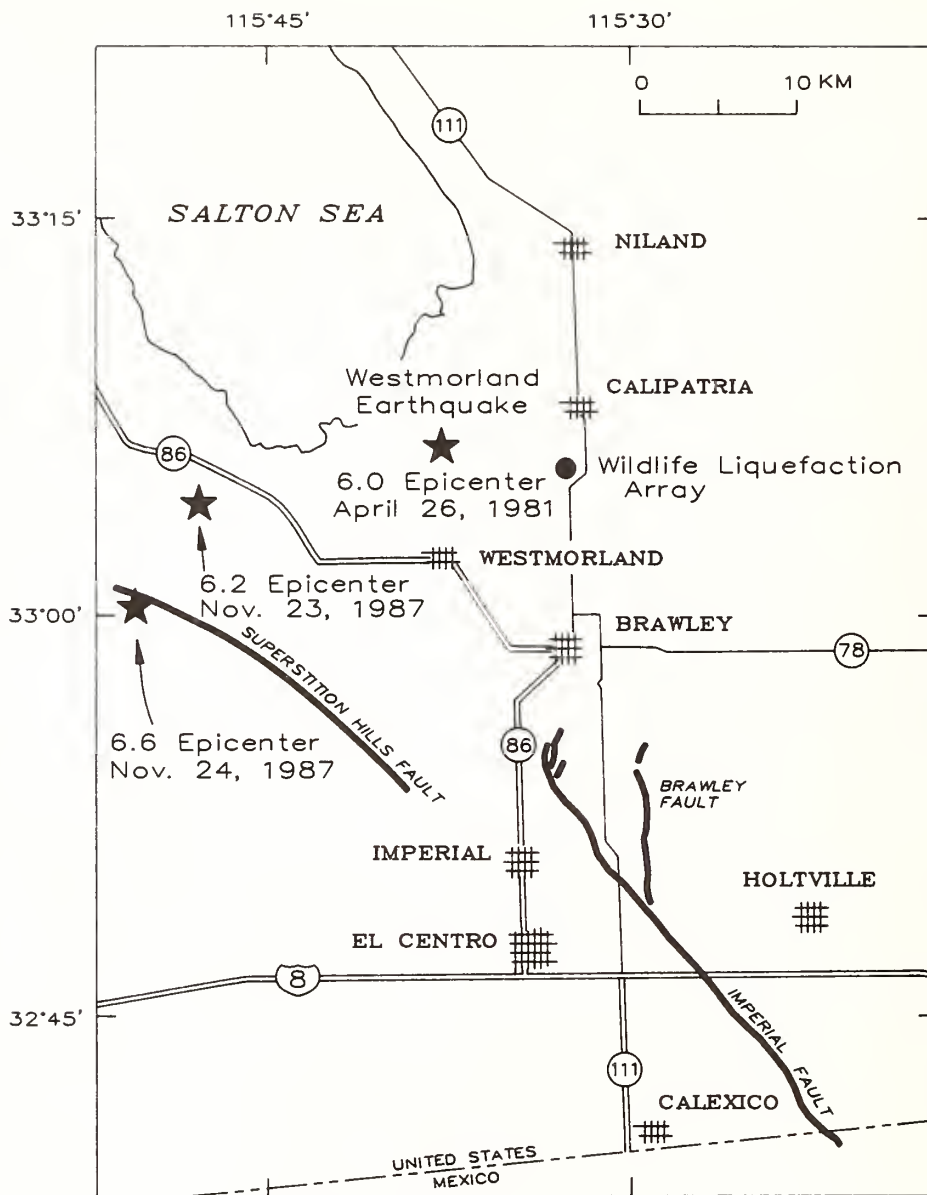


Figure 1. Location map of Wildlife liquefaction array and Superstition Hills fault rupture of November 24, 1987.

# WILDLIFE LIQUEFACTION ARRAY

SAND BOILS AND GROUND CRACKS ASSOCIATED WITH SUPERSTITION HILLS EARTHQUAKE (M6.6), NOVEMBER 24, 1987

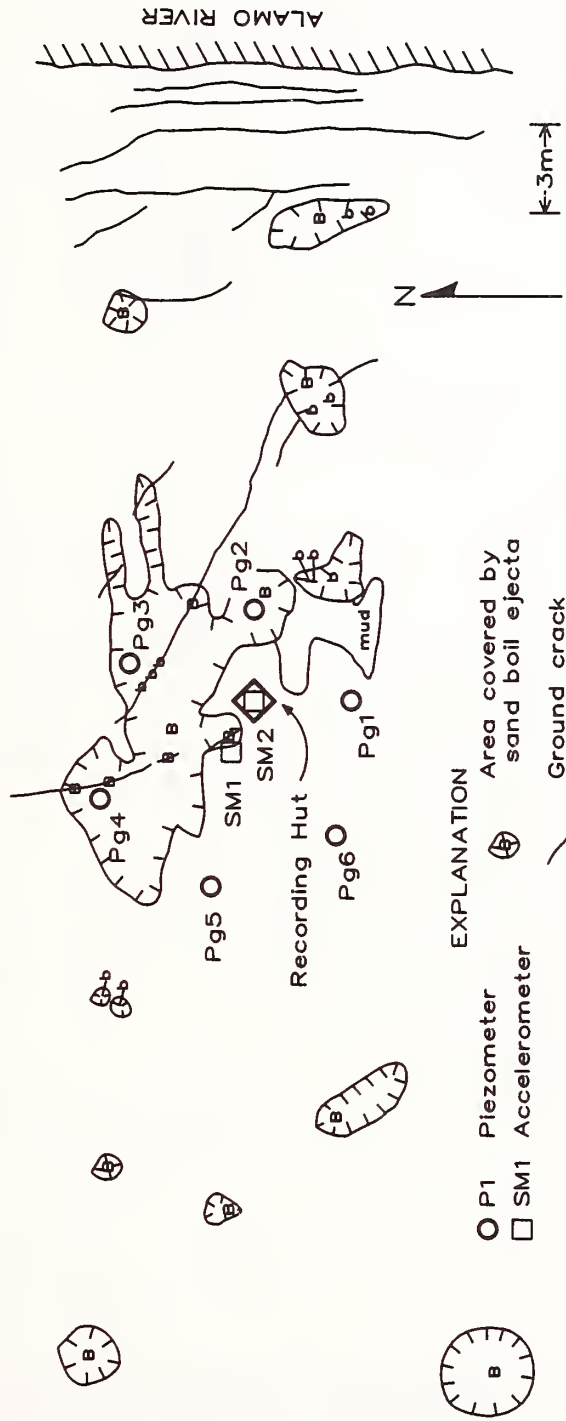


Figure 2. Sand boils and lateral spreading cracks at Wildlife liquefaction array.

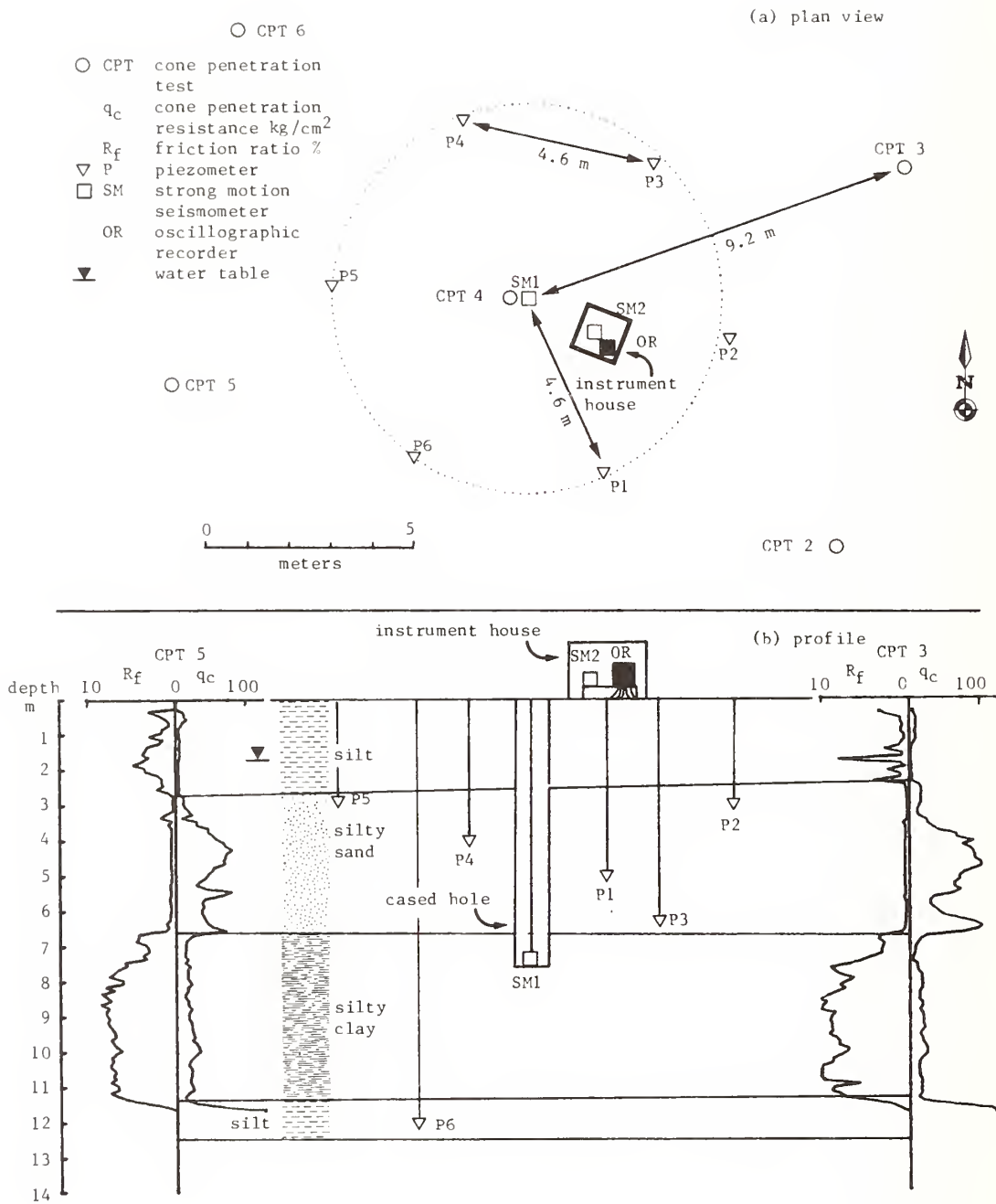


Figure 3. Cross section and map view of liquefaction array (Bennett and others, 1984). Units of  $R_f$  and  $q_c$  are per cent and  $\text{kg}/\text{cm}^2$ , respectively.

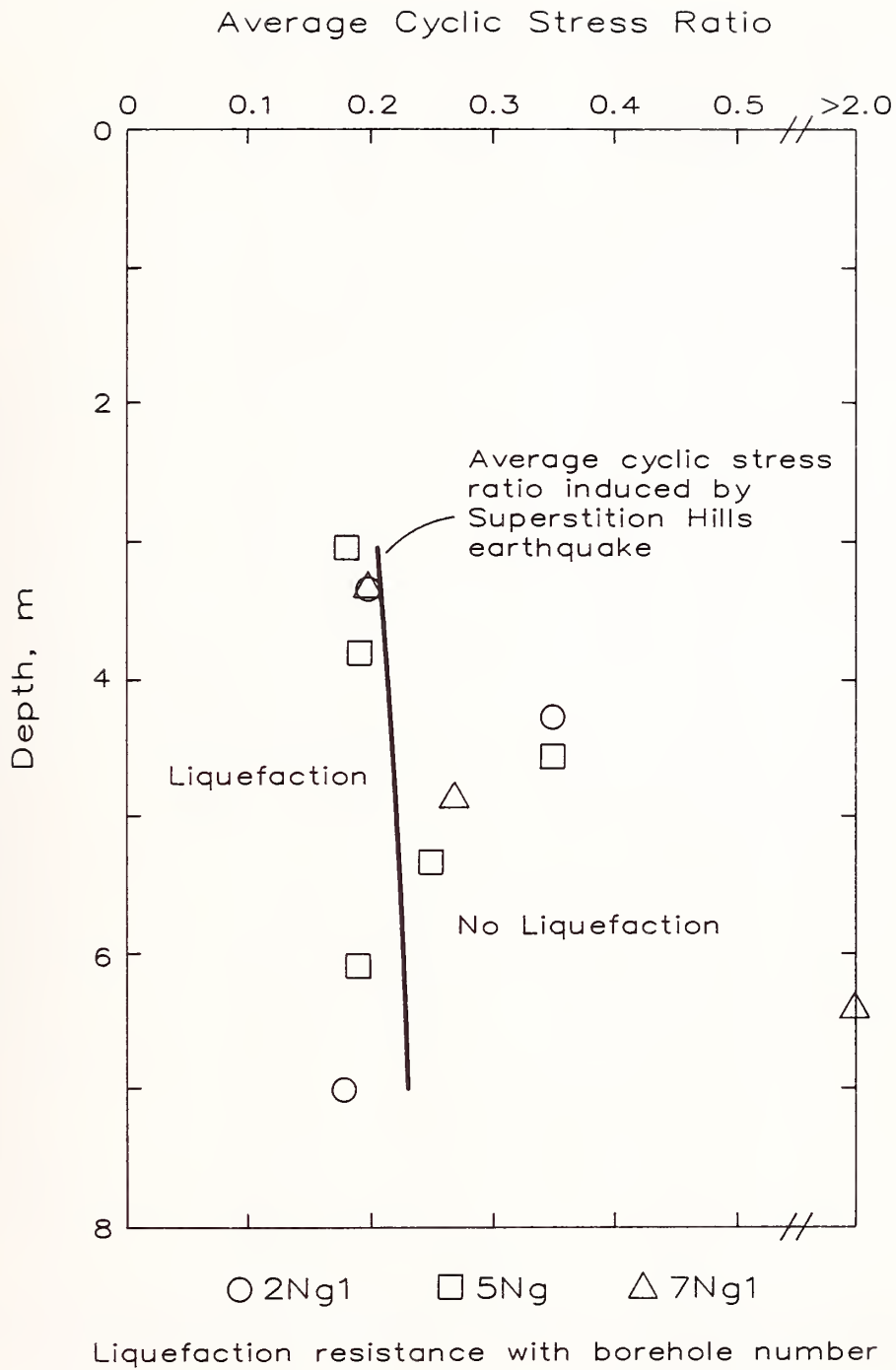


Figure 4. Liquefaction resistance and stress induced by Superstition Hills earthquake as a function of depth. Liquefaction resistance is based on SPT blow counts. Induced stress is the average cyclic stress ratio generated by an earthquake with a 0.21g peak acceleration. See Seed and others (1985) for methodology.

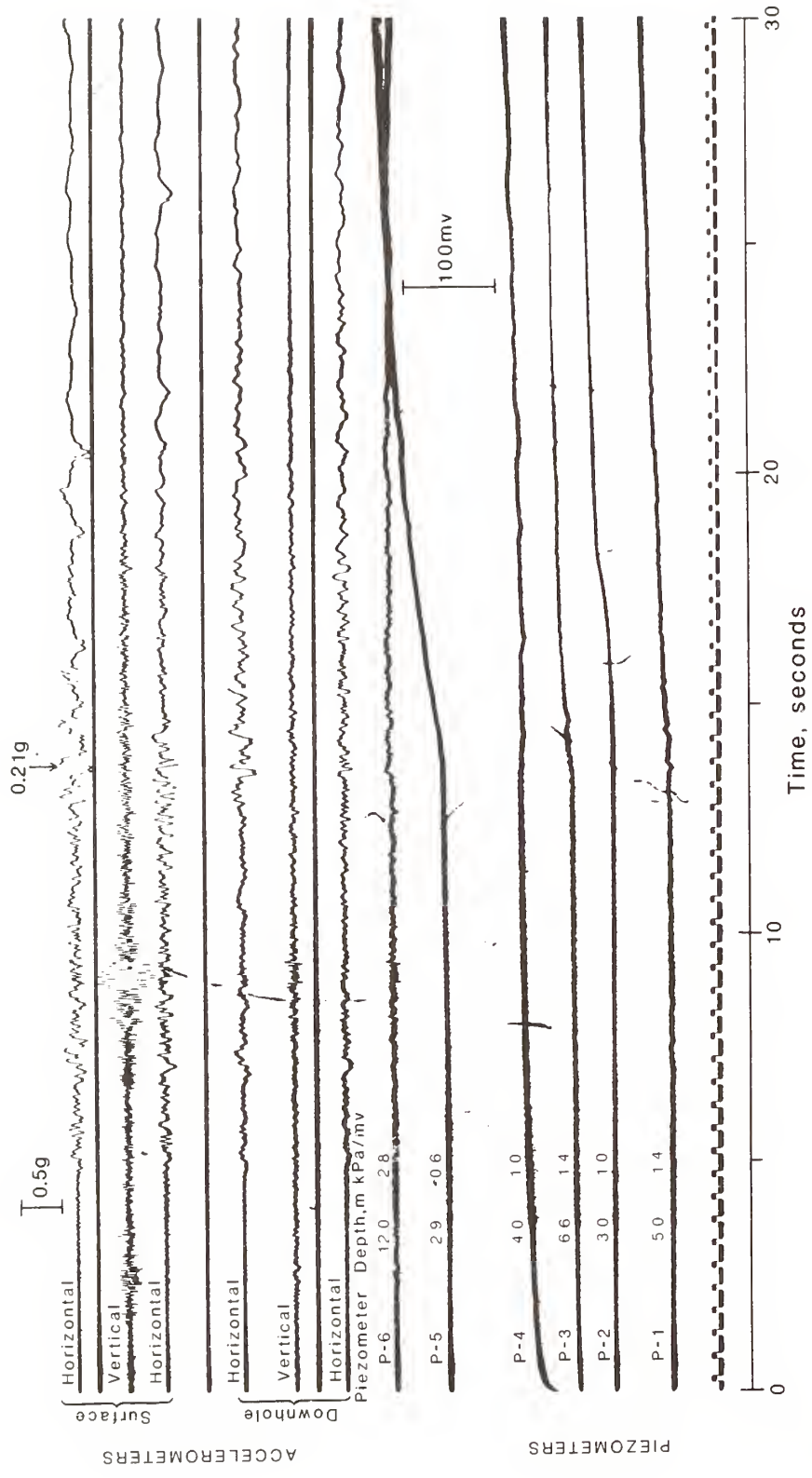


Figure 5. First 30 seconds of the acceleration and pore pressure records at Wildlife from the M 6.6 Superstition Hills earthquake. Note that piezometer record is in millivolts. Scaling for each piezometer is shown in the figure.

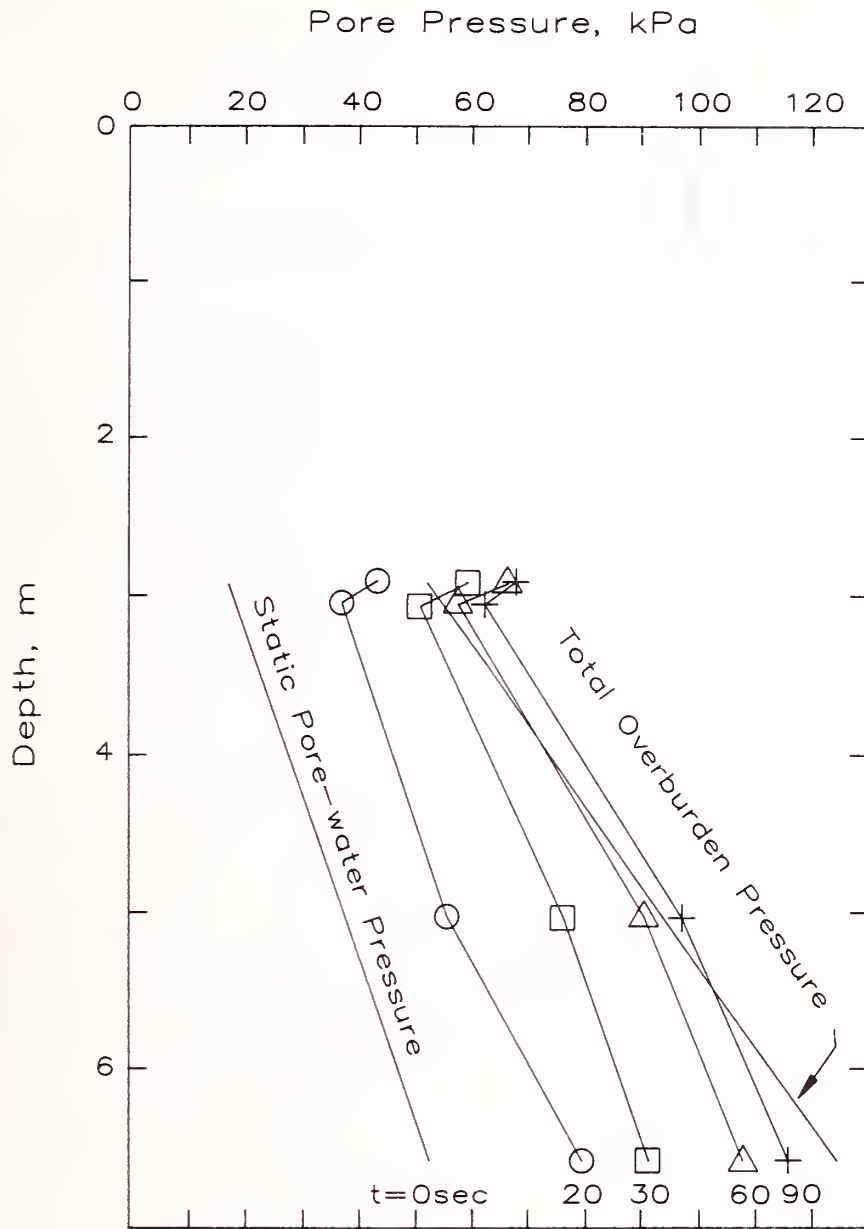


Figure 6. Pore pressure versus depth for selected times after the earthquake triggered the Wildlife array. Zero time is when the recorder triggered.

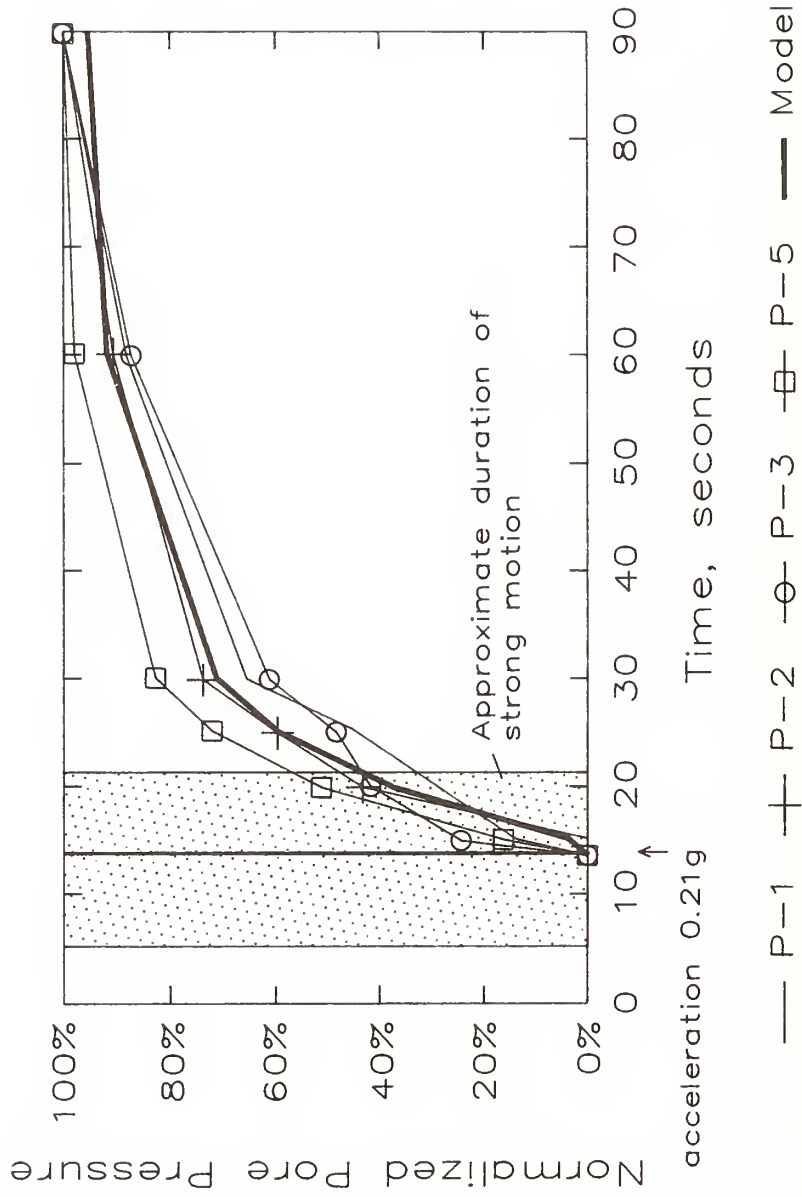


Figure 7. Normalized excess pore pressures from the Superstition Hills earthquake record at Wildlife and model computations. See text for description of model. Pore pressure for each transducer was normalized by dividing values by their value at 90 seconds.

# Two Directional Loading Test for Partially Concrete Filled Steel Columns

by

Shoichi SAEKI<sup>1</sup>, Minoru FUJIWARA<sup>2</sup>,  
Koichi MINOSAKU<sup>3</sup> and Jun HIKINO<sup>4</sup>

## ABSTRACT

The steel pier of Kansai International Airport Bridge, which is now under construction, was designed as a composite structure by filling concrete partially inside it. This aims to resist effectively large bending moment at strong earthquakes. The loading test was carried out to apply this structure to the actual bridge pier, because the behavior of this structure was uncertain before its design. In the loading test, almost 1/5 scale model specimens of the lower column of the actual bridge pier were fabricated, and then lateral load was applied to them under constant vertical load. As a result, it was concluded that this structure with appropriate structural details exhibits smooth stress flow around the boundary between concrete-filled part and non-concrete-filled part, and has ultimate capacity near the full plastic resisting bending moment corresponding to that of wholly-concrete-filled steel columns. This paper presents these test results.

**Keywords:** Partially-concrete-filled steel column, Kansai International Airport Bridge, Two directional loading test, Ultimate capacity

## 1. INTRODUCTION

The type of the steel pier of Kansai International Airport Bridge, which connects the airport island at off the shore of Sensyu within Osaka bay to Izumisano city located in about 40km southwest from Osaka city, is two storied rigid frame structure as shown in Fig. 1. This structure was designed as a composite structure by filling concrete inside the lower column under about sea level. This aims to resist effectively large bending moment at strong earthquakes. The region of the filled concrete was so determined that the increase of pier weight does not make the design of foundation structure uneconomical.

The behavior of wholly-concrete-filled steel columns is already verified<sup>1)</sup>. On the other hand, no study on the behavior of partially-concrete-filled steel columns is reported. For this reason, in applying this structure to the actual bridge pier, it was needed to identify the following items related to its behavior.

(1) Applicability of the calculation method<sup>2)</sup> of ultimate capacity proposed for wholly-concrete-filled steel columns.

(2) State of the stress flow around the boundary between concrete-filled part and non-concrete-filled part, and the effect of a vertical diaphragm attached for making its stress flow smooth.

Accordingly, Public Works Research Institute (say, PWRI), Ministry of Construction, performed two directional loading test for almost 1/5 scale model specimens of the lower column of the actual bridge pier in order to identify these items in collaboration with Kansai International Airport Co., Ltd. This paper deals with this test results.

## 2. TEST METHOD

### 2.1 Specimens

Four specimens, which are almost 1/5 scale model of the lower column of the actual bridge pier, were fabricated. Their dimension is 90×90×350(cm). Fig. 2 and Table 1 show their shape, size and chief properties. A lateral diaphragm was provided for all specimens, and a vertical diaphragm was provided for Type-A, B and D in the same manner as those of the actual bridge pier. As for a lateral diaphragm, a closed type diaphragm was used for the boundary between concrete-filled part and non-concrete-filled part for the purpose of imparting vertical load to the filled concrete, while a hollow type diaphragm was used for other parts. The plate thickness of steel column was determined considering the ratio of the steel column area to the filled concrete area in the actual bridge pier. The steel plate of grade SM41, which is smaller in the yield strength, etc. than the steel of grade SM50Y used for the actual bridge pier, were utilized taking into account the capacity of the loading machine. The concrete used was so mixed that the compression strength (240kg/cm<sup>2</sup>) of the concrete used for the actual bridge pier can be obtained. Table 2 (a) and (b) show material properties of the concrete and the steel plate obtained from the material tests which were done immediately before the loading test.

Each specimen was so designed that the items mentioned in Introduction can be clarified. The features of each specimen are as follows.

Type-A... This specimen, which is identical with Type-B, has almost same structural details as the actual bridge pier. A vertical diaphragm was provided. The thickness of steel plate in non-concrete-filled part was thickened for preventing failure due to substantial local buckling. This specimen and Type-B differ from each

1. Director, Structure and Bridge Department, Public Works Research Institute, Ministry of Construction.
2. Head, Bridge Division, Ditto.
3. Research Engineer, Ditto.
4. Assistant Research Engineer, Ditto.

other in vertical load (the vertical stress under vertical loading in this specimen is almost same as that in the actual pier).

Type-B... This specimen is identical with Type-A. Vertical load in this specimen was raised by five times as high as that of Type-A in order to examine the effect of vertical load on the behavior of partially-concrete-filled steel columns.

Type-C... This specimen does not have a vertical diaphragm. Other structural properties and vertical load are same as those of Type-A.

Type-D... The thickness of steel plate in the boundary between concrete-filled part and non-concrete-filled part was thinned in order to examine the stress flow.

## 2.2 Loading Method

Loading test was performed using the large structural members bi-axial loading machine (loading capacity; 1000ton in vertical direction, 200ton in lateral direction) installed in PWRI. The lower edge of specimens, which is reinforced with double steel plates, was fixed to the bed of the loading machine with bolts, and then lateral load was statically applied to the point of 20cm lower from the upper edge under constant vertical load (100ton for Type A and C, 500ton for Type B). In the case of Type-D, lateral load was applied under the vertical load of 65ton until the specimen yields at the compression side of the lower edge, and subsequently vertical load was increased to 500 ton in order that the specimen may reach its failure within the capacity of loading machine.

## 2.3 Mesuring Method

In the loading test, vertical and lateral displacement of specimens as well as strain in the steel plate of the steel column and the vertical diaphragm were measured. And also strain inside the filled concrete was measured with mould gages which were embeded inside the steel column using prestressing wires.

## 3. TEST RESULTS

### 3.1 Load-Displacement Relationship

Fig. 3 (a)-(d) show the relationship between lateral load and lateral displacement at the loading point for all specimens. In all specimens, a bending crack of the filled concrete firstly occured in the tension side of the lower edge, occurrence of which was estimated from the strain measured by mould gages, and subsequently the yielding and small local buckling of the steel column occured in the compression side of the lower edge. Maximum lateral load for all specimens was observed after these phenomena. Photos 1 and 2 show representative bending cracks of the filled concrete and the local buckling of the steel column, respectively.

Two lines in Fig. 3 (a)-(d) which express the theoretical load-displacement relationship, are drawn on the basis of the elastic theory. A broken

line is drawn considering the flexural rigidity of only steel column, while a chain line is drawn considering the combined flexural rigidity of the steel column and the filled concrete in which the flexural rigidity of the filled concrete is calculated using the secant elastic modulus as shown in table 2 (a). From these figures, it is noticed that the flexural rigidity of the filled concrete leads to the increase of the flexural rigidity of specimens particularly before the occurrence of the bending crack of the filled concrete.

Photos 3 and 4 show failure points of Type-C and Type-D, respectively. Type-C lost its resistance due to the crack of the steel column in the tension side of the lower edge. Type-D lost its resistance due to substantial local buckling of the steel column near the boundary between concrete-filled part and non-concrete-filled part. The ratio of the lateral displacement to the yielding one was about 6.3 for Type-C and 3.5 for Type-D. On the other hand, although the lateral loading for Type-A and Type-B were performed until their lateral displacement respectively reach about 5.3 and 11.3 times the yielding one, their failure points were not observed.

Figs. 4 (a) and (b) show the distribution of lateral displacement in longitudinal direction for Type-A and Type-D, respectively. It is observed from these figures that the distribution of Type-A with a vertical diaphragm is smooth near the boundary between concrete-filled part and non-concrete-filled part compared with that of Type-C without a vertical diaphragm.

### 3.2 Capacity

Table 3 lists concrete cracking load and steel yielding load at lower edge as well as the maximum load. Theoretical values are calculated on the basis of the assumption of the longitudinal strain distributions as shown in Table 4. The theoretical concrete cracking load was calculated on the basis of the assumption that the crack occurs when the stress in the filled concrete reaches the splitting tensile strength (concrete cylinder size; 10×20cm). The value  $P_{tys}$  expresses theoretical steel yielding load in the case that only steel column resists lateral load, while the value  $P_{tysc}$  indicates theoretical steel yielding load in the case that both the steel column and the filled concrete resist lateral load in which the concrete tensile strength is neglected. The value  $P_{uh}$  expresses theoretical maximum load based on the calculation method proposed for wholly-concrete-filled steel columns, while the value  $P_{up}$  indicates theoretical maximum load corresponding to the full plastic resisting bending moment in which the effect of the strain hardening of the steel plates is not considered. Test results for every specimens in Table 3 show that the measured concrete cracking load agrees well with the theoretical value, but the measured steel yielding load is smaller than the value  $P_{tysc}$  and almost equal to the value  $P_{tys}$ . On the other hand, for specimens excluding Type-D which lost

its resistance due to substantial local buckling in non-concrete-filled part, the measured maximum load exceeds the value  $P_{uh}$  and almost reaches the value  $P_{up}$ . Thus, it is realized that partially-concrete-filled steel columns do not entirely behave as a composite structure in the elastic region, but do not lose its resistance abruptly before almost whole cross section reach the plastic region.

### 3.3 Characteristics of Strain Distribution

Figs. 5 (a)-(d) show the longitudinal strain distribution of the steel column and the filled concrete under only vertical loading for all specimens. In this figures, a broken line is drawn assuming that only steel column resists vertical load, while a chain line is drawn assuming that both steel column and the filled concrete resist vertical load. It is observed from these figures that longitudinal strains in the steel column of concrete-filled part exist near the chain line, but approach the broken line as the position gets near the lower edge. It is also noticed that the distribution for Type-B, whose vertical load is larger than that for other specimens, is scattered in non-concrete-filled part, and is close to the broken line around the boundary between concrete-filled part and non-concrete-filled part compared with that of other specimens. In addition, it is observed that longitudinal strains for Type-C and Type-D exist widely around the boundary between concrete-filled part and non-concrete-filled part compared with that for Type-A.

Figs. 6 (a) and (b) show the longitudinal strain distribution of the steel column and the filled concrete under two directional loading for representative specimens, Type-A and Type-C. From these figures, it is noticed that their distributions are similar to those under only vertical load, which approaches the broken line as the position gets near the lower edge. It is also observed that longitudinal strains for Type-C without a vertical diaphragm exist widely in non-concrete-filled part compared with those of for Type-A.

Figs. 7 (a)-(c) indicate the correlations between longitudinal strain and lateral load at representative three points along the flange for Type-A. In these figures, a broken line is drawn assuming that only steel column resists lateral load, while a chain line is drawn assuming that both the steel column and the filled concrete resist lateral load. From these figures, it is noticed that longitudinal strains at the connection point between the flange plate and the vertical diaphragm exist near the chain line, but longitudinal strains at other points exist near the broken line. Thus, the longitudinal strain distribution along the flange plate shows the similar distribution in the case that the shear lag phenomenon occurs.

### 4. CONCLUDING REMARKS

To identify the behavior of partially-concrete-filled steel columns which were applied to Kansai International Airport Bridge under construction, two directional loading test was carried out using almost 1/5 scale model specimens of the lower column of the actual bridge pier. The results obtained are as follows.

- (1) It is realized that partially-concrete-filled steel columns do not exhibit entirely the behavior as a composite structure in the elastic region, because the measured steel yielding load relatively agrees with the theoretical value based on the assumption that only steel column resists lateral load.
- (2) It is, however, verified that partially-filled steel columns do not exhibit substantial local buckling before whole cross section reaches the plastic region, and have high ultimate capacity corresponding to almost full plastic resisting bending moment.
- (3) It is ascertained that the stress flow and the lateral displacement distribution around the boundary between concrete-filled part and non-concrete-filled part become smooth by providing a vertical diaphragm.
- (4) It is observed that vertical load affects on the stress flow and the lateral displacement distribution around the boundary between concrete-filled part and non-concrete-filled part.

#### [Reference]

- 1) Hirohiko Tada, Hiroshi Shinohara, Koichi Minosaku, Akira Takizawa and Jun Hikino; A Study on Behavior of Concrete Filled Steel Tubes, Proc. of the 2-nd Bridge Workshop, 1985.
- 2) Guideline for Design and Construction of Steel Piers consisting of Composite Columns (Concrete Filled Type)-Draft; Hanshin Expressway Public Corporation, 1986,3.

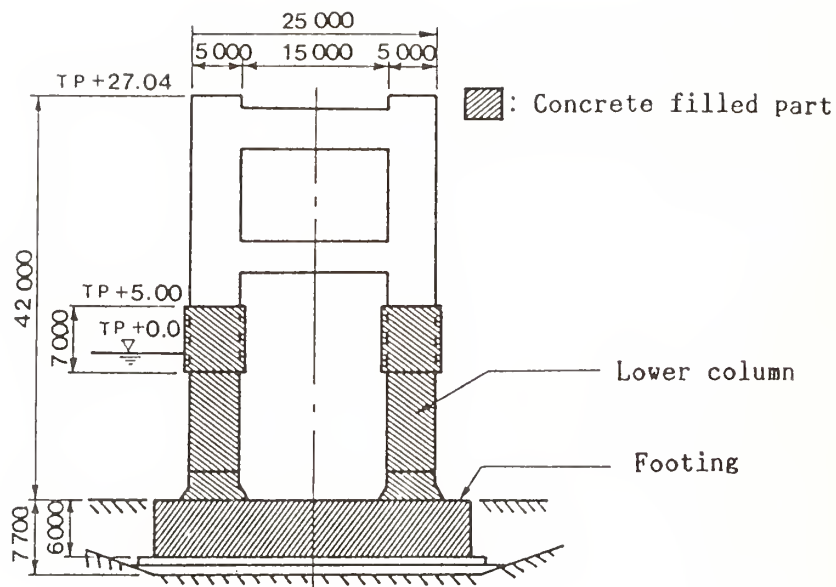


Fig. 1 Front View of the Bridge Pier  
of Kansai International Airport Bridge

Table 1 Properties of Model Specimens

Specimen		Type-A	Type-B	Type-C	Type-D
Height (cm)		350	350	350	350
Cross Section (cm)		90×90	90×90	90×90	90×90
Thickness of steel plate (mm)	Upper	16	16	16	8
	Lower	8	8	8	16
Vertical diaphragm		with	with	without	with
Vertical load (ton)		100	500	100	65⇒500

Table 2 (a) Material Properties  
of Steel Plate (SM 41)

Thickness(mm)	8	16
Yield point(kg/cm <sup>2</sup> )	3,540	2,950
Tensile strength(kg/cm <sup>2</sup> )	4,770	4,480
Young ' s modulus (× 10 <sup>6</sup> kg/cm <sup>2</sup> )	1.98	2.03

Table 2 (b) Material Properties  
of Concrete (concrete cylinder 10×20cm)

Specimen	Type-A	Type-B	Type-C	Type-D
Compression strength(kg/cm <sup>2</sup> )	267	260	253	219
Tensile strength (kg/cm <sup>2</sup> )	26.1	21.6	23.4	25.7
Young ' s modulus (× 10 <sup>5</sup> kg/cm <sup>2</sup> )	2.27	2.17	2.14	2.08



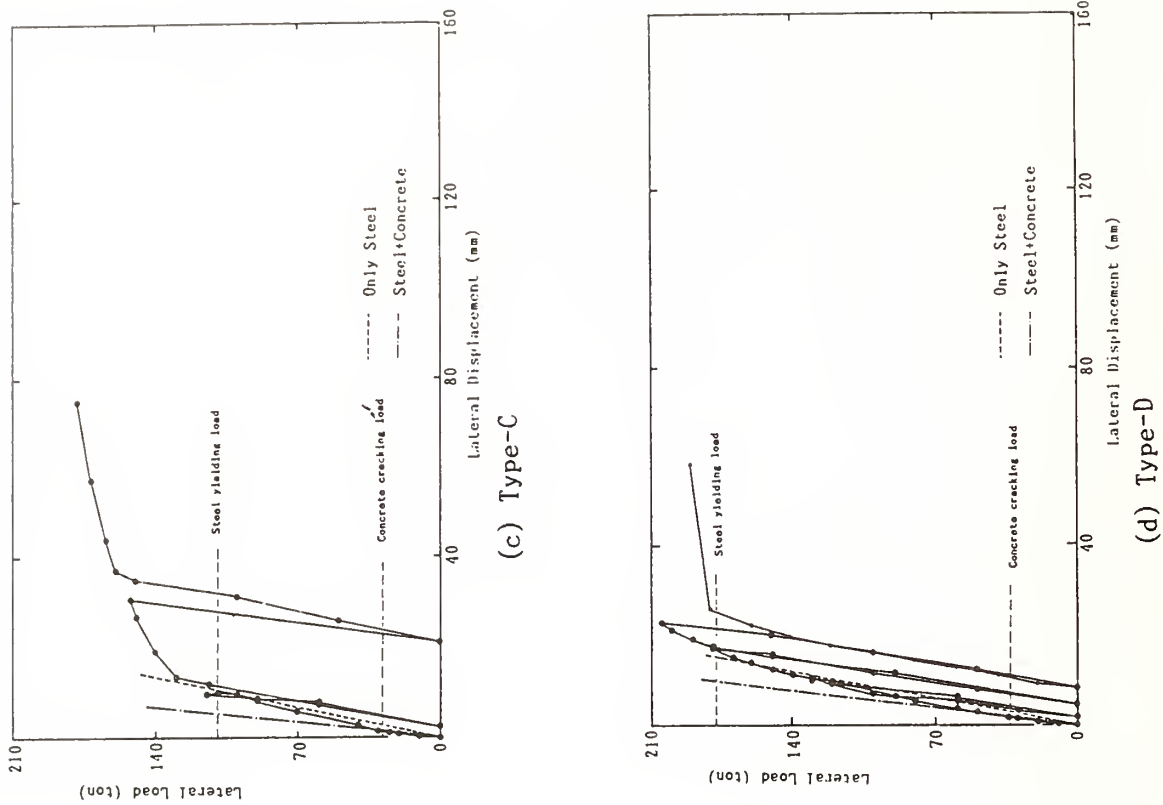


Fig. 3 Relationship between Lateral load and Lateral Displacement

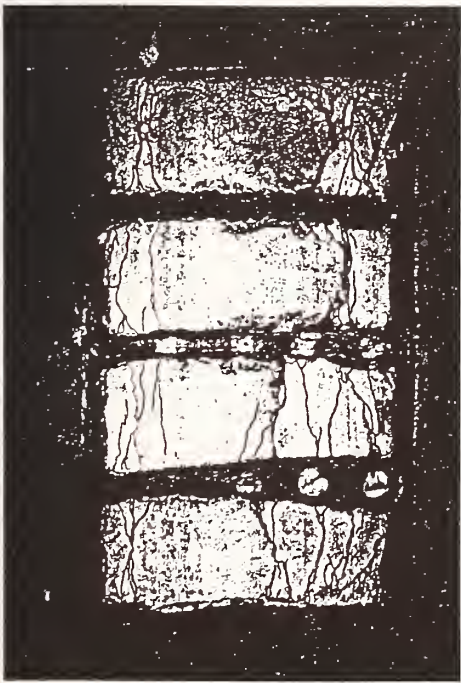


Photo 1 Cracks of Filled Concrete (Type-C)

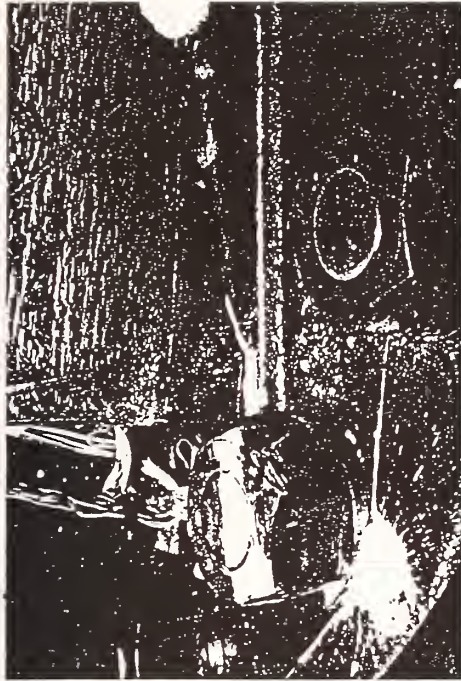


Photo 3 Failure due to Crack of Steel Column near Tension Side of Lower Edge (Type-C)

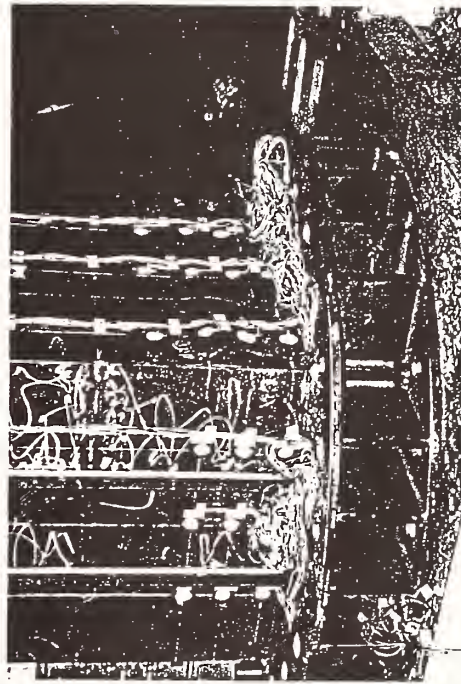
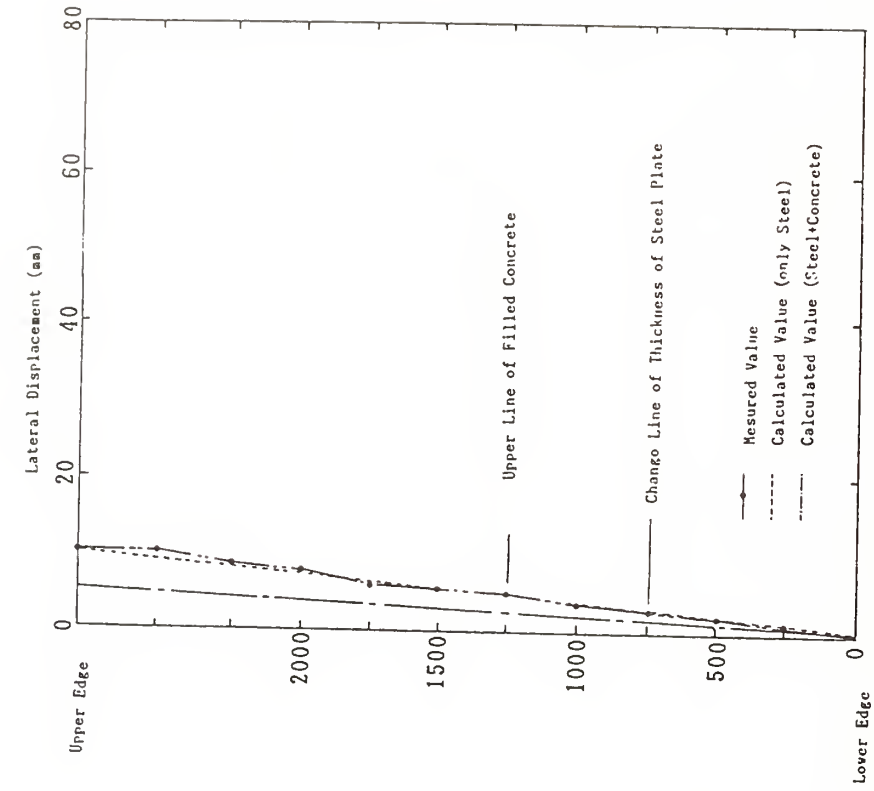


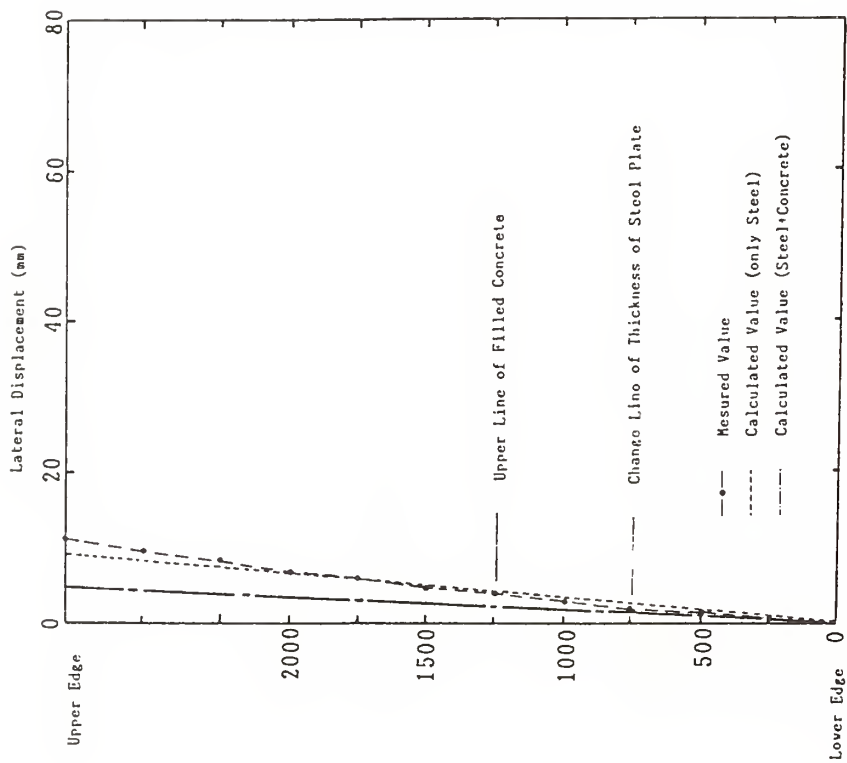
Photo 2 Local Buckling of Steel Column (Type-A)



Photo 4 Failure due to Local Buckling of Steel Column near the Boundary between Concrete-Filled Part and Non-Concrete-Filled Part (Type-D)



(a) Type-A (Lateral Load; 114.5 ton)



(b) Type-C (Lateral Load; 114.8 ton)

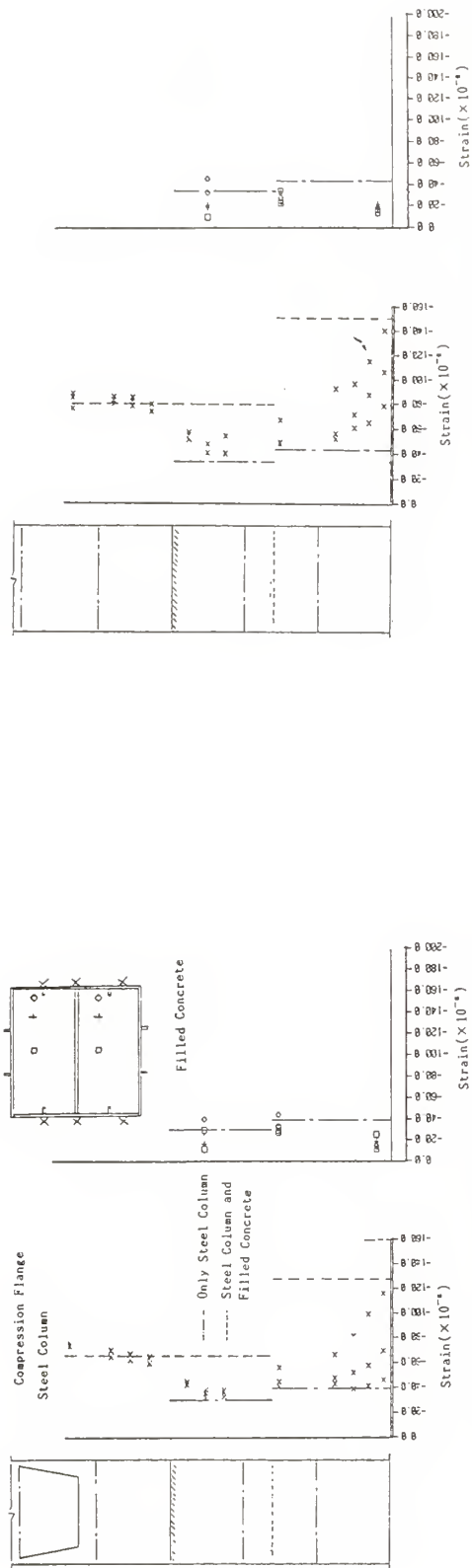
Fig. 4 Lateral Displacement Distribution  
in Longitudinal Direction

Table 3 Test Results(concrete cracking load, steel yielding load, maximum load) unit; ton

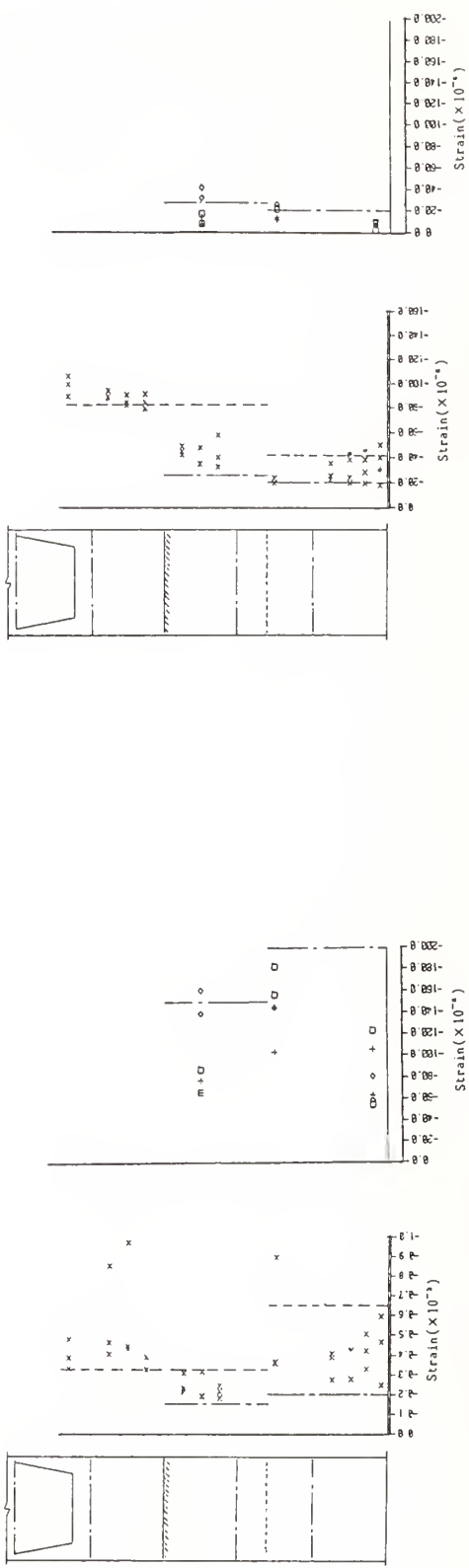
Specimen		Type-A	Type-B	Type-C	Type-D		
Vertical load		100	500	100	65	500	
Concrete cracking load	measured value $P_{cm}$	29.7	54.7	30.0	34.8	-	
	theoretical value $P_{cc}$	32.2	47.5	29.7	38.3	-	
	$P_{cm}/P_{cc}$	0.92	1.15	1.01	0.91	-	
Steel yielding load	measured value $P_{ym}$	114.6	74.7	109.8	179.5	99.8	
	theoretical value	$P_{tys}$	108.3	73.0	98.3	174.4	115.5
		$P_{tysc}$	141.2	137.3	128.9	210.4	179.7
	$P_{ym}/P_{tys}$	1.06	1.02	1.12	1.03	0.86	
	$P_{ym}/P_{tysc}$	0.81	0.54	0.85	0.85	0.56	
Maximum load	measured value $P_{mm}$	192.6	194.5	184.6	-	187.0	
	theoretical value	$P_{uh}$	169.4	168.9	150.1	-	253.9
		$P_{up}$	178.3	201.0	158.2	-	308.2
	$P_{mm}/P_{uh}$	1.14	1.15	1.22	-	0.73	
	$P_{mm}/P_{up}$	1.08	0.97	1.17	-	0.61	

Table 4 Assumed Longitudinal Stress Distributions in Calculating Theoretical Load Values

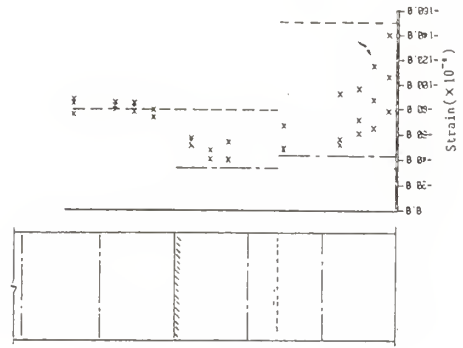
Concrete cracking load	Steel yielding load		Maximum load	
$P_{cc}$	$P_{tysc}$	$P_{tys}$	$P_{uh}$	$P_{up}$
Steel; 	Steel; 	Steel; 	Steel; 	Steel; 
Concrete; 	Concrete; 	Concrete;	Concrete; 	Concrete; 
$\sigma_{ct}$ ; Tensile strength of concrete	$\sigma_{sy}$ ; Yield point of steel	$\sigma_{sy}$ ; Yield point of steel	$\sigma_{lb}$ ; Local buckling strength of steel $\sigma_{cc}$ ; Compression strength of concrete	$\sigma_{sy}$ ; Yield point of steel $\sigma_{cc}$ ; Compression strength of concrete



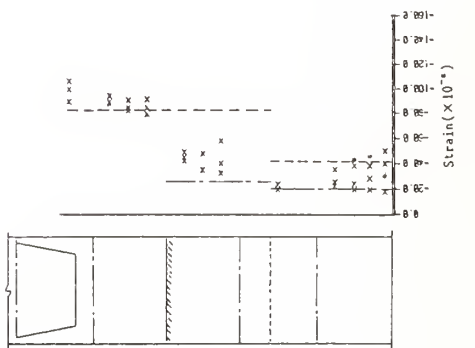
(a) Type-A (Vertical Load; 100ton)



(b) Type-B (Vertical Load; 500ton)



(c) Type-C (Vertical Load; 100ton)



(d) Type-D (Vertical Load; 65ton)

Fig. 5 Longitudinal Strain Distribution in Longitudinal Direction under Vertical Loading

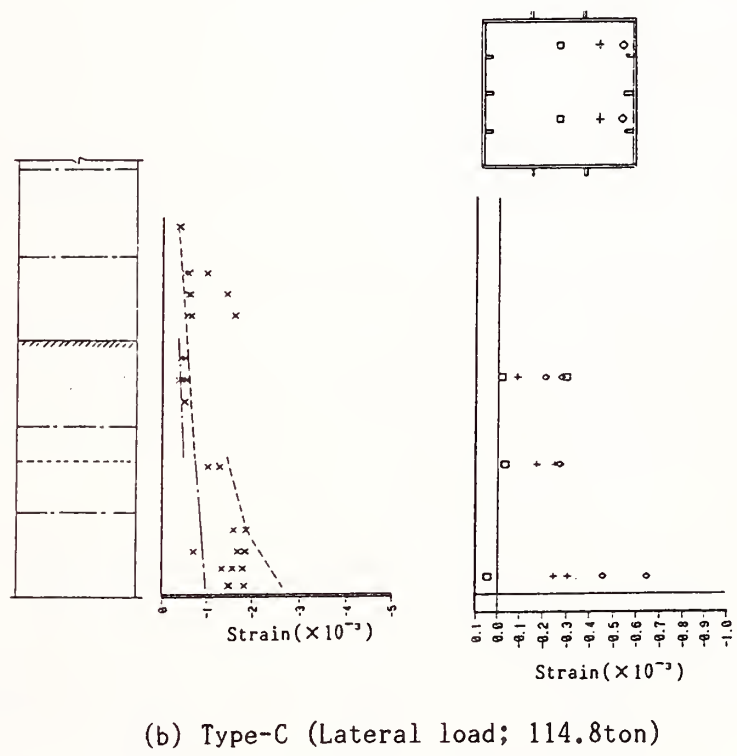
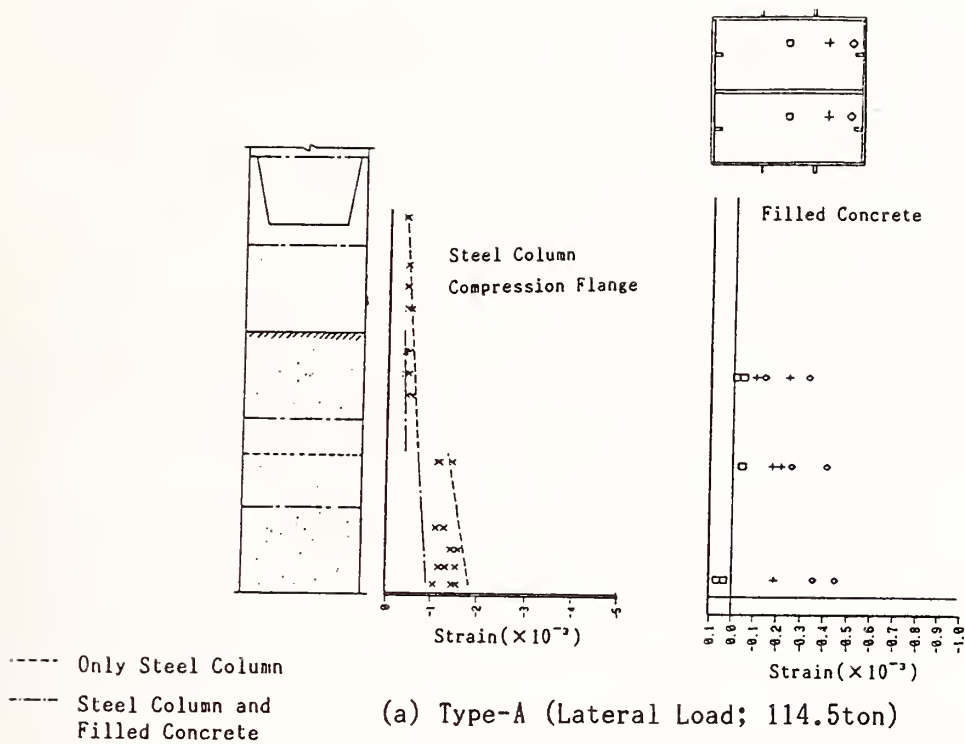
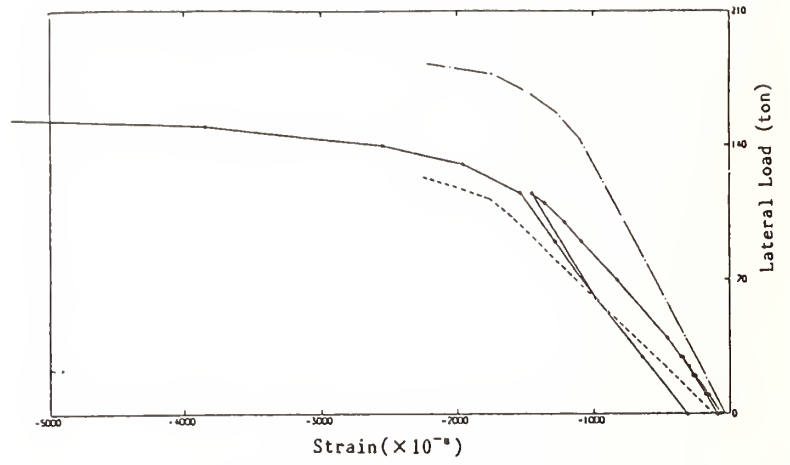
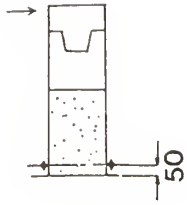
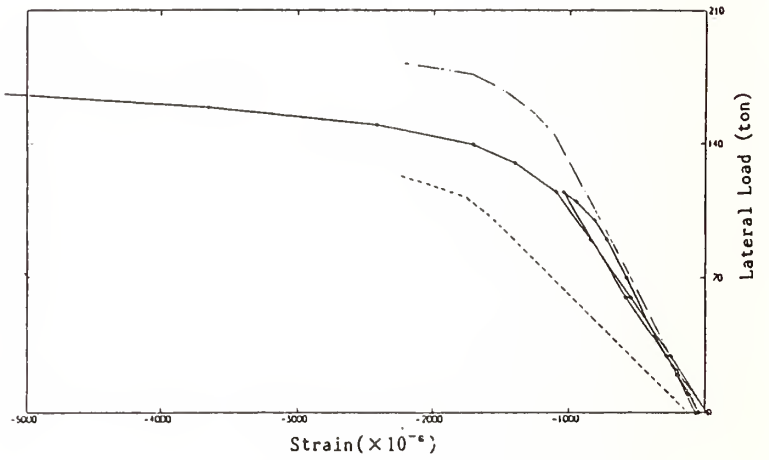
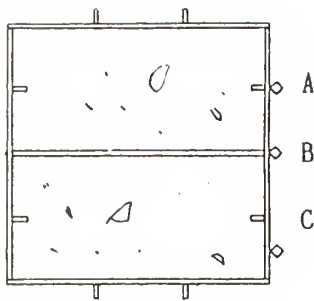


Fig. 6 Longitudinal Strain Distribution in Longitudinal Direction under Two Directional Loading

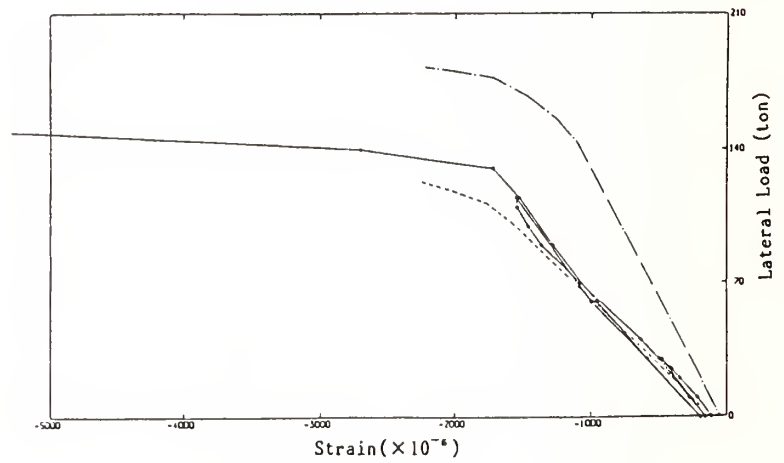


(a) Point A



(b) Point B

----- Only Steel Column  
 - - - - Steel Column and Filled Concrete



(c) Point C

Fig. 7 Relationship between Lateral Load and Longitudinal Strain (Two Directional Loading, Type-A)

# Similitude Studies of Prototype and 1/6-Scale Model Bridge Columns Under Reversed Cyclic Loading

by

William C. Stone, Geraldine S. Cheek and H.S. Lew

## ABSTRACT

Circular, spirally reinforced concrete bridge columns were subjected to cyclic loading in the laboratory. The test specimens were prototype columns designed in accordance with the recent California Department of Transportation (CALTRANS) specifications [1983].

Two full-scale columns, each measuring 5 feet (1.52 m) in diameter with aspect ratios (height/diameter) of 3 and 6, were subjected to slow reversed cyclic lateral load (representing seismic loads) with constant axial load to simulate the weight of the bridge superstructure.

Load-displacement histories, strain energy absorption capacity, and ductility capacity for the prototype columns are presented. Comparisons are made of the ultimate moment capacities, measured displacement ductilities, cyclic energy absorption capacity and the failure modes of the full-scale specimens with those observed from 1/6-scale model tests.

Keywords: Bridge Columns; Cyclic Load; Earthquake Loads; Full-Scale; Inelastic Behavior; Models; Reinforced Concrete; and Seismic Loads.

## 1. INTRODUCTION

As a result of severe damage sustained by many bridge structures during the 1971 San Fernando earthquake, substantial modifications were made to the seismic design guidelines for the state of California [1,2]. The need for experimental verification of these modifications, at full-scale, was first proposed at the Applied Technology Council Workshop on Earthquake Resistance of Highway Bridges held in the spring of 1979 [3]. In response to this need, an experimental test program was initiated by the National Bureau of Standards in the spring of 1983 to investigate the seismic performance of full-scale bridge columns. The test program was sponsored by the National Science Foundation (NSF), the

California Department of Transportation (CALTRANS), the Federal Highway Administration (FHWA) and the National Bureau of Standards (NBS). The program involved the testing of full-scale and 1/6-scale model bridge columns in an effort to determine the effects of scale and the effectiveness of new reinforcement details adopted by CALTRANS and AASHTO [1]. The results of the 1/6-scale model tests were presented at the third U.S.-Japan Joint Bridge Workshop held in 1987 in Tsukuba, Japan [4].

### 1.1 Objectives

The objectives of the full-scale column tests were as follows:

1. To determine the ductility capacity of representative bridge columns designed in accordance with recent CALTRANS standards.
2. To determine the effects of scale on column behavior.
3. To determine the effects of aspect ratio (L/D) on column behavior.
4. To determine the adequacy of transverse reinforcement as presently required by CALTRANS to prevent longitudinal bar buckling.

Evaluation of column performance was based on energy absorption capacity, displacement ductility, ultimate moment capacity, and qualitative observations concerning the ability of the confining reinforcement to prevent buckling of longitudinal steel and to increase ductility.

## 2. DESIGN OF TEST SPECIMENS

The two cantilevered bridge columns described in this report were designed and constructed to meet CALTRANS specifications effective in 1983. On

---

<sup>†</sup>National Bureau of Standards,  
Gaithersburg, MD 20899

the basis of discussions with CALTRANS engineers [5], the final column diameter, aspect ratio, and reinforcing details were selected to reflect standard field practice and representative column sizes. The resulting dimensions were a height of 30 ft. (9.14 m) for the flexure column and 15 ft. (4.57 m) for the shear column with a diameter of 5 ft. (1.52 m) for both columns (see Figures 1 and 2).

The longitudinal reinforcement for both the flexure and shear columns consisted of 25 Grade 60 #14 deformed bars (1.69 in., 430 mm). This resulted in a longitudinal reinforcement ratio,  $\rho_t$ , of 2%. CALTRANS also specifies that lapped splices are not permitted for longitudinal reinforcement larger than #11 bars (1.41 in., 35.8 mm) within a region extending 10 ft. (3.0 m) above the column footing for a fixed base column. The center-to-center spacing of the longitudinal bars was 6.83 in. (173 mm).

The transverse reinforcement for the flexure column was a spiral made from #5 (0.625 in., 15.9 mm) Grade 60 deformed steel bars with a pitch of 3.5 in. (88.9 mm) resulting in a volumetric reinforcement ratio,  $\rho_s$ , of 0.00633. The spiral for the shear column was made from #6 (0.75 in., 19.1 mm) Grade 60 deformed steel bars with a pitch of 2 - 1/8 in. (54.0 mm) giving a volumetric reinforcement ratio of 0.01479. The spirals for both the flexure and shear columns extended from the top of the column into the column footing to the point of tangency of the longitudinal bar hooks as per CALTRANS Design Handbook [5] Section 8.18.2.1.3. The dimensions and steel arrangement for both columns are shown in Figure 3. Model and prototype specifications are given in Table 1.

The columns were fixed at the column base and hinged at the top. These boundary conditions were felt to best model the in-situ boundary conditions for a broad class of bridge columns used in seismic regions, i.e. those which can be assumed to act as single cantilevered sections with the bridge superstructure supported on elastomeric bearing pads. Furthermore an axial column load which simulated the vertical reaction of the bridge superstructure was applied in such a manner as to maintain a vertical reference axis throughout the test.

The prototype columns were first loaded axially to 1000 kips (4,448.2 kN), a value equal to approximately 0.1 f'c Ag. Axial load was held constant during the test and was the same for both specimens. The columns were then subjected to reversed cyclic lateral loads. The yield deflection (referred to as  $\Delta_y$  throughout this paper) was determined experimentally as described in Section 3 below. Thereafter, cyclic lateral deflections were increased by multiples of  $\Delta_y$ . The lateral load was applied at the center of gravity of the column footing. Loading histories for the columns are discussed in Section 3. The cycling of the columns was performed under displacement control using a double acting servo-hydraulic jack. Axial loads were applied under load control using a specially converted servo-hydraulic universal testing machine. Strains in spirals and along the longitudinal bars were measured using strain gages. External displacement transducers were used to measure column rotation, lateral displacement and column curvature. All passive test apparatus (e.g. supports, lateral restraint systems) were instrumented and calibrated for monitoring reactions because the specimen and test apparatus constituted a statically indeterminate system.

### 3. TEST SETUP AND LOADING HISTORY

The method used to determine the yield displacement was the same as that used for the model tests [7]. In brief, the ultimate moment of the column was determined using ACI column charts with  $\phi = 1.0$  [8]. From this moment value, an ultimate lateral load was obtained. The columns were then laterally loaded to 75% of ultimate lateral load in the forward and then in the reverse direction. Displacements were experimentally measured in both directions. The average of the two displacements divided by 0.75 was then used as the yield displacement,  $\Delta_y$ . This definition of the yield displacement was used by Priestley et. al. [9] in their test programs at the University of Canterbury and is graphically defined in Figure 3.

While cyclic load test procedures for steel structures are in the process of standardization [10], no such recommended procedures have yet been agreed upon for testing reinforced

concrete structures. The determination of  $\Delta y$  and the cyclic load history to which the structure was subjected are therefore somewhat arbitrary. Unfortunately, there is evidence that column behavior is dependent upon cyclic load history [11]. For these reasons, and because of the wealth of bridge column test data available for comparison from New Zealand, the procedure described above for the determination of yield deflection and the loading sequence used in the New Zealand tests were adopted.

The columns were tested in the NBS Large Scale Test Facility shown in Figure 4. A photo of the shear column test in progress is shown in Figure 5. Loading history for each prototype column was identical to its corresponding model column. The loading sequences for the flexure and shear column are shown in Figure 6.

In order to determine the effects of scale on the behavior of bridge columns, six 1/6-scale model bridge columns were tested in addition to testing the full-scale specimens. Structural modeling theory calls for the scaling of not only the reinforcing steel, but also the concrete, leading to the use of "microconcrete." The use of microconcrete for specimens subjected to cyclic load, particularly those in which shear effects might be expected to dominate cyclic behavior, was questioned due to the possible differences in the details of the aggregate-interlock mechanism of microconcrete compared with prototype concrete. Two sets of model specimens were thus constructed for the present study, one using microconcrete and one using ready-mix concrete with small size (0.25 in.; 6 mm) river gravel.

The test parameters for the model columns were the same as those used for the prototype columns. The results of the model test program are reported in Reference 7.

#### 4. RESULTS

Plots of load versus column lateral displacement (base of column displacement relative to point of contraflexure) are presented in Figure 7. Significant drops in lateral load during an excursion corresponded to fracturing of the spiral and/or longitudinal reinforcing steel within the plastic hinge region. All the columns, prototype and model, failed in

flexure, although substantial diagonal cracking was observed within the plastic hinge region for the shear columns. Column failure was initiated by fracture of the confining reinforcement followed by buckling of the longitudinal reinforcement (Figure 8). Low cycle fatigue generally resulted in fracture of the longitudinal reinforcement during the next level of displacement ductility above that during which the spiral reinforcement first fractured.

Figure 9 compares performance of the full-scale flexure column with its 1/6-scale models. Lateral load has been normalized by the calculated ACI lateral load  $V_i$  which would cause a moment of  $M_i$  at the column base; thus  $M/M_i$  would have been equally applicable for the y-axis label (see Table 2). This convention will be used throughout the remainder of this paper. The x-axis has likewise been normalized by dividing by  $\Delta y$  and thus represents displacement ductility,  $\mu$ . This permits direct comparison between model and prototype without regard to scaling of results. The maximum moments for both full-scale flexure column and model columns constructed from microconcrete and ready mix concrete (models N3 and N6), respectively were determined to be 1.20, 1.23, and 1.14 times the calculated ultimate moment using ACI procedures. Ultimate displacement ductilities of 6.6, 5, and 4 were recorded for the full-scale flexure column and models N6 and N3, respectively. Note that maximum normalized displacements were approximately 5 and 7 for models N3 and N6. However, these latter values were recorded after moment resistance had dropped below 80% of the peak experimental moment obtained in the first cycle at  $2 \Delta y$ , the criteria used in this report to define column failure. Although there are no present requirements in the United States for column ductility (only for confining reinforcement ratios), at least one country (New Zealand) has adopted design spectra based on ductility with a ductility factor of 6 generally being considered a minimum value. The full-scale flexure column therefore exceeded this criterion but the models did not.

Figure 10 compares performance of the full-scale shear column with corresponding 1/6-scale models, including those for which higher axial

loads were applied ( $0.2f'_cA_g$  versus  $0.1f'_cA_g$ ). The maximum moments for the full-scale shear column and the model columns (N1 and N4) which were constructed from microconcrete and ready mix concrete, respectively, were determined to be 1.18, 1.16, and 1.20 times the calculated ultimate moment using ACI procedures. Models N2 and N5 (identical to N1 and N4, respectively, but with the higher axial load ratio) both showed peak  $M/M_i$  ratios of 1.32 which were substantially higher than for the lower stressed columns.

The moment enhancement ratio for those columns with  $P_e/f'_cA_g = 0.1$  approximately agrees with the value of 1.13 predicted in Reference 12 for columns with  $P_e/f'_cA_g \leq 0.1$ . The value of 1.32 for specimens N2 and N5 is on the high side of the 15% error band predicted in Reference 12 as follows:

$$\begin{aligned} M/M_i &= 1.13 + 2.35 (P_e/f'_cA_g - 0.1)^2 \\ &= 1.15 \end{aligned} \quad (4.1)$$

Ultimate displacement ductilities of 10, 8, and 10 were recorded for the full-scale shear column and models N1 and N4 respectively. Note that maximum normalized displacements were approximately 10 and 12 for models N1 and N4. However, these latter values were recorded after the column had begun to fail and were thus not considered in the evaluation. All of the shear column specimens, both model and prototype, had ultimate displacement ductilities in excess of 6 and thus would appear to be sufficiently reinforced. The amount of spiral reinforcement ( $\rho_s$ ) provided for these columns, however, was substantially in excess of that required by Reference 6 with the final choice for  $\rho_s$  for the shear column specimens being based on recommendations from CALTRANS [5]. The reader should also bear in mind that the loading histories for the shear columns were different than those for the flexure columns. The latter differed only in that 10 cycles were conducted at  $4\Delta_y$  in order to determine the stability of the hysteresis loops at that level of ductility. Model specimens N2 and N5 (which had a  $P_e/f'_cA_g$  value of 0.2) had ultimate displacement ductilities of 10 and 12, respectively, which can be compared with values of 8 and 10 for specimens N1 and N4 ( $P_e/f'_cA_g = 0.1$ ). This indicates that, within the bounds studied in this test program, increased

axial load appears to be beneficial. This hypothesis is further supported by comparing the load-displacement histories in Figure 10 which show consistently wider hysteresis loops for a given displacement ductility, indicating that more strain energy per cycle is dissipated inelastically. The ultimate moment capacities and displacement ductilities described above are summarized in Table 3.

It is useful at this point to make a comparison between the column ductilities measured in this study and their predicted displacement ductilities. Predicted ductilities are determined graphically from a design diagram presented in Reference 12, which is based on the New Zealand code, reproduced here as Figure 11. The x-axis is the ratio of the volumetric ratio of confining reinforcement provided to that specified in NZ-3101 [13]. This ratio is represented by the letter. The dark circles in Figure 11 represent the experimental ultimate displacement ductilities obtained from the NBS tests; the lines show how the predicted values were obtained for the same specimens. The upper diagonal line is for columns with aspect ratios of 3 (the shear columns) the lower diagonal line for an aspect ratio of 6 (flexure columns). It is interesting to note that the ductility of the full-scale flexure specimen, which had approximately the amount of confining reinforcement required by NZ-3101, agrees well with the predicted ductility value. The predicted ductilities for the flexure model specimens were, however, substantially greater than those observed experimentally. The same was true for both the prototype and model shear specimens. One possible reason for the discrepancy in the more heavily confined shear specimens is that large increases in the amount of confining steel become increasingly ineffective and asymptotically approach some maximum ductility. Experimental evidence to support this hypothesis is contained in Reference 14 which suggests a limiting steel ratio for spiral confinement of post-tensioned anchorage zones, beyond which only negligible gains in ultimate load are achieved.

The scaled areas bounded by the hysteresis loops of Figures 8 and 9 can be used to determine energy dissipation per cycle, using the

procedures defined in Reference 7. These values are shown on the bar charts in Figure 12. These charts clearly show that the microconcrete models overpredict the energy dissipation per cycle in the prototype and as evidenced by the rapid degradation in energy dissipation beginning at  $4 \Delta y$  for the flexure column and  $8 \Delta y$  for the shear column, exhibit premature column failure. The early failure of the microconcrete flexure column was caused by fracture of the confining spiral reinforcement in the plastic hinge region during the second cycle at  $4 \Delta y$ . The ready-mix model columns, on the other hand, appear to track the cycle-by-cycle performance of the prototypes quite well, although the ready-mix model flexure column shows some overprediction of energy dissipation per cycle.

The proximity between model and prototype individual cycle energy values in the bar charts represents a measure of the accuracy with which prototype behavior is predicted by model tests. For example, the high values of cyclic strain energy dissipation for the microconcrete models, when compared with the prototype, indicate that the scale factor for energy absorption, based on these tests, is less than the geometric scale factor of 6.1. The geometric scale factor relates the model dimensions to the prototype dimensions. The experimental scale factor for energy absorption,  $s_{1e}$ , calculated on a cycle-by-cycle basis is presented in Table 4 and reflects this aspect of similitude. This calculation is possible because identical load histories were used for both models and prototypes. Averages for  $s_{1e}$  up to the failure of the model specimens are presented at the bottom of the table. An experimental scale factor less than  $s_1$  (which for this set of tests was 6.1) indicates that the models overestimate the prototype absorbed cyclic strain energy. In this sense the microconcrete models are seen to perform poorly with approximately a 30% difference between experimental and practical true model scale factors. Therefore, use of microconcrete test results (based on the limited data available) would likely result in unconservative expectations for prototype energy absorption capacity.

The ready-mix shear model agrees well with the prototype on a cycle-by-cycle

basis and exhibits only a 1% difference between experimental and practical true scale factors. The ready-mix flexure model, while generally tracking prototype behavior (see Figure 12), is shown to have a 12% difference between experimental and practical true scale factors, based on consideration of cyclic absorbed strain energy.

An alternative comparison may be made between the total energy (summation of cycle energies) dissipated by model and prototype columns up to their respective failure points. Column (a) in Table 5 represents unmodified test data, with no corrections made for differences in concrete strength between specimens, nor accounting for friction losses and test machine interaction in the prototype tests. Columns (b) and (c) in Table 5 successively add these corrections. The final values [column (c)] indicate reasonable correlation between the total energy dissipation capacity of the ready-mix model columns and their prototype companions. The experimental scale factor for total energy for the ready-mix shear model column is 8% less than that for the practical true model scale factor (unconservative) while the ready-mix flexure model column leads to a 4% higher (conservative) value. Both of these values are encouraging, given the variance generally associated with testing of reinforced concrete structures, and indicate that total energy absorption capacity can be predicted through the use of appropriate model tests. No comparisons are made in Table 5 between microconcrete model columns and their respective prototypes due to the inability of these models to reproduce the cyclic load-deformation behavior of the prototypes.

Table 6 summarizes two other important specimen parameters relating model-to-prototype performance. The experimental scale factor for yield deflection,  $s_{1d}$ , is shown in column (a). Column (b) modifies  $s_{1d}$  to account for losses due to friction and test machine interaction for the prototype columns. The ratio of  $s_1/s_{1d}$  is a measure of the effectiveness with which the model data can be used to predict prototype yield displacements. Values of this ratio greater than 1.0 indicate conservatism (displacements predicted by model tests would be greater than

actually achieved in the prototype), whereas values less than 1.0 are unconservative (prototype displacements would be greater than predicted on the basis of model tests). Both of the above statements assume that model results would be extrapolated to prototype behavior using the practical true length scale factor,  $s_1$ , and the stress scale factor,  $s_\sigma$ . Use of microconcrete model columns (both flexure and shear) would therefore lead to overestimation of prototype yield deflection -- by an average of 60%. The ready-mix shear model specimen was shown to underpredict prototype yield displacement by 11%, while the ready-mix flexure model over-predicted yield displacement by 4%.

The second part of Table 6 presents information concerning the experimental scale factor for ultimate moment,  $s_{1m}$ . Similar to the calculations for strain energy, two levels of modifications are made to the original column moment data presented in column (c).

Differences in concrete compressive strength are accounted for in column (d) while losses due to friction and test machine interaction in the prototype tests are accounted for in column (e). The ratio of  $s_1/s_{1m}$ , shown in the far right column, indicates that all of the models (both microconcrete and ready-mix) were able to accurately predict prototype ultimate moment using only the considerations for the practical true model (moment scaled by  $s_1^3$ ) and the stress scale factor,  $s_\sigma$ .

## 5. CONCLUSIONS

1. The requirements for longitudinal and confining (spiral) reinforcing steel as defined in Reference 6 [CALTRANS] are sufficient to achieve a displacement ductility factor of 6 for full-scale bridge columns with an aspect ratio (height/diameter) of 6. Also, for full scale bridge columns with an aspect ratio of 3, a displacement ductility factor of 10 was achieved. These values were based on tests of single prototype specimens.
2. Similitude studies were conducted to determine if prototype behavior could be predicted from tests of 1/6-scale model columns. The results of these similitude tests are as follows:

- a) Model specimens constructed from ready-mix concrete were able to consistently reproduce prototype behavior on a cycle-by-cycle basis with scale factors for absorbed strain energy, ultimate moment, and yield displacement falling close to those for the practical true model,  $s_1$ .
  - b) Model specimens constructed from microconcrete were substantially more flexible than both the ready-mix models and prototypes and hence exhibited substantially greater yield deflections. Failure was generally more rapid than for ready-mix specimens and ultimate displacement ductility was 20% less. Because of this, model cyclic absorbed strain energy, when modified to account for scale factor and differences in concrete strength, is shown to overpredict (unconservative) the observed results from prototype tests.
  - c) Both microconcrete and ready-mix models were able to accurately reproduce prototype ultimate moment capacity by using the cube of the scale factor,  $s_1^3$ , and the scale factor for stress,  $s_\sigma$ .
  - d) The importance of the correct selection of materials (i.e. those which can develop aggregate interlock) is shown by the reasonably accurate prediction of the strain energy dissipated per cycle and the total energy dissipated up to column failure of the prototype columns using the results of the ready-mix concrete models.
3. Failure in both model and prototype column specimens was initiated by fracture of the confining reinforcement followed by buckling of the longitudinal reinforcement. Low cycle fatigue generally resulted in fracture of the longitudinal reinforcement during the next level of displacement ductility above that during which the spiral reinforcement first fractured.

4. Yielding of the longitudinal reinforcement in the column foundation was limited to a depth of less than 50% of the column diameter. This represents a distance approximately 40% of the specified (ACI) development length for the longitudinal reinforcement.
  5. Experimentally determined ultimate column moments were substantially greater than the nominal (ACI) calculated moment capacity (with  $\phi = 1.0$ ). The prototype columns (aspect ratios of 6 and 3) exhibited experimental ultimate moment-to-ACI nominal moment ratios (moment enhancement ratio) of 1.20 and 1.46, respectively. Similar ratios were observed for the model specimens. These results are for columns with axial loads of  $P_e/f'_c A_g = 0.1$ .
  6. An increase in column axial load from  $P_e/f'_c A_g = 0.1$  to 0.2 resulted in a 20% increase in ultimate displacement ductility and a 12% increase in moment enhancement ratio. These were based on comparisons between four model bridge columns and support the findings of other researchers [12].
6. REFERENCES
1. "Standard Specifications for Highway Bridges", as amended by AASTHO interims through 1984 with revisions by CALTRANS, AASHTO, 1983.
  2. "Seismic Design Guideline for Highway Bridges", Applied Technology Council, Berkeley, California, October 1981. 200pp.
  3. "Recommendations for Future Research", Applied Technology Council Workshop on Earthquake Resistance of Highway Bridges, Jan. 1979. Applied Technology Council, Berkeley, California. 625pp.
  4. Check, G. S., Stone, W. C., and Lew, H. S., "Behavior of 1/6 Scale Model Bridge Columns Subjected to Cyclic Inelastic Loading", Proceedings of the Third U.S.-Japan Bridge Workshop, Public Works Research Ministry of Construction, 1987, pp 423-448.
  5. Personal communication, Mr. James Gates, Chief Engineer, Structures Division, CALTRANS, 1983.
  6. "Excerpts from the Standard Specifications for Highway Bridges Relating to Seismic Design," 13th Edition, 1983 Adopted by the American Association of State Highway and Transportation Officials with Revisions by CALTRANS, Division of Structures. Version October 1985.
  7. Check, Geraldine S., and Stone, William C., "Behavior of 1/6-Scale Model Bridge Columns Subjected to Cyclic Inelastic Loading", NBSIR 86-3494, U.S. Department of Commerce, November, 1986.
  8. ACI Committee 340, "Design Handbook," in accordance with the Strength Design Method of ACI 318-77, Vol. 2, SP-17A (78), American Concrete Institute, 1978.
  9. Personal Communication with Dr. M.J.N. Priestly, University of Canterbury, Christchurch, NZ, 1985.
  10. "Recommended Testing Procedure for Assessing the Behavior of Structural Steel Elements under Cyclic Loads," ECCS - Technical Committee 1, Structural Safety and Loadings Technical Working Group 1.3 - Seismic Design Report. First Edition No. 45, 1986. European Convention for Constructional Steelwork. Available from A. Plumier, Institut du Genie Civil, 6 Quai Banning, Universite de Liege, Belgium.
  11. Krawinkler, H. et.al., "Recommendations for Experimental Studies on the Seismic Behavior of Steel Components and Materials," Report No. 61, The John A. Blume Earthquake Engineering Center, Department of Civil Engineering, Stanford University, September 1983.
  12. Priestly, M.J.N., and Park, R., "Strength and Ductility of Concrete Bridge Columns Under Seismic Loading," ACI Structural Journal, Title No. 84-S8, Vol.84,

No. 1, American Concrete Institute, Detroit, MI., Jan-Feb 1987, pp 61-76.

13. "NZS-3101: 1982 'Code of Practice for the Design of Concrete Structures'", (Two Volumes: Code and Commentary), Standards Association of New Zealand, 1982.
14. Stone, W.C., and Breen, J.E., "Behavior of Post-Tensioned Girder Anchorage Zones," PCI Journal, Vol. 29, No. 1, Prestressed Concrete Institute, Chicago, Ill., Jan-Feb 1984, pp 64-109.

**Table 1: Column Dimensions**

Specimen	Type of Concrete	Height (feet)	Diameter (inches)	Axial Load (kips)
<b>Model Columns</b>				
N1	Microconcrete	2' - 5.5"	9.8	26.87
N2	Microconcrete	2' - 5.5"	9.8	53.75
N3	Microconcrete	4' - 11"	9.8	26.87
N4	Ready-Mix (1/4" Gravel)	2' - 5.5"	9.8	26.87
N5	Ready-Mix (1/4" Gravel)	2' - 5.5"	9.8	53.75
N6	Ready-Mix (1/4" Gravel)	4' - 11"	9.8	26.87
<b>Prototype Columns</b>				
Flexure	Ready-Mix (3/4" Gravel)	30' - 0"	60.0	1000.00
Shear	Ready-Mix (3/4" Gravel)	15' - 0"	60.0	1000.00

Table 2: Calculated Ideal Strengths of Full-Scale and 1/6-Scale Model Bridge Column Specimens.

Specimen	$P_e$ (kips)	$\frac{P_e}{f'_c A_g}$	$M_i$ (kip-ft)	Column Height (inch)	$V_i$ (kips)	$f'_c$ (ksi)	$f_y$ (ksi)
N1	26.87	.100	32.37	29.5	13.17	3.49	64.7
N2	53.75	.210	35.37	29.5	14.39	3.35	64.7
N4	26.87	.100	32.37	29.5	13.17	3.54	64.7
N5	53.75	.200	35.37	29.5	14.39	3.53	64.7
SHEAR	1000.00	.071	7988.3	180.0	532.55	4.98	68.9
N3	26.87	.100	32.37	59.0	6.58	3.68	64.7
N6	26.87	.110	32.37	59.0	6.58	3.38	64.7
FLEX	1000.00	.068	8041.1	360.0	268.04	5.20	68.9

Where

$P_e$  = applied axial column load

$M_i$  = ideal moment capacity calculated using ACI approach where an ultimate concrete strain of .003 together with a rectangular concrete stress block are assumed.

$P_i$  = ideal lateral load capacity =  $(M_i - P_e \Delta)/h_1$  in general; evaluated here at  $\Delta=0$ , where  $h_1$  = effective height of test column from fixed support to point of contraflexure.

Table 3: Experimental Maximum Moment and Ductility Capacity

Specimen	$\frac{P_e}{f'_c A_g}$	Aspect Ratio ( $h_1/D$ )	Ultimate Moment Capacity			Ductility Capacity		
			$M_i$ (k-ft.)	$M_{exp}$ (k-ft.)	$M_i/M_{exp}$	$\Delta_y$ (in.)	$\Delta_u$ (in.)	$\mu = \Delta_u/\Delta_y$
N1	0.100	3	32.37	38.35	1.18	0.38	3.04	8.0
N2	0.210	3	35.37	46.52	1.32	0.22	2.20	10.0
N3	0.100	6	32.37	39.76	1.23	1.01	4.04	4.0
N4	0.100	3	32.37	37.48	1.16	0.21	2.10	10.0
N5	0.200	3	35.37	46.61	1.32	0.19	2.28	12.0
N6	0.110	6	32.37	36.87	1.14	0.66	3.30	5.0
Shear	0.071	3	7988.30	11640.00	1.46	1.40	14.02	10.0
Flexure	0.068	6	8041.10	9643.00	1.20	3.53	23.30	6.6

Table 4: Experimental Scale Factor for Absorbed Energy\*\*  
[on a cycle-by-cycle basis]

	$s_{1e}$	$s_{1e}$		$s_{1e}$	$s_{1e}$
Cycle <sup>5</sup>	$\left[ \frac{\text{Shear}^1}{N1} \right]^{1/3}$	$\left[ \frac{\text{Shear}}{N4} \right]^{1/3}$	Cycle	$\left[ \frac{\text{Flexure}}{N3} \right]^{1/3}$	$\left[ \frac{\text{Flexure}}{N6} \right]^{1/3}$
11	6.14	4.86	11	4.48	4.84
21	4.14	5.89	21	4.16	5.00
22	3.96	6.07	22	3.85	4.81
41	4.54	6.20	31	4.64	5.27
42	4.41	6.13	32	4.39	5.19
61	4.61	6.18	41	4.77	5.48
62	4.34	6.10	42	5.01	5.47
81	4.99 <sup>2</sup>	6.10	43	5.57	5.45
82	6.14	6.05	44	5.93 <sup>2</sup>	5.44
101		6.18	45	6.26	5.45
102		6.33 <sup>2</sup>	46	6.99	5.46
103		5.94 <sup>3</sup>	47		5.47
			48		5.51
			49		5.60
			410		5.93
			51		6.38 <sup>2</sup>
			52		6.88
			53		7.04
			61		7.75
			62		8.10 <sup>3</sup>
	Micro $s_{1e}$	Ready-mix $s_{1e}$		Micro $s_{1e}$	Ready-mix $s_{1e}$
Avg. <sup>4</sup>	4.6	6.0		4.7	5.4
$S_1/\text{Avg.}$	1.33	1.01		1.30	1.12

- 1: Shear = Full scale shear column, Flexure = Full scale flexure column  
N1 = Microconcrete shear model, N4 = Ready-mix shear model  
N3 = Microconcrete flexure model, N6 = Ready-mix flexure model
- 2: Failure of model.
- 3: Failure of full scale column.
- 4: Averaged up to failure of the model.
- 5: Cycle 41, e.g., is Cycle number 1, displacement ductility of 4 etc.

\*\* Energy calculated by graphically integrating area bounded by lateral load vs column deflection hysteresis loops for each complete lateral excursion at a given displacement ductility using procedures outlined in Reference 6. Cyclic energy for the model specimens was multiplied by  $s_G = f'_c(\text{prototype})/f'_c(\text{model})$ . Prototype cyclic energy was scaled to account for friction and test machine interaction ( $f_{em} = 1.096$  and  $1.305$  for shear and flexure columns, respectively).

Table 5: Scale Factors Relating Prototype and 1/6-Scale Model Column Behavior: Total Strain Energy to Failure\*

Specimen	$f'_c$ (ksi)	(a)		(b) <sup>1</sup>		(c) <sup>2</sup>	
		Energy Absorbed Up to Failure (k-in.)		Column (a) $\times s_\sigma$ (k-in.)		Column (b) $\times f_{em}$ (k-in.)	
N4	3.54	348.70		518.36		518.36	
Shear	4.98	83888.24		83888.24		91914.89	
N6	3.38	351.08		540.12		540.12	
Flexure	5.20	105923.85		105923.85		138270.80	
		$s_{1e}$	$s_1/s_{1e}$	$s_{1e}'$	$s_1/s_{1e}'$	$s_{1e}''$	$s_1/s_{1e}''$
Shear/N4		6.22 <sup>3</sup>	0.98	5.44 <sup>3</sup>	1.12	5.62 <sup>3</sup>	1.08
Flexure/N6		6.71 <sup>3</sup>	0.91	5.81 <sup>3</sup>	1.05	6.34 <sup>3</sup>	0.96

1: The energy absorbed by the model columns has been modified to account for differences in concrete compressive strength between model and prototype.

2: The energy absorbed by the prototype column has been modified to account for losses in lateral load due to friction and test machine interaction when determining  $\Delta_y$  for the prototype columns. Note that  $f_{em} = 1.096$  for the shear column; 1.3054 for flexure column.

3: This value represents the cube root of the ratio of the sum of all prototype cyclic strain energy to the sum of all model cyclic strain energy up to failure of the respective columns (e.g. Shear/N1). Recall that N1 and N3 were constructed with microconcrete; N4 and N6 were constructed using fine aggregate ready-mix. Otherwise these specimens, respectively, were identical.

\*: No comparison is made for microconcrete models, since these were not effective in reproducing prototype behavior on a cycle-by-cycle basis.

Table 6: Scale Factors Relating Full-Scale and 1/6-Scale Model Column Behavior: Displacements and Moments

Specimen	$f'_c$ (ksi)	(a) $\Delta_y$ (in.)	(b) <sup>4</sup> $\Delta_y$ $\times 1/f_{le}$ (in.)	(c) Ultimate Moment (k-in.)	(d) <sup>1</sup> Column (c) $\times s_\sigma$ (k-in.)	(e) <sup>2</sup> Column (d) $\times 1/f_{em}$ (k-in.)		
N1	3.49	0.38	0.38	38.35	54.72	54.72		
N4	3.54	0.21	0.21	37.48	52.73	52.73		
Shear	4.98	1.40	1.44	11640.00	11640.00	12753.95		
N3	3.68	1.01	1.01	39.76	56.18	56.18		
N6	3.38	0.66	0.66	36.87	56.71	56.71		
Flexure	5.20	3.53	3.86	9643.00	9643.00	12584.11		
		$s_{1d}$	$s_{1d}'$	$s_{1d}/s_{1d}'$	$s_{1m}^3$	$s_{1m}'^3$	$s_{1m}''^3$	$s_{1d}/s_{1m}''$
Shear/N1		3.68	3.78	1.61	6.72	5.97	6.16	0.99
Shear/N4		6.67	6.85	0.89	6.77	6.04	6.23	0.98
Flexure/N3		3.50	3.82	1.60	6.24	5.55	6.07	1.00
Flexure/N6		5.35	5.85	1.04	6.40	5.54	6.05	1.01

1: Ultimate moment for model columns has been modified to account for differences in concrete compressive strength between model and prototype.

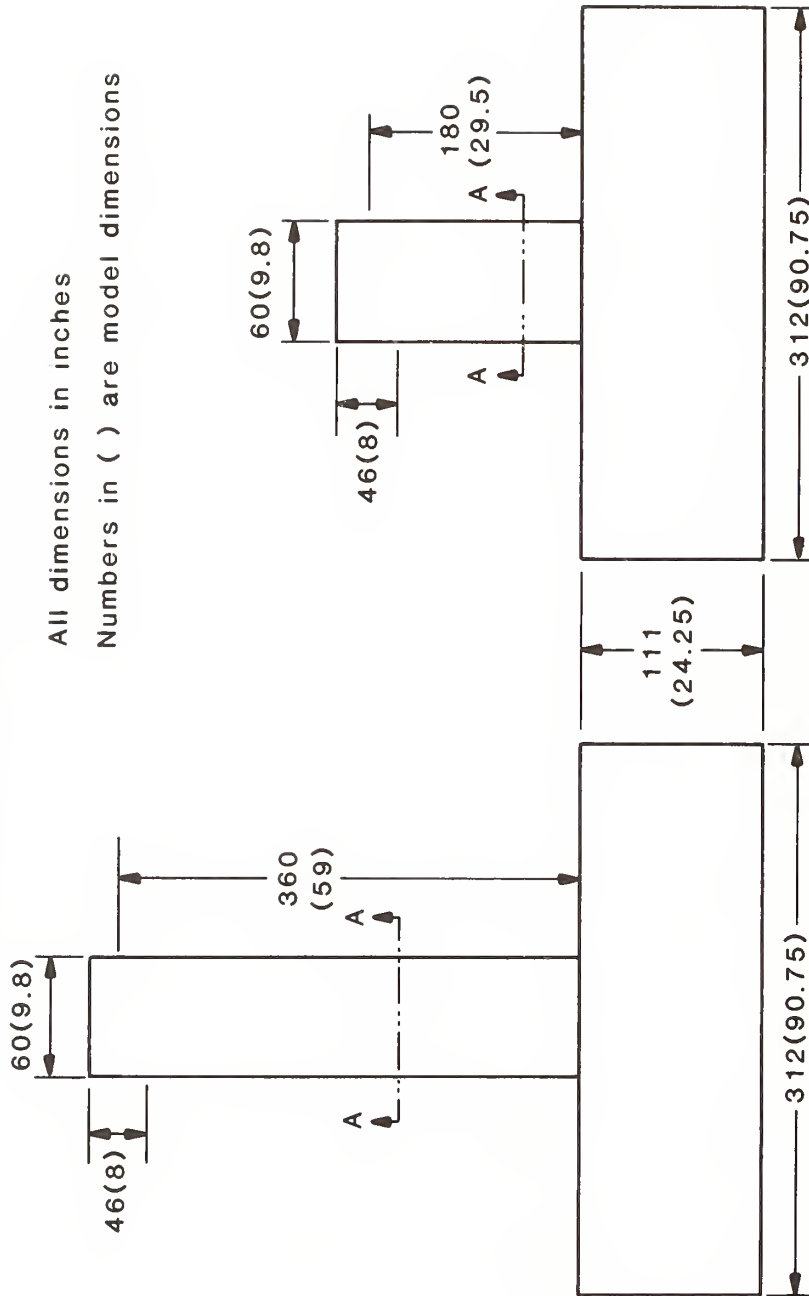
2: Ultimate moment for prototype column has been modified to account for losses in lateral load due to friction and test machine interaction. Note that  $f_{em} = 1.096$  for the shear column; 1.3054 for flexure column.

3: This value represents the cube root of the ratio of the prototype moment to the moment in its corresponding model (e.g. Shear/N1). Recall that N1 and N3 were constructed with microconcrete; N4 and N6 were constructed using fine aggregate ready-mix. Otherwise these specimens, respectively, were identical.

4: Yield displacement for prototype columns has been modified to account for losses in lateral load during determination of  $\Delta_y$  (see note 2 above)

PROTOTYPE AND MODEL DIMENSIONS

All dimensions in inches  
 Numbers in ( ) are model dimensions



NOTE: Base width is 96 (28.375)

Figure 1: Side Profile, Full-Scale and Model Column Specimens

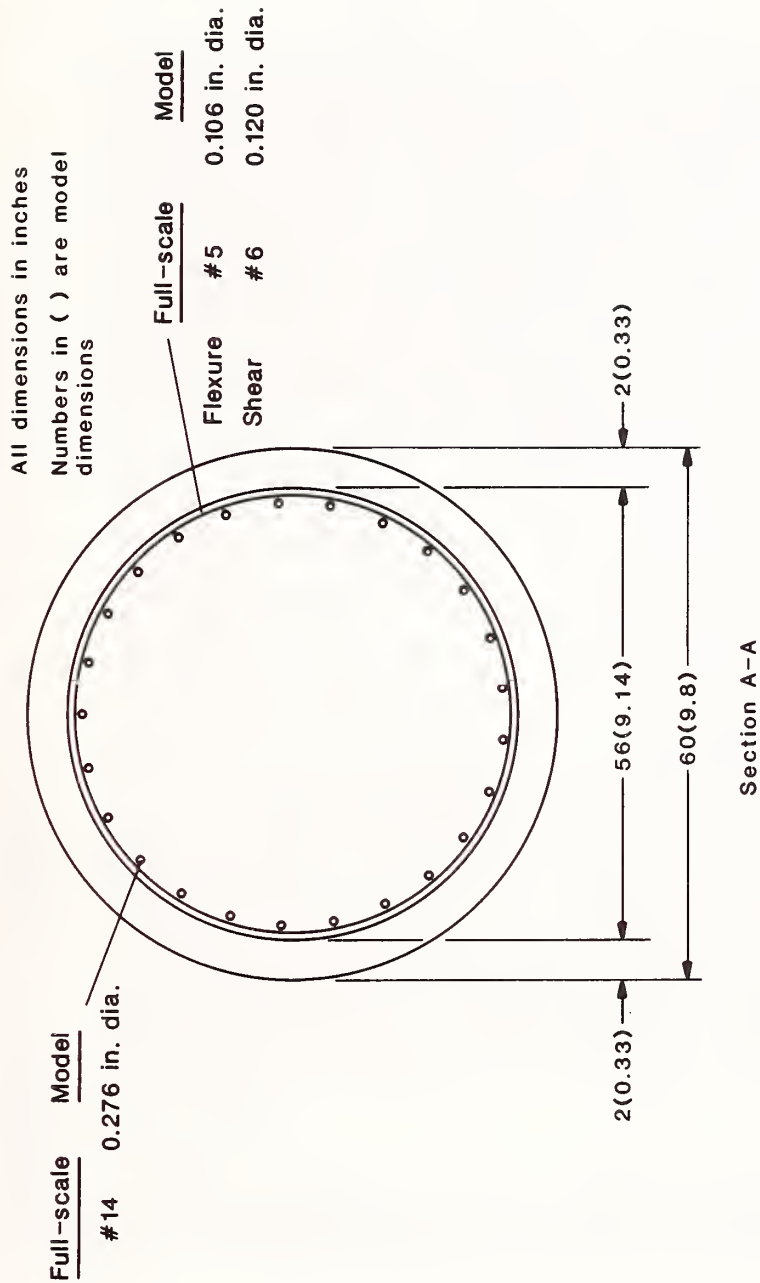


Figure 2: Column Cross-Sections and Reinforcement

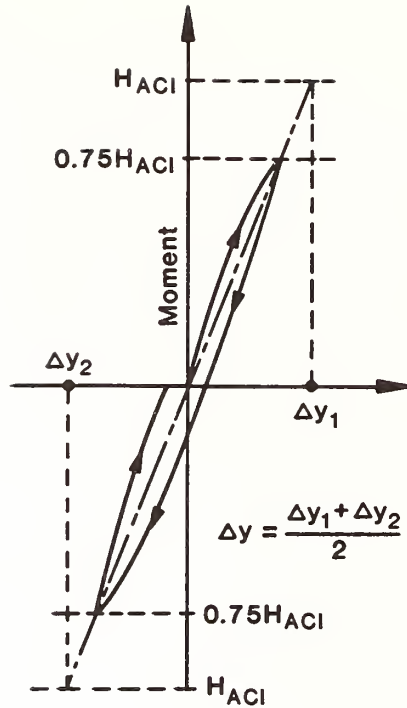


Figure 3: Experimental Definition of Yield Deflection

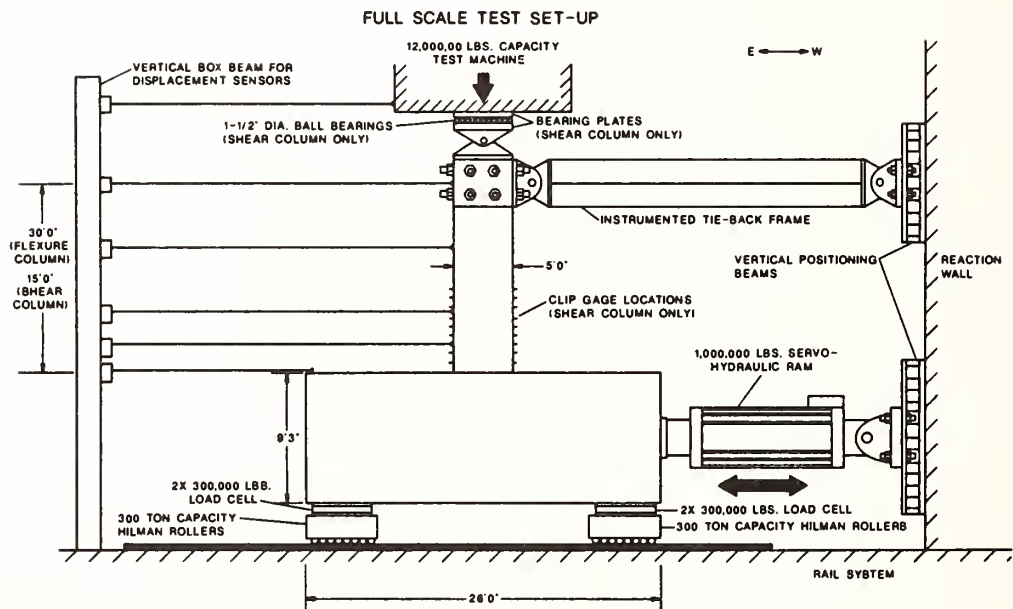


Figure 4: Schematic of Full-Scale Test Apparatus



Figure 5: Prototype Shear Column Under Test in NBS Large Scale Structures Laboratory.

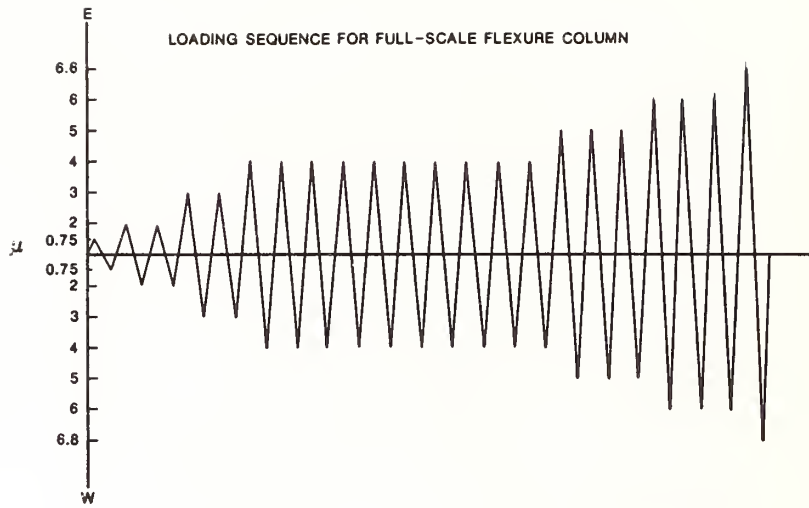


Figure 6a: Loading History for Flexure Columns

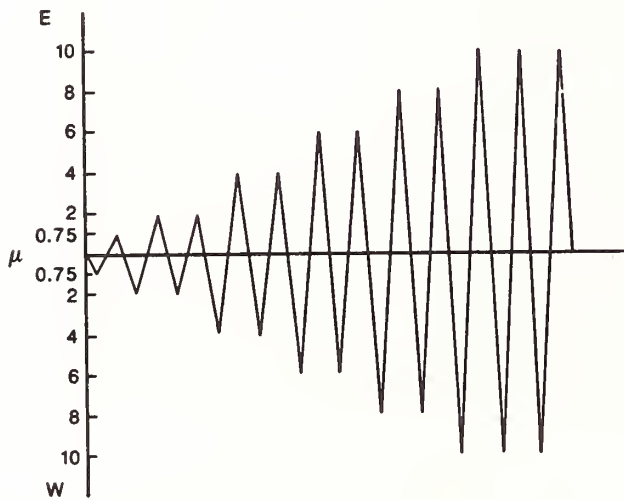


Figure 6b: Loading History for Shear Columns

LOAD DEFLECTION PLOT FOR FLEXURE COLUMN TEST

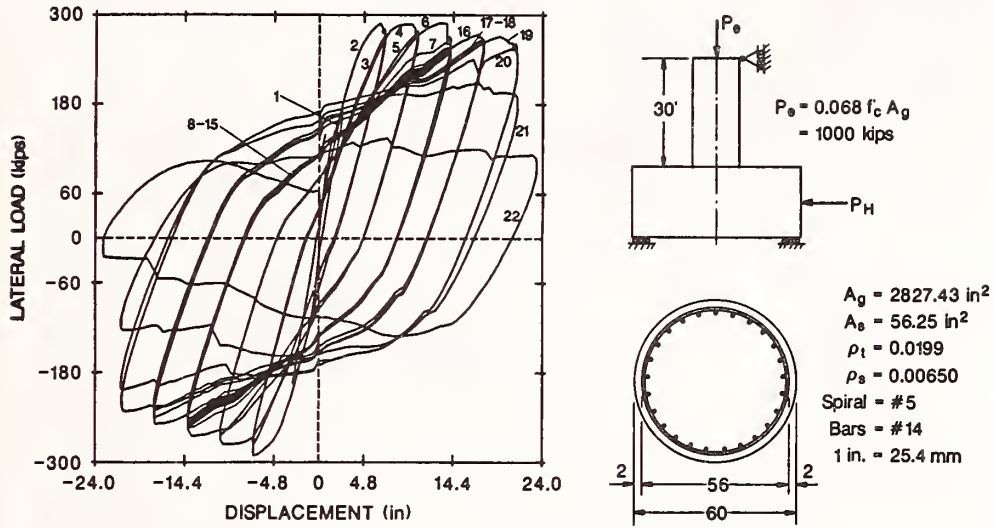


Figure 7a: Lateral Load vs. Displacement plot for Full-Scale Flexure Column. Cycle Numbers 1,2,4,6,16, and 19 correspond to Displacement Ductilities of 1,2,3,4,5, and 6, respectively

LOAD DEFLECTION PLOT FOR SHEAR COLUMN TEST

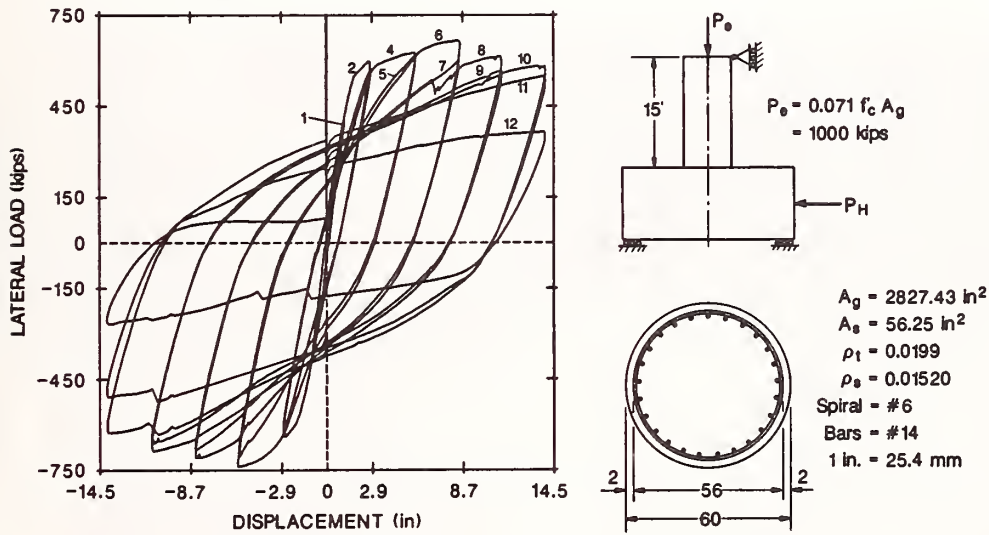


Figure 7b: Lateral Load vs. Displacement plot for Full-Scale Shear Column. Cycle Numbers 1,2,4,6,8, and 10 correspond to Displacement Ductilities of 1,2,4,6,8, and 10, respectively



Figure 8b Full Scale Shear Column at the end of test. Displacement ductility = 10

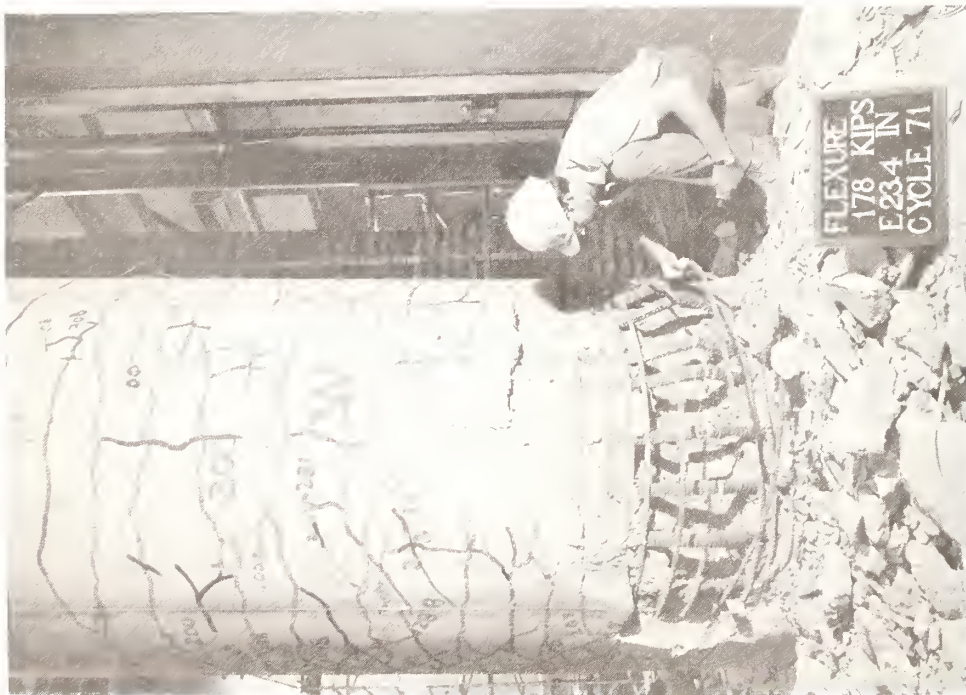


Figure 8a Full Scale Flexure Column at the end of the test. Displacement ductility = 7

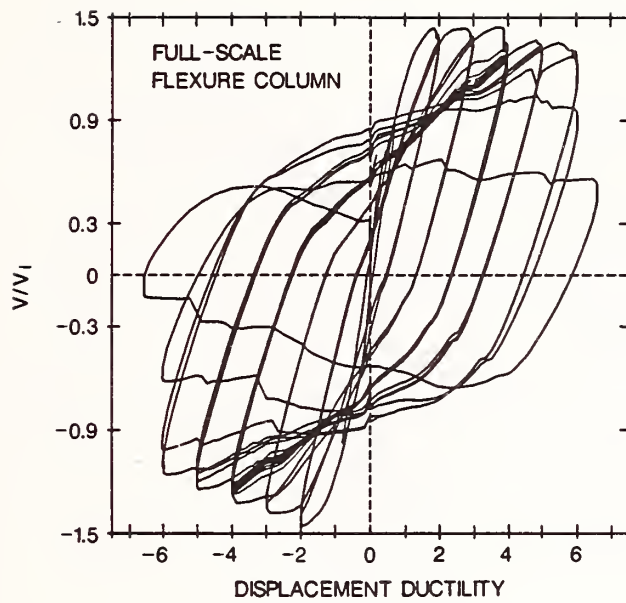


Figure 9a: Normalized Lateral Load ( $V/V_1$ ) versus Displacement Ductility ( $\Delta/\Delta_y$ ) for Full-Scale Flexure Column

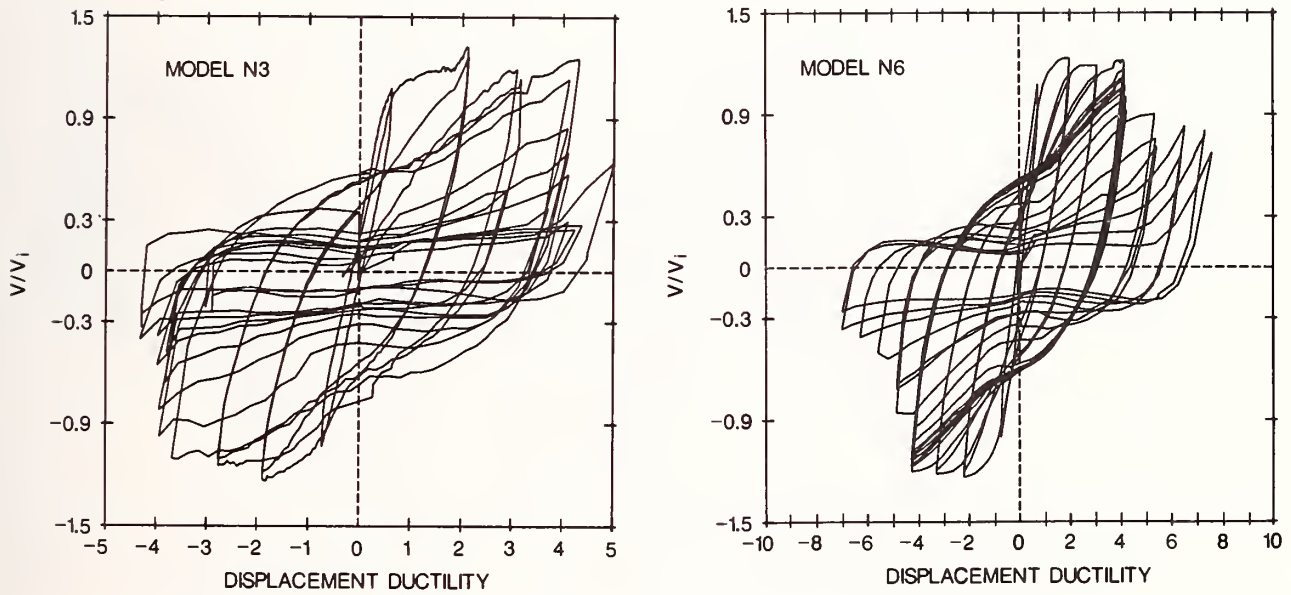


Figure 9b: Normalized Lateral Load ( $V/V_1$ ) versus Displacement Ductility ( $\Delta/\Delta_y$ ) for Model Columns N3 and N6.  
 N3 = microconcrete; N6 = readymix;  $P_e/(f'_c A_g) \approx 0.1$

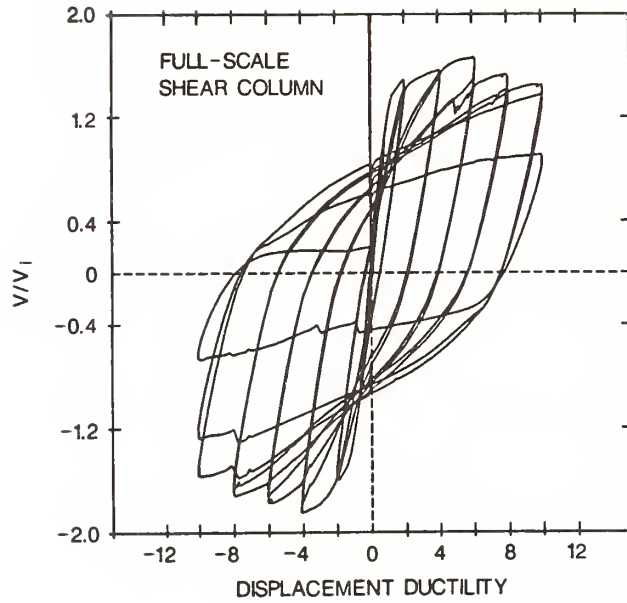


Figure 10a: Normalized Lateral Load ( $V/V_i$ ) versus Displacement Ductility ( $\Delta/\Delta_y$ ) for Full-Scale Shear Column

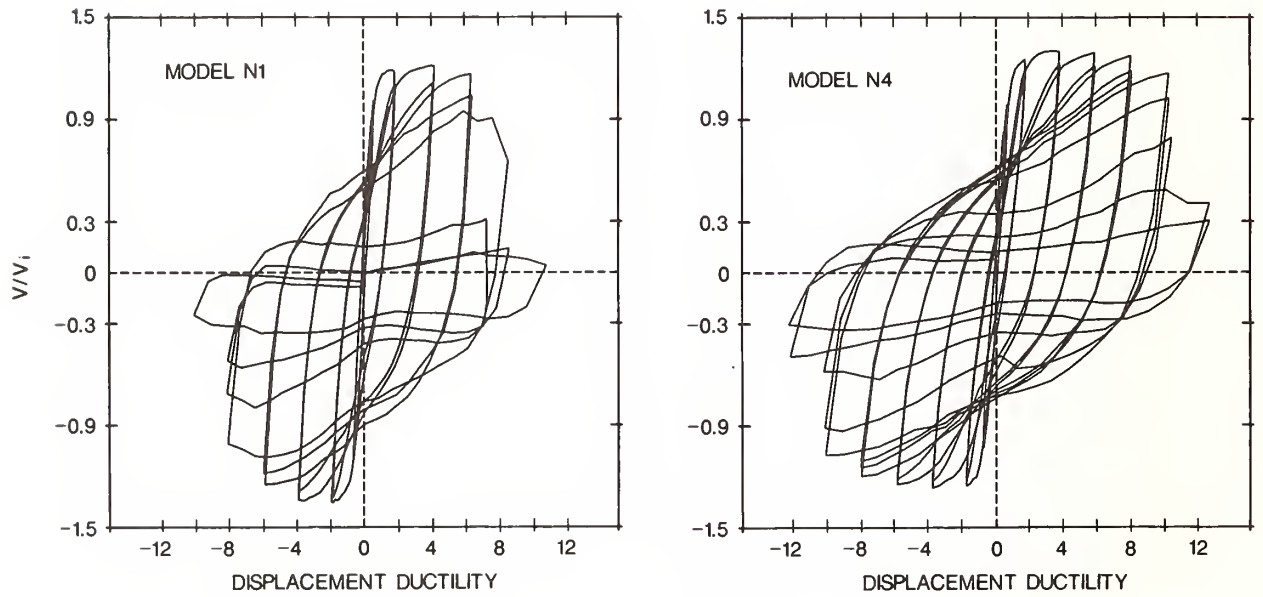


Figure 10b: Normalized Lateral Load ( $V/V_i$ ) versus Displacement Ductility ( $\Delta/\Delta_y$ ) for 1/6-Scale Model Shear Columns. N1 = microconcrete; N4 = readymix;  $P_e/(f'_c A_g) \approx 0.1$

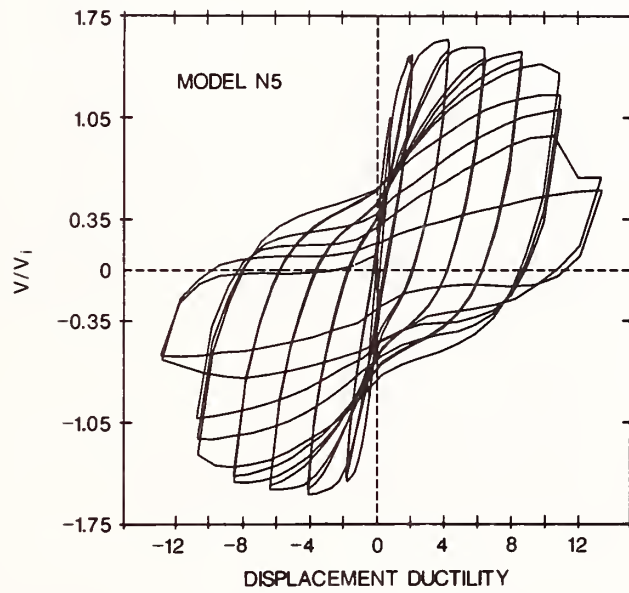
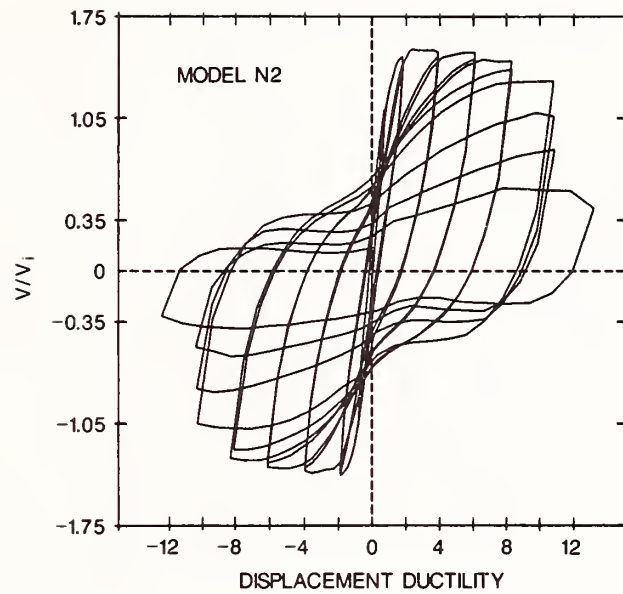


Figure 10c: Normalized Lateral Load ( $V/V_i$ ) versus Displacement Ductility ( $\Delta/\Delta_y$ ) for 1/6-Scale Model Shear Columns. N2 = microconcrete; N5 = readymix;  $P_e/(f'_c A_g) \approx 0.2$

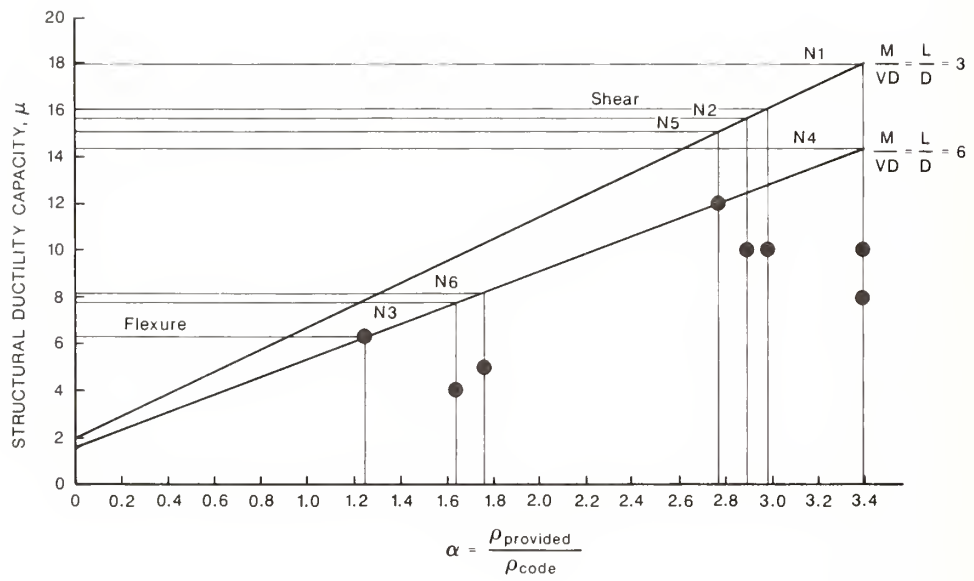


Figure 11: Structure Ductility Capacity Related to Confinement Ratio

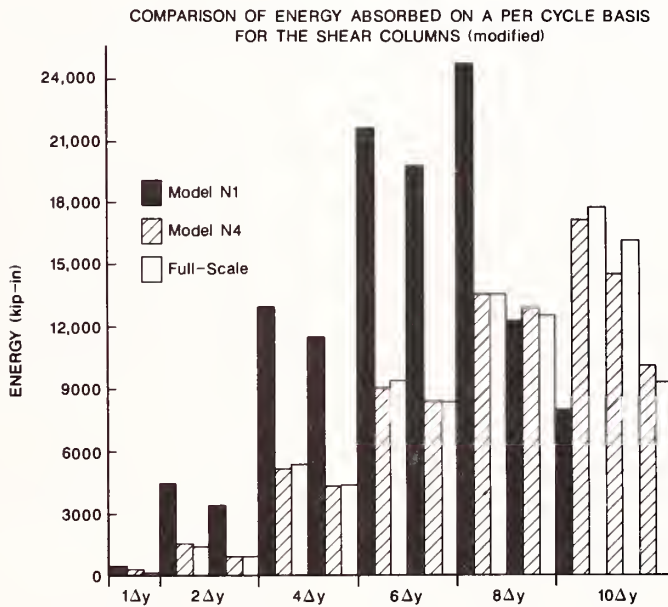
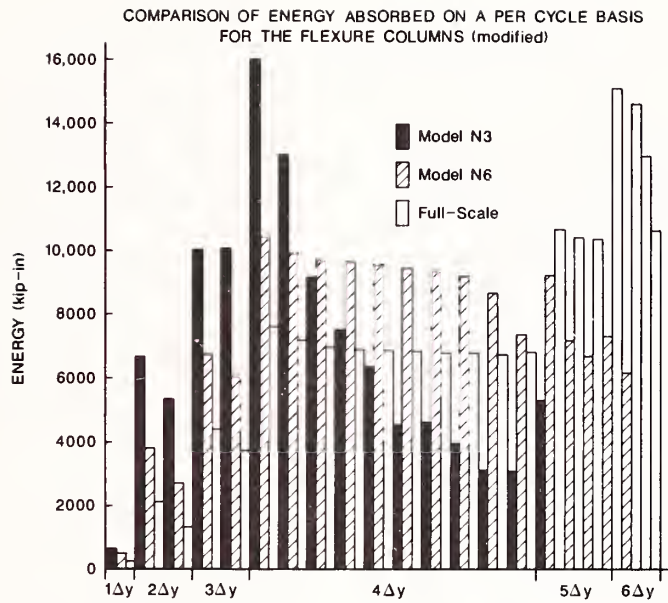


Figure 12: A Comparison of Cyclic Energy Dissipation between Model and Prototype Specimens with Modifications to Account for Differences in Compressive Strength between Models and Prototypes, and for Friction Losses in the Prototype Tests. Top Chart is for Flexure Specimens ( $L/D = 6$ ); Bottom Chart for Shear Specimens ( $L/D = 3$ ).

# Study on the Development of the Mixed Structural System Composed of Reinforced Concrete Column and Structural Steel Girder

BY

Hiroyuki YAMANOUCHI<sup>1</sup>, Isao NISHIYAMA<sup>2</sup>

## ABSTRACT

A new mixed structural system comprised of reinforced concrete columns and structural steel girders is proposed. In order to apply this mixed system to actual structures, a structural evaluation of "joint panels in mixed system" and a quantitative assessment compared to other structural systems were carried out. The investigation results show the advantages of the proposed mixed system for practical application.

KEY WORDS: Mixed System, Panel-Zone, Half-Scale Test, Design Simulation

## 1. INTRODUCTION

Although steel structures have their own advantages in weight, ductility, span length, term of the construction contract etc., compared with reinforced concrete structures, they are not always more competitive in the total construction cost, since the material of reinforced concrete is significantly cheaper than steel. Introduced in this paper is a challenging mixed structural system comprised of reinforced concrete columns and structural steel girders which utilizes both, the advantages of steel and reinforced concrete. In order to apply this mixed system to actual structures, a structural performance evaluation and a quantitative assessment compared to other structural systems are discussed in the following.

The first item discussed in this paper is the structural performance evaluation of the steel girder to reinforced concrete column joint panels. Results from half scale tests on perpendicular girder + column joint sub-assemblages are presented and discussed. The second one is to assess the advantages of the mixed structural system quantitatively and to find out the most effective practical applications, such as the optimal span length. For this purpose, design simulations and comparisons were carried out on a prototype 3x3 bay, three story building, designed in steel, reinforced concrete and as a mixed structural system.

## 2. CYCLIC LOADING TESTS ON GIRDER-TO-COLUMN SUB-ASSEMBLAGES

### 2.1 Joint Panel Details

Typical joint panel details are shown in Fig.1. Depicted are the details of the full-flange-type panel, in which two perpendicular structural steel I-girders penetrate the reinforced concrete column, see Fig.1(a), with the main reinforcing bars (rebars) in the column corners passing through the panel zone, while center line rebars are welded to the top and bottom of the steel girders. Fig.1(b) shows the details of the tapered-flange-type panels, in which girder flanges are tapered by cutting. The taper angle measures 45 degrees. These cut girder flanges assure reliable concrete casting in the panel zone.

### 2.2 Test Specimens And Loading

Five test specimens of one half scale girder-to-column sub-assemblages with short transverse girders were investigated. The ratio of the strength of columns to that of girders and the amount of the flange cutting of the steel girder in the panel zone were selected as test parameters. The shape of the specimens is shown in Fig.2. The mechanical properties of steel, rebar and concrete are shown in Table 1. The specimens, whose columns are weaker than girders, are denoted by "A" and the specimens with strong column and weak girders are affixed with "B". The specimens with full-flange-type panels are denoted by "1", those with tapered-flange-type panels whose taper started from the rebar location are denoted by "2" and the specimen with the taper starting at the column face is denoted by "3". (see Fig.2)

The both ends of the girder were loaded inversely by two actuators simulating seismic forces with a constant axial column load of 620kN, as shown in Fig.3.

### 2.3 Test Results

#### 2.3.1 General Behavior

First, flexural cracks were observed in the columns followed by subsequent diagonal

<sup>1</sup>Dr. of Eng., Head, Structural Dynamics Division, Structural Engineering Department, Building Research Institute, Ministry of Construction, Japan.

<sup>2</sup>Dr. of Eng., Chief, Building Dynamics Division, International Institute of Seismology and Earthquake Engineering, Building Research Institute, Ministry of Construction, Japan.

cracking in the panel zone. Then, the shear yielding of the web plate of the steel girder in the panel zone occurred. Finally, in case of the specimens with full-flange-type panels ("I"), the center line rebars fractured close to the weld point on the top of the girder flange because of poor workmanship of the weld execution. This fracture brought about the spalling of the cover concrete in the panel zone. On the other hand, in case of the specimens with tapered-flange-type panels, the center line rebars did not fracture, forces were transmitted properly from steel girder to reinforced concrete column and the yielding of the tensile reinforcement occurred. Only minor spalling of the concrete cover was observed.

### 2.3.2 Hysteresis Behavior

The hysteresis curves of the column shear force (Qc) vs. story drift angle (R) relationships are shown in Fig.3. Each specimen showed quite stable loops. The maximum strength has the tendency to reduce as the amount of the flange cutting of the steel girder in the panel zone increases. Severe deterioration of load carrying capacity was observed in specimens with full-flange-type panels (A-1 & B-1) at the drift angle of 0.05 radian, where the severe spalling of cover concrete was observed in the panel zone because of the fracture of center line rebars fractured.

### 2.3.3 Maximum Strength and Crack Initiation Strength

The experimental and the calculated strengths of each specimen are summarized in Table 2. The experimental maximum strength to the calculated strength ratios are all larger than unity. This means that even tapered-flange-type joints well satisfy the required maximum strength criteria (eq.(1)) recommended by SRC Standard of ALJ [1],

$$j\mu = cVe ( jFs \cdot j\delta + wP \cdot w\delta_y ) + \frac{1.2 sV \cdot s\delta_y}{\sqrt{3}} \text{ ---- (1)}$$

where,  
 $cVe = \frac{(c_b/2) \cdot s_b^d \cdot m_c^d}{\text{volume}(\text{mm}^3)}$  = effective panel concrete volume (mm<sup>3</sup>),  
 $c_b$  = width of column (mm),  
 $m_c^d (s_b^d)$  = distance from centroid of compression steel to that of tension in column (girder) (mm),  
 $jFs$  = concrete shear strength which is smaller value of 0.12Fc or 1.76 + (3.6Fc/100) (MPa),  
 $Fc$  = nominal design strength of concrete (MPa),  
 $j\delta$  = coefficient dependent on the joint shape (cross-shaped=3),  
 $wP = \frac{w_a}{(c_b \cdot x)}$  = reinforcement ratio of hoops which is less than 0.6%,  
 $w_a$  = 2 times area of the hoop rebar (mm<sup>2</sup>),  
 $x$  = spacing between hoops (mm),  
 $w_y$  = tensile yield strength of hoops (MPa),  
 $sV = \frac{s_b^d \cdot d^c \cdot j_t \cdot t_w}{\text{volume}(\text{mm}^3)}$  = effective panel steel volume (mm<sup>3</sup>),  
 $s_y^d$  = tensile yield strength of the structural steel (MPa), and

$j_t \cdot t_w$  = thickness of steel web panel (mm).

As for the crack initiation strength of the joint panels, the test results are two or three times higher than the calculated ones. The shear stress ( $\tau$ ) at the onset of diagonal cracking is taken as 0.1Fc in Ref.[1]. (see Table 2) Therefore, the experiments show that the crack initiation shear stress might be considered to be 0.3Fc in the case of full-flange-type panels and 0.2Fc in the case of tapered-flange-type panels.

### 2.4 Summary Of Experimental Results

The hysteresis loops are quite stable in all specimens. However, as the amount of cutting of the steel flange increases in the panel zone (tapered-flange-type panels), the maximum strength decreases. The reduction of the maximum strength is associated with the reduction of local bearing force on the steel flange and thus the specimens with tapered-flange-type panels are associated with a reduction of the spalling cracks of the column concrete cover.

Both strength and ductility are acceptable for practical design application in all investigated joint panels. However, the welding of center line rebars to the top of the girder flange must be well executed to eliminate the severe strength deterioration caused by rebar fracture.

## 3. DESIGN SIMULATION

### 3.1 Designed Buildings

Design simulations were conducted on a prototype 3x3 bay, three story building. This structure, shown in Fig.4, was designed with mixed, steel and reinforced concrete structural systems. The span length in the longitudinal direction of the prototype, 8m, was changed to 10m, 12m and 14m. For these three additional model structures, the same design simulations as that done for the prototype model were carried out to examine the effect of span length. The height of the story was set at 2.90m as the clear story height, i.e. the distance from the top of the floor slab to the bottom of the upper floor girder. All assumed design conditions are summarized in Table 3.

### 3.2 Results Of Simulation

Table 4 summarizes the various characteristics of the designed structures; the story height, the story drift, the total weight and the construction cost. The ratios of the calculated panel strengths by eq.(1) to the required panel moments are listed in Table 5.

#### 3.2.1 Girder Height and Story Height

The depth of the girders and the story height

are almost the same in buildings designed with mixed and steel systems. The depth of the girders designed for the reinforced concrete system is not so different from those designed with mixed and steel systems in the case of 10m or less span length. However, as the span length becomes larger than 12m, the required girder depth significantly increases in the reinforced concrete system.

### 3.2.2 Story Stiffness

The story drift angles of designed buildings subjected to seismic force of 20% of the building weight are summarized in Table 4. The inverse of the story drift angle of the mixed system is 70% of that of the reinforced concrete system and about 200% of that of the steel system.

### 3.2.3 Weight of Designed Buildings

The weight per unit floor area is listed in Table 4, where the weight of interior and exterior walls, stairs etc. are not considered. The unit weight of the mixed system, about  $9.8\text{kN/m}^2$ , is rather light compared to that of the reinforced concrete system,  $12.7\text{-}13.7\text{kN/m}^2$ , and is nearly equal to the unit weight of the steel system,  $8.8\text{kN/m}^2$ .

### 3.2.4 Construction Cost

The construction cost per unit floor area are summarized in Table 4, where the following unit costs are used; concrete= $12,300\text{yen/m}^3$ , formwork= $3,600\text{yen/m}^2$ , rebar= $8.57\text{yen/N}$ , structural steel= $18.9\text{yen/N}$ , metal deck =  $17.3\text{yen/N}$  and fire protective covers =  $2,600\text{yen/m}^2$ . The unit cost of the building designed as reinforced concrete system is the cheapest among three systems in all span length simulations. However the unit cost of the mixed system becomes close to that of the reinforced concrete system for buildings with longer span length.

### 3.2.5 Recommended Strength and Required Strength for Joint Panels

The ratios of the calculated strength by eq.(1) to the required strength estimated from the ultimate strengths of adjacent members for the joint panels are summarized in Table 5. The ratios are all larger than unity. This means that the joint panels are not needed to be strengthened for practical use if eq.(1) is satisfied.

### 3.3 Summary Of Design Simulations

The mixed system can keep the story height as small as the steel system. Therefore more stories can be accommodated within the same building height for reinforced concrete systems. The stiffness of mixed system is 70% of reinforced concrete and twice that of steel. Therefore, it can be used for

buildings which require high horizontal stiffness. The weight of the mixed structure is significantly less than that of a reinforced concrete system and, thus, can be applied to soft soils. The construction cost of a mixed system ranges between the reinforced concrete and steel systems.

It was made clear through the design simulations that the strength of the joint panels is not so critical for practical design if it is equal or larger than the recommended strength by SRC Standard of AIJ.

## 4. CONCLUSIONS

The strength of the joint panel decreases as the girder flange is cut in the panel zone. However, the strength satisfies the value recommended by SRC Standard of AIJ. Therefore the strength of the joint panel is not so critical for design applications. The ductility is quite large and it does not deteriorate at least up to a story drift of  $1/20$  radians.

The mixed system showed that it has both, the advantages of reinforced concrete and steel systems, in story height, story stiffness and total weight. It is somewhat inferior to the reinforced concrete system in construction cost, but there are many factors which can not be considered in the cost estimates, such as the terms of the construction contract.

The above mentioned conclusions show the high capability of the advanced mixed system proposed in this paper.

## REFERENCE

- [1] Standard for Structural Calculation of Steel Reinforced Concrete Structures, Architectural Institute of Japan, 1987 (in Japanese).

Table 1 Mechanical properties

Specimen		Steel		Reinforcing bar			concrete
		$\sigma_y$	$\sigma_t$	size	$\sigma_y$	$\sigma_t$	$\sigma_c$
A-1	flange	31.0	45.8	D16	35.6	51.8	2.12
	web	33.6	47.1	D13	37.7	55.4	
A-2	flange	30.1	43.6	D16	35.0	52.2	2.17
	web	33.8	45.2	D13	35.9	50.6	
B-1	flange	34.7	50.3	D16	35.6	51.8	2.10
	web	37.5	51.5	D13	37.7	55.4	
B-2	flange	33.1	44.8	D16	35.0	52.2	2.19
	web	38.6	47.2	D13	35.9	50.6	
B-3	flange	33.1	44.8	D16	35.0	52.2	2.15
	web	38.6	47.2	D13	35.9	50.6	

(unit:MPa)

Table 2 Experimental and calculated strengths

Specimen	Maximum strength (kN)			Diagonal crack strength in panel zone (kN)		
	Exp	Cal	Exp/Cal	Exp	Cal	Exp/Cal
A-1	125.0	96.9	1.29	87.3	32.6	2.68
A-2	105.6	97.5	1.08	66.6	33.4	1.99
B-1	130.1	81.2	1.60	75.3	25.5	2.95
B-2	92.3	83.2	1.11	65.8	26.5	2.49
B-3	85.4	82.6	1.03	51.4	26.1	1.97

\*1 Strengths in the above table are shown as column shear force.

\*2 Maximum strength is calculated from eq.(1).

\*3 Panel shear crack strength is estimated as  $Q_{cra} = \tau \left( \frac{b_c \cdot d + 15 \cdot t_j \cdot d}{m_c \cdot w_{sc}} \right)$ ,  $\tau = 0.1F_c$ .

Table 3 Design conditions

System	moment resisting frame (mixed, steel, reinforced concrete)	
Dimen- sions	3x3 bay, 3 stories clear story height: 2.9m longitudinal span: 8,10,12,14m transverse span: 6m	
Dead Load	floor mixed, steel metal deck + RC slab t=107.5mm reinforced concrete RC slab t=150mm miscellaneous interior/exterior wall, stairs, pent house and parapet are not considered	
Live Load	roof floor	0.59kN/m <sup>2</sup>
	2,3 floor	1.27kN/m <sup>2</sup> (for seismic design)
Mate- rials	steel	SS41(Japan Industrial Standard)
	rebar	SD30(JIS) for slab SD35(JIS) for column
	concrete	F <sub>c</sub> =2.06MPa

Table 4 Summarized characteristics of designed buildings

Item	System Span length (m)	Mixed						Steel						Reinforced concrete					
		8	10	12	14	8	10	12	14	8	10	12	14	8	10	12	14		
Story Height (Girder Depth) (m)	3rd	3.50 (0.40)	3.70 (0.60)	3.70 (0.58)	3.70 (0.59)	3.60 (0.50)	3.70 (0.60)	3.70 (0.58)	3.80 (0.69)	3.60 (0.50)	3.70 (0.60)	3.70 (0.58)	3.80 (0.69)	3.60 (0.70)	3.75 (0.85)	4.00 (1.10)	4.40 (1.50)		
	2nd	3.55 (0.45)	3.70 (0.60)	3.70 (0.58)	3.70 (0.59)	3.60 (0.50)	3.70 (0.60)	3.70 (0.58)	3.80 (0.69)	3.60 (0.50)	3.70 (0.60)	3.70 (0.58)	3.80 (0.69)	3.65 (0.75)	3.75 (0.85)	4.00 (1.10)	4.40 (1.50)		
	1st	3.55 (0.45)	3.70 (0.60)	3.70 (0.58)	3.70 (0.59)	3.60 (0.50)	3.70 (0.60)	3.70 (0.58)	3.80 (0.69)	3.60 (0.50)	3.70 (0.60)	3.70 (0.58)	3.80 (0.69)	3.70 (0.80)	3.75 (0.85)	4.00 (1.10)	4.40 (1.50)		
Story Drift Angle (radian)	3rd	1/447	1/596	1/633	1/602	1/324	1/376	1/411	1/474	1/829	1/791	1/1031	1/1406	1/645	1/577	1/741	1/864		
	2nd	1/375	1/438	1/467	1/480	1/214	1/282	1/307	1/340	1/705	1/594	1/722	1/809	1/645	1/577	1/741	1/864		
	1st	1/543	1/527	1/541	1/582	1/307	1/306	1/301	1/328	1/705	1/594	1/722	1/809	1/645	1/577	1/741	1/864		
Weight (kN/m <sup>2</sup> )		9.83	9.66	9.64	10.04	8.89	9.04	8.91	9.07	13.05	13.02	14.10	16.95	1.64	1.64	1.76	2.15		
Cost (x10 yen/m <sup>2</sup> )		1.93	2.03	2.07	2.21	2.22	2.25	2.24	2.45	1.64	1.64	1.76	2.15	1.64	1.64	1.76	2.15		

Table 5  
 Ratios of calculated strengths  
 to required strength of joint  
 panels in design simulations  
 for the mixed system

		Span length (m)			
Location		8	10	12	14
Roof	y1x1	1.52	1.68	2.24	2.12
Floor	y1x2	1.65	2.03	2.51	1.49
	y2x1	1.14	2.81	1.57	1.56
	y2x2	1.87	3.01	3.09	1.73
3rd Floor	y1x1	2.45	2.01	2.24	2.72
	y1x2	1.56	1.42	1.43	1.67
	y2x1	1.67	1.74	1.49	1.76
	y2x2	1.33	1.63	1.62	1.14
2nd Floor	y1x1	2.86	2.11	2.34	2.72
	y1x2	1.84	1.33	1.46	1.67
	y2x1	1.94	1.81	1.54	1.76
	y2x2	1.20	1.25	1.22	1.18

\*1 The locations of joint panels are expressed by frame numbers in both x and y directions. Frame "1" means exterior frame and "2" means interior frame, where y direction is the longitudinal direction.

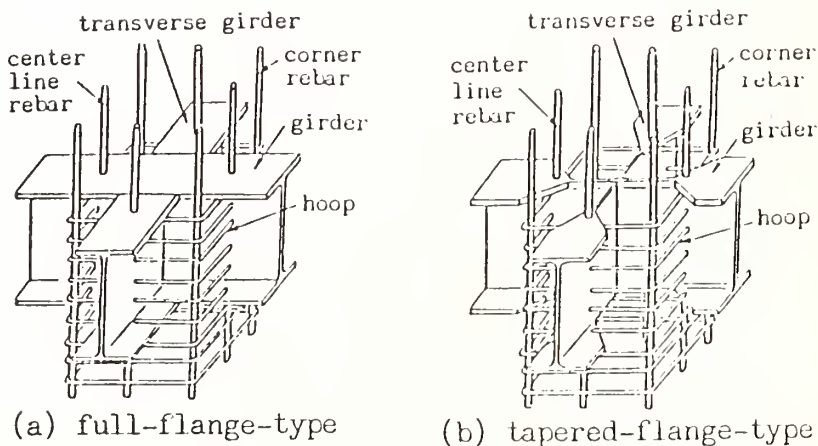


Fig. 1 Details of joint panels

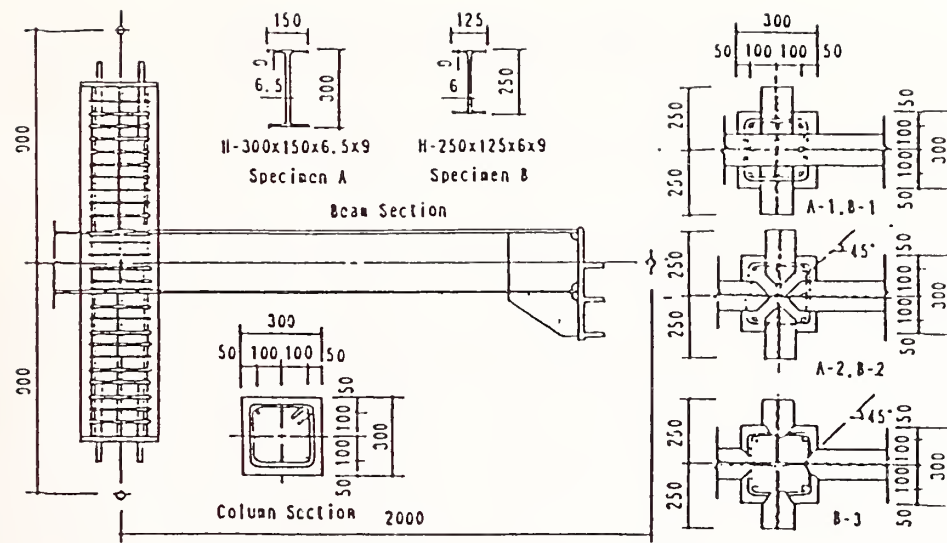


Fig. 2 Shape of specimens

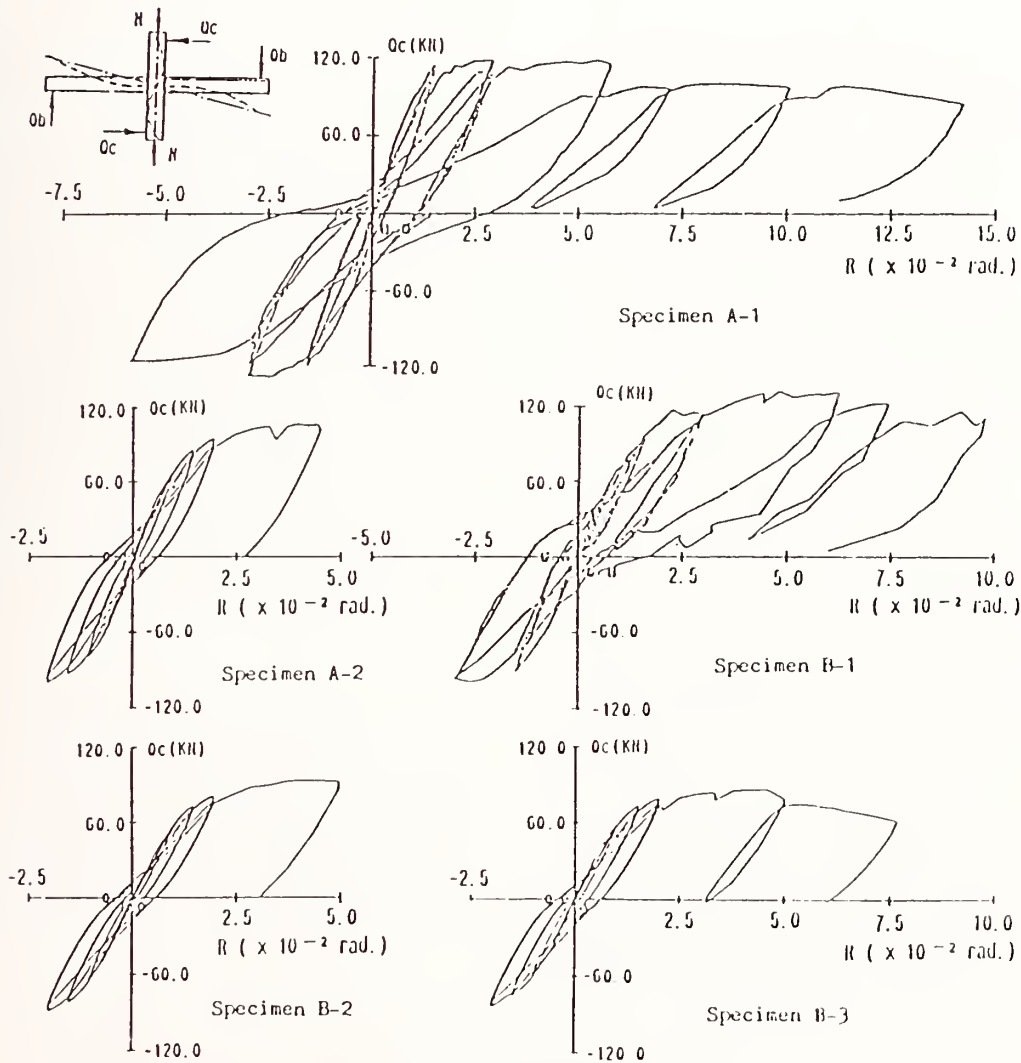


Fig. 3 Hysteresis curves ( $Q_c$ - $R$  relationships)

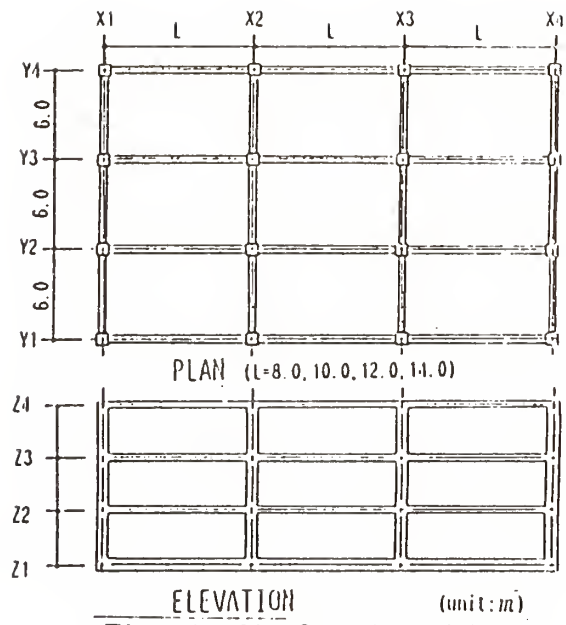


Fig. 4 Simulated building

# Effects of Soil and Rock on Ground Motion and Potential Damage in an Earthquake

by

Walter W. Hays  
U.S. Geological Survey  
Reston, Virginia 22092

## ABSTRACT

Patterns of damage in an earthquake depend on physical parameters of the total earthquake-site-structure system. Interaction between a structure and the underlying soil-rock column involves the frequency- and strain-dependent responses of both the soil-rock column and the structure. When the natural period of vibration of the soil column is equal to or about the same as that of the structure, damage can be severe. A key, therefore, to damage control is to identify the potential for poor site-structure combinations and either to avoid the site or to design and construct the structure so that it has the capacity to withstand the increased demand caused by the effects of site-structure resonance.

## 1. INTRODUCTION

Basic information on site amplification phenomena is needed to improve understanding and engineering-design practice for an effect that occurs at discrete locations in virtually every earthquake. The magnitude 8.1 Mexico earthquake that occurred on Tuesday morning September 19, 1985, at 7:18 a.m. (local time) is one of the most recent reminders that site-amplification effects are important in earthquake-resistant design. The Mexico earthquake illustrated the "worst case"--ground response and the response of some buildings occurring at approximately the same period in one portion of Mexico City, the lake-bed zone. The result was that several hundred buildings, either collapsed or were severely damaged. They were primarily 5-20 story buildings located in the lake-bed zone some 400 km (250 mi) from the epicenter of the earthquake.

### 1.1 Definitions

In order to facilitate understanding of the complicated subject of ground shaking, definitions of important technical terms are provided. In the literature, some terms are used interchangeably with other terms, causing confusion. The terms that are used most frequently in this paper are illustrated in Figures 1 and 2. Important terms include the following:

A. Peak amplitude - This term refers to the maximum value of a time history recorded either at the surface in a free field location or in the basement of a building by a broadband seismograph, usually an accelerograph.

The peak amplitude of an acceleration record (accelerogram) written by a strong-motion accelerograph is a typical example; however, the usage in this paper will be in terms of the peak amplitude of either acceleration, or velocity, or displacement recorded (or derived from one of the other recordings) at the ground surface. The surficial material underlying the accelerograph may be either bedrock or soil; each will introduce a distinctive signature to the time history.

B. Spectral composition - This term refers to the frequency composition of a ground-motion time history (e.g., an accelerogram). The Fourier amplitude spectrum and the response spectrum are the most common representations of the spectral composition and are widely used by scientists and engineers.

The response spectrum depicts graphically the peak amplitude of each time history representing the individual responses of each one of a series of damped, simple harmonic oscillators to the accelerogram input at the base. For zero damping, the response spectrum envelopes the Fourier amplitude spectrum. In this paper, the term response spectrum is always used to denote the spectral velocity (pseudorelative velocity). When spectral velocity is graphed on tripartite logarithmic paper, the values of spectral acceleration (pseudoabsolute acceleration) and spectral displacement (relative displacement) are also described and can be used to estimate the values of the peak amplitudes of horizontal ground acceleration, velocity, and displacement. The spectral ordinates are larger than the peak amplitudes of ground motion because the harmonic oscillator amplifies the input motion.

The peak amplitude of acceleration approaches in the limit the zero-period (high-frequency) asymptote of the response spectrum; whereas, the peak amplitude of displacement approaches in the limit the infinite-period (low frequency) asymptote. The peak amplitude of velocity corresponds to the intermediate-

period portion of the response spectrum, but the peak amplitude of velocity is less (by a numerical constant that depends on the level of critical damping) than the ordinates of spectral velocity which depict the maximum response of the intermediate-period harmonic oscillators. The structural engineer uses the response spectrum to correlate characteristics of ground motion with the elastic response of buildings of various heights and types.

C. Site amplification - Several terms (for example, site response, soil response, ground response, ground-motion response) are used in the ground-motion literature. All of these terms generally carry the same meaning as the term "site amplification" used in this report. Amplification is always relative to a rock site. The surface-soil-to-rock amplification factor is a multiplicative factor ranging from a fraction (deamplification) to values of about 10 (1,000 percent). The multiplicative factor is typically related to a specific part (period band) of the spectrum. Site amplification refers to the frequency- and strain-dependent physical processes that occur when an overlying soil deposit responds to bedrock ground shaking. These physical processes can modify the peak amplitudes of acceleration, velocity, and displacement recorded at the ground surface as well as the spectral velocity or Fourier amplitudes in a discrete period band of the response spectrum. The result is that the ground motions recorded at the surface of a soil deposit differ from the subsurface bedrock ground motions or the ground motion recorded on surface outcrops of bedrock. Whether or not the peak amplitude of surface acceleration is increased or decreased by the soil column is the most controversial aspect of site amplification and is the subject of continuing debate.

D. Soil-to-rock amplification factor - This term describes the amplification factor which is generally computed at each frequency, but reported for a period band (for example, a factor of 5 (500 percent) for the period band 0.2-0.7 s). Unless noted, the soil-to-rock amplification factor describes a frequency-domain effect for the horizontal components of surface ground motion, rather than a time-domain effect. The factor describes empirically what happened at the site underlain by soil relative to the reference site underlain by rock and is described in terms of a specific period band, or the period where the maximum or dominant response occurred.

A factor of 5 in the frequency domain does not correspond to a factor of 5 in the time domain. The extent to which the peak amplitude of ground acceleration is increased

or decreased depends on what happens physically at very low periods (i.e., at the very high frequencies).

E. Transfer function - The concept of a transfer function comes from the theory of linear operators (i.e., Fourier and Laplace transforms). In this paper, the transfer function is used to describe site amplification in the frequency domain, and, unless noted, the soil-to-rock transfer function is always derived. For a site underlain by a soil deposit, the procedure for estimating the transfer function is to divide the response spectrum by the corresponding response spectrum for a nearby site that is underlain by rock. The distance between the two sites must be small in comparison with the epicentral distance to each site. The soil-to-rock amplification factor for a discrete period band is determined from the transfer function. In the Fourier analysis of ground-motion data, the typical procedure is to use the amplitude spectrum and to neglect the phase spectrum. One advantage of using the transfer function is that the source terms (for example, the nuclear-explosion forcing function or earthquake source characteristics) can be eliminated when analyzing site-amplification effects. This process makes the result essentially independent of the energy source.

## 2. CURRENT UNDERSTANDING OF SITE AMPLIFICATION

### 2.1 Worldwide Data

Because site amplification of earthquake ground motion is a controversial subject and the earthquake data are somewhat limited, a brief review will be given to provide a framework of understanding. Such understanding is needed for interpreting and using the site-amplification data. Scientists and engineers throughout the world have recognized and documented since the 1800's that site amplification is a common occurrence in earthquakes (MacMurdo, 1824; Idriss and Seed, 1968; Seed and Idriss, 1969; Seed and others, 1972; Tezcan and others, 1977; Rosenblueth, 1986; Savy and others, 1986). Four earthquakes producing classic examples of site amplification are:

- A. the 1967 Caracas, Venezuela earthquake,
- B. the 1970 Gediz, Turkey, earthquake,
- C. the 1976 Friuli, Italy, earthquake, and
- D. the 1985 Mexico earthquake.

These earthquakes (and others) have shown scientists and engineers that two frequency-dependent phenomena, site response and structural response, must be considered explicitly in earthquake-resistant design. A number of factual statements can now be made about these phenomena. They include:

A. During an earthquake, the characteristics of the earthquake ground motion in any city will vary widely depending on a) thickness and softness of the local soil-rock columns and b) source phenomena such as directivity and focusing of energy (Earthquake Engineering Research Institute, 1986).

B. Damage to a structure at a particular site in an earthquake is complexly related to the dynamic frequency-dependent properties of the earthquake source, the low-pass filtering characteristics of the wave propagation path, and the band-pass filtering characteristics of both the soil-rock column underlying the structure and the structure (Figure 3). The physical parameters of the earthquake and the earth that cause the soil-rock column and the structure to vibrate at the same period increase the potential for damage (Yamahara, 1970).

C. The time histories of acceleration, velocity, and displacement; the response or Fourier spectra; and duration of shaking are the best dynamic representations of how the ground moved during an earthquake. Characteristics of the source, propagation path, and soil-rock column contribute distinctive frequency-dependent signatures to the ground motion recorded at the surface. For example, a) source - increasing the magnitude of the earthquake increases the spectral ordinates of all periods and enhances those in the long periods most, b) wave propagation path - the path acts as a low-pass filter by attenuating the amplitudes of the short periods more rapidly than the amplitudes of the long periods, and c) site - the soil column acts as a band-pass filter by increasing the amplitudes of the bedrock ground motion in a specific band and possibly, but not always, decreasing the amplitudes in other period bands (Hays, 1980). The peak amplitude of ground acceleration recorded on the surface is increased when the amplitudes of the short periods are enhanced; the peak amplitudes of ground velocity and displacement are increased, respectively, when the amplitudes of the intermediate and long periods are enhanced.

D. The level of dynamic shear strain and its effects on soil properties are the most controversial aspects of site amplification. The level of shear strain induced in the soil column by the input bedrock motion increases as the magnitude of the earthquake increases and decreases as the distance from the center of energy release increases.

E. The response of the site to ground shaking depends strongly on the strain-dependent properties of the soil-rock column underlying the site. The level of dynamic

shear strain and the contrast in physical properties of the soil and rock determine whether the soil acts to transmit or to dissipate energy. As an energy transmitter, the soil column acts as a band-pass filter by modifying the amplitude and phase spectra of the incident body and surface seismic waves in selected periods (Murphy and others, 1971) and increasing the duration of shaking (Hays, 1975). As an energy dissipator, the soil column can damp the earthquake ground motion. As a soil-structure system, part of the vibrational energy of both the soil column and the structure can be transmitted back into the Earth, which permits vertical movement, rocking, and side-to-side movement of the structure on its base (Wolf, 1985).

F. Site amplification (the frequency- and strain-dependent response of the soil-rock column to body and surface seismic waves) can increase the amplitude of the surface ground motion in a narrow- or broad-band that can be related to the thickness, shear-wave velocity, bulk density, and geometry of the soil column (Seed and others, 1976). This phenomenon has resulted in some of the most spectacular and devastating effects to man-made structures. The transfer function (See Figure 2) can be used to categorize the dominant spectral response in terms of the period band where it occurs. Although the effect can be characterized for any discrete period band, three period bands are sometimes used: a) short period (0.05-0.5 s), b) intermediate period (0.5-3 s), and c) long period (3-10 s). Each period band correlates with the fundamental mode of response of buildings of increasing heights (Figure 4).

G. The transfer function depends on many physical parameters, including level of dynamic shear strain; shear-wave velocity; density; material damping; thickness; water content; surface and subsurface geometry of the soil-rock column; and the types of seismic waves that excite the soil-rock column--their wavelengths, amplitudes, and directions of vibration.

H. The structure also acts as a band-pass filter as it responds to the ground shaking at its base. The spectral response of the structure can increase or decrease in selected period bands depending on the type of structure, the construction materials, the lateral and vertical dimensions, the physical properties of the soil-rock column, and the wavelengths and amplitudes of the incident seismic waves. The "worst case" is when the dominant period of the bedrock motion, the fundamental natural period of vibration of the structure, and the natural period of the soil column are the same. Such a condition creates a condition for resonance of the entire ground motion-soil-structure system.

Site and building periods - Earthquake-resistant design must take into account the conditions that cause site amplification of ground motion

and damaging soil-structure interaction. Careful evaluation is required to identify the wide range of soil columns and their physical properties, the various types of buildings, and the physical conditions that cause the soil and building responses to occur at or close to the same period. A single soil layer overlying rock, like a building or structure, has a natural period of vibration,  $T_s$ , given by the relation

$$T_s = \frac{4H}{V_s} \quad (1)$$

where H is the thickness of the soil layer and  $V_s$  is the shear-wave velocity measured at low levels ( 0.0001 percent) of strain. Soils, depending on their physical properties, typically have shear-wave velocities ranging from 50 to 600 m/s; whereas, rock-like material and rock have shear-wave velocities greater than about 750 m/s.

Soils exhibit strain-dependent properties. Laboratory tests (Seed and Idriss, 1969) on "undisturbed" samples have shown that as the level of dynamic shear strain increases the material damping increases and the shear modulus decreases. The result is that  $T_s$  increases as the level of shear strain increases. The basic relation has been stated by Seed (1975) as:

$$T_s = \frac{4H}{RV_s} \quad (2)$$

where R is an empirical factor having the following values:

- A. 0.9 for a magnitude 6 earthquake producing a peak effective acceleration of about 0.1 g.
- B. 0.8 for a magnitude 6 earthquake producing a peak effective acceleration of about 0.2 g.
- C. 0.67 for a magnitude 7 earthquake producing a peak effective acceleration of about 0.3-0.4 g.

The fundamental natural period of vibration  $T_b$  of a building is given approximately by the relation

$$T_b = \frac{N}{10} \quad (3)$$

where N is the number of stories. However, the stiffness and flexibility of a building can make its actual fundamental natural period of vibration much shorter or longer. Observations from postearthquake investigations have shown that  $T_b$  lengthens as the thresholds of various states of damage are reached. In an earthquake, the "worst case" for damage is when the value of  $T_s$  coincides with that of  $T_b$ . This situation causes resonance of the building and can result in severe damage or collapse unless the building has been designed to withstand the forces and displacements generated by this phenomenon.

## 2.2 Technical considerations in the evaluation of site amplification

Evaluation of the potential for site amplification requires careful consideration of the following factors:

A. Types of seismic waves - All four types of seismic waves (P, S, Rayleigh, and Love) can be amplified by the soil column, but in different ways (Murphy and others, 1971; Murphy and Hewlett, 1975). Therefore, understanding the physics of site amplification requires consideration of the wave field (Seed and Lysmer, 1986). Typical horizontal acceleration, velocity, and displacement time histories observed at sites located about 20 km from the 1971 San Fernando earthquake are shown in Figure 5. These time histories represent the superposition in time of body and surface waves that have traveled a wide variety of paths between the earthquake source and the recording site. The body waves travel from the source to the recording site along paths extending deep into the Earth's crust, and their energy is vertically incident on the site from below. They cause short-period (high-nearly frequency--greater than 1 Hz.) vibrations, which are most efficient in causing low-rise buildings to vibrate. The surface waves (Love and Rayleigh), on the other hand, propagate through channels or wave guides bounded above by the surface of the Earth, and traverse the site laterally rather than being incident from below. Surface waves are very sensitive to changes in the thickness of the soil column and mainly cause long-period (low-frequency--less than 1 Hz. vibrations), which are most efficient in causing high-rise buildings to vibrate. Because the body and surface waves travel at different velocities, they tend to be separated in time on seismograms recorded 20 or more km from the epicenter. The SH wave is most important in evaluating the potential for site amplification; however, all of the seismic waves must be examined in order to evaluate local site amplification in a comprehensive manner (Hays, 1980). However, the type of structure being sited can reduce the scope of the evaluation. For example, amplification of surface waves is not typically considered in siting a nuclear power plant, which is more sensitive to short-period vibrations than to long-period vibrations. On the other hand, potential site amplification of long-period Rayleigh waves is an important consideration when siting a high-rise building, especially if the building is founded on a deep, soft soil deposit.

B. Level of dynamic shear strain and the dynamic physical properties of the soil column - Assessing the level of dynamic shear strain and its effects on the physical

properties of the soil column requires careful judgment. Laboratory measurements have demonstrated that soils have shear moduli and damping characteristics that depend on the level of strain, which suggests that, under certain conditions, nonlinearities and inelasticities in the soil will attenuate rather than amplify the peak amplitudes of surface ground motion at sites underlain by soil. Current understanding is limited because the high levels of strain produced in the laboratory have apparently not been duplicated by actual strong motion records of past earthquakes. For example, the greatest peak ground velocity ever recorded (in the 1971 San Fernando, California and 1979 Imperial Valley, California earthquakes) is 110 cm/s. The empirical rule that

Strain =  $\frac{\text{peak velocity recorded at the site}}{\text{shear wave velocity of the soil column at the site}}$

leads to the conclusion that the greatest level of strain induced insitu in soil columns in past earthquakes has reached only about 0.5 percent, much less than the level of strain developed in the laboratory environment.

Some researchers (for example, Hays and others, 1979; Hays and King, 1982) have shown that site response is essentially linear up to insitu strain levels of about 0.5 percent for some soil-rock columns. Attenuation relationships suggest that distance to the strain level threshold of 0.5 percent is on the order of a few km for the soil columns having shear-wave velocity of 200 m/s; this distance decreases as the shear-wave velocity of the soil increases to the upper limit of bedrock.

The complexity in the specification of the dynamic properties of the soil is directly related to obtaining an "undisturbed" sample. The complexity increases below depths of 30 m (100 ft) because of the difficulty and expense of sampling. However, for the deep zone, the average shear-wave velocity ( $V_s$ ) can be estimated fairly accurately (using a value of 0.4 to 0.45 for Poisson's ratio) from values of the compressional wave velocity ( $V_p$ ) determined from seismic reflection and seismic refraction surveys, or from measurements in boreholes.

C. Thickness of the soil column - Two different points of view have been used to define the critical thickness of the soil column, the physical parameter that affects the period of the dominant site amplification under conditions of low strain. One view (Seed, 1975) considers that the soil column includes only material having a shear-wave velocity less than 765 m/s (2,500 ft/s). The other view (Kobayashi and Nagahashi, 1982) considers that the soil column extends to bedrock having a compressional wave velocity of at least 3,600 m/s (12,000 ft/s).

In the first case, surface ground motions are assumed to be affected mainly by a short soil column, typically about 30 m (100 ft) thick; whereas, in the second case surface ground motions are assumed to be affected by a much thicker soil column. The short soil column will mainly affect the short periods and the peak amplitudes of acceleration; whereas, the thick soil column will mainly affect the intermediate- and long-period bands and the peak amplitudes of velocity and displacement.

D. Near field - The near field of an earthquake (or "near-source" region) is the most complex part to evaluate for potential site-amplification. The site is defined as being in the far field of an earthquake (or "far-source" region) when it is located sufficiently far from the physical extent of the earthquake source that the solid angle subtended by the source and the site is very small. In the far field, estimation of the characteristics of ground motion is much easier than in the near field (or "near-source" region) where seismic energy arrives nearly simultaneously from many different directions. The difference is essentially one of using a point-source approximation (the far field) and an extended source (the near field). Analyses of strong-ground-motion data close to the causative fault have been made by a number of investigators (for example, Idriss, 1978; Hays, 1980; Singh, 1985). For the near field, these analyses indicate that:

- o Separation of the frequency-dependent effects of the source from the effects of the soil-rock column is very difficult to perform analytically. Near the fault, the source tends to dominate the path and site effects. The directivity of the source appears to cause most of the large variability in the values of the peak amplitudes of ground acceleration, velocity and displacement, and the ordinates of spectral velocity (Singh, 1985).
- o A "killer pulse," a pulse of approximately one second duration that typically does not have the greatest peak amplitude of acceleration but which has the greatest kinetic energy, is generated in some cases in the near field (for example, in the 1971 San Fernando, California earthquake) as a consequence of the "fling" of the fault (Bertero and others, 1978). Breakout and stopping phases of the fault rupture can also affect the near-field ground motion and complicate the analysis.

E. Bedrock Motions - Estimating bedrock ground motions is also a difficult task in evaluating site-amplification effects. The frequency-dependent characteristics of the bedrock motion that is input to the soil column depend on the details of the geology of the propagation path. These details are usually imprecise.

Therefore, analytical calculations must be bounded, using a suite of strong-motion accelerograms acquired in past earthquakes at sites underlain by rock as the constraint.

The ideal data are from sites underlain by the same type of rock, located at about the same distance from the zone of energy release, and having the same geology underlying the propagation path as for the path to the site being evaluated.

F. Aftershock ground-motion data - Broadband records of the aftershock sequences of earthquakes can be used in the analysis; however, the strengths and weaknesses of the analytical procedure must be carefully considered. The strength is that some of the aftershock ground-motion records have the signature of the travel path and soil-rock columns traversed by seismic waves generated in the main shock, and only the source parameters differ. The weakness is that the lower levels of dynamic shear strain developed in an aftershock may cause overestimation of the amplification factor and underestimation of the dominant period of the site response.

G. Angle of incidence - Analysts generally assume vertical incidence of the body waves at the base of the soil column. Violation of this assumption does not introduce significant error (Murphy and others, 1971) for most applications.

H. Variability in site-amplification effects - Several investigators (for example, Murphy and others, 1971; Hays, 1980) have shown that site-amplification effects are fairly repeatable if the soil is soft, the level of strain is low (e.g., 0.0001 to 0.5 percent), and the site is not in the near field of the fault. The degree of repeatability of the site transfer function is currently unknown for sites near the fault when the shear strain exceeds 0.5 percent.

### 2.3 Empirical Data on Site Amplification

Worldwide data - Four examples of site amplification are described below:

A. The 1967 Caracas, Venezuela earthquake - Soil-structure interaction occurred in Caracas, 56 km (35 mi) from the epicenter of this moderate (Ms 6.4) earthquake. Severe damage was mainly restricted to tall buildings (buildings greater than 12 stories) sited on soft soil columns that were at least 160 m (520 ft) thick. The dominant site response occurred in the intermediate period band, centered around 1.2-1.6 s (Seed and others, 1972).

B. The 1970 Gediz, Turkey earthquake - Soil-structure interaction caused the collapse of a one-story garage and paint workshop (a part of the Tofias automobile factory) located 225 km (135 mi) from the epicenter of this large (Ms 7.0) earthquake. The cause was the similarity

of the predominant periods of: a) the bedrock motions, b) the response of the 120-135 m (390-440 ft) column of alluvium, and c) the response of the building. The responses of the soil and building occurred in the intermediate-period band and were centered around 1.2 s (Tezcan and others, 1977).

C. The 1976 Friuli, Italy earthquake - Site amplification of a factor of 4 (400 percent) occurred in the short- to intermediate-period band (0.2-0.7 s) for a site underlain by 15 m (50 ft) of alluvium located 25 km (15 mi) from the epicenter. The peak amplitude of bedrock accelerations ranged from 0.10 to 0.53 g (Savy and others, 1986). The magnitude (Ms) of the main shock was 6.9.

D. The 1985 Mexico earthquake - This great (Ms 8.1) earthquake produced two surprises: a) the low value of the peak amplitude of acceleration (0.18 g) in the near source region, and b) the high (0.18 g) value of the peak amplitude of acceleration in certain parts of Mexico City located 400 km (250 mi) from the epicenter (Figure 6). Extensive damage occurred in 5- to 20-story buildings sited in the lake-bed zone of Mexico City underlain by soft lake-bed deposits (Rosenblueth, 1986). This zone had been recognized in the 1960's (Zeevaert, 1962) as one that enhanced 2-second periods (i.e., a 2-second band-pass filter). The largest ground motions in Mexico City occurred at sites underlain by 35 to 50 m of soft lake-bed deposits having a shear-wave velocity of about 100 m/s. The dominant period of accelerogram recorded in the lake-bed zone was 2 s. The lake-bed deposits amplified the peak amplitude of acceleration (caused by Rayleigh waves) by about a factor of 5 (500 percent) relative to the level of peak acceleration observed at nearby sites underlain by stiffer, rock-like material (Rosenblueth, 1986). The ordinate of 5 percent damped spectral acceleration at 2 s reached 1 g, a factor of 5 greater than the peak ground acceleration in the lake-bed zone and a factor of 30 greater than the peak surface bedrock acceleration. The similarity of the soil response and the building response at many locations in the lake-bed zone resulted in severe damage and collapse of about 400 engineered buildings. These buildings generally had fundamental natural periods ranging from 0.5 to about 2 s. The number of severely damaged and collapsed buildings represented less than one percent of the total number of engineered buildings in Mexico City, which indicates that buildings constructed according to the Mexican building code performed well everywhere but in the lake-bed zone.

### 2.4 United States data

Many investigators have studied site-amplification in various parts of the United States. Although the data are limited and vary in completeness, some useful observations have emerged.

A. San Francisco Bay Region - The 1906 San Francisco earthquake, the 1957 Daly City earthquake, and the extensive program of geologic and engineering seismologic data acquisition conducted by the U.S. Geological Survey in the 1970's led to the following observations on site amplification:

- o Analyses of the effects of the 1906 (Ms 8.3) San Francisco earthquake showed that the soil-rock column underlying a structure can have a significant effect on the input ground motions and the damage patterns (Wood, 1908).
- o Strong-ground-motion data from the 1957  $M_L$  5.4 Daly City earthquake provided a basis for concluding that the peak amplitudes of acceleration and the spectral composition of the ground motions varied as a function of the wave propagation path and the physical properties (softness) of the soil-rock column (Idriss and Seed, 1968).
- o Correlation of empirical ground motion data and physical properties data showed that each geologic unit in the San Francisco Bay region has a characteristic and predictable response to low-strain seismic excitation (Borcherdt, 1975; Borcherdt and others, 1975; 1978; Joyner and others, 1981).
- o Empirical ground motion data showed that the San Francisco Bay sediments and fill can be expected to amplify all frequencies of ground motion in varying degrees. For example, the short-period energy from distant nuclear-explosion ground motions was amplified by the bay mud by a factor of about 10 (1,000 percent) under conditions of low-strain ground shaking.

B. Los Angeles Region - The most significant contributions to knowledge on site-amplification effects resulted from: a) the February 9, 1971 San Fernando earthquake, which triggered 241 three component strong-motion accelerographs located at the base of buildings and in free-field locations within 75 km (45 mi) of the epicenter of the Ms 6.4 earthquake; b) the extensive program of the National Oceanic and Atmospheric Administration to monitor the aftershocks of the San Fernando earthquake at more than 100 locations; and c) comprehensive data acquisition by the U.S. Geological Survey in the 1970's and 1980's. Important observations included the following:

- o Transfer functions derived from ground-motion data recorded at the same locations in the San Fernando Valley from the San Fernando earthquake, selected aftershocks, and nuclear explosions at the Nevada Test Site were very similar. The similarity of the site response is notable even though the levels of bedrock

ground motion and shear strain varied markedly (Hays and others, 1979; Rogers and others, 1982, 1985).

- o Amplification of short-period seismic energy occurred along the boundary of the San Fernando valley where the alluvium is stiff and thin (Hays, 1977). Amplification occurred also in Glendale where the thickness of the soft alluvium varied from 29-65 m over a distance of only several km (Murphy and others, 1971b).
- o The thick alluvium in the center of the Los Angeles basin amplified the long-period surface waves (Hanks, 1976).
- o The ground motion was amplified across the entire spectrum by some topographic features (Boore, 1973; Davis and West, 1973).
- o Soil columns in the Long Beach (Rogers and others, 1982) and Los Angeles areas (Rogers and others, 1985) caused site amplification. The amplification factors in the short, intermediate, and long-period bands ranged from 2 (200 percent) to 5 (500 percent).

C. Nevada - The main contributor to knowledge on site-amplification effects was the Ground Motion and Structural Response Program of the U.S. Atomic Energy Commission, conducted primarily in the 1960's and 1970's. More than 3,000 strong motion records of explosions were obtained at near- and far-source locations, including locations such as Tonopah, Las Vegas, and Beatty, where the regional geology and the characteristics of the soil-rock columns were well defined. The most significant observations included the following:

- o The similarities of the strong-ground-motion records and response spectra of earthquake- and nuclear-explosion ground motions were demonstrated at distances ranging from a few kilometers to a few hundred kilometers from the source (Hays, 1975; 1980).
- o Site amplification agreed well with theory and was demonstrated for locations having widely different soil-rock columns (Murphy and others, 1971; Hays and others, 1979). Levels of strain ranged from 0.001 to 0.5 percent.
- o A classic example of short-period body-wave amplification was verified in Tonopah (Figure 7). The amplification factor of 7 (700 percent) (Murphy and others, 1971) correlated with the thickness and physical properties of the fill and agreed with that predicted on the basis of theory.

This effect was repeated many times with small variability under low-strain ground shaking.

- o Observations of intermediate- to long-period

surface wave amplification were documented in Las Vegas and shown to agree with theory (Figure 8).

The maximum amplification factor of 10 (1,000 percent) was caused by the thick alluvium in the center of the valley (Murphy and Hewlett, 1975) and varied as a function of the thickness. These effects were repeated many times with small variability under low-strain levels of ground shaking.

- o The variation of site amplification with depth was demonstrated at Beatty, where the bedrock motions were a factor of 4 (400 percent) less than the surface motions at 0.3 seconds, the characteristic site period,  $T_s$  (Figure 9) (Murphy and West, 1975). These effects were shown to agree with theory, and were repeated many times with small variability under low-strain levels of ground shaking.

D. Salt Lake City-Ogden-Provo - Hays and King (1982, 1984) used nuclear-explosion ground motion data recorded at sites underlain by soil and rock in this urban corridor adjacent to the 370-km-long (222 mi) Wasatch fault zone to evaluate soil response.

Their analysis showed that the ground-shaking hazard is worst for sites in the centers of the valley underlain by thick, soft silts and clays (Figure 10, 11, and 12). These soft soil deposits cause frequency-dependent amplification of ground motion relative to a bedrock site on the Wasatch front. The soil-to-rock amplification factors reach 10 (1,000 percent) in the period band 0.2-0.7s, under conditions of low (0.0001 to 0.1 percent) levels of shear strain where the soil deposits are thin gravels and sands near the Wasatch front, the soil-to-rock amplification factors only reach 2 (200 percent). Because the thickness of the silts and clays increases toward the valley centers, the amplification factors also increase as distance from the surface trace of the Wasatch fault zone increases out to a distance of about 35 km. The unknown at this time is the extent to which site-amplification factors would change under high-strain ground shaking, especially if a large ( $M=7.5$ ) earthquake nucleates underneath one of the cities on the Wasatch Fault which is thought to become listric with depth.

E. Seattle, Washington - Ihnen and Hadley (1984) modeled the strong ground motion of the 1965 magnitude ( $M_s$ ) 6.5 Seattle earthquake using a ray-tracing technique. Their analytical results suggested that the thick, soft soil deposits of the Duwamish River caused an amplification factor of 5 (500 percent) in the short- to intermediate-period band in western Seattle, the part of Seattle experiencing the greatest damage from ground shaking in 1965. Strong-ground motion data in the region are too limited to provide definitive empirical confirmation of these results at this time.

F. Other Urban Areas - Although ground-motion data are limited and incomplete, some investigators have shown in at least a preliminary way that Boston, Massachusetts (Whitman, 1983); Memphis, Tennessee (Sharma and Kovacs, 1980); Charleston, South Carolina (Elton and Martin, 1986); San Juan, Puerto Rico (Molinelli, 1985), and Chicago, Illinois, have soil-rock columns that will cause amplification of ground motion under conditions of low- to intermediate-strain ground shaking in some period band.

### 3. CONCLUSIONS AND RECOMMENDATIONS

Site-amplification effects in various urban areas of the United States can be categorized in terms of the period bands where the predominant soil-to-rock amplification factors occur. Table 1 summarizes this information, which provides a basis for evaluating the possibility of poor soil-structure combinations; that is, the response of the soil to earthquake ground shaking and the response of existing and new buildings occurring at the same period, leading to a condition of resonance, as in the September 19, 1985, Mexico earthquake.

The greatest need is for acquisition and analysis of a ground motion data base that is adequate for resolving the technical issues of strain dependence and nonlinearity now associated with site amplification. Resolution of the issues would benefit the design process with respect to site effects and lead to standardization and codification. At the present time, the ground motion data sample in the United States is inadequate and too inconsistent for resolving questions such as:

A. How different are the amplitude, spectral, and temporal characteristics of site amplification in an earthquake having fixed source properties (for example, a magnitude of 7.5) when the given soil-rock column is located at distances ranging from near source to far source?

B. How different are the amplitude, spectral, and temporal characteristics of site amplification for the given soil-rock column located at a fixed source-to-site distance (for example, 10 km) when the magnitude varies over the range 5.0 to 8.0?

One way to accelerate the growth of the data base is to take advantage of the International Decade of Natural Hazard Reduction (IDNDR) proposed for the period 1990-2000. Many opportunities for cooperative research on all aspects of earthquake engineering including site amplification during the IDNDR. For example, extensive strong motion instruments are now available in Algeria, Chile, China, Italy, Jordan, and Yugoslavia. Through cooperative planning, data-acquisition programs can be devised to collect the type of ground motion data that would help to resolve the technical issues.

## References

- 1) Algermissen, S. T., and Perkins, D. M., 1976, A probabilistic estimate of maximum acceleration in rock in the contiguous United States: U.S. Geological Survey Open-File Report 76-416, 45 p.
- 2) Algermissen, S. T., Perkins, D. M., Thenhaus, P. C., Hanson, S. L., and Bender, B. L., 1982, Probabilistic estimates of maximum acceleration and velocity in rock in the contiguous United States: U.S. Geological Survey Open-File Report 82-1033, 99 p.
- 3) Bertero, V. V., Mahin, S. A., and Herrera, R. A., 1978, Aseismic design implications of near-field San Fernando records: *Journal of Earthquake Engineering and Structural Dynamics*, v. 6, pp. 31-42.
- 4) Boore, D. M., 1973, The effect of simple topography on seismic waves: implications for the acceleration recorded at Pacoima Dam, San Fernando Valley, California: *Seismological Society of America Bulletin*, v. 63, pp. 1603-1610.
- 5) Borchardt, R. D., (Editor) 1975, Studies of seismic zonation of the San Francisco Bay region: U.S. Geological Survey Professional Paper 941-A, 102 p.
- 6) Borchardt, R. D., Joyner, W. D., Warrick, R. E., and Gibbs, J. F., 1975, Response of local geologic units to ground shaking, *in* Borchardt, R. D., (Editor), Studies for Seismic Zonation of the San Francisco Bay Region: U.S. Geological Survey Professional Paper 941-A, pp. 52-67.
- 7) Elton, D. J., and Martin, J. R., 1986, Site Period Study for Charleston, S.C.: 3rd U.S. Conference on Earthquake Engineering, Proceedings, Charleston, S.C., v. 1, pp. 497-504.
- 8) Hanks, T. C., 1976, Observations and estimation of long period strong ground motion in the Los Angeles Basin: *International Journal of Earthquake Engineering and Structural Dynamics*, v. 4, pp. 473-488.
- 9) Hays, W. W., 1975, A note on the duration of earthquake and nuclear explosion ground motions: *Seismological Society of America Bulletin*, v. 65, pp. 875-844.
- 10) Hays, W. W., 1977, Evaluation of the seismic response in the Sylmar-San Fernando area, California, from the 1971 San Fernando earthquake: American Society of Civil Engineers, Mechanics Division Specialty Conference on Dynamic Response of Structures, Los Angeles, Proceedings, pp. 502-511.
- 11) Hays, W. W., 1986, The importance of post earthquake investigations: *Earthquake Spectra*, V. 2, pp. 653-668.
- 12) Hays, W. W., 1980, Procedures for estimating earthquake ground motions: U.S. Geological Survey Professional Paper 1114, 77 p.
- 13) Hays, W. W., Algermissen, S. T., Miller, R. D., and King, K. W., 1978, Preliminary ground response maps for the Salt Lake City area: International Conference on Microzonation, 2nd, San Francisco California, Proceedings, v. 2. pp. 487-508.
- 14) Hays, W. W., and Gori, P. L., (Editors), 1984, Evaluation of regional and urban earthquake hazards and risk in Utah: U.S. Geological Survey Open-File Report 84-763, 687 p.
- 15) Hays, W. W., and King, K. W., 1984, Seismic microzonation along the Wasatch fault zone, Utah: World Conference on Earthquake Engineering, 8th Proceedings, v. 1, pp. 1-12.
- 16) Hays, W. W., and King, K. W., 1982, Zoning of the earthquake ground-shaking hazard along the Wasatch fault zone, Utah: International Conference on Microzonation, 3rd, Seattle, Washington, Proceedings, v. 3, pp. 1307-1317.
- 17) Hays, W. W., Rogers, A. M., and King, K. W., 1979, Empirical data about local ground response: Earthquake Engineering Research Institute, National Conference on Earthquake Engineering, 2nd, Stanford, California, Proceedings, pp. 223-232.
- 18) Idriss, I. M., 1978, Characteristics of earthquake ground motions: *Earthquake Engineering and Soil Dynamics*, Proceedings of Specialty Conference, American Society of Civil Engineers, v. 3, pp. 1151-1267.
- 19) Idriss, I. M., and Seed, H. B., 1968, Analysis of ground motions during the 1957 San Francisco earthquake: *Seismological Society of America Bulletin*, v. 58, pp. 2013-2032.
- 20) Innen, Steven, and Hadley, D. M., 1984, Prediction of strong ground motion in the Puget Sound region: The 1965 Seattle earthquake: Sierra Geophysics Report, SGI-R-84-113 to U.S. Geological Survey, 38 p.
- 21) Joyner, W. B., Warrick, R. E., and Fumal, T. E., 1981, The Effects of Quaternary Alluvium on Strong Ground Motion in the Coyote Lake, California Earthquake of 1979: *Seismological Society of American Bull.*, v. 71, pp. 1333-1349.
- 22) Kobayashi, Hiroyoshi, and Nagahashi, Sumio, 1982, Response spectra on seismic bedrock during earthquakes: *Engineering Seismology*, Tokyo Institute of Technology, pp. 22-27.

- 23) MacMurdo, J., 1824, Papers relating to the earthquake which occurred in India in 1819, Philadelphia Magazine, v. 63, pp. 105-177.
- 24) Miller, R. D., 1980, Surficial geologic map along part of the Wasatch Front, Salt Lake Valley, Utah: Miscellaneous Field Studies Map, MS-1198, (scale: 1:100,000).
- 25) Molinelli, Jose, 1985, Earthquake Vulnerability Study for the Metropolitan Area of San Juan, Puerto Rico: in Hays, W. W., and Gori, P. L., (Editors), A Workshop on Reducing Potential Losses from Earthquakes in Puerto Rico, Proceedings of Conference XXX, USGS, Open-File Report 85-731, p. 211-277.
- 26) Murphy, J. R., and Hewlett, R. A., 1975, Analysis of seismic response in the city of Las Vegas, Nevada: A preliminary microzonation: Seismological Society of America Bulletin, v. 65, pp. 1575-1598.
- 27) Murphy, J. R., Lynch, R. D., and O'Brien, L. J., 1971, Predicted San Fernando earthquake spectra: Environmental Research Corporation Report NVO-1163-TM30, to U.S. Atomic Energy Commission, 38 p.
- 28) Murphy, J. R., and West, L. R., 1974, An analysis of surface and subsurface seismic measurements demonstrating the amplification effect of near-surface geology: Environmental Research Corporation Report NVO-1163-TM41 to U.S. Atomic Energy Commission, 21 p.
- 29) Murphy, J. R., Weaver, N. L., and Davis, A. H., 1971, Amplification of seismic body waves by low-velocity layers: Seismological Society of America Bulletin, v. 61, pp. 109-146.
- 30) Rogers, A. M., and Hays, W. W., 1978, Preliminary evaluation of site transfer functions developed from nuclear explosions and earthquakes: International Conference on Microzonation, 2nd, San Francisco, California, Proceedings, v. 2., p. 753-764.
- 31) Rogers, A. M., Tinsley, J. C., and Borchardt, R. D., 1985, Predicting relative ground response, in Ziony, J. F., (Editor), Evaluating earthquake hazards in the Los Angeles region--An earthquake science perspective: U.S. Geological Survey Professional Paper 1360, pp. 221-248.
- 32) Rosenblueth, Emilio, 1986, The Mexican earthquake: A first-hand report: Civil Engineering, American Society of Civil Engineers, New York, January, pp. 38-40.
- 33) Savy, Jean, Bernreuter, Don, and Chen, J. C., 1986, Site effects: A generic method for modeling site effects in seismic hazard analyses, in Hays, W. W., (Editor), Proceedings of Conference XXXIV, USGS Open File Report 86-185, pp. 249-284 35 p.
- 34) Schwartz, D. P., and Coppersmith, K. J., 1984, Fault behavior and characteristic earthquakes: examples from the Wasatch and San Andreas faults: Journal of Geophysical Research, v. 89, no B7, pp. 5681-5698.
- 35) Seed, H. B., and Lysmer, John, 1986, Site response - A critical problem in soil-structure interaction analyses for embed structures: Workshop on Soil-structure Interaction, Brookhaven National Laboratory and U.S. Nuclear Regulatory Commission, Proceedings, pp. 233-250.
- 36) Seed, H. B., 1975, Design provisions for assessing the effects of local geology and soil conditions on ground and building response during earthquakes, in New earthquake design provisions: Proceedings of seminar sponsored by Professional Development Committee of Structural Engineers Association of Northern California and San Francisco Section of America Society of Civil Engineers, pp. 38-63.
- 37) Seed, H. B., and Idriss, I. M., 1969, Influence of soil conditions on ground motions during earthquakes: Journal on Soil Mechanics and Foundations Division of America Society of Civil Engineers, v. 95, pp. 1199-1218.
- 39) Seed, H. B., Murarka, R., Lysmer, John, and Idriss, I. M., 1976, Relationships of maximum acceleration, maximum velocity, distance from source, and local site conditions for moderately strong earthquakes: Seismological Society of America Bulletin, v. 66, pp. 1323-1342.
- 40) Seed, H. B., Whitman, R. V., Dezfulian, H., Dobry, R., and Idriss, I. M., 1972, Soil Conditions and building damage in the 1967 Caracas earthquake, Journal of the Soil Mechanics Foundations Division, America Society of Civil Engineers, v. 98, pp. 787-806.
- 41) Singh, J. P., 1985, Earthquake ground motions: Implications for designing structures and reconciling structural damage: Earthquake Spectra, v. 1, pp. 239-270.
- 42) Sharma, S., and Kovacs, W. D., 1980, The Microzonation of the Memphis, Tennessee Area: U.S. Geological Survey Open-File Report 80-914, 129 p.
- 43) Smith, R. B., Richins, W. D., and Dose, D. I., 1985, The 1983 Borah Peak, Idaho Earthquake: Regional seismicity, kinematics of faulting, and tectonic mechanics: in Stein, R. S. and Bucknam, R. C., (Editors), On the Borah Peak, Idaho, earthquake, U.S. Geological Survey Open-File Report 85-290, p. 236-263.
- 44) Tezcan, S. S., Seed, H. B., Whitman, R. V., Serff, N., Christian, J. T., Durgunoglu, H. T., and Yegian, M., 1977, Resonant period effects in the Gediz, Turkey earthquake of 1970: Earthquake Engineering and Structural Dynamics, v. 5, pp. 157-179.

- 45) Whitman, R. V., 1983, An Engineer's Perspective on the Cape Anne, Massachusetts Earthquake of 1755: Earthquake Notes, v. 54, no. 1, p. 8 (Abstract).
- 46) Wolf, J. P., 1985, Dynamic Soil-Structure Interaction, Prentice-Hall Publishing Company, Englewood Cliffs, New Jersey, 466 p.
- 47) Wood, H. O., 1908, Distribution of Apparent Intensity in San Francisco, in The California Earthquake of April 18, 1906: Report of the State Earthquake Investigation Commission, Carnegie Institution of Washington, Washington, D.C., pp. 220-245.
- 48) Yamahara, H., 1970, The interrelation between frequency characteristics of ground motion and earthquake damage to structure: Soils and Foundations, v. 10, pp. 57-74.
- 49) Zeevaert, L., 1964, Strong ground motions recorded during earthquakes of May 11 and 19th, 1962 in Mexico City: Seismological Society of America Bulletin, v. 54, pp. 209-232.

Table 1.--SITE AMPLIFICATION EFFECTS IN VARIOUS URBAN AREAS

LOCATION	PERIOD BAND OF DOMINANT RESPONSE		
	SHORT (0.05 - 0.5 SEC.)	INTERMEDIATE (0.5 - 3.0 SEC)	LONG (3.0 - 10 SEC)
SAN FRANCISCO, CALIFORNIA	X	X	X
LOS ANGELES, CALIFORNIA	X	X	
SEATTLE, WASHINGTON	X	X	
LAS VEGAS, NEVADA	X	X	X
SALT LAKE CITY, UTAH	X	X	
MEMPHIS, TENNESSEE	X	X	
ST. LOUIS, MISSOURI	X	X	
CHARLESTON, SOUTH CAROLINA	X	X	
BOSTON, MASSACHUSETTS	X	X	
SAN JUAN, PUERTO RICO	X	X	

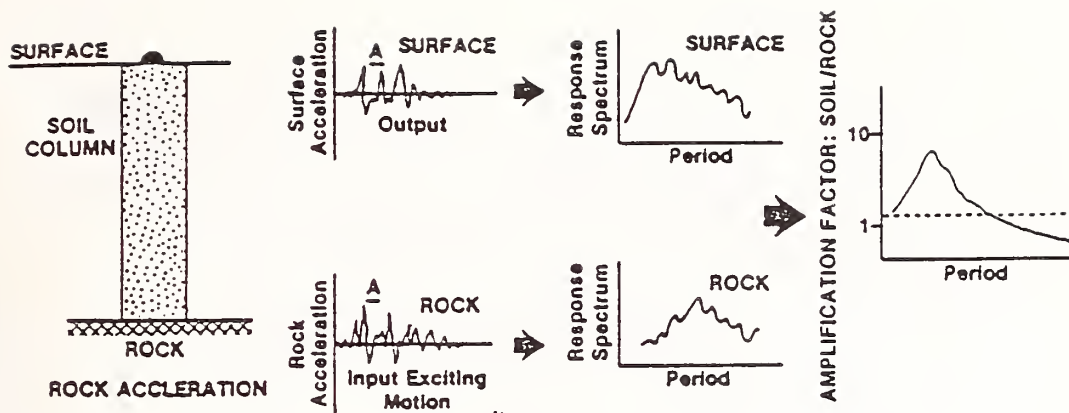


Figure 1.--Schematic illustration showing (from left to right) the soil-rock column, the bedrock and surface acceleration time histories, the corresponding response spectra derived from them, and the spectral amplification factor transfer function). The peak amplitude of acceleration is read from the acceleration time histories. The soil-to-rock amplification factor for a discrete period band is read from the transfer function.

## GROUND MOTION AND THE RESPONSE SPECTRUM

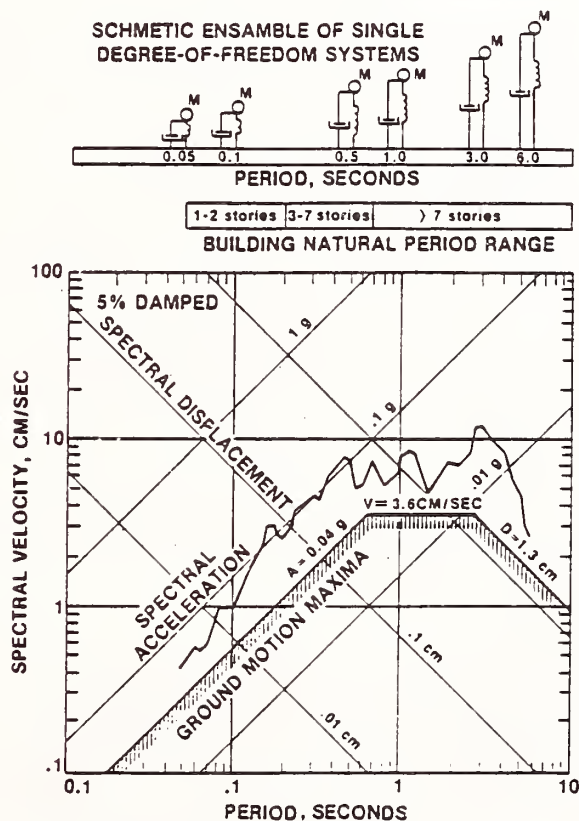


Figure 2.--Schematic illustration showing the correlation of the response spectrum derived from a strong-motion accelerogram with a series of damped, single degree-of-freedom, harmonic oscillators. The peak amplitude of acceleration is the zero-period asymptote of the spectrum. The peak amplitude of displacement is the infinite-period asymptote. The ground motion can be correlated with site and building response through the response spectrum.

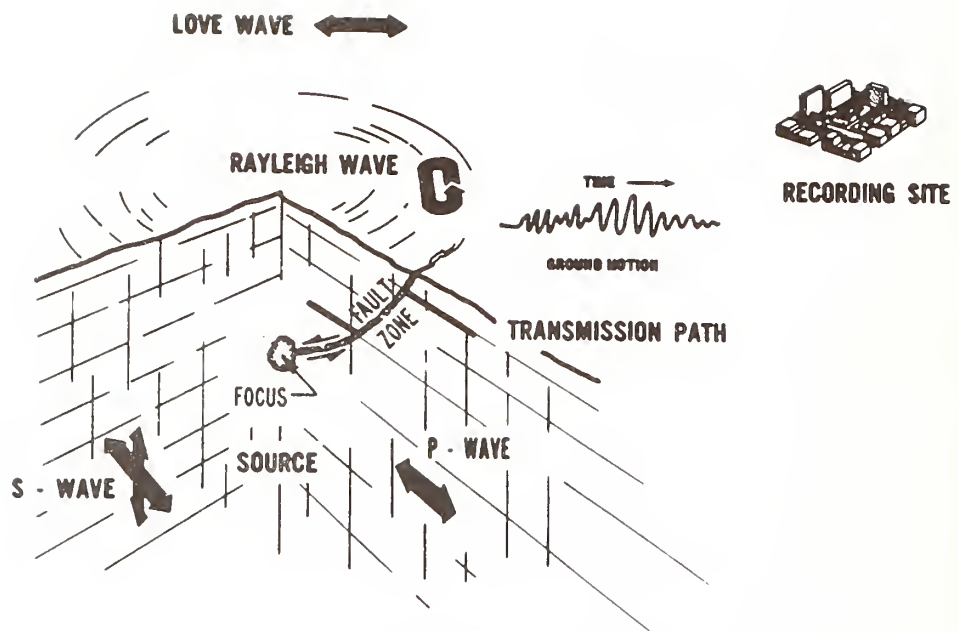


Figure 3.--Schematic illustration showing the earthquake-path-site-structure system.

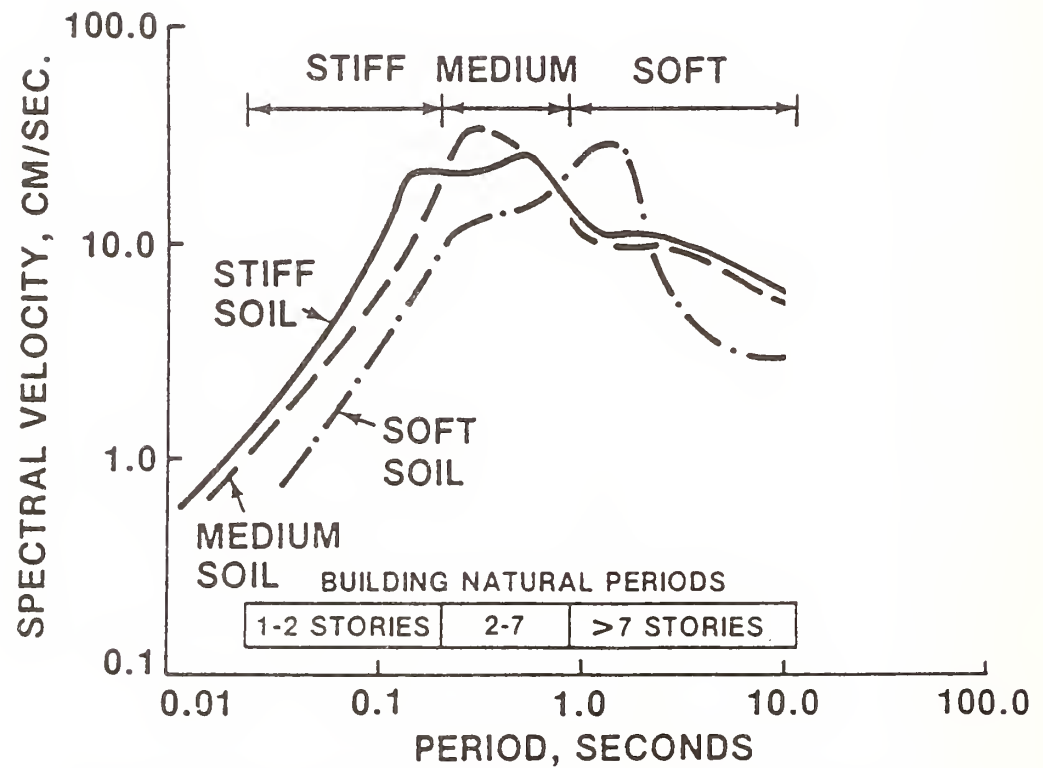


Figure 4.--Graph showing the effect of different types of soil columns on the spectral composition of ground motion. The general correlation with the height of the building is also shown for comparison.

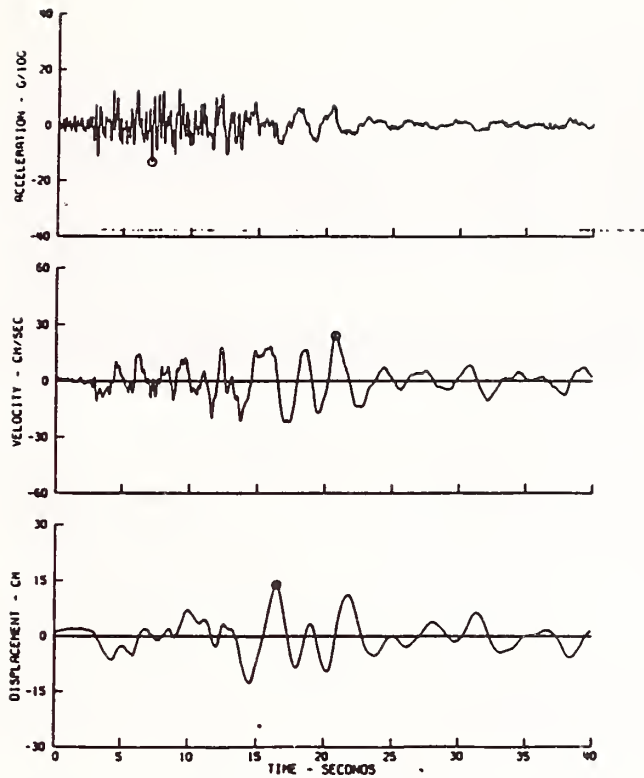


Figure 5.--Display showing the horizontal component of ground acceleration (top) and the derived velocity (center) and displacement (bottom) time histories. These records show the high-frequency body waves and low-frequency surface waves observed at a distance of about 20 km for a moderate magnitude earthquake.

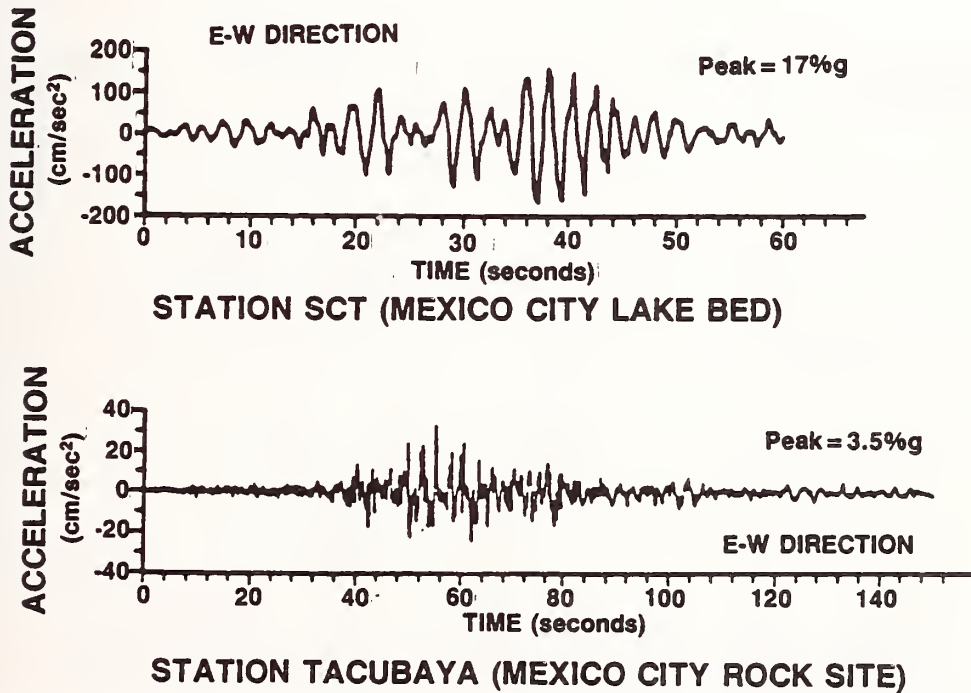


Figure 6.--Comparison of the strong motion accelerograms recorded on rock-like material and in the lake-bed zone. The soft soil in the lake-bed zone amplified the 2-second ground motion.

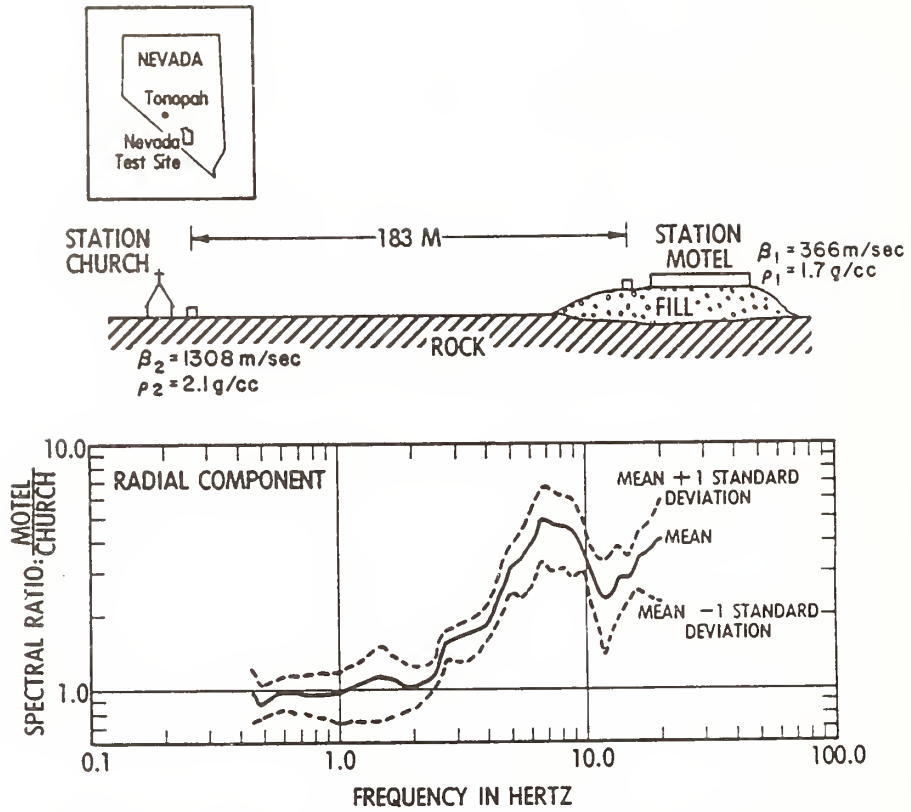


Figure 7.--Examples of short-period body wave site-amplification effects in Tonopah, Nevada. The soil-to-rock amplification factor of 7 is centered around a frequency of 7 Hz.

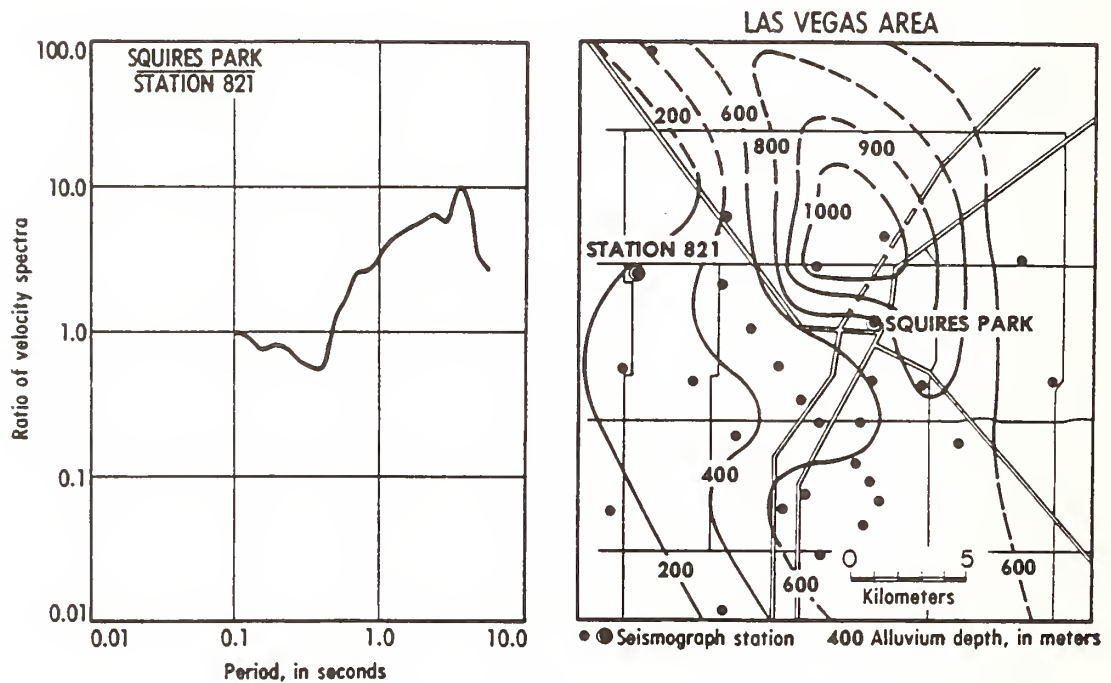


Figure 8.--Map showing the thick-to-thin soil transfer function in Las Vegas.

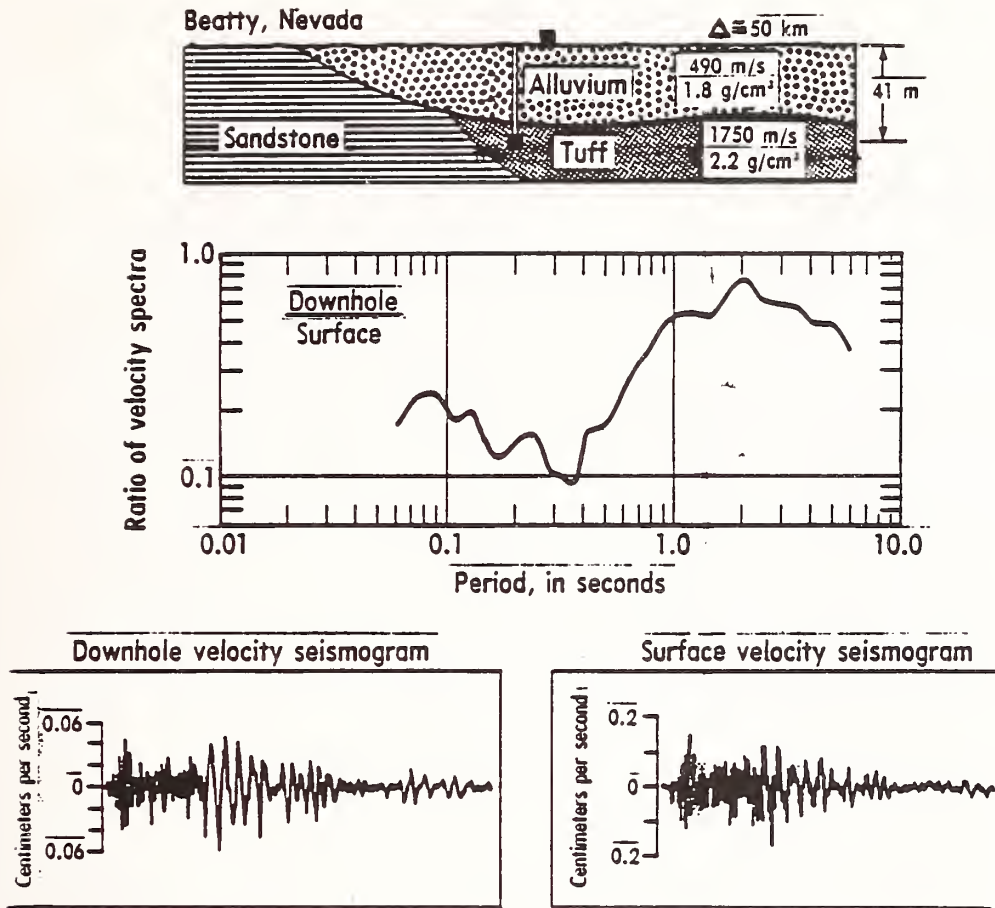


Figure 9.--Site amplification observed at Beatty, Nevada, from measurements in an uphole-downhole seismic array.

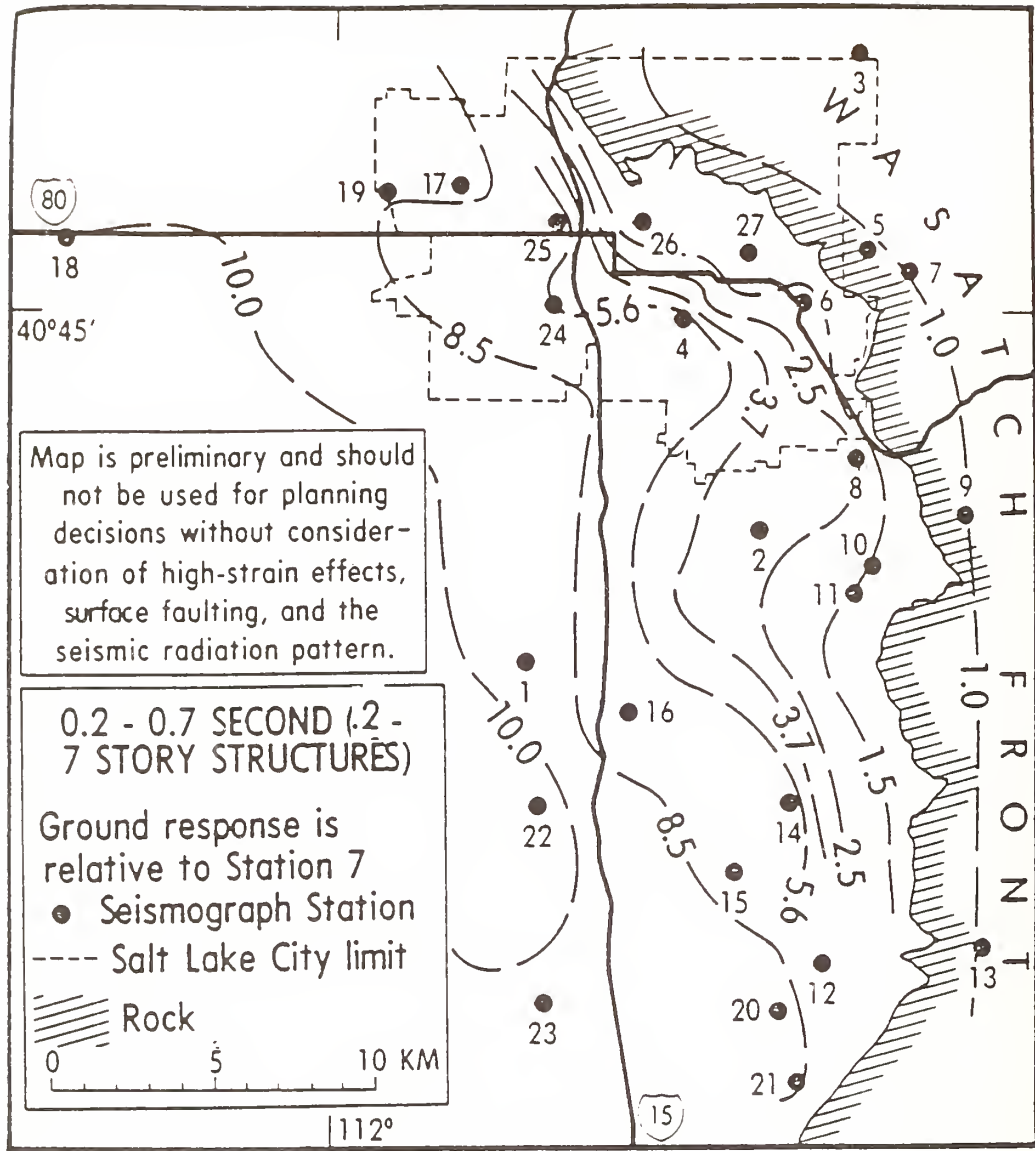


Figure 10.--Map showing the site amplification factor for the period band 0.2-0.7s, Salt Lake City area. Values on contours indicate the radii of velocity response spectra that would be expected relative to rock on the Wasatch Front. These values provide an estimate of the spatial variation of ground motion in the period band in which the 2-7 story buildings have their fundamental natural period of vibration.

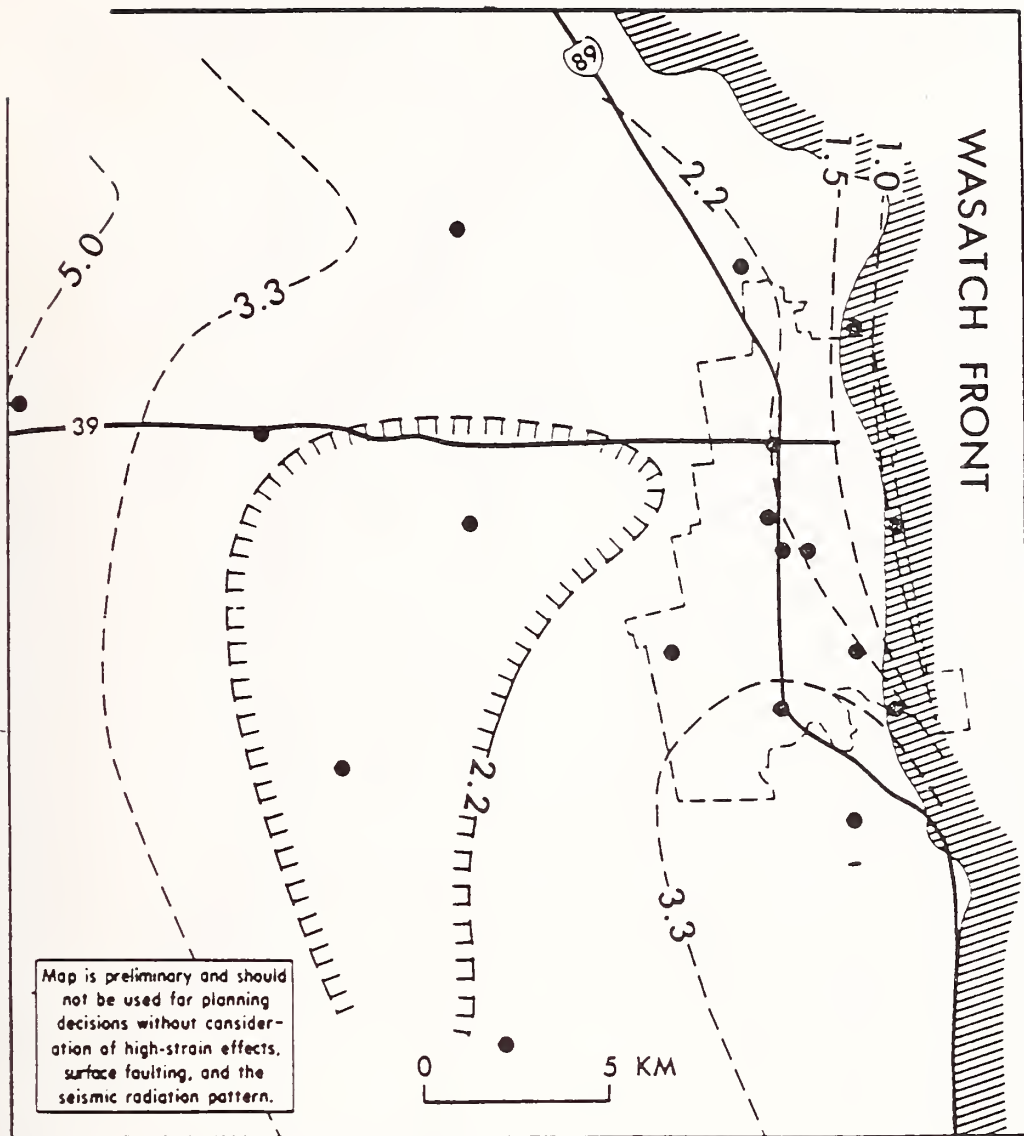


Figure 11.--Map showing the site amplification factors for the period band 0.2-0.7s, Ogden area. Values on contours indicate the ratios of velocity response spectra that would be expected relative to rock on the Wasatch Front. These values provide an estimate of the spatial variation of ground motion in the period band in which the 1-7 story buildings have their fundamental natural period of vibration.

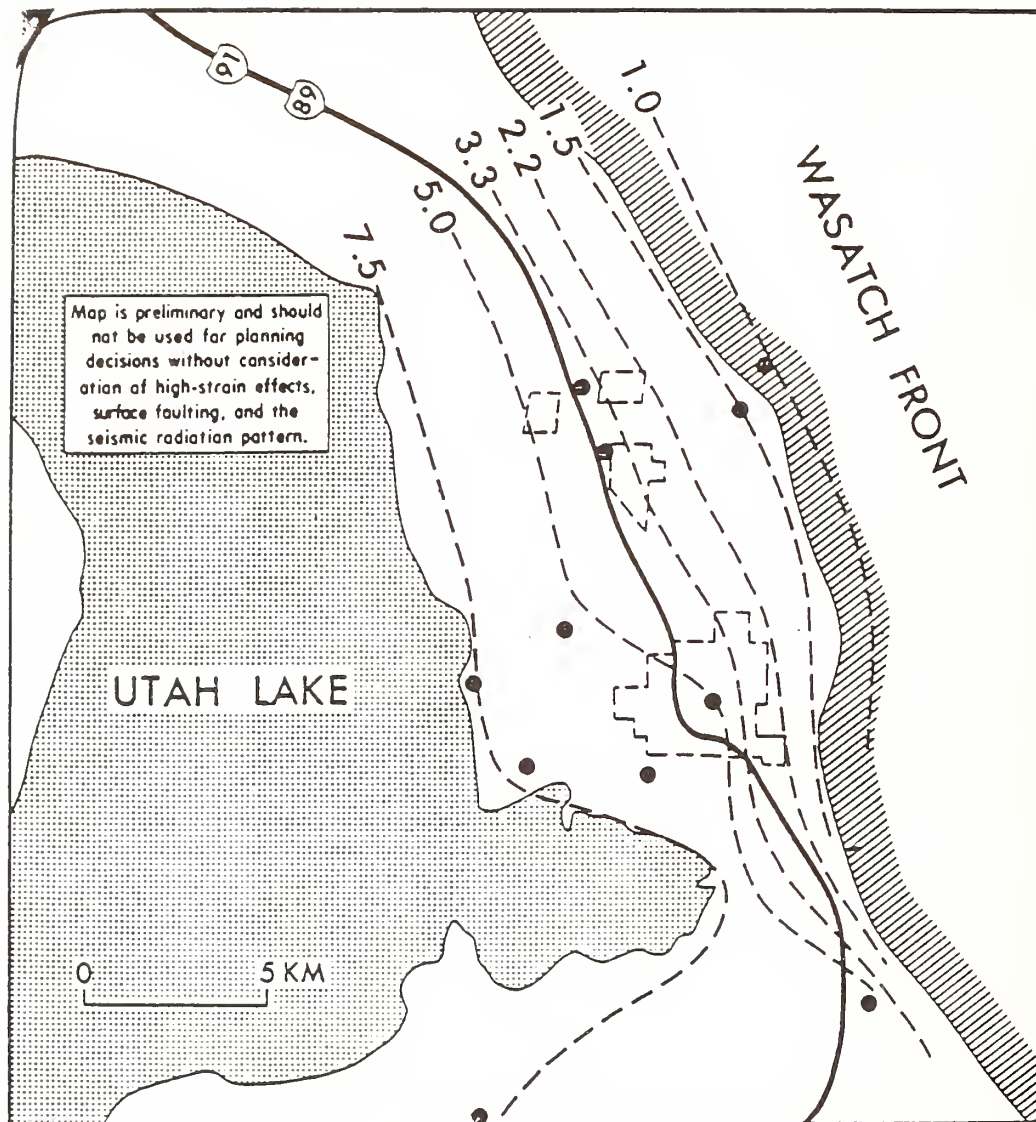


Figure 12.--Map showing the site amplification factors for the period band 0.2-0.7s, Provo area. Values on contours indicate the ratios of velocity response spectra that would be expected relative to rock on the Wasatch Front. These values provide an estimate of the spatial variation of ground motion in the period band in which the 1-7 story buildings have their fundamental natural period of vibration.

# Seismic Performance of Reinforced Concrete High-Rise Frame Structure with Wall Columns—Part 1: Deformation Capacity of Critical Structural Elements such as Wall Columns, Beams and Shear Walls

By

Masaya Hirose<sup>1</sup>, Hisahiro Hiraishi<sup>2</sup>  
Masashi Fujisawa<sup>3</sup>, Manabu Yoshimura<sup>4</sup>

## ABSTRACT

For apartment houses from 10-storied to 15-storied high, research and development were done of reinforced concrete buildings of wall frame structure with walled frames in the ridge direction and independent shear walls in the span direction, a design guideline was compiled in 1987 for buildings of up to 11 stories for the time being. Of the structure discussed herein, we try to secure a seismic performance of yield base shear coefficients of 0.35 & more in the ridge direction and of 0.40 & more in the span direction, plus a plastic deformation ability with a story drift angle of 1/100 or so. In this paper principal research results will be presented of the parametric experimental research done on such main seismic structural members as wall columns, beams in the ridge direction, and shear walls in the span direction. Those research results served as "back data" of the technical guideline mentioned above.

This research project was one of Japan's recent typical overall technical development projects which are carried out in order to develop ductile medium to high-rise R/C structures.

**Key Words :** RC structure, apartment house, T-beam, wall column, shear wall, seismic performances, plastic deformation ability, overall technical development project.

## 1. Preface

Recently in Japan the demand for high-rise apartment houses has been gradually increasing in order to make effective use of the urban space, which has become more and more badly crowded. In terms of construction cost reduction, the reinforced concrete (R/C) construction has come to attract more attention than the steel construction and the steel framed RC construction. In Japan medium-rise apartment houses have originally been cast-in-site or precast wall RC constructions, which have a good seismic capacity and have suffered very few seismic damages. For that reason, national-scale technical development projects have been carried out so as to improve this structural system mainly in terms of ductility and use it for high-rise apartment houses. Here some examples will be given of apartment houses built in this structural system with some dynamic characteristics thereof then the results will be presented of large-scale experimental studies of the main structural members of the system namely, the T-beam, the wall column with a flat section and the shear wall.

## 2. Outline of the Structural System and its Dynamic Characteristics

### 2.1 Outline of the Structural System

This structural system was developed for medium to high-rise apartment houses. The plan is shown in Fig. 1.1 Next, Fig. 1.2 shows the plan (display) of main structural members. As can be seen in these figures, the ridge direction of this system has a frame structure with flat wall columns and relatively even span lengths; the span direction has independent shear walls with flat periphery columns at either end. As for this structural system, the following structural standard have been set up in order to ensure an appropriate horizontal bearing capacity and good ductility. If we follow the standard, we are given permission for each structural design without carrying out special structural experiments or dynamic analyses.

- a. Lower limits of wall ratio ( $a_w$ ) \* and wall column ratio ( $a_{wc}$ ) \*\*: at the 1st floor of an N-storied building,  $a_w \geq 25N$  and  $a_{wc} \geq 20N$ . This stipulation a. and the following e. will limit the mean shear stresses ( $\bar{\tau}_u$ ) of the shear wall and the wall column at the maximum horizontal capacity of a building to about 17kg/cm<sup>2</sup>, and about 24kg/cm<sup>2</sup>, respectively, which allows us to expect improved ductility.
- b. lower limits of depth of beam ( $D_g$ ) and length of the span ( $l_g$ ) :  $D_g \geq 65\text{cm}$  and  $l_g \geq 4D_g$ , which will make the ultimate mean shear stress at beam yield  $\tau_{ug}$ , less than about 20 kg/cm<sup>2</sup>. Items a., e. and this b. will limit the tensile reinforcement ratio of beam to 1.5% at the most. This item b. allows us to expect prevention of early shear failure and bond-split plitrailure of beam.

$$* a_w = \frac{\text{Sum of sectional area of shear walls} (\sum A_{ws})}{\text{Total floor area} (A_f)}$$

$$** a_{ws} = \frac{\text{Sum of sectional area of walled columns} (\sum A_{ws})}{A_f}$$

1. Dr. of Eng., Director, International Institute of Seismology and Earthquake Engineering, Ministry of Construction, Japan.
2. Dr. of Eng., Head, Structure Division, Structural Engineering Department, BRI, MOC
3. Chief Researcher, Structure Division, Structural Engineering Department, BRI, MOC
4. Dr. Eng. Associate Professor, Faculty of Engineering, Tokyo Metropolitan University

- c. Lower limit of width of wall column (b) of ridge direction and range of ratio of depth (D) to width of wall column : the width of the wall column in the ridge direction  $b \geq 30\text{cm}$ , which is to make the wall column double reinforcing and to widen the effective extent to confine concrete. Moreover,  $2 \leq D/b \leq 5$  (1st floor) ;  $2 \leq D/b \leq 8$  (other floors).

The lower limit is to ensure the rigid zone for reducing the beam reinforcement and the upper limits are to avoid extreme flatness so as to ensure ductility. Besides, there is a regulation on reinforcing bars to confine concrete in the compression zone of the wall column with possibility to yield in flexure.

- d. Cross section and thickness of shear wall : shear wall shall be with peripheral wall columns at both ends of horizontal section and thickness of wall and wall reinforcement ratio shall be not less than  $15\text{cm}$  and  $0.25\%$ , respectively. These items were regulated to keep adequate flexure capacity and ductility for the whole structure.
- e. Required minimum yield base shear coefficient ( $C_B$ ) : Minimum values of  $C_B$  required in the ridge and span directions are  $0.35$  and  $0.40$ , respectively. These values are regulated according to expected degrees of ductility in both directions. Besides, the following items are regulated in the guideline.
- f. Details of non-structural wall
- g. Simplicity of plan and elevation of a building
- h. Lower limit to number of spans in ridge direction
- i. Lower limit to ratio of length to height of a building in span direction

#### Dynamic Behavior

Structural characteristics of this system is that it is composed, relatively in a uniform way, of structural members of which structural performance seems to be made clear by experiment. Therefore, we can expect to make clear with few errors the seismic performance necessary to each structural members by non-linear static and dynamic analyses of the whole structure. Here, several items on the dynamic behavior of the structure, which were made clear by several preliminary analyses and estimated as back data for the regulations in the guideline, are described. In the analytical studies, the assumed external force distribution for the static analyses was the same as regulated in the enforcement order of the Building Standard Law, and in the dynamic response analyses, the following observed waves were used with modification of the maximum acceleration to  $350\text{gal}$ .

- |                  |         |
|------------------|---------|
| a. El Cento      | 1940 NS |
| b. Sendai THO 30 | 1978 NS |
| c. Hachinohe     | 1968 NS |
| d. Hachinohe     | 1968 EW |

As examples of analytical results, Figs. from 2.4 to 2.7 show several results on an 11-storied building which plan and section are illustrated in Fig. 2.3.

This building was designed based on the structural guideline with  $C_B = 0.35$  in ridge direction and  $0.40$  in span direction.

Principal items are as follows.

- a. The horizontal rigidity of a building by this structural method is so high that the fundamental vibration period in both directions of the super structure with fixed end is roughly estimated by  $0.012h$  (sec), where  $h$  (m) means the total height of a building.
- b. Failure mechanism in ridge direction is a so-called total failure mechanism where flexure yielding occurs in beams prior to wall columns at each nodal point except the column top at the highest story,

column base at the ground story and column ends of external columns in tension side. And failure mechanism in span direction is flexure yielding or shear failure at the base of shear walls, or total rotational mechanism of footing.

- c. In case of the ridge direction of the building shown in Fig. 2.3, yielding hinges begin to appear at beams of intermediate stories when static monotonous load reaches  $0.23$  in base shear coefficient  $C_B$  and  $0.2\%$  in drift angle at the top,  $R_T$ . When  $R_T$  and  $C_B$  get to about  $0.3\%$  and  $0.3$ , respectively, yielding hinges appear at  $50\%$  of all beams, and yielding hinges appear at base of columns only when  $R_T$  is about  $0.7\%$  and horizontal load reaches  $90\%$  of the maximum bearing capacity (Fig. 2.4).
- d. Existence of structural elements perpendicular to framing members, such as floor slabs to beams and peripheral wall columns to shear walls, enlarge remarkably the bearing capacity of a building.
- e. The maximum response relative displacements to the observed waves with  $350$  gal as the maximum acceleration are confined to about  $2.7\text{cm}$ ,  $1\%$  in drift angle in ridge direction (Fig. 2.5, 2.6). And the maximum response drift angles in span direction are less than  $0.3\%$ .
- f. The maximum rotation angle of beams at the maximum response deflection, obtained by dynamic response analyses on frame models in ridge direction, are confined to  $2\%$  and the maximum responses of shear forces of each wall column are within  $1.4$  times the shear forces in such a failure mechanism as described in the item C. It means that so-called dynamic amplification factors of shear force in wall columns are around  $1.4$ .
- g. Dynamic amplification factors of shear force in shear walls, obtained by the dynamic response analyses on flexure-shear models in span direction, are within  $1.2$ .

### 3. Experimental Results on Girder

#### Introduction

In Japan, high-rise reinforced concrete buildings have become popular in recent years. In the structural design of those buildings it is usual that "Strong Column and Weak Girder" philosophy is employed and girders are designed to have sufficient ductility. On the other hand, longitudinal reinforcement of girders tends to increase as a building becomes higher, and past studies have revealed that girders with large amount of main bars are apt to fail in a brittle manner such as shear or bond splitting. It is, therefore, important for high rise R/C buildings to prevent such brittle failure of girders and to secure ductility of them.

Results of experimental studies conducted from the above view point as to ductility of highly reinforced girders are stated in this chapter. Note the tests reported herein are those done at the Building Research Institute, Ministry of Construction (BRI), University of Tokyo (UT) and Tokyuu Construction Company (TCC).

#### Specimens and Loading Methods

Specimens, being all "T-beam" and twenty-five in total number, were designed to simulate girders in lower stories of a fifteen story building. Scale of them were one-third for BRI, one-half for UT and full for TCC. Main parameters of the tests were a. amount of stirrup (BRI), b. arrangement of stirrup (UT) and c. size of main bars (TCC). The specimens were subjected to reversals of double curvature loading. As to details of loading methods, refer to

the past papers [1][2][3].

Major Findings from Tests

Major findings from the tests at the three research institutes are outlined below.

- a. As amount of stirrup increased, bond-splitting failure became hard to occur.
- b. The specimens, computed shear strength of which were less than computed flexural strength, mostly failed in bond splitting and such specimens showed significant strength decay at drift level of more than 1%. And bond-splitting failure was observed even in the specimens with computed shear strength over flexural strength.
- c. Although bond-splitting failure was observed both at the bottom of girder and at the intersection of girder and slab, the latter case was much larger in number. This is probably due to the fact that bad condition was less favorable at the top of girder than at the bottom of girder because the specimens were fabricated in a horizontal position.

Studies on Bond-Splitting Failure

a. Effect of stirrup

Several series of tests were conducted in BRI. Among them a series of tests using specimens (No. 1 to No. 4) with same amount of main bars ( $p_c = 1.2\%$ ) and different amount of stirrup. ( $p_w = 0.3\% - 0.9\%$ ) was introduced herein.  $p_w$  of the specimens No. 1 ~ No. 4 were respectively, 0.3% (No. 1), 0.6% (No. 2), 0.9% (No. 3), and 0.3% for middle region but 0.6% for end region (No. 4).

Envelope of P-δ relations and final damage were compared in Fig. 3.1 and 3.2. No. 1 and No. 2 suffered severe bond-splitting failure and showed significant strength decay after drift level of 1% (No. 1) and 3% (No. 2). However, No. 3, although suffered some bond cracks, did not fail in bond splitting until the end of the test. Note that No. 4 with more stirrup in the end region than No. 1 showed some improvements ductility while it also failed in bond splitting at the middle region.

Figure 3.3 compares strain distribution of bottom main bars at several drift levels for No. 1 and No. 3.

The bottom bar of No. 1, which failed in bond-splitting at the bottom, showed tensile strain even in the region expected to be in compression. This was due to bond deterioration of this bar. On the contrary such observation was not made for No. 3. The Above results clearly indicate that the amount stirrup had a significant effect on bond splitting behavior of girders.

b. Bond-Splitting Failure at Intersection of Girder and Slab

In the BRI tests, bond-splitting failure at the intersection of girder and slab was often observed.

One of the sources of such failure is that slab bars of the specimens were of single layer, as shown in Fig. 3.4(a). To see the influence of this, additional tests using specimens (No. 2A and No. 3A) with the same amount of slab bar ratio with the previous specimens (No. 2 and No. 3) but double slab-bar-layers were conducted. In these tests bottom slab-bar-layer in the transverse direction was expected to contribute to improving bond-splitting behavior of girder because it was placed across the bond-splitting face.

Note concrete compressive strength of the additional tests was 236kg/cm<sup>2</sup> which was almost equal to that of the previous test (230kg/cm<sup>2</sup>).

P-δ relations of the additional tests and previous tests are compared in Fig. 3.5. Final damage of No. 2A is also shown in Fig. 3.2. The specimens with double slab-bar-layers were significantly improved in ductility as compared to the specimens

with single slab-bar-layer. And No. 2A did not suffer bond-splitting failure while No. 2 suffered.

Fig. 3.6 shows strain distribution of bottom transverse slab-bar at several drift levels for No. 2A.

This figure clearly demonstrate that strains of this bar nearly reached yielding strain at drift level of more than 2%. The above results strongly suggest that bottom transverse slab bars resisted in widening of bond-splitting cracks and contributed in improving bond-splitting behavior of girder.

c. Relations of Shear Strength Ratio and Deformability

Relations of shear strength ratio and deformability are plotted in Fig. 3.7 as to all specimens, in which shear strength ratio was defined as deformability was defined as deformation at which load dropped up to 80% of the maximum load on the envelope of P-δ relations. Note that symbols in the figure correspond to failure mode shown below;

- : flexural failure
- : bond-splitting failure after flexural yielding
- : bond-splitting failure before flexural yielding

It is apparent from the figure that when the shear strength ratio was more than 1.1, deformability was more than 4% and failure mode of these more than 1, 1, deformability was more than 4% and failure mode of these specimens was flexure or bond-splitting after flexural yielding, in other word, not pure bond-splitting.

Conclusion

From these test results, the following findings were obtained;

- a. As amount of stirrup increases, bond-splitting failure becomes hard to occur,
- b. When the shear strength ratio exceeds 1.1, favorable ductility is expected, and
- c. Bottom transverse slab bars have a significant effect on bond-splitting behavior of girder. Therefore, when girders are tested, it is desirable that slab bars of specimens be of double layers even when they are small scale model.

4. Results of Experiments on Deep Columns [5][6][7]

Outline

Combined bending-shear cycle loading tests of 38 deep column specimens were conducted to examine their seismic performances. The main variables are : a. level of axial compressive stress ( $\sigma_0 / F_c$ ), b. aspect ratio (D/b), c. shear span ratio (M/(Q·D), d. extent to confine concrete and e. with or without perpendicular wall. Influences of these variables on the bending capacity, shear capacity and ductility of deep columns were examined.

Flexure Capacity

Based on the test results of the 33 specimens of which tensile reinforcements yielded, observed maximum bearing flexure capacities were compared with the calculated values by several kinds of theoretical methods. As a result, the following simplified equation (1) was found adaptable for practical use (Fig. 4.1).

$$\mu = 0.9a_t \cdot \sigma_y \cdot D + 0.4a_w \cdot \sigma_{wy} \cdot D + 0.5N \cdot D$$

$$(1 - N / (b \cdot D \cdot F_c)) \dots \dots \dots (1)$$

where,  
 $a_t, \sigma_y$  : sum of sectional area of tensile reinforcements and the yielding point strength, respectively

$a_w, \sigma_{wy}$  : sum of sectional area of intermediate vertical reinforcements and the yielding point strength, respectively

N : axial force  
F<sub>c</sub> : compressive strength of concrete

b, D : width and depth of deep column, respectively

Shear Capacity

Concerning the test results of shear capacity ( $tQ_{su}$ ) of 4 T-sectioned deep column specimens with perpendicular wall, effects of perpendicular walls to shear capacity of rectangular deep column and the ratio of  $tQ_{su}$  to calculated value ( $cQ_{su}$ ) by the proposed equation (2) were examined and the followings were made clear (Fig.4.2). Here, eq. (2) is an experimental one which would fall around the lower limit of the shear capacity of rectangular-sectioned member.

$$Q_{su} = \left\{ \frac{0.053p_t \cdot 0.23(Fc+180)}{M/(Q \cdot d)+0.12} + 2.7\sqrt{p_{wh} \cdot \sigma_{wh} + 0.1 \sigma_{oe}} \right\} \times be \cdot j \quad (2)$$

M, Q : bending moment and shear force at critical section, respectively

d, j : effective depth and distance between the center of tensile stress and that a compressive stress of the section, respectively

be :  $\Sigma A/D$  ( $be < 1.2b$ ), width of the equivalent rectangular section with depth, D and total area,  $\Sigma A$ ,  $\Sigma A$  means total area of the deep column and the effective portion of perpendicular walls, where the effective extent shall be not larger than  $6t$  ( $t$ :thickness)

$p_{te}$  : effective tensile reinforcement ratio in %,  $100 \times a_t / (be \cdot D)$

$p_{we}$  : effective web reinforcement ratio  $a_w / (be \cdot S)$ ; where  $a_w$  is the area of a pair of web reinforcement and S is their spacing

$\sigma_{oe}$  : effective axial compressive unit stress,  $N/(be \cdot D)$

The main finding are,

- a. Ratios of  $tQ_{su}$  on T-sectioned specimens to  $cQ_{su}$  on rectangular-sectioned are 1.25 ~ 1.38 in the cases where perpendicular walls exist on compressive side and 1.06 ~ 1.15 in the cases on tension side.
- b. Eq. (2) gives conservative values, that is, the ratio of  $tQ_{su} / cQ_{su}$  is about 1.5 in rectangular column and the ratios are about 1.5 ~ 1.8 in T-sectioned column.

Deformation Ability

The authors defined "the stable limit" as the deflection point where clear compressive failure is observed in compressive zone of critical section after flexure yielding. Concerning the drift angle  $R_u$  at the stable limit, the following results were obtained (Fig.4.3 ~ 4.7).

- a. Confinement of concrete in the compressive zone of deep column is very effective to increase  $R_u$ . Increase of confined zone is also effective especially in columns with a high axial stress or with a high D/b ratio (Fig.4.3, 4.4).
- b. Values of  $R_u$  tend to decrease with increase of D/b ratio (Fig.4.5).
- c. Values of  $R_u$  of the specimens with perpendicular walls in compression side are larger than those of rectangular columns, but perpendicular walls in tension side are not effective to increase  $R_u$  (Fig.4.6).
- d. Arranging transverse ties and existence of perpendicular walls in the middle of section are both effective to prevent members from sudden deterioration of bearing capacity after the stable limit.
- e. The stable limit of deep column with effective confining reinforcements can be generally estimated by the combination of the ratios of D/b and  $\sigma_o / Fc$  (Fig.4.7).

Outline

Combined bending-shear cycle loadings tests of 21 shear wall specimens without openings and 5 specimens with openings were conducted to discuss mainly their flexure capacity, shear capacity, deformation ability and so on. The main variables are a.  $\sigma_o / Fc$ , b. ( $A_c$  : sectional area of peripheral column) / ( $A_w$  : sectional area of shear wall), c. existence of floor beams and the amount of axial reinforcing bars, d. existence of intermediate column, e. scale effect.

Flexure Capacity

By comparison of the test results of flexure capacity of the 27 shear wall specimens with peripheral wall columns including 22 past specimens, with the calculated values by several kinds of empirical equations, the following eq. (2) was found adaptable for practical use (Fig.5.1).

$$M_u = (a_t \cdot \sigma_y) l_w + 0.5(a_t \cdot \sigma_y) \cdot l_w + 0.5 N \cdot l_w \quad (1)$$

where,

$a_t$  : Sum of sectional area of all vertical reinforcements in the peripheral column in tension side

$l_w$  : distance of center-to-center of the peripheral columns at both ends of wall section

Others are the same as in eq. (1)

Concerning the specimens with openings, their flexure capacities were calculated based on the assumed failure mechanism where the specimens were replaced with frames with rigid zone and where all beams at the openings were assumed to yield in flexure at faces.

The calculated results agreed fairly well with the test results and the ratios of the tested to the calculated were 0.98 ~ 1.08.

Shear Capacity

Comparing the experimental shear capacity of shear wall specimens without openings with the calculated values by eq. (2) and the following equation (4), the followings were made clear. Here, eq. (4) is proposed to get mean value of shear capacity on I-sectioned shear walls.

$$cQ_{su} = \left\{ \frac{0.0679p_t e^{0.23} (Fc+180)}{\sqrt{M / (Q \cdot D)+0.12}} + 2.7\sqrt{p_{wh} \cdot \sigma_{wh} + 0.1 \sigma_{oe}} \right\} \times be \cdot j \quad (4)$$

where,

D : total length (=depth) of shear wall

j : may be equal to 0.85 (D-b/2), here b means width of peripheral wall column

$p_{wh}$  : effective horizontal wall reinforcement ratio containing axial bars in beams

$b_o$  : effective thickness of shear wall, counteracting effective area of peripheral columns with effective width of (t+2b) ; where t means thickness of wall

Other notations are the same as in eq. (2) except D shall be used for d.

The main findings are as follows.

- a. Eq. (2) gives conservative values, i.e., the ratios of  $tQ_{su} / cQ_{su}$  range from 1.16 to 1.56. Mean value,  $m$  is 1.38 and standard deviation,  $\sigma$  is 0.133.
- b. The ratios of  $tQ_{su} / cQ_{su}$  range from 0.87 to 1.19,  $m$  is 1.04 and  $\sigma$  is 0.19.
- c. Between the specimen reduced to 1/5 and the one to 1/10, the influence of scale effect to the ratios of  $tQ_{su} / cQ_{su}$  was not significant.

Deformation Ability

Fig. 5.4 illustrates the  $\tau - R$  relationship of

the 21 above-mentioned shear wall specimens without openings. Further, the relationship between the deflection angle limit,  $R_{um}$  and the compressive capacity coefficient  $\bar{\sigma}_c$  by the following definition is illustrated in Fig. 5.5. That is,

$$\bar{\sigma}_c = (a_c \cdot \sigma_y + a_w \cdot \sigma_{wy} + N) / (a_c \cdot \sigma_y + b \cdot D \cdot F_c) \quad \text{----- (5)}$$

where,

$a_c$  : sum of sectional area of all vertical reinforcements in the peripheral column in tension side

Others are the same as defined before.

$R_{um}$  : horizontal drift angle when shear capacity deteriorated to 80% of the maximum

The main findings are as follows,

- a. Test specimens of which average unit shear stress at the maximum shear strength,  $\bar{\tau}_u = Q_u / (t \cdot l_w)$ , is more than around 40kg/cm<sup>2</sup> reach the maximum capacity by shear failure at  $R=1/200 \sim 1/100$  and many of them show sudden deterioration of capacity after  $R=1/100$  (Fig. 5.4).
- b. On the contrary, specimens with  $\bar{\tau}_u \leq 20\text{kg/cm}^2$  fail in flexure and reach  $R_u=1/50 \sim 1/30$  without significant capacity deterioration (Fig. 5.4).
- c. As  $\bar{\sigma}_c$  increases,  $R_u$  tends to decrease. And when  $\bar{\sigma}_c$  is less than 0.7,  $R_u$  of many specimens reach more than 15/1000.
- d. Specimens with openings reach the maximum capacity at  $R=1/200 \sim 1/100$  and after that, their capacity deteriorate gradually because of progressive shear failure in short span beams. It is effective for making the deterioration mild to put column-type ribs at the corners of openings or to arrange diagonal reinforcing bars in the short beams.

## 6. Ending Remarks

Besides the above-mentioned researches, many experimental works on wall column-beam subassemblages, non-structural walls and bearing piles, several static and dynamic tests on scaled models of the whole or a part of solid static and dynamic tests on scaled models of the whole or a part of solid structure and many analytical studies related to nonlinear static or dynamic behavior of the structure were conducted concerning this structural system and a lot of findings were obtained.

This research project was carried out as a cooperative project by Architectural Institute of Japan, Building Research Institute, Urban and Housing development cooperation and Japan Constructor's society under the leadership of Prof. H. Umemura, Prof. H. Aoyama, Prof. K. OGURA, prof. Y. Sonobe and Y. Kanoh and a huge member of professors and researchers joined the project.

The authors express their deepest thanks to all of the persons concerned.

## 7. References

- [1] S. Fuchikawa, et al.: Effect of stirrup on Ductility of T-Beams (Part 1, 2), Proceedings of AIJ Annual Meeting, 1987
- [2] S. Kouda, et al.: Arrangement of Lateral Reinforcement in T-Beams and Ductility, Proceedings of AIJ Annual Meeting, 1987
- [3] T. Iwakura, et al.: Experimental Study on Full Scale T-Beam with Large-Diameter Deformed Bars, Proceedings of AIJ Annual Meeting, 1987
- [4] Building Center of Japan : Guidelines for Structural Design and Construction of Medium-to-High-rise R/C Building with Broad Columns, and their Commentary, 1987
- [5] H. Hiraishi, T. Kawashima, et al.: Experimental Study on Deformation Capacity of Wall Columns (Part

- 1, 2, 3), Proceedings of AIJ Annual Meeting, 1987
- [6] K. Murakami, H. Imai, : An Effect of Inner Confining Reinforcement and Shear Span Ratio, Proceedings of AIJ Annual Meeting, 1987
- [7] H. Tamura, K. Minami, et al.: Inelastic Behavior of Wall Columns under Shear Reversal with Varying Axial load (Part 1,2), Proceedings of AIJ Annual Meeting, 1987
- [8] H. Tomatsuri, H. Hiraishi et al.: Experimental Study on Deformation Capacity of Shear Walls After Flexural Yielding (Part 1, 2,3), Proceeding of AIJ Annual Meeting, 1987
- [9] H. Takagi, Y. Kanoh, et al.: Experimental Study on Effect of Interior Beams on Shear Strength of Shear Walls Failing in Shear (Part 1, 2), Proceedings of AIJ Annual Meeting, 1987
- [10] S. Mochizuki, Y. Nakajima, et al.: Restoring Force Characteristics of Shear Walls Failing in Shear (Part 1, 2), Proceedings of AIJ Annual Meeting, 1987
- [11] K. Iso, K. Matsuo et al.: Experimental Study on Strength and Deformation Behavior of "Fork-Shaped Shear Walls", Proceedings of AIJ Annual Meeting, 1987

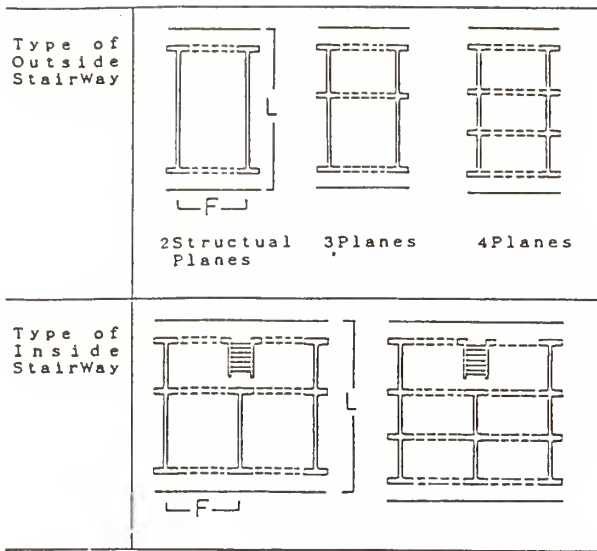


Fig. 2.1 Example of Typical Plan

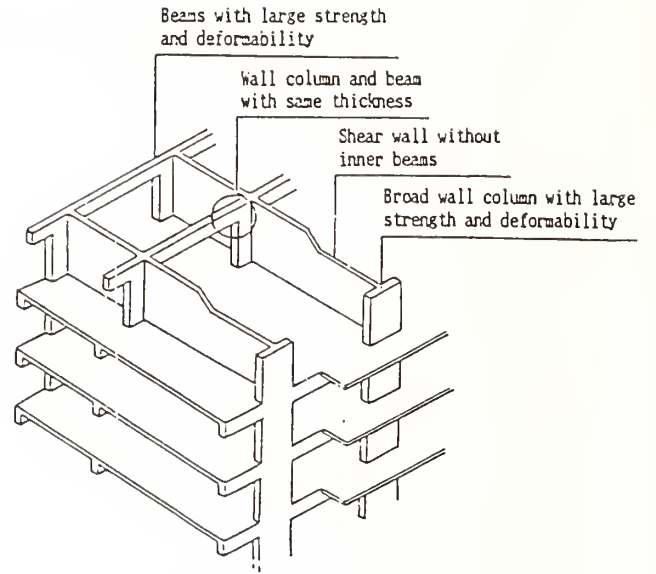


Fig. 2.2 Outline of Structural System of the R/C Frame Structure with Wall Column

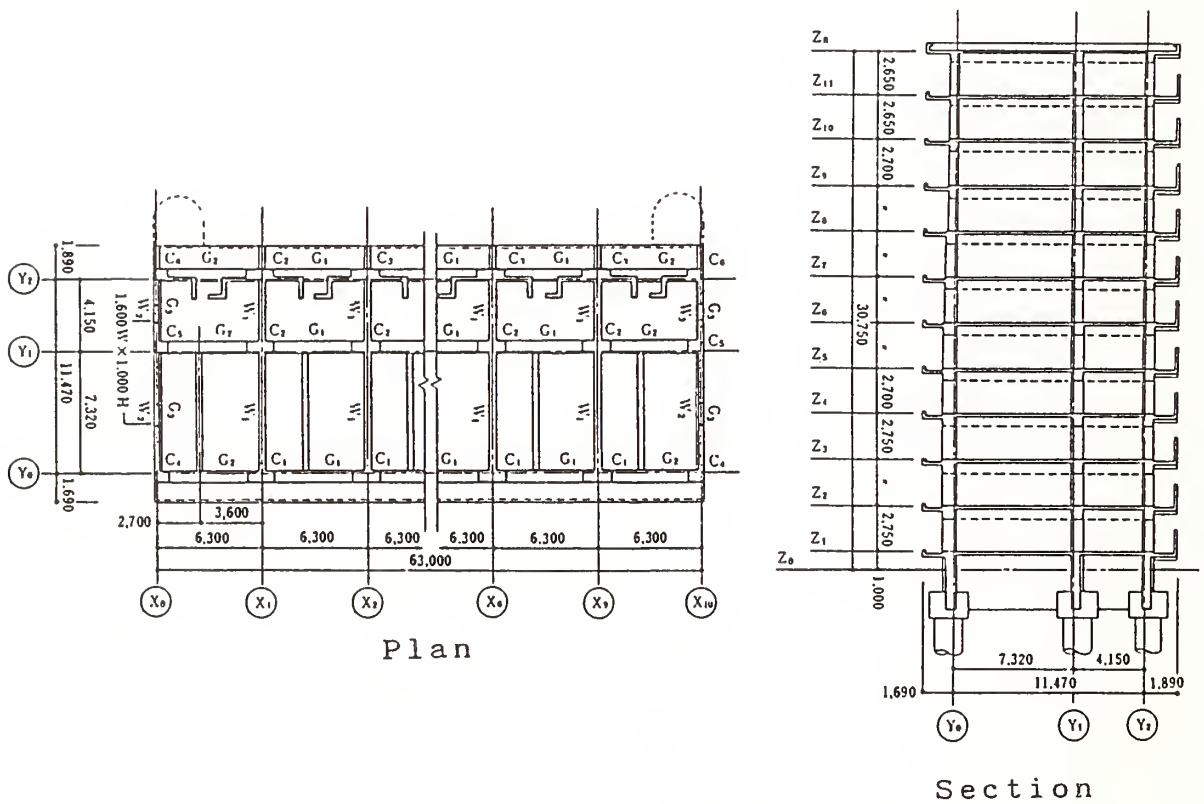


Fig. 2.3 Outline of a Building used for Analysis

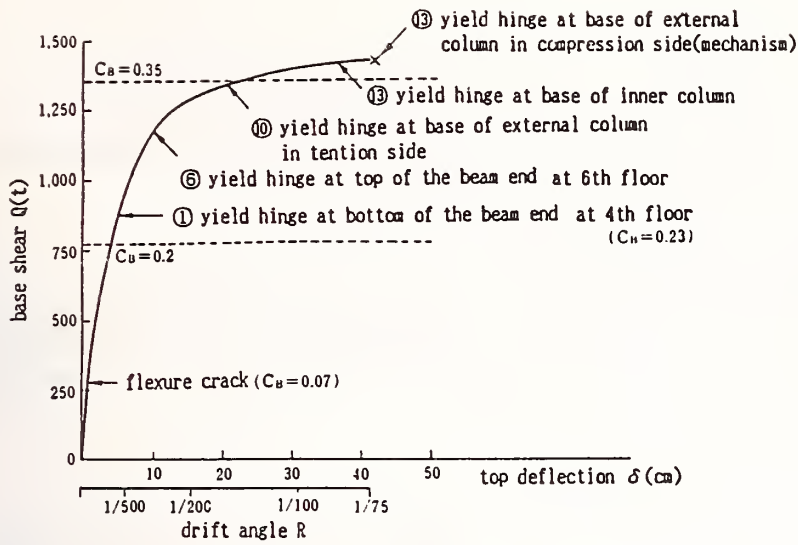
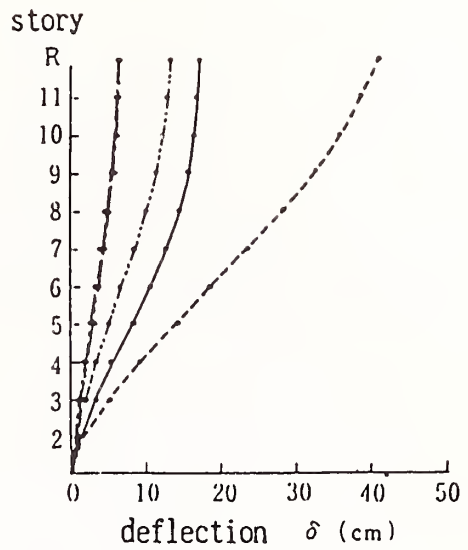
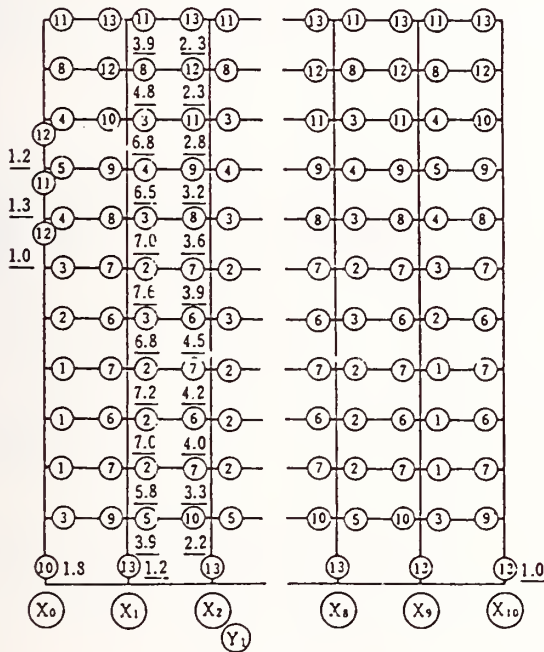


Fig. 2.4 Top Deflection-Base Shear Force Relationship



- - - - El Centro NS  
 - - - - Sendai TH030 NS  
 - - - - Hachinohe NS  
 - - - - Hachinohe EW  
 - - - - mechanism (nonlinear static analysis)

Fig. 2.6 Maximum Deflection at Each Floor



(n) : position and order of yield hinge  
 n : ductility factor at mechanism

Fig. 2.5 Occurrence Order of Yield Hinge

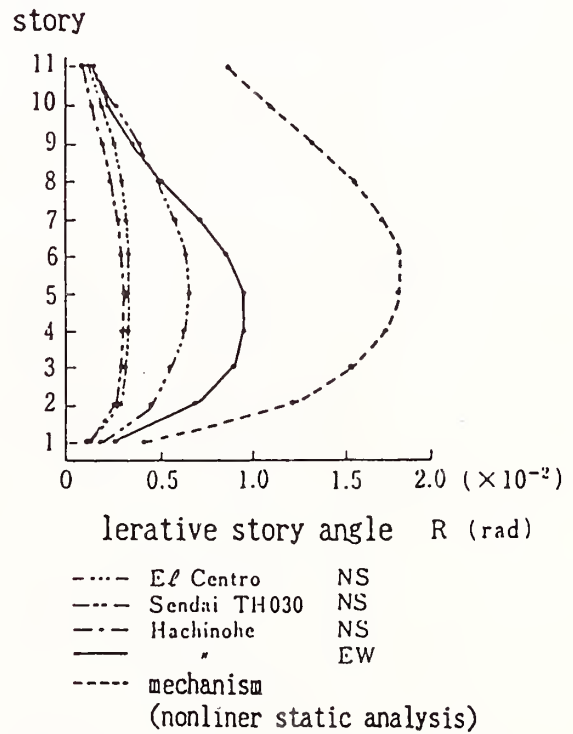


Fig. 2.7 Maximum Relative Drift Angle at Each Floor

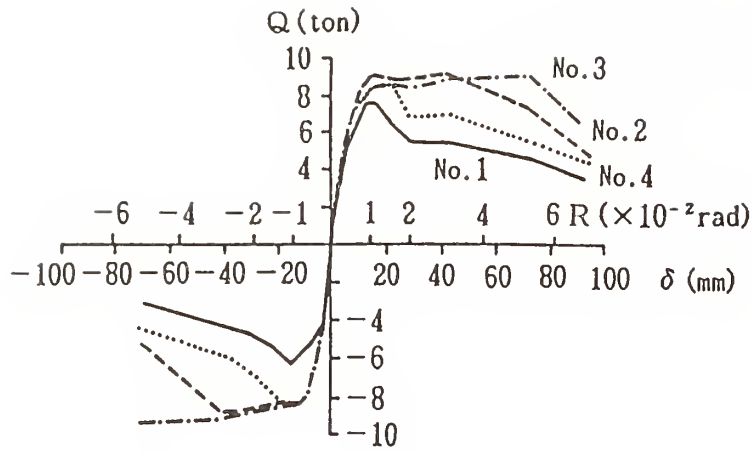
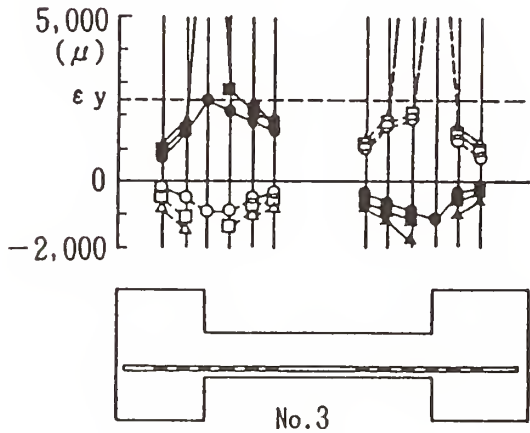
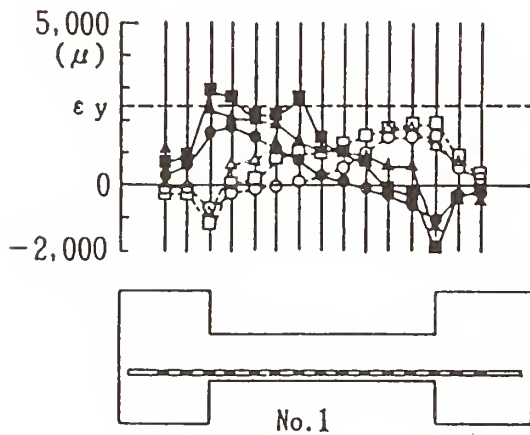


Fig. 3.1 Envelope of P- $\delta$  Curve



- R=1/200    ○---○ R=-1/200
- R=1/100    □---□ R=-1/100
- ▲—▲ R=1/67    △---△ R=-1/67

Fig. 3.3 Strain Distribution of Main Bars

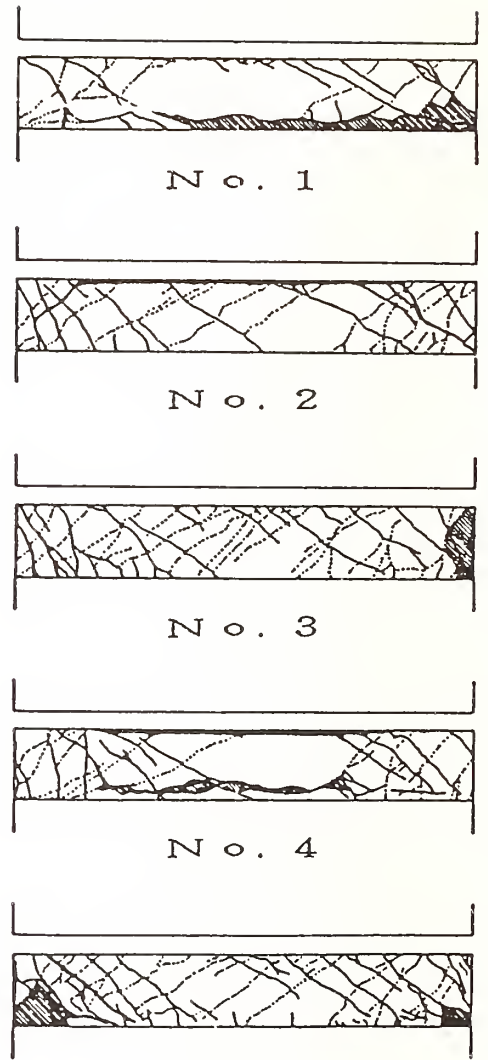


Fig. 3.2 Final Damage

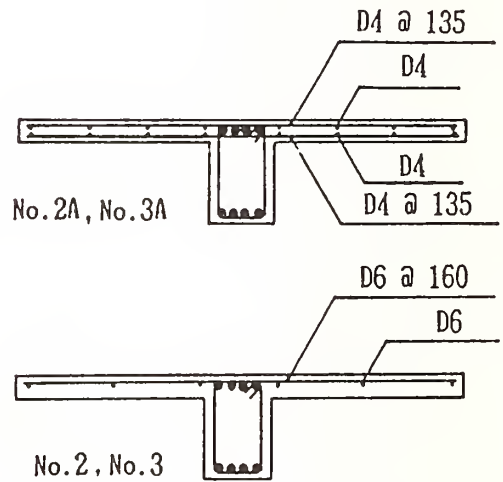


Fig. 3.4 Reinforcement Details

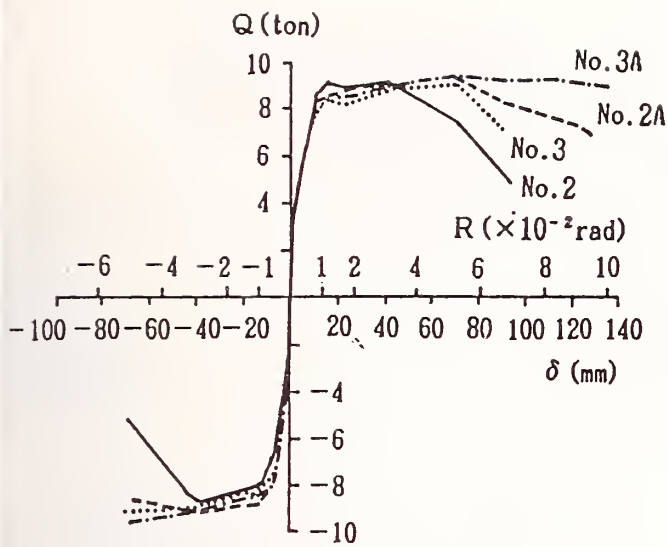


Fig. 3.5 Comparison of Envelopes

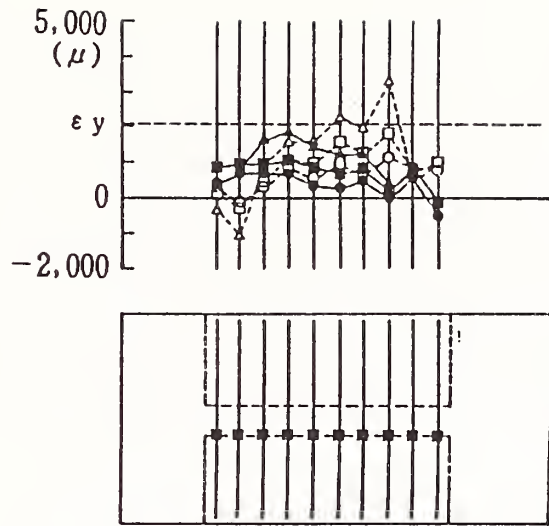


Fig. 3.6 Strain Distribution of Bottom Bars in Transverse Slab (No. 2A)

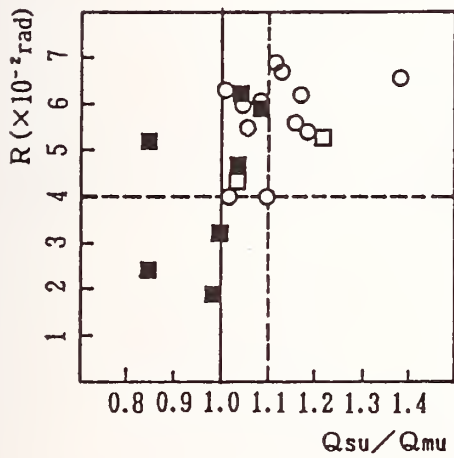
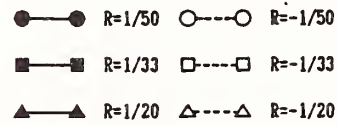


Fig. 3.7 Shear Strength-Ratio v. s. Deformation Capacity

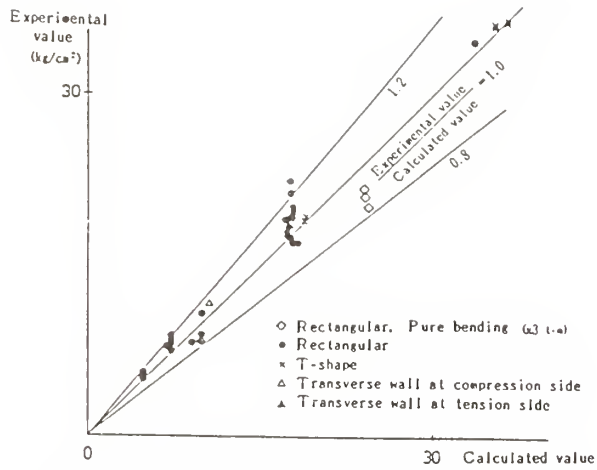


Fig.4.1 Maximum flexural strength  
 $(\tau_{Mu} = M_u / (bdh))$

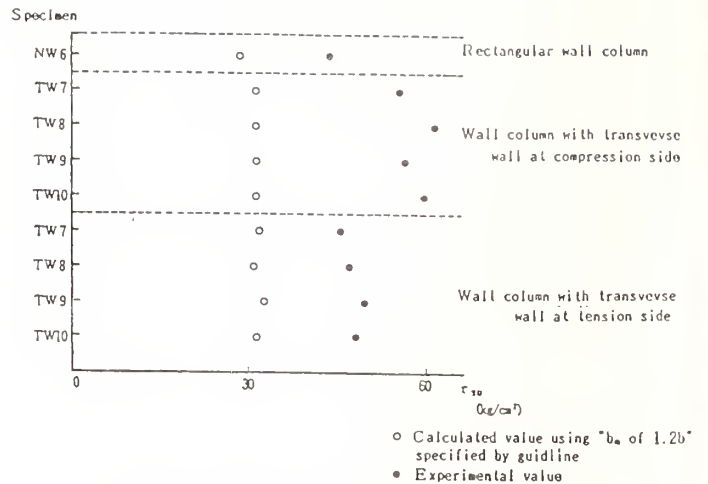


Fig.4.2 Maximum shear strength  
 $(\tau_{su} = Q_{su} / (bD))$

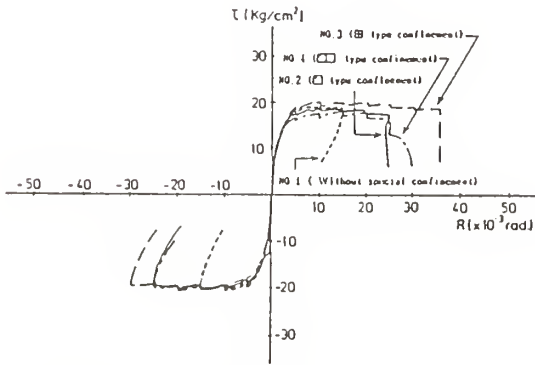


Fig.4.3  $\tau$  versus R relations  
 (Effect of confinement at edge zone)

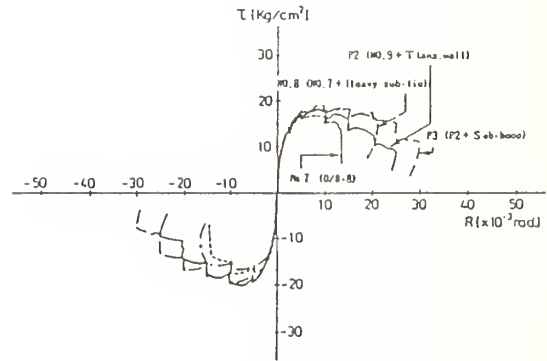


Fig.4.4  $\tau$  versus R relations  
 (Effect of tie bars and sub tie bars)

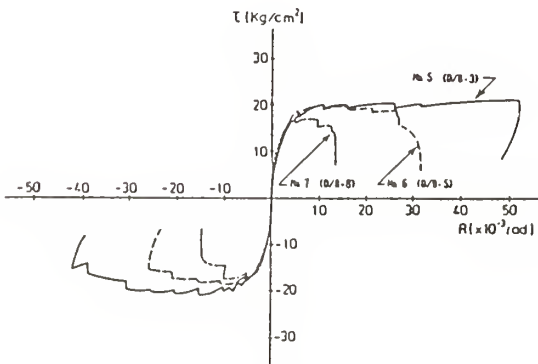


Fig.4.5  $\tau$  versus R relations  
 (Effect of ratio of depth to width)

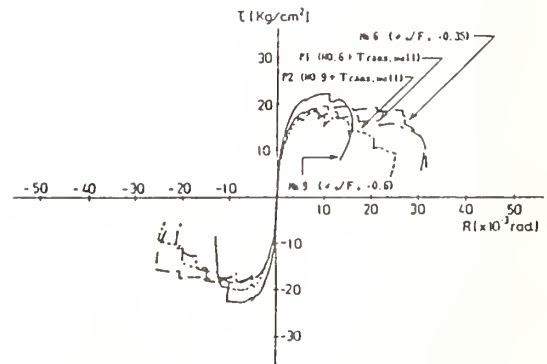


Fig.4.6  $\tau$  versus R relations  
 (Effect of transverse wall  
 and axial stress level)

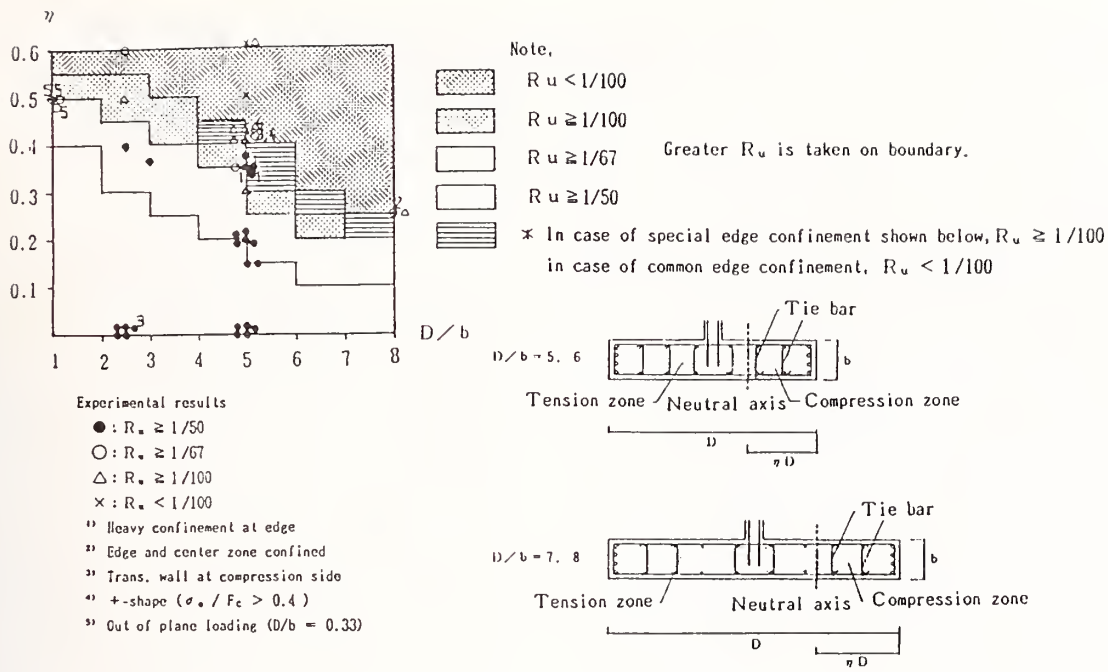


Fig.4.7 Deformation capacity of wall columns

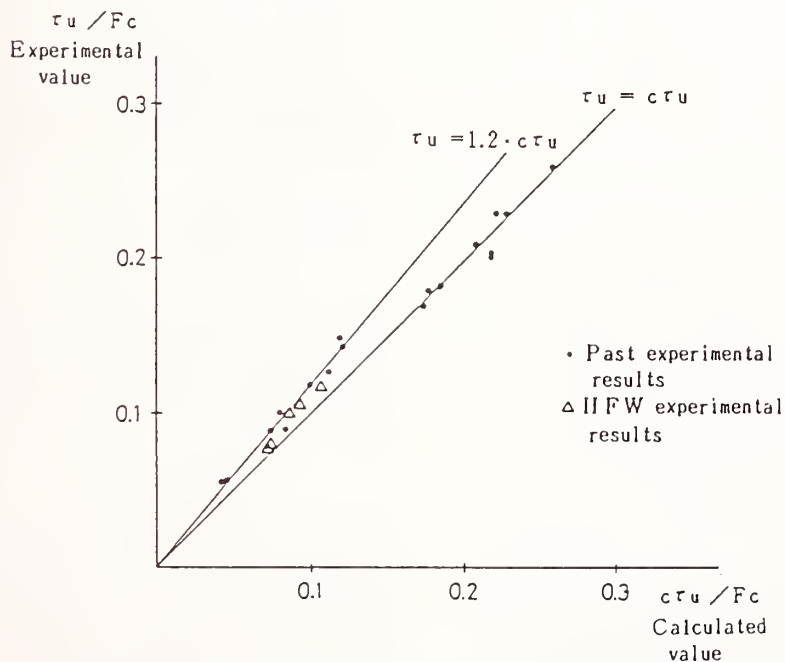


Fig.5.1 Maximum flexural strength

# Vibration Studies of Richard B. Russell Concrete Gravity Dam

by

Dr. Robert Hall, Messrs. Tommy Bevins, and Stephen Wright

## ABSTRACT

The Richard B. Russell Concrete Gravity Dam was subjected to a forced vibration test before and after reservoir impoundment. The results of these prototype vibration tests were compared with linear-elastic three-dimensional dynamic finite-element (FE) analyses. This comparison provides a basis for assessing the accuracy of linear-elastic FE models for predicting dynamic response of concrete gravity dams. During the vibration tests, relative joint motion arrays were positioned at three locations for the forced vibration before reservoir impoundment and at two locations after the reservoir impoundment. The tests were used to determine the natural frequencies, damping ratios, mode shapes, and relative joint motions. A comparison of the measured hydrodynamic pressures with the theoretical values was based on an approximate method by Fenves and Chopra. Calculation and tests illustrated that the hydrodynamic effects did cause a decrease in the natural frequencies due to the added mass of the reservoir. The vibration tests revealed relative motion between the monoliths which resulted in some nonlinear structural response. The pressure distribution predicted by Chopra's simplified procedure was not completely verified.

**KEYWORDS:** Damping Ratios; Finite Element Analysis; Forced-Vibration Test; Frequencies; Mode Shapes.

## 1. INTRODUCTION

The Richard B. Russell Dam, built by the U.S. Army Corps of Engineers (CE) is located approximately 170 miles from the mouth of the Savannah River between Georgia and South Carolina. The crest of the concrete gravity dam is 1,884 feet in length. The concrete gravity section of the dam consists of a spillway section, a nonoverflow section, and an intake section. Figure 1 shows the 13 nonoverflow, 8 intake, and 11 spillway monoliths. The tallest of those is approximately 200 feet high at an elevation of 495 feet.

Forced-vibration tests were made on the dam before and after reservoir impoundment to determine the natural frequencies, damping ratios, mode shapes, and relative joint motions (1) (2). The first series of low-level, forced-vibration tests was conducted

in January and February 1982, before reservoir impoundment, with a mean headwater elevation of 343 feet; and a second series of tests were performed in June and July 1984, after reservoir impoundment, with a mean headwater elevation of 470 feet. This provides an experimental measure of the hydrodynamic interaction by comparing the dynamic properties from the two tests.

The dynamic properties of the dam will also be used to provide a record of the dam's structural condition as built. In the event that an earthquake should damage the dam in the future, the test data will be useful in determining the significance of the damage.

## 2. EXPERIMENTAL EQUIPMENT

The dam was excited by a 17,000-lb inertial mass welded to a steel plate that was epoxied to the mass concrete of the dam. The force input to the dam was computed as the product of the measured acceleration and the 17,000-lb mass. Figure 2 is a typical force spectrum showing maximum force input as a function of frequency of vibration.

Accelerometers were used to measure the horizontal accelerations of the dam. Most of these accelerometers have a sensitivity of approximately 5 V/g. A few of the close-in measurements were taken using 0.25-V/g accelerometers. The accelerometers have a frequency response range from 0 to 500 Hz. Analog signals were recorded on magnetic tape and later digitized using a structural dynamic analyzer.

Piezoelectric pressure transducers were used to measure the hydrodynamic pressures during the vibration tests of monolith 7. The transducers were mounted in special waterproof canisters bolted to the upstream face by divers.

## 3. FINITE-ELEMENT PROGRAM

A structural analysis program for the static and dynamic response of linear systems was used to calculate the natural frequencies and mode shapes of the dam (3). The program is coded in FORTRAN 66 and was run on the Honeywell DPS 8 mainframe computer at the U.S. Army Engineer Waterways Experiment Station.

The structural mode shapes and frequencies can be obtained by two distinct algorithms:

a. The determinant search method is used for small problems in which the total stiffness matrix can be kept in the core of the computer.

b. The subspace iteration method is used for large problems in which only portions of the stiffness matrix can be retained in the core of the computer.

A subspace iteration method was used to solve for the undamped natural frequencies and mode shapes presented in this report.

### 3.1 Parameter Studies

The grid for the FE model (Figure 3) was developed by conducting parameter studies of isolated nonoverflow, spillway, and intake monoliths. Modal analyses were used to obtain appropriate FE grid sizes for each of the monoliths. A compatible grid was found for all of the monoliths, thus making possible the generation of the modal and element data with the computer (4). Favorable results were obtained when modal analyses of each monolith using uniform grids were compared with analyses using the grid for the entire three-dimensional FE model. Figures 4 through 6 show typical sections of the monoliths and the resulting three-dimensional grids of each monolith.

Figure 5 shows the penstock tube opening in the intake monolith modeled as solid or "smeared-hole" elements with 29 percent less stiffness and density than the mass concrete. Modal analyses showed good agreement between a finer FE grid that included the penstock opening and the grid using solid elements.

Studies were also performed to obtain a suitable Winkler spring representation of the foundation. Comparisons of two-dimensional and three-dimensional FE dynamic analyses on the nonoverflow section using Winkler springs with analyses using an FE foundation grid in order to determine a correct Winkler spring model of the foundation.

The concrete properties used in the FE analyses were taken from previous measurements on 6- 12-inch concrete cylinders (5). Dynamic modulus of elasticity values used were  $5.1 \times 10^6$  psi for exterior mass concrete and  $4.26 \times 10^6$  psi for interior mass concrete. From previous foundation tests the dynamic elastic modulus of the foundation used to compute the spring constant was  $6.05 \times 10^6$  psi. Using elastic theory, the average horizontal and vertical spring

constant was  $4 \times 10^{10}$  lb/ft in the flexible base model (6).

### 3.2 Element Types

Four element types were used to model the dam. Variable-number-nodes (8 to 21 nodes) three-dimensional solid elements were used to model the mass concrete of the nonoverflow, intake, and spillway monoliths (3). Plate elements were used to model the concrete spillway piers, the concrete training walls at spillway monoliths 16 and 26, and the concrete deck of the spillway bridge. Beam elements were used to model the steel girders of the spillway bridge, and Winkler springs were used along the base of the model in the flexible base analysis.

### 3.3 Boundary Conditions

By definition, only the X, Y, and Z translations were defined on the three-dimensional thick-shell elements. All degrees of freedom were deleted along the base of the model for the fixed base analyses. For the flexible base analyses, the longitudinal (Y) translations and all rotations were fixed along the base of the model. Except at the dam abutment interface, horizontal and vertical springs were placed at all nodes on the base in the X and Z directions.

In order to model the restraint due to the abutments, nodes along the two end sections (monoliths 1 and 32) had all degrees of freedom deleted (i.e., nodes fixed). However, a few of the nodes had translational degrees of freedom defined on the Georgia side for the model of the dam without reservoir. This abutment was not complete at the time of the first vibration test.

For the model without reservoir, 5,127 and 5,609 degrees of freedom were used for the fixed base and flexible base FE models, respectively. For the model with reservoir, 5,100 and 5,582 degrees of freedom were used for the fixed base and flexible base FE models, respectively.

### 3.4 Modeling Of Added Mass

Concentrated masses were added at nodes thought to be in contact with the reservoir to model the reservoir mass and the tainter gates. A constant 49.6-ft-wide mass of reservoir was applied to the model with reservoir. Studies (5) showed that this constant width of reservoir added the same amount of mass as a modified Westergaard (7) analysis. A typical nonoverflow monolith for the dam was analyzed with a constant 49.6-ft-wide mass of reservoir. The fundamental

frequency compared well with the result obtained from an approximate procedure by Chopra (8). The mass of the reservoir acting on the tainter gates and the mass of the gate was applied at the trunnion locations on the spillway piers.

#### 4. COMPARISON OF FINITE ELEMENT MODEL TO PROTOTYPE TEST RESULTS

##### 4.1 Dam Without Reservoir

Comparisons of the dam crest mode shapes are shown in Figures 7 through 11. Note that the mode numbers correspond to bending modes of the dam crest. The fourth mode was not measured experimentally, but was determined analytically. Table 1 summarizes the results of these analytical and experimental mode shape comparisons. Based upon the results of the Modal Assurance Criteion (MAC) values (9), the correlation between analytical and experimental mode shapes was favorable. Overall, the model with a fixed base had slightly better mode shape correlation than did the model with a flexible base, possibly because the base of the dam was more rigid than modeled by the FE flexible base analysis. For a qualitative comparison, the mode shapes all appear to have the largest amplitude in the same general location on the crest of the dam. The MAC does indicate quantitatively how good the comparison is among modes.

As shown in Table 2, the frequencies estimated by the FE models were higher than frequencies measured experimentally (16 to 30 percent higher for the FE fixed base model, and 9 to 18 percent higher for the flexible base model). This is reasonable since the FE models are approximations of the dam using a discrete number of degrees of freedom. The FE model in this case is stiffer than the actual dam. The flexible base model estimated frequencies closer to the experimentally measured frequencies than did the fixed base model because foundation interaction decreases the frequency (10).

Comparisons of the experimental mode shapes in cross section with results from the FE model with fixed foundation were also conducted. The frequencies of the cross-sectional modes correspond with the crest modal frequencies. Table 3 summarizes the results (5). The correlation between most mode shapes was favorable, and the governing mode shape in cross section resembled the fundamental mode shape of a cantilever beam. However, at the lower frequencies, the mode shapes for spillway monolith 22 exhibited discontinuities at the bottom of the pier. This is probably because the force input was not large enough to completely

excite the entire monolith at the lower frequencies. The spillway monoliths are the stiffest part of the dam. From a three-dimensional dynamic FE analyses of an isolated spillway monolith, the fundamental frequency was 11.3 Hz. This is higher than the first four experimentally measured natural frequencies of the dam without reservoir (5.9 Hz to 8.2 Hz).

##### 4.2 Dam With Reservoir

Comparisons of the dam crest mode shapes are shown in Figures 12 through 16. Note that the mode numbers correspond to bending modes of the dam crest. Table 4 summarizes the results of these comparisons. (The response at monolith 22 was not used in computing the MAC because excessive local responses were recorded in test 2 at this monolith.) Crest mode shape correlation between experiment and analysis was not as favorable as with the dam without reservoir. The fixed model had higher MAC values than the flexible base model for the first three modes, possibly because the prototype foundation stiffness was greater than modeled in the FE flexible base analyses.

Various factors may have caused the low correlation between experimental and analytical mode shapes. Errors in the experimental mode shapes may be due partly to a force input that was not large enough to completely excite the entire dam at the lower frequencies. Also, a high degree of modal coupling (closely spaced resonance frequencies) existed at a higher frequencies.

Hydrodynamic effects did cause a decrease in the natural frequencies from the first test series. The frequencies and damping values from both test series are listed in Tables 2 and 5, respectively. This decrease in frequencies was expected to occur. The percentage change in frequencies was largest for the first mode and less for the higher modes. With the exception of mode 5, the damping estimates were increased by 0.2 to 0.5 percent of critical damping.

A finite-element analyses (5) indicated that the change in frequencies increased as the frequency increased (Table 2). The disagreement between the analytical and experimental effects is due to using the added mass concept (7) to account for hydrodynamic effects. Westergaard's method assumes that water is incompressible. This assumption is valid when the forcing frequency is less than the fundamental natural frequency of the dam/reservoir system, but for frequencies higher than this, the method overestimates the hydrodynamic effects (11). Also, when the driving

frequency of the forced-vibration test exceeds the fundamental frequency of the dam, Westergaard's assumption is no longer valid.

Another influence of the frequencies and mode shapes between the two test series is a change in the friction forces between monoliths. The first series of tests was conducted in the winter, and the second series of tests was conducted during the summer.

The relative motions were monitored for monoliths 14, 15, and 16. The measurements were made when the exciter was at drive point 16, which would give the most relative motion. The transfer functions on each side of the joint were measured. If there is no relative motion, the transfer functions on each side of a joint will be identical.

For the relative motion measurements at joint 14-15, transfer and coherence functions are shown in Figures 17 and 18, respectively. The transfer functions have the same shape (i.e., the peaks occur at the same frequencies), but monolith 15 undergoes a larger magnitude of response. The phase angles of the two measurements are the same. This combination of magnitude and phase information indicates that the monoliths are moving together (in phase), but monolith 15 is experiencing a large amplitude of motion.

Similar to joint 14-15, joint 15-16 demonstrates the same type of behavior. Here, monolith 16 undergoes the largest magnitude of response. The transfer and coherence functions for joint 15-16 are shown in Figures 19 and 20, respectively. The differences in the response magnitudes increase as the frequency increases. The increasing amount of relative motion is caused by a change in monolith section stiffnesses. Monolith 15 is an intake section, and monolith 16 is a transition section. As pointed out before in the discussion about the mode shapes, each section tends to act separately at the higher frequencies.

From these joint measurements, even for the low level of forces input to the structure, there is relative motion between monoliths. Not only does the relative motion occur, but there is a decrease in the energy transferred to an adjacent monolith. This is demonstrated by the fact that the monoliths closest to the drive point have the highest responses. These data demonstrate that the frictional forces at the joints will produce nonlinear behavior in the dam.

Another interesting aspect of the joint

measurements is that the centerline of the monolith has higher amplitude motions than the edges. This is shown in Figure 21 for monolith 15. The accelerometer at the center of the monolith has a larger amplitude response than the edges at monoliths 14 and 16, and the phase at the edges of the monolith lags behind the center gage. This apparent amplification at the center of the monolith is another indication of relative joint motions. The motion of a monolith is a combination of the forced response due to the force being transferred across the joint and some independent motion of the monolith with the restraints at the joints imposing a drag on the motion at the edges.

A comparison of the measured hydrodynamic pressures with the theoretical values based on an approximate method by Fenves and Chopra (12) is shown in Figure 22. The extremely large response at elevation 430 ft (normalized height = 0.65) seemed to be in error and is not included in the comparison. This method computes pressures for the first mode of vibration using the equation:

$$f_{\ell}(y) = \frac{\tilde{L}}{M} \frac{S_a(\tilde{T}_1, \xi)}{g} [w_s(y)\phi(y) + gp(y, \tilde{T})]$$

where

$\tilde{L}$  = generalized earthquake force coefficient

$M$  = generalized mass coefficient

$S_a(\tilde{T}, \xi)$  = pseudo acceleration ordinate of EQ Spectrum

$\tilde{T}_1$  = period of dam/reservoir system

$\xi$  = damping of dam/reservoir system

$g$  = acceleration due to gravity

$w_s(y)$  = weight per unit height

$\phi(y)$  = normalized fundamental mode shape

$p(y, \tilde{T})$  = hydrodynamic pressure function

For these computations, only the second term inside of the brackets that involves  $p$  contributes to the pressures. This term is the hydrodynamic pressure for the dam vibrating in its first mode shape.

Therefore, the pressure equation is now:

$$f_{\ell}(y) = \frac{\tilde{L}}{M} \frac{S_a(\tilde{T}_1, \xi)}{g} [gp(y, \tilde{T})]$$

The term,  $w_s(y)\phi(y)$ , represents equivalent forces to account for the inertial effects of the dam. The term  $S_a$  is the maximum response of the monolith at the fundamental frequency of the dam (5.3 Hz). The two curves shown are for concrete with  $E_c$  of  $2.5 \times 10^6$  and  $4.0 \times 10^6$  psi. This establishes a band within which the experimental pressures should fall since the monolith was constructed using different concretes with a modulus between the two values used in the computations. The ratio  $L/M$  used in the computations was 3.5. This value was computed following the procedure presented by Fenves and Chopra (12). The ratio falls between the approximate value for dams with empty reservoirs (3.0) and the approximate value for dams with the reservoir impounded (4.0).

Although the experimental pressures were low, 0.002 psi, they are of the same magnitude with hydrodynamic pressures predicted by theory and with pressures measured during vibration testing of the Pine Flat Dam (13). The maximum pressures at Pine Flat were larger, 0.005 psi, but this is expected since Pine Flat is a taller and more flexible dam.

## 5. CONCLUSIONS

By visual inspection of the mode shapes with and without reservoir, hydrodynamic interaction changed the mode shapes of the dam, with the largest differences occurring at the ends of the dam. The dam's midsection had similar responses with and without reservoir interaction; however, slight shifts in the maximum response points towards the ends of the dam indicate that hydrodynamic effects added mass to the dam's midsection. Various factors could have caused fairly low correlations between experimental mode shapes for the tests with and without reservoir. The force input was not large enough to completely excite the entire structure at the lower frequencies, causing scatter in estimates of the mode shapes. Ideally, two or more force inputs would be better. Also, a high degree of modal coupling existed at the higher frequencies, and the friction forces between monoliths may have been different because the tests were conducted during different seasons.

The experimental natural frequencies were reduced by the hydrodynamic effects, with the percent change in the first mode the largest (10.1 percent). With the exception of the fifth mode, the reservoir impoundment had little effects on the damping estimates.

The hydrodynamic pressures measured in the second test with reservoir were close to the

predicted values for the fundamental frequency (except at elevation 430), and the pressure distribution was similar to distributions measured at the Pine Flat Dam (13). The theoretical hydrodynamic pressures were based on a two-dimensional response of an isolated nonoverflow monolith (monolith 7). The fundamental mode shape of a cantilever beam was used to compute the theoretical pressure distribution. Because the experimental and analytical cross-sectional mode shapes of the entire dam resembled the fundamental mode shape of a cantilever beam, the use of a two-dimensional model was valid for predicting the pressure distribution on this nonoverflow monolith. Further pressure measurements and analyses would be needed to confirm if the theoretical pressure distribution is valid for the other parts of the dam.

Measurements from both tests at the relative joint motion arrays indicated relative motions between monoliths. The nonlinear behavior of the dam is attributed primarily to the monoliths' joint behavior.

Despite a few experimental errors, no gross anomalies existed, and the dynamic properties determined are reasonable. It can be concluded that the dam appears to be structurally sound as built.

Three-dimensional linear FE analyses have been compared with previous experimental estimates of the modal parameters of a concrete gravity dam. Using available dynamic material properties of the dam concrete and the foundation, a three-dimensional FE modal was successfully developed to estimate the linear-elastic modal properties of the dam. The fourth mode shape was not measured experimentally for the dam without reservoir but was computed by the three-dimensional FE analyses.

The MAC was useful for evaluating the correlation between the experimental and the FE mode shapes. Favorable correlations of the crest mode shapes were computed for the dam without reservoir, indicating that a reasonable three-dimensional FE model was developed for computing the first three natural modes of vibrations. Various factors may have caused a lower correlation between the experimental and analytical crest mode shapes for the dam with reservoir. Low force input at lower frequencies caused poorer estimates in experimental mode shapes at certain locations, and a high degree of modal coupling existed at the higher frequencies. The effects of the soil-dam interaction at the abutments and the effects of reservoir may not have been modeled adequately. Also, nonlinearities due to joint slippage were not

modeled. The correlation between most cross-sectional shapes was favorable, and the governing mode shape in cross section resembled the fundamental mode shape of a cantilever beam.

It has been shown that a proposed design cross-sectional mode shape by Chopra (1978) is sufficiently accurate for design purposes. Chopra presents a simplified analysis procedure for computing stresses due to earthquake ground motion in the horizontal direction. The simplified procedure uses the fundamental mode of vibration of a two-dimensional model of the dam. The design mode shape resembles the fundamental mode shape of a cantilever beam. As discussed by Chopra, the response of concrete gravity dams to earthquake ground motion is primarily due to the fundamental mode of vibration. The experimental cross-sectional mode shapes of the entire dam resembled Chopra's design mode shape (i.e., the fundamental mode shape of a cantilever beam). Further studies would have to be performed to determine the validity of Chopra's method versus the analysis of the entire dam. These further studies would compare the stresses from the analysis of the entire dam with the stresses from Chopra's simplified procedure.

Analyses of isolated nonoverflow, intake, and spillway monoliths were useful because they showed the relative stiffness of the parts of the dam. The calculated fundamental frequencies of the isolated monoliths indicated that the intake sections were the most flexible part of the dam and that the spillway monoliths were the stiffest part of the dam. Furthermore, the calculated fundamental frequency (7.1 Hz) of the entire dam without reservoir for a fixed foundation was less than the fundamental frequencies of the nonoverflow and spillway monoliths (9.8 Hz and 11.3 Hz, respectively) but slightly more than the fundamental frequency of the intake monolith (6.9 Hz). It can be concluded from these analyses that the intake sections increased the flexibility of the entire dam.

The three-dimensional analyses estimated frequencies up to 30 percent higher than those measured experimentally. This is reasonable since the FE models are an approximation of the dam using a discrete number of degrees of freedom. Due to foundation interaction, the FE mode with flexible foundation predicted natural frequencies closer to the experimentally measured values than did the FE model with rigid foundation.

In general, it appears that three-dimensional linear FE analyses can give a good estimate

of the natural frequencies of concrete gravity dams with or without reservoir effects. The FE analyses can adequately estimate the bending mode shapes of concrete gravity dams without reservoir impoundment. These analyses can adequately estimate the bending mode shapes of concrete gravity dams with reservoir if the reservoir effects are appropriately modeled.

## 6. ACKNOWLEDGEMENTS

The results presented herein, unless otherwise noted, were obtained from research conducted under the Structural Engineering Research Program of the US Army Engineer Waterways Experiment Station, Vicksburg, Mississippi. Permission was granted by the Office, Chief, of Engineers to publish this information.

## 7. REFERENCES

1. Chiarito, Vincent P., and Mlakar, Paul F. 1983. "Vibration Test of Richard B. Russell Concrete Dam Before Reservoir Impoundment," Technical Report SL-83-2, U.S. Army Engineer Waterways Experiment Station, Vicksburg, MS.
2. Bevins, Tommy L., Chiarito, Vincent P., and Hall, Robert L. "Vibration Test of Richard B. Russell Concrete Dam After Reservoir Impoundment," Technical Report SL-87- , in preparation, U.S. Army Engineer Waterways Experiment Station, Vicksburg, MS.
3. Bathe, K. J., Wilson, E. L., and Peterson, F. E. 1973. "SAPIV: A Structural Analysis Program for Static and Dynamic Response of Linear Systems," University of California, Earthquake Engineering Research Center, Richmond, CA.
4. Chiarito, Vincent P. 1985 (Jan). "Linear Finite Element Comparison with Experimental Modal Analysis for a Concrete Gravity Dam," Proceedings of the Third International Modal Analysis Conference, Vol 1, pp 59-65.
5. Wright, R. S., Chiarito, V. P., and Hall, R. L., 1988 (Feb). "Summary of the Richard B. Russell Concrete Dam Vibration Study," Technical Report SL-88-10, U.S. Army Engineer Waterways Experiment Station, Vicksburg, MS.
6. Timoshenko, S. P., and Goodier, J. N. 1970. Theory of Elasticity, 3d ed., McGraw-Hill, New York.
7. Westergaard, H. M. 1933. "Water Pressure on Dams During Earthquakes," Transactions, American Society of Civil Engineers, Vol 98, pp 418-433.

8. Chopra, Anil K. 1978. "Earthquake Resistant Design of Concrete Gravity Dams," Journal of the Structural Division, American Society of Civil Engineers, Vol 104, No. ST6, pp 953-971.

9. Allemang, R. J., and Brown, D. L. 1982 (Nov). "A Correlation Coefficient for Modal Vector Analysis," Proceedings of the 1st International Modal Analysis Conference, pp 110-116.

10. Norman, C. Dean, and Stone, Harry E. 1979. "Earthquake Analysis of the Gravity Dam Monoliths of the Richard B. Russell Dam," Technical Report SL-79-8, U.S. Army Engineer Waterways Experiment Station, Vicksburg, MS.

11. Chakrabarti, P., and Chopra, Anil K. 1974 (June). "Hydrodynamic Effects in Earthquake Response of Gravity Dams," Journal of the Structures Division, American Society of Civil Engineers, Vol 100, No. ST6, pp 1211-1224.

12. Fenves, Gregory, and Chopra, Anil K. 1986. "Simplified Analysis for Earthquake Resistant Design of Concrete Gravity Dams," Report No. EERC-85/10, University of California, Berkeley, CA.

13. Rea, D., Liaw, C. Y., and Chopra, Anil K. 1972. "Dynamic Properties of Pine Flat Dam," Report No. EERC-72/7, University of California, Berkeley, CA.

Table 1. Crest Mode Shape Comparisons - Dam without Reservoir.

Crest Mode No.	Prototype Vibration Test Frequency, Hz	Three-Dimensional Finite Element Analyses			
		Fixed Base Frequency, Hz	MAC*	Flexible Base Frequency, Hz	MAC*
1	5.9	7.1	0.73	6.6	0.74
2	6.8	7.9	0.63	7.4	0.63
3	7.6	9.3	0.64	8.7	0.61
4	Not measured	10.4	--	9.6	--
5	8.2	10.7	0.41	10.0	0.13

\* Modal Assurance Criterion.

Table 2. Summary of Experimental and Analytical Frequencies, Hz.

Crest Mode No.	Prototype Vibration Test Without Reservoir	Finite Element Analysis Without Reservoir		Prototype Vibration Test With Reservoir	Finite Element Analysis With Reservoir	
		Fixed Base	Flexible Base		Fixed Base	Flexible Base
1	5.9	7.1	6.6	5.3	6.2	5.7
2	6.8	7.9	7.4	6.2	6.8	6.4
3	7.6	9.3	8.7	7.3	7.8	7.3
4	Not measured	10.4	9.6	7.5	8.2	7.6
5	8.2	10.7	10.0	8.1	8.7	8.0

Table 3. Cross-Section Comparisons without Reservoir.

Crest Mode No.	Experimental Frequency, Hz	Finite Element Fixed Base Frequency, Hz	Modal Monolith 7	Assurance Monolith 16	Criterion Monolith 22
1	5.9	7.1	0.73	0.37	0.00
2	6.8	7.9	0.40	0.74	0.00
3	7.6	9.3	0.73	0.94	0.47
4	Not measured	10.4	--	--	--
5	8.2	10.7	0.72	0.79	0.84

Table 4. Crest Mode Shape Comparisons - Dam with Reservoir.

Crest Mode No.	Prototype Vibration Test Frequency, Hz	Three-Dimensional Finite Element Analyses			
		Fixed Base Frequency, Hz	MAC*	Flexible Base Frequency, Hz	MAC*
1	5.3	6.2	0.20	5.7	0.19
2	6.2	6.8	0.44	6.4	0.38
3	7.3	7.8	0.63	7.3	0.51
4	7.5	8.2	0.15	7.6	0.36
5	8.1	8.7	0.09	8.0	0.33

\* Modal Assurance Criterion.

Table 5. Experimental Damping Estimates.

Crest Mode No.	Damping Before Impoundment percent	Damping After Impoundment percent
1	4.29	4.41
2	2.07	2.76
3	3.11	3.69
4	Not measured	1.52
5	5.16	2.90

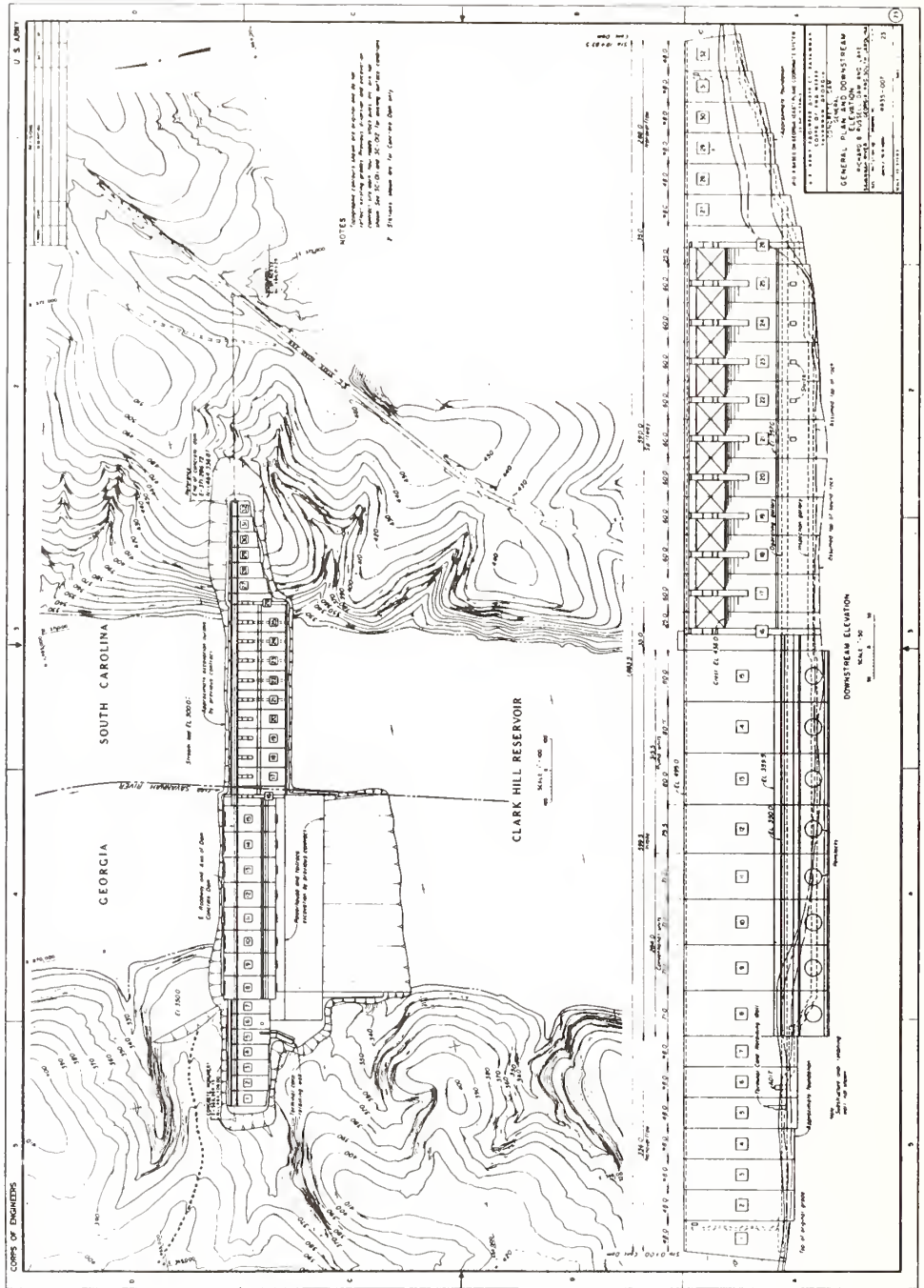


Figure 1. Plan and Elevation Views of Richard B. Russell Dam.

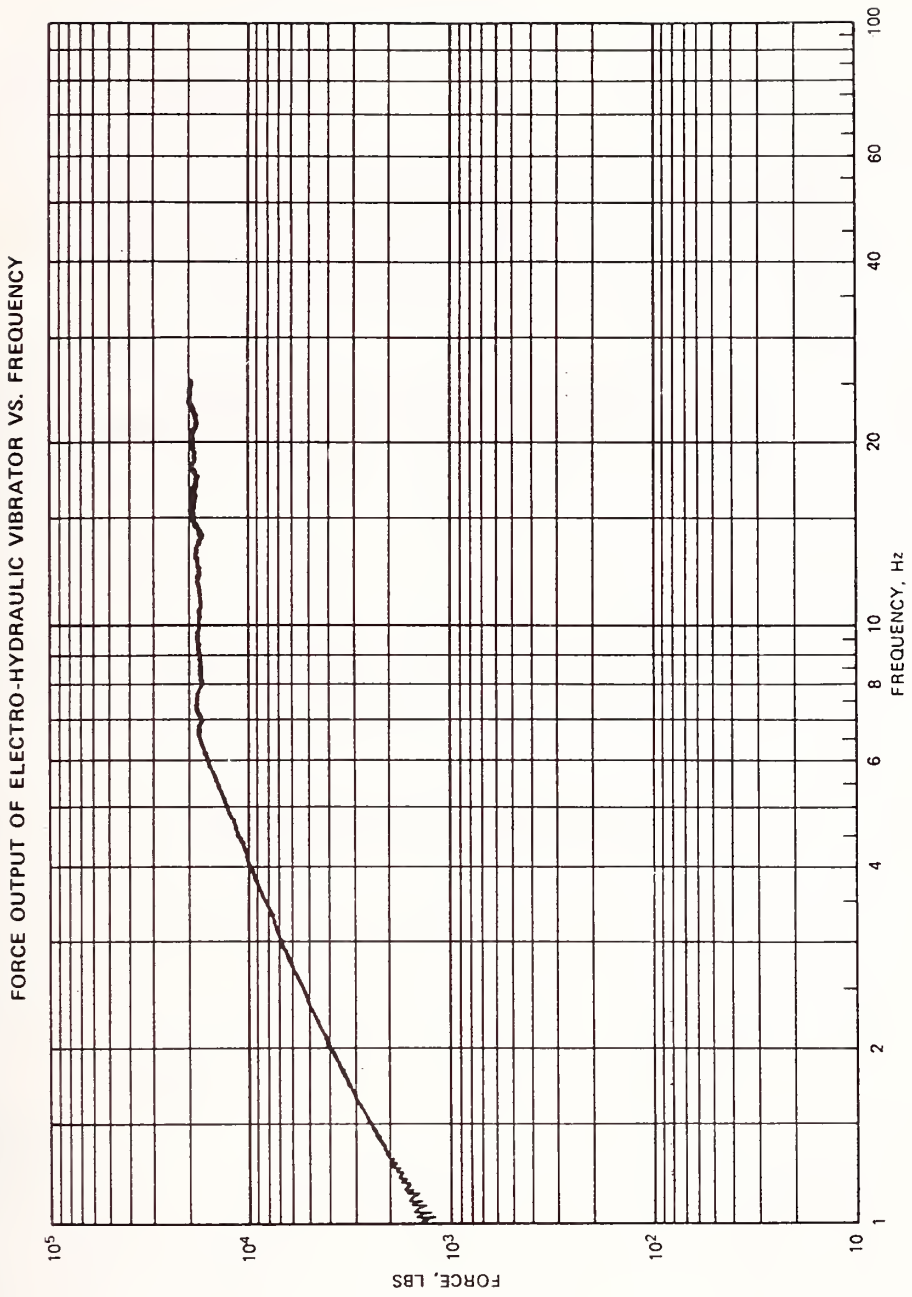


Figure 2. Typical Force Spectrum

# MONOLITHS

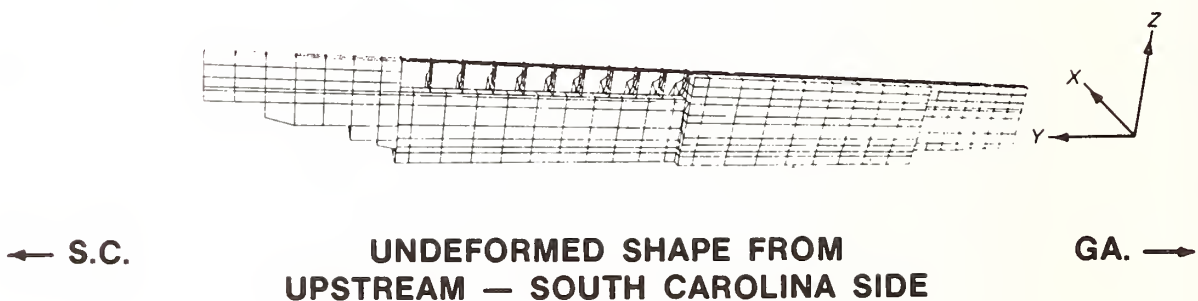
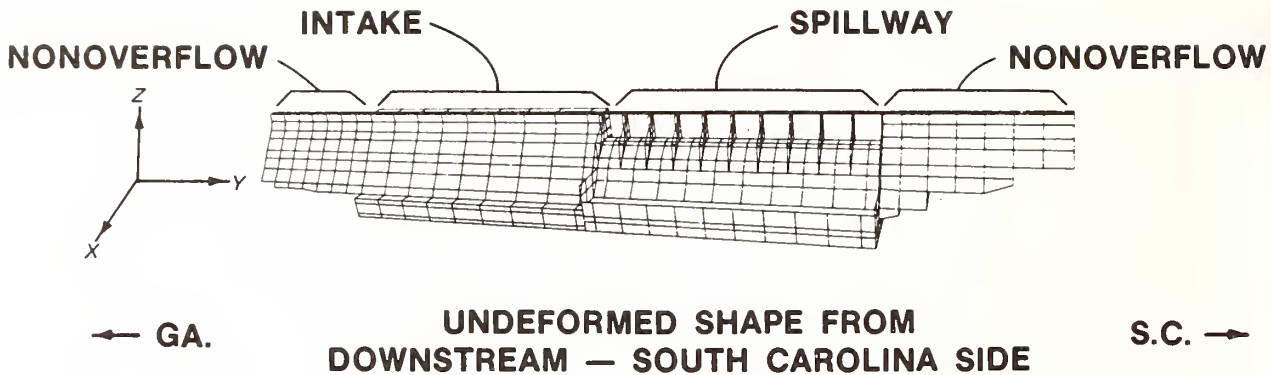


Figure 3. Finite-Element Grid of Entire Dam.

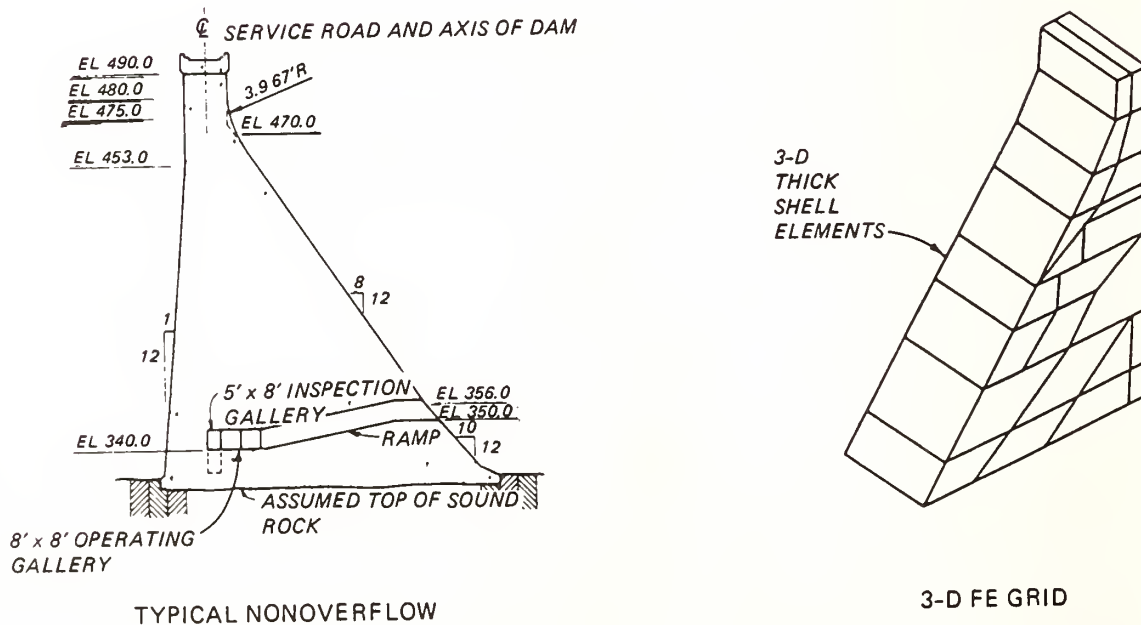
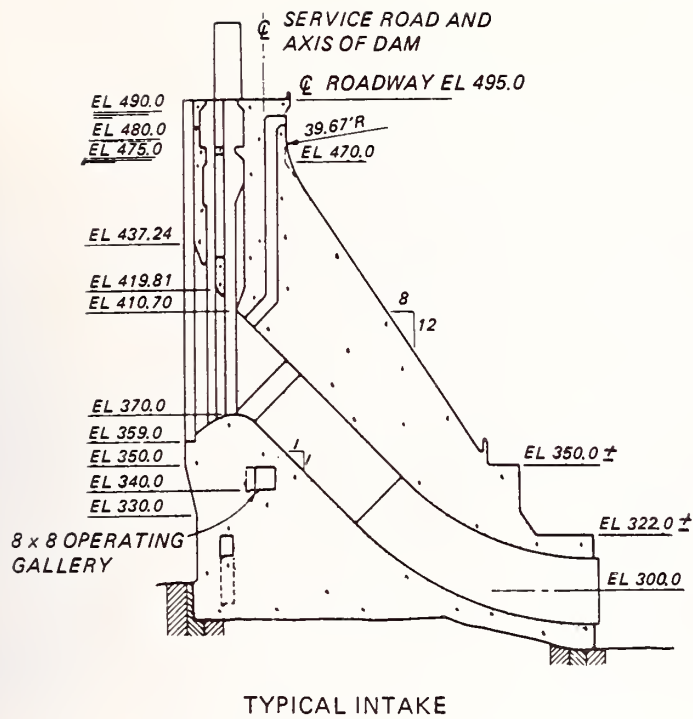
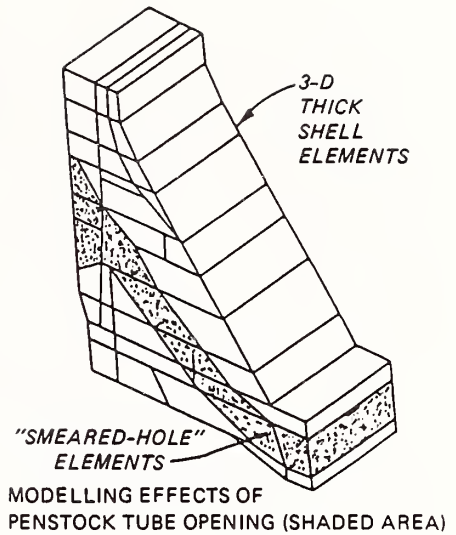


Figure 4. Typical Nonoverflow Monolith.

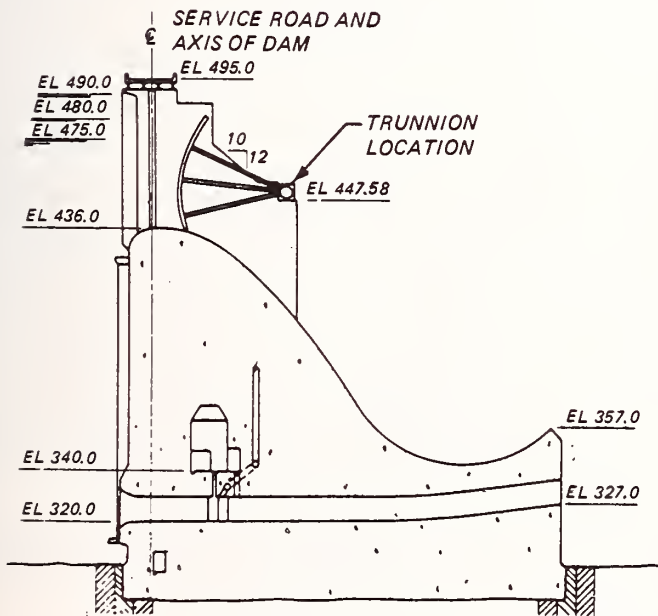


TYPICAL INTAKE

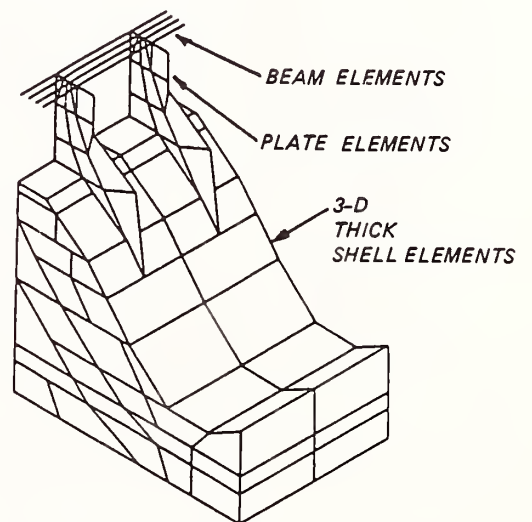


3-D FE GRID

Figure 5. Typical Intake Monolith.



TYPICAL SPILLWAY



3-D FE GRID

Figure 6. Typical Spillway Monolith.

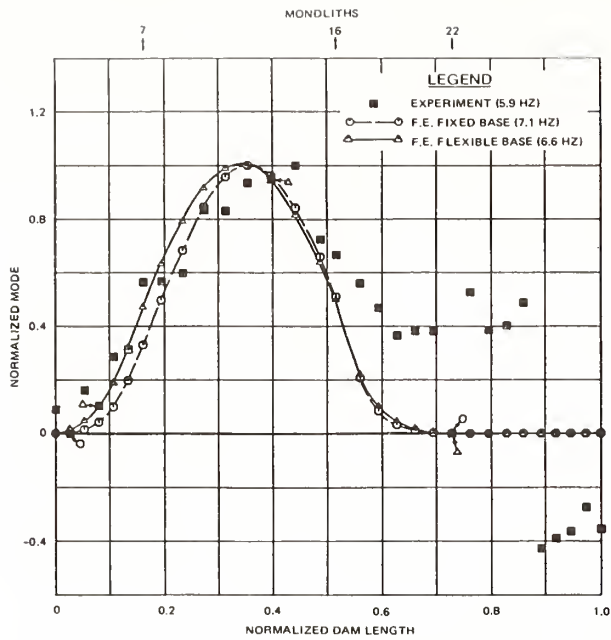


Figure 7. Mode 1 - Dam without Reservoir.

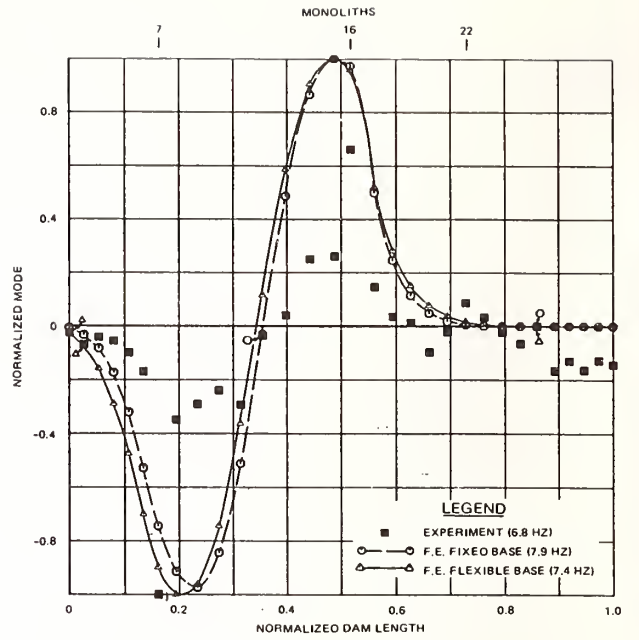


Figure 8. Mode 2 - Dam without Reservoir.

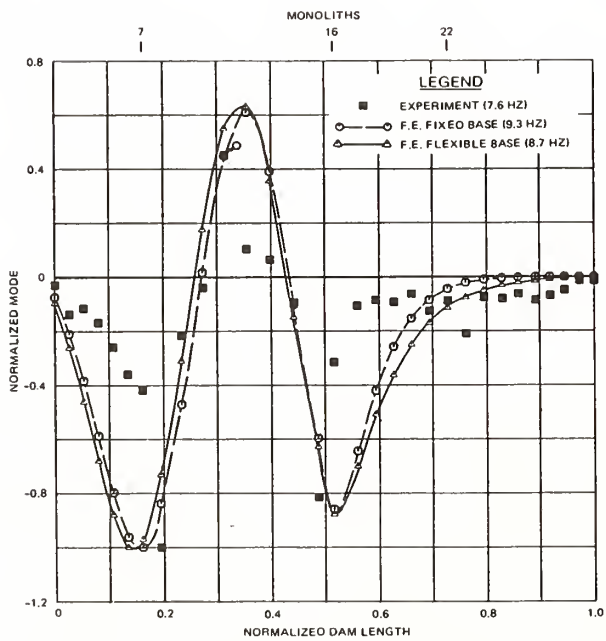


Figure 9. Mode 3 - Dam without Reservoir.

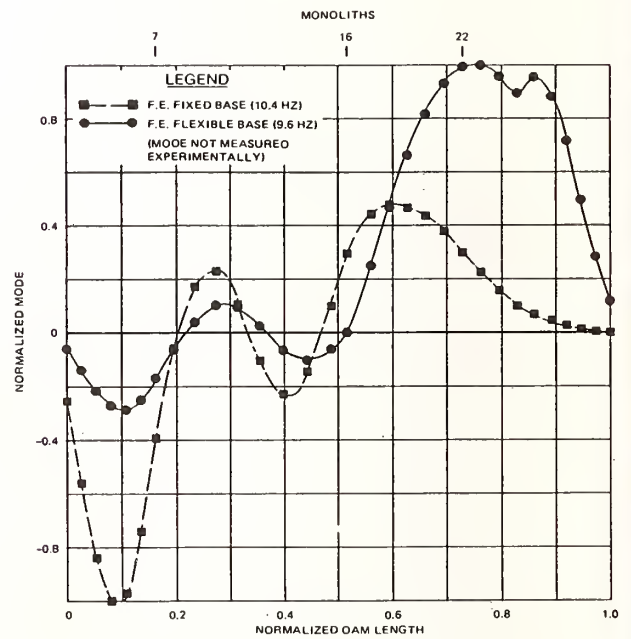


Figure 10. Mode 4 - Dam without Reservoir.

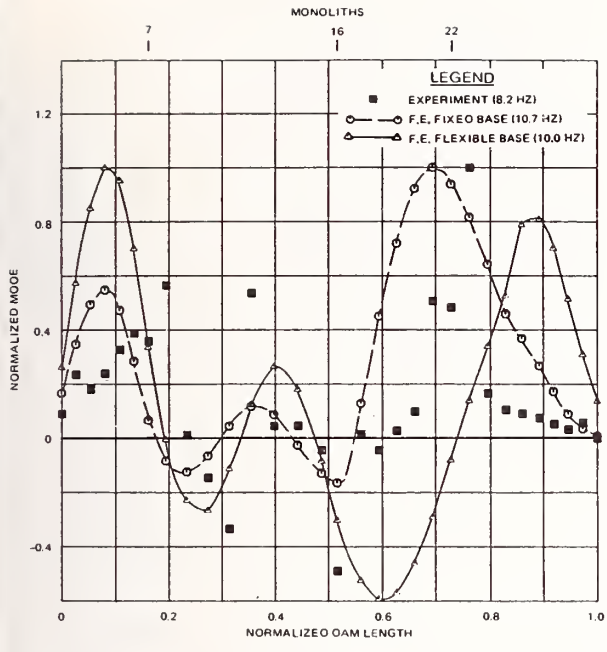


Figure 11. Mode 5 - Dam without Reservoir.

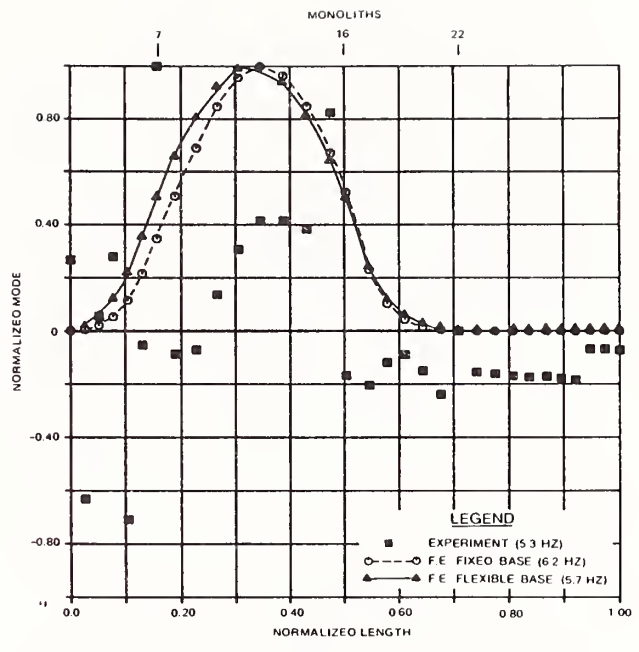


Figure 12. Mode 1 - Dam with Reservoir.

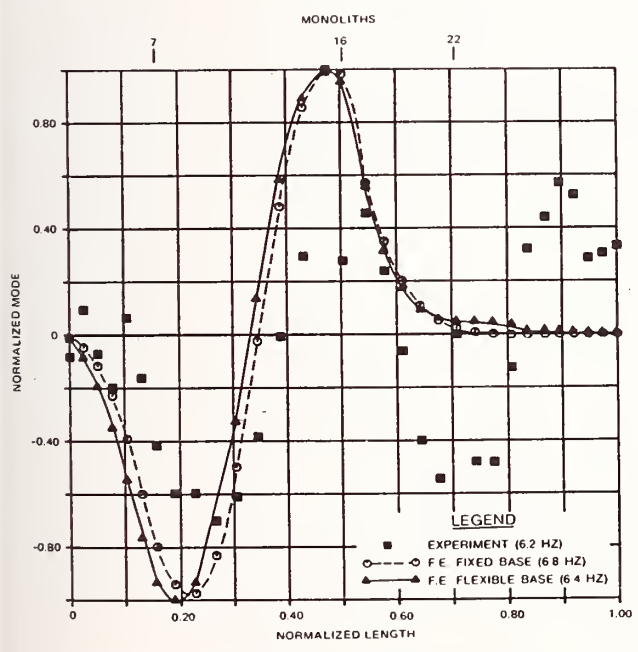


Figure 13. Mode 2 - Dam with Reservoir.

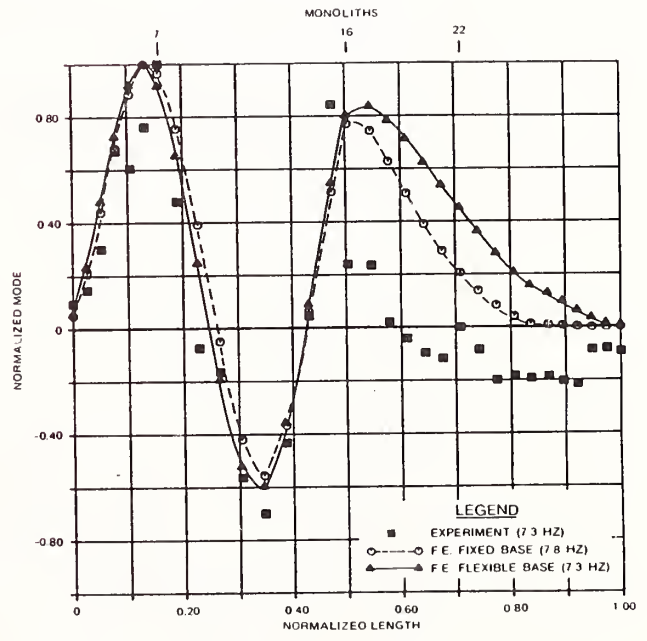


Figure 14. Mode 3 - Dam with Reservoir.

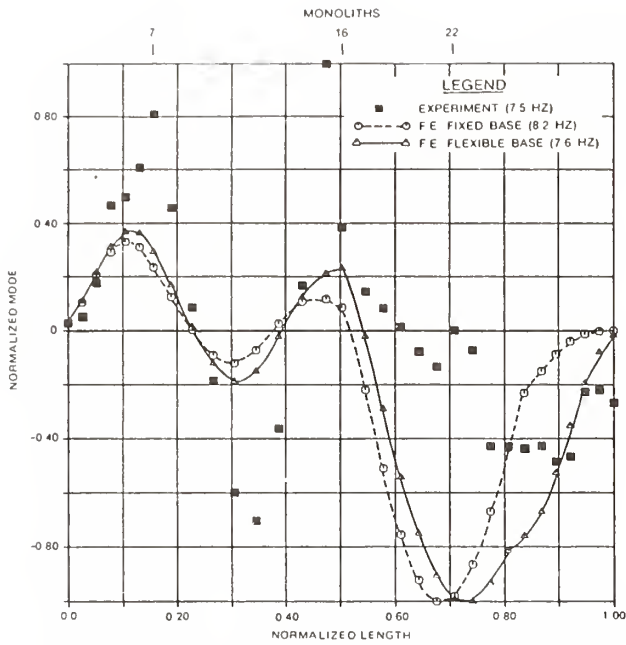


Figure 15. Mode 4 - Dam with Reservoir.

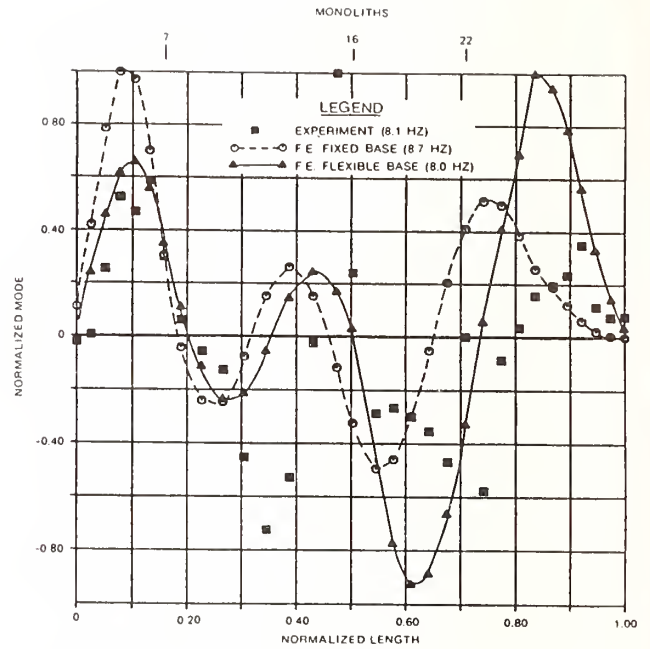


Figure 16. Mode 5 - Dam with Reservoir.

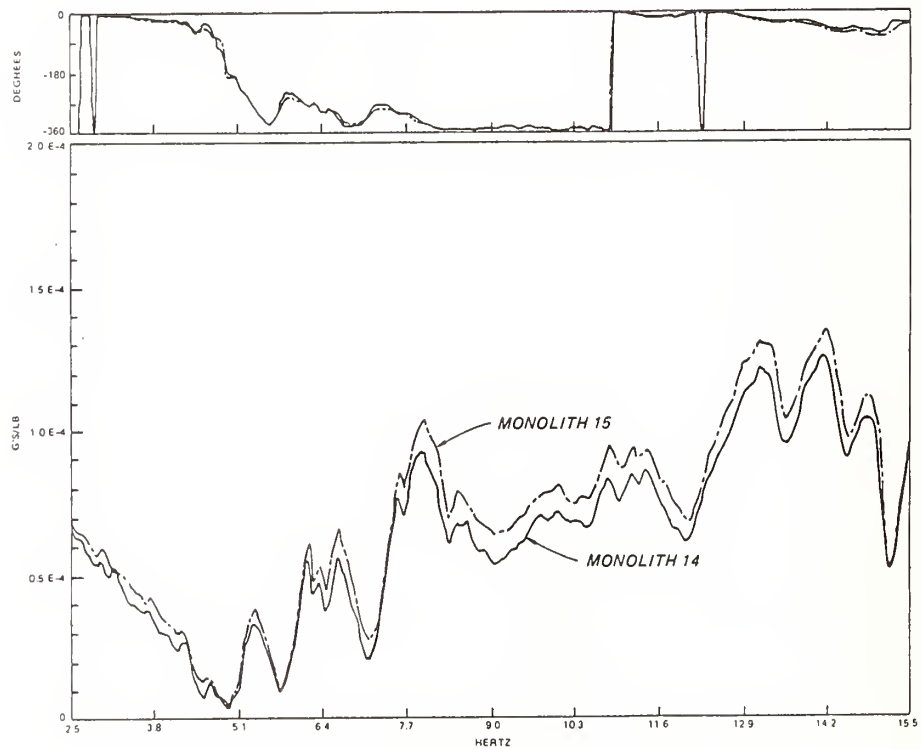


Figure 17. Transfer Functions for Joint 14-15.

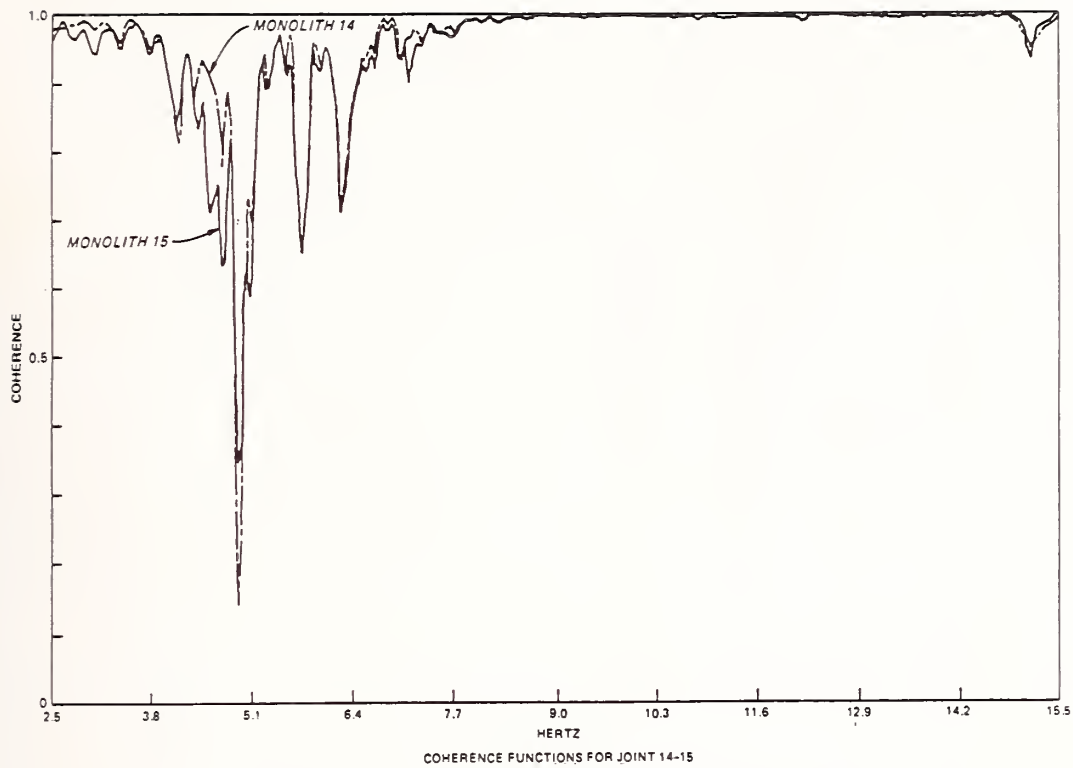


Figure 18. Coherence Functions for Joint 14-15.

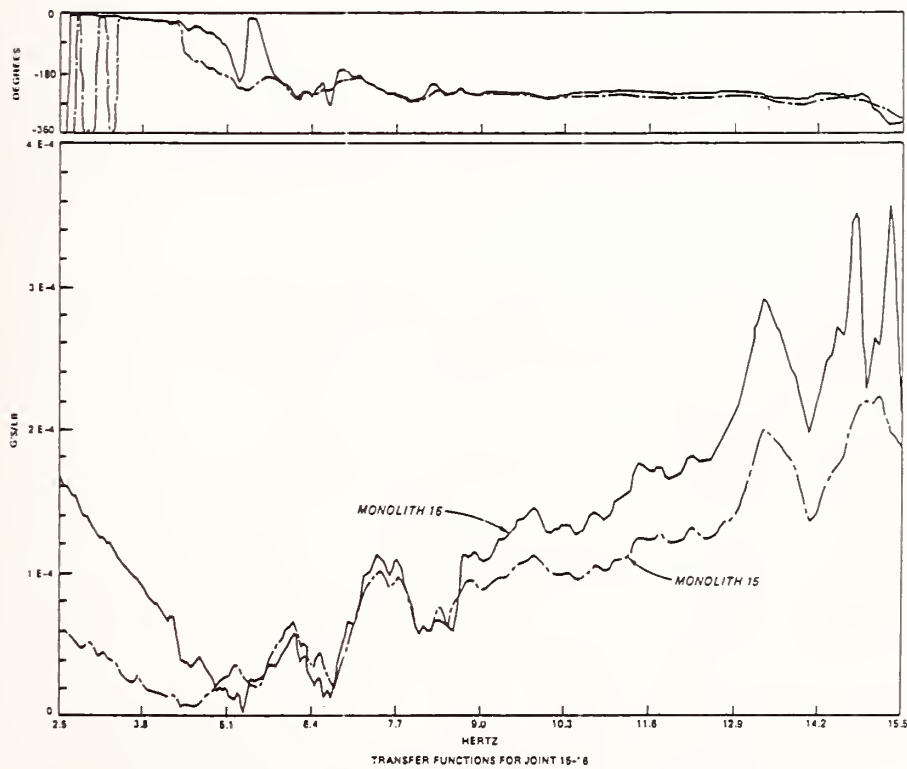


Figure 19. Transfer Functions for Joint 15-16.

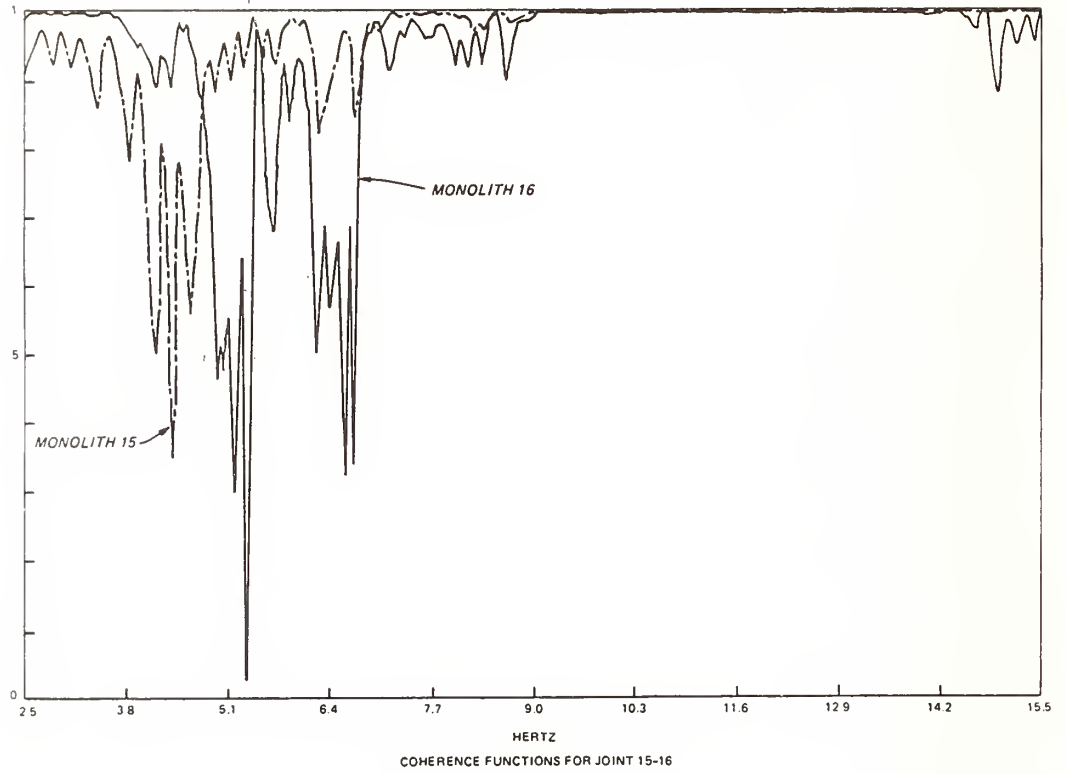


Figure 20. Coherence Functions for Joint 15-16.

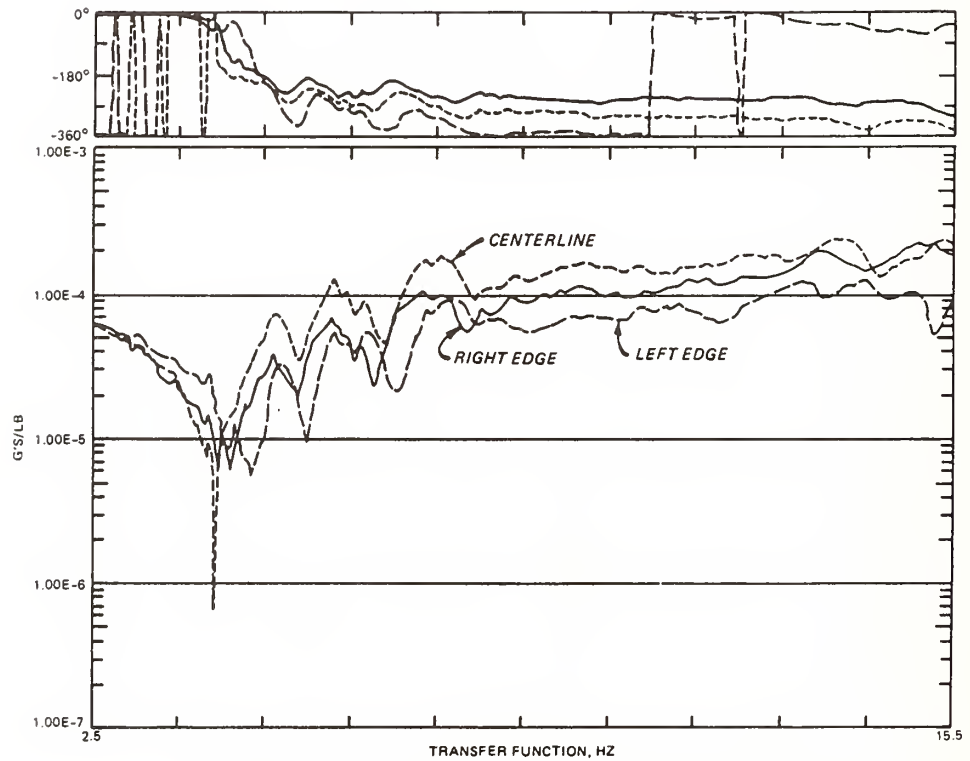


Figure 21. Transfer Functions for Monolith 15.

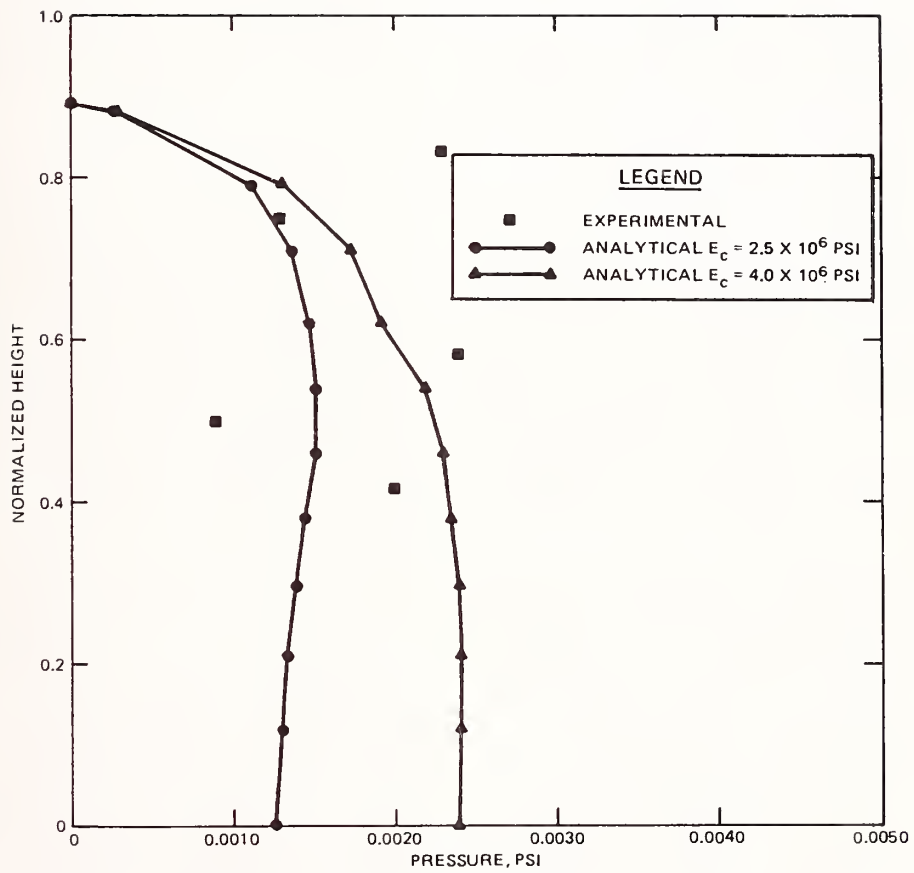


Figure 22. Hydrodynamic Pressures.

# Base Isolated Building Structures in Japan

BY

1) Yoshikazu KITAGAWA and Masaya HIROSAWA 2)

## ABSTRACT

This paper presents a brief introduction of the base isolated building structure in Japan. First, the classification of seismic response control system and the present state of base asolation system are roughly reviewed, and second, examples of existing base isolated building structure are introduced with figures.

KEY WORDS: Seismic Response Control System, Base Isolation System, Passive Way, Active Way Classification, Present State

## 1. INTRODUCTION

Many studies and proposals concerned with the base isolation system have been carried out. Some of those studies and proposals were realized by actual structures in New Zealand, France, U.S.A., Japan and other countries.

Recently, base isolated structures have been proposed and enthusiastically put into practice in Japan, although the ball bearing system was proposed by Dr. Kito in 1924. In this paper, some structures with base isolation in the field of building structures are briefly classified and introduced.

## 2. CLASSIFICATION OF SEISMIC RESPONSE CONTROL SYSTEM

Although there have been many proposals and studies concerning both the seismic response control system and the base isolation system, definitions and the usage of technical terms were not the same, entirely depending upon the use of individual researchers. Also there have been many different classifications and many different view points.

In order to understand the present status of the seismic response control system, the following classification based upon three points of view is introduced in this paper.

- 1) Classification due to Basic Principles of Dynamics
- 2) Classification due to Realization
- 3) Classification due to Installed Location

- |   |   |   |
|---|---|---|
| 1) Classification due to Basic Principles of Dynamics | { | 1) A Method to Control and Adjust Restoring Force Characteristics |
|   | { | 1i) A Method to Control and Adjust Damping                        |

- |   |   |   |
|---|---|---|
|   | { | 1ii) A Method to Control and Adjust Mass  |
|   | { | 1iv) A Method to Control and Adjust Input Motion (Combination of above methods) |
| 2) Classification due to Realization        | { | 1) Passive Way  |
|   | { | 1i) Active Way  |
| 3) Classification due to Installed Location | { | 1) Outer Type (Base Isolated Type)  |
|   | { | 1i) Inner Type (Non-base Isolated Type)   |

According to this classification, base isolation system can be defined as the combination of outer type, passive way, and a method to control and adjust rigidity and damping.

The examples with a figure of seismic response control system, which is already classified based upon three points of view are shown in Table 1.

## 3. PRESENT STATE OF BASE ISOLATION SYSTEM

In the aseismic design, structures are generally fixed to the ground and are susceptible to deformation and stress due to earthquake motion. Thus the aim of aseismic design is to withstand these forces and avoid destruction. On the other hand, the base isolation system to reduce horizontal seismic force on the structure has been developed. This system is set at the base of the structure and must support the dead weight of the structure in the vertical direction and be able to move easily in the horizontal direction.

Usually, the natural period of the whole structure becomes long, and the acceleration of the structure is reduced. But the displacement at the position of the base isolation will be very large due to the earthquake motion with the long period component of earthquake motion. Therefore, much attention must be paid to this point with

1) Dr. of Eng., Head of Second Earthquake Engineering Division, International Institute of Seismology and Earthquake Engineering, Building Research Institute, Ministry of Construction, Japan.

2) Dr. of Eng., Director, I.I.S.E.E., Building Research Institute, Ministry of Construction, Japan.

regards to the energy absorption mechanism.

The laminated rubber isolation is most popular, and many types of energy absorption mechanism have been developed, such as visco-elastic material damper, viscose damper, steel damper, sliding bearing and so on. Furthermore, the control of displacement due to wind force is also required.

The structure with the base isolation system will require special permission from the Minister of Construction following a detailed review of the dynamic behavior of the whole structure by the board of technical members (chairman: Prof. H. Aoyama, University of Tokyo). At present, more than 18 base isolated structures have been constructed in Japan (see Table 2). And analytical studies, experiments and earthquake observations on these structures are being carried out.

#### 4. EXAMPLES OF BASE ISOLATED STRUCTURE

##### Dwelling House (Ref. 1, see Figs. 1 and 2)

A two-storey RC structure isolated on laminated rubber bearings placed on the foundation under each of the 6 columns was constructed at Yachiyo-City, Chiba Pref., in 1982. After the completion of the building, the free and forced vibration tests and microtremor measurements were carried out. Seismographs were also installed at the base mat, the first floor and the roof for carrying out the observations.

##### Institute Building (Ref. 2, see Figs. 3,4 and 5)

A four-storey RC building was constructed at Tsukuba-City, Ibaraki Pref., in 1986. The base isolation system in this building consists of laminated elastomeric bearings and steel hysteretic dampers. These devices are installed between the first floor and the base mat. After completion, the free and forced vibration tests, static test were carried out in order to evaluate the reliability of the dynamic isolation system in the linear range. Earthquake observation in and around this building has been carried out.

##### Laboratory Building (Ref. 3, see Figs. 6,7 and 8)

A base isolated five-storey RC building was constructed at Kiyose-City, Tokyo, in 1986. The base isolation system in this building consists of laminated rubber bearings and steel bar dampers. After completion, static and forced vibration tests were carried out, and the results of these tests were compared and analyzed. Earthquake observation in and around this building has been carried out.

##### Laboratory Building (Ref. 4, see Figs. 9, 10 and 11)

A base isolated five-storey building was

constructed at Fujisawa-City, Kanagawa Pref., in 1987. This 7500ton reinforced concrete frame building rests on 35 lead rubber bearings. After completion, free and forced vibration tests, and microtremor measurements were carried out. And the dynamic characteristics of this building were compared with the designed values. Earthquake observation is has been carried out.

##### Boarding House (Ref. 5, see Figs. 12 and 13)

A three-storey RC building was constructed at Funabashi-City, Chiba Pref., in 1985. The base isolation system in this building consists of laminated rubber bearings and viscose dampers. The viscose damper does not have noticeable initial stiffnees and the movement is smooth, and enables the base isolation to be effective against large or small earthquakes. After completion, microtremor measurements and manual vibration tests were carried out, and earthquake observation at the base mat, the first floor and the roof has been carried out.

##### Institute Building (Ref. 6, see Figs. 14,15 and 16)

A base isolated two-storey RC building was completed at Chofu-City, Tokyo, in 1986. The base isolation system in this building consists of laminated rubber bearings, hysteretic dampers and fail-safe supports. This system was designed to maintain the function of not only acceleration response reduction in a severe earthquake, but also to keep horizontal and vertical vibration isolated from the ground micro-vibration. The shaking table tests using a scale model and forced vibration tests of this building were carried out. Earthquake observation has also been conducted in and around the building.

##### Full-scale Test Building (Ref. 7, see Figs. 17, 18 and 19)

Development of the base isolation system is intended for practical use, and in line with this purpose two identical three-storey RC full-scale test building were constructed at Sendai-City, Miyagi Pref., in 1986. One was built with the base isolation system and the other with an ordinary foundation. The base isolation system in this building consists of laminated rubber bearings and oil dampers. After the completion of these buildings, free and forced vibration tests, and a static test were carried out. Observation for earthquake motion and for response due to strong wind was also conducted.

##### Institute Building (Ref. 8, see Figs. 20,21 and 22)

A base isolated four-storey RC building will be constructed at Yokohama-City, Kanagawa Pref., in 1988. The base isolation system in this building consists of sliding bearings, bearing plates and horizontal springs. PTFE(

Poly Tetra Fluoro Ethlere) resin ball bearings are used for sliding bearings. Steel plates, bars or chloroprens rubbers are used for horizontal springs. Sliding bearings are attached to the bottom of the columns of a superstructure and slip occurs between the PTFE plants and bearing plates in the foundation. Horizontal springs are fixed between the superstructure and the foundation, connecting both parts. Shaking table tests using a reduced scale model were carried out. And a force vibration test, microtremor measurements and earthquake observation has also been conducted.

#### 5. CONCLUDING REMARKS

The base isolated building structure in Japan is briefly introduced. The number of the base isolated structure has increased rapidly. In order to evaluate the reliability of the dynamic isolation system, the earthquake observation in and around this building has been carried out and high quality data will be accumulated in the near future. In relation to the increase of data, disclosure of the data is necessary for cooperation and coordination between each other. Free use of these data would be fruitful for the progress of research.

#### 6. ACKNOWLEDGEMENTS

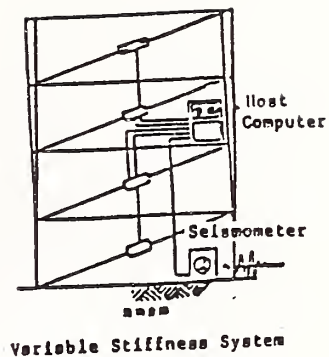
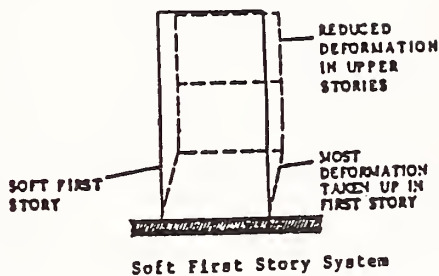
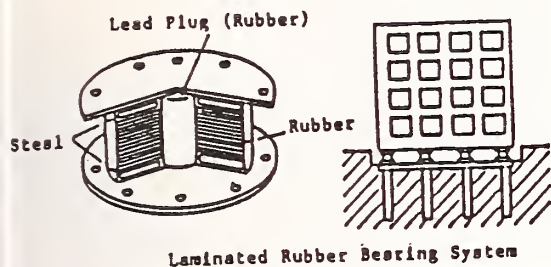
The author would like to acknowledge gratitude to the following persons; Mr. S. NAKAE, Okumura Co.; Dr. T. TAKEDA, Ohbayashi Co.; Mr. M. MIYAZAKI, Sumitomo Construction Co.; Mr. H. HAYAMIZU, Takenaka Co.; Mr. A. Yasaka, Kajima Co.; Mr. H. YOKOTA, Shimizu Co.; Dr. S. KAWAMURA, Taisei Co., for offering the Data in this report. The author also wishes to express my sincere thanks to Miss Y. TAKASHIMA for typing and drawing.

#### 7. REFERENCES

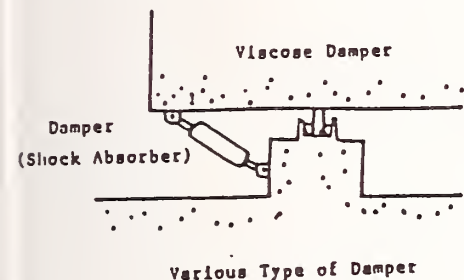
- 1) H. TADA, A. SAKAI, M. TAKAYAMA, A. WADA et al; Research Study on Aseismic Isolation System by Enforcement Construction Part(1~13), Annual Meeting, Arch. Inst. Japan, 1983~86.
- 2) I. ABE, S. OTSUKA, O. HARADA et al; A Study on Dynamic Behavior of Base Isolated Structure (Part 1.2), Annual Meeting, Arch. Inst. Japan, 1987.
- 3) T. TAKEDA, H. OKADA, T. NAKAMURA, M. SEKI et al; Study on Earthquake Base Isolation System for Structure (Part 1~12), Annual Meeting, Arch. Inst. Japan, 1984~86.
- 4) I. SHIMODA, M. MIYAZAKI, K. NAKANO, Y. KITAGAWA, K. IBE et al; Experimental Study on A Base Isolated Building Using Lead Rubber Bearing (Part 1~5), Annual Meeting, Arch. Inst. Japan, 1987.
- 5) S. AIZAWA, M. TONO, H. HAYAMIZU, Y. ABE; A Study on Earthquake Base Isolation System Using Laminated Rubber Bearing on Large Scale Specimen (Part 1~6), Annual Meeting, Arch. Inst. Japan, 1983~86.
- 6) H. KOSHIDA, A. YASAKA, M. IIZUKA, T. YANO et al; Vibration Tests of The Base Isolated Building, 7th JEES, 1986.
- 7) M. SUKAGAWA, Y. NAKAMURA, H. MORIOKA, M. KANEKO et al; Study on Base Isolation System of Buildings, Annual Meeting, Arch. Inst. Japan, 1986.
- 8) K. KITAZAWA, A. IKEDA and S. KAWAMURA; Study on A Base Isolation System, 8th WCEE, 1984.
- 9) Investigation Report on Establishment of Guide-Line Concerning with Technical Development for Base Isolated Structure (in Japanese), BCJ, 1987.

1) Classification due to Basic Principles of Dynamics

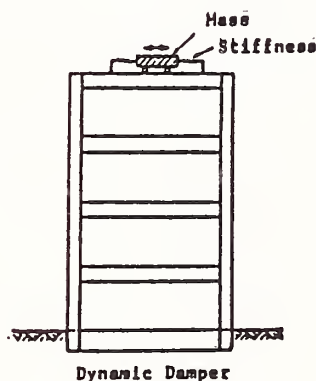
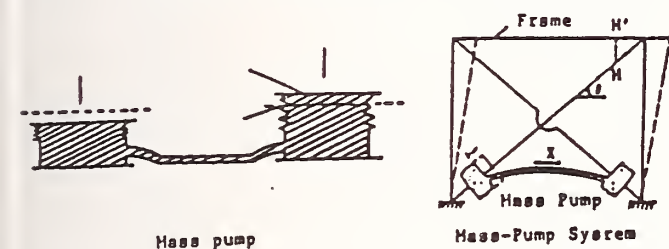
i) A Method to Control and Adjust Restoring Force Characteristics



ii) A Method to Control and Adjust Damping



iii) A Method to Control and Adjust Mass



iv) A Method to Control and Adjust Input Motion

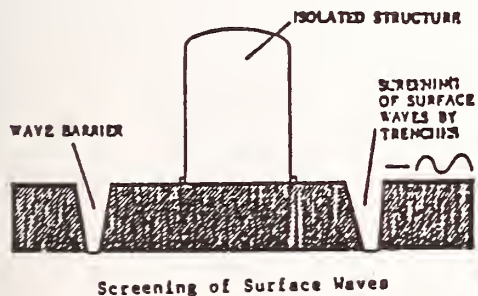
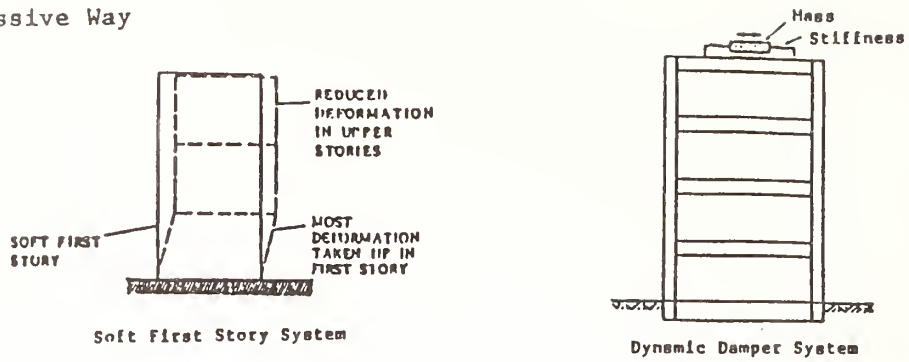


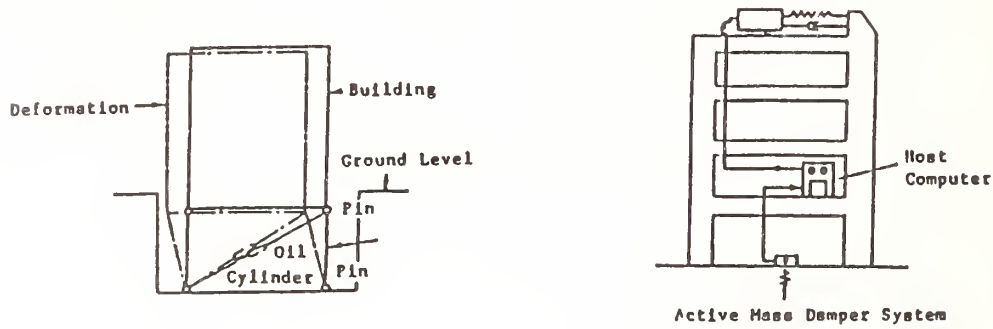
Table 1 EXAMPLES OF CLASSIFICATION (Part-1)

2) Classification due to Realization

i) Passive Way

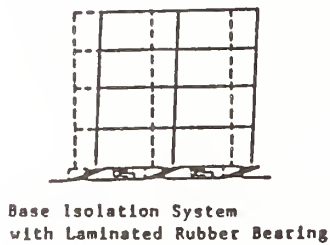


ii) Active Way



3) Classification due to Installed Location

i) Outer Type (Base Isolated Type)



ii) Inner Type (Now-base Isolated Type)

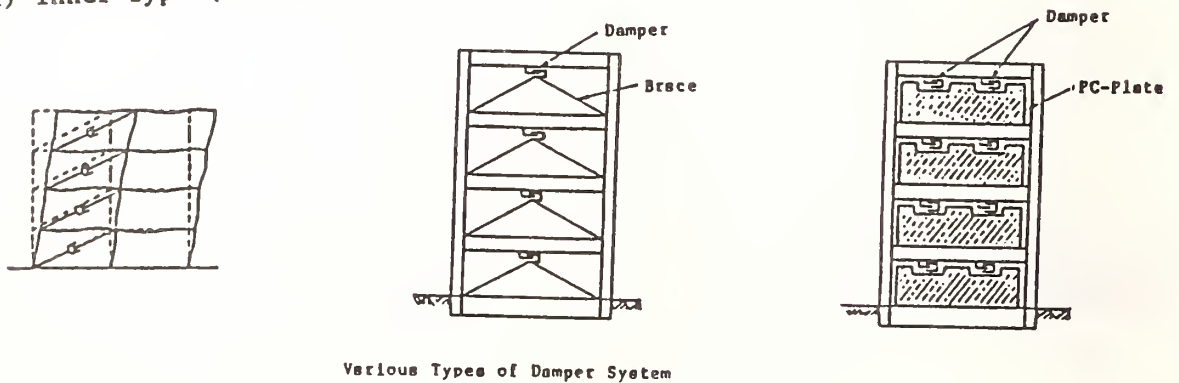


Table 1 EXAMPLES OF CLASSIFICATION (Part-2)

Table 2. List of Base Isolated Structure Permitted from The Minister of Construction (Part 1)

Design	Tokyo Kenchiku Structure Engineers	Tokyo Kenchiku Str. Eng. Yunichika	Tokyo Kenchiku Str. Eng. Okumura Co.	Ohbayashi Co.	Oiles Industry Co. Sumitomo Construction Co.	Takenaka Co.
Number of Permission	BCJ-LC-99	BCJ-Mei 1	BCJ-Mei 2	BCJ-Mei 3	BCJ-Mei 4	BCJ-Mei 5
Date of Permission	1982.4	1985.7	1985.11	1986.2	1986.3	1986.4
Stories	+2	+2, -1	+4	+5	+5	+3
Building Area	60.18 m <sup>2</sup>	226.23m <sup>2</sup>	348.18m <sup>2</sup>	351.92m <sup>2</sup>	1,136.5 m <sup>2</sup>	719.28m <sup>2</sup>
Uses	Dwelling	Museum	Institute	Multi Purpose Laboratories	Laboratory	Boarding House
Structure	RC	RC	RC	RC	RC	RC
Foundation	Mat	Caisson Type-Pile	Cast-in-Place bored Pile	PHC-Pile	Cast-in-Place bored Pile	Cast-in-Place bored Pile
Isolator	Dimension	82 x 300 φ	Rubber Thickness 5 x 300 φ (12 layers)	Rubber Thickness 4.4 x 740 φ (61 layers)	Rubber Thickness 10 x 24 layers (H-363) Diameter (650, 700, 750, 800 φ)	Thickness 7 x 670 φ x 19 layers (H-187) Thickness 9 x 700 φ x 18 layers (H-195)
	Number	6	32	25	14	14
Damper	Axial Pressure or Force	$\sigma = 45 \text{kg/cm}^2, 0.5 \text{t/cm} (32 \text{t})$	$\sigma = 60 \text{kg/cm}^2, 0.5 \text{t/cm} (42.5 \text{t})$	$\sigma = 60 \text{kg/cm}^2, 0.86 \text{t/cm} (120 \text{t})$	$\sigma = 50 \sim 80 \text{kg/cm}^2, 150 \sim 380 \text{t}, (650, 700, 750, 800 \phi)$	$\sigma = 43.3 \text{kg/cm}^2, 150 \text{t} (8 \text{ pieces}), 200 \text{t} (6 \text{ pieces})$
		Friction between Concrete Elements and so on	Round Steel Bars bended as Coil (8 pieces)	Round Steel Bars bended as Coil (12 pieces)	Rounded Steel Bars (96 Pieces)	Viscose Dampers (8 pieces)
Design Base Shearing Force Coefficient		0.2	0.15	0.15	0.2	0.15
	at Small Deformation	1.83sec.	1.4 sec.	1.4 sec.	X 0.895sec. (at 50% strain level) Y 0.908sec.	X direc. 2.09sec. Y direc. 2.10sec.
	at Large Deformation		1.9 sec.	2.1 sec.	X 2.143sec. (at 100% strain level) Y 2.148sec.	
Input Earthquake Motion		EL CENTRO 1940 (NS) HACHINOHE 1968 (NS) HACHINOHE 1968 (EW) TAFT 1952 (EW)	EL CENTRO 1940 (NS) HACHINOHE 1968 (NS) HACHINOHE 1968 (EW) TAFT 1952 (EW)	EL CENTRO 1940 (NS) HACHINOHE 1968 (NS) HACHINOHE 1968 (EW) TAFT 1952 (EW) Artificial Seismic Waves-2types	EL CENTRO 1940 (NS) HACHINOHE 1968 (NS) HACHINOHE 1968 (EW) TAFT 1952 (EW) Artificial Seismic Waves-2types	EL CENTRO 1940 (NS) TAFT 1952 (EW) TOKYO 101 1956 (NS) HACHINOHE 1968 (NS) Artificial Seismic Waves 4types
	Input Level	300gal	300gal, 450gal	300gal, 450gal	25cm/sec., 50cm/sec.	25cm/sec., 50cm/sec.
Reference	1		2	3	4	5

Table 2 List of Base Isolated Structure Permitted from The Minister of Construction (Part 2)

Design	Kajima Co.	Tokyo Kenchiku Str.-Eng.	Okumura Co.	Ohbayashi Co.	Fujita Co.	Ohbayashi Co. Min. of Const.
Number of Permission	BCJ-Mei 6	BCJ-Mei 7	BCJ-Mei 8	BCJ-Mei 9	BCJ-Mei 10	BCJ-Mei 11
Date of Permission	1986.5	1986.7	1986.12	1987.2	1987.2	1987.6
Stories	+2	+2	+4	+5, -1	+3	+1
Building Area	379.10m <sup>2</sup>	149.53m <sup>2</sup>	225.40m <sup>2</sup>	560.30m <sup>2</sup>	102.21m <sup>2</sup>	8,341.50m <sup>2</sup>
Uses	Institute	Museum	Apartment House	Office	Laboratory	Institute
Structure	RC	RC	RC	RC	RC	RC
Foundation	Cast-in-Place bored Pile	Caisson Type Pile	Cast-in-Place bored Pile	Cast-in-Place bored Pile	PHC-pile (A, B Types)	PHC-pile (A Type)
Isolator	Dimension	320 x 1340φ (Thickness 48x5 layers) 308 x 1080φ (Thickness 38x6 layers)	Thickness 4x435 (25 layers, 16 layers)	Thickness 5x620 φ (50 layers) Thickness 6x740 φ (45 layers)	Thickness 4x450 φ (44 layers)	Thickness 32x420 φ (62 layers)
	Number	18	12	20	4	32
Damper	Axial Pressure or Force	155t: 1340φ 100t: 1080φ	σ = 60kg/cm <sup>2</sup> , 140t	100 ~ 150t: 620φ 200 ~ 250t: 740φ	85t: 450 φ	65t
		Round Steel Bars (14 pieces)	Round Steel Bars bended as Coil (6)	Round Steel Bars bended as Coil (7)	Round Steel Bars (108 pieces)	Lead Rubber Bearings (4 pieces)
Design Base Shearing Force Coefficient		0.2	0.15	0.15: 1FL 0.183: 3FL 0.205: 5FL	0.15: 1FL 0.17: 2FL 0.20: 3FL	0.15
	at Small Deformation	X direc. 0.828sec. Y direc. 0.809sec.	1.3sec. 1.9sec.	X direc. 1.30sec. Y direc. 1.24sec.	X direc. 1.30sec. Y direc. 1.24sec.	1.17sec
Natural Period	at large Deformation			X direc. 2.99sec. Y direc. 2.97sec.	X direc. 2.99sec. Y direc. 2.97sec.	2.26sec
	Input Earthquake Motion	EL CENTRO 1940(NS) TAFT 1952(EH) TOKYO 101 1956(NS) SENDAI TH038-1 1978(EH)	EL CENTRO 1940(NS) TAFT 1952(EH) TOKYO 101 1956(NS) HACHINOHE 1968(NS)	EL CENTRO 1940(NS) TAFT 1952(EH) HACHINOHE 1968(NS) SDKANRIG SDKANRIG SDKANRIG (Artificial Seismic Waves)	EL CENTRO 1940(NS) TAFT 1952(EH) HACHINOHE 1968(NS) HACHINOHE 1968(EH) ART79100 (Artificial Seismic Waves)	EL CENTRO 1940(NS) TAFT 1952(EH) HACHINOHE 1968(NS) HACHINOHE 1968(EH) TSUKUBA 85NS, 85EH, 86NS, 86EH Observed Earth. Motions
Input Level	25cm/sec., 50cm/sec.	300gal, 450gal	25cm/sec., 50cm/sec.	25cm/sec., 50cm/sec.	25cm/sec., 50cm/sec.	25cm/sec., 50cm/sec.
Reference	6					

Table 2 List of Base Isolated Structure Permitted from The Minister of Construction (Part 3)

Design	Shimizu Construction Co. LTD.	Taisei Co.	Okumura Co.	Ohbayashi Co.	Sunitomo Const. Co.	Kumagai Co.
Number of Permission	BCJ-Mei 12	BCJ-Mei 13	BCJ-Mei 14	BCJ-Mei 15	BCJ-Mei 16	BCJ-Mei 17
Date of Permission	1987.6	1987.7	1987.7	1987.12	1988.2	1988.2
Stories	+4	+4	+3	+8	+10	+3
Building Area	170.366 m <sup>2</sup>	323.0m <sup>2</sup>	191.83m <sup>2</sup>	461.3	467.7	278.1
Uses	Office, Boarding House	Institute	Apartment House	Office	Office Apartment House	Office Boarding House
Structure	RC	RC	RC	RC	RC	RC
Foundation	PHC-pile (B, C Types)	Footing	Mat	Cast-in-Place boarded Pile	Cast-in-Place boarded Pile	Cast-in-Place boarded Pile
Isolator	Dimension	Thickness 6x450 φ, 6 x 500 φ, 6 x 550 (31 layers)	Thickness 7x500 φ (14 or 16 layers)	Thickness 5.4, 6.2, 6.0 x 880 φ, 960 φ, 1030 φ, (30 layers)	Thickness 8x900 φ (30 layers)	Thickness 5x550 φ (53 layers)
	Number	14	10	12	14	12
Damper	Axial Pressure or Force	51~165(t)				
		Lead Rubber Bearings	Sliding Bearing	Round Steel Bars	Lead Rubber Bearings (14 pieces)	Round Steel Bars (14 pieces)
Design Base Shearing Force Coefficient		0.15	0.15	0.15	0.2	0.15
	at Small Deformation	0.77sec	1.2sec.	1.3sec	0.61sec	1.14sec
Input Earthquake Motion		2.33sec	2.2sec	2.55sec	2.08 at 50% Strain Level 2.54 at 100% Strain Level	2.47sec
		EL CENTRO 1940 (NS) TAFTA 1952 (EH) HACHINOHE 1968 (NS) IBARAGI 606 1964 (NS)	EL CENTRO 1940 (NS) TAFTA 1952 (EH) HACHINOHE 1968 (NS) AKITA 1983 (NS) Artificial Seismic Waves (2 Types)	EL CENTRO 1940 (NS) TAFTA 1952 (EH) HACHINOHE 1968 (NS) TOKYO101 1956 (NS)	EL CENTRO 1940 (NS) TAFTA 1952 (EH) HACHINOHE 1968 (NS) TOKYO101 1956 (NS) Artificial Seismic Waves-2 types	EL CENTRO 1940 (NS) TAFTA 1952 (EH) HACHINOHE 1968 (NS) Artificial Seismic Waves-2 types
Input Level	35cm/sec., 50cm/sec.	100gal., 25cm/sec., 50cm/sec.	25cm/sec., 50cm/sec.	35cm/sec., 50cm/sec.	25cm/sec., 50cm/sec.	25cm/sec., 50cm/sec.
Reference	7	8				



Fig. 1 General View

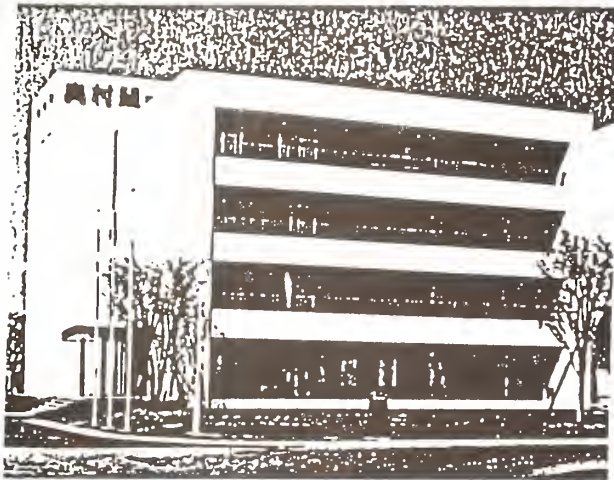


Fig. 3 General View

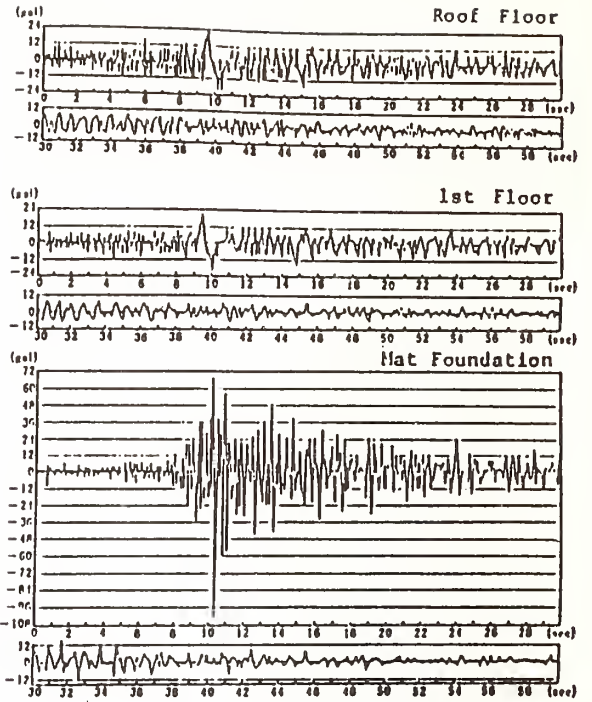


Fig. 2 Example of Observed Motions

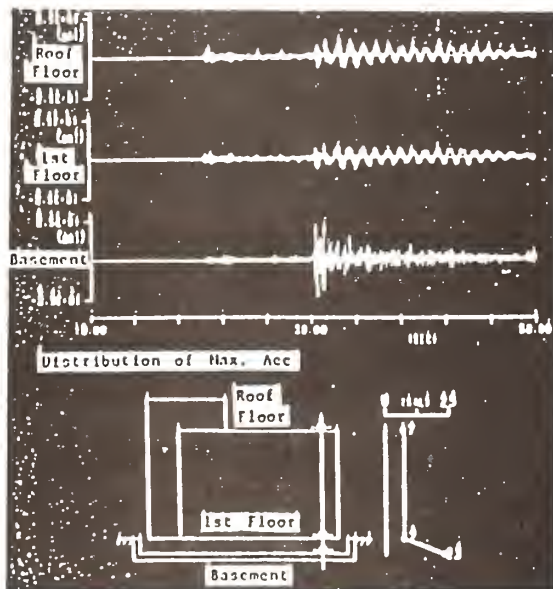


Fig. 4 Example of Observed Motion

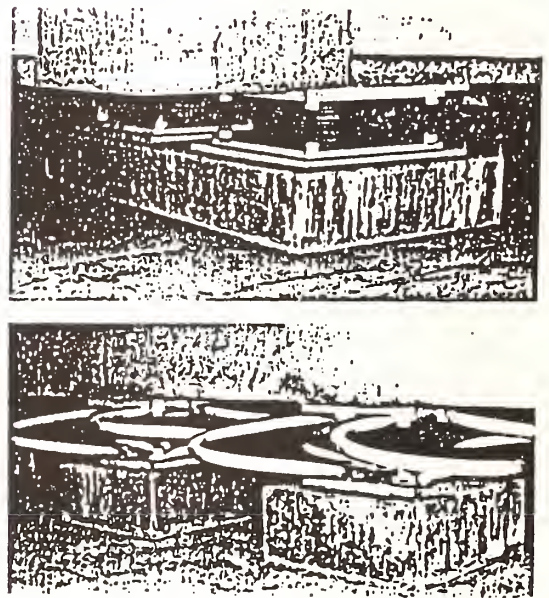


Fig. 5 Installed Devices

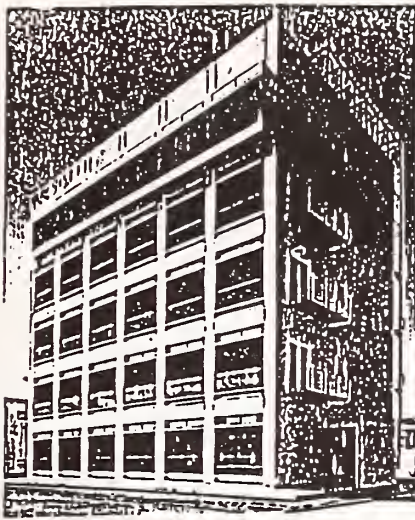


Fig. 6 General View

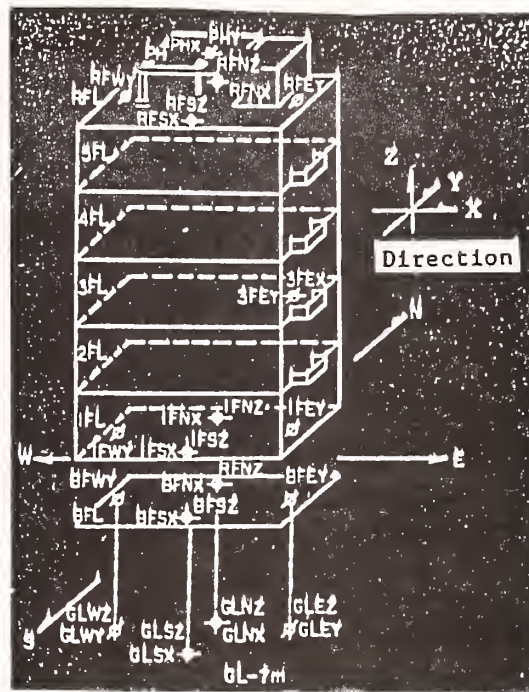


Fig. 7 Outline of Earthquake Observation System

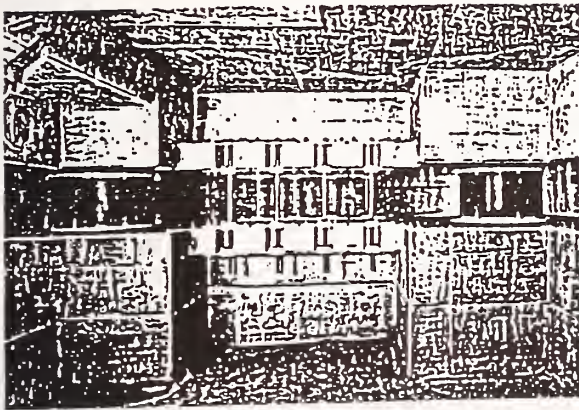


Fig. 8 Installed Devices

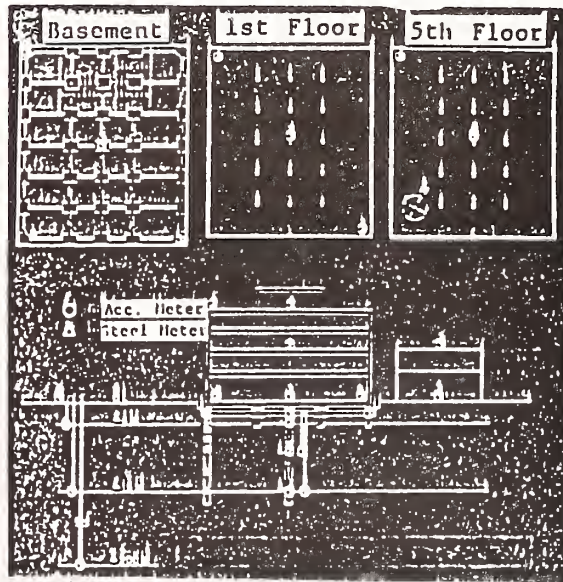


Fig. 10 Outline of Earthquake Observation System

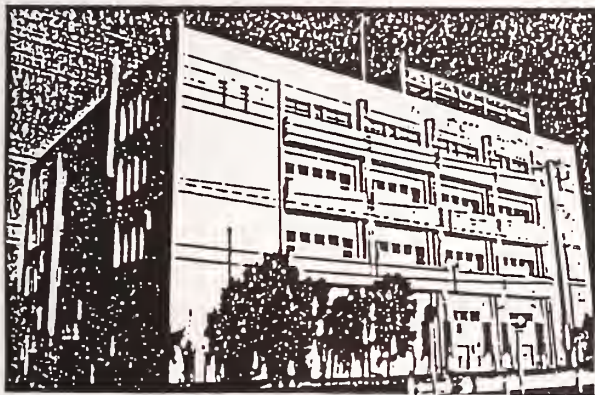


Fig. 9 General View

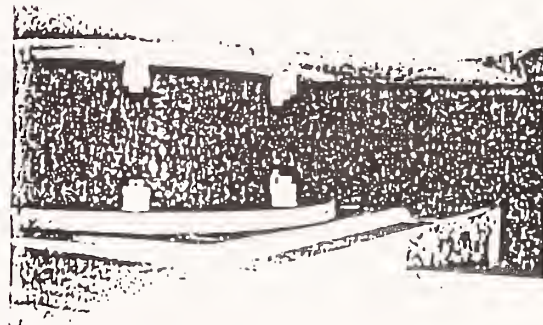


Fig. 11 Installed Devices

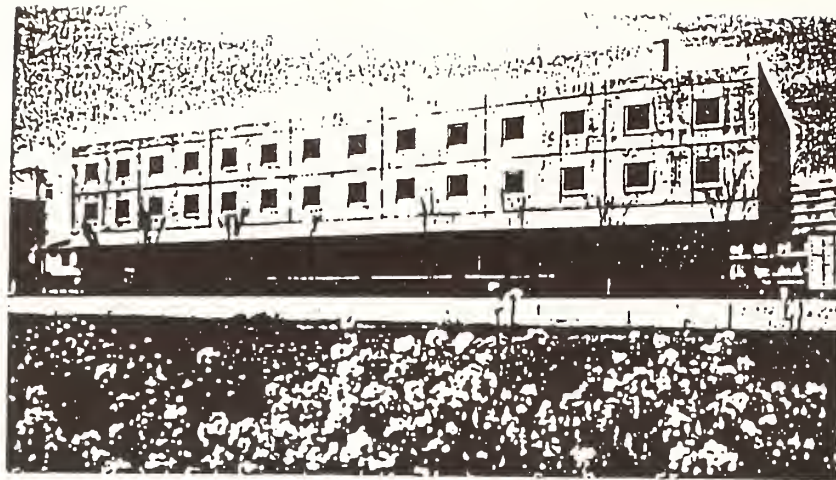


Fig. 12 General View

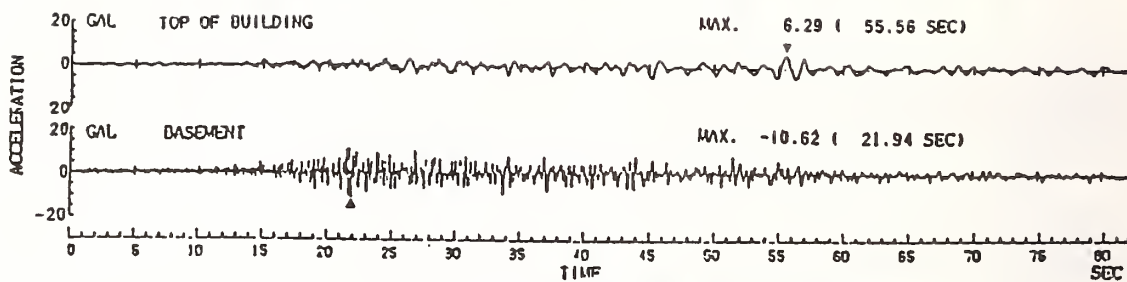


Fig. 13 Example of Observed Motions

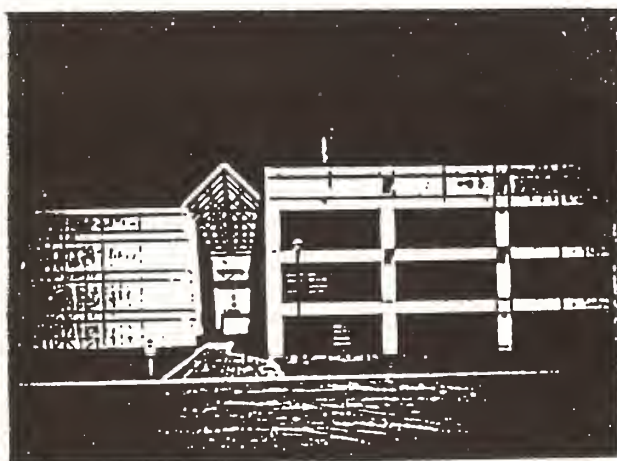


Fig. 14 General View

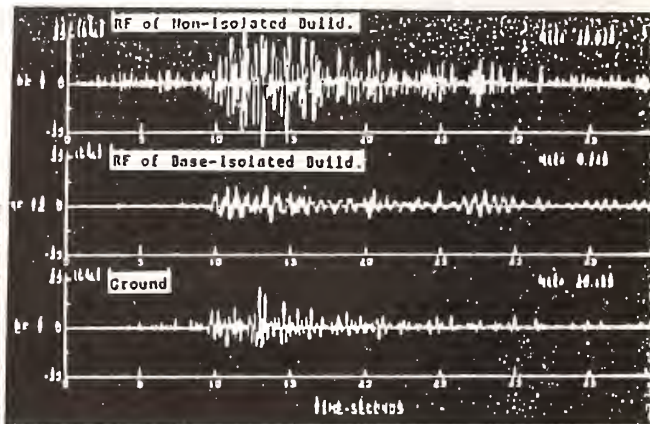


Fig. 15 Example of Observed Motions

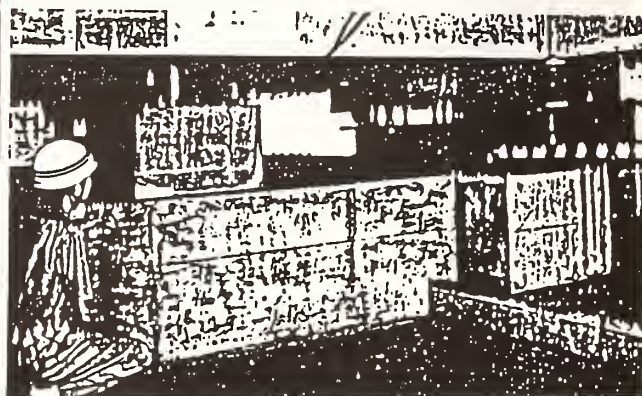


Fig. 16 Installed Devices

Shimizu Base Isolation System

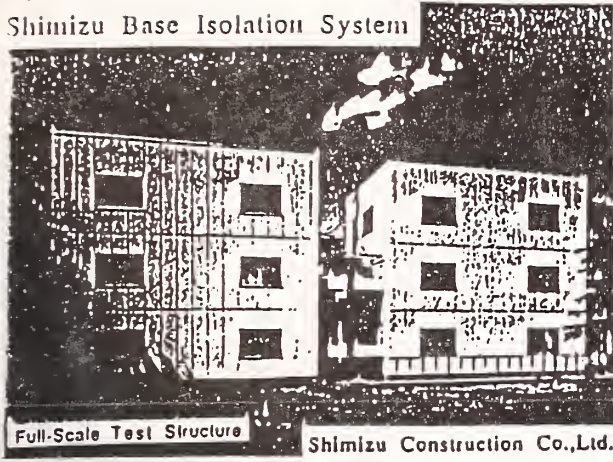


Fig. 17 General View

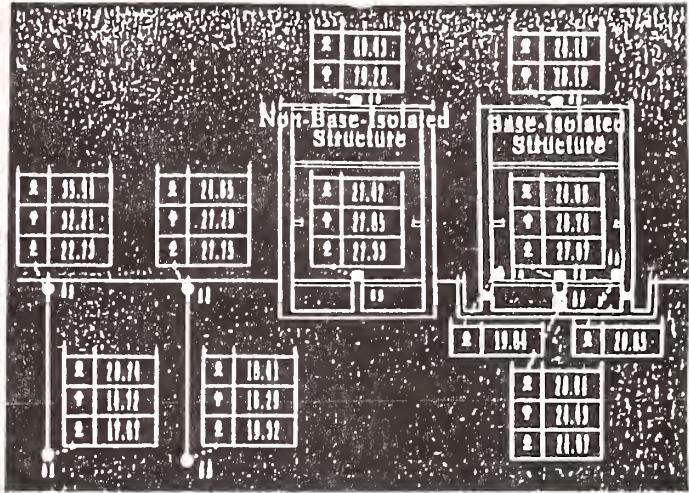


Fig. 18 Example of Observed Motions

Shimizu Base Isolation System

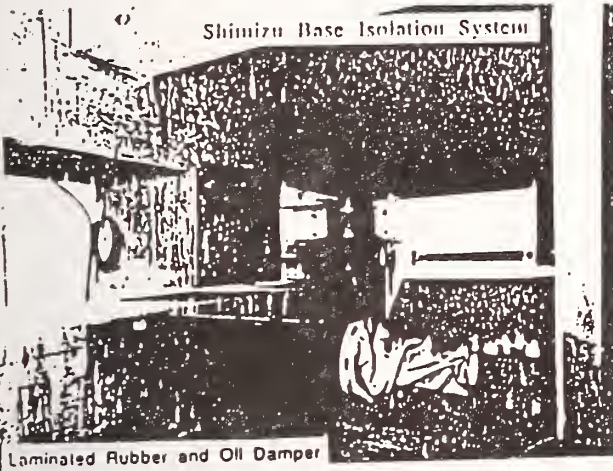


Fig. 19 Installed Devices

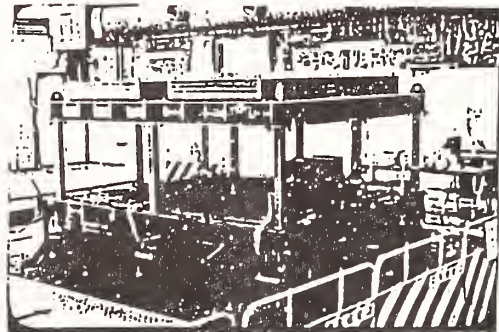


Fig. 21 General View of Shaking Table Testing Using Scale Model

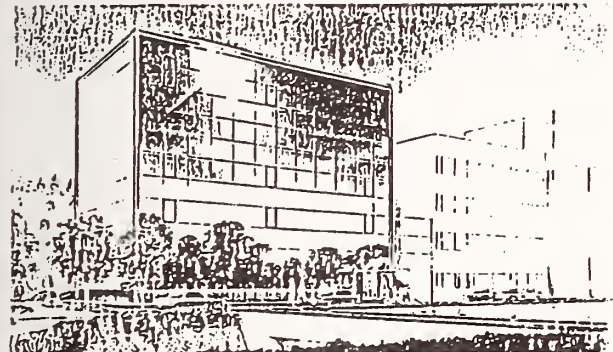


Fig. 20 Perspective View of Planning Building

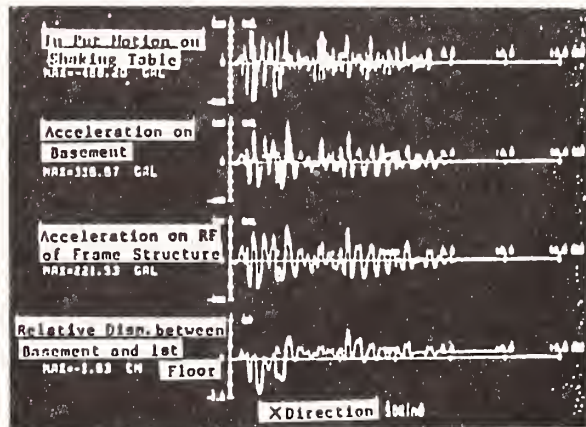


Fig. 22 Measured Accelerograms

# Shaking Table Test on the Ridge Response During Earthquake

By

Yasushi Sasaki<sup>1</sup>, Tetsuro Kuwabara<sup>2</sup> and Seitaro Yoshimi<sup>3</sup>

## SUMMARY

The large-scale slope failure that occurred at the southern flank of Mt. Ontake on the occasion of the Nagano-ken-seibu Earthquake of 1984 caused much loss of life as well as property. This report presents the results of the model vibration tests conducted for the purpose of examining the dynamic response characteristics of large-scale slopes, including acceleration response characteristics, vibration modes and strain distribution.

KEY WORDS: Large-scale Slope, Dynamic Response Characteristic, Model Vibration Test, Vibration Mode, Strain Distribution.

## 1. FOREWORD

On the occasion of the Nagano-ken-seibu Earthquake (M=6.8) of September 14, 1984, a large-scale slope failure occurred at the southern flank of Mt. Ontake, about 10 km distant from the epicenter, with the collapse volume estimated at about  $3.4 \times 10^7 \text{ m}^3$ , as shown in Photo 1. Such a large-scale slope failure has been examined from various viewpoints, but the dynamic response characteristics of the slope have not yet been fully examined. Thus, in order to obtain the fundamental knowledge for clarifying the mechanism of generation of a large-scale slope failure by an earthquake, a series of model vibration tests were carried out. Using an elastic silicone rubber, six scale models of a slope including the ridge were each fabricated on a frame having a rigid boundary between the bottom and the side. For the tests, a large shaking table in the vibration laboratory of the Public Works Research Institute was used. It was designed for vibration in two directions, horizontal and vertical, and each model was sinusoidally vibrated in the direction of the ridge and the direction at right angles to the ridge, or the vertical direction. The excitation frequency was changed over 3-60 Hz at intervals of 0.5 Hz, and the response acceleration in one or two directions inside the model and on the surface of the model were measured. From the response accelerations of measurement and observation

by means of stroboscope, the condition of vibration of the large-scale slope, the strain distribution, resonant frequency by configuration of the slope and the change of the response acceleration ratio were examined to find the fundamental characteristics of the dynamic response of the large-scale slope.

## 2. TESTING PROCEDURE

### 2.1 Model Dimensions

The slope models were fabricated in the form of a simplified triangular pyramid of the ridge including the large scale slope. An outline of the slope model is shown in Photo 2. The model dimensions were determined with the height of the maximum vertical cross-section fixed at 21.2 cm and by giving the angle  $\alpha$  at which the ridge line makes the horizontal plane (referred to as "ridge angle" in the following), and the angle  $\beta$  at which the slope makes with the horizontal plane in the maximum vertical cross-section (referred to as the "slope angle" in the following). The models were designed for a total of six cases, (i.e. four cases with the slope angle  $\beta$  fixed at  $45^\circ$  and the ridge angle  $\alpha$  changed for  $15^\circ$ ,  $20^\circ$ ,  $25^\circ$  and  $30^\circ$  and two cases with the ridge angle  $\alpha$  fixed at  $25^\circ$  and the slope angle  $\beta$  changed for  $30^\circ$  and  $60^\circ$ ). Figure 1 and Table 1 show the dimensions of the slope models. The frame was of steel with a bottom 120 cm wide and 220 cm long, and for the ground having an angle of  $45^\circ$  to the bottom, gypsum and a wooden flask were used. To the surface of the steel sheet of the bottom and the ground slope surface, a hard PVC sheet was cemented to prevent adhesion to the silicone rubber used as model material and improper hardening due to catalytic toxicity.

---

<sup>1</sup>Dr. Eng., Head, Ground Vibration Division, Earthquake Disaster Prevention Department, Public Works Research Institute, Ministry of Construction

<sup>2</sup>Research Engineer, Ground Vibration Division, ditto

<sup>3</sup>Ground Vibration Division, ditto

## 2.2 Model Fabrication

Elastic silicone rubber was used for the model material. This silicone rubber is expensive, but it allows the easy fabrication of a model of low elasticity and has the feature that the characteristics change little with elapse of time. For Case 6, the model was fabricated in eight layers as the accelerometers were all installed inside the model. For the other five cases, the model was fabricated in three layers to embed the accelerometers in the model, while the accelerometers to be installed on the model surface were installed in the notches on the model surface after completion of the model. For the model flask, a thick acrylic sheet was used, and silicone rubber in the form of a liquid was placed and cured thoroughly, while an accelerometer was installed at the specified position before the next layer was placed. After placement, the silicone rubber was cured thoroughly, the flask removed, and in order for observation of the movement of the model, 2 mm white thick lines were drawn on the model at intervals of 5 cm.

## 2.3 Physical Properties of Silicone Rubber

For the models of Cases 1 through 5, three test pieces were prepared for each layer, and for the model of Case 6, one test piece prepared for each layer. These test pieces were in the form of a cylinder of 5 cm diameter and 10 cm height, and from the size and weight of such test piece and by cyclic unconfined compression testing, the unit volume mass  $\rho$  ( $\text{g/cm}^3$ ), shearing modulus  $G$  ( $\text{kgf/cm}^2$ ) and damping factor  $h$  (%) were obtained. Here, for the diameter and height of test piece, the mean values of three measurements with vernier calipers used at every  $120^\circ$  in the peripheral direction were used. The modulus of elasticity  $E$  ( $\text{kgf/cm}^2$ ) was obtained from the axial stress and axial strain which were obtained by using the load and displacement in the cyclic unconfined compression test, while the shearing modulus  $G$  ( $\text{kgf/cm}^2$ ) was taken to be of a value obtainable by dividing the modulus of elasticity by 3, with Poisson's ratio assumed to be 0.5. Furthermore, for the damping factor  $h$ , the damping energy  $\Delta W$  obtained from the result of the cyclic unconfined compression test was used. From the foregoing, the mean values of the unit volume mass  $\rho$  ( $\text{g/cm}^3$ ), shearing modulus  $G$  ( $\text{kgf/cm}^2$ ) and damping factor  $h$  (%) were obtained. The results are shown in Table 2.

## 2.4 Measurement Items and Measurement Methods

The response acceleration was measured by the accelerometers installed inside the model, on

the model surface and on the frame. The accelerometer is of a miniature size of 5 mm square x 10 mm and is adapted for measurement of  $+2G$  in one direction. The positions of installation of the accelerometers in Case 1 are shown in Figure 2. In Case 6, the accelerometers were installed at 12 points in the model for measurement of the response acceleration in the direction at right angles to the ridge. In Cases 1 through 5, the accelerometers were installed at two places in the model so that the response acceleration in the direction at right angles to the ridge could be measured. At the same time, they were installed on the model surface in either of the following two modes. In the unidirectional test, the accelerometers were installed at 10 places (11 places for Case 3) on the model surface so that the response acceleration in the excitation direction, that is, the direction of the ridge, the direction at right angles to the ridge or the vertical direction, could be measured. In the two-directional measurement, they were installed at 6 places on the model surface of Case 1, or points 3, 6, 8, 10, 11 and 14 as shown in Figure 2, so that the response accelerations in the excitation direction and the direction orthogonal to the exciting direction could be measured. At resonant frequency, photographic and video pictures were taken to observe the vibrating conditions of the model. Particularly, in the video recording, a stroboscope was used for minute observation of the vibrating conditions of the model.

## 2.5 Excitation Conditions and Data Recording Conditions

For excitation, a large shaking table in the vibration laboratory of the Public Works Research Institute was used as it enabled exciting in both horizontal and vertical directions, and the excitation was made in one direction of (a) ridge direction, (b) direction at right angles to ridge or (c) vertical direction shown in Figure 1. In the unidirectional measurement, the model was subjected to 115 frequencies of excitation acted by a sinusoidal input motion of 200 gal in maximum acceleration which was varied over 3-60 Hz at a pitch of 0.5 Hz, and the response acceleration at the respective parts of the model were digitally recorded for 2 seconds at 400 Hz sampling frequency.

## 2.6 Methods of Calculation of Acceleration Response Ratio, Displacement and Strain

The acceleration response ratio in the resonant test was obtained as a power ratio of the acceleration data to the response acceleration data in the frame excitation direction by the formula (1),

$$\alpha_j = \sqrt{\frac{\sum_{i=1}^n a_j(i \cdot \Delta t)^2}{n}} \quad (1)$$

where  $\alpha_j$ : Acceleration response ratio at measurement point  $j$ ;  
 $a_1(t)$ : Input Acceleration data (cm/sec<sup>2</sup>);  
 $a_j(t)$ : Acceleration data at measurement point  $j$  (cm/sec<sup>2</sup>);  
 $n$ : Number of acceleration data (400 Hz X 2 sec = 800 points).

Displacement of the measurement point was taken to be the relative displacement to the frame and was obtained, in view of the sinusoidal excitation, by the formula (2),

$$d_j(t) = \frac{10 \times (a_j(t) - a_1(t))}{-(2\pi f)^2} \quad (2)$$

where  $d_j(t)$ : Relative displacement of measurement point  $j$  to frame (mm);  
 $a_1(t)$ : Input Acceleration (cm/sec<sup>2</sup>);  
 $a_j(t)$ : Response acceleration of measurement point  $j$  (cm/sec<sup>2</sup>);  
 $f$ : Excitation frequency (Hz).

Furthermore for examination of the shear strain distribution in the model, the shear strain was approximately obtained in use of the displacement data according to the two-directional measurement. Assuming that the displacement ( $u$ ,  $v$ ) of a vertex of the triangle shown in Figure 3 could be expressed by linear equations of the coordinates  $X$  and  $Y$  of the vertex, as shown by formula (3).

$$\begin{aligned} u &= \alpha_0 + \alpha_1 X + \alpha_2 Y \\ v &= \alpha_3 + \alpha_4 X + \alpha_5 Y \end{aligned} \quad (3)$$

The coefficient  $\alpha$  in formula (3) would be obtainable by using the coordinates and the displacement of three points. Next, the strain component of the triangle would be obtained by formula (4).

$$\begin{aligned} \epsilon_x &= \frac{\partial u}{\partial X} = \alpha_1, \quad \epsilon_y = \frac{\partial v}{\partial Y} = \alpha_5, \\ \gamma_{xy} &= \frac{\partial u}{\partial Y} + \frac{\partial v}{\partial X} = \alpha_2 + \alpha_4 \end{aligned} \quad (4)$$

From the foregoing, the maximum shear strain of the triangle could be calculated by the formula (5).

$$\gamma_{\max} = \epsilon_1 - \epsilon_3 = 2 \cdot \sqrt{\left(\frac{\epsilon_x - \epsilon_y}{2}\right)^2 + \frac{1}{4} \gamma_{xy}^2} \quad (5)$$

### 3. TEST RESULTS

#### 3.1 Vibrating Conditions

A diagram of the acceleration response ratios at ch 11 which was installed the maximum vertical cross-section is shown according to the direction of excitation, viz. (a) excitation in ridge direction, (b) excitation in direction at right angles to the ridge and (c) excitation in the vertical direction, in Figure 4. From the diagram, a resonant frequency is noted at 17.0 Hz at which the acceleration response ratio becomes 4.0 times in (a) the excitation in ridge direction. In (b) excitation in the direction at right angles to ridge, a resonant frequency is noted at 15.0 Hz at which the acceleration response ratio becomes 5.4 times. Furthermore, in (c) excitation in vertical direction, although the acceleration response ratio is smaller than those in the excitations in the horizontal direction, the ratio becomes 2.7 times and 2.5 times at about 16.5 Hz and 24.5 Hz. The vibrating conditions of the model at these resonant frequencies are shown below.

##### 3.1.1 Excitation in Ridge Direction

The region where the model displacement is great under the sinusoidal excitation of 17.0 Hz in the ridge direction is at about the maximum vertical cross-section along the ridge line or at about the upper part along the maximum vertical cross-section for the side. Figure 5 shows the conditions of vibration under the excitation in the direction of the ridge. Here, the displacements of the measurement points are exaggerated when compared with the model size. From the side view (b) of the drawing, at the front part of the ridge, the movement in the horizontal direction is predominant under the excitation in the ridge direction, while at the upper part of the maximum vertical cross-section, the displacement amplitudes in both the horizontal and vertical directions are increasing to vibration approximately in the ridge direction. Summing up the foregoing results of measurement and the results of observation by stroboscope, the vibration under excitation in the ridge direction is a movement in the form of an arc at the central part of the ridge, and at the front part of the ridge, the movement in the horizontal direction is predominant, while at the central and upper parts of the ridge, the movement in the direction of the ridge line is predominant, and the displacement amplitude is maximum at the central part of the ridge.

### 3.1.2 Excitation in Direction at Right Angles to Ridge

The region where the model displacement is great under the sinusoidal excitation of 15.0 Hz in the direction at right angles to the ridge is at about the maximum vertical cross-section along the ridge line, and in the maximum vertical cross-section, at about the upper part. The conditions of vibration under the excitation in direction at right angles to the ridge are shown in Figure 6. From the plan (a) in the same drawing, the displacement is the largest at the central part of the ridge line under the excitation in direction at right angles to the ridge, and the displacement at the upper part of the ridge line is smaller than that at the lower part of the ridge line. Also, from the conditions of displacement in the maximum vertical cross-section shown in the drawing at (b), the increase of the displacement at the central lower part of the cross-section is noticeable.

### 3.1.3 Excitation in Vertical Direction

In the model vibration under the sinusoidal excitation of 16.5 Hz in the vertical direction, it was difficult to confirm the model displacement by observation as compared with that under excitation in the direction of the ridge and that at right angles to ridge, but the vibration at about 16.5 Hz was nearly similar to that at about 17.0 Hz under excitation in the ridge direction.

## 3.2 Strain Distribution

Comparison of the strains varying with the direction of excitation was made with the different excitation frequencies and excitation accelerations by the direction of excitation converted to those of 16.5 Hz, 200 gal for the horizontal directions and 16.5 Hz, 100 gal for the vertical direction. For excitation in direction at right angles to the reidge, in consideration of the acceleration response ratio at the measurement point (ch 11) at the upper part of the maximum vertical cross-section changing to 0.83 time with change of the excitation frequency from 15.0 Hz to 16.5 Hz and also the actual excitation acceleration of 168 gal with respect to the target excitation acceleration of 200 gal, a multiplying factor of  $0.83 \times 1.19 = 0.99$  time was taken. For excitation in the ridge direction, in consideration of the actual excitation acceleration of 400 gal with respect to the target excitation acceleration of 400 gal, a multiplication factor of 0.49 time was taken, and for the excitation in vertical direction, in consideration of the actual excitation acceleration of 420 gal

with respect to the target excitation acceleration of 500 gal, a multiplication factor of 0.24 time was taken. Then, by multiplying the strain values in the excitations of the different directions by the foregoing multiplication factors, the varying strains by the direction of excitation was examined. The strain distributions obtained by the foregoing procedure are shown in Figure 7. From the drawing, a large strain is occurring in the region not adjacent to the side boundary under the excitation in the ridge direction and also at the lower central part of the maximum vertical cross-section under the excitation in direction at right angles to ridge, while the strain along the ridge line under the excitation in the direction at right angles to ridge and that under the excitation in the vertical direction are not so large. However, the strain under the excitation in vertical direction presents a similar distribution to that of the strain under the excitation in the ridge direction, and the acceleration in the vertical direction is estimated to be about 1/2 of that in the horizontal direction, and so where the vertical movement is similarly great to the horizontal movement, the strain generated by the simultaneous excitation in both the ridge direction and the vertical direction will increase further.

## 3.3 Acceleration Response Ratios and Resonant Frequencies by Model Shape

Figure 8 shows the acceleration response ratios by the excitation direction and model shape for each case. The plot point of the acceleration response ratio is ch 11 (or ch 14 for Case 3) which was installed on the maximum vertical cross-section, and the acceleration response ratios under (a) excitation in ridge direction, (b) excitation in the direction right angles to ridge and (c) excitation in the vertical direction are shown together. From the diagrams, each case shows the primary resonant frequencies in the respective excitation directions present between 13 Hz and 18 Hz. Particularly, in Case 5 for the ridge angle of 25° and slope angle of 30°, the resonant frequencies in the respective excitation directions are very close to one another. Furthermore, in the order of Cases 1, 2 and 3, or in order of the ridge angles of 25°, 20° and 15°, the acceleration response ratio at the primary resonant frequencies under the excitation in the direction at right angles to ridge tends to decrease, while the acceleration response ratio at the secondary resonant frequencies tends to increase. This may be accounted for by the increasing distance between the midpoint of the ridge line and the measurement point with the decreasing ridge

angle. Effects of the ridge angle and slope angle on the acceleration response ratio and resonant frequency were examined for each direction of excitation. The results are shown in Figures 9 and 10. With the increasing ridge angle, the acceleration response ratio showed the tendency to decrease in the case of the excitation in the ridge direction, no change in the case of the excitation in the direction at right angles to ridge, or increase in the case of the excitation in the vertical direction. The resonant frequency tended to increase with an increasing ridge angle in the case of any direction of excitation. Changes with increasing slope angle were not so appreciable as those in the case of the ridge angle.

#### 4. CONVERSION OF THE TEST RESULTS TO THE PROTOTYPE

When a vibration test is made with a scale model used, the law of similarity applicable is a problem. In the present tests, however, the equation governing the phenomena is the "equation of vibration," and so as a principle for obtaining the law of similarity, the equation of vibration should be used. However, the vibration of a slope observed in a model vibration test is three-dimensional, and formulation of the phenomena in use of such a vibration equation is difficult. Then, assuming two-dimensional shearing vibration, the similarity ratio was determined for the equation of motion of such shearing vibration<sup>1), 2)</sup>. The equation of shearing vibration motion is shown by the formula (6),

$$\frac{\partial^2 X}{\partial t^2} = \frac{G}{\rho} \frac{\partial^2 X}{\partial Z^2} \quad (6)$$

where  $X$ : Horizontal displacement;  
 $t$ : Time;  
 $G$ : Shearing modulus  
 $\rho$ : Density;  
 $Z$ : Height.

The constants of the model against those of the prototype slope are determined as below.

$$\kappa = Z_p/Z_m \quad (7.1)$$

$$\mu = \rho_p/\rho_m \quad (7.2)$$

$$\alpha = t_p/t_m \quad (7.3)$$

$$\nu = G_p/G_m \quad (7.4)$$

$$\beta = X_p/X_m \quad (7.5)$$

where  $p$ : Constants of prototype slope;  
 $m$ : Constants of model.

By substituting formulas (7) in formula (6), there is obtained formula (8).

$$\frac{\partial^2 X_m}{\partial t_m^2} = \frac{\nu \cdot \alpha^2}{\mu \cdot \kappa^2} \cdot \frac{G_m}{\rho_m} \cdot \frac{\partial^2 X_m}{\partial Z_m^2} \quad (8)$$

Then, with the shear motion assumed, the following formula (9) is valid for between the slope size, physical property and the time axis.

$$\frac{\nu \cdot \alpha^2}{\mu \cdot \kappa^2} = 1 \quad (9)$$

The height  $Z_m$  of the model slope is about 40 cm, and so if  $Z_p=500$  m, then  $\kappa=1,250$ . Similarly, if  $\rho_m=0.98$  g/cm<sup>3</sup> and  $\rho_p=2.5$  g/cm<sup>3</sup>, then  $\mu=2.55$ , and if  $G_m=0.2$  kgf/cm<sup>2</sup> and  $G_p=100,000$  kgf/cm<sup>2</sup>, then  $\nu=500,000$ .

Then, the value of  $\alpha$  for satisfying formula (9) is obtainable by the formula (10).

$$\alpha = \sqrt{\frac{\mu \cdot \kappa^2}{\nu}} = \sqrt{\frac{2.55 \times (1,250)^2}{500,000}} = 2.82 \quad (10)$$

By substituting  $\alpha=2.82$  in formula (7.3), there is obtained the formula

$$t_p = 2.82 t_m \quad (11)$$

From formula (11), the primary resonant frequency for a slope of  $Z_p=500$  m,  $\rho_p=2.5$  g/cm<sup>3</sup> and  $G_p=100,000$  kgf/cm<sup>2</sup> is, as the model frequency is 13-18 Hz about 4.6-6.4 Hz. Figure 11 shows the range of primary resonant frequencies of slopes with the actual slope height taken as a parameter.

#### 5. CONCLUSION

Through the present tests, the following was clarified.

- (1) The model resonant frequencies under excitation in the direction of the ridge are noted at about 16.0-17.5 Hz, and the form of vibration is an arc movement at the central part of the ridge. At the front of the ridge, motion in the horizontal direction is predominant, while at the central and upper parts of the ridge, motion in a direction of the ridge line is predominant, and the displacement amplitude is maximum at the central part of the ridge.
- (2) Under excitation in the direction at right angles to the ridge, the resonant frequencies are noted at about 13.0-15.0 Hz, and the form of vibration is such that the horizontal displacement is maximum at the central part of the ridge line and that the displacement at the upper part of the ridge line is smaller than that at the lower part of the ridge line. Furthermore, in the maximum

vertical cross-section, the displacement increases appreciably at the central lower part of the cross-section.

- (3) Under excitation in the vertical direction, the resonant frequencies were noted at about 15-16.5 Hz and 22-26 Hz, and at about the primary resonant frequencies, arc movement at the central part of the ridge was noted as in the case of excitation in the direction of the ridge.
- (4) For comparison of the strains according to the direction of excitation with one another, they were reduced to those under the excitation frequency of 16.5 Hz and under 200 gal for the two horizontal directions and 100 gal for the vertical direction. Consequently, it is noted that a relatively large strain occurs in the regions at the central and lower part of the ridge line in the case of excitation in the ridge direction or at the central lower part of the maximum vertical cross-section in the case of the excitation in the direction at right angles to the ridge.
- (5) Under the excitation in the ridge direction, the resonant frequencies were 16.0-17.5 Hz, and the acceleration response ratios were 4.0-6.2, and under the excitation in the direction at right angles to the ridge, the resonant frequencies were 13.0-15.0 Hz, and the acceleration response ratios were 5.2-6.7. Under excitation in the vertical direction, the primary resonant frequencies were 15.0-16.5 Hz, and the acceleration response ratios were 2.0-2.7.
- (6) With the increasing ridge angle, the acceleration response ratio showed the following trend of change: decreasing in the case of the excitation in the ridge direction; no change in the case of the excitation in the direction at right angles to the ridge; and increasing in the case of the excitation in the vertical direction. For the resonant frequency, a trend to increase with the increasing ridge angle was noted in all the directions of excitation. For the change of the resonant frequency and acceleration response ratio with the increasing slope angle, no significant trends were noted within the range of the present tests.
- (7) With the model vibration assumed to be of shearing vibration, the resonant frequencies of the prototype slopes obtained with a law of similarity applied were about 4.6-6.4 Hz against

the model resonant frequencies of 13-18 Hz when the prototype slope height was assumed to be 500 m.

In the present model vibration tests, the boundary conditions are simplified, and an elastic material is used as the model material, and so it is difficult to say that the behavior of actual slopes are correctly reproduced, but this much may be said that the fundamental matters have been determined with respect to the forms of vibration by the direction of excitation, strain distribution, strains according to the direction of excitation and difference in the form of vibration due to the model shape, and it will be necessary to further examine the dynamic response characteristics of large-scale slopes in earthquake with the effects of the law of similarity and boundary conditions taken into consideration.

#### REFERENCES

- 1) K. Matsumura: Deformation of Soil Embankment by Seismic Movement, Journal of Research, Public Works Research Institute, No. 28, October 1934
- 2) Report on Model Vibration Tests of Embankment Having Profile Properties Changed: Soil Dynamic Division, Public Works Research Institute, January 1981



Photo 1 Large-scale Slope Failure at Southern Frank of Mt. Ontake

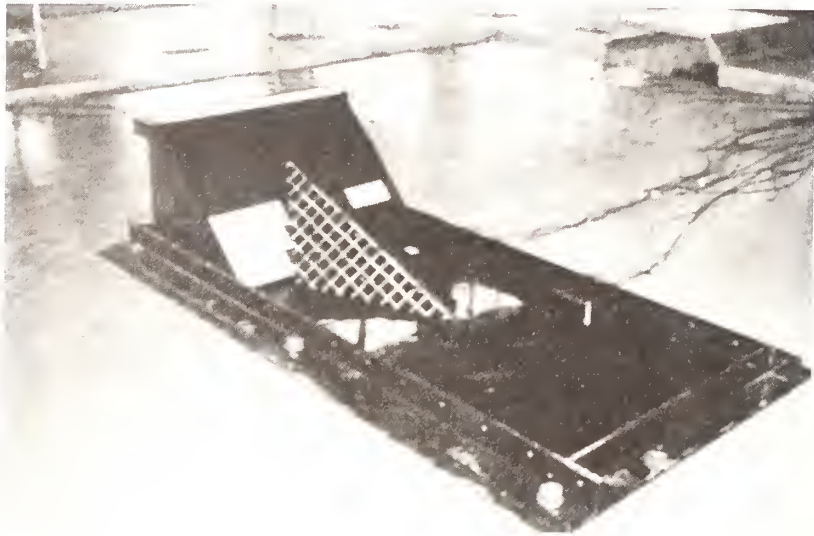


Photo 2 Overall View of Slope Model

Table 1 Slope Model Dimensions

Model No.	Model Dimensions				
	$W$ (cm)	$L$ (cm)	$h$ (cm)	$\alpha$	$\beta$
Case 1	42.4	85.2	39.7	25°	45°
Case 2	42.4	91.5	33.3	20°	45°
Case 3	42.4	108.1	29.0	15°	45°
Case 4	24.4	85.2	39.7	25°	60°
Case 5	73.4	85.2	39.7	25°	30°
Case 6	42.4	86.6	50.0	30°	45°

Table 2 Mean Values of Model Properties

Model No.	Unit Volume Mass $\rho$ (g/cm <sup>3</sup> )	Shear Modulus $G$ (kgf/cm <sup>2</sup> )	Damping Factor $h$ (%)
1	0.98	0.27	4.9
2	0.98	0.27	4.9
3	1.01	0.22	5.1
4	0.98	0.26	5.0
5	0.98	0.26	5.0
6	0.99	0.19	5.4

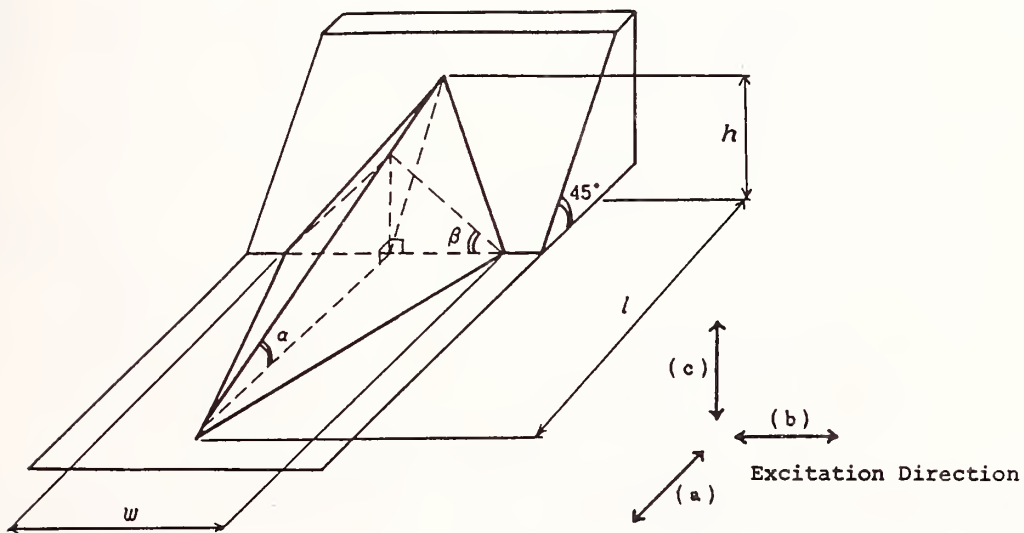


Fig. 1 Slope Model Dimension

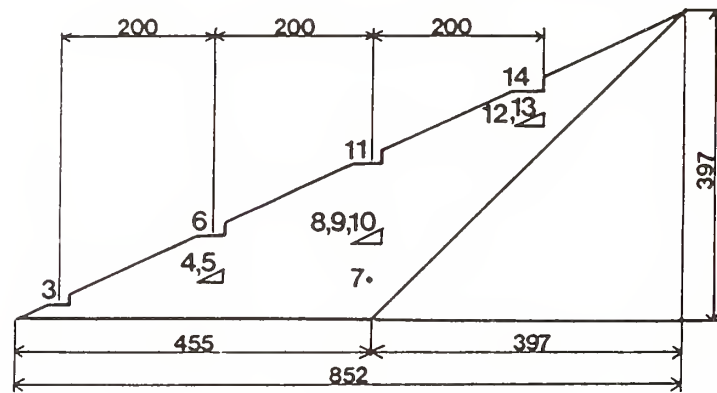
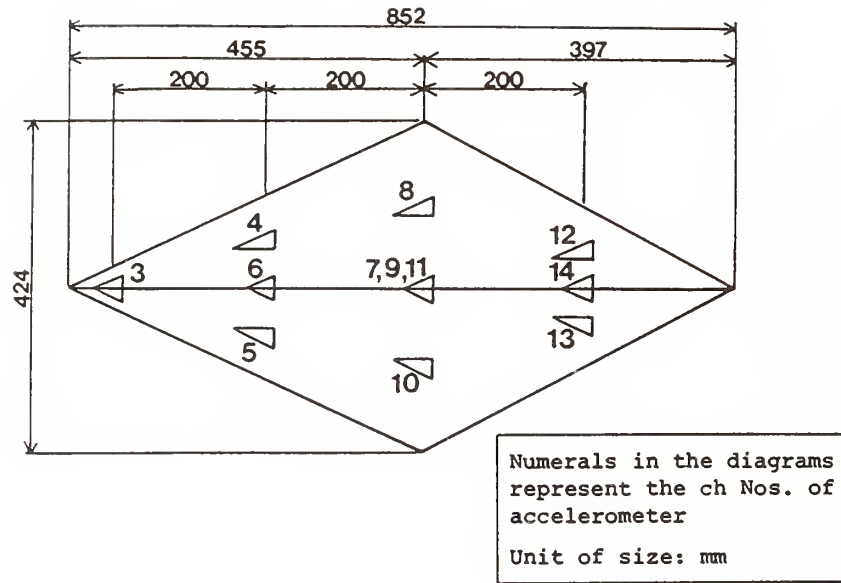


Fig. 2 Locations of Accelerometers (Case 1)

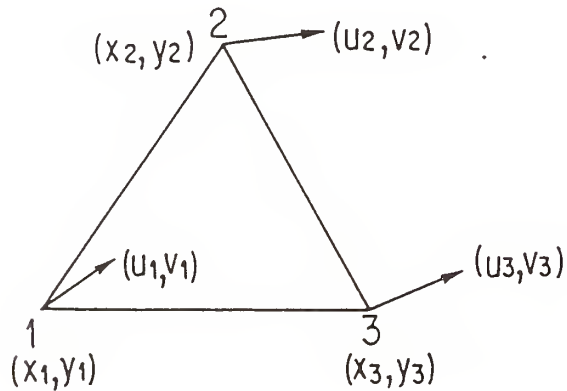


Fig. 3 Element for Strain Calculation

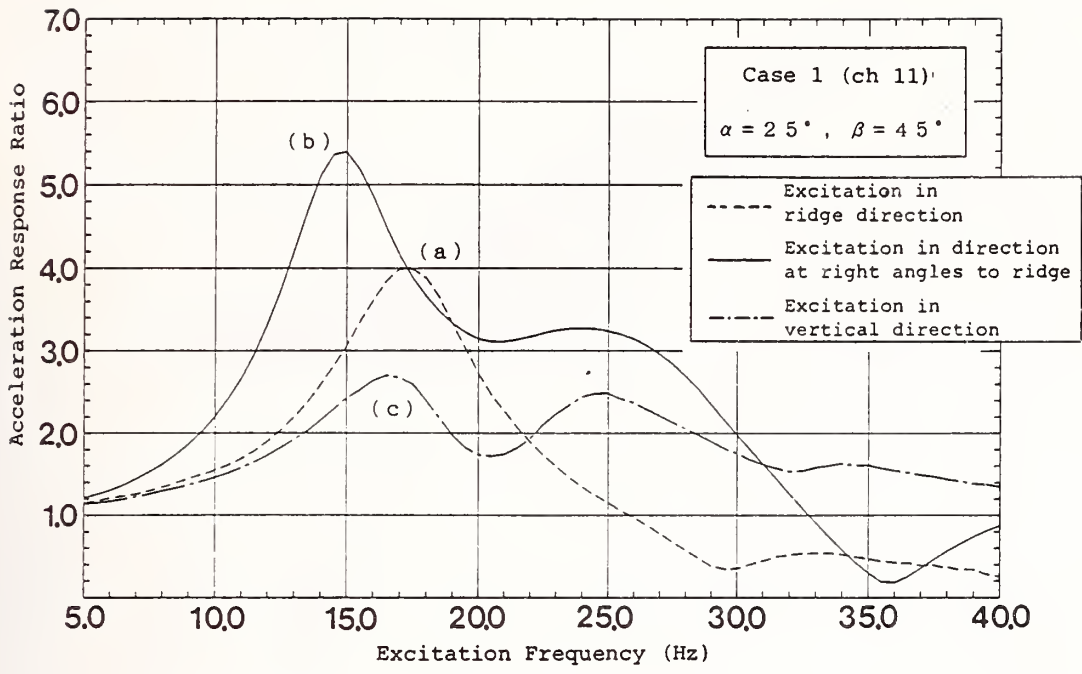


Fig. 4 Acceleration Response Ratio Curves by Direction of Excitation

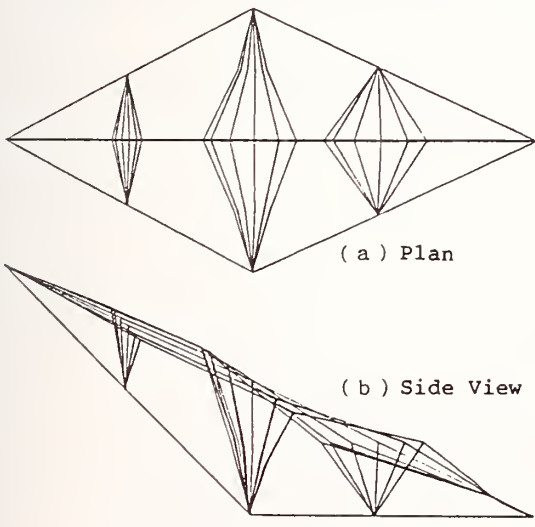


Fig. 5 Vibration Mode of Model under Excitation in Ridge Direction (Case 1, 17Hz)

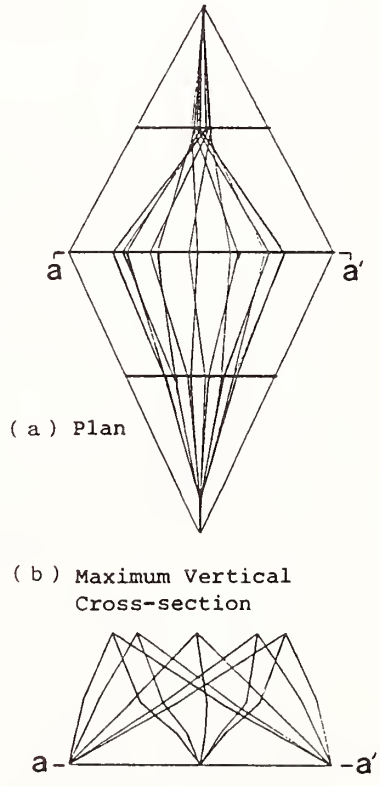
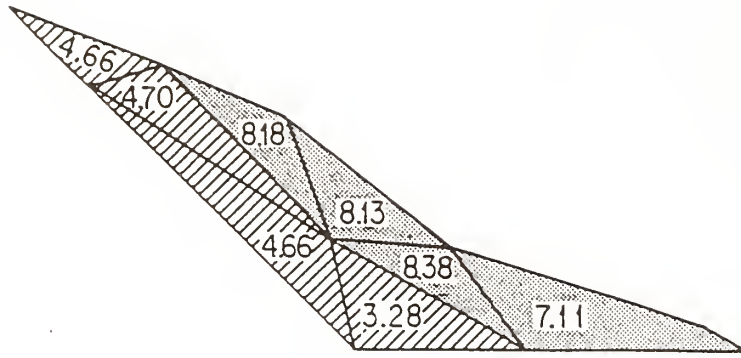
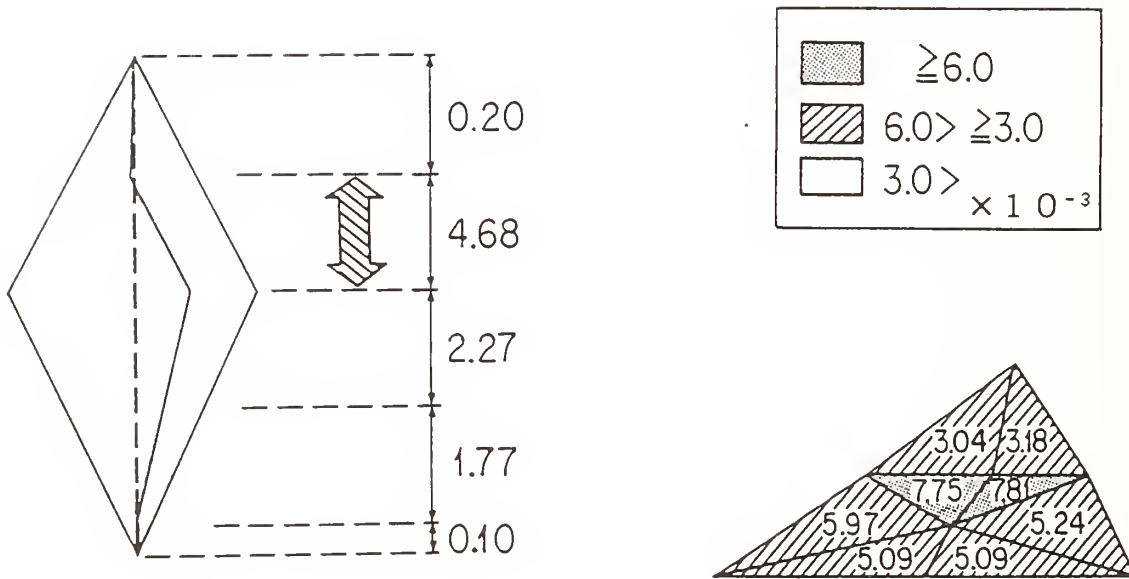


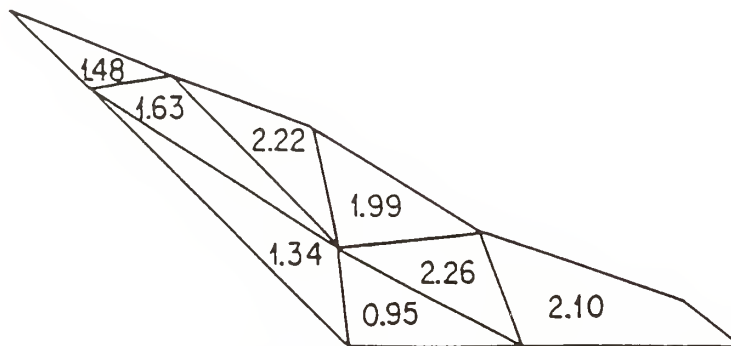
Fig. 6 Vibration Mode of Model under Excitation in Direction at Right Angles to Ridge



(a) Excitation in Ridge Direction

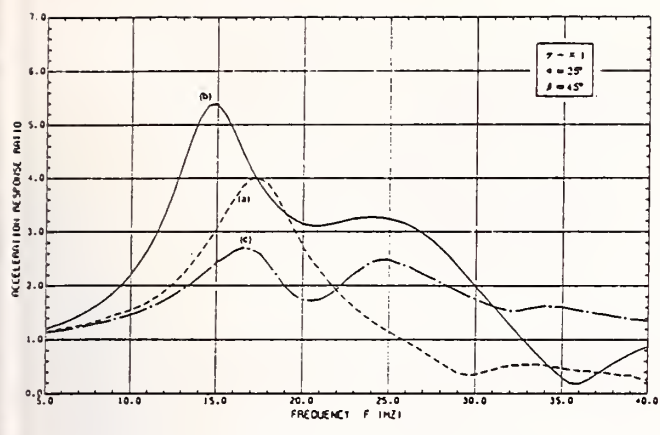


(b) Excitation in Direction at Right Angle to Ridge

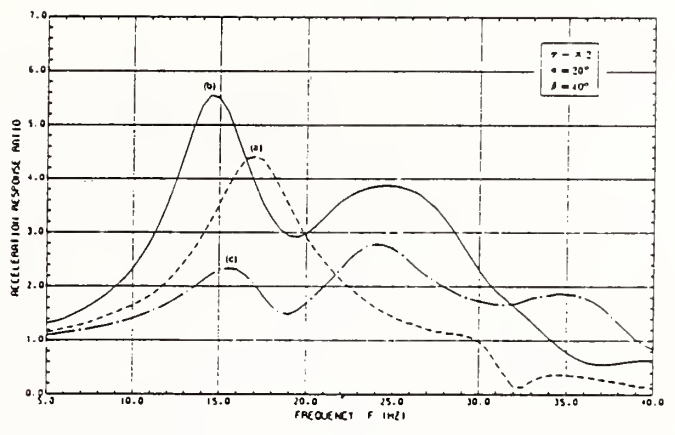


(c) Excitation in Vertical Direction

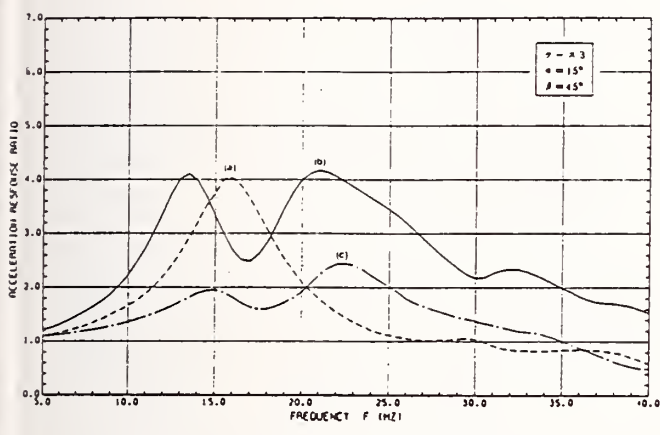
Fig. 7 Shear Strains by Direction of Excitation



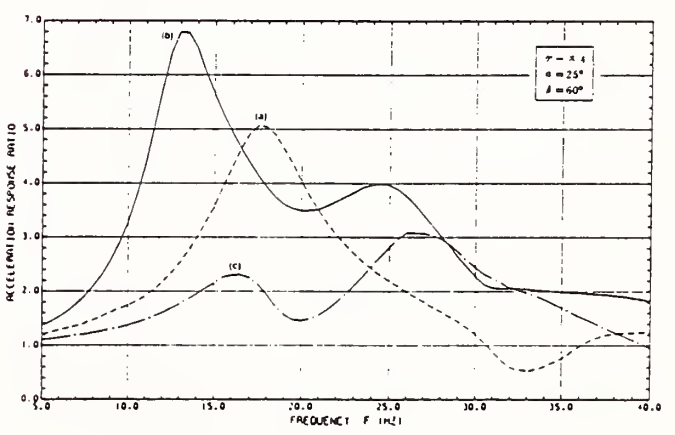
Case 1 ( $\alpha = 25^\circ$ ,  $\beta = 45^\circ$ )



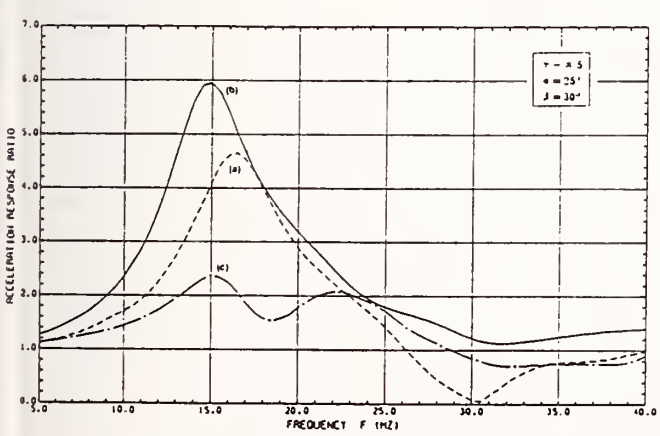
Case 2 ( $\alpha = 20^\circ$ ,  $\beta = 45^\circ$ )



Case 3 ( $\alpha = 15^\circ$ ,  $\beta = 45^\circ$ )

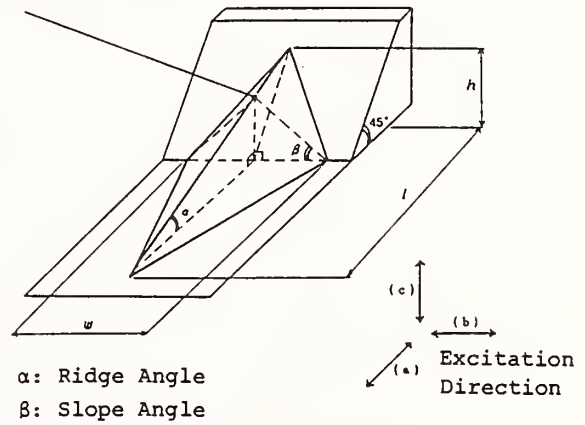


Case 4 ( $\alpha = 25^\circ$ ,  $\beta = 60^\circ$ )



Case 5 ( $\alpha = 25^\circ$ ,  $\beta = 30^\circ$ )

Measurement Point ch 11  
(ch 14 for Case 3)



- $\alpha$ : Ridge Angle
- $\beta$ : Slope Angle
- (a) Excitation in Ridge Direction
- (b) Excitation in Direction at Right Angles to Ridge
- (c) Excitation in Vertical Direction

Fig. 8 Acceleration Response Ratios by Direction of Excitation and Shape of Model

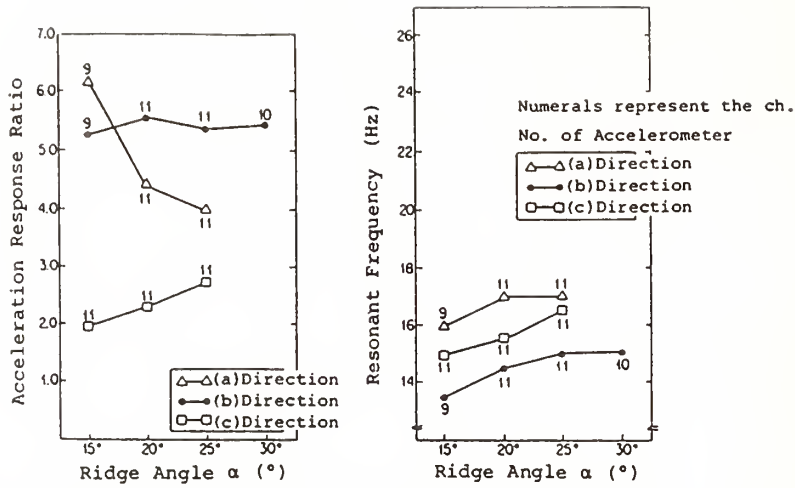


Fig. 9 Effect of Ridge Angle on Acceleration Response Ratio and Resonant Frequency

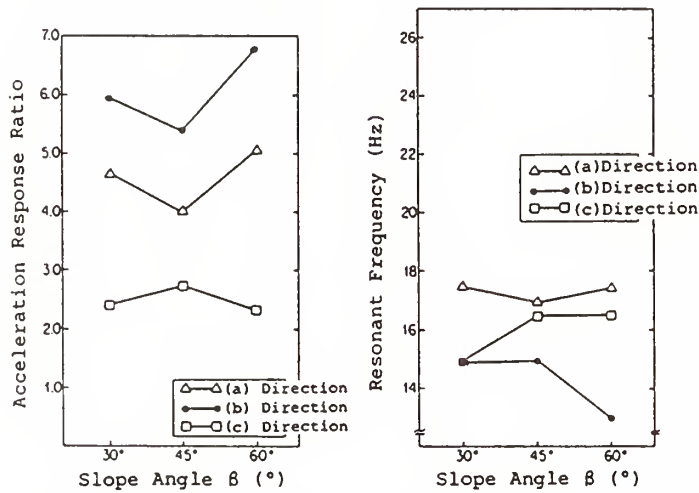


Fig. 10 Effect of Slope Angle on Acceleration Response Ratio and Resonant Frequency

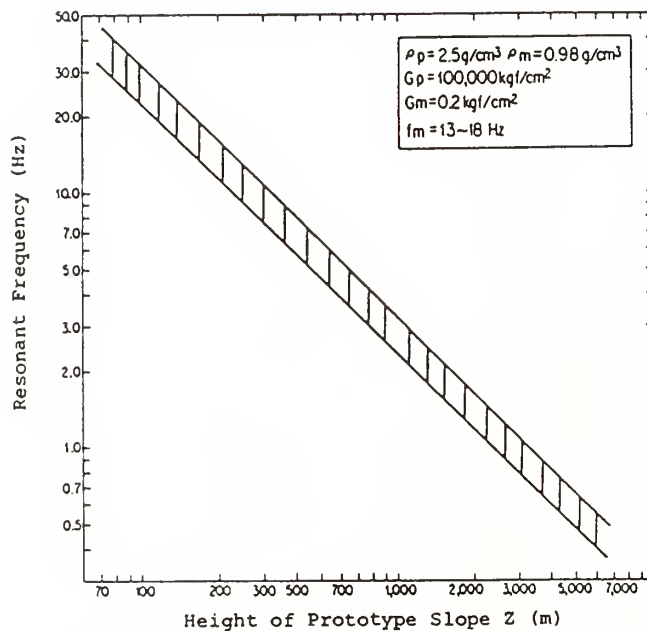


Fig. 11 Resonant Frequency Estimation of Prototype Slope

# Investigation of Two Buildings Shaken During the 19 September 1985 Mexico Earthquake

BY

Douglas A. Foutch<sup>1</sup>, Keith D. Hjelmstad<sup>1</sup> and Enrique Del Valle Calderon<sup>2</sup>

## ABSTRACT

A great earthquake such as the 19 September 1985 Mexico Earthquake is a tragic event that takes thousands of lives and destroys buildings and other structures worth many millions of dollars. In the aftermath of such an event, it is vital that as many lessons as possible be learned from the tragedy, so that new buildings might be designed and constructed better or existing structures strengthened against future shocks.

The main purpose of this research is to evaluate the performance of two reinforced concrete buildings that were strengthened using structural steel members prior to the 19 September 1985 earthquake. The strengthening systems for both buildings were designed by Professor Enrique Del Valle of UNAM. Both buildings suffered major damage during a moderate earthquake that occurred in 1979. Even though these structures were in the vicinity of several collapsed buildings, they suffered very little damage during the 1985 earthquake. Forced vibration tests of the buildings and geotechnical investigations of the buildings were undertaken to evaluate the retrofit schemes that were used. The reasons for the excellent performance of these buildings will be ascertained and recommendations for similar schemes will be proposed and evaluated for U.S. practice.

## 1. DESCRIPTION OF THE STRUCTURES

Building B is a nine-story reinforced concrete frame building that stands 24.05m above grade. The building is irregular in plan, but measures roughly 10.8m x 17.6m as shown in Fig. 1. The floor system was a waffle slab, and additional reinforcing was provided in the slab along the frame lines to form the girders of the framing systems. The exterior frames in the longitudinal direction were infilled with syporex blocks. These were not considered in the seismic resistance of the building. However, no separation between the walls and the frame were provided.

As it vibrated in the transverse direction during the 1979 earthquake, the building impacted a four-story structure that was built next to it with a separation of only a few centimeters. This caused fracture in the some columns at that level as well as damage to the longitudinal walls. Transverse and longitudinal partition walls suffered damage at many levels. In order to add stiffness and strength to the buildings, diagonal cross bracing was added to the central bay of three of the transverse frames as shown in Fig. 1. The braces were fabricated by

continuously welding angles together toe-to-toe to form rectangular sections. The reinforced concrete columns of these bays were also reinforced using a lattice-type detail composed of angles at the corners and diagonal plates. This was necessary to accommodate high column axial forces that would result from the additional overturning moment and from the narrow bay size in the braced bay. Reinforced concrete shear walls 60mm thick were added to the exterior longitudinal walls. A small amount of damage occurred in the fourth story due to pounding with the adjacent building during the 1985 earthquake. It is conceivable that an upper story collapse would have occurred at this level if the retrofit system had not been installed.

The investigation to date has concentrated on Building A, a twelve-story reinforced concrete frame building that measures 11.4m x 21.3m in plan and stands 36.4m above the foundation level, excluding the penthouse. This building also has waffle slab floors which serve as the girders in the transverse and longitudinal frames. Syporex infills were added to the external walls in the longitudinal direction but were not considered as structural elements. Plan views of the foundation and typical floor of the retrofit structure are shown in Fig. 2. Elevation views of the original building are shown in Fig. 3.

Extensive damage was done to the building during the moderate earthquake that struck Mexico City on March 14, 1979. Beams and columns in the first three stories suffered severe flexural and shear cracking due to E-W (transverse) shaking. The damage was repaired using epoxy injection. New steel braced frames were attached to the exterior of the building at the north and south ends to resist E-W motion. This required strengthening the slabs at points of attachment to the new frames. New RC infilled walls 60mm thick were added to the 1-2 and 4-5 bays of Frames A and C to resist N-S motion. New footings and piles were also added under the columns of the new steel frames. An elevation view of the new steel frames is shown in Fig. 4.

## 2. EXPERIMENTAL AND ANALYTICAL INVESTIGATIONS

During January 1987, forced vibrations tests of the two buildings were conducted. Thanks to the

<sup>1</sup>University of Illinois at Urbana-Champaign, 208 Romine, Urbana, IL 61801, USA

<sup>2</sup>Universidad Nacional Autonoma de Mexico (UNAM), Mexico City, MEXICO

excellent preparations done by Professor Del Valle of UNAM, the testing program was completed with very few problems. Preliminary results for Building A are shown in Table 1. Prior to the addition of the new walls and frames, the period of the building in the E-W direction was measured to be about 1.85 seconds for ambient levels of vibration. The story weights before and after strengthening are shown in Table 2. Thus, the steel frames increased the stiffness of the building considerably as indicated by the current period of 1.25 seconds. The low damping in the E-W direction is also an indication that the steel frame dominates the response in this direction. Since the period of the site is thought to be about over 2.0 seconds, the stiffening effect of the steel frame which shifted the period of the building away from the danger region was the primary cause of the excellent behavior during the 1985 earthquake. The additional strength also played an important role. The building suffered no structural damage and only slight cracking of the new infill walls around the boundary.

One surprising result of the tests was the relatively large amount of foundation compliance present in both buildings. The translation and rotation of the base contributed over 50% of the roof motion as shown in Fig. 5. The first E-W mode for the structure before retrofit was calculated and is shown in Fig. 6. Note that, as expected, the foundation flexibility does not have as much effect on the flexible frame structure as it does on the stiff, braced frame building. The geotechnical studies reconfirmed the soft nature of the soil at the site. The soft clay is about 42m deep at the site and is characterized by blow count values of one or less for most of this depth and a water content that was as high as 465% at one location.

An analytical model of the building has been developed. Preliminary studies indicate that the steel frame carries over 90% of the seismic forces in the E-W direction. Also, the foundation flexibility increases the period of the structure from about 0.90 seconds to 1.25 seconds in the E-W direction. The preliminary analysis indicates that the base shear would be around 27% of the total weight of the building for the accelerogram recorded at the SCT location. Geotechnical studies at the site of Building A and at SCT indicate that the depth of soft clay and the water content is almost identical at each site. At 0.30W, the forces in the steel members are just at the allowable levels by AISC specifications. The base shear during the 1979 earthquake was estimated to have been about 0.09W. The strength of the building was calculated to be about 0.11W. This appears to be consistent with the observed damage. Had the structure not been retrofit, the base shear would have been around 0.80W during the 1985 earthquake. Thus, had the structure not been strengthened, it is quite likely that the building would have collapsed. The strengthening system was designed in accordance

with the 1976 Mexico City code, but with a ductility factor of 2, rather than 4, which would have been allowed. The average shear stress in the walls in the N-S direction was estimated to be about 200-300 psi for the SCT ground motion.

### 3. PRELIMINARY IMPLICATIONS FOR DESIGN

1. Where a few very stiff elements are added to flexible structures, the diaphragms should be checked to ensure that the inertial forces from mass evenly distributed throughout the building may be transmitted to these discrete locations. The connections between the stiff elements and the existing structure must also be carefully designed.

2. For buildings where stiffening is the primary effect that is sought from the retrofit, the addition of massive elements, such as RC shear walls, is counterproductive since the increase in mass diminishes the effect of the increased stiffness on the period of the building. Steel bracing systems are particularly effective for stiffening and strengthening buildings if architectural and detailing requirements can be met.

3. For soft soil sites, the effects of foundation flexibility can have a dominating influence on the building's response and it must be considered in the analysis. This is especially true where stiffening of the structure is the desired effect.

4. Strengthening the foundation may be one of the most important aspects of any retrofit solution. It may also be the most difficult. If very stiff and strong elements are added to the building, it is important that a realistic estimate of the forces that the foundation may be asked to carry be made. The foundation should be checked and strengthened to carry these forces, rather than those specified by code. It will be easier to repair structural damage above ground than foundation damage underground.

### 4. FURTHER STUDIES

A dynamic analysis of both structures remains to be done. The as-designed buildings will be analyzed for the 1979 and 1985 earthquakes and the retrofit structures will be analyzed for the 1985 earthquake. A detailed analysis of the member and connection performance for each will be undertaken. Recommendations for similar schemes will be proposed and evaluated for U.S. practice.

### ACKNOWLEDGEMENTS

Financial support for this research was provided by the National Science Foundation under grant NSF ECE85-11315. Any findings, conclusions or recommendations expressed in this paper are those of the authors and do not necessarily reflect the views of the National Science Foundation.

Table 1  
Measured dynamic properties for Building A

Mode	Period (seconds)	Damping (% critical)
1 EW	1.26	3
2 EW	0.28	5
1 NS	1.00	5
2 NS	0.21	9
1 Torsion	0.48	6

Table 2  
Story weights before and after retrofit

Level	Before Weight (kips)	After Weight (kips)
P.H.	135.4	135.4
Roof	406.3	425.1
10	425.6	455.3
9	425.6	455.3
8	425.6	455.3
7	425.6	455.3
6	425.6	455.3
5	425.6	455.3
4	425.6	455.3
3	425.6	455.3
2	425.6	455.3
1	467.2	503.0
P.B.	393.9	412.0
Base	1136.90	1356.9
Total	6370.1	6930.1

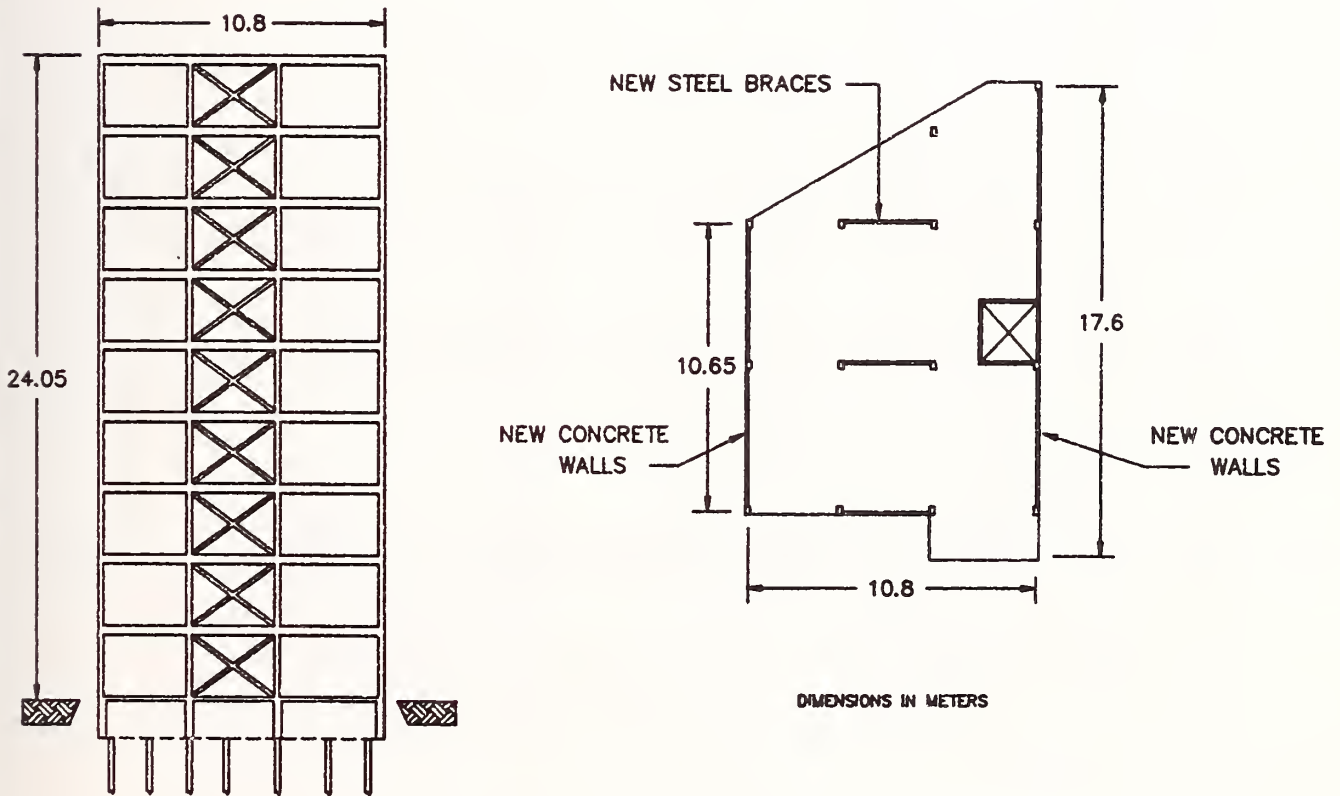
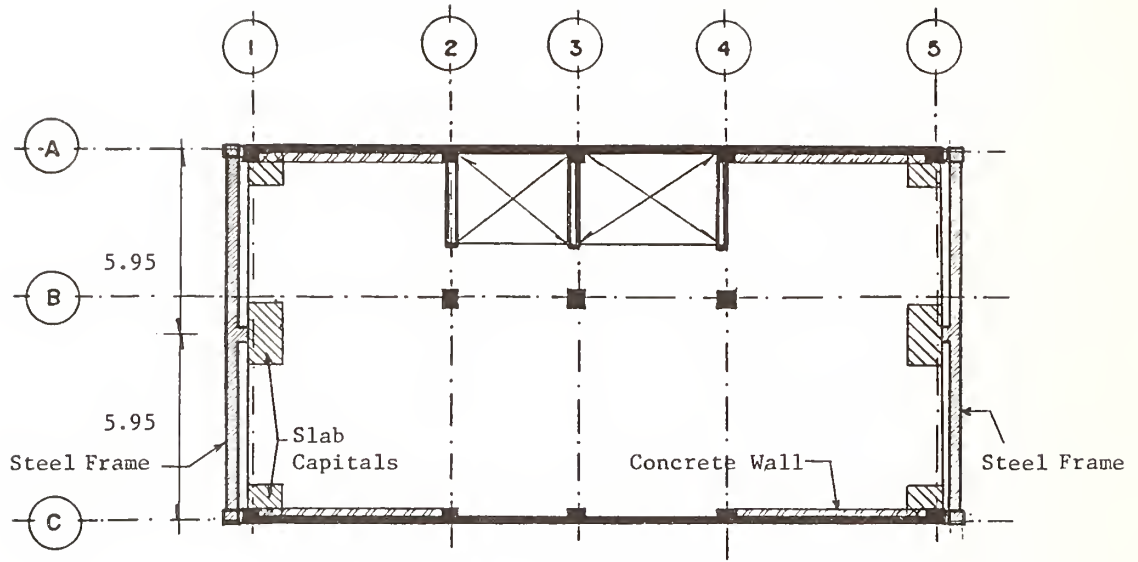
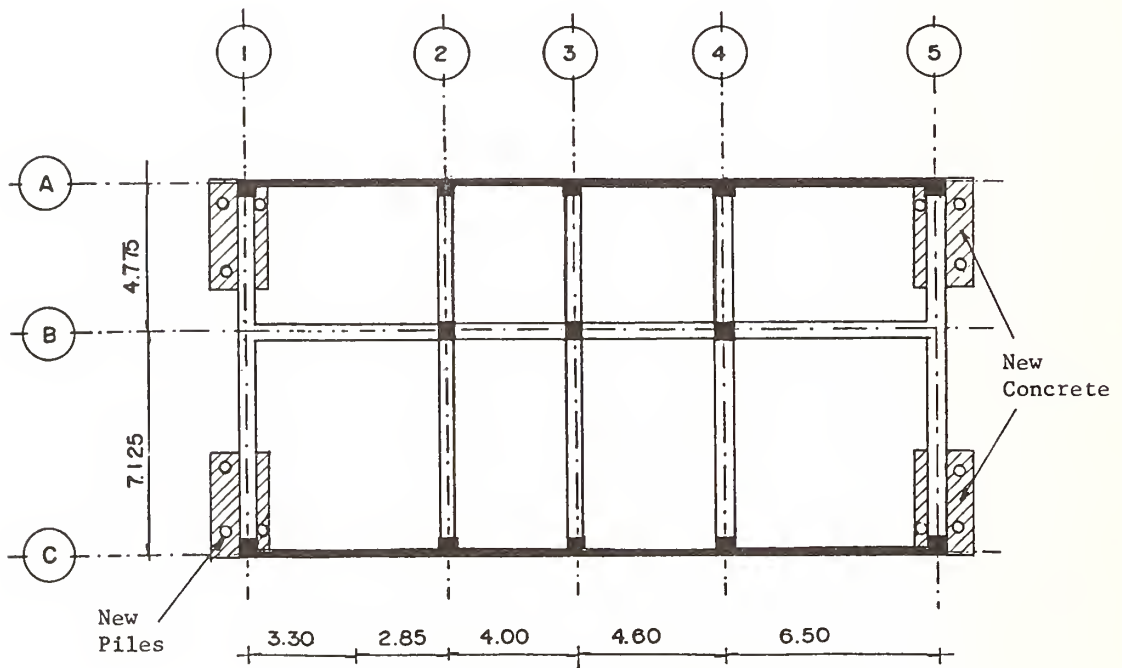


Figure 1 Plan and elevation views of Building B



Typical Plan After Retrofit



Foundation After Retrofit

Figure 2 Plan views of Building B after retrofit

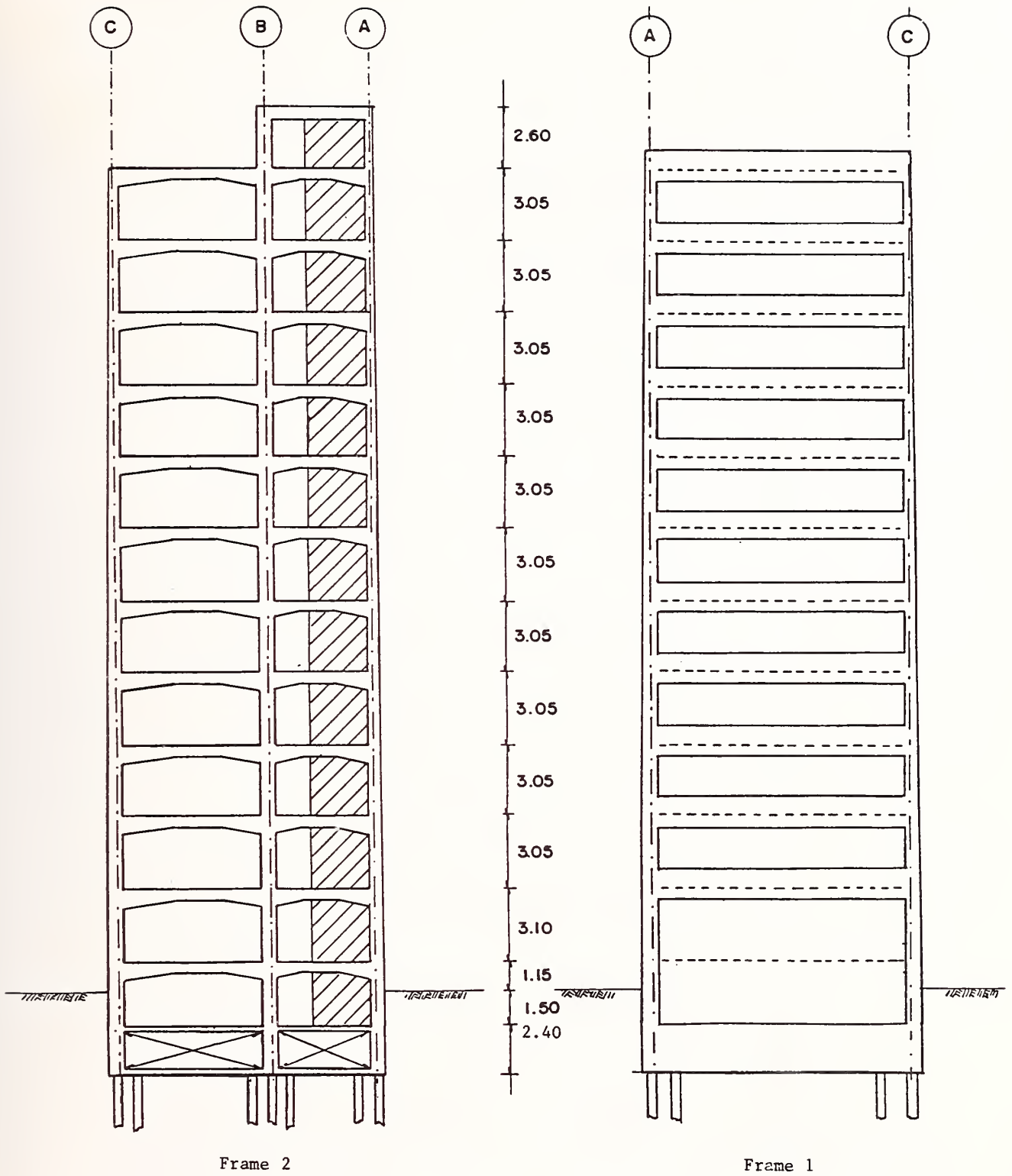


Figure 3 Elevation views of Frame 2 and Frame 1 before retrofit

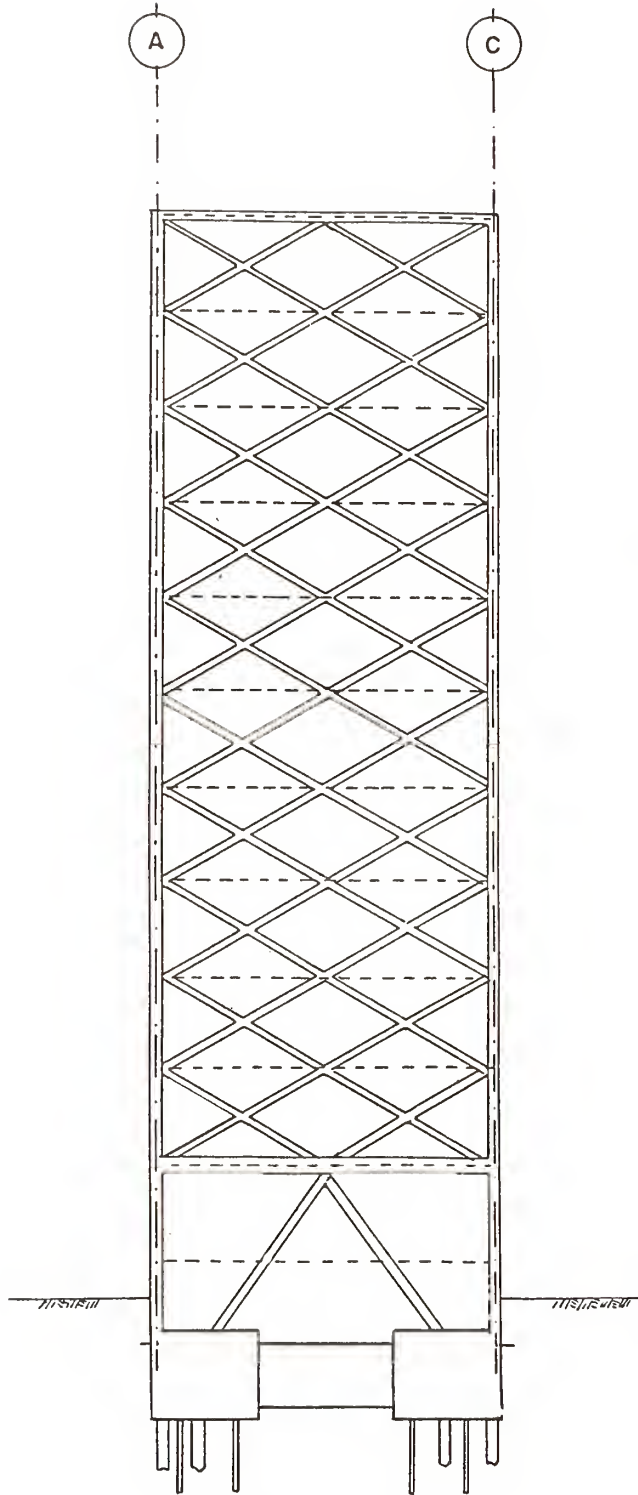
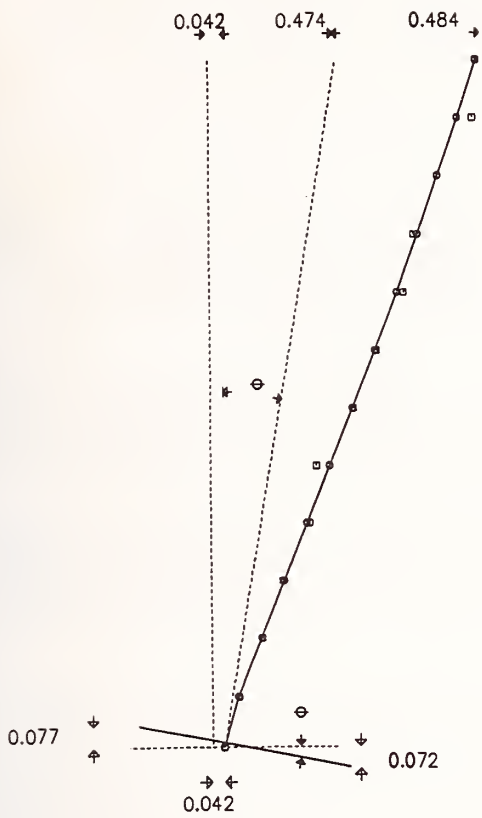


Figure 4 Elevation view of steel frame attached to Frame 1 and to Frame 2 as part of the strengthening scheme for the transverse direction

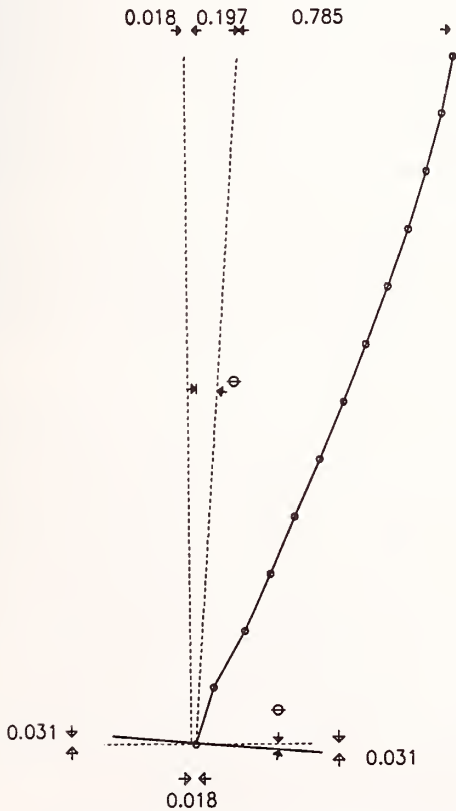


- ▣ MEASURED VALUES
- COMPUTED VALUES

MEASURED PERIOD = 1.25 sec.  
 MEASURED DAMPING = 2.75 %  
 COMPUTED PERIOD = 1.26 sec.

LEVEL	COMPUTED	MEASURED
ROOF	1.0	1.0
10	0.9284	0.986
9	0.8553	
8	0.7784	0.763
7	0.6974	0.725
6	0.6139	0.620
5	0.5288	0.535
4	0.4420	0.393
3	0.3541	0.366
2	0.2677	0.264
1	0.1826	0.188
P. B.	0.0966	0.099
BASE.	0.0421	0.042

Figure 5 Measured and computed mode shape for the first E-W mode after retrofit



- COMPUTED VALUES

COMPUTED PERIOD = 1.91 sec.

LEVEL	COMPUTED
ROOF	1.00
10	0.9553
9	0.8948
8	0.8258
7	0.7468
6	0.6649
5	0.5795
4	0.4889
3	0.3941
2	0.3026
1	0.2059
PB	0.0871
BASE.	0.0182

Figure 6 Calculated mode shape for the first E-W mode before retrofit

# Recorded Behavior of Structures—Whittier Narrows Earthquake, 1 October 1987

by

A. Gerald Brady<sup>1</sup>

## ABSTRACT

More than 250 stations were triggered in the Los Angeles metropolitan area and its surroundings by the M 5.9 Whittier Narrows earthquake of 1 October 1987. The large networks maintained by the California Division of Mines and Geology (CDMG), the U.S. Geological Survey (USGS), and the University of Southern California (USC), and many smaller networks, provided a collection of records that may be as important to the research community as the records from the San Fernando earthquake of 1971. Vibrational modes of buildings having multichannel records are investigated from their signatures on analog film records during the strong motion response. It is possible to identify the first, second, and, in one case, third translational modes, associated at times with in-plane bending of floors. In the two extensively instrumented buildings studied, with symmetric plans, no torsional modes are prominent enough to be identified.

## 1. INTRODUCTION

Figure 1, from Hauksson and others (1988), shows the peak horizontal ground level accelerations of the main shock (shown by an open star) recorded at stations operated by the USGS and CDMG. Accelerations are given in fractions of  $g$ , the acceleration due to gravity. Closed circles indicate hard-rock sites and crosses indicate soft-rock sites. Various abbreviations are used for the indicated faults: WF - Whittier, RHF - Raymond Hill, SMDF - Sierra Madre, NIF - Newport-Inglewood, SAF - San Andreas, and PVP - Palos Verdes.

Included in the stations plotted in Figure 1 are the basement records, or other ground records, from the instrumented buildings and other structures that form the basis of this report. These structures fall into four categories and are plotted in Figure 2.

1. Moderately instrumented buildings, having eight or more stories and with three triaxial accelerographs placed at three different heights in the building as required by the applicable building codes. The instruments are at the lowest level (in every case herein, the basement), the top story (its floor or ceiling), and at midheight.
2. Extensively instrumented buildings having four or more stories, and with at least nine channels of data feeding to at least one central recorder. Several triaxial

accelerographs may be placed, in addition, at ground or basement levels. Accelerometers are placed to answer specific response questions associated with individual buildings.

3. Dams having moderate instrumentation, namely, a triaxial accelerograph at a crest station, and at least one other at an abutment, or upstream or downstream at a hard rock site.
4. Structures with extensive instrumentation, excluding the buildings in item 2 above, having twelve data channels feeding a central recorder, and having an abutment triaxial accelerograph.

This paper stresses the ability to gather important information on vibrational behavior of well instrumented buildings, whether moderately or thoroughly instrumented (as defined in the categories above) from the analog film records themselves, prior to any digitization and computer processing. For the past fifty years, and for the life of the currently installed film accelerographs, basic structural behavior can often be obtained from the films (for example, see Housner and Jennings, 1982). The results in this report can be derived from the film copies in Etheredge and Porcella (1987), together with more precise information on the sensitivity, or scaling factor for each data trace. Careful processing of digitized film data, or of digitally recorded data, can of course provide orders of magnitude more results than appear here. But delays due to the numbers of records from large magnitude events in well instrumented areas, and due to funding and personnel constraints, renders an understanding of the film records particularly important.

Another factor to consider is that within the concepts of earthquake engineering and the reduction of earthquake hazards, we are interested in the larger responses of these structures, particularly during the arrivals of the strongest ground motions. Portions of these strong-motion responses are readily identified as modal responses (all points passing through their origins simultaneously) and amplitudes can be scaled with acceptably small errors, even several modal responses are in effect at the same time. With a film speed of 1 cm/s, frequencies of interest are readily measured, with accuracy maintained by averaging over as wide a time interval as necessary.

---

<sup>1</sup>U.S. Geological Survey, Menlo Park, CA 94025

Most triaxial accelerographs are wired together for simultaneous starts and for common time marks, usually at 0.5 s intervals. Both of these features are imperative for modal response identification, particularly for locations on the films many seconds after triggering, and also particularly if the film speeds are not all accurately equal. Alignment for simultaneity is built-in in the case of central recorders.

In none of the symmetric buildings studied here was there any significant strong-motion torsion about a vertical axis identified. Torsion is not identifiable in buildings with moderate instrumentation, for on no floor are there two parallel, separated, accelerometers.

None of the records gives any indication of structural damage occurring during the strong motion portion of the response. This would have been evident from the appearance of very high frequency for short durations at several sites in a building, caused by shattering concrete at critical locations, and also evident from the lengthening of fundamental modal periods, caused by loss of stiffness.

## 2. BUILDINGS WITH MODERATE INSTRUMENTATION

Table 1 lists the buildings with moderate instrumentation. They range in height from 8 to 12 stories and in epicentral distance from 8 to 31 km. The last column of the table refers to the detailed placement of the three accelerographs. Although the ideal position, to avoid the contamination of translational motion by torsion, is at the center of the building plan, the actual locations are considered satisfactory. These buildings are plotted in Figure 2.

Figure 3 is a sketch of possible mode shapes for translational motion. Table 2 lists the identi-

fied translational modes in these moderately instrumented buildings. The identifying procedure is relatively simple. In first modes, the upper level motions, although partially contaminated by higher frequencies, pass through their static positions simultaneously, and reach local peaks, in or out of phase, also simultaneously. Transient motions during the strong motion arrivals often force these measurements to be taken subsequent to the strongest structural responses. Second and third mode motions are superimposed on the first mode. Amplitude measurements for these are best made when the first mode motions are changing least, that is, close to the first mode peaks. Peak-to-peak amplitudes are scaled; the amplitudes listed in Table 2 are derived from one-half these scaled peak-to-peak amplitudes. Provided the modal response is reasonably well established the motions will be sinusoidal, and the displacement amplitudes in the last column can be calculated. These last two columns provide a sense of the amplitudes experienced at the top floor in the various modes for these buildings.

In the case of the Alhambra and Whittier buildings, computer processing has provided prominent frequencies (from Fourier spectra) and longer period displacement amplitudes (from corrected data). These are included in Table 2, when clearly associated with the particular mode under investigation, and can be compared with the scaled and calculated values.

No attempt has been made to scale the amplitudes at midheight, except for the third mode for the Alhambra building; only the phasing with respect to the top-most motion is checked. Although such measurement might help determine a more accurate first mode shape, the shapes of higher modes would clearly need more thorough instrumentation (see Figure 3).

Table 1. Peak ground level horizontal accelerations for buildings having moderate triaxial instrumentation required by codes.

ID	Address	Epicentral Stories	distance (km)	Acceleration (g)	Digitized	Instrument detail
1	Alhambra; 900 S. Fremont	12	8	0.30	D	(1)
2	Whittier; 7215 Bright	10	10	0.63	D	(2)
3	Norwalk; 12400 Imperial	8	15	0.29	D	(2)
4	Los Angeles; 1111 Sunset	8	16	0.16	D	(3)
5	Long Beach; VA Hospital	11	31	0.10	D	(1)

Notes: (1) Upper floor instruments on a vertical line at the center of an exterior wall; basement instrument is not in line.

(2) All 3 instruments lie on a central vertical line.

(3) All 3 instruments lie on a vertical line at the center of the longer exterior wall.

Table 2. Identified translational modes in moderately instrumented buildings - frequencies, and top floor acceleration and displacement amplitudes.

Address	Component	Mode	Freq <sup>(1)</sup> (Hz)	Accln ampl.(g) <sup>(1)</sup>	Displ. ampl. (cm) <sup>(2)</sup>
Alhambra 900 S. Fremont	090°	1	0.52	0.06	5.5
		2	0.5 <sup>(3)</sup>		5.8 <sup>(3)</sup>
	360°	1	1.4	0.03	0.4
		1	0.5	0.11	10.9
			0.5 <sup>(3)</sup>		8.8 <sup>(3)</sup>
		2	--	--	--
3 <sup>(4)</sup>	4.15	0.18	0.26		
		4.2 <sup>(3)</sup>	0.3 <sup>(5)</sup>	0.45 <sup>(5)</sup>	
Whittier 7215 Bright Ave.	180°	1	0.78	--	--
		2	2.1	0.30	1.7
		2.1 <sup>(3)</sup>		1.5 <sup>(3)</sup>	
	090°	1	--	--	--
2		4.0	0.48	0.7	
Norwalk 12400 Imperial	090°	1	0.66	0.07	4.0
		2	--	--	--
	360°	1	0.67	0.10	5.5
		2	1.84	0.31	2.3
Los Angeles 1111 Sunset Blvd.	348°	1	0.58	0.07	5.2
		2	1.96	0.07	0.5
	258°	1	0.74	0.07	3.2
		2	1.99	0.11	0.7
Long Beach VA Hospital	360°	1	1.67	0.21	1.9
		2	--	--	--
	270°	1	1.87	0.13	0.9
		2	6.72	0.10	0.1

- Notes: (1) Frequencies averaged over several cycles; acceleration amplitude at top-most instrument from most prominent cycle.  
(2) Displacement amplitude at top-most instrument, assuming sinusoidal motion.  
(3) Digitized and processed data provide frequencies from Fourier amplitude spectrum and displacement amplitudes from integrated corrected data (Brady and others, 1988).  
(4) Whereas the two upper level instruments record opposite accelerations for 2nd mode motion, they record same directions for 1st and 3rd mode motion.  
(5) Midheight amplitudes in 3rd mode motion.

### 3. BUILDINGS WITH EXTENSIVE INSTRUMENTATION

The buildings listed in Table 3 have been instrumented with the intent of studying specific structural response. The details of their individual accelerometer locations in Etheredge and Porcella (1987) clearly show efforts to record higher translational modes, torsion about a vertical axis, in-plane bending of floors, rocking of foundations, soil/structure interaction effects, and the different responses at either side of major geometrical or structural discontinuities. The buildings are plotted in Figure 2.

Building heights range from four to seven stories, in addition to one 33-story high-rise in Los Angeles. Epicentral distances range from

15 to 76 km, with an accompanying drop in peak horizontal ground-level acceleration from 0.24 to 0.03 g. The first three buildings on the list are planned for computer processing; two of these are studied in this report: 12440 Imperial Highway in Norwalk, and the Wadsworth VA Hospital. The high-rise at 1100 Wilshire, Los Angeles, is clearly shaped to have complicated couplings of torsion and translation in all modes, and is not conducive to the investigative process of this report.

The last column of Table 3 indicates the number of channels directed to the central recorder (two recorders for the Norwalk building) and the number of additional triaxial accelerographs, in basements or the surrounding ground, tied into the recording system.

Table 3. Peak ground level horizontal accelerations for buildings having extensive instrumentation (12 data channels, min.)

ID	Address	Stories	Epicentral distance (km)	Acceleration (g)	Digitized	Instrument detail
6	Norwalk; 12440 Imperial	7	15	0.24	D	24 ch + Bsmt. + 2 Gd sites
7	Los Angeles; 1100 Wilshire	33	17	0.21	D	12 ch + 3 Bsmts.
8	Los Angeles; Wadsworth VA Hosp.	6	35	0.09	D	9 ch + 2 Gd sites
-	Newport Beach; 840 Newport Center Dr.	7	52	0.06	-	12 ch
-	San Bernardino; County Govt. Bldg.	5	73	0.03	-	12 ch + Gd floor
-	Loma Linda; VA Hospital	4	76	0.04	-	9ch + 2 Gd sites

### 3.1. Norwalk, 12440 Imperial

The instrumentation for this building is a cooperative project between the USGS and Bechtel. The structure has a steel, ductile, moment-resisting frame, whose foundation includes 30 ft. deep caissons, drilled in place. The alluvium is very deep throughout this area of the Los Angeles basin. The center caisson contains a downhole triaxial accelerometer package. A total of 24 channels are directed to two central recorders. Three triaxial accelerometers located several hundred feet from the building provide ground level records. A neighboring building at 12400 Imperial has moderate instrumentation and is considered in the earlier section.

Figure 4 shows a south elevation of the 463'-long building. It is 136' in the north-south direction. The accelerometers recording motion in the north-south direction are indicated, with numbers corresponding to their traces in Etheredge and Porcella (1987). No. 18 accelerometer failed early in the record. Displacements calculated from the scaled accelerations, as in the section above, are indicated on the sketches of the mode shapes under consideration. The first mode frequency of 0.76 Hz does not alter as the strong motion passes, although the in-plane bending which is present during the strong motion slowly decreases, so that 10 or 12 seconds after triggering it is not discernable. Negligible amounts of torsion are detectable from these figures, namely 0.2 cm in the 463' length in the 1st mode and 0.1 cm in the second mode.

Instrumentation was also available for translational modes in the east-west direction. A first mode at 0.77 Hz was associated with an acceleration amplitude of 0.08 g and displacement of 3.5 cm at roof level (that is, the 7th

floor ceiling). A second mode at 2.35 Hz has acceleration amplitudes of 0.08 g, corresponding to displacement amplitudes of 0.4 cm.

### 3.2. VA Hospital, Los Angeles (Wadsworth)

This structure has a rectangular plan base and square cross-shaped towers from the 2nd to 6th floors. The core is a steel frame, while the wings, or arms of the cross are steel-braced towers. The building rests on reinforced concrete piles. Accelerometers in a straight line at roof level (the 6th story ceiling), in three different sections of the structure, are designed to record torsion, in-plane bending of the roof, and the motion of the roof of a cross wing relative to the core at the junction. Basement records provide the usual input in a triaxial package, affected, also as usual, by the structure's interaction with the soil at the basement level.

The recorded motions at the roof indicate strong resonant behavior, lightly damped, between 11 and 16 s after triggering. The frequency measures 1.15 Hz, the acceleration amplitude is 0.066 g corresponding to a displacement amplitude of 1.2 cm. A higher mode is also possible earlier, during the strong motion, but lack of midheight records makes a confident identification impossible. Its frequency ranges from 4.2 to 5.7 Hz with acceleration amplitudes of approximately 0.13 g, corresponding to displacements ranging from 0.1 to 0.2 cm.

There was no significant in-plane bending at the roof level, nor, at these amplitudes, was there any indication of torsion, or unexpected behavior at the junction of the core with the building wing.

One additional accelerometer is recording along

the line of these roof accelerometers. Since the building is symmetric in plan, it would be expected that structural behavior would be basically the same in this perpendicular direction. The first mode frequency scales at 1.11 Hz, compared with 1.15 Hz, and any differences, during the strong motion portion, between acceleration amplitudes are not discernable.

#### 4. SIMPLY INSTRUMENTED DAMS AND AN EXTENSIVELY INSTRUMENTED DAM AND BRIDGE

In this last section are included several dams and a bridge for which the methods of this report are not attempted, for reasons of insufficient information for true mode identification, or insufficient amplitudes for sufficiently accurate results. After computer processing of the records, these stations might well be reincluded in this project.

Most dams with triaxial accelerographs at the crest, and at least one from an abutment, upstream, or downstream, have been instrumented basically for monitoring purposes. Accelerations reaching specified levels indicate to the authorities that inspection is advisable. In some cases, however, sinusoidal behavior at the

crest can be associated with frequencies that have been calculated from the dam design stages, or from in-situ dynamic tests on the completed dam.

Table 4 lists six dams with a crest record and at least one other from the abutment, upstream, or downstream. Epicentral distances range from 4 to 44 km, and horizontal accelerations, from instruments other than the crest, drop from 0.31 to 0.04 g. Although it would be possible to measure the frequencies of various occurrences of sinusoidal motion at the crest, this will not be attempted here, and should await such time as more preliminary knowledge of the dynamic behavior of the dams is available.

Table 5 lists two more structures that fit the above category of having acceleration amplitudes too low for sufficiently accurate scaling results. They are included here in case the records prove to be sufficiently interesting to warrant digitization and computer processing for dynamic behavior. Even at low amplitudes, the records must be capable of confirming any basic computed modal properties generated by computer processing.

Table 4. Peak abutment or ground level horizontal accelerations for dams having moderate instrumentation (triaxial crest instrument, and at least one from abutment, upstream, and downstream).

ID	Dam	Epicentral distance (km)	Acceleration (g)	Digitized	Instrument locations
9	Whittier Narrows Dam	4	0.31	D	Cr., Upstr.
10	Brea Dam	23	0.16	D	Cr., Abut., Downstr.
11	Carbon Canyon Dam	27	0.22	D	Cr., Abut.
12	Sepulveda Dam	38	0.15	D	Cr., Downstr.
-	San Antonio Dam	38	0.04	-	Cr., Abut., Downstr.
-	Prado Dam	44	0.07	-	Cr., Abut., Downstr.

Table 5. Structures with extensive instrumentation, excluding buildings.

Structure	Epicentral distance (km)	Peak gd. accln. (g)	Digitized	Instrumentation details
Live Oak Reservoir Dam	31	0.04	-	12 ch + Abut.
Santa Ana River Pipeline Bridge	59	0.05	D	12 ch + Abut.

5. CONCLUSIONS

During earthquakes in which instrumented structures suffer structural responses approaching those that might damage the structure, the record amplitudes are sufficiently high that visual inspection of them and careful measurements can provide accurate estimates of mode shapes and frequencies as these modal resonances occur. Opportunities for these studies will recur as long as analog film recorders are a part of structural instrumentation networks and this would appear to be many years' duration - at least 25 years, the expected life of film recorders currently in operation and being installed.

First and second translational modes are identified and their frequencies and shapes measured. The amplitude of in-plane bending, coupled in all cases with translations, can be measured. No significant torsion was discernable in the symmetric structures studied here.

6. REFERENCES

1. Brady, A. G., Mork, P. N., Seekins, Linda C., 1988, Processed strong-motion records; Whittier Narrows, California, earthquake; October 1, 1987; Vol. 1, USGS-NSMIN stations within 15 km of the epicenter: U.S. Geological Survey Open-File Report 88-354.
2. Etheredge, E., and Porcella, R., 1987, Strong-motion data from the October 1, 1987, Whittier Narrows earthquake: U.S. Geological Survey Open-File Report 87-616.
3. Hauksson, E., Jones, L. M., Davis, T. L., Hutton, L. K., Brady, A. G., and others, 1988, The 1987 Whittier Narrows earthquake in the Los Angeles metropolitan area, California: Science, V. 239, No. 4846, March 18, p1409-12.
4. Housner, G. W., and Jennings, P. C., 1982, Earthquake design criteria: Earthquake Engineering Research Institute monograph series, El Cerrito, Calif.

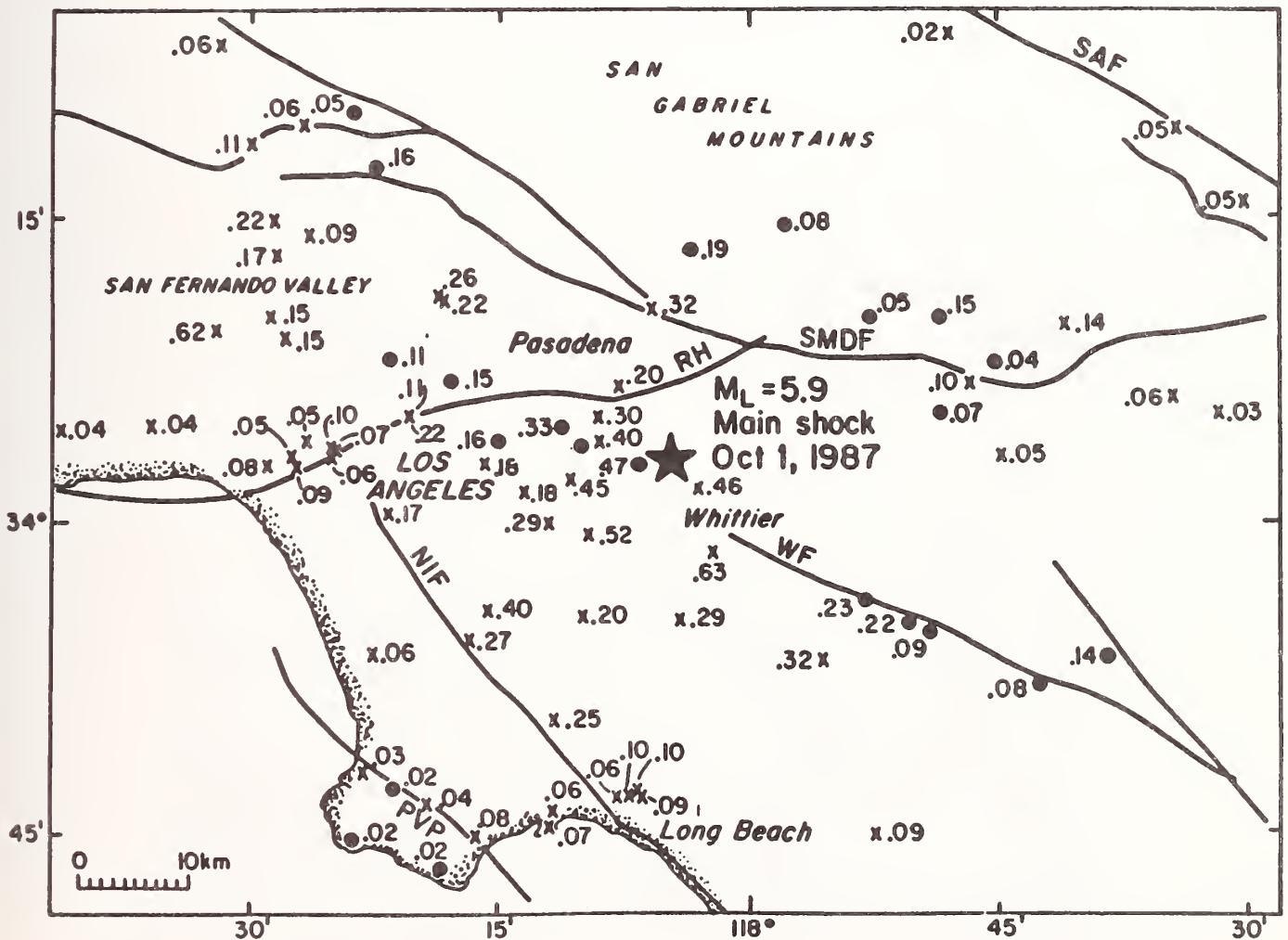


Figure 1. Peak horizontal ground level accelerations (g), at stations operated by USGS and CDMG. Solid circles indicate hard rock sites, crosses otherwise. Indicated faults are explained in the text. (Hauksson and others, 1988)

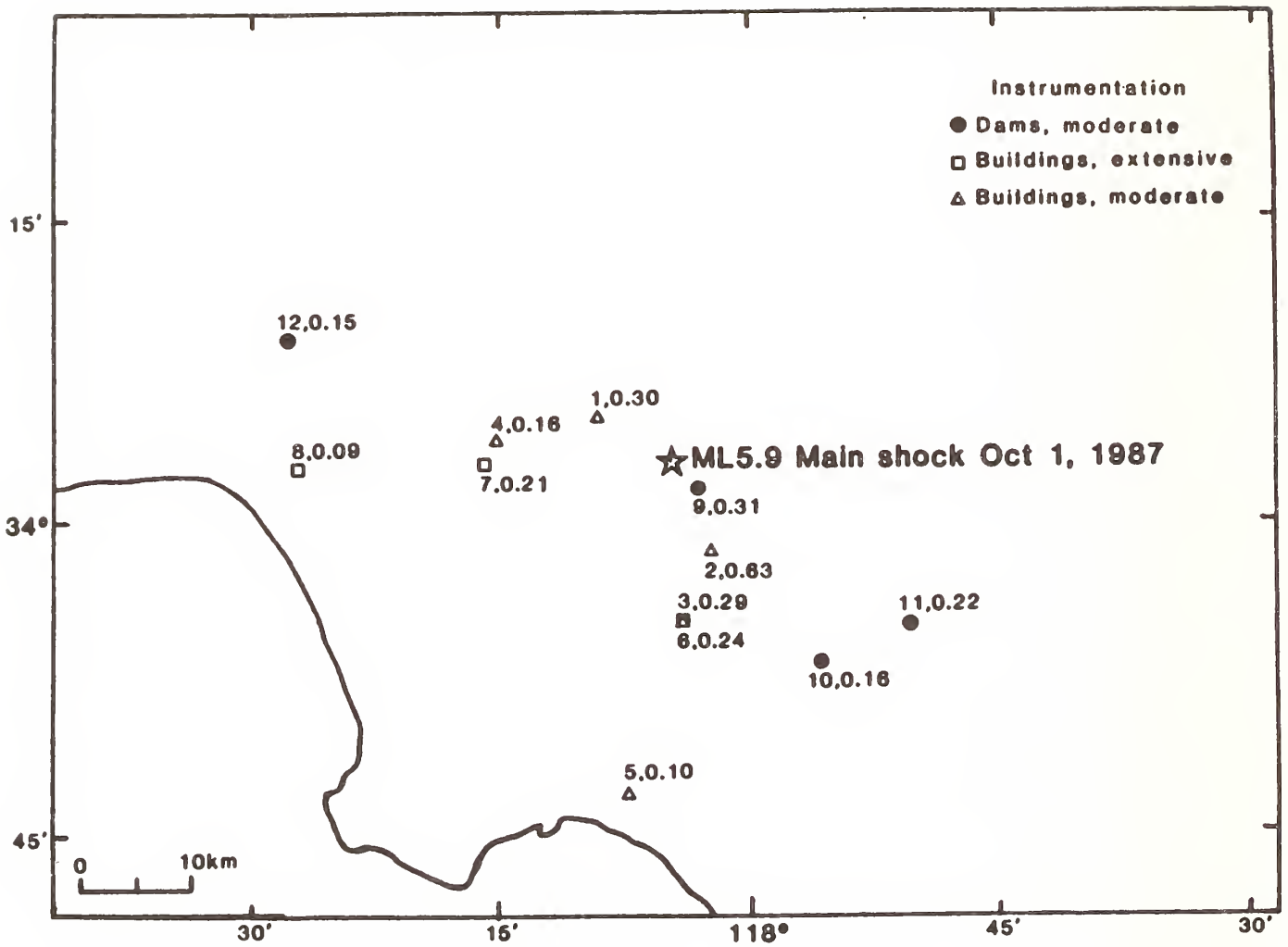


Figure 2. Locations of stations operated by USGS and discussed in this report. An identification number (for Tables 1, 3 and 4) is followed by peak horizontal ground acceleration.

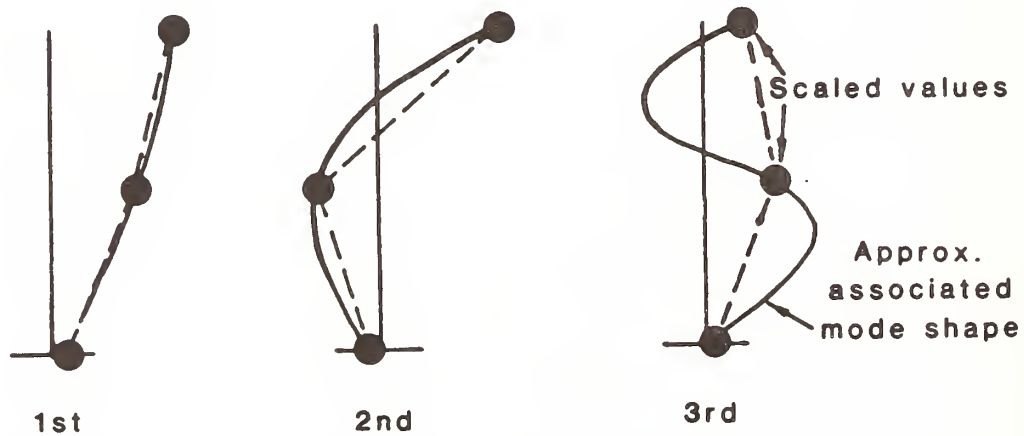
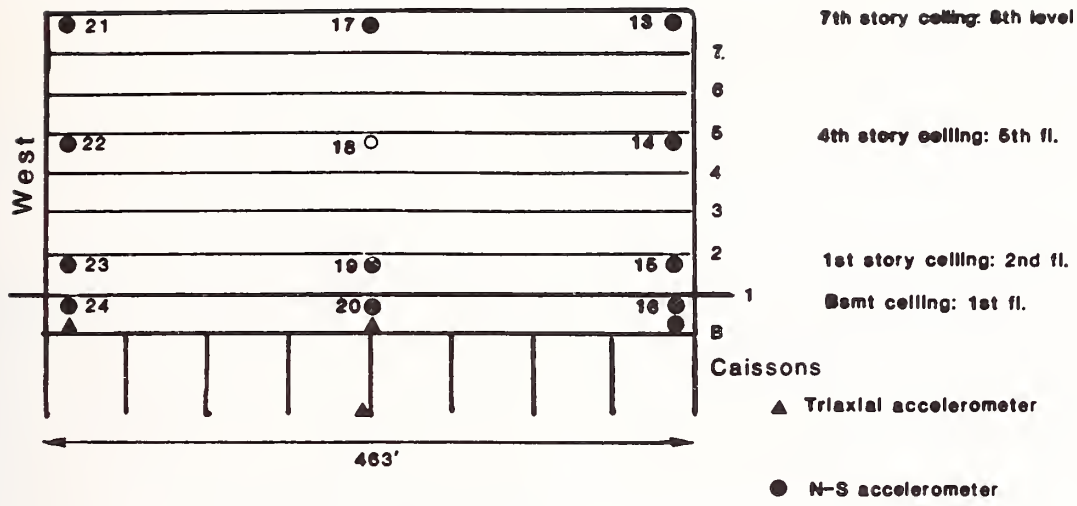
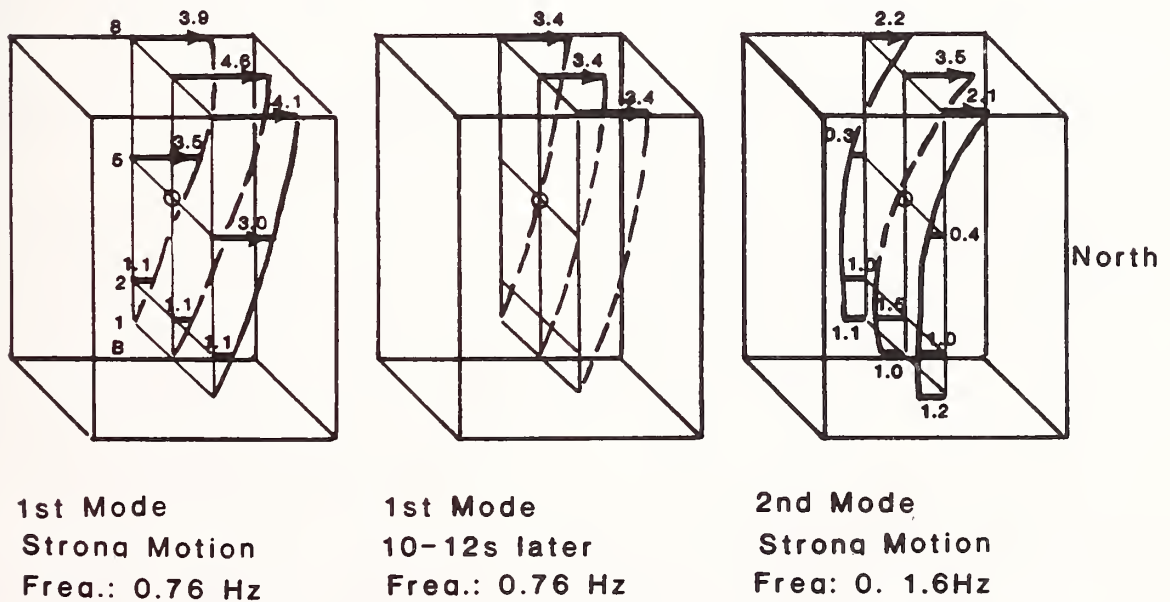


Figure 3. Sketch of the lower translational modes sought for moderately instrumented buildings.



A. South Elevation



B. Modal Deflections - cm.

Figure 4. A, South elevation of 12440 Imperial, Norwalk, with accelerometer placements for N-S translational modes. B, Deflected mode shapes with displacements in cm., calculated from modal accelerations.

# Field Experiments on Pipelines in the Parkfield Earthquake Zone

BY

J. Isenberg<sup>(1)</sup> and E. Richardson<sup>(2)</sup>

## ABSTRACT

Welded steel and ductile iron pipeline segments have been constructed at Owens Pasture near Parkfield, CA, where the US Geological Survey has predicted a recurrence of the 1966 magnitude 6.0 earthquake. Measurements include strain on welded steel pipe, joint displacement and rotation in ductile iron pipe, fault offset and acceleration-time histories.

KEYWORDS: Fault Offset; Field Experiment; Pipelines

## 1. INTRODUCTION

Surface expressions of fault movement such as lateral offsets and ground rupture and lateral spreading pose major threats to pipelines. For example, lateral offsets of up to 20 ft were considered in the design of the Trans-Alaska pipeline.

Recently, the seismic performance of sewage and high pressure gas pipelines in urban areas crossed by fault zones such as the Newport-Inglewood fault zone in Los Angeles have received attention. Ground rupture was considered in the design of an underwater sewer outfall that crosses the San Andreas fault (Ref. 1). In addition to lateral offset, the effects of ground shaking due to wave propagation must be considered as was done in the design of the Trans-Bay tunnel for BART (Ref. 2) in San Francisco.

Models of pipeline behavior at fault crossings have been proposed to help understand pipe-soil interaction at fault crossings and to provide conservative designs in cases where detailed geotechnical information is lacking (Refs. 3 and 4). These models and others, of which Ref. 5 is representative, embody assumptions about pipe-soil interaction, including friction at the pipe-soil interface and coefficients of passive soil resistance that have been investigated under laboratory conditions (Refs. 6 and 7), but have never been

tested at field scale under earthquake conditions. The predicted recurrence of the 1966 Parkfield-Cholame earthquakes (Refs. 8 and 9) and the associated experiments (Ref. 10) provide an opportunity to study these assumptions. The experiment which is described below is designed to capitalize on the earthquake prediction by studying the behavior of two types of pipelines that cross a strand of the San Andreas Fault near Parkfield, CA. The experimental pipelines are collocated with a USGS creepmeter that indicates fault creep is occurring at the site. A maximum of four inches lateral offset is expected to accompany the earthquake. Passive and active instrumentation have been installed to measure local ground shaking, the lateral offset and the deformations of joints and strains in the pipes.

In addition to lateral offset, pipelines are exposed to ground shaking due to wave propagation. Models have also been proposed to support design of pipelines exposed to shaking (Refs. 2, and 11 through 16). A common assumption of such models is that the ground deformation is due to a wave train propagating with a predominant frequency and group velocity and is imposed on the pipeline with negligible dynamic pipe-soil interaction. Field experiments to investigate the relationship between ground shaking and the response of continuous pipelines are being conducted in Tokyo at a site where surface rupture is not expected (Ref. 17).

The present experiment complements the Japanese work by measuring ground shaking close to the zone of surface rupture and relating the response of the pipeline to both effects.

---

<sup>1</sup> Principal, Weidlinger Associates  
Palo Alto, California  
<sup>2</sup> Associate, Weidlinger Associates  
Palo Alto, California

## 2. WAVE PROPAGATION EFFECTS

A typical model of wave propagation effects is illustrated in Fig. 1, Ref. 15. Here, a wave train propagates with peak displacement  $A$  and predominant wavelength  $L$  at an angle  $\theta$  with respect to the axis of a straight length of pipe.

In the absence of slip at the pipe-soil interface, axial and transverse components of displacement can be used to compute axial strains and curvatures. In Ref. 14, the shear stress at the pipe-soil interface is computed and used to identify cases where slip occurs and to modify the strain induced in the pipe; bent pipe segments are also considered.

Several elements of the model involve assumptions that require further study, such as the predominant wavelength (which may be derived from the predominant frequency and the group velocity) and the direction of propagation. A step toward improved estimates of ground strain has recently been taken by Barenberg, Ref. 18, who found that ground strain derived from particle velocity and wave speed agrees well with average ground strains found by subtracting integrated accelerometer records and dividing by the distance between them. Other studies aimed at identifying predominant frequencies and their group velocities include Refs. 11, 19, and 20. Experimental correlation between free field ground motion parameters and pipeline strains is the subject of previous work, such as Ref. 21, and of ongoing work such as Ref. 17 and the present study.

An example of how such information is used to examine the serviceability of pipeline networks following an earthquake is provided by Shinozuka and co-workers (Ref. 13) who investigated the responses of networks subjected to vertically propagating SH waves. The ground strain is assumed to be equal to the particle velocity divided by the local shear wave speed and pipeline damage is assumed to occur when the ground strain exceeds 0.3%; after qualifying this model by comparing it with observation in the 1923 Kanto earthquake, Shinozuka and colleagues applied it to a Los Angeles water transmission network.

### 2.1 Lateral Offsets

In the approach developed by Newmark and Hall (Ref. 3) for continuously welded steel pipes and initially applied to

design of the Trans-Alaska pipeline, the pipe is oriented with respect to the fault strike such that offset puts the pipe in tension. Flexure of the pipe is neglected.

The geometry envisioned in the model is shown in Fig. 2. An effective anchor length is defined as the distance away from the fault over which friction between soil and pipe is mobilized, meaning that the frictional stresses acting over this length are constant and equal to the maximum that confinement will support. The average plastic strains in the pipe over this length depend on the properties of the pipe (thickness, yield strength, hardening stiffness), the characteristics of the soil (friction, unit weight) and the amount of fault offset. The Newmark-Hall approach has been amended by Kennedy-Chow-Williamson to take into account the increased frictional resistance that occurs near the fault crossing due to local flexure of the pipe.

The Newmark-Hall approach tends to give longer anchor lengths and lower strains than the Kennedy-Chow-Williamson method; the latter is regarded as conservative for design. In some cases, the difference in anchor length is significant. A major goal of the present field test is to provide data that will allow these and other design and assessment methods to be evaluated.

The seismic performance of ductile iron pipes is related to the capacity of joints to accommodate relative displacement and rotation. Reaches of pipe are considered to be much stiffer and stronger than flexible joints. In regions of unstable ground, replacement of flexible joints with restrained joints leads to a more rigid pipeline system resembling the welded steel pipeline. Modern ductile iron pipe for water distribution uses rubber gasket push-on joints, which can accommodate several inches of extension and up to about 5° of rotation without leaking. Under conditions of fault movement which exceed these reserves, leakage and joint rupture are expected. One aspect of joint behavior in situ that is not well understood is how combinations of extension and rotation interact to influence joint capacity; laboratory studies indicate that interaction decreases capacity (Ref. 22). In the present experiment, pipes are oriented at various angles to the fault strike in order to subject joints to various combinations of rotation and extension. In addition to flexible joints, rigid couplings of the type commonly used in unstable ground are employed in some lengths of pipe.

## 2.2 Needed Experimental Data

For continuously welded pipelines, experimental data are needed to correlate group velocity and particle velocity data with strain in the pipe and to measure the effective anchor distance from surface rupture where lateral offset has occurred. For pipelines with flexible joints, data are needed to show how lateral offset is accommodated at the joints in combination of extension and rotation.

## 3. PARKFIELD PIPELINE EXPERIMENT SITE

The site of the present field test is Owens Pasture, which is about 2 km N.W. of Parkfield, CA. Ground rupture was observed here in the June-August 1966 Parkfield-Cholame earthquakes. The USGS has identified Owens Pasture as a possible zone of surface rupture during a recurrence of that earthquake sequence. The pasture is level and is bounded on the north by a range of hills and on the east by a swale and shallow pond which is dry most of the year. The soil is adobe clay mixed with pebbles and gravelly sediments washed down from the hills. There are no obvious features that mark the location of the fault strand in the pasture. A USGS creepmeter in the southeast corner of the pasture is oriented at 30° to the assumed local strike of a San Andreas Fault strand.

The creepmeter currently indicates that about 11 mm of fault creep per year is occurring between the two faults which are located about 10 mm apart. This is substantially less than the value of 15-18 mm annual creep that is observed at sites to the south and less than the 25 mm annual creep that is observed at the Middle Mountain site to the north. The low creep rate at Owens Pasture may be due to locating the creepmeters only partially inside the creep zone or to division of the surface fault into multiple strands, only one of which intersects the creepmeter.

To find the most likely zone of rupture, trenches were dug orthogonally to the assumed fault strike at the north and south ends of the pasture. The sides of the trenches were inspected for fault gouge and other subsurface evidence of localized displacement. Such evidence is ideally found in a zone about one meter wide. Since the fault zone acts as a barrier to water and water borne sediments, the zone may be marked by a change in color of soil and by the abrupt disappearance of sand and gravel lenses, which in the present case would have been washed down from the hills.

Such a zone was found in the North Trench at the location shown roughly in Fig. 3, although evidence was weaker than had been hoped. No evidence was found in the South Trench. In order to define the strike as shown in Fig. 3, geological evidence in the swale and further to the southeast was considered, as was the location of the creepmeter and the records obtained from it; based on these considerations, including important subjective judgments, the strike is assumed to be as shown in the figure.

### 3.1 Pipeline Segments

The design models referred to above specify that the pipeline should be put into tension by fault offset. Accordingly, a welded steel pipeline segment has been constructed and instrumented which will be put into tension by right lateral strike slip. In Fig. 4, this segment is designated T (for tension) and is oriented at 40° to the assumed fault strike. It is instrumented to measure bending in the horizontal plane and extension. A companion segment, designated C (for compression) is oriented at -40° to the fault strike and will be subject to compression. The steel pipe segments were delivered in 40 ft lengths and welded at ground level. End plates were welded to provide a bond for the concrete anchors.

Eight ductile iron segments were also emplaced; see Fig. 5. Each segment is comprised of two or three 18 ft pipe lengths oriented at 60° and 30° to the fault strike. Two length segments are placed such that the joint is at the assumed fault crossing; three length segments are placed such that the assumed fault crossing is at the middle of the middle length. Individual pipe lengths were put in the trench and joints were formed under supervision of representative of US Pipe and Foundry Co., which donated the pipe and fittings. The pipes with restrained joints, Fig. 5, were filled with water and pressurized to seat the seals. The pipes with unrestrained joints were not pressurized.

The pipe segments were laid in a two foot wide trench excavated to a depth of at least four feet. Then a six inch layer of river sand was poured in the bottom of the trench to provide a bed and the pipe was placed in the trench. The trenches were widened to four feet at locations where strain gages (welded steel) or displacement transducers (ductile iron) are attached in order to provide room for the installers to work. The trenches were backfilled with river

sand up to three to six inches above the crown. Then native spoil from the trench excavation was replaced and compacted by driving the tractor-backhoe over it.

All pipeline segments have restrained ends provided by concrete anchors in order to simulate a great length of pipe. Anchors for the push-on ductile iron pipe are of modest size because deformation is concentrated at the joint. Anchors for welded steel provide 48 square feet of bearing in order to resist axial forces of 200 kips accompanying axial strains of 0.2% to 0.3%; friction provides additional resistance of 50-60 kips. The design of the anchor is based on measurements of stress-strain properties of steel and coefficient of friction between sand backfill and the steel pipe. These measurements were made at Cornell University under supervision of Prof. T. D. O'Rourke.

### 3.2 Measurements and Instrumentation Plan

Passive instrumentation consists of survey monuments which have been placed according to USGS practice roughly perpendicular to the fault strike as shown in Fig. 6. These monuments are surveyed every three to four months by USGS and will be surveyed after the earthquake. These will be the principal measurements of lateral offset.

The welded steel pipes are instrumented with weldable strain gages. A one-quarter bridge is used, making each gage self-compensating for temperature changes. At burial depth of 3 1/2 to 4 ft, temperature variations are probably negligible. As an independent check, two thermocouples have been attached near the ends of the pipe to measure temperature directly.

The ductile iron pipes are instrumented with displacement transducers. Each joint has one transducer designed to measure extension and another attached to an arm to measure rotation. Waterproofing is done inside each transducer. The entire assembly is covered by a smooth shroud to keep soil from interfering with the movement of such transducer components as the wire.

Finally, three 3-axis seismometers are placed as shown in Fig. 6. These are supplied by the Kyoto University under a US-Japan cooperation agreement developed for the present project by Kyoto University and NCEER. Each is mounted on a concrete pad as shown in the figure. Each is self-recording, and there is a

link to the data acquisition system which permits common timing to be established between the strains on the welded steel pipe, relative displacements at joints in ductile iron pipe and the ground shaking as recorded by the seismometers.

The data acquisition system was designed by Campbell Scientific Co. to specifications developed by Weidlinger Associates in conjunction with its instrumentation subcontractor, Torque and Tension Systems, Inc. The system is divided into two recording units of 25 channels each. Each unit is activated when one of six trigger channels exceeds a predetermined threshold value corresponding to earthquake or creep induced strain. A number of 60-second events can be recorded. Currently, the threshold triggers are set at 100 microstrain.

## 4. STATUS AND FUTURE PLANS

Seismic activity has been low in Parkfield recently. A few earthquake swarms have been recorded; however the alert level remains normal. Long term fault creep displacements recorded north of Owens Pasture are of order 22 mm/year; at Owens Pasture, the rate is 12-13 mm/year; south of Parkfield the rates are 3-10 mm/year (Ref. 23). After a pause following the 1985 Coalinga, CA earthquake, the creep rate in Owens Pasture has returned to the previous rate.

Future activities include surveying the alignment array and tying it into the monuments on the pipelines. A data interpretation plan will be developed in cooperation with Japanese workers for relating seismometer records to pipe strains and joint deformations. A finite element analysis is being considered which will include the details of the anchors and 3-D pipe-soil interaction effects.

## 5. ACKNOWLEDGMENT

This work was conducted at Weidlinger Associates, Palo Alto, CA under NCEER Contract No. 86-3044, and NSF Master Contract No. ECE 86-07591. Partial support to Weidlinger Associates was also furnished by the National Science Foundation under Grant No. CES 86 16822.

The cooperation and assistance of the US Geological Survey has been indispensable to this experiment. The assistance of US Pipe and Foundry Co. of Union City, CA and Birmingham, AL in supplying ductile iron pipe segments, joints, transportation and on-site assistance in

laying the pipe is gratefully acknowledged. The assistance of Northwest Pipe and Casing Co. of Portland, OR in supplying steel pipe segments and transportation is also gratefully acknowledged.

Dr. Thomas D. O'Rourke, Associate Professor of Civil Engineering at Cornell University, is consultant to Weidlinger Associates on this project. His contributions in deciding orientation of the welded steel pipe, in designing the anchors and selecting instrumentation have increased greatly the value of the experiment.

Torque and Tension Systems, Inc. of Campbell, CA is subcontractor to Weidlinger Associates of instrumentation and data recording. Mr. Jack Jones is responsible for design and supervision. Mr. Craig Vossbrinck is responsible for installation.

Three strong motion seismometers have been provided by the Kyoto University, Prof. H. Kameda, principal investigator, under a US-Japan cooperation agreement implemented for the present project by the University of Kyoto, Japan and the US National Center for Earthquake Engineering Research.

#### 6. REFERENCES

1. Murphy, G. J., G. E. Hervert, Y. Eisenberg, and D. D. Treadwell, "Ocean Outfall Across the San Andreas Fault," Lifeline Earthquake Engineering, Proceedings of the Second Specialty Conference of the Technical Council on Lifeline Earthquake Engineering, Oakland, CA August 1981.
2. Kuesel, T. R., "Earthquake Design Criteria for Subways," Journal of the Structural Division, ASCE, Vol. 95, No. ST6, June 1969, pp. 1213-1231.
3. Newmark, N. M. and W. J. Hall, "Pipeline Design to Resist Large Fault Displacement," Proceedings U.S. National Conference on Earthquake Engineers, June 18-20, 1975, Ann Arbor, MI.
4. Kennedy, R. P., A. W. Chow, and R. A. Williamson, "Fault Movement Effects on Buried Oil Pipelines," Journal of the Transportation Engineering Division, Proceedings of ASCE, Vol. 103, 1977.
5. Wang, L. R-L., "Role and Development of Soil Parameters for Seismic Responses of Buried Lifelines," Presented at 1983 International Symposium on Lifeline Earthquake Engineering, Portland, OR, June 19-24, 1983.
6. Takada, S., "Experimental Study on Mechanical Behavior of PVC Pipelines Subjected to Ground Subsidence," Presented at 1983 International Symposium on Lifeline Earthquake Engineering, Portland, OR, June 19-24, 1983.
7. Trautmann, C. H. and T. D. O'Rourke, "Load-Displacement Characteristics of a Buried Pipe Affected by Permanent Earthquake Ground Movements," Presented at 1983 International Symposium on Lifeline Earthquake Engineering, Portland, OR, June 19-24, 1983.
8. Brown, R. D. et al., "The Parkfield-Cholame California Earthquakes of June-August 1966 - Surface Geologic Effects, Water Resources Aspects and Preliminary Seismic Data," US Geological Survey Professional Paper 579, US Government Printing Office, 1967.
9. Bakun, W. H. and A. G. Lindh, "The Parkfield, California, Earthquake Prediction Experiment," Science 229, 1985, pp. 619-624.
10. \_\_\_\_\_, "A Proposed Initiative for Capitalizing on the Parkfield, California Earthquake Prediction," Board of Earth Sciences, Commission on Physical Sciences, Mathematics and Resources, National Research Council. National Academy Press., Washington, D.C., 1986.
11. O'Rourke, M. J., G. Castro, I. Hossain, "Horizontal Soil Strain Due to Seismic Waves," Journal of Geotechnical Engineering, V110, No. 9, September 1984, pp. 1173-1187.
12. Shinozuka, M., S. Takada, and H. Ishikawa, "Seismic Risk Analysis of Underground Lifeline Systems with the Aid of Damage Probability Matrix," Columbia University in the City of New York, Department of Civil Engineering and Engineering Mechanics, Technical Report No. NSF-PFR-78-15049-CU-2, September 1978.
13. Shinozuka, M., R. Y. Tan and T. Koike, "Serviceability of Water Transmission Systems Under Seismic Risk," Proceedings of the 2nd Specialty Conference of the Tech-

- nical Council on Lifeline Earthquakes Engineering, ASCE, August 1981.
14. Shinozuka, M. and T. Koike, "Estimation of Structural Strains in Underground Lifeline Pipes," Technical Report No. NSF-PFR-78-15049-CU-4, Dept. of Civil Engineering and Engineering Mechanics, Columbia University, March 1979.
  15. Iwasaki, T., "Earthquake Resistant Design of Underground Pipelines in Japan," Proceedings of the US-Japan Workshop on Seismic Behavior of Buried Pipelines and Telecommunications Systems, Tsukuba Science City, Japan, December 5-7, 1984.
  16. Datta, S. K., A. H. Shah, and N. El-Akily, "Dynamic Behavior of a Buried Pipe in a Seismic Environment," Journal of Applied Mechanics, Trans. ASME, Vol. 49, 1982, pp. 141-148.
  17. Kawashima, K., "Public Works Research Institute," Ministry of Construction, Government of Japan, Private Communication, July 16, 1987.
  18. Barenburg, M. E., "Correlation of Pipeline Damage with Ground Motions," Journal of Structural Div., Proceedings ASCE to be published as a Technical Note.
  19. Shinozuka, M., H. Kameda, and T. Koike, "Ground Strain Estimation for Seismic Risk Analysis," Journal of Engineering Mechanics, ASCE, Vol. 109, No. 1, February 1983, pp. 135-191.
  20. Harada, T., T. Oda, and T. Shimada, "Determination of Apparent Wave Propagation Velocity from Damage Statistics for Buried Pipelines," Earthquake Behavior and Safety of Oil and Gas Storage Facilities, Buried Pipelines and Equipment, PVP-Vol. 77, American Society of Mechanical Engineers, 1983, pp. 209-216.
  21. Iwamoto, T., N. Wakai, T. Yamaji, S. Nagao, "Observation of Dynamic Behavior and Safety of Oil and Gas Storage Facilities, Buried Pipelines and Equipment," PVP-Vol. 77, American Society of Mechanical Engineers, 1983, pp. 285-293.
  22. O'Rourke, T. D. and C. H. Trautmann, "Earthquake Ground Rupture Effects on Jointed Pipe," Proceedings of the 2nd Specialty Conference of the Technical Council on Lifeline Earthquake Engineers, American Society of Civil Engineers, August 1981, pp. 65-80.
  23. Shulz, S., G. M. Mavko, R. O. Burford and W. D. Stuart, "Long Term Fault Creek Observation in Central California," Journal of Geophysical Research, V87, No. B8, August 10, 1982, pp. 6977-6982.

#### NOTICE

This paper was prepared by Weidlinger Associates as a result of research sponsored by the National Center for Earthquake Engineering Research (NCEER). Neither NCEER, associates of NCEER, its sponsors, Weidlinger Associates, nor any person acting on their behalf:

- a. makes any warranty, express or implied, with respect to the use of any information, apparatus, method, or process disclosed in this report or that such use may not infringe upon privately owned rights; or
- b. assumes any liabilities of whatsoever with respect to the use of, or for damages resulting from the use of, any information, apparatus, method or process disclosed in this report.

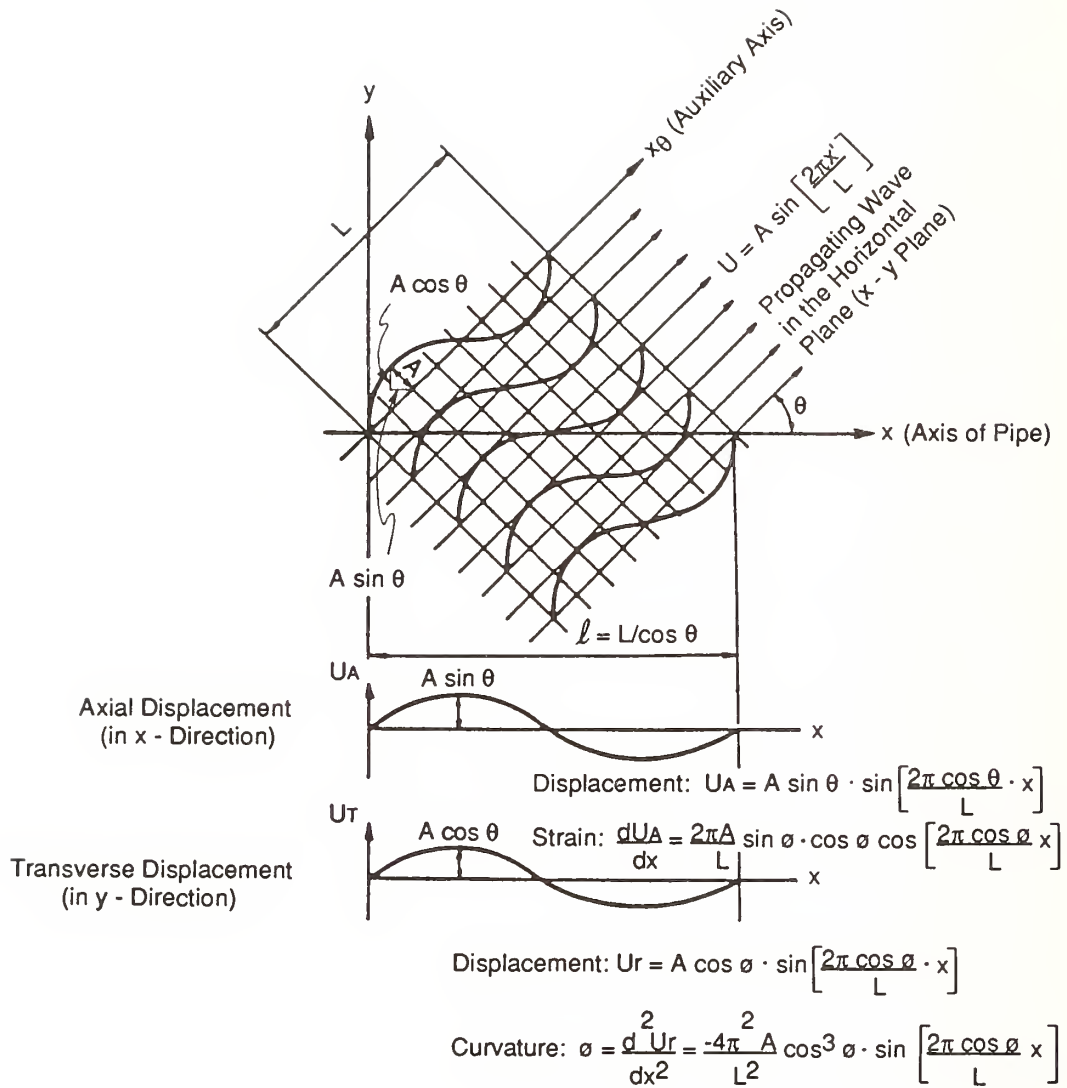
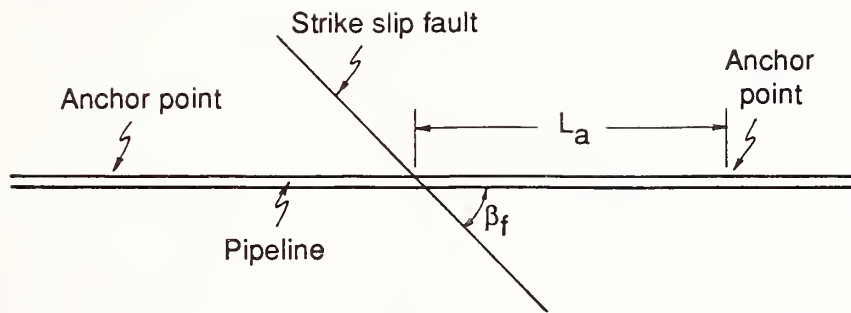
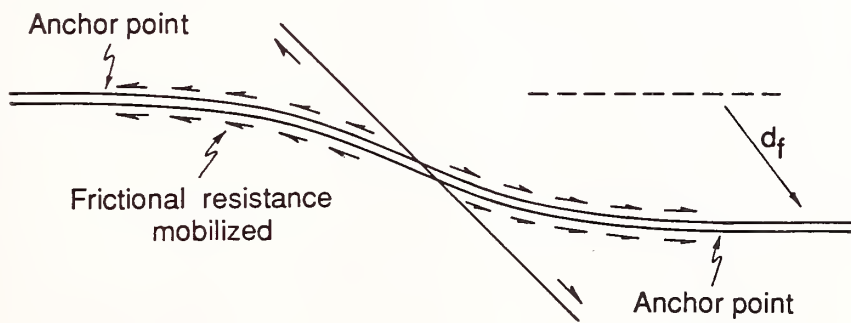


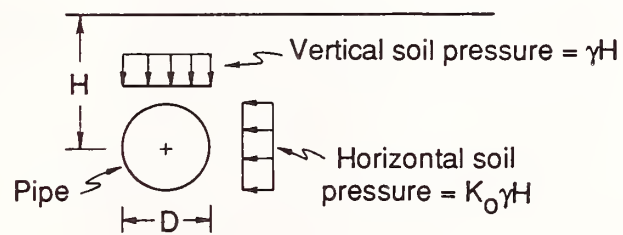
Figure 1. Model of wave propagation effects for pipeline analysis (after Ref. 15).



a) Before Fault Movement



b) After Fault Movement



c) Transverse Cross-Section

Figure 2. Plan and sectional views of continuous pipeline envisioned in Newmark-Hall design approach.

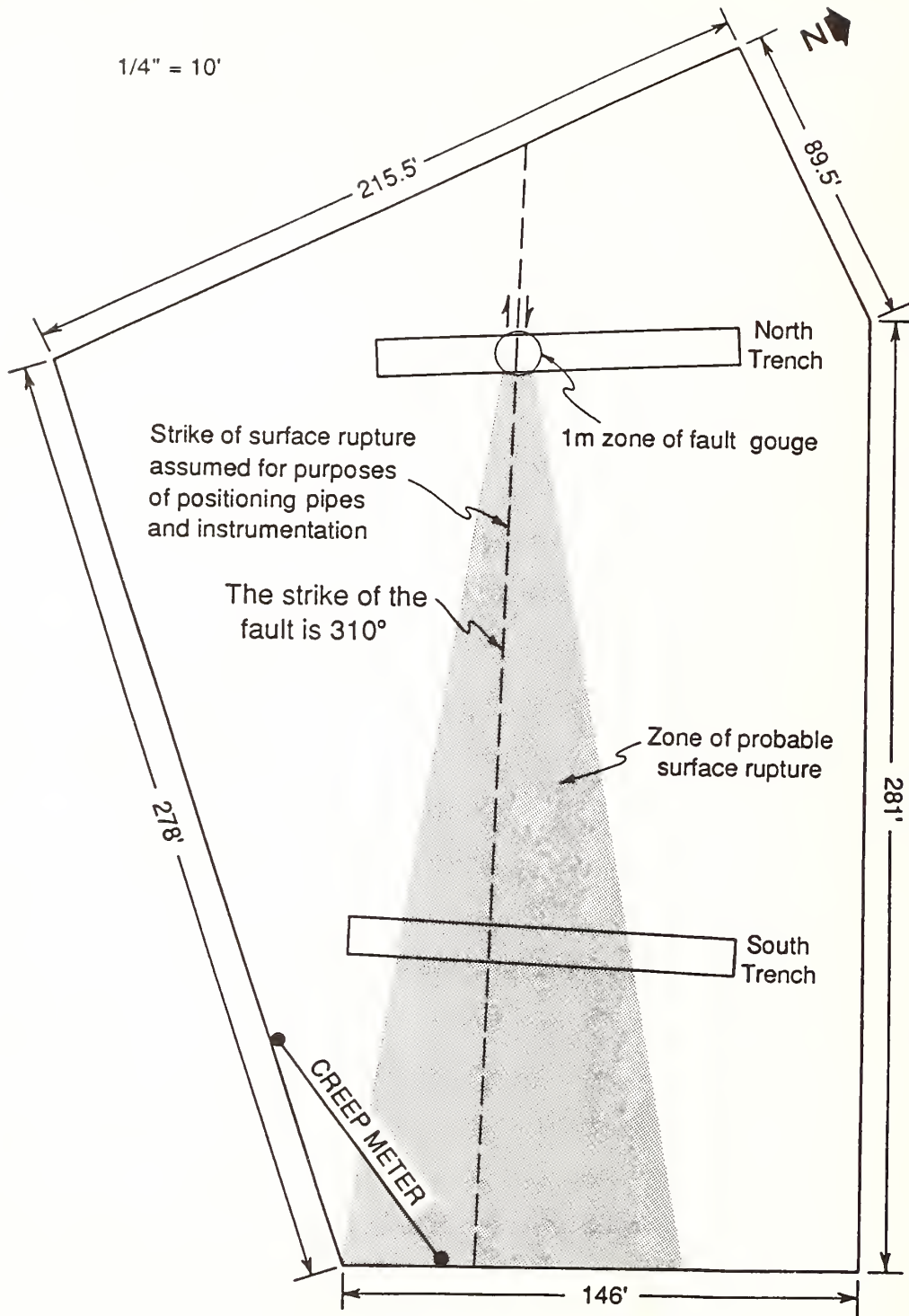


Figure 3. Assumed zone of surface rupture, Owens Pasture.

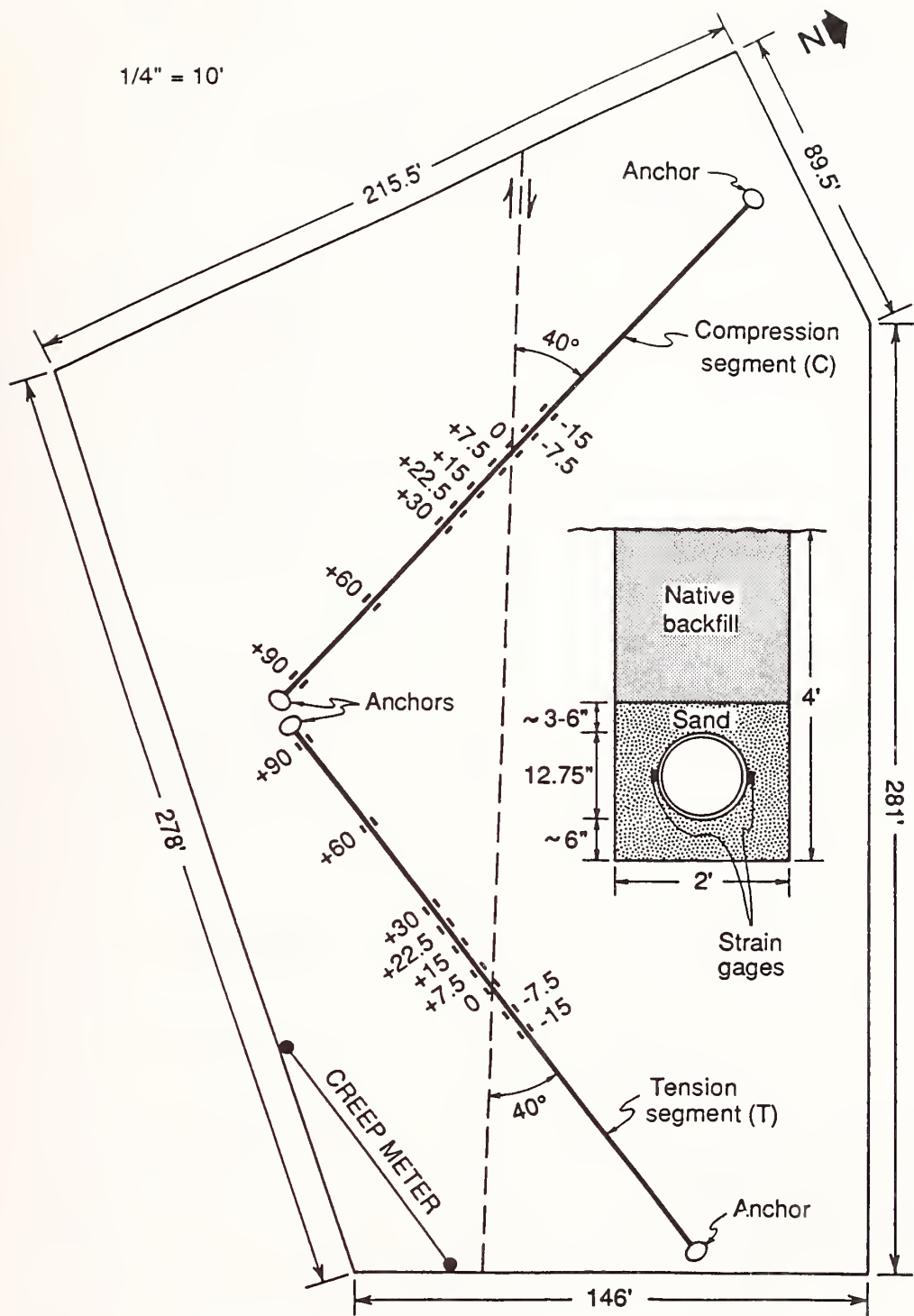


Figure 4. Orientation and strain gage locations, welded steel pipe segments.

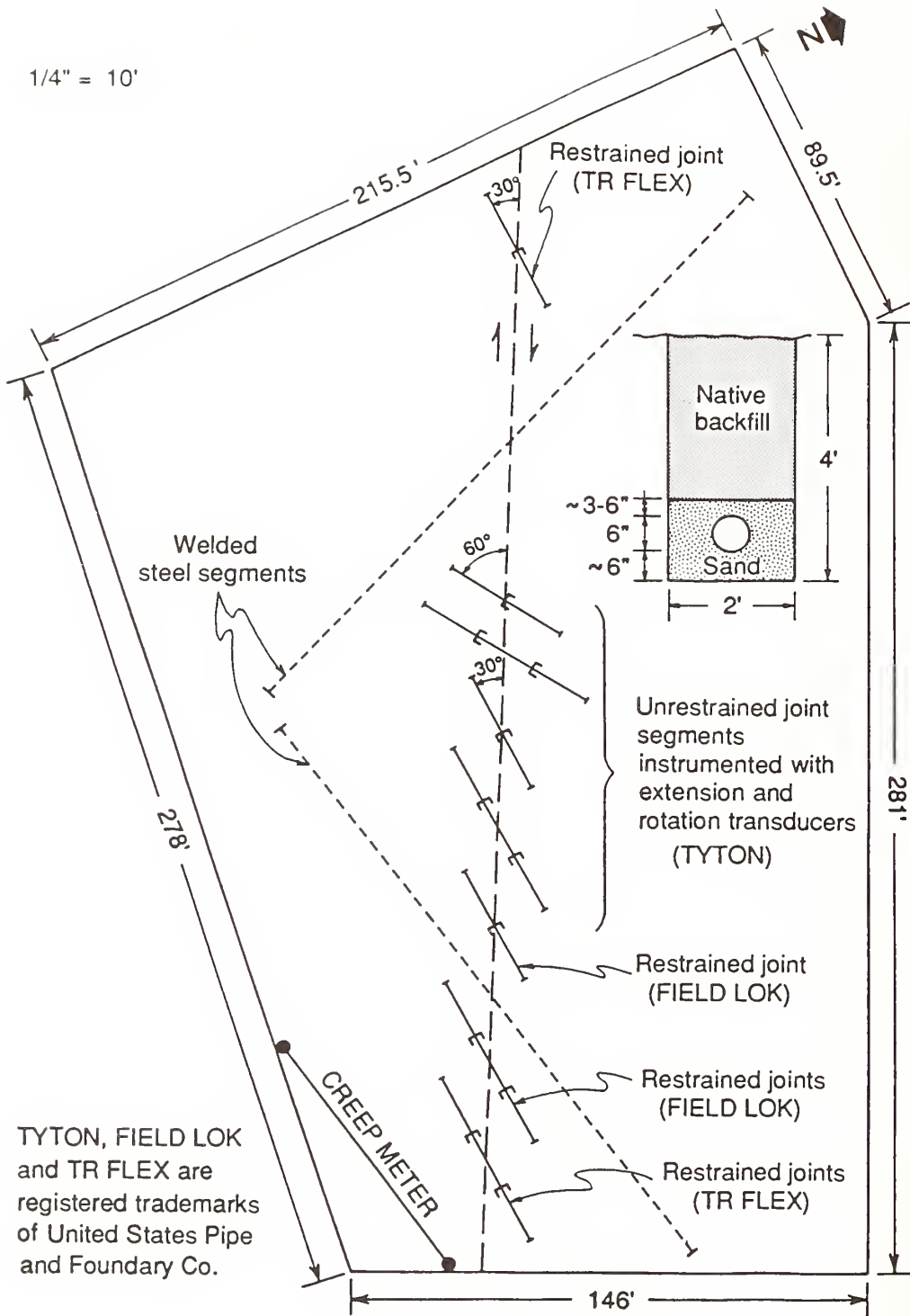


Figure 5. Orientation and joint types for iron pipe segments.

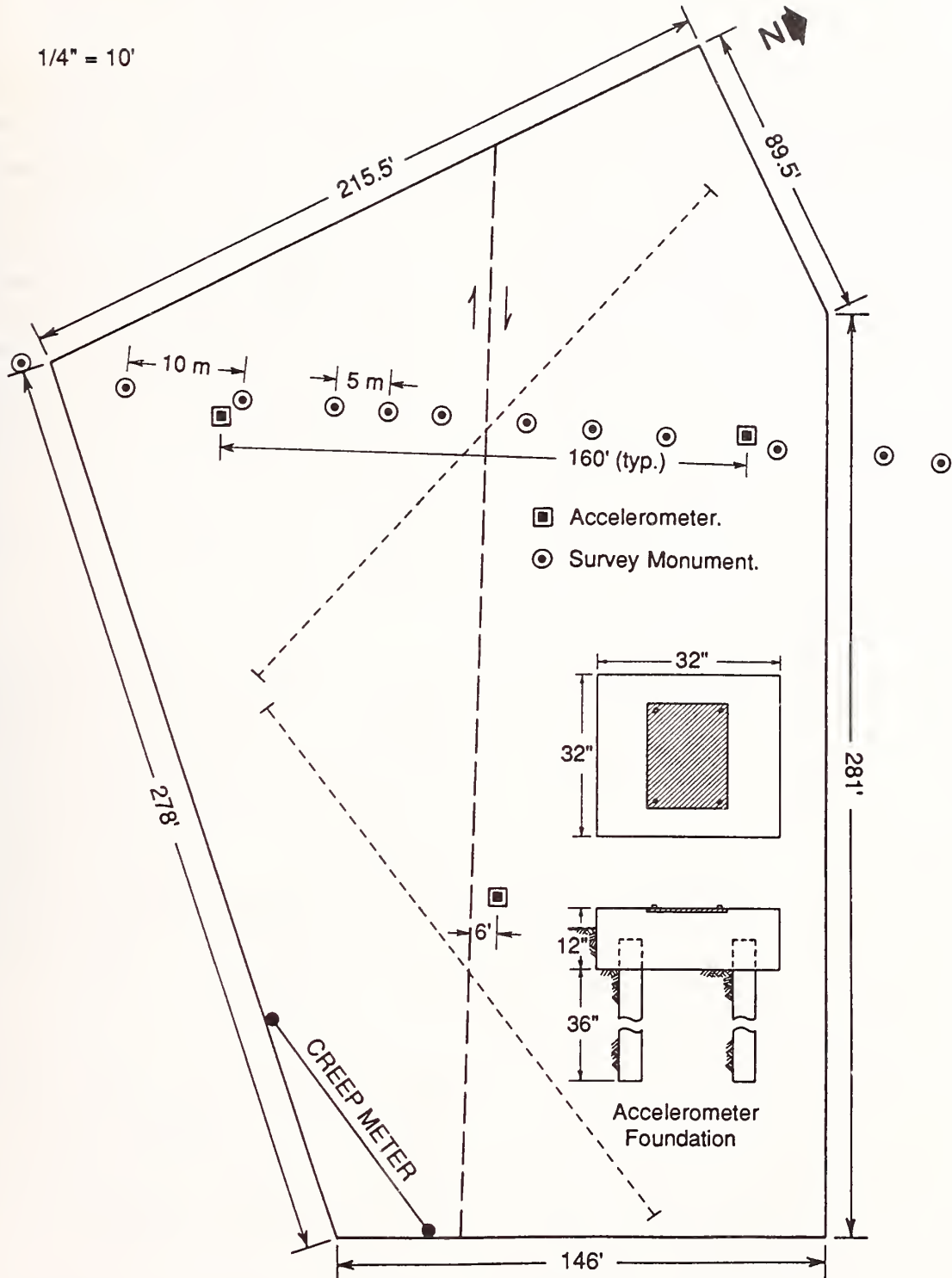


Figure 6. Locations of survey monuments and of accelerometers and details of their foundations.

# The Drawing Image of Earthquake Hazard

By

Keiichi OHTANI<sup>1</sup>, Hiroshi TAKAHASHI<sup>2</sup>

## ABSTRACT

The aspects of disaster were changed according to the changes of times and the variations of social structure. Otherwise, the numbers of casualties and injuries and damaged structures were mainly reported to the scale of the hazard, therefore it is difficult to take the total image of the hazard at the present time. The earthquake hazard has the different two sides; the one is the damaging process which is grown up the first, second and third disasters by the passage of times, and the other one is the restoring process which is the functional recovery according the progress of time. It is a important factor to make the countermeasures of earthquake disaster prevention for the provide for earthquake of which is done to clear and accurate the total image of the earthquake hazards. This paper describe the introductory research to search the method to take the total image of the earthquake hazards. We consider that the accumulation of these research will be contributed the substantiality of the countermeasures for earthquake hazards.

**KEYWORDS:** Earthquake hazard, Countermeasure of earthquake disaster, Mitigation of earthquake hazard.

## 1. INTRODUCTION

The scope of researches and countermeasures of disaster prevention consists of the elucidation of the process by which a natural hazard develops into a disaster, and the prevention of its developments. This is thus an essential responsibility of a modern country. Nevertheless, the aspects of disaster were changed according to the changes of times and the variations of social structures. Otherwise, the numbers of casualties and injuries and damaged structures were mainly reported to the scale of the hazard, therefore it is difficult to take the total image of the hazard at the present time. The earthquake hazard has the different two sides; the one is the damaging process which is grown up to the first, second and third disasters by the passage of times, and the other one is the restoring process which is the functional recovery according the progress of time. It is a important factor to make the countermeasures of

earthquake disaster prevention for the provide for earthquake of which is done to clear and accurate the total image of the earthquake hazards. This paper describe the introductory research to search the method to take the total image of the earthquake hazards. We consider that the accumulation of these research will be contributed to the substantiality of the countermeasures for earthquake hazards.

In Japan, we are often discussed that if the Kanto earthquake will be attacked in future, we will estimate how many and what kind of disaster will be occurred. The problems of these discussions are the indefiniteness of the mutual relations of each kind of disaster. Therefore, it is need that the construction of the model which is taken the total image of the overall disasters. This model will be given the important data to consider the earthquake disaster prevention.

It is the present situation that the insufficient method developed for the huge city, such as Tokyo, is partially applied the drawing of the planning of community earthquake disaster prevention. The earthquake disaster are controlled by the nature of occurrence of earthquake which is a natural phenomena, and the resistance force to the earthquake of the received area (vulnerability function, damaging characteristics). This characteristics are determined the condition of the each area. Therefore, the fundamental factor of the planning of the area earthquake disaster prevention is based on the exact understanding of the area characteristics against the earthquakes.

This paper describe the appropriate method of drawing the model, which is considered the progress of times, for the taking the total image of earthquake hazards. This research is started recently, this paper is the introductory report of the construction of model of the total earthquake hazards.

1) Head, Earthquake Engineering Laboratory, National Research Center for Disaster Prevention, Science and Technology Agency.

2) Dr. of Sci, Director-General, NRCDP, STA

## 2. CHAIN CHARACTERISTICS OF EARTHQUAKE HAZARDS

The earthquake hazards are formed by the directly damages, such as human and structural damages, the outbreak and the spreading of fire, the hindrance of life by the stoppage of lifelines, the influence of economical activities of the area. By the grown up of the earthquake scale, the grade and the area of damages are expanded. At the very severe earthquake, the damage grade is reached to the national size.

The total damages from first to third stages caused by the earthquake is arranged to time series of the relation between the each damage item and the each vulnerability function. Fig.1 shows the disaster chain model for earthquakes. The items are correlated with each other through the vulnerability characteristics. Then, the earthquake disaster is explained the multi-input and multi-output system, generally. Here, we are assumed that the model has not feedback loop. For this model, 8 damage items and 8 vulnerability functions are considered as follows;

- 1) Damage to ground and slopes  
(ground)  
Ground condition
- 2) Damage to Houses (dwelling)  
Housing condition
- 3) Damage to life line system (supply)  
Supply system
- 4) Damage to dangerous facilities  
(production)  
Industrial production
- 5) Fire and Diffusion (accumulation)  
Social background
- 6) Casualties (welfare)  
Welfare and rescue
- 7) Social disruption (Society)  
Social life
- 8) Extra-regional impacts (relevancy)  
Core functionality

It is possible to make a model of the chain characteristics of disaster. the each vulnerability has the factor to expand the disaster and the factor to restrain the disaster. The size of disaster are determined by the combination of these two factors.

The model of these type are often used for the research of hazard mitigation. this model is effective to the research of the occurrence behaviour of the disaster, but it is difficult to insert the restoring process for these model. Therefore, we will consider the other model to estimate the total process from the occurrence of disaster to the convergence of disaster.

## 3. DAMAGING AND RESTORING PROCESS

We were considered the construction of the model which can be estimate the damaging and restoring processes according the time change. The earthquake disaster of each kind of damage is increased to the damaging ratio according the time progress, is reached the maximum damaging ratio is decreased after the time of maximum point and finally is not occurred the damage. Fig. 2 shows the functional model of damaging process. The upper and lower figures in Fig. 2 are the momentary and cumulative functions of damaging process, respectively. It is assumed that these processes can be explained the exponential functions as follows;

$$\text{Momentary function} \\ F(t+d) = C \times t \times e^{-t/b} \quad (1)$$

$$\text{Cumulative function} \\ G(t) = \int_0^t \{F(t+d)\} \times dt \quad (2)$$

where C denotes the constant to prescribe the grade of damage, b the duration from the start time of the occurrence of damage to the time of the maximum occurrence of the damage and d the starting time of the occurrence of damage. It is possible to consider the total image of the damaging process by using this type of model.

Fig.3 shows the restoring process as same as the consideration of the damaging process. The similar function is assumed as follows;

$$\text{Momentary function} \\ F(t+d_r) = C_r \times t \times e^{-t/br} \quad (3)$$

$$\text{Cumulative function} \\ G(t_r) = \int_0^t \{F(t+d_r)\} \times dt \quad (4)$$

where the subscript  $r$  of  $r$  denote the restoring process.

The grasps of the total image of the disaster will be able to use the functional model in Figs. 2 and 3. The total process from the occurrence of damage to the convergence of damage by the superposing of the damaging and restoring processes is shown in Fig. 4. The functional description of the total process can be explained by using Eqs. (2) and (4).

$$G_t(t) = G(t) + G(t_r) \quad (5)$$

The total image of earthquake hazard will be calculated the superposition of the total processes to be calculated each damage using Eq. 5. the horizontal axis in these descriptions denotes the time passages. If it is assumed to occurrence the large earthquake, the duration from the time of occurrence of earthquake to the time of convergence of hazard will be reached several or nearly 10 years.

#### 4. CHANGE OF STANDARD LIFE LEVEL

It is possible to close the total image of the earthquake hazard by using the functional models. However, the estimation of the effects of earthquake hazard for individual or community, is necessary to consider the change of standard life level. The consideration of the changing grade of standard life level is important thing. The degrees of decline of level and duration are determined by the scale of earthquake. The grade of the effects at the large earthquake is greater than the one at smaller earthquake, as shown in Fig. 5. The basics of the countermeasures of earthquake disaster prevention is bring the trend of large earthquake close to the trend of medium and small earthquakes.

The flowchart which is calculated the fluctuation of the comity's or individual's level according the earthquake hazard, is shown in Fig. 6. The overall level change is calculated to sum up by weighting method the calculated results for each damage item. The total sum of hazard will be calculated by the integration of the decrease part of standard life level in the time domain, and multiplied the amount of living expenses for individual or sum of budget for community. To apply the estimation for real earthquake hazard, it is necessary to collect the many data and to built the many assumption for the calculation of above mentioned procedures. The example of the calculated result of overall image for the seismic intensity 6 (JMA scale). This figure is shown the ability of expression of the overall image of earthquake hazard. The assumption method of the coefficient and application method of each datum are the future research objects.

#### 5. CONCLUSION

We were examined the modelling method of taking the overall image of earthquake hazard and the total process of the earthquake damages. This paper describe only the consideration method. We will plan to study the more detailed problem such as the application method of real data.

- |   |  |
|---|--|
| Y <sub>1</sub> : Damage to Ground and Slopes    | X <sub>1</sub> : Ground Condition      |
| Y <sub>2</sub> : Damage to Houses               | X <sub>2</sub> : Housing Condition     |
| Y <sub>3</sub> : Damage to Life Line System     | X <sub>3</sub> : Supply System         |
| Y <sub>4</sub> : Damage to Dangerous Facilities | X <sub>4</sub> : Industrial Production |
| Y <sub>5</sub> : Fire and Diffusion             | X <sub>5</sub> : Social Background     |
| Y <sub>6</sub> : Casualties                     | X <sub>6</sub> : Welfare and Rescue    |
| Y <sub>7</sub> : Social Disruption              | X <sub>7</sub> : Social Life           |
| Y <sub>8</sub> : Extra-Regional Impacts         | X <sub>8</sub> : Core Functionality    |

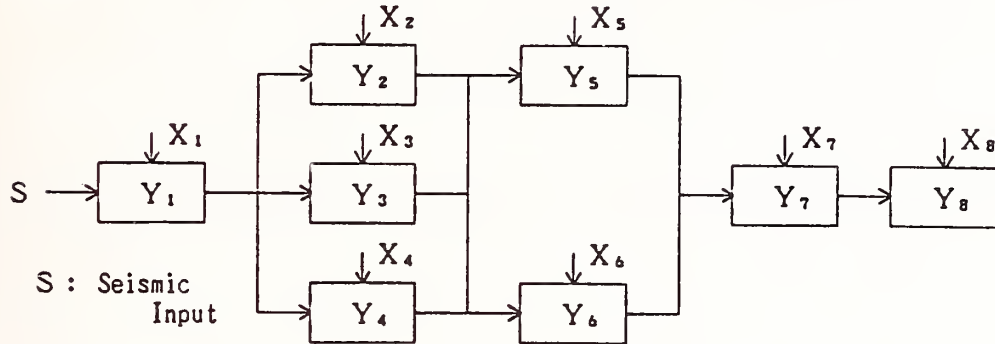


Fig. 1. Disaster Chain Model

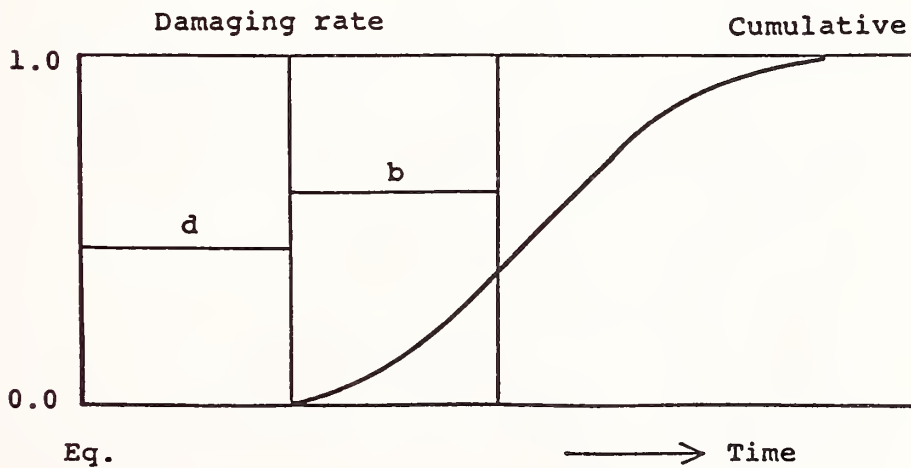
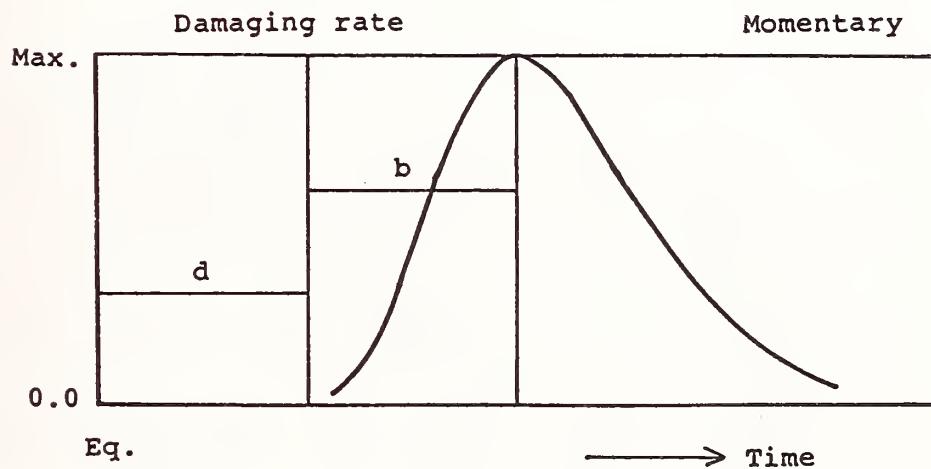


Fig. 2. Functional Model of Damaging Processes

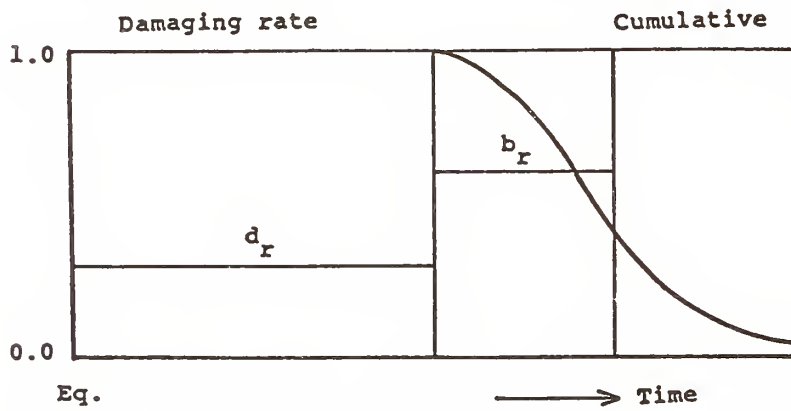
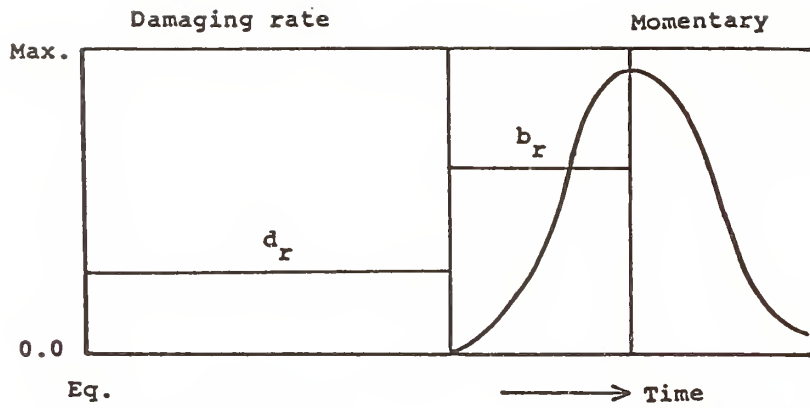


Fig. 3. Functional Model Of Restoring Processes

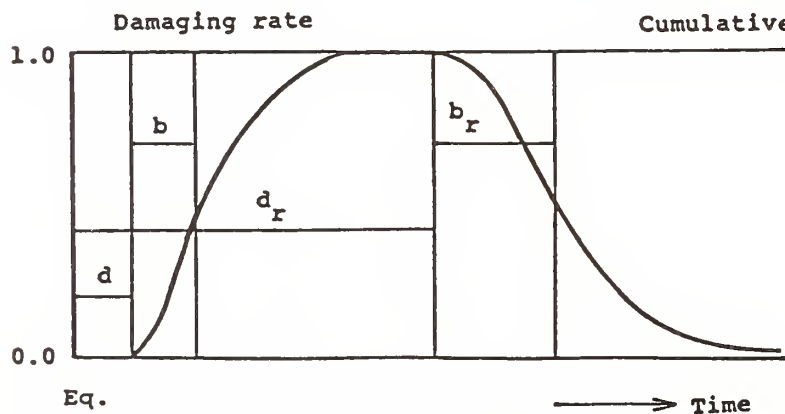
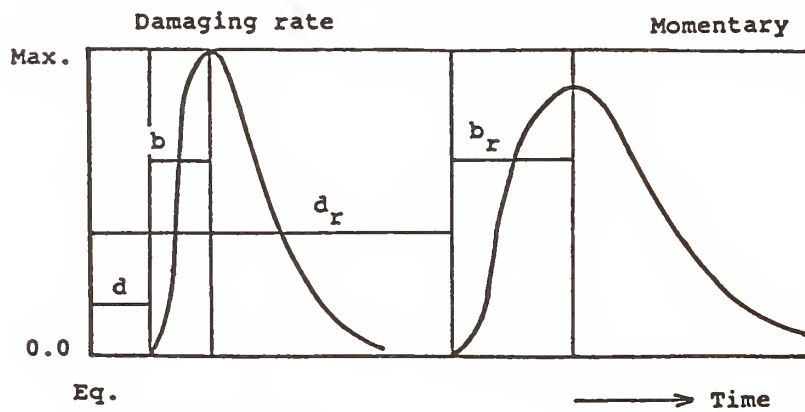


Fig. 4. Functional Model of Total Disaster Processes

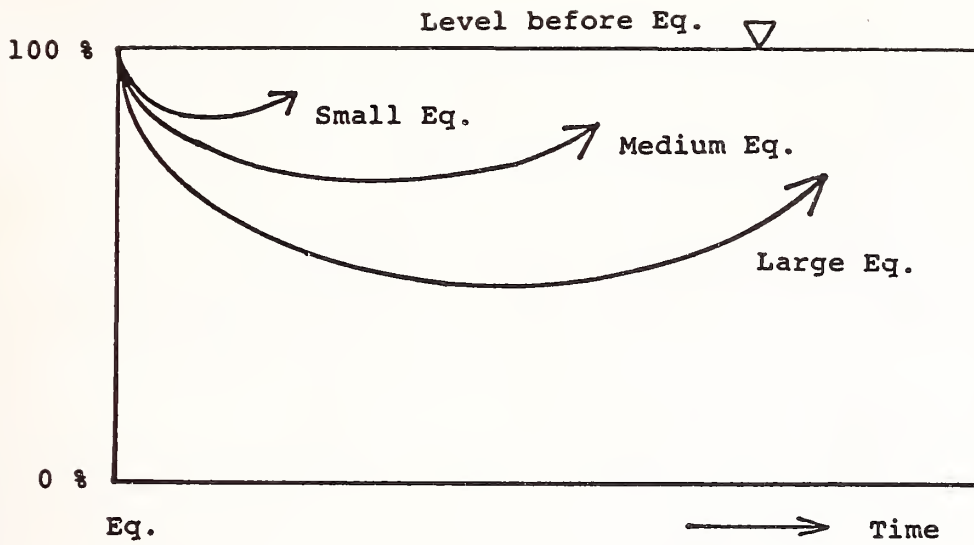


Fig. 5. Change of Standard Life Level

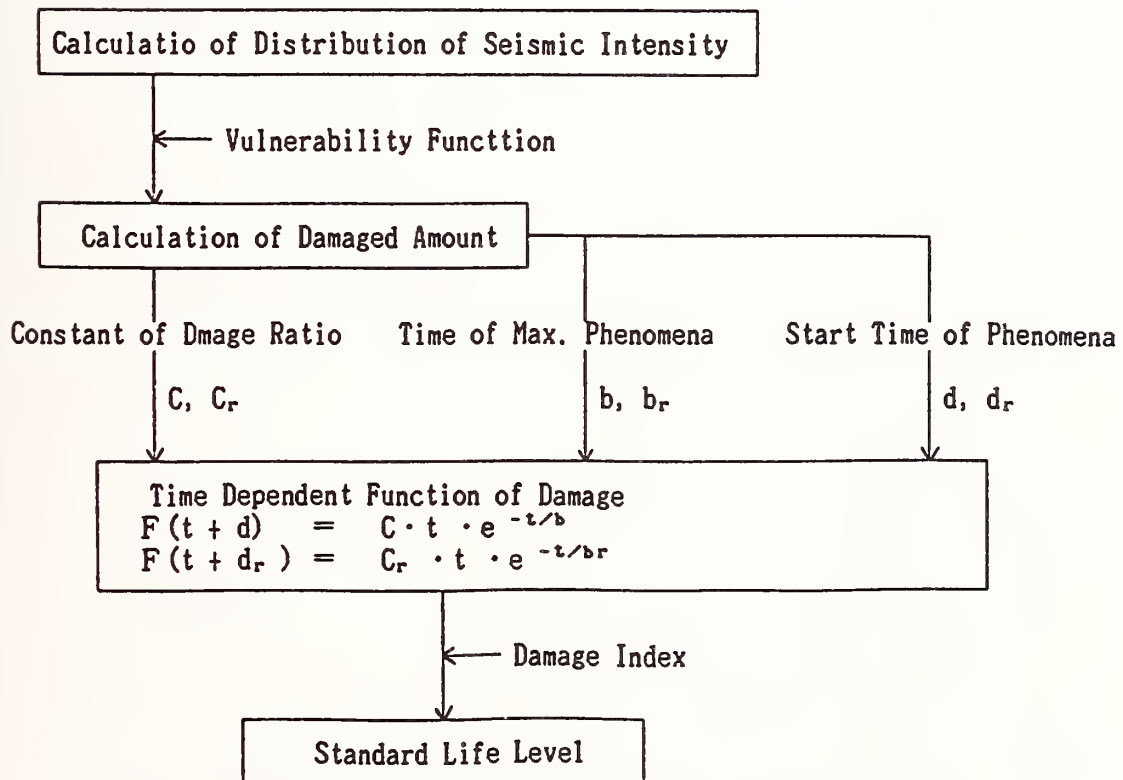


Fig. 6. Flowchart of Calculation of Standard Life Level

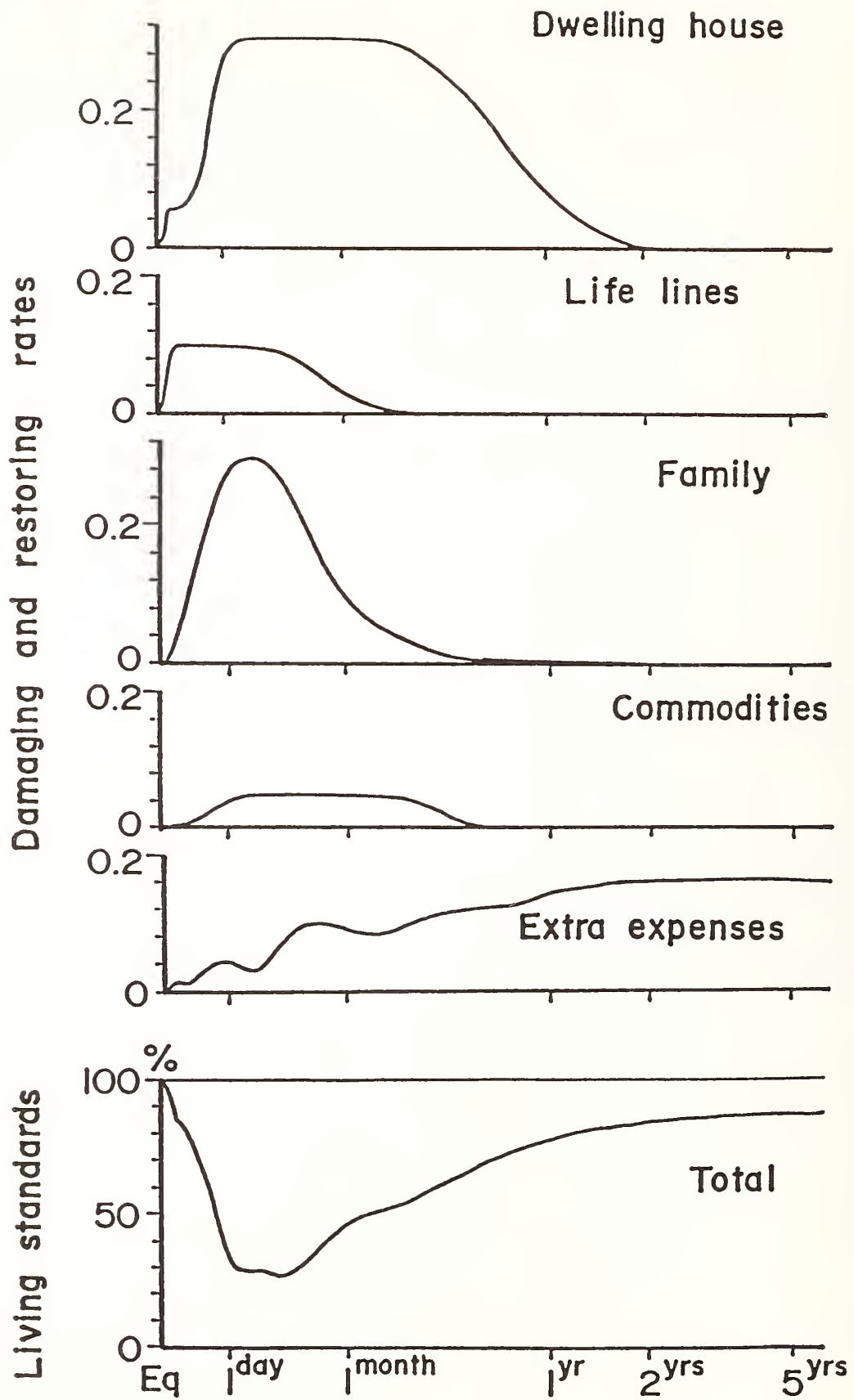


Fig. 7. An Example of Calculated Total Image of Earthquake Disaster

## **Theme III**

---

### **Storm Surge and Tsunamis**



# Combined Effect of Storm Waves and Surge

BY

Paul D. Farrar and H. Lee Butler<sup>1</sup>

## ABSTRACT

This paper describes techniques used by the Coastal Engineering Research Center (CERC), U.S. Army Engineer Waterways Experiment Station, for modeling combined storm waves and surge. Numerical models for spectral wave climate and for long-wave response, with flooding, are applied separately and the results combined. Examples of recent project studies are presented, and limitations of the modeling techniques used are discussed. A current CERC research program to integrate wave and surge numerical models for more accurate simulation of their combined effect is described.

**KEYWORDS:** Storm Surge; Waves; Hurricane; Coastal Flooding; Numerical Modeling

## 1. INTRODUCTION

The U.S. Army Corps of Engineers (CE), as the U.S. Government agency responsible for protection of the coasts of the nation, must be able to accurately predict the likelihood and effects of the destructive storms which shape the coast, damage property and structures, and endanger lives. In addition, the CE provides research support to other Federal, state, and local agencies, such as the Federal Emergency Management Agency and the National Park Service, when they require information on coastal processes or coastal flooding.

A storm surge will produce higher water levels on which short-period surface waves can propagate, subjecting beaches and structures to wave forces not experienced under ordinary water-level conditions. There is a pressing need for procedures to determine the impacts of storm surge and related wave forces for the purpose of establishing design criteria for coastal structures, providing data for economic analysis of coastal projects, and developing evacuation plans.

Use of time-dependent numerical models for simulating water levels and wave propagation in open coastal waters, estuaries, bays, or lakes has become a standard practice. Information on physical response produced by these numerical codes is combined using statistical analysis of event probabilities to estimate the total magnitude and frequency of occurrence of storm-induced water levels in coastal regions. This paper describes both present practice and a development project to enhance the CE's ability to numerically model the combined effects of storm surges and waves on coastal areas.

## 2. STORM SURGE MODELING TECHNIQUES

The numerical modeling system now used by the CE for storm surges and other long waves (such as tides, seiches, and tsunamis) is the Coastal Modeling System or CMS (1). CMS was developed by the Coastal Engineering Research Center (CERC) of the U.S. Army Engineer Waterways Experiment Station (WES). It comprises a set of numerical routines supporting a long wave model, known as the WES Implicit Flooding Model (WIFM) (2).

WIFM solves the standard long wave equations for a body of water (see Reid and Bodine (3)) using an alternating-direction implicit finite-difference scheme. Forces modeled are wind stress, water flows and elevations at boundaries, air pressure variations, rain accumulation, advection and eddy diffusion of momentum, and bottom friction. CMS includes a hurricane wind model and a tidal model which can be used to generate the forcing for the long wave model. Alternatively, wind and tidal forcing functions can be entered from other sources.

A distinguishing feature of WIFM is that it simulates the flooding and drying of land areas, which is an extremely important factor in most storm surges. Flooding and drying rates are determined diagnostically using weir-type equations in which the flow is prescribed on the basis of water level differences, flow type (submerged or overtopping) and boundary characteristics. Special barrier boundaries are allowed between cells to simulate structures such as dikes or dune ridges, which would otherwise be too narrow for representation in the finite difference grid, but which, nonetheless, are important for proper modeling of flooding. As with the boundaries between ordinary cells, the flow across these barriers is determined using weir-type equations. If a formerly dry model grid cell accumulates water to a prescribed depth, it is added to the region in which the wave equations are solved (rather than weir equations). Likewise, when a wet cell's water level drops to a critical level, the wave equations are turned off.

---

<sup>1</sup>Coastal Engineering Research Center, U.S. Army Engineer Waterways Experiment Station, P.O. Box 631, Vicksburg, MS 39180-0631.

Another important feature of WIFM is the capability to use a stretched grid. The region to be studied is covered by a rectangular grid, but one in which the spacing of cells may vary. CMS contains routines for creating these grids. This enables the model to cover a large area while maintaining high resolution in areas of interest, but without having to use enormous (and expensive) grids.

### 3. STORM WAVE MODELING TECHNIQUES

A storm will produce not only a long wave surge, but also short-period wind-driven waves (periods of less than 30 sec, approximately). These waves can cause significant damage by wave impact and flooding because of their unusual size, and because a surge may raise the mean water level, allowing waves to reach previously unexposed areas and structures. The modeling of storm surge processes must therefore include these effects.

The current technique used for modeling wind-driven waves by the CE, is the use of spectral wave models. The wave energy-density spectrum is divided into discrete bands in both frequency and direction (usually 20 frequency and 16 direction bands). The numerical model calculates wave propagation and dissipation in each of these spectral elements, the nonlinear wave-wave interactions between them, and the input of energy by wind. The CE spectral wave model most appropriate for coastal studies is SHALWV (4). This model takes into account reshaping of the spectrum by varying bottom depth and the refraction and dispersion of the wave energy.

SHALWV and similar deep-water wave models have been used by CERC to produce a number of long-term wave climate hindcasts for use in planning by various CE field and engineering end users. A hindcast of waves from hurricanes in the Gulf of Mexico and U.S. Atlantic Coast has been completed (5) covering the years 1956-1975, the same period used in earlier hindcast studies for these regions with hurricanes excluded. SHALWV was used as the wave model in order to include the effect of the continental shelf on the waves. The hindcast areas were covered using grids with 30 n.m. spacing.

### 4. CASE STUDIES

#### 4.1 Long Island, New York

A study to investigate the frequency of storm plus tide flood levels along the coast and within the bays of southern Long Island, New York, was conducted at WES (6). The study involved development of two model grids (global and nearshore models), collection of field data for model calibration, computation of coastal and back-bay stage frequencies, and analysis of alternative barrier and inlet configurations. A combination of the joint probability method and a modified historical method was used to develop

the combined stage frequencies for hurricanes and extratropical storms (called northeasters for the study area). Due to the severity of the historical and hypothetical storms to be simulated for developing the statistical data base, a scheme to model breaching of the barrier island system was implemented. This empirical procedure combined surge tide and wave setup to trigger dune destruction and breaching. For nearshore and back-bay simulations, it was necessary to represent the statistics of the thousands of possible global surge-tide events with a much smaller ensemble of events for actual computer simulation. For all storm simulations, the contribution to flood water potential from wave effects was taken into account. Wave setup estimates were made by applying standard practices in the Shore Protection Manual (7). A procedure was developed which would process previously generated storm simulation output and compute additional bay elevations on a storm-by-storm basis. The accuracy of these results suffers because of the simplifying assumptions made, as well as a lack of information available as to the physical processes involved. The results did provide a good indication of the size of the influence of wave setup on back-bay stage frequencies.

#### 4.2 Roughans Point, Massachusetts

A second example of the separate calculation of storm surge and waves is described in Hardy and Crawford (8). The purpose of this study was to determine flood levels in the back-bay reaches of the Saugus-Pines River system, as well as to determine the frequency of water volumes caused by storm waves overtopping seawalls protecting a residential area called Roughans Point, located just north of Boston, Massachusetts.

To study the wave overtopping problem and frequency of the resulting flood conditions, five models were used in conjunction. An ensemble of northeasters, developed from a set of 28 historical storms, was simulated using WIFM to determine storm surge levels. Deepwater spectral wave model hindcasts, which were available for 26 of the events, were transformed into shallow water wave conditions at the shoreline using the methods of Jensen (9) and of Hubertz (10). Flooding due to overtopping of various proposed structures was determined using overtopping coefficients obtained by tests of physical scale models of the structures. A flood routing model calculated the maximum stage in the interior of Roughans Point caused by each simulated event. A representative set of events was chosen for simulation, and stage-frequency curves were determined based on the probabilities of the events and the response to them.

#### 4.3 Agana, Guam

Mark et al. (11) determined the stage frequency of tropical storm water levels for the area of Agana Harbor, Guam. An ensemble of 168 hypo-

thetical tropical storm events, determined to statistically represent the events affecting the harbor, was assembled. WIFM was used to calculate the storm surge corresponding to each event. The time series of elevation of surge for each case were then added to 100 tidal time series randomly selected from tide records for the site, resulting in an ensemble of 16,800 combined tide-surge events.

SHALWV was used to determine the spectral wave conditions for the storms at the edge of the coral reef at the site. A deepwater grid of 30 by 14 cells with 30 n.m. spacing, and a near-shore grid of 9 by 9 cells with 2.16 n.m. spacing nested in the larger grid provided coverage of both the full area of the typhoon and topographic detail near the harbor.

A physical scale model was used to estimate water level contributions due to ponding and setup on the reef. The results of all these models were then combined with a statistical model of storm frequency to produce stage frequency estimates for local planning purposes.

## 5. DISCUSSION OF CURRENT TECHNIQUES

Although the studies described above represent a progression of the best techniques available for engineering applications, certain weaknesses are apparent in these approaches. These investigations have treated storm surge and the wind-driven short-period surface wave field as non-interacting, linearly-additive phenomena. If the two are considered together, the usual technique is to calculate the storm surge and then, for each time increment, calculate values of wave breaking, runup, setup, and overtopping based on the current surge water level. Any mutual feedback effects are neglected. If, however, the surge modifies the wind-wave field, which, in its turn modifies the surge this simplification may not be justifiable.

Wave overtopping of natural and man-made structures, such as dune ridges or dikes, can cause flooding which would not be predicted by an ordinary storm surge model. WIFM determines the flooding rates of model regions using weir-type equations based on the still-water surface level of the surge. If wind waves in the direction of flooding are present, flooding rates will increase. Flooding by wave overtopping can occur in cases where the still-water level is below the level of structure.

Wind waves directed against land or a structure will generate wave setup, in which the stress caused by the shoaling and breaking waves is balanced by a surface slope, and wave-induced currents, in which the stress drives the flow. Stress contributions of the wind-wave field should be added to the surge model in areas where the wind-wave field is significantly modified by shoaling and breaking.

The wind-wave field will change on time scales of the order of the storm (1000 sec or greater) due to changes in the water depth caused by the storm surge. In some locations, especially near structures and inlets, the surge will also generate currents strong enough to modify the wave field.

Much of the physical damage caused by a storm surge is caused by wind waves which, because of changes in water levels, propagate into areas which normally would be protected or completely dry. A model used to predict damage should include effects of both waves and surge, and should accurately model breaking and dissipation of waves moving through obstructed areas (such as marsh, woods, or urban areas).

## 6. RESEARCH ACTIVITIES

In order to improve CE capabilities in the area of modeling storm surges and their effects, CERC is now engaged in a research project to develop a combined wind-wave, storm-surge numerical modeling system, using already developed and tested methods of modeling these phenomena. The short-wave method will be that of SHALWV, and the long-wave that of WIFM. The system will be integrated into CMS to allow use of system features for data entry, interchange, and display. The initial stage of combination of the models will be the isolation of water-level dependent portions of SHALWV (such as the wave propagation portions) and wave-field stress dependent portions of WIFM followed by the development of replacement routines. Subsequent phases will include development of wave-dependent flooding and overtopping routines for the long-wave and flooding model.

### 6.1 Comparison with Observations

The research program is now making a thorough comparison of the results of current techniques with field observations taken during a hurricane. The Hurricane Surge Prototype Data Collection Work Unit of CERC has placed wave and water-level gages in the path of hurricanes approaching the U.S. coast. The gages were installed in previously prepared sites shortly before a hurricane's arrival. The hurricane being used for comparison is Danny, 1985 (12). At present wind and wave hindcasts have been completed, but analysis of the results has not been completed. These results will be used for comparing the effectiveness of current techniques and those to be developed under this project.

### 6.2 Numerical Methods

The system will run the surge and wave models simultaneously, as co-resident intercommunicating processes, rather than by combining the two into one huge model. In other words, each model will run independently of the other until it needs results from the other, at which point

the process will remain inactive until the data is received. As each component model generates data needed by the other, that data will be transmitted. Thus the two models will run simultaneously during independent portions of the computations, and alternately during the interdependent portions. This protocol should not only save much development time, but allow the combined system to take advantage of further developments in the two components as they are made by other CERC research groups.

## 7. ACKNOWLEDGMENTS

The research presented in this paper, unless otherwise noted, was sponsored by the Office Chief of Engineers, U.S. Army, and is published by its permission.

## 8. REFERENCES

- (1) Leenknecht, D. A., D. J. Mark, and H. L. Butler, "Coastal Modeling System (CMS), Theory and Program Documentation," U.S. Army Engineer Waterways Experiment Station, Vicksburg, MS, Report in preparation.
- (2) Butler, H. L., "Evolution of a Numerical Model for Simulating Long-Period Wave Behavior in Ocean-Estuarine Systems," Estuarine and Wetland Processes with Emphasis on Modeling, Marine Science Series, Vol. 11, Plenum Press, New York, NY, 1980.
- (3) Reid, R. O., and B. R. Bodine, "Numerical Model for Storm Surges in Galveston Bay," Journal of Waterways and Harbors Division, ASCE, Vol. 94, No. WW1, Proc. Paper 5805, February 1968, pp. 33-57.
- (4) Hughes, S. A., and R. E. Jensen, "A User's Guide to SHALWV: Numerical Model for Simulation of Shallow-Water Wave Growth, Propagation, and Decay," U.S. Army Engineer Waterways Experiment Station, Vicksburg, MS, Report CERC-86-2, 1986.
- (5) Abel, C. E., B. A. Tracy, C. L. Vincent, and R. E. Jensen, "Hurricane Hindcast Methodology and Wave Statistics for Atlantic and Gulf Hurricanes from 1956-1975," U.S. Army Engineer Waterways Experiment Station, Vicksburg, MS, Report in preparation.
- (6) Butler, H. L., and M. D. Prater, "Innovative Determination of Nearshore Flood Frequency," Proceedings of the 20th International Conference on Coastal Engineering, ASCE, Taipei, Taiwan, 9-14 November 1986, pp. 2463-2475.
- (7) Shore Protection Manual, 4th ed., 2 Vols., U.S. Army Engineer Waterways Experiment Station, Coastal Engineering Research Center, CE, U.S. Government Printing Office, Washington, DC, 1984.
- (8) Hardy, T. A. and P. L. Crawford, "Frequency of Coastal Flooding at Roughans Point, Broad Sound, Lynn Harbor, and the Saugus-Pines River System," U.S. Army Engineer Waterways Experiment Station, Vicksburg, MS, Report CERC-86-8, 1986.
- (9) Jensen, R. E., "Methodology for the Calculation of a Shallow-Water Wave Climate," U.S. Army Engineer Waterways Experiment Station, Vicksburg, MS, WIS Report 8, 1983.
- (10) Hubertz, J. M., "A Users Guide to a Steady-State Shallow-Water Directional Spectral Wave Model," U.S. Army Engineer Waterways Experiment Station, Vicksburg, MS, Report CERC-86-1, 1986.
- (11) Mark, D. J., J. M. Smith, and T. A. Hardy, "Typhoon Stage-Frequency Analysis for Agana Bay, Guam," U.S. Army Engineer Waterways Experiment Station, Vicksburg, MS, Report in preparation.
- (12) Garcia, A. W. and W. S. Hegge, "Hurricane Danny Storm Surge Data," U.S. Army Engineer Waterways Experiment Station, Vicksburg, MS, Report CERC-87-11, 1987.

# Stability of Submerged Dike at the Opening Section of Tsunami Protection Breakwaters

BY

Katsutosi Tanimoto<sup>1</sup> and Katsutoshi Kimura<sup>2</sup>

## ABSTRACT

The deepest breakwaters in the world are under construction in Kamaishi Bay in order to protect the port area from tsunamis as well as storm waves. The deepest depth is 63 m and a submerged dike with the crest depth of 19m is planned to be built at the central opening section of 300m wide to close the bay mouth of 2100m wide as much as possible. Because of the narrowness, strong current of 8.2 m/s is expected at the occasion of the design tsunami attack. The submerged dike consisting of a rubble mound foundation and a crown caisson must be stable against the strong current.

In the present paper, the outline of an experimental study which has been carried out to give the design information is introduced. The model scale is 1/50 and the following subjects are investigated:

- a. flow pattern around the opening section due to steady flow,
- b. stability of armour units for the submerged rubble mound foundation against periodic flows,
- c. hydrodynamic forces and stability of the submerged caisson.

KEY WORDS: Tsunami Breakwater, Submerged Dike, Armour Units, Caisson, Hydrodynamic Forces, Stability, Sliding

## 1. INTRODUCTION

The most common facility to prevent or reduce tsunami run-up on the land is seawalls which are built along the waterline. In a port area, however, seawalls with a high crest causes hindrance and inconvenience the daily port operation. Reduction of tsunami height by means of offshore breakwaters provides a solution for the protection of the port area against tsunamis. Tsunami breakwaters restrict the inflow of tsunami waves into harbours by narrowing the entrance and make change the mode of harbour resonance. The theoretical calculations establish that amplification of tsunami height does not materialize because of the energy loss at the entrance.

The typical example of tsunami breakwaters is found in Ofunato Bay along the Sanriku Coast (see Fig.1), where the tsunami breakwater was completed at the bay mouth in 1967 after the Chilean Earthquake Tsunami in 1960. The Tokachi-oki Earthquake Tsunami in 1968 provided the opportunity to demonstrate the effectiveness of this breakwater for the reduction of tsunami height in the bay.

A new tsunami breakwater is under construction in Kamaishi Bay where is located at the distance of 30km in the north from Ofunato Bay. Figure 2 shows the plan of Kamaishi Bay. The site of breakwaters is the bay mouth of 2100m wide. The breakwaters consist of the north breakwater of 990m long and the south breakwater of 670m long, and have a central opening of 300m wide as well as two side narrow openings. The layout of breakwater is the best among several alternatives in tsunami reduction capability and minimization of eddy currents around the entrance. Figure 3 shows the longitudinal section of the tsunami breakwaters. As seen in this figure, 70% of the total breakwater length is located at the depth deeper than 50m and the deepest portion is extended to the depth of 63m. At the central opening, the submerged dike with the crest depth of 19m below the low water level is planned to be built. The construction of the breakwaters reduces the opening section at the bay mouth to 5.4%, which is much smaller than 14.7% in case of Ofunato Bay. Because of the narrowness, a strong current of 8.2 m/s is expected at the occasion of the design tsunami attack. The submerged dike must be stable against the strong current. In order to give the design information, the authors have carried out the experimental study on the stability of submerged dike against tsunamis at the opening section of tsunami breakwaters. The present paper introduces the outline of the study.

<sup>1</sup> Dr. of Eng., Director, Hydraulic Engineering division, Port and Harbour Research Institute, Japan.

<sup>2</sup> Research Engineer, Maritime Structure Laboratory, Hydraulic Engineering Division, Port and Harbour Research Institute, Japan.

## 2. EXPERIMENTAL BASIN AND MODEL

The experiments have been carried out in the deep water basin (50m long, 20m wide) of the Offshore Structure Experimental Basin (50m long, 45m wide) at the Port and Harbour Research Institute, Ministry of Transport. Figure 4 shows of the plan of the basin together with the arrangement of breakwater model. In the basin, currents are generated with arbitrary direction and speed as well as irregular waves. The model scale is 1/50 and the cross sections of breakwaters at the trunk and the central opening section are shown in Fig.5. Breakwaters are the mixed type which consists of a rubble mound foundation and an upright section. The lower part of the upright section at the trunk is shaped as a trapezoid and the upper part is a wave dissipating type of double horizontal slit walls. The submerged dike at the opening section consists of a rubble mound foundation and a rectangular crown caisson of which the crest depth is 38cm (19m in the prototype) below the low water level.

The experiments have been carried out for the following three subjects:

- a. flow pattern around the opening section due to steady flow,
- b. stability of armour layer of the submerged rubble mound foundation against periodic flow,
- c. hydrodynamic forces and stability of the submerged crown caisson.

## 3. FLOW AROUND THE OPENING SECTION

The flow was measured by electro magnetic current meters. Figure 6 shows a horizontal distribution of velocity averaged over the depth. In the downstream region, the contracted stream zone with a high velocity and the separation zone with a low velocity are formed, and the observed live stream boundaries are drawn in the figure. Compared with the side of the south breakwater, the live stream boundary at the side of the north breakwater is more shifted to the center, because the north breakwater is projected to the oncoming flow.

Figure 7 shows the distribution of equi-velocity contours at various vertical sections, of which the location is indicated by the Y-coordinate (see Fig.6). In upper zone around the crown caisson, a strong flow with the velocity of 100 ~ 120 cm/s is observed and the maximum velocity is appeared at slightly downstream side from the crown caisson. Figure 8 demonstrates

the distribution of velocity vector at the section of Y=100. Relatively strong flow with the velocity of about 50cm/s hits locally to the rear slope of the rubble mound foundation, where armour units are apt to be scoured as shown later.

The profile of water surface is also measured. Figure 9 shows the profiles measured at Y=300 for different conditions of the representative velocity which is defined as the X-direction velocity measured at the location above the crest of crown caisson by 20cm. When the velocity exceeds about 80cm/s, a sudden drop of the water surface in the downstream is appeared to cause a hydraulic jump.

## 4. STABILITY OF ARMOUR UNITS FOR THE RUBBLE MOUND FOUNDATION

The stability of the rubble mound foundation has been tested under the action of five cycles of periodic flows having a period of 16 minutes in the prototype (see Fig.14 appeared later). Tested armour units are two ranks of quarry stones (300~800kg, and 2t in the prototype) and three ranks of deformed concrete blocks (tetrapods; 2t, 5t, and 10t). Photo 1 displays the experimental setup of the stability test for the quarry stones of 300 ~ 800kg. In the tested region, the armour layer forms grid meshes by painting with different colours, so that the movement of armour units can be observed easily.

Figure 10 shows an example of the deformation of the rubble mound foundation (300~800kg) after the action of tsunamis with the peak velocity of about 10m/s in the prototype, which is larger than the design velocity. The deformation is measured with ultrasonic depth meter. The contour lines in the figure indicate the scour depth or the accumulation height from the original depth before the tsunami action. At the time of inflow, the downstream region along the live stream boundary from the north breakwater is scoured. Vice versa, the downstream region along the live stream boundary from the south breakwater is scoured at the time of outflow. The largest scour depth reaches to 5~7m in the prototype. Since such a deformation with slightly less magnitude is caused by the design condition, it is necessary to protect the rubble mound foundation with the larger size of armour units.

Figure 11 shows experimental relations between the peak velocity and the damage percent for various armour units. The damage percent is defined as the ratio of the number of moved units to the total number of armour units in the observation area (30 cmX 30cm) where the severest scour is caused around the harbour side of the north breakwater. According to the results, quarry stones are more stable than deformed concrete blocks, when the weight is the same. However it is decided that deformed concrete blocks are used as armour units for the scouring area, because the large size of quarry stones are not available with a low cost.

##### 5. HYDRODYNAMIC FORCES AND STABILITY OF THE SUBMERGED CROWN CAISSON

Hydrodynamic forces on the submerged crown caisson due to steady flows have been measured with the aids of pressure transducers for the straight arrangement of tsunami breakwaters (see Fig.16 appeared later). Figure 12 shows an example of the measured pressure distribution. Positive pressures act on the vertical wall at the upstream side and negative pressures act on the vertical wall at the downstream side. Pressures are negative on the crest slab. Pressures on the bottom slab are positive at the upstream side and negative at the downstream side.

In general, hydrodynamic forces due to steady flows are expressed by the following drag force ( $F_H$ ) and lift force ( $F_V$ ):

$$F_H = (w_o / 2g) C_D A_H U^2 \quad (1)$$

$$F_V = (w_o / 2g) C_L A_V U^2 \quad (2)$$

where,  $w_o$  is the specific weight of fluid,  $g$  is the gravitational acceleration,  $C_D$ ,  $C_L$  are the drag and the lift coefficients,  $A_H$ ,  $A_V$  are the projected areas to the vertical and the horizontal planes,

In Fig.13, the drag and lift forces are plotted against the velocity with the standard deviation, where the forces are expressed as the intensity  $F$  divided with the corresponding projected area. The relations calculated for appropriate hydrodynamic coefficients are also shown by solid lines in the figure. According to the results, the value of the drag coefficient is in the range of 1.0 to 1.5, and the value of the lift coefficient is in the range of 0.5 to 0.8.

Hydrodynamic forces have been also measured for periodic flows. Figure 14 shows examples of time variations of the velocity and pressures at the representative points for a periodic flow. The periodic flow is fairly stable and the absolute peak velocities are in the range of 110 to 120 cm/s. The pressures at two vertical walls ( $P_2$ ,  $P_3$ ) variate similarly with the velocity, although the phase of  $P_3$  is shifted by a half cycle because of the difference of the direction definition. On the contrary, the pressure at the crest slab ( $P_5$ ) is always negative (upward) and has two negative peaks in one cycle of the flow. The appearance time of the peak, however, agrees with that of the velocity. The hydrodynamic coefficients have been analyzed for the phase of the peak velocity. Then, the drag coefficient is in the range of 1.2 to 1.5, and the lift coefficient is in the range of 0.5 to 0.8. They are almost same to those due to steady flows.

The stability of the submerged crown caisson against steady flows has been observed for both breakwater arrangements of straight and Kamaishi Breakwaters. In the tests, the weight of the crown caisson as well as the flow velocity are changed. Figure 15 shows the results for Kamaishi Breakwaters. The caisson weight is denoted by  $W_1$ ,  $W_2$ ,  $W_3$ ,  $W_4$  in the figure, and  $W_2$  is the lightest and  $W_4$  is the heaviest among them. The velocity above the caisson is in the range of 97 to 104 cm/s for the case of  $W_2$ , and in the range of 115 to 124 cm/s for the cases of  $W_3$  and  $W_4$ . In the results, slidings are caused only in the north breakwater side.

In general, the following relation is given for the threshold state against sliding:

$$F_H + \mu F_V = \mu W' \quad (3)$$

where,  $F_H$  and  $F_V$  are the horizontal force and the upward vertical force per unit length of the caisson,  $\mu$  is the friction factor between the concrete slab and the rubble mound foundation ( $=0.6$ ),  $W'$  is the weight of the caisson per unit length in the water (namely, the buoyancy is subtracted). Figure 16 shows the experimental results of stability (non-sliding, threshold, sliding) of the caisson with various weight ( $\mu W'$ ) against the various velocity ( $U$ ), together with the threshold relations calculated for several combinations of hydrodynamic coefficients. The experimental stabilities for the weights of  $W_2$  and  $W_3$  in the arrangement of Kamaishi Breakwaters are well explained by the

calculation with  $C_D = 1.2$  and  $C_L = 0.6$ . The threshold state for the weight  $W_4$  is near to the relation calculated for  $C_D = 1.5$  and  $C_L = 0.8$ . In all, the threshold states fall in the range between these two calculated relations, when the high velocity corresponding to the design condition is considered.

#### 6. CONCLUDING REMARKS

The outline of an experimental study on the stability of a submerged dike at the opening section of tsunami breakwaters has been introduced. The study results have been made use to the design of Kamaishi Tsunami Breakwaters. In the design, storm waves and earthquakes are considered as well as tsunamis. As a result, it is confirmed that tsunami forces are the severest. Figure 17 shows the designed opening section. Three kinds of armour units (300 ~ 800kg quarry stones, 2t and 10t tetrapods) are planned to be placed for the appropriate areas of the rubble mound foundation. The size of the submerged crown caisson, which is decided for the present, is 13m wide and 13m high.

At present, the construction of the rubble mound foundation is completed by 50% as a whole. In this year of 1988, the fabrication of a large size caisson of 30m high is to be started for the breakwater trunk. As to the opening section, the fabrications of concrete armour units and submerged caissons are scheduled so as to be started in 1995.

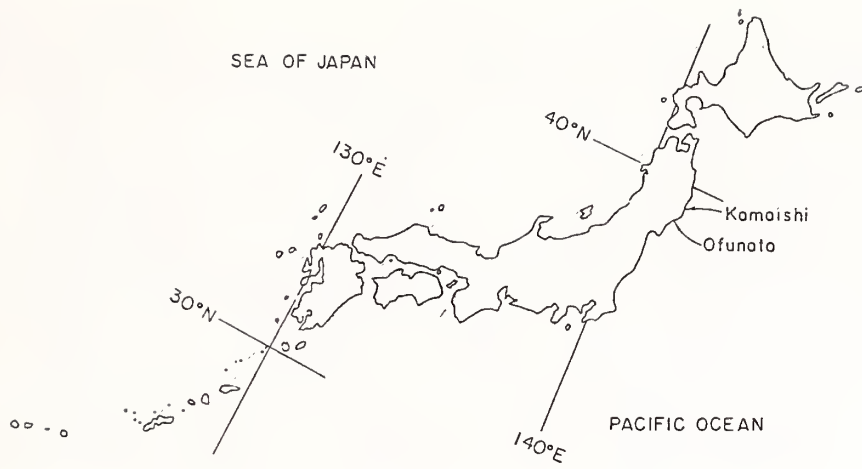


Fig.1 Location Map of Japan

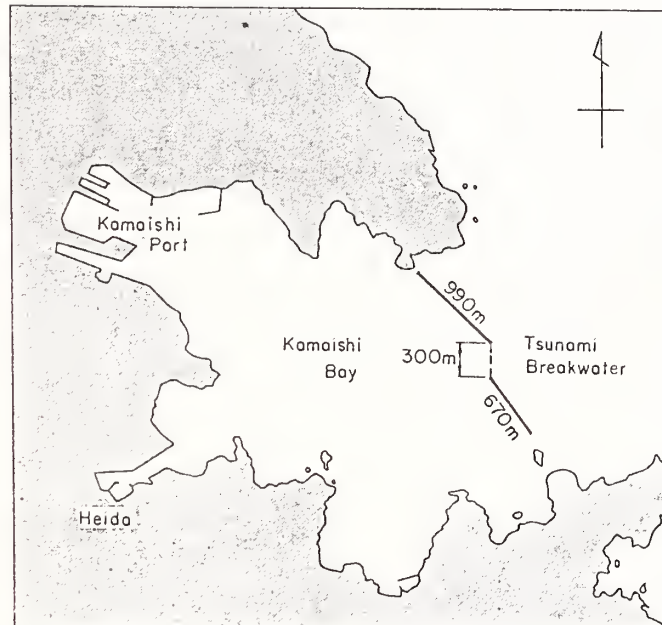


Fig.2 Plan of Kamaishi Bay

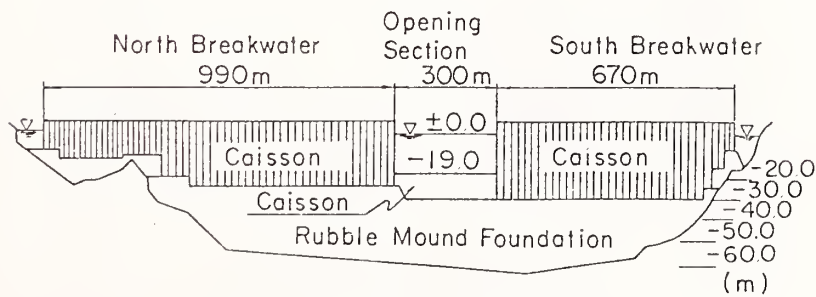


fig.3 Longitudinal Section of Breakwaters

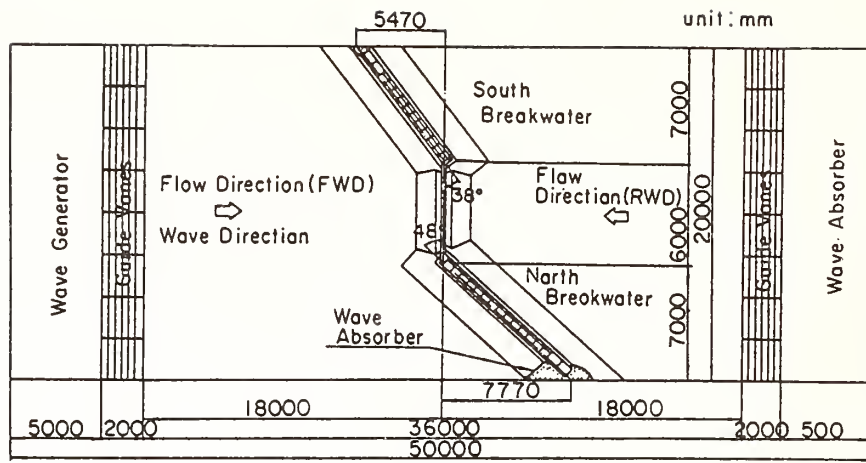


Fig. 4 Breakwater Arrangement in Experimental Basin

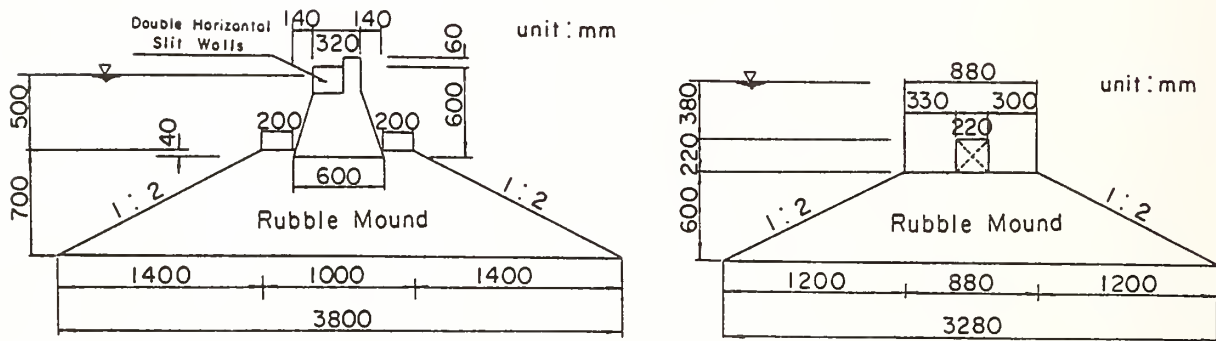


Fig. 5 Cross Sections of Breakwaters

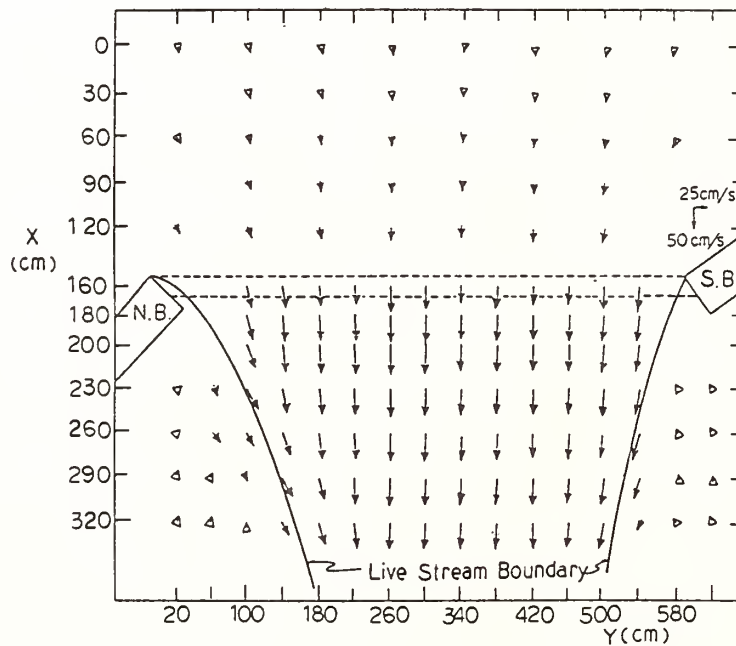


Fig. 6 Flow Pattern around Opening Section

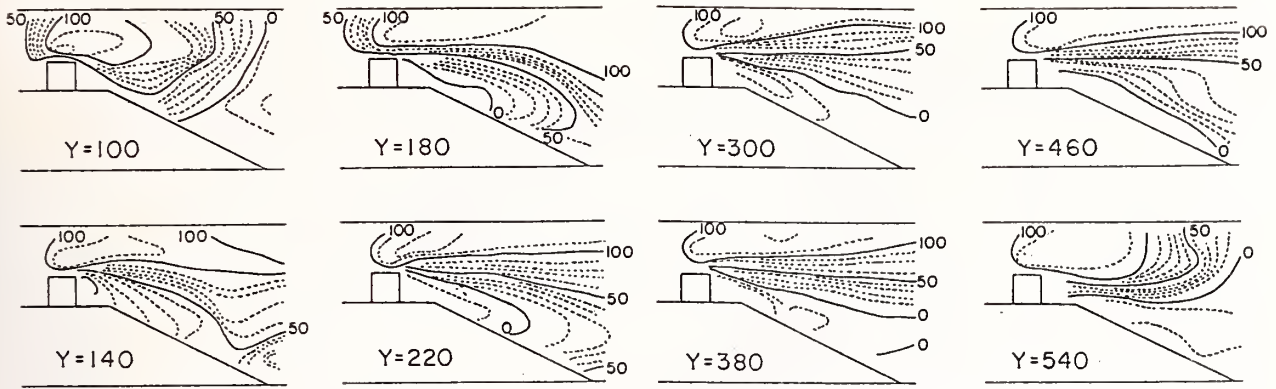


Fig.7 Equi-velocity Contours in Vertical Sections

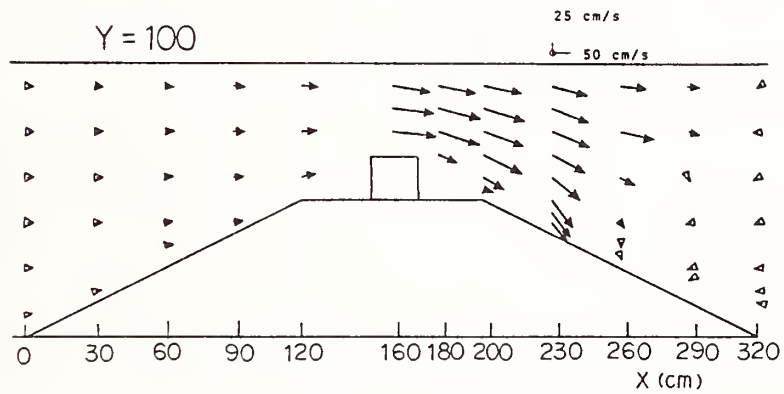


Fig.8 Velocity Vector at Section of Y=100

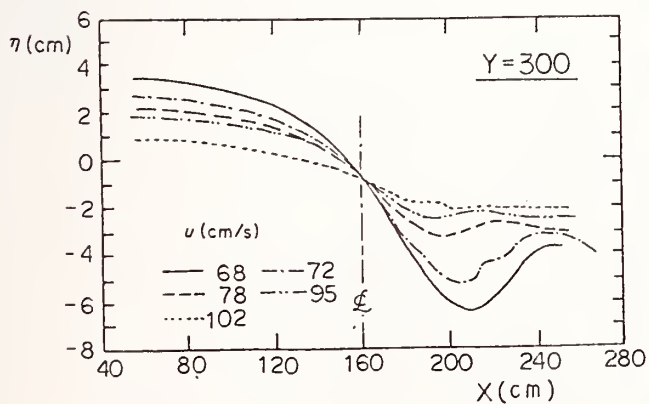


Fig.9 Water Surface Profiles at Y=300

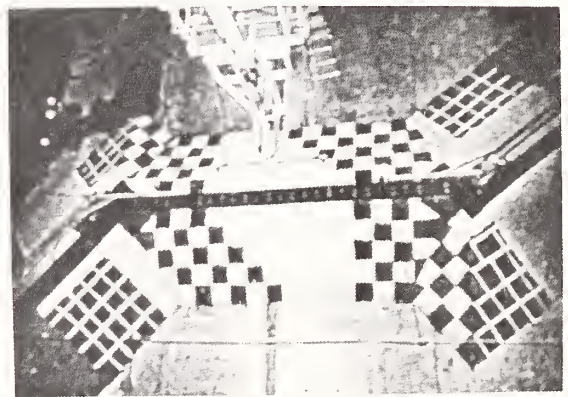


Photo 1 Stability Test of Rubble Mound Foundation

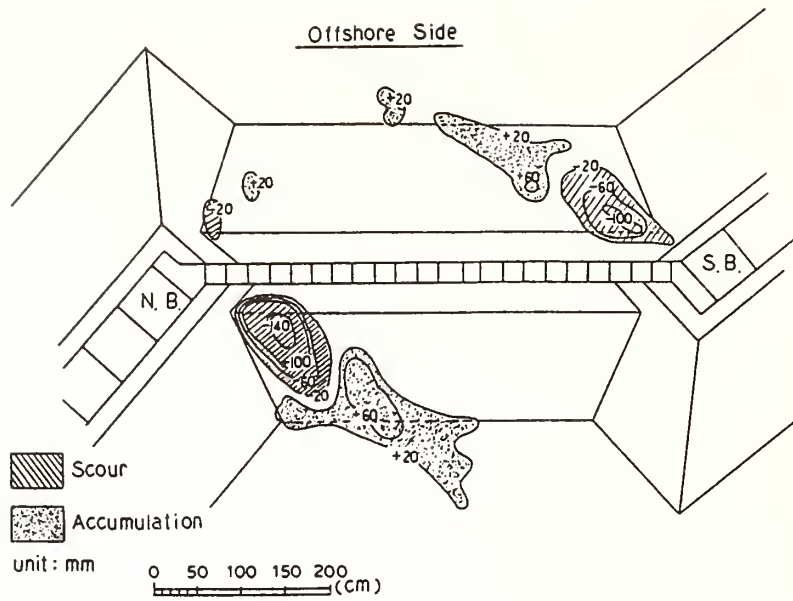


Fig.10 Deformation of Rubble Mound Foundation

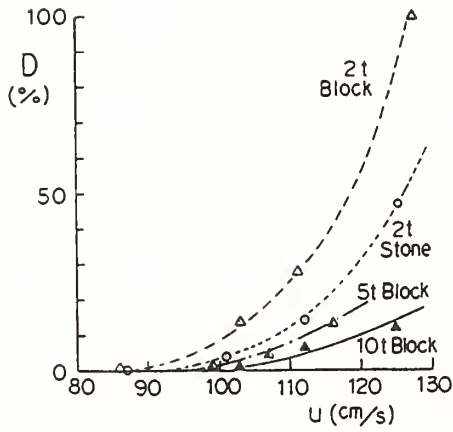


Fig.11 Experimental Relations between Peak Velocity and Damage Percent

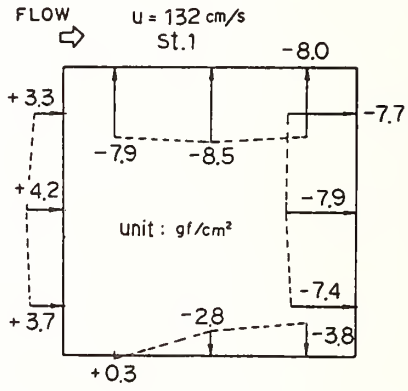


Fig.12 Pressures on Submerged Caisson

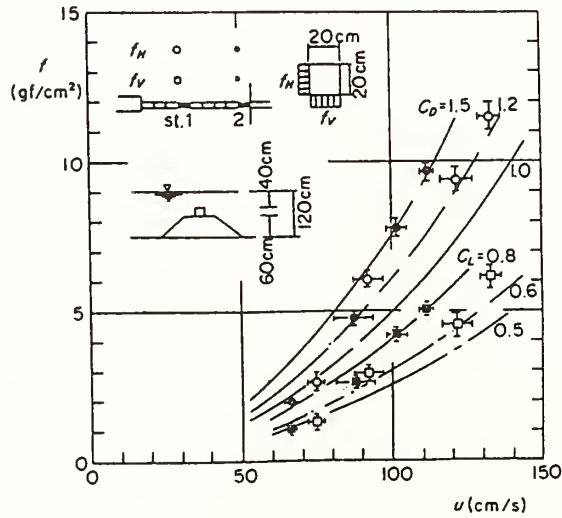


Fig.13 Hydrodynamic Forces vs Velocity

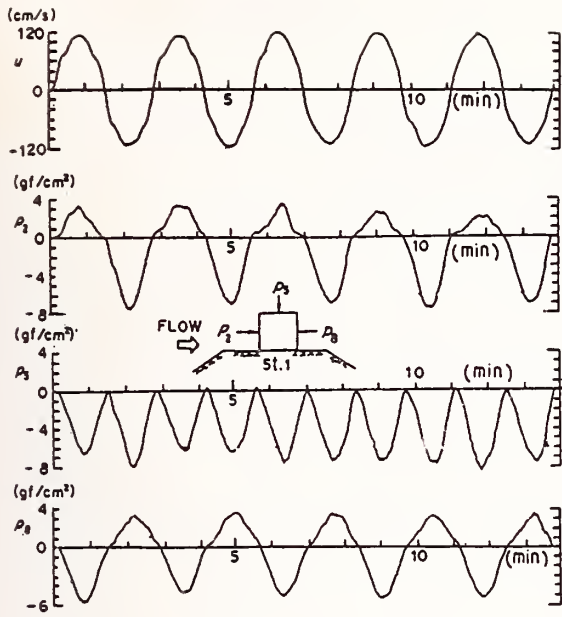


Fig. 14 Time Histories of Velocity and Pressures

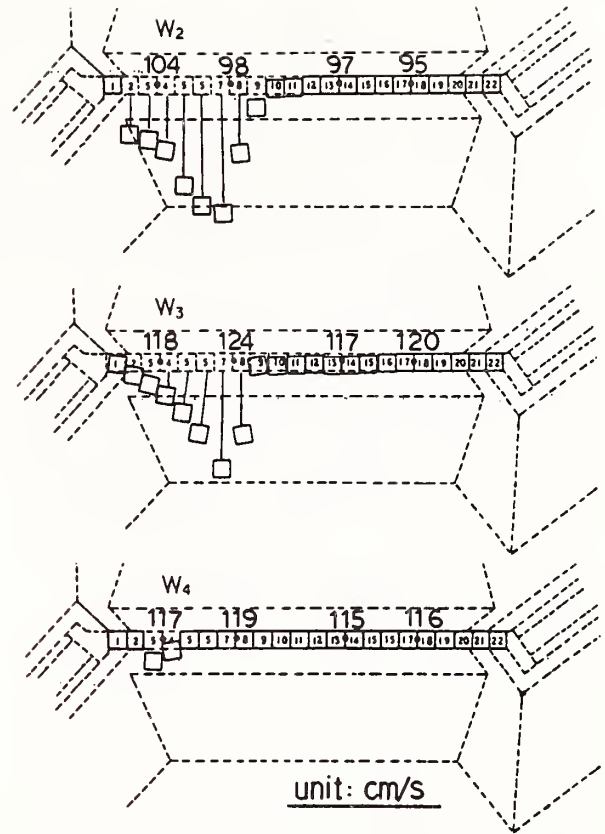


Fig. 15 Sliding of Submerged Caissons

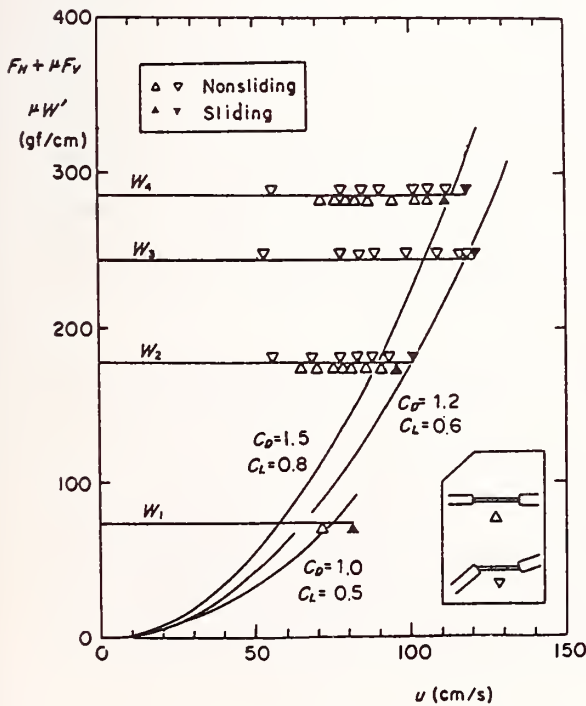


Fig. 18 Stability of Submerged Caisson

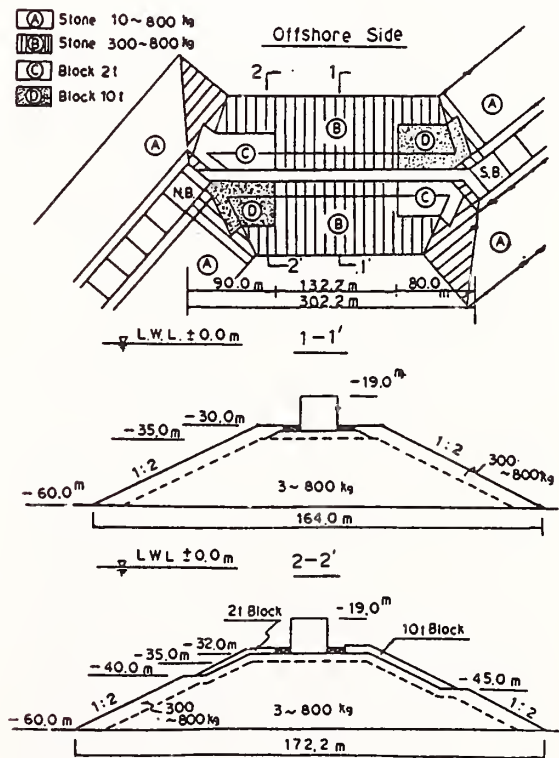


Fig. 17 Designed Opening Section for the Present

# Marine Applications of Geographic Information System

BY

Celso S. Barrientos  
Marine Environmental Assessment Division  
National Environmental Satellite,  
Data, and Information Service  
National Oceanic and Atmospheric Administration  
Washington, DC

## 1. ABSTRACT

This paper describes the application of computer technology to the analysis and synthesis of different types of data and information derived from the marine environment. The results are different forms of display and summary to facilitate the understanding of processes and synthesis of the information.

We present a summary of the information to be used in the study and discuss the process of analysis used. We review the geographic information system and present a case study for the East Coast of the United States in relation to the unusual environmental events during the summer of 1987 and in particular as related to the dolphin deaths episode.

## 2. INTRODUCTION

The Marine Environmental Assessment Division (MEAD), of NESDIS, NOAA, has been active in applying satellite data analyses to fisheries problems. Two years ago we began implementing Geographic Information System (GIS) routines on an image processing system using a combination of VAX 780 and a PC-AT clone. The specific GIS in use is the Aeronca package which came with our image processing software, EASI/PACE.

The problems investigated by MEAD include applications of satellite imagery to west African fisheries, analysis of the upwelling off Peru and Ecuador, larval recruitment at the mouth of Chesapeake Bay, and the large marine ecosystems around Antarctica. For each of these projects, a geographic overlay of land masses, cloud areas, geography boundaries, and labels is an important tool in our analytical technique.

A GIS software package processes large volumes of different spatial data. Data from various and diverse sources must be synthesized and presented to the user in a useful and consistent fashion. In our analysis we deal with different types of data including output of numerical models, observations of physical variables, remote sensing data, and biological and chemical data.

Data were generated from different sources with different time and spatial scales. Meteorological observations were made during set times for operational forecasting use. Polar orbiting satellites make two passes a day and theoretically can take measurements twice a day. Biological and chemical data are taken by special cruises and not readily available. Oceanographic observations are made in widely spaced stations and only limited number of parameters are measured. During oceanographic cruises, then more parameters are observed, however, cruises are infrequent due to big expense. Output of numerical models are the most widely available type of data. Meteorological variables are archive from the operational runs of weather models while oceanographic data can be generated from physical/dynamical model.

GIS process is to put the varied types of data and information in the same frame of reference that can be manipulated in a convenient fashion. Several computer software packages are used in our GIS. We purchased the image processing package and the basic GIS package from software manufacturers. All the other programs that we are using were developed in-house.

### 3. ILLUSTRATION OF GIS

We will illustrate our GIS applications for the marine environment by looking at the east coast and Gulf of Mexico region of the U.S. This region covers from the Yucatan Peninsula of Mexico to the United States/Canadian border. We can begin by displaying one field—the sea surface temperature. We initiate our image enhancement by making a land mask using the high-resolution geographical data base of the Central Intelligence Agency to eliminate all land pixels for easier interpretation and analysis. By properly masking land areas, the coastal boundary is delineated even with just one field displayed. Next we added the geographic boundary and contoured the sea surface temperature field. Then we added the computed monthly geostrophic transport for April 1987 and the climatological transport vectors for April. We added the two vectors and displayed the results. We have combined six fields in the process. These are the geographic boundary, land mask, sea surface temperature, geostrophic and climatological transports, and the vector difference. Our system can display eight fields. However, we can have many more fields stored.

### 4. THE EAST COAST EVENTS OF 1987

Beginning at the spring of 1987 and continuing to the fall season, many environmental events occurred in the East Coast of the U.S. These include the dolphin deaths episode, anoxia conditions, garbage beaching, and the "red tide" occurrence in North Carolina coast. These unusual environmental events attracted wide public attention particularly with the press.

When unusual events occurred like in 1987, scientists from different disciplines were mobilized to understand the events, establish causal relationships, and hopefully propose some alleviating measures.

MEAD obtained the dolphin beaching data from the Smithsonian Institution who is the repository for this information. We plotted in histogram format the weekly number of dolphins beaching beginning in the week of June 6 and ending in the week of September 13. The highest number of beaching occurred during the week of August 2-8. During the 1987 summer period, about 300 dolphins beached. The beaching moved southward with time from the New Jersey coast to the Virginia coast consistent with the seasonal migration pattern of the dolphins.

We used our GIS capability and plotted the location of the beaching. With proper color scheme, we can see clearly the southward movement of the beaching and the increase in number of beaching to the peak in early August and then diminishing.

NOAA has the statutory responsibility to study these unusual events. In the case of the dolphin deaths, NOAA established a team in coordination with other agencies to look in all aspects of the episode. In my Office, we have the task of analyzing the physical data so that the other scientists, particularly the biologists, may have some information on finding the causes of these episodes, i.e. the dolphin deaths.

### 5. ENVIRONMENTAL CONDITIONS

We begun by saying that there were unusual events in 1987. Certainly, our focus here, the dolphin deaths appeared unusual. Therefore, our premise in environmental analysis is to look for something unusual in the environment.

There are various environmental parameters that should be analyzed to look at unusual environmental conditions. These include temperature, wind, wave, ocean current, salinity, river runoff, and precipitation. We have different data sources:

1) remote sensing, 2) observations, 3) model output, and 4) analysis. All the available data and information were collected and analyzed.

We collected the AVHRR (Advanced Very High Resolution Radiometer) data taken by the NOAA Polar Orbiter Satellites. We analyzed the imageries and tie the information together with other physical data. AVHRR data can give us the sea surface temperature, phytoplankton, and sediment load of the water.

Sea surface temperature (SST) were derived mainly from the satellite imageries. We examined the satellite data archives and selected clear images (no or few clouds). SST were derived from the AVHRR data using the Multi-Channel Sea Surface Temperature (MCSST) analysis technique. SST analyses are available at least every ten days period from May to September.

One way to look at unusual SST is to study the anomaly. We compared the monthly SST with long term monthly mean for June, July, and August. The chart of the SST anomalies for June is fairly flat - no major difference shown. However, the SST anomaly chart for July showed major areas of warmer water than normal. The magnitude of the warming is over 2°C in some places. This warming is quite significant considering that this is a monthly mean. The warming anomaly continued through August but the magnitude has decrease. SST analysis was compared with ship observations and the agreement was good.

We archive output of the Limited area Fine Mesh (LFM) numerical model. With this data we computed the wind field over the water. The significant result was that during the 1987 summer, there were prolonged periods (about a week) when the wind was coming from the northeast quadrant. This was particularly pronounced during early August.

If we compare this persistent wind statistics with the monthly mean data, these may not appear significant since the mean showed that about 20% of the time the wind is coming from the NE quadrant. However, 1987 might still be unusual because of the persistence of the wind during prolonged periods. To examine this situation requires further study.

With the wind and temperature data, we calculated the water transport and surface trajectory. The results showed that floatable were brought to the coastal region by the surface currents. These included the dead and sick dolphins. A question can be raised whether there are dolphin deaths every year and they don't beached because the wind is blowing from the opposite direction. We have no answer in MEAD to that question, however, the biologists indicated that should not be the case. That the dolphin deaths are unusual. If the episode is a yearly event, then there would have been no more dolphins left or the stock estimate is wrong to a very low side.

Precipitation was below normal in the East Coast of the U.S. during the summer of 1987. This has significant consequences - the river runoff is low, salinity is high, and intrusion of sea water is further up the bays and estuaries. Was the low precipitation unusual? No. There were years with less rainfall than in 1987, for example, 1980 but there was no dolphin deaths episode then.

## 6. SUMMARY

Geographic Information System software was used in conjunction with an image processing routines to analyze the environmental conditions in the east coast of the United States in relation to the unusual events during the 1987 summer and, in particular the dolphin deaths episode.

Preliminary results of the study are:

- 1) Ocean temperature was warmer than normal, especially in July when the anomalies were greater than 2°C in some places.
- 2) There were prolonged periods (about a week) when the wind is from the NE quadrant. Computed surface transport and trajectory could have brought the dead and sick dolphins in the east coast beaches.
- 3) Below normal precipitation resulting in low river runoff and higher salinity in the mixing zone.

Our study of the 1987 summer is continuing. We are working closely with other scientists in other disciplines. Hopefully, we will learn more about the dolphin deaths episode.



## **Theme IV**

---

### **Summary of U.S.-Japan Cooperative Research Program**

:



# U.S.-Japan Coordinated Earthquake Research Program on Masonry Buildings—Seismic Test of the Five Story Full-Scale Reinforced Masonry Buildings

By

Shin Okamoto<sup>1</sup>, Yutaka Yamazaki<sup>2</sup>

Takashi Kaminosono<sup>3</sup> and Masaomi Teshigawara<sup>4</sup>

## ABSTRACT

A Large number of tests on reinforced masonry (RM) structural elements, such as walls and beams etc., were carried out under the Japanese side program of the U.S.-Japan Coordinated Earthquake Research Program on Masonry Buildings. On the basis of these test results, a draft of the design guidelines for medium-rise RM buildings is now ready to be proposed.

In order to investigate the validity of the design method and to know the total behavior of a RM building which consists of RM structural elements, a five story full scale RM building was tested by applying lateral forces corresponding to inertia forces caused by earthquake ground motion.

The five story test building is 14m in height, 13.79m in length in the loading direction, 15.19m in width in the transverse direction. The prototype structure is a typical apartment building in Japan.

In this paper, the design and construction of the test building, as well as the overall test plan of the test specimen are presented. The test was carried out from mid-November 1987 to the end of January 1988. The test results of the static (cyclic) loading phase, which is the main part of the entire test program, are briefly presented and discussed.

KEY WORDS: Experimental Testing, Full Scale Test, Reinforced Masonry

## 1. INTRODUCTION

Under the auspices of the UJNR on Wind and Seismic Effects, both, the U.S. and Japan are working since 1984 on a coordinated earthquake research program on masonry structures. The target of the Japanese program is the development of comprehensive design guidelines for medium rise RM structures, in particular, the five story apartment building, to meet the country's need of high density residential construction. Based on a detailed understanding of the structural behavior of RM buildings derived from analytical and experimental research programs on materials, components, sub-assemblages and planar frame structures, the design guidelines (draft) was developed.

The five story full scale prototype test on a reinforced concrete masonry building was planned and carried out in order to experimentally verify analytical models which are assumed and dealt with in the draft of the design guidelines.

In the main portion of the full scale test, the test structure was subjected to increasing cyclic

lateral load with the lateral load distribution derived from the Japanese Building Code.

In this paper, the design and the construction of the test specimen is first described, and next, the test plan is introduced. The test results of the static cyclic loading phase also are briefly presented and discussed.

## 2. DESIGN OF THE TEST BUILDING

### 2.1 Design Criteria

The test building (Photo. 1) was designed in accordance with the concepts of a draft of the design guidelines for medium-rise RM buildings [Ref.1].

The main concepts of the design guidelines are as follows;

- 1) Ratios of sum of wall length in each direction to floor area of a RM building (wall length rate) should be more than  $15.0\text{cm/m}^2$  when the masonry prism strength is assumed to be  $240\text{kg/cm}^2$ .
- 2) Allowable stress design concepts should be used for temporary design load.
- 3) Base shear capacity should be more than 50% of the total building weight.
- 4) Rapid strength degradation should not occur in RM members up to the drift angle of  $1/100$  rad. Thus, flexural yield should take place prior to shear failure in most of all RM members. And the strength ratio of shear strength to flexural strength,  $Q_{su}/Q_{mu}$ , is required to be more than 1.2 in walls and 1.1 in beams respectively in order to design a RM building using the structural performance factor,  $D_s$ , of 0.5.

### 2.2 Design of Test Building

The test specimen represents one module of a typical 5-story apartment building in Japan. The floor plan and elevations of the test specimen are shown in Figs. 1 and 2. The test specimen consists of four frames, Y1-Y4, in the lateral direction which is the selected loading direction for the full scale test. The typical story height is  $2.80\text{m}(9'-2")$  including a  $150\text{mm}(6")$  reinforced

<sup>1</sup>Dr. of Eng., Director, Research Planning & Information Department, Building Research Institute, Ministry of Construction, Japan.

<sup>2</sup>Dr. of Eng., Head, Production Department, Building Research Institute, Japan.

<sup>3</sup>Senior Research Engineer, Production Department, Building Research Institute, Japan.

<sup>4</sup>Dr. of Eng., Research Engineer, Production Department, Building Research Institute, Japan.

concrete floor slab which increases in thickness to 200mm (8") along the central loading strip, see Fig. 1, and above the masonry walls to accommodate the vertical 200mm (8") module in masonry concrete block construction.

The test building was designed by the following manner:

- 1) Design strength and elastic module are listed in Table 1.
- 2) Working stress and ultimate horizontal story shear strength were calculated under the external forces whose distribution along the height of the test building is specified by the Japanese Building Code. The distribution of lateral force and story shear force are presented in Table 2.
- 3) In the allowable stress design of individual structural elements for the temporary design load level (nominal shear stress level of  $4\text{kg/cm}^2$ ), the design shear stress for walls and beams had to be sum of 1.5 times the shear stress due to seismic load and the shear stress due to the permanent load.

- 4) Ultimate flexural strength of each wall and beam was calculated by Eq. 1) [Ref.1]:  

$$M_u = \Sigma(A_t \cdot \sigma_y)lw + 0.5 \Sigma(A_w \cdot \sigma_{wy})lw + 0.5 \cdot N_c \cdot lw + N_w \cdot e$$

where

$A_t$ : cross sectional area of flexural reinforcement ( $\text{cm}^2$ ) (including cross section of reinforcement in transverse wall, which effective width is up to 1m on each side.)

$\sigma_y$ : yield stress of flexural rebar ( $\text{kg/cm}^2$ )

$A_w$ : cross sectional area of vertical reinforcement ( $\text{cm}^2$ )

$\sigma_{wy}$ : yield strength of vertical reinforcement ( $\text{kg/cm}^2$ )

$N_c$ : axial force (kg)

$lw$ :  $0.9L_w$

$N_w$ : axial force of transverse wall (kg)

$e$ : distance between compression end of wall and working point of  $N_w$

Reinforcing bars in the transverse members, such as walls and floor slabs, were taken into account. Effective width of RM transverse members was taken as the lesser value of either 1.0m from the face of a RM member in loading direction or 0.25 times the clear span between the RM member in loading direction and the next frame which is parallel to the RM member. The ultimate horizontal strength at each story were estimated by applying the virtual work method to each wall line including boundary beams. The calculated value of ultimate horizontal strength is shown in Table 3.

- 5) In order to carry out the full scale test under severe condition, it was planned to provide some members whose strength ratio,  $Q_{gu}/Q_{mu}$ , did not satisfy the specification of a tentative RM design guidelines. The strength ratio of these members are listed in Table 4.

### 3. DETAILS OF TEST BUILDING

#### 3.1 Profile

Test building has two dwelling units and a stair

case well for each story. The floor area is 13.79m (loading direction) x 15.19m (transverse direction, including 2.4m wide balcony) and the total building height is 14m from the top of foundation to the roof slab (each story is 2.8m in height).

The standard and corner concrete units used in the test building are shown in Fig. 3. Running bond was used in the test building as shown in Fig. 4. Both vertical and horizontal rebars were arranged in 20cm spacing module basically. Wall length rates are  $15.20\text{cm/m}^2$  in the loading direction, and  $23.30\text{cm/m}^2$  in the transverse direction respectively. If the test building consists of 8 dwelling units per floor plan (4 of the test building modules side by side), those values are  $14.89\text{cm/m}^2$  and  $18.15\text{cm/m}^2$  in each direction, respectively.

#### 3.2 Reinforcement

An overview of the reinforcement for frames Y1-Y4 is shown in Fig. 5, and detailed lists of reinforcement for individual wall and beam elements are depicted in Tables 5 and 6, respectively. Basically deformed reinforcing bars, 19mm (D19, #6), were arranged in walls as flexural reinforcement. But D16(#5) reinforcement was used as flexural reinforcement in fourth and fifth story I shaped walls, in walls with cross-walls, and in the flange/wall intersection of flanged walls. Vertical reinforcing bars D16(#5) were arranged with a spacing of 400mm(16"). Horizontal reinforcing bars D10(#3) and D13(#4) were arranged with a spacing of 200mm(8") alternately ( $p_w=0.25\%$ ). In the fourth and fifth story, D10(#3) with a spacing of 200mm ( $p_w=0.18\%$ ) were arranged.

The vertical reinforcement in wall elements is divided into end or main flexural reinforcement which is arranged in the extreme cells of the wall element and standard vertical reinforcement arranged in interior cells. In addition to the member reinforcement indicated in Tables 5 and 6, spirals were provided around the bottom flexural reinforcement in all beams, where flexural yield hinges are expected. Spirals of length  $L=800\text{mm}$  (31.5"), which corresponds to 40d for a D19 (#6) bar, consisted of S4 (0.16") undeformed reinforcement with 100mm (4") inside diameter and 40mm (1.6") pitch. Only one beam, namely  $G_{2A}$  in the second story ( $2G_{2A}$ ), was not provided with spiral reinforcement, in order to determine behavior differences. Spirals were also provided at the base of all walls at the ground floor level around the splices of the main flexural reinforcement (extreme bars) except for the flanged wall ends. In addition, joint reinforcement consisting of S4 (0.16") diameter bars was placed in walls  $1W_{2A}$  and  $1W_5$  and in the lower parts of beam  $1G_{2A}$ . This joint reinforcement was ladder shaped for the walls and U-shaped for the beam.

Transverse walls X1-X3 were typically reinforced with D13, D16@400mm (#4&#5@16") vertically and D10@200mm (#3@8") horizontally with one D19 (#6) bar horizontally at every floor level. In the

1st-3rd story, however, every alternate vertical and horizontal reinforcing bar was changed from D13 to D16 (#4 to #5) and from D10 to D13 (#3 to #4), respectively to increase the reinforcement ratio from 0.18% to 0.25%. Flexural floor reinforcement consisted typically of D10 @200 (#3@8") in both directions, top and bottom.

The short beams  $G_{5A}$  and  $G_{5B}$  were reduced in depth to two courses or 39cm (15.35"), in order to prevent shear failure at low load levels. Spandrel walls with various connection details to the adjacent wall elements  $W_{9B}$  and  $W_{10B}$  were arranged in frame Y4 to study the respective design details. Steel frames and doors were installed in frame Y3 between walls  $W_{7A}$  and  $W_8$  to study their performance at various deformation levels.

Additional design details to be investigated during the full scale test are the top flexural rebar arrangement in the bond beam-R/C slab assemblages, see Table 6, and the effect of small openings in structural components arranged at various locations throughout the test building.

#### 4. CONSTRUCTION OF THE TEST BUILDING

##### 4.1 Reinforcement Setting

The starter bars for the lateral load resisting masonry frames were anchored in a 1.2m (46") deep and 0.9m (35") wide reinforced concrete foundation beam grillage which was tied to the box girder test floor by means of 310 high strength 32mm (1-1/4") diameter post-tensioning bars, prestressed with 40tons (88kips) each.

Construction of the masonry walls commenced by placement of the story high vertical main flexural reinforcement prior to unit placement, in order to protect rebar strain gages and to allow the installation of spiral reinforcement around the 40d (d=diameter of reinforcing bar) lap joints in the critical hinge zones of the first story walls.

##### 4.2 Shear Keys and Inspection Holes

Shear keys, 25mm deep x 80mm wide @ 400mm (1"x3"@16"), perpendicular to the wall axis were formed at the top of the foundation beams and at every floor level in the reinforced concrete slab to prevent slippage between walls and slabs at high load levels.

Inspection holes (clean-outs) were provided at the foot of the walls and the bottom of the bond beams in order to clean out construction debris and joint mortar residue prior to grouting, and to inspect the proper placement of the reinforcement. These clean-outs were arranged every 400mm (16") or where vertical rebar was located.

Prior to grouting of the walls, approximately 25mm (1") of high slump mortar was poured into the cells to minimize segregation effects of coarse aggregate at the slab interface during the placement of the grout concrete. Grouting commenced in two lifts of 1/2 the story height to allow partial setting of the first grout layer

prior to subsequent grouting. The design strength of the grout concrete was  $240\text{kg/cm}^2$  (3400psi), the maximum aggregate size was 20mm (3/4"), and 4% of air entrainment was used to obtain slump levels of approximately 210mm (8.3"). Compaction of grout was achieved by internal vibrating of each with 28mm diameter rod vibrator. Grouting was stopped 100mm (4") below the top of each wall to allow slab concrete to penetrate into the walls. Masonry units, where part of the inside face shell was cut out, were used at the floor levels to establish additional bond between the reinforced concrete floor slab and the walls.

#### 5. MATERIAL PROPERTIES AND QUALITY CONTROL

##### 5.1 Ultrasonic Grout Inspection

After construction of the test specimen, ultrasonic grout inspections in the vicinity of the spiral reinforcement in the first story walls revealed grout flaws in 6 of 32 inspection points. These grout flaws indicate potential problems with grout placement due to the reinforcement congestion in the end cells, caused by the spiral reinforcement. The detected problem areas were subsequently injected with cement grout.

##### 5.2 Concrete

Compressive strength of concrete was designed so that the masonry prism strength should reach  $240\text{kg/cm}^2$  at the time of the loading test.

Twenty seven cylinders, 100mm and 200mm high (4"x8"), of grout concrete for standard material tests and 12 three course, stack bonded, grouted masonry prisms were produced for each story; all test specimens were air cured in the laboratory next to the test building. Compressive tests of the concrete cylinders were carried out 7 and 28 days after the grouting operation, and the prisms were tested in compression after 28 days. Additional materials tests half way through the full scale test program were performed to determine the actual properties at the time of testing. The 28 day tests, as well as test results obtained during the static load testing of the research building, are summarized by story level in Table 7.

The prism compressive test results showed the lower value than the design strength due to making a prism strength just close to and below  $240\text{kg/cm}^2$ . For this purpose, low strength grout concrete with high W/C ratio was used intentionally. The concrete mix design for the floor slabs directly followed the grout mix design of the corresponding story.

##### 5.3 Joint Mortar and Reinforcing Bars

Compressive strength tests of joint mortar specimens, 40x40x160mm (1.5x1.5x6"), after 28 days are also summarized in Table 7. The mechanical properties of the utilized reinforcing bars, obtained experimentally from 6 specimens for each rebar diameter, showed an actual yield stress level of approximately  $39\text{kg/mm}^2$  (54ksi) independent of the rebar size.

## 6. TEST PLAN

The overall test plan consists of the following three phases: 1) the static loading test, 2) the forced vibration test, and 3) the pseudo dynamic tests. The overall test sequence is summarized in Table 8.

### 6.1 Static Loading Test

During the static load testing, increasing cyclic lateral loads following the Japanese Building Code distribution were applied to the test structure by means of servo controlled hydraulic actuators, as schematically shown in Fig. 6. The loading history followed the pattern depicted in Fig. 7, with the first phase of cyclic load levels controlled by nominal base shear stress levels of 1, 2, 3, 4, 6, and  $8\text{kg/cm}^2$  (14, 28, 43, 57, 85, and  $114\text{psi}$ ), respectively. The  $4\text{kg/cm}^2$  ( $57\text{psi}$ ) level represents approximately one of the design limit states, namely the service limit state with a corresponding base shear coefficient of 0.2. Two cycles at this level of service limit stress were repeated at the onset of the yield limit state and the ultimate load limit state of the structure, as shown in Fig. 7, to simulate moderate seismic loading subsequent to various levels of damage accumulation.

In addition to these service load level cycles after each of the outlined limit states, low level individual floor loads were applied in order to establish flexibility coefficients and thus a global stiffness matrix for the lateral floor degrees of freedom.

In the inelastic deformation phase of the structure, the load cycles, while still following the code load distribution, were generally determined by total building drift angle (horizontal roof displacement/height of the structure), as indicated in Table 8, rather than by nominal base shear stress levels.

This static load sequence provides information on: 1) the building response up to service load levels, 2) a trace of the resistance mechanism for increasing lateral force and deformation levels including maximum lateral load capacity, 3) strength degradation and deformation capacity characteristics, and 4) a performance assessment of special design details such as small openings in walls, spandrel wall design, flexural rebar arrangement in beams and service performance of doors at various deformation levels.

### 6.2 Forced Vibration Test

The main objective for the forced vibration tests is a state determination of the test structure at various design limit states by establishing the dynamic response characteristics. Actual stiffness data of the test structure at different damage accumulation levels is important for the calibration of analytical correlation models, and natural frequency and damping information is used in the assessment of subsequent seismic response of the structure. A 10ton, 1-15Hz oscillator permanently installed at the roof level of the test structure was used to obtain the dynamic

response of the test structure including torsional modes and base rocking through steady state vibration and run-down tests.

Component characteristics of floor slabs were also measured through drop weight tests in selected areas at the second and top floor levels.

### 6.3 Pseudo Dynamic Test

The PSD (pseudo dynamic) test phase has two objectives, namely to check the application of the B.R.I. (Building Research Institute) PSD loading system to relatively rigid structures such as this reinforced masonry shear wall structure, and to determine the structural response behavior during a subsequent earthquake or aftershock, following significant damage accumulation during the main event. The pseudo dynamic test followed the yield load limit state, as shown in Table 8 and Fig. 7.

## 7. LOADING

The 5-story full scale test structure was loaded by 11 one hundred ton (220kip) capacity actuators, 3 at the roof level and 2 at the first through fourth floor level, as schematically shown in Fig. 6. All actuators have a stroke of 500mm (20") except for the two exterior roof level actuators 5E and 5W which have stroke ranges of 1000mm (40").

The actuators were connected to a structural steel load beam assembly, as shown in Fig. 8, which transfers the loads to  $0.9 \times 1.0 \times 1.6\text{m}$  ( $35 \times 39 \times 63\text{in}$ ) reinforced concrete load blocks connected monolithically to the 200mm (8") thick and 2.99m (9'-10") wide reinforced concrete floor loading strip along the centerline of the building. In order to preserve the structural integrity of the concentrated load application system after the development of cracks in the floor slab, a high strength thread bar system connecting the load blocks with exterior load distribution beams, as shown in Fig. 8, was provided. The sixteen 32mm (1-1/4") diameter high strength bars at each floor level were only hand tight and not post-tensioned, to limit the introduction of unrealistic axial stress levels in the horizontal beam elements.

The servo valves for the 11 hydraulic actuators are controlled by a MX-3000 Super Mini Computer which receives feedback control information from the load cells incorporated into the actuator assembly and from external magnescales which measure the displacements of each floor level with high accuracy. The magnescales were positioned, one per floor level, between a stiff external reference frame and the geometric center of the test building plan. Only at the roof level, two additional magnescales were installed to measure also the displacements of the two exterior load application points. Each actuator was computer adjusted in a force or displacement control mode.

For the static (cyclic) load testing, two exterior actuators at the roof level, see Fig. 6, were operated under displacement control to prevent the introduction of a torsional deformation mode, and

all other actuators were force slaved to the total measured roof load following the lateral load distribution for the actual test building as specified in the Japanese Building Code. The total roof load contribution factors for the individual floor loads, as indicated in Fig. 6, are 0.40, 0.49, 0.59, and 0.72 for floor levels 1 through 4, respectively.

In the pseudo dynamic test, the actuators were basically displacement controlled from the magnescale readings. However, at floor levels 1 to 4, where only one magnescale measured each center displacement of the floor slab, only one of the two floor actuators was directly displacement controlled from the magnescale with the other actuator in a force slaved mode with respect to the displacement controlled actuator at this floor level.

## 8. INSTRUMENTATION AND DATA ACQUISITION

### 8.1 Instrumentation

Figure 9 shows locations of LVDT's and magnescales. Almost 200 LVDT's were prepared to measure the overall structural response relative to external reference points and the response of selected individual structural components.

Due to the large number of individual elements comprising the test structure, the limited number of instrumented structural components was determined based on the expected deformation limit states of each individual load resisting frame, as indicated in Fig. 10. In order to capture these assumed deformation states, displacement transducers were arranged as shown in Fig. 10, with instrumented components indicated by solid lines.

Flexural (F), diagonal (S), and rotational (R) instrumentation in Fig. 10 refers to LVDT's arranged in series along the extreme fibers of the flexural element, diagonally between the corner points of the element, and perpendicular to the member axis, respectively.

Almost 600 strain gages were attached to the reinforcing bars in critical sections where the formation of flexural yield hinges is expected. For some reinforcing bars many strain gages were used in order to trace the bond-slip behavior, and to obtain the strain distribution in the hinge zone. Concrete surface gages were attached to the block face of walls where direction reversal in shear force is expected. The typical locations of the strain gages are shown in Fig. 11.

### 8.2 Data Acquisition

Eight hundred data points were measured by the high speed data acquisition system which can read 1000 points/second. The data was processed in a super mini computer, and then transmitted to personal computers (PC). In the PCs, 200 data points were selected in order to monitor the experiment. Selected data were displayed on 5 graphic displays. One PC has the capacity to monitor 48 points.

## 9. OUTLINE OF TEST RESULTS

Since the testing came to an end January 1988, all the data obtained through the testing are still being processed. The data correction especially for static cyclic loading test data is required due to following many reasons. Those are:

- i. drift of external reference points (frame) estimated to be caused by movement of the test laboratory structure-reaction floor slab & wall system by temperature fluctuation

All the data were measured 48 hours continuously when the test building took a rest without any testing. The predominant period of the measured drift time history in displacement was just 24 hours, and the level of the maximum peak-peak displacement was 1mm at the top of the test structure. This drift exerts a seriously influence on test data obtained during service load phase because the displacement at the roof floor slab level is in the range of several millimeters.

- ii. connection of the first measured data in a day with the corresponding last measured one in the last day
- iii. connection of a data measured before a displacement transducer repositioning, which is needed due to a stroke limit under large movement of the test building, with the corresponding data measured after the repositioning
- iv. zero adjustment of a data disturbed due to unit loading tests for individual floor levels which were carried out to obtain a stiffness matrix of the test building, pseudo dynamic testing, and forced vibration tests

In principle, data correction in this case is common to the one described in term iii.

- v. error correction  
The high speed data acquisition system produced a few error in time history data when processing. This process error is to be corrected manually one by one.

In this paper, limited test results are introduced in the following. Detailed data analyses for test results have, at present, been continued and will be reported in the next meeting.

Figure 12 shows the loading sequence through overall testing. The test was carried out exactly under the scheduled loading plan as shown in Table 8 and Fig. 7 except last loading cycles in the ultimate load phase. The static loading test was over when the top displacement reached 7/800 rad. drift angle due to concentration of inelastic deformation on the first story. The corresponding first story displacement at this stage was about 60mm, 1/50 rad. drift angle, which is approximately 50% of the top displacement.

Hysteresis curves for the base shear vs. the top displacement and vs. the first story displacement are shown in Fig. 13. Figure 14 shows the base shear vs. the top displacement envelop curve with description of major events during loading. The

test structure behaved almost linear in force vs. displacement relationship for the nominal shear stress level below 10  $11\text{kg}/\text{cm}^2$ .

During and after the loading under the top displacement corresponding to 1/800 rad. drift angle, stiffness degradation became to be remarkable, and shear crack was produced in wall-beam joint elements and also diagonal crack in wall elements.

At this stage, most of all main flexural reinforcement located at the base of the first story wall yielded. Yielding in those located in beam elements occurred at nearly 3/800 rad. drift angle displacement, and at the same displacement level toe crush due to high compression occurred at the base of the first story long wall. Diagonal crack occurred also in a short beam  $G_{5B}$  in the frame Y3 when displacement reached 2/800 rad. drift angle, and face shells on the beam started to fall down after 3/800 rad. drift angle displacement.

The maximum strength of the test structure was 960 ton in base shear which corresponds to total weight of the structure approximately. The top and the first story displacements corresponding to the maximum strength was 70mm (1/200 rad. drift angle) and 22.4mm (1/125rad.) respectively. The first story tangential stiffness at this displacement level decreased in approximately 400ton/cm from initial elastic stiffness, 4000ton/cm.

In the third phase loading (ultimate load phase), the test structure responded for cyclic loading with stable force vs. deflection loop up to about 5/800rad. drift angle displacement. It changed, however, into unstable response after 6/800 rad. displacement, namely deflection concentrated on the first story as shown in Fig. 15 and strength also greatly decreased. Figure 16 shows crack pattern in selected frames.

#### 10. CONCLUDING REMARKS

The Japanese 5-story full scale reinforced concrete masonry test building was designed based on the proposed draft of the new Japanese design guidelines for medium rise (up to 5 stories) RM structures and was tested to provide relevant behavioral response data for the verification of design models for the structures.

Since the data obtained through the testing are still being processed, brief introduction of the test results only was described in this paper. It was found, however, that the test structure showed very good response behavior against static cyclic loading as expected before the test started.

Detailed data analyses and the precise structural analyses for the test structure have been continued and those will be reported in the next meeting.

#### ACKNOWLEDGEMENTS

The writers would like to express their gratitude

to the Promotion Committee for Masonry Research (PROCMAR, chaired by Prof. H. Umemura), for providing the 5-story full scale masonry test building. Special thanks and appreciation goes to all the Technical Coordinating Committee for Masonry Research (TECCMAR, chaired by Prof. T. Okada) and the Building Construction Committee for Masonry Research (BLDCMAR, chaired by Prof. K. Kamimura) members who contributed invaluable to the design and the testing of the full scale masonry research building.

#### REFERENCES

- [1] T. Kaminosono, et al., "Draft of Design Guidelines for Reinforced Masonry Buildings", Proceedings of the Third Joint Technical Coordinating Committee on Masonry Research, Tomamu, Japan, 1987



photo 1 Five-Story Full Scale RM Test Building

Table 1 Design Strength and Elastic Modulus of Materials

Material	Design Strength [kg/cm <sup>2</sup> ]	Young's Modulus [kg/cm <sup>2</sup> ]	Shear Modulus [kg/cm <sup>2</sup> ]	Poisson's Ratio
Masonry prism	240	1.8x10E5	0.80x10E5	1/6
Grout concrete	240	2.3x10E2	0.99x10E5	1/6
Reinforcement	SD30 SD35	2.1x10E6	--	--

Table 2 Determination of Lateral Design Loads

Level i	Weight W <sub>i</sub>	R Σ W <sub>i</sub>	Shear Force Distribution Factors [3]	Shear Force Q <sub>i</sub>	Lateral Loads P <sub>i</sub>	Service Limit State 0.2xP <sub>i</sub>	Ultimate Limit State 0.5xP <sub>i</sub>
	ton	ton		ton	ton	ton	ton
R	176	176	1.70	301	301	60	150
4	205	381	1.39	529	230	46	114
3	205	585	1.23	720	191	38	96
2	205	791	1.11	877	157	32	79
1	205	996	1.00	996	117	23	59
Total	996	-	-	-	996	199	498

Table 3 Calculated Lateral Capacities

Frame Story	Y1	Y2	Y3	Y4	Summation
	[ton]				
5th	37.1	51.1	42.2	31.2	161.6
4th	65.4	89.9	34.2	54.7	284.2
3rd	88.6	122.1	100.8	74.4	385.9
2nd	108.1	148.1	122.8	91.5	470.5
1st	122.8	168.5	139.2	102.7	533.2

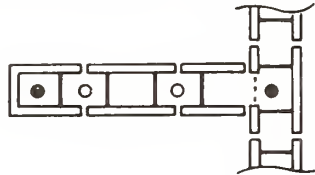
Table 4 List of Members with Limited Ductility

Member	Story	τ <sub>u</sub> [kg/cm <sup>2</sup> ]	Q <sub>su</sub> /Q <sub>mu</sub>
Beam G3	4th	13.9	1.0
Wall W10	2nd	15.2	1.1
	1st	17.2	1.0

Table 5 List of Wall Reinforcement

Story	Wall	W1AB, W6AB	W2AB	W3, W5	W4AB	W10AB
		W9AB, W11AB	W7AB	W8		
5th	Main Flexural	D19, D16*	D16	D16	D19, D16*	D16
	Vertical	D16 @400	D16 @400	D16, D13 @400 alternately	D16, D13 @400 alternately	D16 @400
	Horizontal	D10 @200				
4th	Main Flexural	D19, D16*	D16	D16	D19, D16*	D19
	Vertical	D16 @400	D16 @400	D16, D13 @400 alternately	D16, D13 @400 alternately	D16 @400
	Horizontal	D10 @200				
3rd	Main Flexural	D19, D16*	D16	D16	D19, D16*	D19
	Vertical	D16 @400				
	Horizontal	D13, D10 @200 alternately				
2nd	Main Flexural	D19, D16*	D19	D16	D19, D16*	D19
	Vertical	D16 @400				
1st	Horizontal	D13, D10 @200 alternately				

\* Flanged end



● Main Flexural Reinforcement  
○ Vertical Reinforcement

Table 6 List of Beam Flexural Reinforcement

Beam	G1	G2		G3	G4	G5	G6		G7
		W2 side	W3 side				W9 side	W10 side	
5th	T	D19	D19		2-D19*3 (2-D19*2)	D19	D19		D19
	B	D19	D19		D22	D16	D16	D19	D19
4th	T	D19	D19	D19, D16*1 (D22)	2-D22*1 (2-D22*2)	D19	D16	D19	D19
	B	D19	D19		D25	D16	D16	D19	D19
3rd	T	D22	D22	D22, D16*2 (D22, D16*1)	D25, D22*1 (D25, D22*2)	D22	D19	D16, D22*1	D22
	B	D19	D19	D16, D19*1	2-D19*1	D19	D16	D19	D19
2nd	T	D25	D25		D25, D22*2 (D25, D22*1)	D22	D19	2-D19*1 (D22, (D22) D16*1)	2-D19*3 (D22)
	B	D22	D22		D22, D19*1	D19	D16	D16, D22*1	D22
1st	T	2-D19 (D25)	2-D19 (D25)		D25, D22*2	D16, D19*3 (2-D19*1)	D19	2-D19*3 (D16, (D22) D22*1)	2-D19*3
	B	D22	D22		D19, D22*1	D19	D16	D16, D22*1	D22

T:TOP B:Bottom  
( ): Dwelling unit B

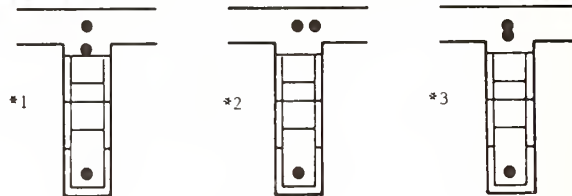


Table 8 Test and Loading Sequence

Test Phase	1. Static (cyclic)			2. FORCED VIBRATION	3. PSEUDO DYNAMIC
	Service Load Level	Load Tests	Displ. Tests		
Response Level	[kg/cm <sup>2</sup> ]	[kg/cm <sup>2</sup> ]	[rad]		
elastic		1 2 3			
cracking		4			
yield		6 8			
ultimate Load		4	9 10 or	1/800 2/800 3/800 4/800	
ultimate displacement				5/800 6/800 7/800 8/800 4/800	

Table 7 Compression Test Results [Kg/cm<sup>2</sup>]

Test	Concrete Grout		Masonry Prisms			Mortar
	28days	testing	28days	testing	testing*	
Time	28days	testing	28days	testing	testing*	28days
Number of Specimens	6/story	6/story	6/story	6/story	3/story	13/story
5th story	262.1	320.7	210.1	204.1		416.2
4th	255.0	304.7	190.7	203.2		466.1
3rd	251.9	293.7	160.1	199.3		370.3
2nd	240.7	350.8	174.4	193.8		372.3
1st	207.1	326.2	157.1	184.7	178.5	420.2
Measn	243.8	319.2	178.5	197.0	178.5	409.0

\* cut from test building at the beginning of the test program

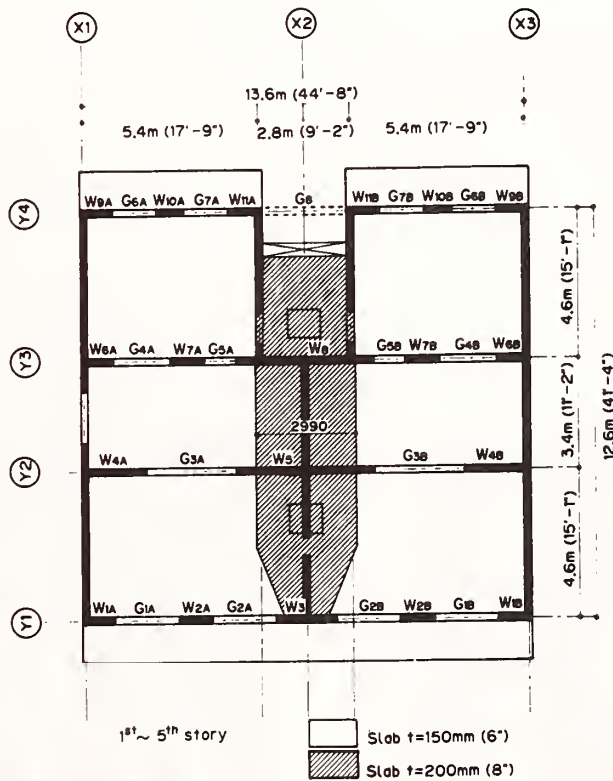


Fig.1 Plan of the Test Building and Member Designation

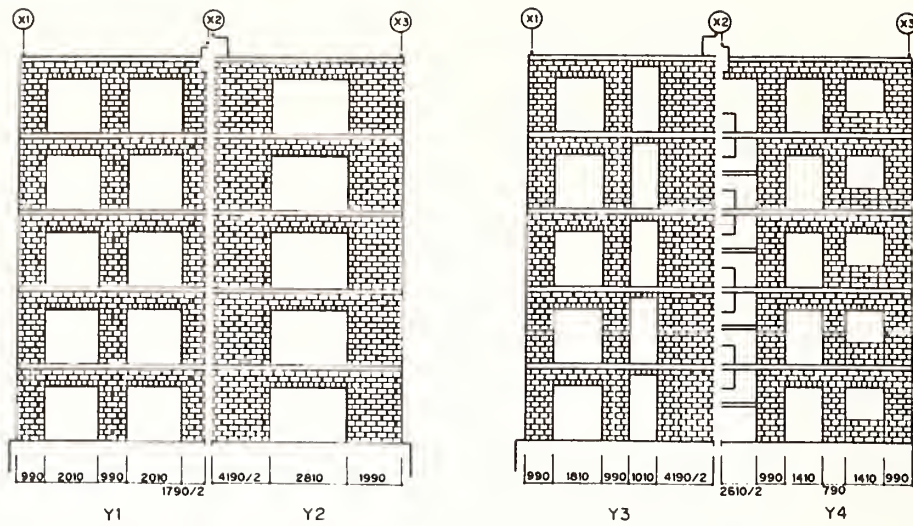


Fig. 2 Lateral Load Resisting Frames Y1 through Y4 [scale in mm]

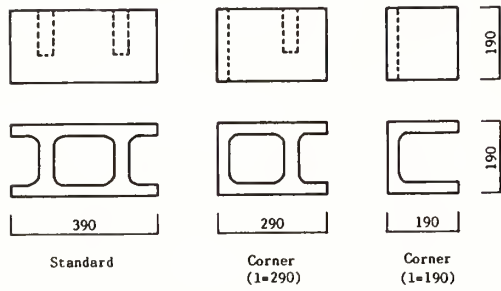


Fig. 3 Concrete Block Units [scale in mm]

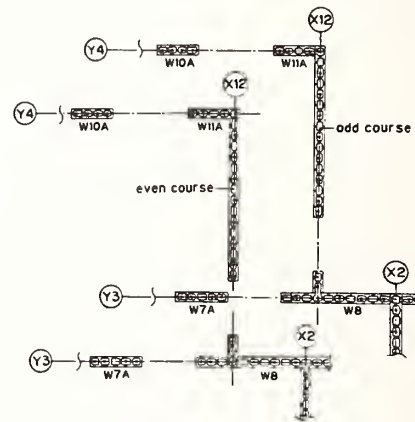


Fig. 4 Typical Bonding and Reinforcing Patterns

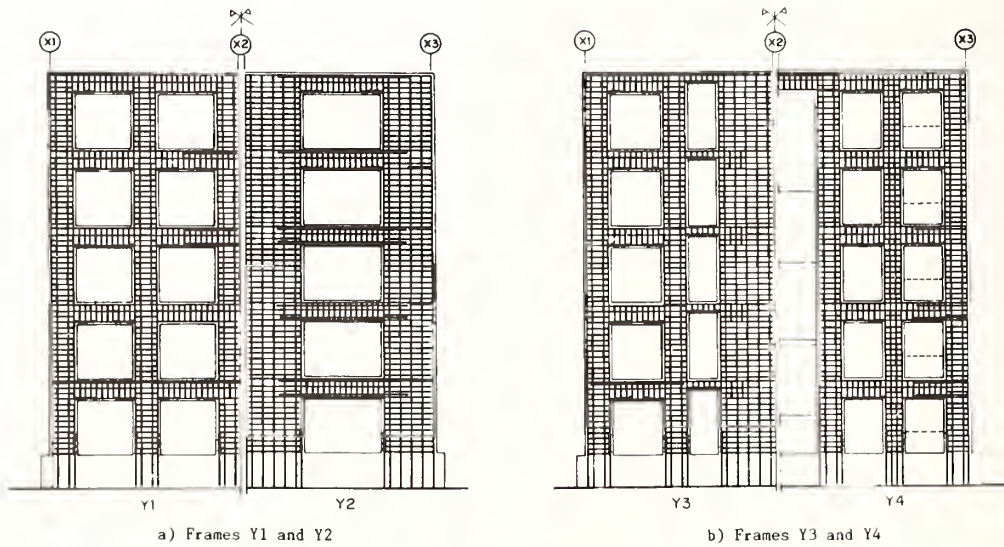


Fig. 5 Reinforcement Layout in Lateral Resisting Frames

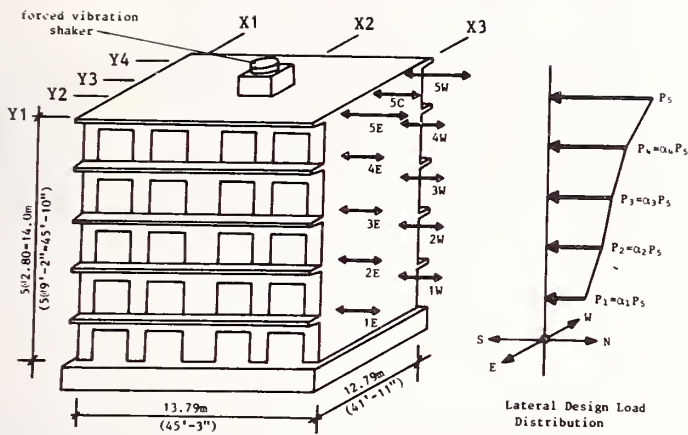
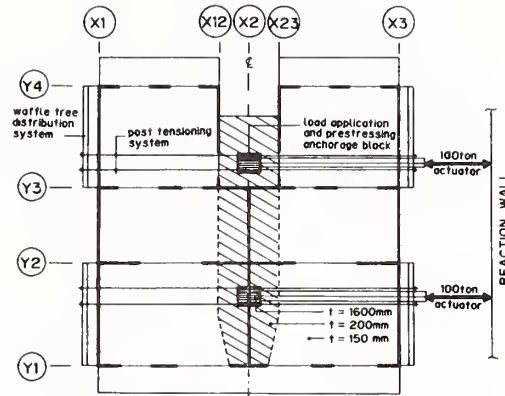


Fig.6 Loading Sketch of Five-Story Full Scale RM Test Building

a) plan view of typical floor slab



b) vertical section through load assembly

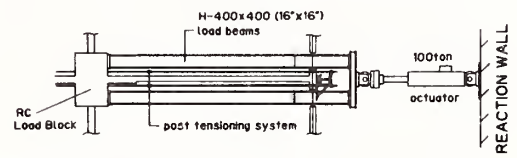


Fig.8 Load Application System

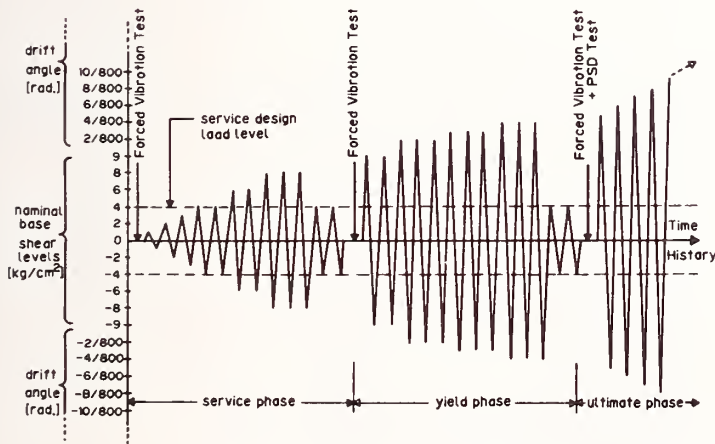


Fig.7 Test Plan and Load History

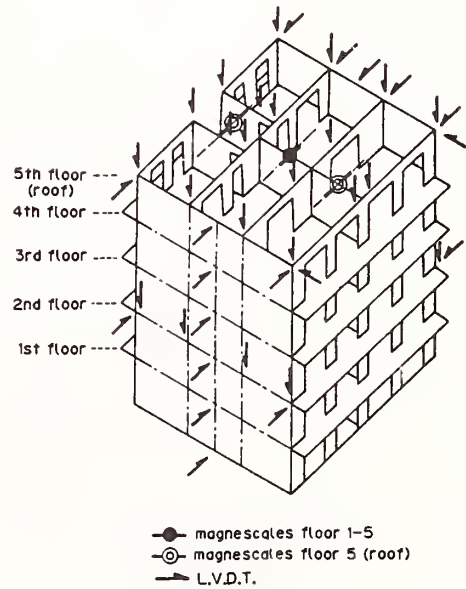


Fig.9 Location of External Displacement Transducers

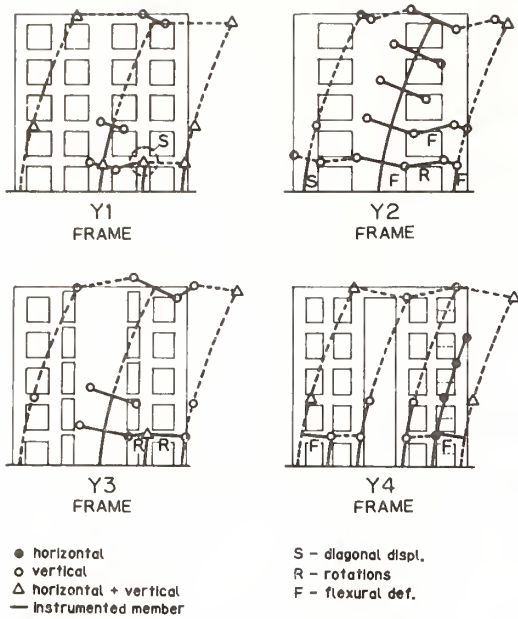


Fig.10 Expected Deformation Patterns and Displacement Instrumentation

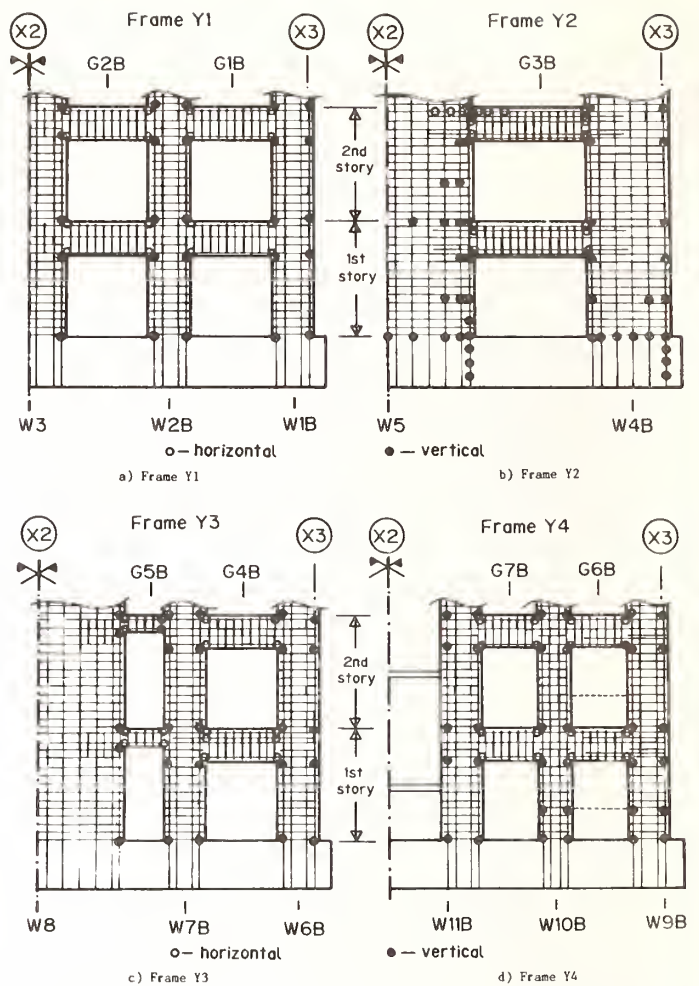


Fig.11 Example of Rebar Strain Gage Locations

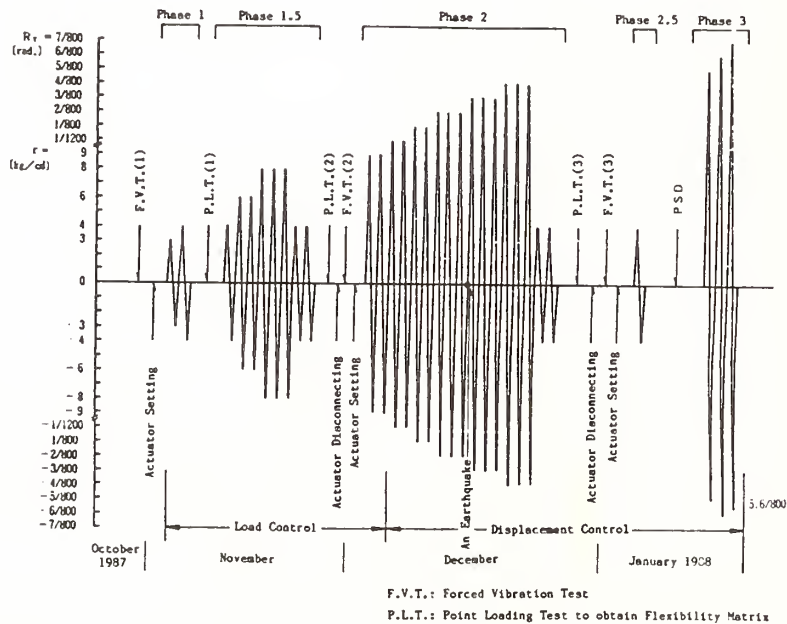
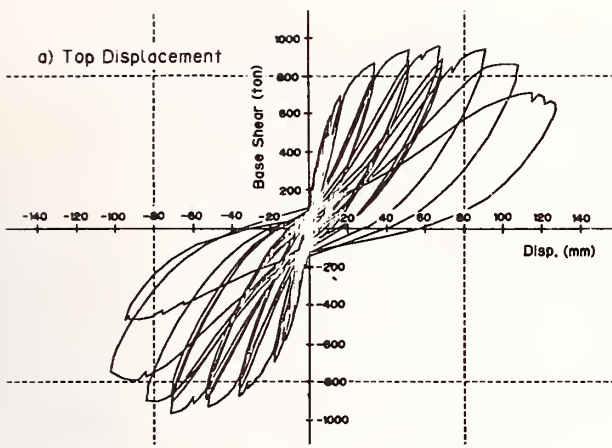
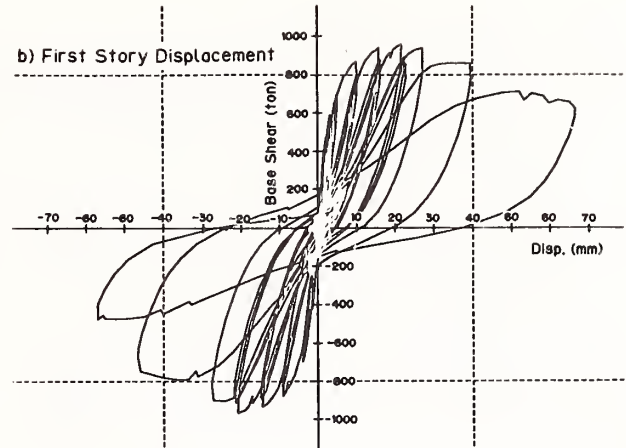


Fig.12 Loading Sequence through Overall Testing



a) Top Displacement



b) First Story Displacement

Fig.13 Base Shear vs. Displacement Relationship  
Obtained through Static Cyclic Loading Tests

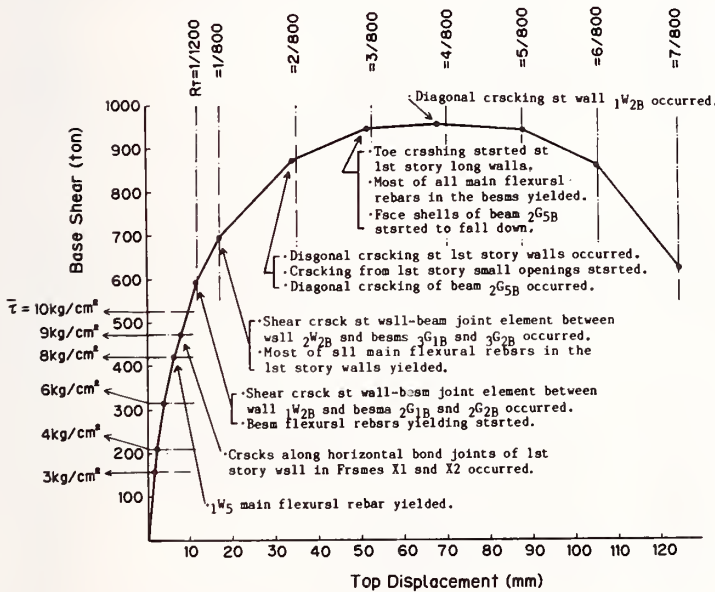


Fig.14 Base shear vs. Top Displacement  
Envelop Curve for Static Cyclic  
Loading Tests

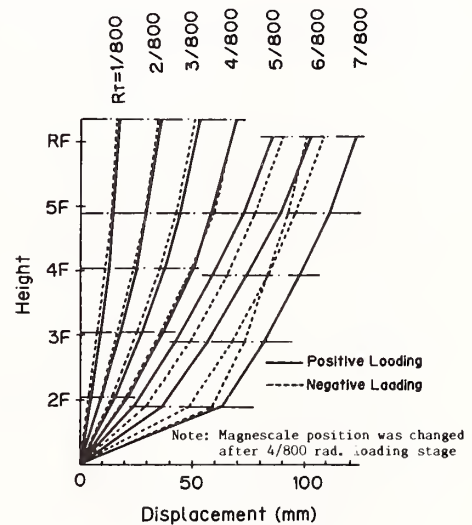
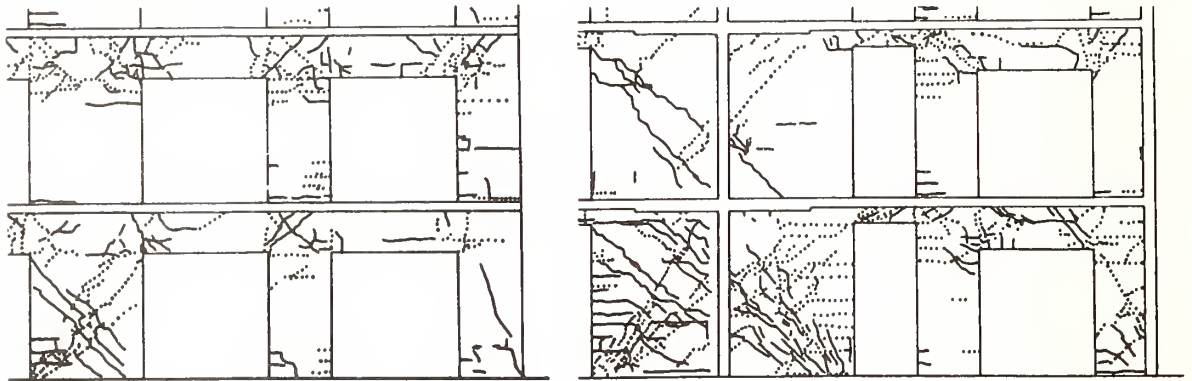


Fig.15 Change in Deflection  
Mode with Increasing  
Top Displacement

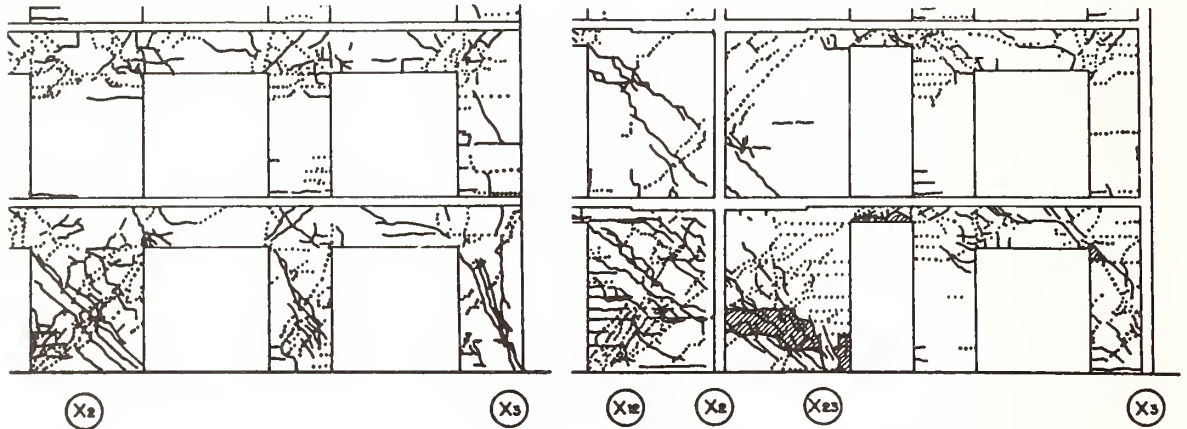
$R_T=2/800\text{rad.}$



$R_T=4/800\text{rad.}$



$R_T=7/800\text{rad.}$



a) Frame Y1

b) Frame Y3

Fig.16 Crack Pattern

# Current Status of the U.S. Coordinated Program for Masonry Building Research

BY

James L. Noland<sup>1</sup>

## ABSTRACT

The U.S. Coordinated Program for Masonry Building Research is an integral set of twenty-eight specific research tasks. The tasks addressed or have addressed topics ranging from material behavior to component behavior to building system behavior using both experimental and analytical approaches. Preparation of a coherent design methodology is the final goal. The work began in the fall of 1985 and is in progress. Phase Two began in January 1988 and includes four new research tasks. Two tasks originally planned have been deleted and two previously separate tasks have been combined.

KEYWORDS: Design; Masonry; Research;  
U.S.-Japan

## 1. INTRODUCTION

The U. S. Coordinated Program for Masonry Building Research is a comprehensive program of research into the structural aspects of reinforced masonry. It addresses the needs of the United States for improved technology applicable to the design and construction of reinforced masonry buildings. Improved masonry structural technology is expected to enable masonry buildings to become a more viable alternative to steel and concrete buildings, hence stimulate competition and foster reduced building costs. It is also expected to stimulate engineering education in structural masonry because of the availability of a more cohesive and well-founded limit state design methodology.

Because materials are often locally available, extensive or sophisticated construction equipment is not mandatory, and forming is not required, masonry construction is possible in most parts of the world and constitutes a significant portion of world building inventories. However, masonry design and construction technology has not kept pace with that developed for buildings of other materials, e.g., steel and concrete. This is especially of concern for construction in seismically active locations.

Existing design codes and design methods are a mixture of empirical rules and linear-elastic working stress methods neither of which is satisfactory for designing reinforced masonry buildings with the proper level of ductility and strength for seismic and other conditions.

While reinforced masonry buildings have generally performed satisfactorily in previous earthquakes, the present state of reinforced masonry building design and analysis methods is not adequate to predict seismic response and safety. Much additional information and work is required to support the development of a limit state design methodology and analytical procedures which are necessary to bring masonry structural technology up to a level compatible with steel and concrete structural technology.

With NSF support, the Technical Coordination Committee for Masonry Research (TCCMAR) was formed in February 1984 for the purpose of defining and performing both analytical and experimental research and development necessary to improve masonry structural technology. TCCMAR was not intended to be a fixed group; new members have been added as needs arose. The current roster of TCCMAR is given in Table 1.

TCCMAR identified, and with NSF funding, began conducting research Tasks in the fall of 1985. Since then two research tasks originally planned have been deleted, i.e., Task 2.4 - Dynamic Properties of Masonry Systems and Task 4.1 - Wall to Wall Intersections and four tasks added. Added Tasks are 2.4(a), 2.4 (b), 3.1 (c) and 5.3. Task 2.3 was expanded to include the work originally planned under Task 2.4 and Task 4.1 was redefined to address static and dynamic response of flanged walls. Table 2 presents the current list of research tasks and the responsible researchers.

A systems approach is being taken to perform the research, i.e., the individual tasks are time-phased and coordinated to avoid duplication of effort and to provide information when it is needed for continuing activities. It is a building block approach in which the initial work supports the succeeding work.

The program is being conducted on a project basis as depicted by Figure 1. The interaction between tasks is a multi-noded process represented by Figure 2 and the time-phasing of tasks is shown in the schedule (Figure 3).

## 3. ADMINISTRATIVE CHANGES

It may be noted that the schedule has been revised to reflect funding conditions. The

<sup>1</sup> Atkinson-Noland & Associates,  
Boulder, Colorado, U.S.A.

result is that the program has been extended one year with the completion date now of December 31, 1992 instead of December 31, 1991 as reported at the nineteenth UJNR meeting.

Because of overwhelming commitments both Dr. Robert Hanson and Dr. Bertero are unable to continue serving as project consultants. They have been replaced by Dr. Mete Sozen, University of Illinois and Dr. James Jirsa, University of Texas, both of whom are highly qualified.

Dr. M.J.N. Priestley has been added to the project Executive Panel and represents many years of masonry research and testing. Jon Traw, recently named Vice President of Codes and Engineering at the International Conference of Building Officials has replaced Frank Drake who has retired from ICBO.

#### 4. PROGRESS

Research Task Principal Investigators submit progress statements annually and are current as of August 31. Table 3 presents a status summary as of August 31, 1987.

#### 5. U.S.-JAPAN RESEARCHER EXCHANGE

Dr. Masaomi Teshigawara (BRI-Tsukuba, Japan) spent the fall of 1985 in the U.S. primarily at the University of Colorado. He involved himself in both Tasks 3.1(a) and 6.2 and was helpful in relating the Japanese experiences on the subjects of these Tasks.

Arrangements were made for Dr. Teshigawara to visit several U.S. organizations concerned with masonry, i.e., NCMA, BIA, NBS, PCA as well as the University of California in San Diego and Berkeley.

Dr. Frieder Seible spent an extra week in Japan immediately prior to the joint U.S.-Japan meeting in August 1985 to review the large-scale test facilities. This was done to discover any information which could affect the design of the large-scale test laboratory which has been built at UCSD.

Dr. Osamu Senbu visited the U.S. in August-September 1986. Arrangements were made for him to stay in Boulder and to subsequently attend the joint meeting on September in Keystone, Colorado.

Hart, Kariotis, Ewing and Noland visited BRI briefly (two days) in May 1986 as a stop-over on the way to a NSF-sponsored U.S.-China masonry structures meeting in Harbin, China. It was an opportunity to review Japanese test results and to continue with arrangements for the next joint U.S.-Japan meeting to be held in September 1986.

Dr. Kyle Woodward visited BRI for two weeks in June-July 1986 to investigate, in detail, the experimental equipment, instrumentation, data

acquisition, etc., in use there for large scale testing. This was done to support planning of the experimental equipment acquisition for the laboratory at UCSD and planning of the large-scale masonry tests to be done there.

Dr. Seible was the recipient of a Japanese government research award and of additional support by the Japanese industry to support a four-month residency at the Building Research Institute, Tsukuba, Japan from mid-August 1987 to mid-December 1987. This enabled him to observe and participate in the Japanese tests of a full-sized masonry building. His experience will greatly benefit the U.S. in its tests of a full-sized five story building specimen in 1990.

#### 6. MEETINGS

TCCMAR-U.S. meets twice a year for 2½ days each to present results of work done and for meetings of subgroups to resolve technical issues. Meetings of the entire group were held in February and August of 1987 and in January of 1988. Several meetings of technical sub-groups were also held.

The Third Meeting of the U.S.-Japan Joint Technical coordinating Committee was held in Hokkaido, Japan during October 1987. The proceedings of that meeting were published which contain technical reports from each side. A copy of the Resolutions of the meeting are attached to this report. Technical tours to production plants and construction sites were made after the meeting to familiarize the U.S. participants with Japanese practice.

The Fourth Joint Meeting has been scheduled for October 17-19, 1988 and will be held in the San Diego area. Visits to masonry unit production facilities and to masonry construction sites are planned to acquaint the Japanese participants with U.S. practice in the Southern California area.

#### 7. PROJECT REPORTS

Several Reports have been published by TCCMAR/U.S. They are listed below in the order they were published:

Atkinson and Kingsley, Comparison of the Behavior of Clay and Concrete Masonry in Compression, September 1985. (Task 1.1)

Seible, F., Report on Large Structures Testing Facilities in Japan, September 1985. (Task 9.2)

Scrivener, J., Summary of Findings of Cyclic Tests on Masonry Piers, June 1986. (Task 3.1(a))

Scrivener, J., Bond of Reinforcement in Grouted Hollow-Unit Masonry: A State-of-the-Art, June 1986. (Task 6.2)

Woodward, K., Report on a Site Visit to Building Research Institute, Ministry of Construction, Tsukuba, Japan, July 1986. (Task 9.2)

TCCMAR, Summary Report: U.S. Coordinated Program for Masonry Building Research, September 1985 to August 1986. (Task 11.1)

Seible, F., Design and Construction of the Charles Lee Powell Structural Systems Laboratory, November 1986, Report 9.2-2. (Task 9.2)

Seible, F. and LaRovere, H., Summary of Pseudo Dynamic Testing, February 1987. (Task 3.1(b))

Soric, Z. and Tulin, L., Bond Splices in Reinforced Masonry, August 1987. (Task 6.2)

Ewing, R.; Kariotis, J.; El-Mustapha, A., LPM/I, A Computer Program for the Nonlinear, Dynamic Analysis of Lumped Parameter Models, August 1987. (Task 2.3)

Nakaki, D. and Hart, G., Uplifting Response of Structures Subjected to Earthquake Motions, August 1987. (Task 2.1)

Hart, G. and Basharkhah, M., Slender Wall Structural Engineering Analysis Computer Program (Slwall, Version 1.01), September 1987. (Task 2.1)

Hart, G. and Basharkhah, M., Shear Wall Structural Engineering Analysis Computer Program (Shwall, Version 1.01), September 1987. (Task 2.1)

Kariotis, J. and Johnson, A., Design of Reinforced Masonry Research Building - Phase 1, September 1987. (Task 9.1).

Hart, G., Sajjad, ., Basharkhah, M., Inelastic Column Analysis Computer Program (incap, Version 1.01), March 1988. (Task 2.1-3).

#### 8. INDUSTRY SUPPORT

Support of the masonry and masonry-related industry increased during the last year and was most welcome. Contributions have been in the form of materials, labor, and funds. Contributions include the Concrete Masonry Association of California and Nevada, Western States Clay Products Association, Masonry Institute of America, National Concrete Masonry Association, Delaware Valley Masonry Institute, Brick Institute of America - Region 12, and Prestressed Concrete Operations.

#### 9. ACKNOWLEDGEMENT

Primary financial support for the U.S. side of the joint program has been provided by the National Science Foundation. Dr. A.J. Eggenberger is the cognizant Program Manager. The Council for Masonry Research contributed

funds in 1987 to support review and improvement of standard material tests and plans to do so in 1988.

#### THIRD MEETING OF THE JOINT COORDINATING COMMITTEE ON MASONRY RESEARCH (JTCCMAR)

TOMAMU, HOKKAIDO, JAPAN  
OCTOBER 15, 16 AND 17, 1987

#### RESOLUTIONS

1. The third meeting of JTCCMAR was held in Tomamu, Hokkaido, Japan on October 15, 16 and 17, 1987. The meeting was attended by nine researchers from the United States and twenty researchers and twelve observers from Japan.
2. At the meeting there was a successful exchange of information and ideas between the researchers from both countries on the subjects of masonry material behavior, behavior of assemblies, testing procedures, analytical/modeling methods, and seismic design procedures.
3. It is recognized that, while progress has been made in developing an understanding of the behavior of masonry, there is still an urgent need for additional information. The participants therefore recommend that sponsoring agencies take appropriate measures to continue support for masonry research.
4. The participants recognize that both countries have many common research needs regarding masonry construction as well as mechanical properties of masonry units, components, and systems.
5. It is recognized that continuous and in-depth effort is required to establish the seismic performance characteristics of existing masonry structures and to develop improved construction and design procedures for new masonry structures.
6. The participants realize that the research programs of both countries primarily address central issues. They also recognize that, while the knowledge developed will provide a basic foundation for improved masonry technology, many other important issues exist which should be addressed.
7. The participants recognize that tests of masonry structures on full-scale specimens are necessary to understand the overall behavior and performance of masonry structural systems. They recommend that each of the two countries continue with plans to conduct at least one full-scale seismic test of a masonry structural system designed in accordance with procedures adopted in each country.
8. The technical communication which has been carried out by sub-groups and individuals of

TCCMAR/U.S. and TCCMAR/Japan has been valuable and should be continued. Researchers should be exchanged as required to enable a meaningful exchange of concepts and information between individuals and groups with similar research interests.

The participants appreciate that in order to attain these objectives, the Japanese side dispatched two researchers to the U.S. in 1985-1986, and the U.S. sent one researcher to observe Japanese laboratory procedures and four researchers for a two-day working group.

In 1987 one Japanese researcher attended the August meeting of TCCMAR/US in San Diego, and one U.S. researcher spent 4 months at BRI in Tsukuba to participate in the Japanese full-scale test.

9. The participants recognize that methodologies for the evaluations of seismic safety of masonry structures should be established based upon the results of this coordinated program.

10. It was recognized that many differences exist between the design procedures in each country, however, both countries agree that the required ultimate seismic performance in each country is almost at the same level.

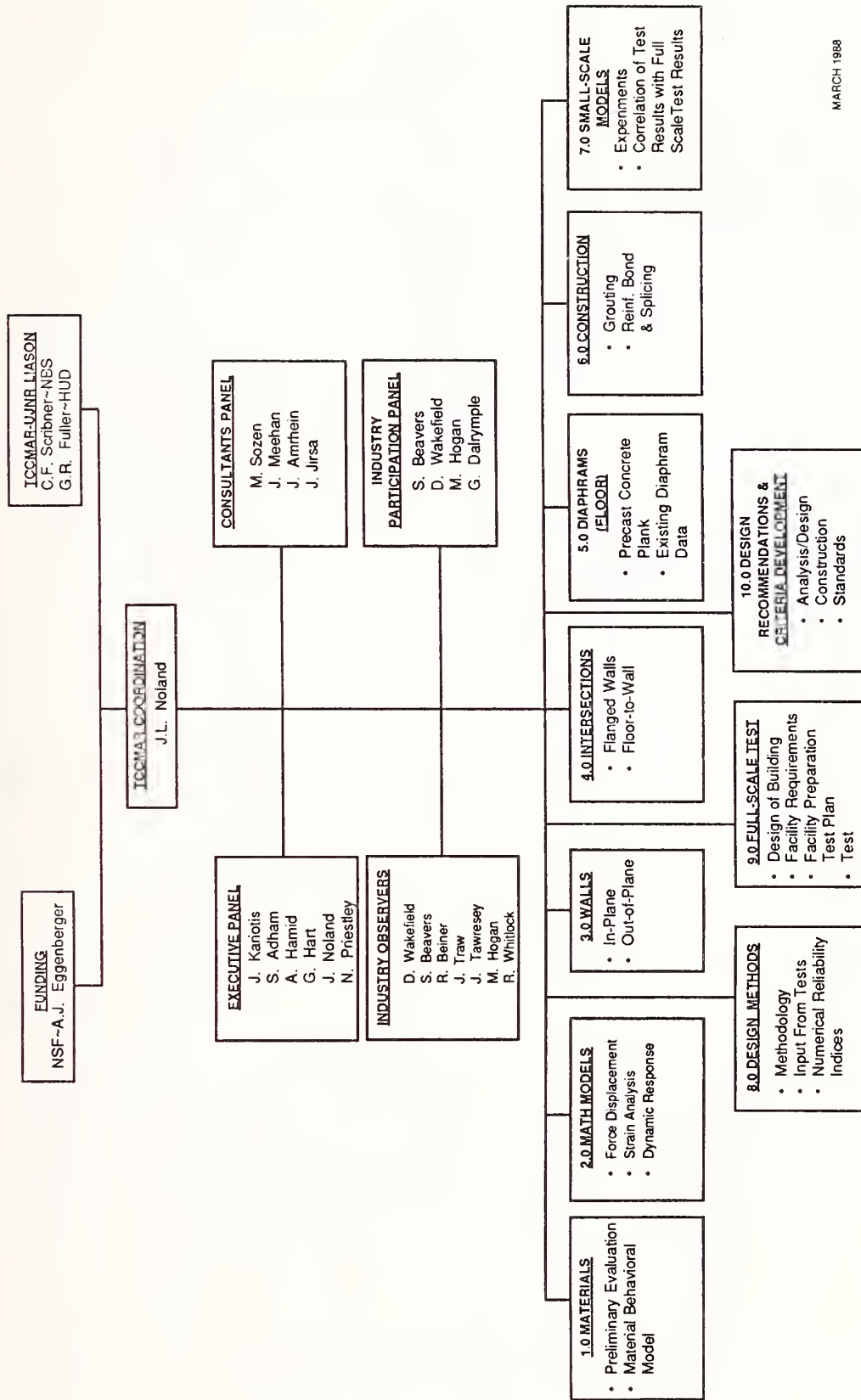
11. Significant progress has been made by both sides in testing and modeling masonry materials, components, subassemblages, and prototypes which will lead to a better understanding of masonry structural behavior and to development of adequate seismic design procedures for masonry buildings.

12. Considering that the U.S. program is planned to continue until 1992 and considering the benefits of the mutual exchange between the US and Japanese programs, it is hoped that the joint relationship be continued so the mutual benefits may be maximized.

13. It was recognized that the results of this coordinated research program could also be beneficial to other countries which have a seismic hazard.

14. The Fourth meeting of JTCCMAR will be held in the U.S. in the Fall of 1988.

# U.S. - JAPAN COORDINATED PROGRAM FOR MASONRY BUILDING RESEARCH



MARCH 1988

FIGURE 1 - ICCMAR ORGANIZATION (U.S.)

U.S.-JAPAN COORDINATED PROGRAM FOR MASONRY BUILDING RESEARCH

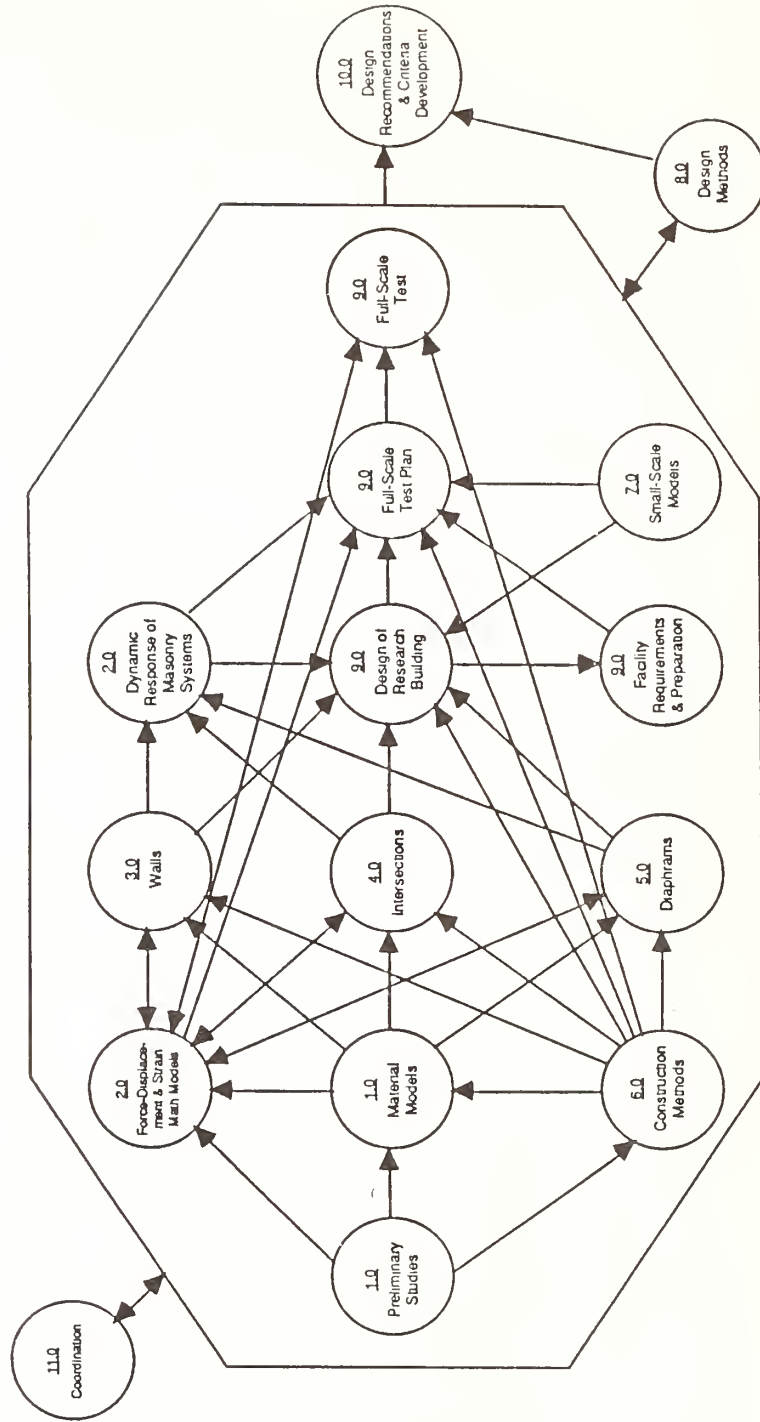
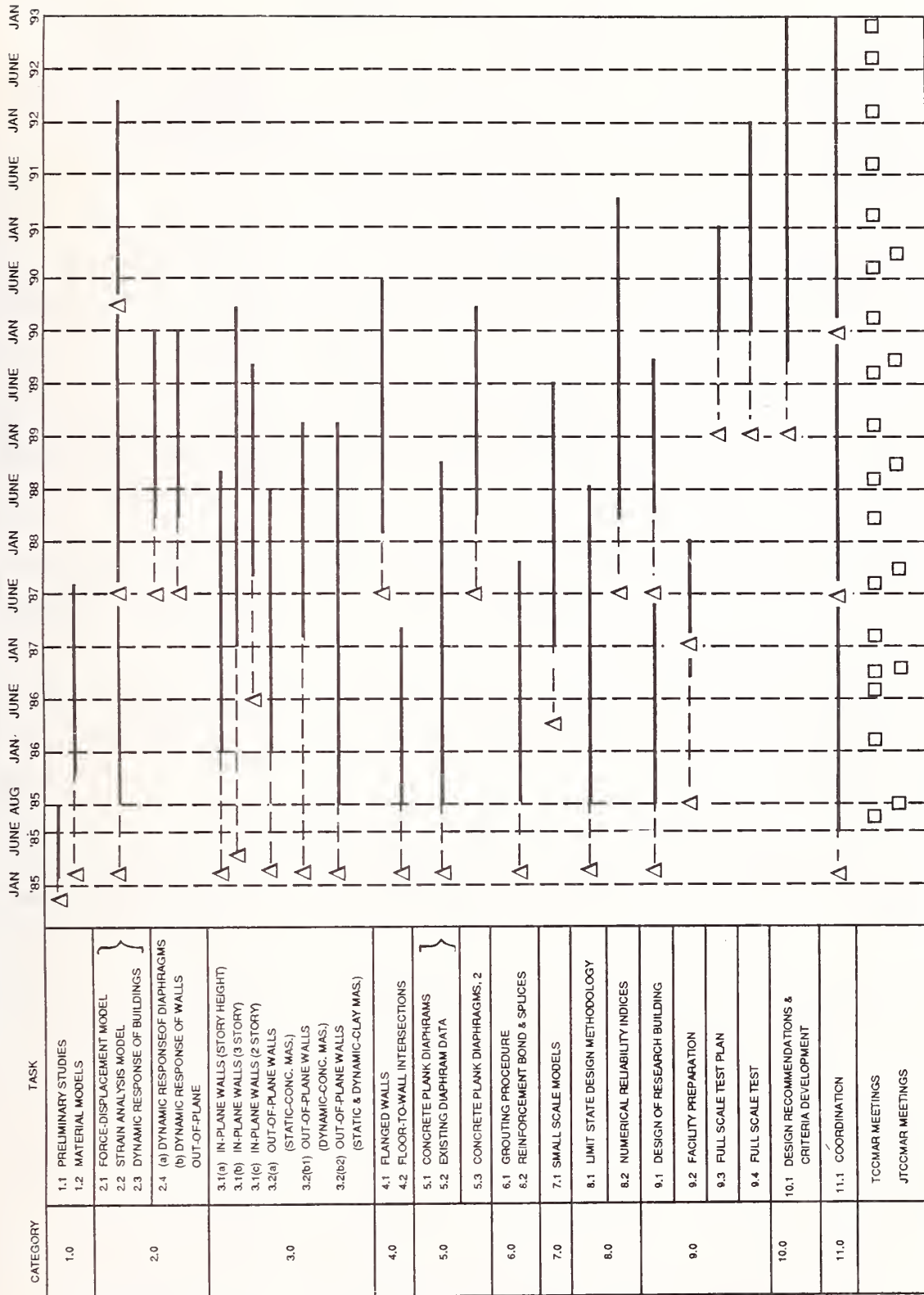


FIGURE 2 — TASK INGREDIENTS-DEPENDENCE CHART (U.S. PROGRAM)

MAY 1987

# U.S.-JAPAN COORDINATED PROGRAM FOR MASONRY BUILDING RESEARCH



△ = PROPOSAL SUBMITTAL

FIGURE 3 — TASK SCHEDULE (U.S. PROGRAM)

MARCH 1988

TABLE 1 - TCCMAR RESEARCHERS

Daniel Abrams  
Newmark Laboratory  
Dept. of Civil Eng.  
Univ. of IL  
208 N. Romine St.  
Urbana, IL 61801  
217-333-0565

Russell Brown  
Civil Engineering Dept.  
Clemson University  
Clemson, SC 29631  
803-656-3000 ex 3314

Ahmad Hamid  
Department of Civil Eng.  
Drexel University  
Philadelphia, PA 19104  
215-895-2342

Gilbert Hegemier  
Dept. of Eng. Sciences B-010  
Univ. of Calif.-San Diego  
La Jolla, CA 92093  
619-534-4280

Richard Klingner  
Phil Ferguson Eng. Lab  
University of Texas-Austin  
10100 Burnet Road  
Austin, TX 78758-4497  
Lab-512-471-3062/4577  
UT-512-471-7259

Max Porter  
Dept. of Civil Engineering  
416A Town Eng. Bldg. ISU  
Ames, IA 50011  
515-294-7456

P.B. Shing  
University of Colorado  
Dept. of CEAE, Box 428  
Boulder, CO 80309  
303-492-8026

Kyle Woodward  
Eng. Sciences Dept. B-010  
Univ. of Calif.-San Diego  
La Jolla, CA 92093  
619-452-4640

Samy Adham  
Agbabian Associates  
250 N. Nash  
El Segundo, CA 90245  
213-640-0576

Robert Englekirk  
Englekirk & Hart  
2116 Arlington Ave.  
Los Angeles, CA 90018-1397  
213-733-2640

Harry Harris  
Department of Civil Eng.  
Drexel University  
Philadelphia, PA 19104  
215-895-2364

Albin W. Johnson  
S. B. Barnes & Assoc.  
2236 Beverly Blvd.  
Los Angeles, CA 90057  
213-382-2385

Ronald Mayes  
Computech Engin. Services  
2855 Telegraph Ave. #410  
Berkeley, CA 94705  
415-843-3576

M.J.N. Priestley  
Eng. Sciences Dept. B-010  
Univ. of Calif.-San Diego  
La Jolla, CA 92093  
619-534-5951

Bjorn Sveinsson  
Computech Engin. Service  
2855 Telegraph Ave. #410  
Berkeley, CA 94705  
415-843-3576

Richard Atkinson  
Atkinson-Noland & Assoc.  
2619 Spruce St.  
Boulder, CO 80302  
303-444-3620

Robert Ewing  
Ewing & Assoc., Inc.  
28907 Doverridge Dr.  
Rancho Palos Verdes, CA  
90274  
213-541-3795

Gary Hart  
Englekirk & Hart  
2116 Arlington Ave.  
Los Angeles, CA 90018-1397  
UCLA-213-825-1377  
E&H -213-733-2640

John Kariotis  
Kariotis & Associates  
711 Mission St. #D  
South Pasadena, CA 91030  
213-682-2871

James L. Noland  
Atkinson-Noland & Assoc.  
2619 Spruce St.  
Boulder, CO 80302  
303-444-3620

Frieder Seible  
Eng. Sciences Dept. B-010  
Univ. of Calif.-San Diego  
La Jolla, CA 92093  
619-534-4640

Leonard Tulin  
University of Colorado  
Dept. CEAE, Box 428  
Boulder, CO 80309  
303-492-7994

TABLE 2 -- RESEARCH TASKS

Category	Task (Researcher)	Title-Purpose
1.0	<u>1.1</u> (Atkinson)	<b>Preliminary Material Studies</b> -- To establish the range of continuity of masonry behavior to provide a basis for selection of the type or types of masonry to be used. To establish standardized materials test procedures for all the experimental tasks.
1.0	<u>1.2</u> (Hamid) (Brown)	<b>Material Models</b> -- To evaluate K1, K2 and K3 for the flexural stress-block. To determine uniaxial and biaxial material properties for analytical models (Tasks 2.1 and 2.2) including post-peak behavior. To evaluate non-isotropic behavior.
2.0	<u>2.1</u> (Englekirk)	<b>Force-Displacement Models for Masonry Component</b> -- To develop force-displacement mathematical models which accurately characterize reinforced masonry components under cyclic loading to permit pretest predictions of experimental results. To develop models suitable for parameter studies and models suitable for design engineering.
2.0	<u>2.2</u> (Ewing)	<b>Strain Analysis Model for Masonry Components</b> -- To develop a strain model for reinforced masonry components in conjunction with Task 2.1 to enable regions of large strain to be identified thus assisting in experimental instrumentation planning. To develop a simplified model to be used to provide data for strength design rules and in-plane shear design procedures.
2.0	<u>2.3</u> (Kariotis)	<b>Dynamic Response of Masonry Buildings</b> -- To develop a generalized dynamic response model to predict interstory displacements using specified time histories. To correlate force-displacement models and to investigate force-displacement characteristics of structural components in the near-elastic and inelastic displacement range. To provide data for building test planning.
2.0	<u>2.4(a)</u> (Porter)	<b>Dynamic Response of Diaphragms</b> -- To develop an analytical model of load displacement history of floor and roof diaphragms to provide associated displacements and stiffnesses for the dynamic model of masonry buildings (Task 2.3). This includes determination of complete hysteretic load displacements for floor diaphragms of masonry buildings. The Task will provide a computer model extension of Tasks 5.1 and 5.2 and interface with Task 2.4(b).
2.0	<u>2.4(b)</u> (Mayes) (Sveinsson)	<b>Dynamic Out-of-Plane Response of Reinforced Masonry Walls</b> -- To develop analytical models based upon the results of Task 3.2(b) which can be used to predict out-of-plane response of masonry walls of various shapes, sizes, and internal construction. To conduct response studies based on independent variation of parameters. The models will serve the purposes of Task 2.3 and 2.4(a).
3.0	<u>3.1(a)</u> (Shing)	<b>Response of Reinforced Masonry Story-Height Walls to Fully Reversed In-Plane Lateral Loads</b> -- To establish the behavior of story-height walls subjected to small and large amplitude axial force, and bending moments considering aspect ratios, reinforcement ratios and patterns, and the effect of openings.

Table 2 Continued-

Category	Task (Researcher)	Title-Purpose
3.0	<u>3.1(b)</u> (Hegemier) (Seible) (Woodward)	Development of a Sequential Displacement Analytical and Experimental Methodology for the Response of Multi-Story Walls to In-Plane Loads--To develop a reliable methodology for investigating, through integrated analytical and experimental studies of three-story reinforced hollow unit masonry walls. The methodology will be the basis of studying the response of a full-scale masonry research building in Task 9.4
3.0	<u>3.1(c)</u> (Klingner)	Response of Reinforced Masonry Two-Story Walls to Fully Reversed In-Plane Lateral Loads -- To establish the behavior of two-story walls subjected to small and large amplitude reversals of in-plane lateral deflections, axial force and bending moments considering the effect of openings, floor-wall joint details and reinforcement ratios.
3.0	<u>3.2</u> (Hamid) (Mayes) (Harris)	Response of Reinforced Masonry Walls to Out-of-Plane Static Loads -- To verify the behavior of flexural models developed using material models, to evaluate the influence of unit properties, bond type and reinforcement ratios upon wall behavior. To provide stiffness data for correlation with dynamic wall test results (Task 3.2 (b)).
3.0	<u>3.2</u> (Adham) (Mayes)	Response of Reinforced Masonry Walls to Out-of-Plane Dynamic Excitation --To determine effects of slenderness, reinforcement amounts and ratios, vertical load and grouting on dynamic response, to verify mathematical response models, to develop design coefficients for equivalent static load methods.
4.0	<u>4.1</u> (Priestley)	Response of Flanged Masonry Shear Walls to Dynamic Excitation -- To experimentally investigate the dynamic behavior of flanged shear walls, in particular, the behavior of T-section walls and the significance of dynamic, as opposed to static or quasi-static testing, for in-plane loading. To develop analytical models to investigate the flange-web shear lag phenomena, and to identify the interaction between flange width, height, reinforcement content, and ductility level.
4.0	<u>4.2</u> (Hegemier)	Floor-to-Wall Intersections of Masonry Buildings -- To determine the effectiveness of intersection details to connect masonry wall components, to construct a nonphenomenological analytical model of intersection behavior for use in building system models.
5.0	<u>5.1</u> (Porter)	Concrete Plank Diaphragm Characteristics -- To investigate experimentally concrete plank diaphragm floor diaphragms with stiff supports to determine modes of failure and stiffness characteristics including yielding capacity in terms of distortion as needed for masonry building models.
5.0	<u>5.2</u> (Johnson) (Porter)	Assembly of Existing Diaphragm Data--To assemble extensive existing experimental data on various types of floor deforms, to reduce to a form required for static and dynamic analysis models.
5.0	<u>5.3</u> (Porter)	Concrete Plank Diaphragm Characteristics Continuation -- To investigate experimentally concrete plank floor diaphragms with flexible supports to determine modes of failure and stiffness characteristics including yielding capacity in terms of distortion as needed for masonry building models.

Table 2 Continued-

Category	Task (Researcher)	Title-Purpose
6.0	<u>6.1</u> (TBD)	<b>Grouting Procedures for Hollow Unit Masonry</b> -- To identify methods of grouting hollow unit masonry such that the cavity is solidly filled and reinforcement is completely bonded.
6.0	<u>6.2</u> (Tulin)	<b>Reinforcement Bond and Splices in Grouted Hollow Unit Masonry</b> -- To develop data and behavioral models on the bond strength and slip characteristics of deformed bars in grouted hollow unit masonry, to develop data and behavioral models on the bond strength and slip characteristics of deformed bar lap splices in grouted hollow unit masonry as needed for building modeling.
7.0	<u>7.1</u> (Abrams)	<b>Small Scale Models</b> -- To experimentally observe the dynamic behavior of three-story concrete masonry buildings built with 1/4 scale hollow concrete units. The response will be compared to that of full-scale specimens previously tested. It is expected that dynamic tests of scale model building will reveal fundamental response modes.
8.0	<u>8.1</u> (Hart)	<b>Limit State Design Methodology for Reinforced Masonry</b> -- To select an appropriate limit state design methodology for masonry. To select and document a procedure to compute numerical values for strength reduction factors. To review program experimental research tasks to assure that statistical benefits are maximized and proper limit states are investigated.
8.0	<u>8.2</u> (Hart)	<b>Numerical Reliability Indices</b> -- To develop numerical values of statistically-based strength reduction (i.e. 0) factors using program experimentally developed data, other applicable data, and judgment. To complete development of the methodology.
9.0	<u>9.1</u> (Kariotis)	<b>Design of Reinforced Masonry Research Building</b> -- Phase 1 - - to develop the preliminary designs of the potential research buildings which reflect a significant portion of modern U.S. masonry construction. To select a single configuration in consultation with TCCMAR which will be used as a basis for defining equipment and other laboratory facilities in displacements using methods developed in Category 2 tasks and the associated load magnitudes and distributions. Phase 2 - To prepare final drawings and specifications for construction of the five-story test specimen.
9.0	<u>9.2</u> (Hegemier) (Seible)	<b>Facility Preparation</b> -- Define, acquire, install and check-out equipment required for experiments on a full-scale reinforced masonry research building.
9.0	<u>9.3</u> (TCCMAR)	<b>Full Scale Masonry Research Building Test Plan</b> -- To develop a detailed and comprehensive plan for conducting static load-reversal tests on a full-scale reinforced masonry research building.
9.0	<u>9.4</u> (TCCMAR)	<b>Full Scale Test</b> -- To conduct experiments on a full-scale reinforced masonry research building in accordance with the test plan and acquiring data indicated. To observe building response and adjust test procedures and data measurements as required to establish building behavior.

Table 2 Continued-

Category	Task (Researcher)	Title-Purpose
10.0	<u>10.1</u> (TCCMAR)	<b>Design Recommendations and Criteria Development</b> -- To develop and document recommendations for the design of reinforced masonry building subject to seismic excitation in a manner conducive to design office utilization. To develop and document corresponding recommendations for masonry structural code provisions.
11.0	<u>11.1</u> (Noland)	<b>Coordination</b> -- To fully coordinate the U.S. research tasks to enhance data transfer among researchers and timely completion of tasks. To schedule and organize TCCMAR and Executive Panel meetings. To establish additional program policies as the need arises. To stimulate release of progress reports and dissemination of results. To coordinate with industry for the purposes of informing industry and arranging industry support. To interface with NSF and UJNR on overall funding and policy matters.

TABLE 3 - SUMMARY OF FUNDED TASK STATUS AS OF 31 AUGUST 1987

TASK	TITLE	PERCENT COMPLETE	STATUS
1.1	Preliminary Material Studies	100	Complete. Report 1.1-1 published.
1.2(a)	Materials Models -- Concrete Masonry	85	Test machine stiffness problem fixed. All experimental procedures developed. Eccentric loading testing complete by Aug. 31. Concentric loading testing complete by Sept. 30. Final report outlined.
1.2(b)	Material Models - Clay Masonry	60	Problems with test equipment resolved. Apparatus checked out. Testing to be completed by Sept. 30. Final report by June 1988
2.1	Force Displacement Models (Phase I)*	80	Research and evaluation indicated that "Structural Component Models" (SCM) are the best approach. Correlation studies using results of Task 3.1(a) begun. Results promising. Reports 2.1-1, 2.1-2, and 2.1-3 published.
2.2	Strain Analysis Models (Phase I)	80	Basic technical approach developed based upon extensive evaluation of alternatives. FEM will be used to understand in-plane response of reinforced masonry walls. Analytical model will replicate degrading force-displacement. Model will follow Vecchio and Collins approach as modified considering other work.
2.3	Dynamic Response of Masonry Building Systems (Phase I)	80	Integrated approach developed to formulate lumped parameter models for building response analyses. Builds upon Tasks 2.1 and 2.2. Families of ground motion time-history records selected for use in building system studies. LPM with foundation flexibility studies defined.
3.1(a)	In-Plane Walls -- Story Height	40	11 of 26 walls tested. Fixture and procedure satisfactory. Photos taken for photogrammetric analysis. Supplement received to add clay unit walls. Donation received to test one wall with joint reinforcement as shear steel.
3.1(b)	In-Plane Walls -- Three-Story and GSD Method	5	Methodology for tests defined to develop Generated Sequential Displacement test method. Specimens defined. No further progress possible until Task 9.2 complete. Reports 9.2-1, 9.2-2 published.
3.1(c)	In-Plane Walls -- Two-Story	20	Specimen design complete. Materials ordered. Design and construction of test set-up in progress. Specimen construction beginning Feb 1988, testing beginning April 1988.
3.2(a)	Out-of-Plane Walls -- Static Tests (Concrete Masonry)	60	Planning Complete. Test set-up complete. Pilot tests done by August 31. One-half of specimens will be tested in Sept.; one-half in Oct. Report complete by Jan. '88.

\*Phase I refers to the period fall 1985 to December 31, 1987.

TABLE 3 -

TASK	TITLE	PERCENT COMPLETE	STATUS
3.2(b1)	Out-of-Plane Walls -- Dynamic Tests (Concrete Masonry)	30	Tests not yet begun. Base support assemblies for walls contracted. Free labor for wall construction arranged. All wall materials donated and on-site program in-progress).
3.2(b2)	Out-of-Plane Walls -- Static and Dynamic Tests (Clay Masonry)	30	Planning completed. Testing apparatus prepared. Load history implemented. Instrumentation checked out. Four walls built and two tested. Data reduction begun. Plans made for construction of next four walls.
4.2	Wall-to-floor Intersections	80	Last part of analysis to be completed. Report expected in Sept. '87.
5.1	Concrete Plank Diaphragms	65	Test fixture completed and checked out. Pilot tests completed. 3-4 additional floors to be tested. Analysis begun.
5.2	Review of Existing Data on Diaphragms	85	Open literature acquired. Seeking proprietary data.
6.2	Reinforcement Bond and Splices	100	Completed. Reports 6.2-1 and 6.2-2 published.
7.1	Small Scale Models -- Dynamic Tests	15	Model material studies completed. Design of first dynamic test structure completed. Construction of first model 1/3 complete. First test in early October.
8.1	Limit State Methodology	95	Draft of final report prepared -- will be revised in accordance with research and with comments received at Aug. meeting of TCCMAR.
9.1	Design of Research Building -- Phase I	100	Complete.
9.2	Test Facility Preparation (Equipment)	25	Equipment defined, selected, and ordered. Expected to be operational by Sept. '88. Check-out will be done using Task 3.1(b) specimens.
11.1	Coordination	90	(Phase I) On-going activity. Next major event is JTCCMAR Oct. '87 in Japan.

# Dynamic Strength and Ductility of Reinforced Concrete Bridge Piers

BY

Toshio Iwasaki<sup>1</sup>, Osamu Ueda<sup>2</sup>, Kazuhiko Kawashima<sup>3</sup>,  
Kinji Hasegawa<sup>4</sup> and Takeshi Yoshida<sup>5</sup>

## ABSTRACT

A series of dynamic loading tests with use of large-scale reinforced bridge piers had been conducted in Public Works Research Institute, and the precision in estimating the strength and ductility of reinforced concrete bridge piers according to the Specification for Highway Bridges in Japan was investigated in this paper, using the data of these experiments.

It was understood that the calculated bending strength according to the Specification is similar to the experimental maximum strength, and that the experimental ultimate displacement and the calculated ultimate displacement according to the Specification (including the displacement by the slipping-off of the longitudinal reinforcements from the footing) are almost the same in spite of the difference of the definition for the ultimate.

## 1. INTRODUCTION

In the seismic design of reinforced concrete bridge piers, they are designed to make the stress by the seismic force corresponding to 0.2G-0.3G smaller than the allowable stress. The real seismic force worked to the bridges near the epicenter during the large earthquake such as Miyagiken-oki-earthquake of 1983, was bigger than the above-mentioned design seismic force, and some reinforced concrete bridge piers are considered to have yielded. Most of the reinforced concrete bridge piers, however, were not suffered severe damages by the earthquake. They vibrated not so much during the earthquake because of the hysteresis damping after yield, and they had also enough ductility without degrading of strength. Therefore, it is important to estimate the strength and ductility of reinforced concrete bridge piers in plastic region in order to prevent the bridge from having severe damages such as the falling of the girder during the large earthquake. Earthquake Engineering Division, PWRI, conducted many dynamic reversal loading experiments of reinforced concrete piers to investigate experimentally their strength and ductility. Using the data of these experiments, this paper investigates the precision in estimating the strength and ductility of reinforced concrete piers according to the Specification for Highway bridges, which consists of Part I Common Part, Part II Steel Bridge, part III Concrete Bridge, Part IV Substructure and Part V Seismic Design, stipulated by Japan Road Association.

## 2. EXPERIMENTS OF REINFORCED CONCRETE PIERS

Table 1 shows some items of twenty-five reinforced concrete pier models used in this paper. The purpose of these experiments is to study systematically various effects such as the effect of the number of the loading repetition, the loading velocity, the ratio of the tie hoop and the shear resistance reinforcements, etc. Each parameter mentioned above is varied from the lower value to the upper value in the practical range and each specimen has a special feature according to the purpose of the experiment.

The specimen No. shown in Table 1 is given to the serial specimens and some Nos. are excluded from Table 1, because some specimens subjected to the biaxial loading

in horizontal plane, some specimens with the cut-off of longitudinal reinforcements and some other specimens for special purpose can not be used in this paper. Fig. 1 shows the distribution of the shear span ratio, the ratio of the longitudinal reinforcement and the ratio of the tie hoop, and this figures indicate the general features of the specimens.

The definition of the yield and ultimate point in experiments is important in comparing the strength and ductility in experiments and in calculations. Some methods to define them are proposed and the following method is used in this paper. Fig. 2 shows the envelope of load and displacement hysteresis loops at the loading point in experiments, in which the displacements were step-wise increased monotonically. The yield strength  $P_y$  and displacement  $\delta_y$  is defined as the load and displacement when the strain of the longitudinal reinforcements at the tension side goes up to the 1800 micro-strain. The strain of 1800 micro is an average yield strain in tensile tests of the longitudinal reinforcements used in the specimens. The load goes up to the maximum load after yield and falls down, as shown in Fig. 2. The maximum strength  $P_M$  is defined as a maximum load and the ultimate displacement  $\delta_u$  is defined as a displacement when the load falls down to the yield strength. It should be noticed that the specimens have the enough capacity of the strength and ductility after they go over the ultimate displacement and the ultimate point does not mean the collapse of the bridge, and it should be also noticed that the capacity for supporting the load in the horizontal direction is different from that in the vertical direction.

As for the fracture mode, three specimens of P. 18, 21 and 30 failed in shear and the other specimens failed in bending.

## 3. CALCULATION METHOD OF STRENGTH AND DUCTILITY

The maximum bending strength and ultimate displacement by the bending moment is calculated according to the appendix in Part V of the Specification as the following. A pier column is divided into some sections in the longitudinal direction and each section is divided into some elements. Assuming the stress-strain diagram of concrete and reinforcement as shown in Fig. 3., a neutral axis of each section is decided to satisfy the following equation of equilibrium for the axial load under the condition that the strain is proportional to the distance from the neutral axis.

$$N = \sum_{i=1}^n \sigma_{ci} \Delta A_{ci} + \sum_{i=1}^n \sigma_{si} \Delta A_{si} \dots \dots \dots (1)$$

- 1 Dr. of Engr., Assistant Director-General, Public Works Research Institution, Ministry of Construction Japan
- 2 Director, Earthquake Disaster Prevention Department, Public Works Research Institute, Ministry of Construction, Japan
- 3 Dr. of Engr., Head, Earthquake Engineering Division, Earthquake Disaster Prevention Department, Public Works Research Institute, Ministry of Construction, Japan
- 4 Research Engineer: ditto
- 5 Assistant Research Engineer, ditto

in which,  $N$  is an axial load worked to the section,  $\delta_{ci}$  and  $\delta_{si}$  are stress of concrete and reinforcement in the  $i$ th element, respectively, and  $\Delta A_{ci}$  and  $\Delta A_{si}$  is an area of concrete and reinforcement in the  $i$ th element, respectively. Bending moment  $M$  and curvature  $\phi$  are calculated by the following equations after deciding the neutral axis.

$$M = \sum_{i=1}^n \sigma_{ci} x_i \cdot \Delta A_{ci} + \sum_{i=1}^n \sigma_{si} x_i \cdot \Delta A_{si} \quad \dots \dots \dots (2)$$

$$\phi = \epsilon_{co} / x_0 \quad \dots \dots \dots (3)$$

in which,  $X_1$  is a distance from the neutral axis to the  $i$ th element  $\epsilon_{co}$  is the extreme fiber strain of concrete at the compression side and  $X_0$  is a distance from the extreme end of the compression side to the neutral axis. The yield bending moment  $M_y$  and curvature  $\phi_y$  can be calculated by Eq. (2) and Eq. (3), substituting the strain of the tensile longitudinal reinforcements for the yield strain  $\epsilon_{sy} = \delta_{sy} / E_s$  ( $\delta_{sy}$ : the yield stress of the reinforcement,  $E_s$ : Young's modulus of the reinforcement), and the ultimate bending moment  $M_u$  and curvature can be calculated by Eq. (2) and Eq. (3), substituting the extreme fiber strain of concrete at the compression side for the ultimate strain of 0.0035. The value of the ultimate strain of concrete is according to Part III and Part V of the Specification. It is important that the definition of "ultimate" in the experiment and in the calculation are not the same. As it is mentioned above, the ultimate is defined in the experiment as when the load falls down to the yield strength after it goes up to the maximum strength in the load-displacement diagram at the loading point. The ultimate is defined, however, in the calculation as when the extreme fiber strain of concrete at the compression side reaches the value of 0.0035. The ultimate is defined by various ways and the way for the experiment and for the calculation in this paper is most popular one. It should be noticed, however, that the definition of the ultimate point in the experiment and in the calculation is not equal.

The pier column rotates at the bottom because of the slipping-out of the longitudinal reinforcements from the footing and the displacement by this rotation at the loading point,  $\delta_2$  can be calculated by the following equation.

$$\delta_2 = \theta \cdot H \quad \dots \dots \dots (4)$$

in which,  $H$  is a height of pier column and  $\theta$  is an angle of rotation at the bottom of the pier column.  $\theta$  can be calculated from the average bond stress of the reinforcement according to the references 4) and 5). The total displacement  $\delta$  at the loading point can be calculated by adding up the displacement by bending moment,  $\delta_1$  and the displacement by slipping-out of the reinforcements,  $\delta_2$  as the following equation.

$$\delta = \delta_1 + \delta_2 \quad \dots \dots \dots (5)$$

The shear strength of the specimens are calculated by the following equation according to the Part III of Specification.

$$P_s = \frac{A_w \sigma_{sy} \cdot d}{1.15a} + \tau_a b_w d \quad \dots \dots \dots (6)$$

in which,  $A_w$  is an area of the tie hoops,  $\sigma_{sy}$  is the yield stress of the tie hoop,  $d$  is the effective height of the cross section,  $a$  is a space of tie hoops,  $\tau_a$  is an allowable

shear stress and  $b_w$  is a width of the pier column. The yield stress of the tie hoop,  $\sigma_{sy}$  is measured by the tension tests and the allowable shear stress is calculated by the following equation according to the reference 6).

$$\tau_a = 0.015 \sigma_{ck} \quad \dots \dots \dots (7)$$

## 4. INVESTIGATION ON STRENGTH AND DUCTILITY OF SPECIMENS

### 4.1 Load and Displacement Relation

Table 2 shows the calculated strength and ductility of twenty five specimens, by the method shown in the preceding chapter. Fig. 4 compares the experimental load-displacement relation and the calculated relation on some typical specimens.

As shown in Fig. 4(a), in the experimental relation of Specimen (P.4) which does not have longitudinal reinforcements along the lateral side like a beam, the load increases not so much after the yield, and as shown in Fig. 4(b), in the experimental relation of Specimen (P.10) which has longitudinal reinforcements along the lateral side like a column, the load increases to the maximum strength after yield and decreases gradually to the ultimate point. On the other hand, the load increases gradually to the ultimate strength after yield in the calculated relation, and the large increasing of the load after yield as observed in the columnlike specimens and the decreasing of the load after the maximum strength are not found in the calculated relation. The calculated relation is similar to the experimental relation comparatively in the beamlike specimens, and the calculated relation is not similar to the experimental relation in the columnlike specimens, as mentioned above. The reason why the load increases with the increasing of the displacement in the calculation, is that the degradation of concrete and the fracture of reinforcements by the cyclic loading are not taken into the calculation and the improvement of the calculation is needed in future.

The decreasing of the load at the ultimate stage in the specimens which fail in bending, is generally brought by the fracture of the longitudinal reinforcements and Fig. 5 compares the calculated ultimate displacement and the displacement when the longitudinal reinforcements start fracturing. As shown in Fig. 5, two displacements are comparatively almost the same, and it is found that the calculated ultimate displacement corresponds to when longitudinal reinforcements start fracturing.

The experimental relation of the load and displacement shown in Fig. 4(c) in Specimen (P.18) which failed in shear, is naturally different from the calculated displacement, since the calculation assumes the flexural deformation by the bending moment. It should be noticed, however, that the calculated relation not disagree to the experimental relation at all, but approximates it to a certain extent.

### 4.2 Maximum Strength

This paragraph investigates the experimental maximum strength  $P_M$ , the load corresponding to the calculated ultimate bending moment  $M_u$ ,  $P_B (= M_u/H$ , it will be called the bending strength later) and the shear strength  $P_s$ .

Fig. 6 shows the relation of the experimental maximum strength  $P_M$  and the bending strength  $P_B$ . As shown in this figure,  $P_s$  and  $P_M$  are almost the same in all specimen, including even the three specimens which failed in shear, (P.18, 21 and 30) as well as the specimens which failed in bending. The it is very interesting that  $P_B$  is similar to  $P_M$  in the specimens which failed in shear but have the tie hoop with the ratio of 0.1% at

least. If the shear strength  $P_s$  are not equal to the bending strength  $P_B$ , the actual strength should be the lower value of  $P_B$  or  $P_s$ . Therefore, Fig. 7 shows the relation of the experimental maximum strength  $P_M$  and the lower strength of  $P_B$  or  $P_s$ . The shear strength  $P_s$  is lower than the bending strength  $P_B$  in Specimens P.17 (shear span ratio  $h/d = 3.8$ ), P.18 ( $h/d = 2.2$ ), P.20 ( $h/d = 3.8$ ), P.21 ( $h/d = 2.2$ ), P.27 ( $h/d = 2.5$ ) and P.30 ( $h/d = 1.9$ ) and it is concluded by the calculation that these specimens will fail in shear. Specimens P.16, 21, and 30 actually failed in shear, as it was mentioned above, and Specimens P.17 and 20 with the shear span ratio of 3.8 failed in bending and Specimen P.27 with the shear span ratio of 2.5 failed also in bending, since it has the diagonal reinforcements. Apart from Specimen P.27, in which the diagonal reinforcements are not taken into the calculation, the calculated value and the experimental value is almost the same in twenty-one specimens except the Specimens P.18, 21 and 30 which failed in shear. In Specimens (P.18, 21 and 30), the experimental maximum strength  $P_M$  is about two times bigger than the calculated shear strength  $P_s$ .

#### 4.3 Ductility

Fig. 8 compares the experimental value and calculated value of the yield displacement  $\delta_y$ . As shown in this figure, the calculated value is similar to the experimental value even in the specimens which failed in shear as well as in the specimens which failed in bending, since the longitudinal reinforcements actually yielded in the specimens which failed in shear, and the assumption in calculating the yield displacement is considered to be reasonable.

Fig. 9 compares the experimental value and calculated value of the ultimate displacement  $\delta_u$ . The calculated value is generally similar to the experimental value and the deviation is, however, bigger than that of the yield displacement, and the calculated values deviate in the range of  $1/2 \sim 2$  times of the experimental value. The calculated ultimate displacement  $\delta_u$  corresponds to the displacement when the longitudinal reinforcements start fracturing as mentioned above, and it depends on various conditions such as the ratio of the tie hoop, the number of the loading repetition, the spiral reinforcements, and the ratio of the longitudinal reinforcements, etc., when the fracture of the longitudinal reinforcements starts.

##### 1) Effect of ratio of tie hoop and number of loading repetition on ultimate displacement $\delta_u$ .

Specimens P.10, 11, 12, 13, 16, 19 and 22 have the same shear span ratio  $h/d$  of 5.4, the same ratio of the longitudinal reinforcement  $P_l$  of 2.03% and the same shape of the section, so the calculated ultimate displacements are the same value. On the other hand, the experimental values vary in the wide range of 85.5 ~ 125.9 mm as shown in Fig. 9. Table 3 arranges the causes of the difference between the calculated ultimate displacement and the experimental ultimate displacement, and there are some special features as the following.

i)  $\delta_u$  increases as the ratio of the tie hoop  $P_w$  increases, that is to say,  $\delta_u$  increases from 92.6 mm to 102.5 mm by about 10% as  $P_w$  increases from 0.1% (P.10) to 0.3% (P.13).

ii)  $\delta_u$  increases as the number of the loading repetition  $n$  with the same amplitude of displacement, decreases in experiments, in which the displacement was increased step-wise monotonically.  $\delta_u$  of Specimen P.19 ( $n = 3$ ) and P.22 ( $n = 5$ ) are 114.5 ~ 125.9 mm, and about 30% bigger than that of Specimens P.10~22 ( $n = 10$ ), which are 85.5 ~ 92.6 mm.

The number of the loading repetition  $n$  has a great effect on the fracture of the longitudinal reinforcements. It is

delayed as the number of the loading repetition is decreased, and consequently  $\delta_u$  becomes larger.

##### 2) Effect of spiral hoop on ultimate displacement $\delta_u$

Specimens P.26, 31 and 32 have the spiral hoop, which corresponds to the tie hoop with the ratio of 1.02%, at the bottom of the pier columns and these experimental ultimate displacements  $\delta_u$  are much bigger than these calculated ultimate displacement. Table 4 compares the result of specimens with spiral reinforcements and without spiral reinforcements, which have the same dimension and the same shear span ratio. The ultimate displacement of the specimens with the spiral hoop, is 40% bigger than that with the tie hoop of the ratio of 0.1% ~ 0.5%.

##### 3) Effect of ratio of longitudinal reinforcements on ultimate displacement $\delta_u$

The calculated ultimate displacements  $\delta_u$  of Specimens P.8 and 9 are much bigger than the experimental ultimate displacements, contrasted with the above-mentioned specimens with spiral hoops. Since the extreme fiber strain of concrete in specimens with the low ratio of the longitudinal reinforcement of 0.48% does not readily reach to the ultimate strain of 0.0035 and only the strain of the reinforcements increases in the calculation, the calculated ultimate displacement  $\delta_u$  becomes very big. It is needed to define the ultimate on the different point of view from the strain of concrete, for the piers with the low ratio of the longitudinal reinforcement.

The purposes of these specimens in this paper are to investigate the effect of various parameters by changing widely these parameters. The calculated ultimate displacement  $\delta_u$  is very similar to the experimental ultimate displacement  $\delta_u$ , excluding P.13 with the high ratio of the tie hoop, P.19 and 22 with the few number of the loading repetition, P.26, 31 and 32 with the spiral reinforcements, and P.8 and 9 with the low ratio of the longitudinal reinforcement.

In addition, it is noticed that the calculated values of Specimens P.18, 21 and 30 which failed in shear, are also similar to the experimental value.

Arranging the yield displacement and the ultimate displacement, Fig. 10 compares the calculated value and the experimental value in terms of the ductility factor  $\mu$  ( $= \delta_u/\delta_y$ ). There is considerably some divisions, and they have, however, generally good similarity.

## 5. CONCLUDING REMARKS

The applicability of the estimation method for the strength and ductility according to Part III and Part V of the Specification for Highway Bridges was investigated, using the experimental results of twenty-five specimens conducted by Earthquake Engineering Division, PWR1. The following conclusions may be deduced:

1) The calculation method according to Part V of the Specification is generally reasonable, if the slipping-off of the longitudinal reinforcements from the footings is taken into the calculation. Investigating into the details, the calculated relation of the load and displacement is very similar to the experimental relation in the specimens without the longitudinal reinforcements along the lateral side, and in the specimens with the longitudinal reinforcements along the lateral side, however, the increase of the load after yield and the decrease of the load after the maximum strength in experiments can not be calculated. This is owing to not taking the decrease of the effective area of concrete by spalling and the degradation of concrete strength into the calculation, and it is needed to improve the calculation method in future.

2) The calculated bending strength  $P_B$  according to the Part V of the Specification is similar to the experimental maximum strength  $P_M$ . It should be noticed that the experimental maximum strength  $P_M$  is almost equal to the calculated bending strength  $P_B$  even in the specimens which failed in shear. The mechanism of shear fracture is different from the mechanism of bending fracture, and it is, however, pointed out that the maximum strength of the piers which has the tie hoops with the higher ratio than 0.1% but will fail in shear, can be calculated according to Part V of the Specification with a certain extent of accuracy.

3) The equation for calculating the shear strength in Part III of the Specification gives about the half value of the experimental shear strength.

4) The experimental ultimate displacement and the calculated ultimate displacement according to Part V of the specification (including the displacement by the slipping-off of the longitudinal reinforcements from the footing) are almost the same in spite of the difference of the definition for the ultimate.

#### REFERENCES

- 1) Kawashima, K. and Koyama, T.: Effect of Number of Loading Cycles on Dynamic Characteristics of Reinforced Concrete Bridge Pier Columns, Civil Engineering Journal. Vol. 29, No. 6, 1987 (in Japanese).
- 2) Kawashima, K., Hasegawa, K., Koyama, T. and Yoshida, T.: Effects of Cyclic Loading Hysteresis on Dynamic Behavior of Reinforced Concrete Bridge Piers, Civil engineering Journal. Vol. 29, No. 8, 1987 (in Japanese).
- 3) Mahin, S.A. et al.: Rate of Loading Effects on Uncracked and Repaired Reinforced Concrete Members, Report No. EERC 72-9, Univ. of California, Berkeley, 1972.
- 4) Ohta, M.: Experimental Study on Behavior of Reinforced Concrete Bridge Piers under Cyclic Loading. Proc. of Japan Society of Civil Engineers, Vol. 292, 1979 (in Japanese).
- 5) New Proposed Seismic Design Method, No. 1185 of the Technical Memorandum, Public Works Research Institute, Ministry of Construction, 1977.
- 6) Design Manual for Concrete Highway Bridges: Japan Road Association, 1980.

Table 1 Specimens

No.	Dimension of Section $D \times w$ [cm]	Covering Depth (cm)	Height of Column (cm)	Shear Span Ratio $h/a$	Longitudinal Reinforcement				Tie Hoop			Concrete			Strength Loading		
					Material and Diameter $\phi$ (cm)	Cut-off	Lateral Reinforcement	Ratio (%)	Yield Strength $\sigma_y$ [ $\text{kgf/cm}^2$ ]	Material and Diameter $\phi$ (mm)	Ratio (%)	Yield Strength $\sigma_y$ [ $\text{kgf/cm}^2$ ]	Material	Diameter of Maximum Coarse Aggregate (mm)	Compression Strength [ $\text{kgf/cm}^2$ ]	Velocity [cm/sec]	Number of Repetition (cycles)
P-4	40x80	5	240	6.9	SD30,19	-	-	1.79	3792	SR24,9	0.08	3660	High Early Strength Portland Cement	20	290	0.24	10
P-5	40x80	5	240	6.9	SD30,19	-	-	1.79	3792	SR24,9	0.08	3660	"	20	258	25	10
P-6	40x80	5	240	6.9	SD30,16	-	-	0.87	3625	SR24,9	0.08	3660	"	20	290	0.24	10
P-7	40x80	5	240	6.9	SD30,16	-	-	0.87	3625	SR24,9	0.08	3660	"	20	258	25	10
P-8	40x80	5	240	6.9	SD30,13	-	-	0.48	3704	SR24,9	0.08	3660	"	20	290	0.24	10
P-9	40x80	5	240	6.9	SD30,13	-	O	0.48	3704	SR24,9	0.08	3660	"	20	258	25	10
P-10	50x50	3.5	250	5.4	SD30,13	-	O	2.03	3144	SR24,9	0.1	2776	"	10	319	25	10
P-11	50x50	3.5	250	5.4	SD30,13	-	O	2.03	3144	SR24,9	0.2	2776	"	10	327	25	10
P-12	50x50	3.5	250	5.4	SD30,13	-	O	2.03	3144	SR24,9	0.2	2776	"	10	321	25	10
P-13	50x50	3.5	250	5.4	SD30,13	-	O	2.03	3144	SR24,9	0.31	2776	"	10	334	25	10
P-16	50x50	3.5	250	5.4	SD30,13	O	O	2.03	3144	SR24,9	0.1	2776	"	10	325	25	10
P-17	50x50	3.5	175	3.8	SD30,13	-	O	2.03	3144	SR24,9	0.1	2776	"	10	338	25	10
P-18	50x50	3.5	100	2.2	SD30,13	-	O	2.03	3144	SR24,9	0.1	2776	"	10	334	25	10
P-19	50x50	3.5	250	5.4	SD30,13	-	O	2.03	3144	SR24,9	0.1	2776	"	10	340	25	3
P-20	50x50	3.5	175	3.8	SD30,13	-	O	2.03	3144	SR24,9	0.1	2776	"	10	324	25	3
P-21	50x50	3.5	100	2.2	SD30,13	-	O	2.03	3144	SR24,9	0.1	2776	"	10	321	25	3
P-22	50x50	3.5	250	5.4	SD30,13	-	O	2.03	3144	SR24,9	0.1	2776	"	10	320	25	5
P-25	50x50	3.5	116	2.5	SD30,13	-	O	2.03	3144	SR24,9	0.51	3494	"	10	390	25	10
P-26	50x50	3.5	116	2.5	SD30,13	-	O	2.03	3144	SR24,9	1.02	3494	"	10	390	25	10
P-27	50x50	3.5	116	2.5	SD30,13	-	O	2.03	3144	SR24,9	0.1	3494	"	10	390	25	10
P-28	$\phi 56.4$	3.5	250	4.7	SD30,13	-	O	2.03	3144	SR24,9	0.1	3494	"	10	406	25	10
P-29	$\phi 56.4$	3.5	175	3.3	SD30,13	-	O	2.03	3144	SR24,9	0.1	3494	"	10	406	25	10
P-30	$\phi 56.4$	3.5	100	1.9	SD30,13	-	O	2.03	3144	SR24,9	0.1	3494	"	10	406	25	10
P-31	$\phi 56.4$	3.5	250	4.7	SD30,13	-	O	2.03	3144	SR24,9	1.02	3494	"	10	406	25	10
P-32	$\phi 56.4$	3.5	175	3.3	SD30,13	-	O	2.03	3144	SR24,9	1.02	3494	"	10	406	25	10

Notes 1)  $d=D/4$

2) P-1 ~ P-3 (not correcting the inertia force), P-14, P-15 (Fracture at the cut-off).

P-23, P-24 (biaxial loading) and, P-33, P-34 (diagonal loading) are not the objectives of this study.

No.	Calculated Value According to Part V of Specification (Slipping-off is according to Reference 5))															Calculated Value According to Part III of Specification			Experimental Value		
	Displacement by Bending $\delta_1$ [mm]					$\delta = \delta_1 + \delta_3$ (mm)					Strength [t]					Displacement [mm]		Strength [tf]			
	Cracking $\delta_{1c}$	Yield $\delta_{1y}$	Ultimate $\delta_{1u}$	Cracking $\delta_{2c}$	Yield $\delta_{2y}$	Ultimate $\delta_{2u}$	Cracking $\delta_c$	Yield $\delta_{y\delta}$	Ultimate $\delta_u$	Cracking $f_c$	Yield $f_y$	Ultimate $f_u$	Bending Strength $P_B$ [tf]	Shear Strength $P_S$ [tf]	Yield $\delta_y$	Ultimate $\delta_u$	Yield $P_y$	Ultimate $P_u$			
P-4	1.02	12.76	24.8	0.37	8.93	64.03	1.39	21.69	88.8	3.4	13.8	14.8	4.6	19.26	19.0	69.0	14.3	15.5			
P-5	0.97	13.08	24.01	0.36	9.1	64.65	1.33	22.18	85.7	3.3	13.7	14.7	14.5	17.92	19.0	79.0	13.8	16.8			
P-6	1.03	9.07	34.13	0.31	6.33	66.22	1.34	15.4	100.4	3.1	6.8	7.6	7.5	19.26	12.2	80.0	7.1	8.8			
P-7	0.97	9.41	31.55	0.3	6.42	63.24	1.27	15.83	94.8	3.0	6.7	7.5	7.4	17.92	12.2	86.0	7.1	10.1			
P-8	1.03	5.15	51.7	0.25	4.9	72.74	1.28	10.05	124.4	3.0	4.0	4.7	4.7	19.26	5.4	55.0	4.3	4.8			
P-9	0.97	5.7	44.18	0.24	4.97	64.68	1.21	10.67	108.4	2.8	4.0	4.7	4.6	17.92	5.4	55.0	3.9	5.0			
P-10	0.94	8.1	48.46	0.22	3.43	36.98	1.16	11.53	85.4	3.6	11.1	14.4	14.3	16.84	13.0	92.6	11.6	16.8			
P-11	0.94	8.1	48.46	0.22	3.43	36.98	1.16	11.53	85.4	3.6	11.1	14.4	14.3	22.83	13.0	85.5	11.5	16.8			
P-12	0.94	8.1	48.46	0.22	3.43	36.98	1.16	11.53	85.4	3.6	11.1	14.4	14.3	22.62	13.0	86.4	11.5	16.9			
P-13	0.94	8.1	48.46	0.22	3.43	36.98	1.16	11.53	85.4	3.6	11.1	14.4	14.3	28.85	13.0	102.5	10.3	16.3			
P-16	0.95	8.21	48.76	0.22	3.43	36.98	1.17	11.64	85.7	3.6	11.1	14.4	14.3	17.15	13.0	97.4	10.3	17.0			
P-17	0.46	3.95	23.88	0.15	2.4	26.18	0.61	6.35	50.1	5.1	15.9	20.5	20.4	17.5	7.5	59.2	15.9	24.2			
P-18	0.15	1.29	7.78	0.09	1.37	14.94	0.24	2.66	22.7	8.8	27.7	35.8	35.5	17.36	3.9	20.2	27.6	39.1			
P-19	0.94	8.1	48.46	0.22	3.43	36.98	1.16	11.53	85.4	3.6	11.1	14.4	14.3	17.57	13.0	125.9	10.9	16.6			
P-20	0.46	3.95	23.88	0.15	2.4	26.18	0.61	6.35	50.1	5.1	15.9	20.5	20.4	17.01	7.5	70.8	15.5	24.6			
P-21	0.15	1.29	7.78	0.09	1.37	14.94	0.24	2.66	22.7	8.8	27.7	35.8	35.5	16.91	3.9	19.9	27.7	42.7			
P-22	0.94	8.1	48.46	0.22	3.43	36.98	1.16	11.53	85.4	3.6	11.1	14.4	14.3	17.29	13.0	114.5	10.9	16.7			
P-25	0.22	1.88	10.61	0.11	1.62	17.67	0.33	3.5	28.3	8.3	26.3	33.8	33.5	49.54	5.7	37.5	27.3	37.4			
P-26	0.22	1.88	10.61	0.11	1.62	17.67	0.33	3.5	28.3	8.3	26.3	33.8	33.5	85.48	5.8	50.0	26.6	38.4			
P-27	0.22	1.88	10.61	0.11	1.62	17.67	0.33	3.5	28.3	8.3	26.3	33.8	33.5	20.79	5.1	29.5	28.5	42.5			
P-28	0.93	7.33	37.84	0.21	3.09	20.65	1.14	10.42	58.5	3.2	10.1	14.9	14.7	21.35	12.0	70.5	11.8	17.2			
P-29	0.45	3.58	18.57	0.15	2.16	14.49	0.6	5.74	33.1	4.6	14.4	21.2	20.9	21.35	6.6	51.5	14.6	25.1			
P-30	0.15	1.17	6.07	0.09	1.23	8.3	0.24	2.4	14.4	8.0	25.1	37.1	36.5	21.35	3.8	22.5	25.8	42.7			
P-31	0.93	7.33	37.84	0.21	3.09	20.65	1.14	10.42	58.5	3.2	10.1	14.9	14.7	86.04	11.6	104.5	10.4	16.9			
P-32	0.45	3.58	18.57	0.15	2.16	14.49	0.6	5.74	33.1	4.6	14.4	21.2	20.9	86.04	7.1	74.0	14.7	25.4			

Table 3 Effect of Tie Hoop Ratio and Loading Repetition on Ultimate Displacement

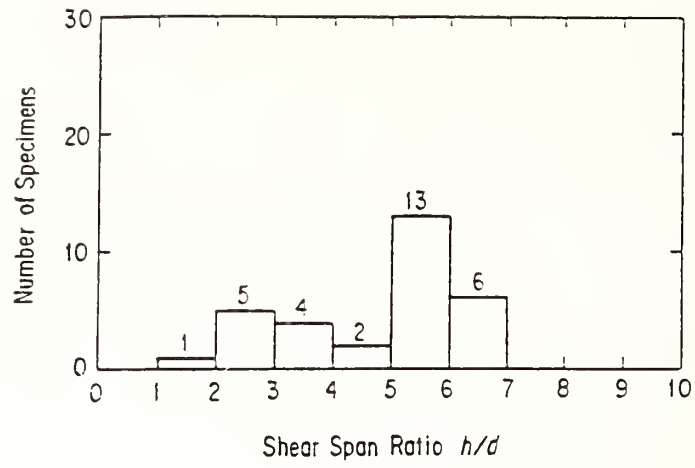
No.	Ultimate Displacement $\delta_u$ [mm]		Calculation Experiment	Feature of Specimen
	Experiment	Calculation		
P-10	92.6	85.4	0.92	Standard Specimen
P-11	85.5	85.4	1.00	$P_w = 0.2\%$
P-12	86.4	85.4	0.99	$P_w = 0.2\%$
P-13	102.5	85.4	0.83	$P_w = 0.3\%$
P-16	97.4	85.7	0.88	Standard Specimen
P-19	125.9	85.4	0.68	Number of Loading Repetition $n = 3$
P-22	114.5	85.4	0.75	" $n = 5$

(Notes) Standard Specimen  $P_f = 2.03\%$ ,  $P_w = 0.1\%$ ,  $n = 10$ ,  $h/d = 5.4$

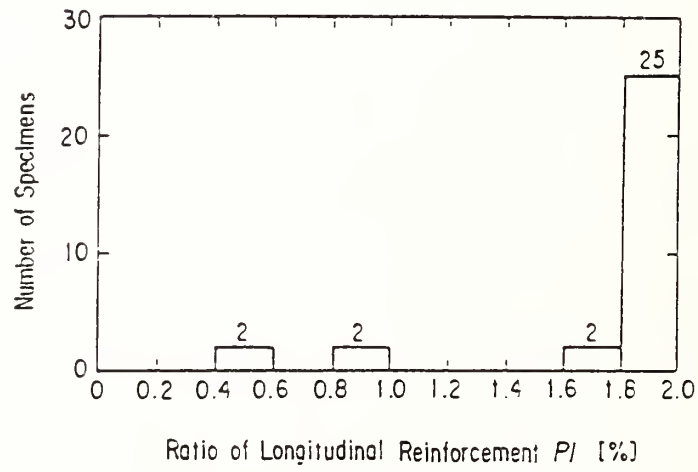
Table 4 Effect of Spiral Hoop on Ultimate Displacement

No.	Ultimate Displacement $\delta_u$ [mm]		Calculation Experiment	Feature of Specimen
	Experiment	Calculation		
P-18	20.2	22.7	1.12	$h/d = 2.2$
P-25	37.5	28.3	0.75	$h/d = 2.5$ High Ratio of Tie Hoop ( $P_w = 0.5\%$ )
P-26	50.0	28.3	0.57	$h/d = 2.5$ Spiral Hoop ( $P_w = 1.0\%$ )
P-28	70.5	58.5	0.83	$h/d = 4.7$
P-29	51.5	33.1	0.64	$h/d = 3.3$
P-31	104.5	58.5	0.56	$h/d = 4.7$ Spiral Hoop ( $P_w = 1.0\%$ )
P-32	74.0	33.1	0.45	$h/d = 3.3$ Spiral Hoop ( $P_w = 1.0\%$ )

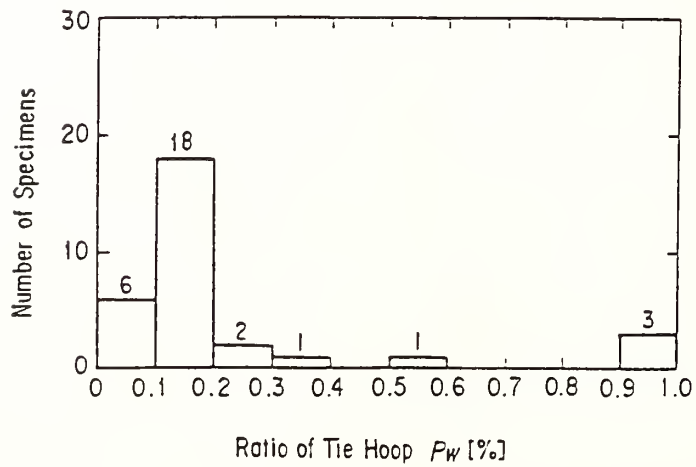
(Notes) Ratio of Longitudinal Reinforcement in All Specimens  $P_f = 2.03\%$ ,  
Ratio of Tie Hoop in P-18, 28, 29,  $P_w = 0.1\%$



(a) Distribution of Shear Span Ratio



(b) Distribution of Ratio of Longitudinal Reinforcement



(c) Distribution of Ratio of Tie Hoop

Fig. 1 Feature of Specimens

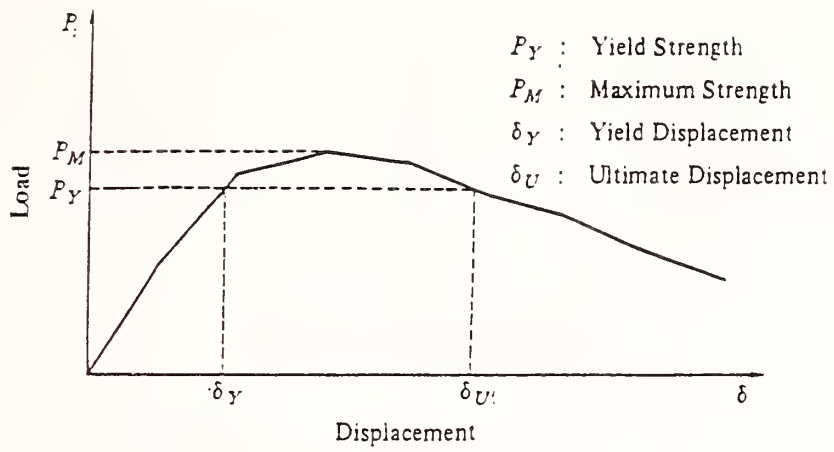


Fig. 2 Definition of Ultimate

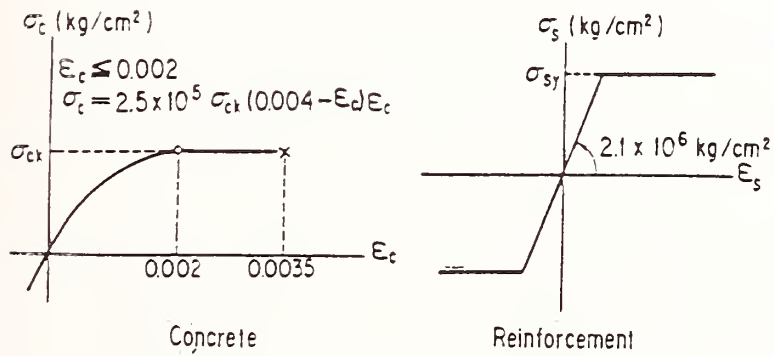
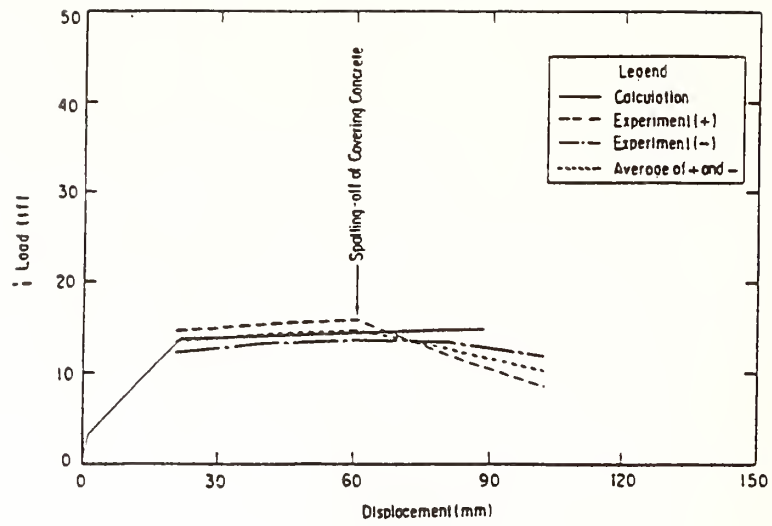
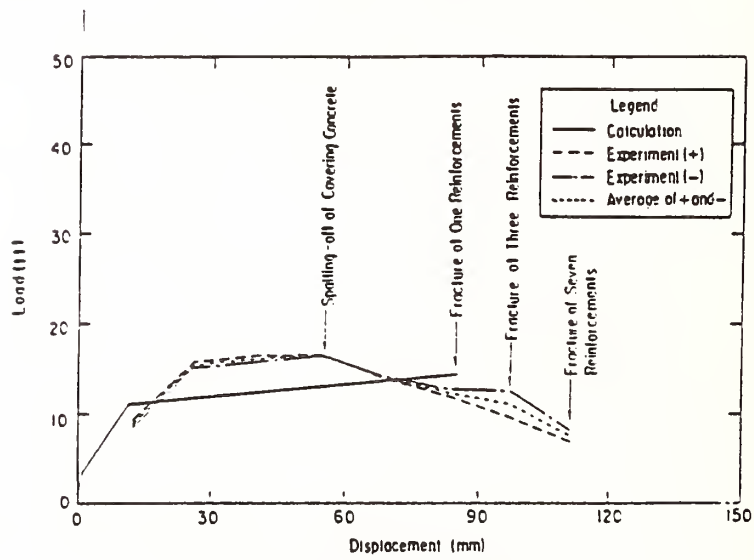


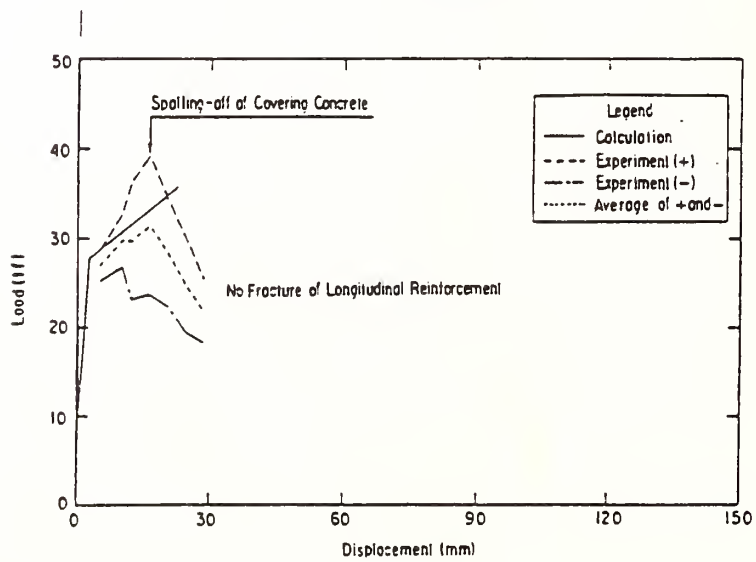
Fig. 3 Stress-Strain Diagram of Concrete and Reinforcement



(a) Beamlike Specimen (P-4)



(b) Columnlike Specimen (P-10)



(c) Shear Filled Specimen (P-18)

Fig. 4 Comparison of Experimental Relation and Calculated Relation of Load and Displacement

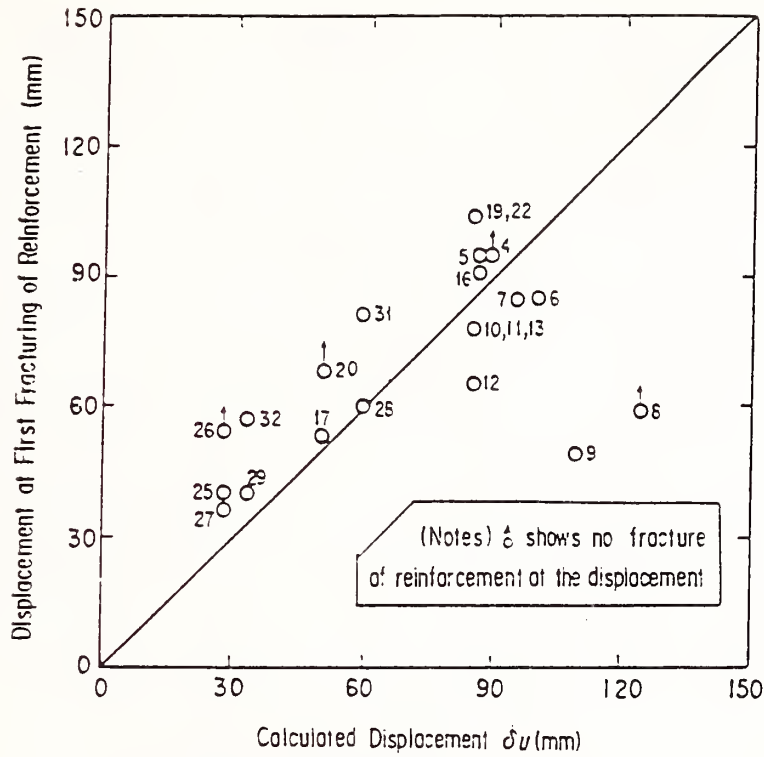


Fig. 5 Displacement at First Fracturing of Reinforcement and Calculated Ultimate Displacement

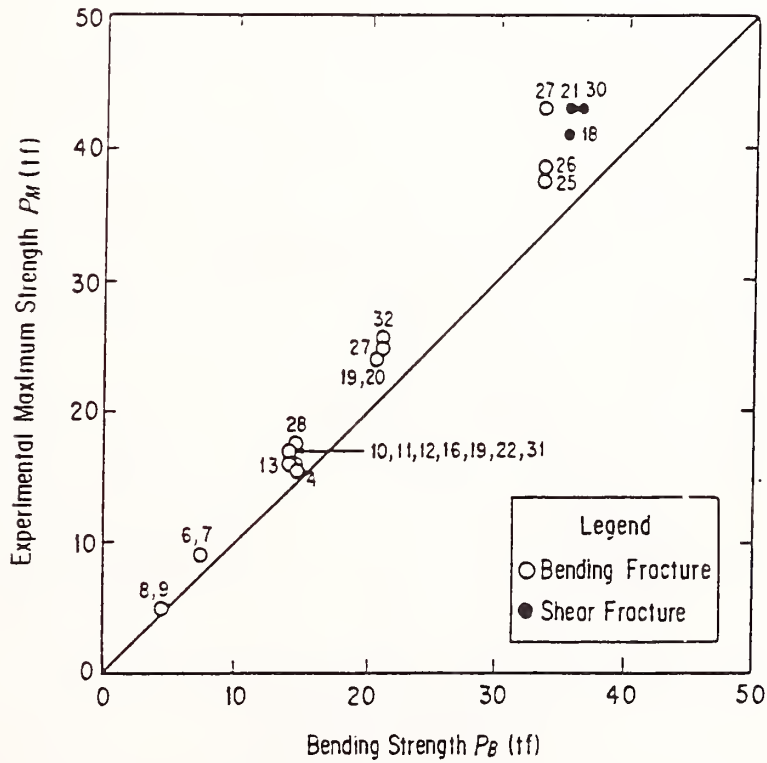


Fig. 6 Bending Strength and Experimental Maximum Strength

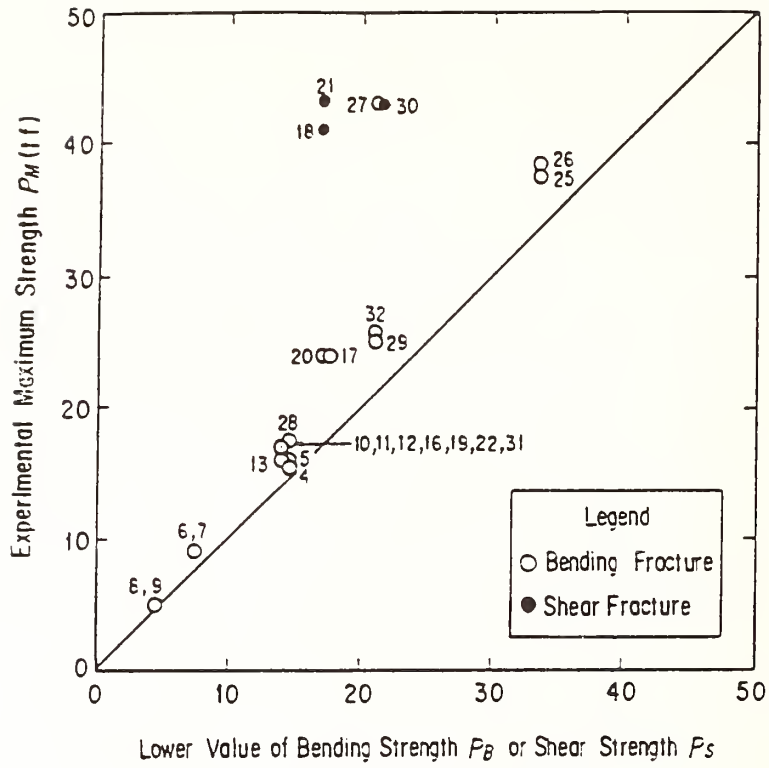


Fig. 7 Lower Value of Bending Strength  $P_B$  or Shear Strength  $P_s$  and Experimental Maximum Strength  $P_M$

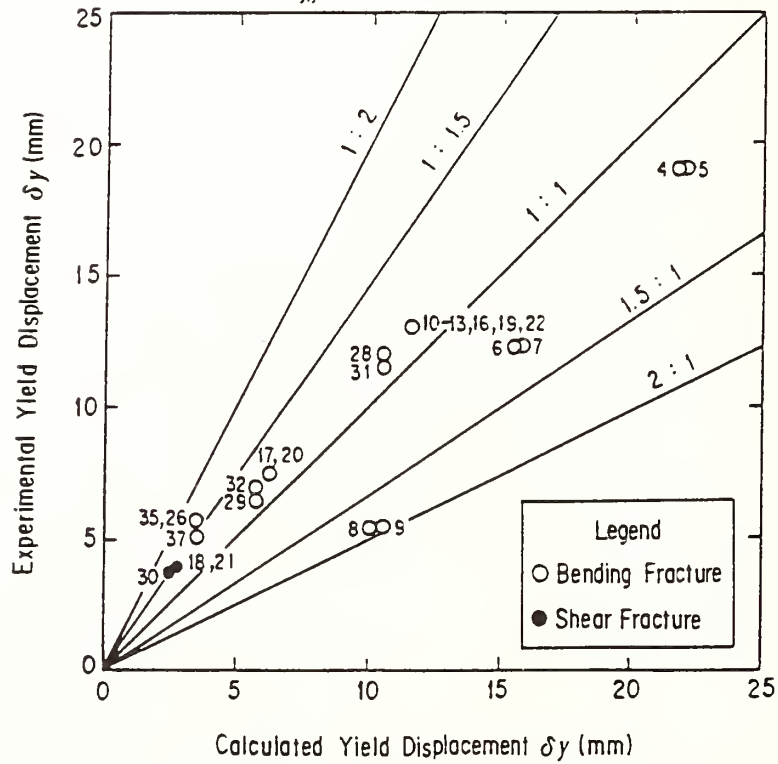


Fig. 8 Yield Displacement of Experiment and Calculation

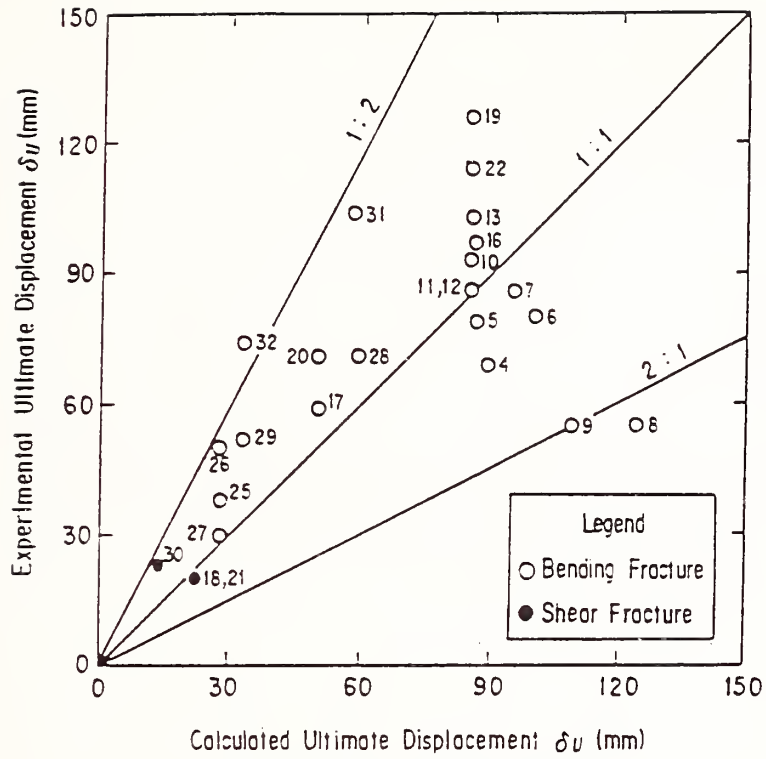


Fig. 9 Ultimate Displacement of Experiment and Calculation

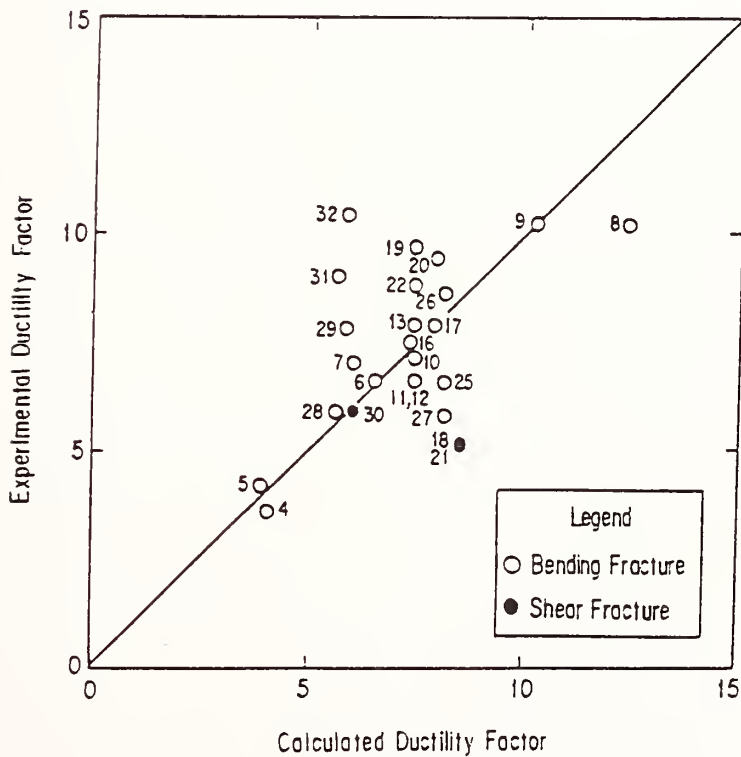


Fig. 10 Ductility Factor of Experiment and Calculation



## **Theme V**

---

# **Two Decades of Accomplishments and Challenges for the Future**



# U.S. Side: Accomplishments and Challenges—Panel on Wind and Seismic Effects

BY

Noel J. RAUFASTE<sup>1</sup>  
Richard N. WRIGHT<sup>2</sup>

## ABSTRACT

The US-JAPAN Panel on Wind and Seismic Effects was created in 1968; it provides for cooperative activities of fifteen US and six Japanese agencies with participating representatives of private sector organizations. Annual meetings alternate between JAPAN and the US (odd numbered years in JAPAN; even numbered years in the US). These one-week technical meetings provide the forum to discuss recent research results; one-week technical study tours follow the meetings.

The Panel develops important technologies that advance engineering design and construction practices and improve the quality-of life. This knowledge is produced by the collaboration of the US and JAPAN members working in ten task committees which focus on specific technical issues, e.g., earthquake strong motion data. The results of task committees are shared at annual joint meeting and often published as proceedings.

The National Bureau of Standards provides the US-side chairman and secretariat. The Public Works Research Institute, JAPAN provides the JAPAN-side chairman and secretariat.

KEYWORDS: Earthquake; seismicity; storm surge; tsunamis; US-JAPAN Panel; wind loads

## 1. BACKGROUND

Responding to the need for improved engineering and scientific practices through exchange of research personnel, technical data, information, and research equipment, the United States and JAPAN in 1961 created the US-JAPAN Cooperative Science Program. Three collateral programs comprise the Cooperative Science Program. The US-JAPAN Natural Resources Development Program (UJNR), one of the three, was created in January 1964. The objective of UJNR is to exchange information on research results and exchange scientists and engineers in the area of natural resources for the benefit of both countries. UJNR is composed of 17 Panels each responsible for specific technical subjects.

The Panel on Wind and Seismic Effects was established in 1968 to provide technologies, for US and Japanese governments, to reduce damages from high winds, earthquakes, storm surge, and tsunamis. The Panel also provides the vehicle to exchange technical data and information on design and construction of civil engineering lifelines, buildings, and water front structures, and to exchange high wind and seismic measurement records.

---

<sup>1</sup>Head, Cooperative Research Programs, Center for Building Technology, National Bureau of Standards

<sup>2</sup> Director, Center for Building Technology, National Bureau of Standards

This report addresses the Panel's impact on US and some Japanese building practices and provides suggestions for future thrusts. A counterpart report, prepared by the JAPAN-side, will highlight impacts of the Panel's work on JAPAN's building practices.

A few years after the Panel's creation, US and Japanese researchers had visited many of the leading laboratories of both countries and began joint monitoring of performance of buildings and public works. Both countries had need for improved strong-motion instrumentation arrays and data. This need resulted in creating the first Task Committee (TC); it provided a vehicle to perform joint research. Likewise, the need for data from large-scale testing resulted in the second TC. Others followed a similar process. Six TCs were created by 1975. The 10th TC was created in 1981. TC results are presented at annual Panel meetings. In 1978 TC's began submitting formal reports for inclusion in the Proceedings.

TCs change in response to member's needs and research opportunities. As illustrations: in the mid-1970's the TC on Disaster Prevention Methods for Lifeline Systems split off a TC on High Speed Wind Data. In 1979, the TC on High Speed Wind Data changed its name to Wind Characteristics and Structural Response and spun off a TC on Storm Surge and Tsunamis. The TC on Disaster Prevention Methods for Lifeline Systems in 1981 refocused to the present TC on Wind and Earthquake Engineering for Transportation Systems.

The Panel organized formal joint research programs. In 1981 an agreement was signed for cooperation in Large-Scale Testing under the auspices of the Panel. Also in 1981, joint research on Reinforced Concrete Structures was initiated; full-scale testing was performed at the Building Research Institute (BRI), JAPAN with supporting tests in JAPAN and in the US. Two years later the joint research program on Steel Structures was initiated. Full-scale testing again was led by BRI with supporting tests in the US and JAPAN. The US-JAPAN coordinated program for Masonry Building Research was started in 1985. A coordinated program for testing lifeline structures resulted in NBS' testing of full-scale bridge piers in its 50Mn universal testing facility to

evaluate post-1972 seismic design criteria.

TC's hold periodic workshops with participation of non-governmental experts to share information from research and practice, and develop research agendas to solve current and anticipated problems. Results are shared through prepared papers and written workshop summaries, and through published proceedings and presentations at annual Joint-Panel meetings.

These meetings, alternating between the US and JAPAN, have been conducted since the Panel's inception. Task Committee meetings, exchanges of data and information through technical presentations at the annual Panel meetings, exchanges of guest researchers, visits to respective research laboratories and informal interactions between Panel meetings, joint workshops and seminars, and joint cooperative research programs have contributed immensely to the development and effective delivery of knowledge that has influenced design and construction practices in both countries.

The direct communications between counterpart country organizations is the cornerstone of the Panel. Effective information exchanges and exchanges of personnel and equipment have strengthened domestic programs of both countries. There have been opportunities for experts in various technical fields to get to know their foreign counterparts, conduct informal exchanges, bring their respective views to the frontiers of knowledge, and advance knowledge of their specialties.

A Department of State evaluation of the Panel in 1983 commended the Panel's work as "...one of the best, both in terms of activity and of value to the US" and "...as the epitome of the way an international technical cooperation program should be operated."

The Panel has been very active during its two decades:

- o over 35 workshops and conferences and more than 50 joint publications
- o over 1000 technical papers published as a result of the Panel's work
- o about 100 researchers and engineers each from the US

and JAPAN participated in joint programs and investigations in counterpart laboratories

- o produced method to exchange strong-motion earthquake data between the US, JAPAN, and other countries.

The Panel's results have supported building and structure code improvements in both countries, for example:

1. Created and exchanged digitized earthquake records for use as the basis of research for Japanese and US geotechnics and structures;
2. Produced data that advanced US design and construction of bridge columns;
3. Produced large-scale testing data that advanced the seismic design code for buildings;
4. Created a database comparing Japanese and US standard penetration tests to improve seismic design criteria for soil liquefaction;
5. Created databases on storm surge and shore line interaction and on tsunamis and tsunami warning systems for use by designers to verify mathematical models of tsunamis and storm surge.

Section 2 addresses Panel accomplishments which contributed to advancing US and Japanese engineering practices. Future Panel work is presented in Section 3. The Appendix lists panel conferences, meetings, researcher exchanges, publications during 1978-1987. Information on Panel activities during its first decade was less formally documented; hence it is not included in this paper.

## 2. PANEL ACCOMPLISHMENTS

Accomplishments are listed under their respective task committees.

### A. Strong-Motion Instrumentation Arrays and Data

- o developed manuals on strong-motion earthquake record digitization for design professionals to improve earthquake design criteria and improved state-of-knowledge.

### B. Large-Scale Testing Program

- o established multi-year comprehensive joint research program to evaluate performance of various building structure types, provided mechanisms for effective joint research programs, and stimulated communication between researchers in both countries.
- o developed improved design criteria for reinforced concrete and steel building structures through joint research program on full-scale testing. Results contributed significantly to updating US and Japanese seismic codes and standards.
- o provided mutual guidance in planning and executing the coordinated research program on performance of full-scale structures that maximized use limited research funds in both countries, particularly the complementary use of country's unique testing facilities.

### C. Repair and Retrofit of Existing Structures

- o stimulated US research develop criteria for repairing reinforced concrete, masonry, and steel buildings and bridges.
- o provided recommendations incorporated into building codes and professional practices, illustrated by rehabilitation program used by the city of Los Angeles to upgrade existing masonry buildings to resist earthquake forces.
- o influenced US design practices to upgrade existing structures e.g, the new State of California bridge design criteria for tying girders to better resist earthquake forces.

### D. Evaluation of Performance of Structures

- o developed data base of methods to evaluate existing buildings and analyze experimental testing

programs for structures. This data contributed to new risk analysis and screening methods to determine earthquake resistance of buildings.

- o contributed to analysis of physical testing and correlating results of large-scale and component testing programs.
- o developed, in cooperation with other Task Committees, a procedure to produce a file of "bench-mark structures" which were evaluated for resistance to seismic loads; structures were instrumented for evaluation after future events.

E. Natural Hazard Assessment and Mitigation Through Land Use Programs

- o exchanged technical papers and ideas in the area of earthquake hazard and risk assessment e.g.,
  - scientific personnel
  - information to implement the Earthquake Hazards Reduction Act in the United States and the Large-scale Earthquake Countermeasures Act in Japan
  - information on techniques for seismic risk mapping (ground shaking) and maps of liquefaction hazards
  - information on evaluation of specific earthquakes in the US and JAPAN.

F. Disaster Prevention Methods for Lifeline Systems

- o translated PWRI's "Manual of Repair Methods for Civil Engineering Structures Damaged by Earthquakes" (in cooperation with the National Center for Earthquake Engineering Research [NCEER] SUNY, Buffalo). The manual has engineering guidelines and practices for maintenance, emergency inspection, damage detection and estimation methods to restore, repair, and retrofit lifeline systems. It will be a valuable reference for development of US practices.
- o contributed to assessment of the design and operating standards for lifeline systems. This effort was led by the Building Seismic Safety Council (BSSC) under sponsorship of the Federal

Emergency Management Agency (FEMA) with participation of UJNR Panel members and other professionals.

- o stimulated increased public attention to safety problems of lifeline systems using results from workshops and seminars e.g., workshop on abatement of earthquake hazards to lifelines (November, 1986 in Denver, Colorado).

- o research on the behavior of lifeline systems under seismic forces using instrumented ductile pipes at different orientations to faults at Parkfield, CA (sponsored by NCEER) will produce performance criteria on pipe resistance to ground displacement.

G. Wind Characteristics and Structural Response

- o contributed to producing benchmark data to assess the validity of physical and analytical models of wind and its effects on building structures.

- o performed measurements of basic wind speeds in tropical and extra-tropical storms, response of tall slender structures to wind loads, and localized effects of wind on cladding elements and on solar collectors.

- o exchanged significant data on wind speeds obtained by the Meteorological Research Institute on its tower at Tsukuba by post-storm damage assessments performed in the US by various government agencies, and by full-scale measurements of wind forces on low-rise buildings in the US and wind speed measurements at coastal exposures in JAPAN.

H. Soil Behavior and Stability During Earthquakes

- o produced recommendations for interpretation of the Standard Penetration Test which were generally accepted by the design and construction profession in the U.S.

- o advanced the state-of-art of in-

situ testing of soils to evaluate their behavior and stability under severe earthquake shaking through a cooperative program on in-situ testing of soils. A workshop was conducted on in-situ testing of soils in 1984.

- o advanced the state-of-art of in-situ testing of soils through the cooperative research program and exchange of personnel following the 1983 Nihonkai-Chubu earthquake which caused widespread liquefaction of soils. Advances were made in part by four guest researchers: Messrs. Tatsuo UWABE, Takashi TSUCHIDA, and Yoshitaka HACHIYA to WES and Mr. Jeffrey FARRAR to PWRI.

#### I. Storm Surge and Tsunamis

- o strengthened US data base on effects of tsunamis. Joint Panel effort supplemented NOAA's development to determine risks and design parameters. This data base made it possible to develop improved models to predict the occurrence of tsunamis during the first hour and to predict their run-up heights at various locations.

#### J. Wind and Earthquake Engineering for Transportation Systems

- o prepared recommendations for new seismic design specifications for bridges; they were adopted by the States (research sponsored by FHWA).
- o contributed to development of changes in seismic design criteria for transportation systems through 18 years of joint investigations of natural disasters starting with the 1971 San Fernando and subsequent earthquakes. US and JAPAN research complemented each other's efforts to identify needed specification changes.
- o completed a series of laboratory tests on large-scale models of concrete piers and columns.
- o contributed to the repair and strengthening procedures for existing bridges, field testing of bridges, analytical and laboratory tests, instrumentation development and placement, and the development and adoption of design specifications.

- o contributed to the completion of joint comparisons of wind tunnel test results, exchanges of guest researchers in the field of aerodynamics, performance of formal training at Princeton and Johns Hopkins Universities. With the cooperation of NBS, NSF, and FHWA have enabled students to experiment and advance the state-of-knowledge.
- o sponsored various workshops that identified needs and planned for technical information exchanges and field visits to public works.

### 3. FUTURE PANEL ACTIVITIES

The Panel members annually evaluate their work questioning issues such as what can be done to better meet the Panel's needs? What are areas that no longer need be done? What are the challenges requiring attention that are not being addresses? Answers to these questions are acted on by the 10 T/C's.

#### A. For T/C, Strong-Motion Instrumentation Arrays and Data continue:

- performing data analysis/processing from downhole 3D arrays for the geophysical research community and the structural engineering design and analysis community.
- assessing structural behavior of base-isolated structures during strong-motion earthquakes by critical evaluation of processed records from structures instrumented for earthquake response.
- comparing digitizing and processing techniques through workshops.

#### B. For T/C, Large-scale Testing Program activities will include:

- performing a coordinated study to determine the performance of pre-cast/pre-stressed structures in high seismic areas of the world.
- performing a coordinated

study to develop economical composite structural systems for multi-story building construction.

C. For T/C, Repair and Retrofit of Existing Structures emphasize:

- studying new materials and methods to accomplish repair and retrofit operations on buildings and bridges e.g., fiberglass reinforced plastic, composite bridge decks, and exploiting use of automation and robotics for repair and retrofit.
- coordinating research projects with Japanese researchers and researchers from other countries to minimize duplication and maximize benefits obtained by participating countries.

D. For T/C, Evaluation of Performance of Structures continue:

- improving the screening and evaluation methods to determine seismic resistance and identifying research needs to improve evaluation technology.
- expanding the catalog of "benchmark" structures in each country that have been evaluated and instrumented. Evaluate other buildings in JAPAN and US using Japanese and US methods, including provisions of ATC-14.
- coordinating workshops and other activities with task committees on large-scale testing and repair and retrofit to develop and refine test methods for analyzing seismic resistance of buildings.

E. For T/C, Natural Hazard Assessment and Mitigation Through Land Use Programs focus on:

- conducting a workshop on seismic hazard and risk (loss) estimations (planned for 1989). Thrusts to include but not limited to:

1. Probabilistic earthquake (ground motion) hazard assessment
2. Attenuation of seismic waves
3. Site response
4. Earthquake losses
5. Delineation of seismotectonic elements
6. Application of hazard assessment to seismic provisions of building codes.

The workshop will help shape the following activities:

- adopting and preparing technical material for mitigating earthquake effects, to be published in a format for easy application for a broad range of mitigation activities--land use programs, building codes, disaster preparedness, and new research results, particularly in the area of attenuation of seismic waves and the estimation of response of individual sites to shaking.
- evaluating the potential economic and life loss associated with earthquakes and the application of techniques that reduce these losses.
- promoting exchanges of scientific and technical personnel to better understand techniques for hazard and risk assessment and mitigation.
- continuing exchanges of scientific and technical literature.

F. For T/C, Disaster Prevention Methods for Lifeline Systems there is need for greater joint participation and data exchanges of field tests of pipelines and other lifeline systems by:

- increasing joint development and use of laboratory experiment facilities (i.e. multiple shaking tables) required for various lifeline systems.
- planning and implementing joint

research program on a selected lifeline system similar, in concept, to the Large-Scale Testing Program. This new program expects to produce knowledge of behavior of lifeline systems under simulated earthquakes and provide a basis for design guidelines which reduce deficiencies in design practices.

- developing and executing joint demonstration projects of emergency evaluation and of on-line control monitoring systems for lifeline operation using state-of-the-art sensors and computer technology. This effort is expected to produce a diagnostic capability for lifeline conditions and a decision method to repair lifelines for restoration of services.
- developing performance standards and a manual for repair, restoration, and retrofit. The work will integrate current knowledge into guidelines for safety design and retrofit of lifelines.

G. For T/C, Wind Characteristics and Structural Response, five areas are critical to advancing the state-of-art in wind engineering:

- obtaining reliable and comprehensive wind speed measurements at offshore locations.
- collecting pressure data (external and internal) on full-scale buildings located in areas representing a wide range of surface roughness.
- improving wind tunnel modeling techniques (from full-scale wind data representing a wide range of surface roughness) and developing standards to conduct wind tunnel tests.
- developing improved procedures for incorporating wind engineering knowledge in building codes and standards.

- supporting joint programs to make use of existing research facilities in the US and JAPAN and to provide greater exchange of research personnel.

H. For T/C, Soil Behavior and Stability During Earthquakes, primary technical challenges for the next decade are in-situ testing of soils and remedial treatment of unstable soils. Work should be focused on:

- developing measurement methods to improve in-situ testing of soils, obtaining basic observational data on the behavior of soils under earthquake shaking, and validating analytical models of soil behavior.
- devising new modes of cooperative research building on the strengths of the US and JAPAN research organizations, planning better strategies to fund cooperative research, and improving ability to deliver knowledge produced during the research phase.
- conducting a workshop on remedial treatment of soils, a US-JAPAN cooperative research program on remedial measures, and more frequent exchanges of researchers on long-term working visits between US and JAPAN research organizations.
- addressing remedial treatment of unsatisfactory soils, including those with inadequate resistance to earthquake-induced liquefaction. Remedial treatment is needed in older works and in new projects on construction sites with marginal conditions. Near term goals are to hold workshops that focus on better transferring information, establishing effective cooperative program, and increasing exchanges of researchers for long-term visits.

- I. For T/C, Storm Surge and Tsunamis emphasize:
- planning a 2nd workshop on tsunami and storm surge.
  - developing a database (global inventory) of storm surge and tsunamis to support the engineering and research needs of US, JAPAN, and other countries.
  - forecasting global climate change to predict changes in sea level and on-shore run-up for mitigating damage from high water.
  - improving methods for data collection, recording, and reduction for consistency so countries users may better interpret and use the data.

J. For T/C, Wind and Earthquake Engineering for Transportation Systems, the technical challenge of forecasting, measuring, and characterizing natural events, such as earthquakes and winds on bridges and transportation systems, will continue to exist. There is need for:

- performing research on soil-structure interaction on bridge foundations during earthquakes which will result in less expensive full-scale bridge field tests.
- developing better and more reliable instrumentation for unattended field use to record natural events.
- understanding the behavior of cable-stayed bridges, the inspection of large cables, and the protection of cables from corrosion.

#### 4. ACKNOWLEDGEMENTS

The production of this summary paper resulted from a team effort by the ten US Panel Task Committee Chairmen and from guidance provided by Dr. Charles SCHEFFEY (charter Panel member), Dr. H.S. LEW past US Secretary, and Dr. Edward PFRANG US Panel Chairman (1969-1984).

Technology development was nurtured by the technical discussions and the comradeship developed at annual meetings, field trips, and cultural affairs which provided the environment for peers to get to know each other and to develop lasting friendships. The technically substantive work occurred primarily in their respective laboratories; yet, without friendships and mutual trust which grew out of the joint Panel activities, laboratory research alone could not have had the direction, synergistic effects, nor the success of delivery into practice into both countries. Moreover, Panel activities and accomplishments have stimulated support of the participating organizations from policy-makers in their respective countries.

The dedicated support, intellectual contributions, and work of the Panel Chairmen and Secretariats, from both sides, were instrumental in maintaining a high level of activity leading to the many accomplishments of this Panel.

ATTACHMENT

US-JAPAN PANEL ON WIND AND SEISMIC EFFECTS  
1978 - 1988

1. EXCHANGE ACTIVITIES

The past decade saw many exchanges of researchers and cooperative research from both countries.

- 1978 May: 2nd Committee Meeting for the Joint Research Program on Large-scale Testing of Structures, San Francisco  
Dec: 3rd Committee Meeting for the Joint Research Program on Large-scale Testing of Structures, Tokyo
- 1979 Jul: 4th Committee for the Joint Research Program on Large-scale Testing of Structures, San Francisco
- 1980 May: 1st Seminar on Repair and Retrofit of Structures, Los Angeles
- 1981 May: 2nd Seminar on Repair and Retrofit of Structures, Tsukuba
- 1982 May: 3rd Seminar on Repair and Retrofit of Structures for Earthquake Resistance, San Francisco  
Sept-Dec: Joint Program on evaluation of Japanese state-of-art of wind tunnel applications to industrial aerodynamics research
- 1983 May: 1st US Japan Joint Workshop on Evaluation of Performance of Existing Buildings, Tsukuba  
1st Joint Workshop on Storm Surge and Tsunami, Tsukuba  
Nov: Joint Research Program on In-Situ Testing Methods for Determining Soil Liquefaction Potential
- 1984 Feb: 1st Workshop on Bridge Structures, Tsukuba  
Mar: 1st Workshop on US Japan Masonry Program, Tsukuba  
May: 1st Workshop on Life Line Systems, Washington  
Jul: 2nd Workshop on Evaluation of Performance of Existing Buildings, San Francisco  
Aug: Joint Research Program on Large-Scale Testing of Multi-Story Structures. Results presented at the 8th World Conference on Earthquake Engineering  
Joint Research Program on Large-Scale Testing of Steel Structures  
Dec: 2nd Joint Workshop on Seismic Behavior on Buried Pipelines and Telecommunication

- Systems, Tsukuba
- 1985 May: 3rd Workshop on Evaluation of Performance of Existing Buildings, Tokyo
- Aug: Joint Research Program on Large-Scale Testing of Masonry Structures; 1st Joint Technical Coordinating Committee, Tokyo
- 2nd Joint Workshop on Bridge Structures, San Francisco
- Joint Workshop on In-Situ Test Methods for Determination of Soil Liquefaction Potential, San Francisco
- 1986 Aug: Planning Conference on Disaster Prevention for Lifeline Systems held in conjunction with 3rd US National Conference on Earthquake Engineering, Charlston, SC
- 1987 May: 3rd Workshop on Repair and Retrofit of Existing Structures, Tsukuba
- 3rd Workshop on Performance and Strengthening of Bridge Structures, Tsukuba
- Planning Conference on Evaluation of Seismic Resistance of Existing Buildings, Tsukuba
- Aug: Workshop on Strong Motion Earthquake Recording, Menlo Park, CA
- Oct: 3rd Meeting of the Joint Technical Coordinating Committee on Masonry Research, Tsukuba

## 2. RESEARCHER EXCHANGES

- 1978 Jun: B.R. ELLINGWOOD, NBS; A.G. BRADY, E.L. HARP, D.K. KEEFER, and C.M. WENTWORTH, USGS; C. ARNOLD, J.A. BLUME, J.D. COOPER, H.H. FOWLER, and P.I. YANEV performed joint investigation of the Miyagiken-Oki Earthquake
- 1978-79 Jul-Jul: T. UWABE, PHRI\*\*\* guest researcher at WES performing research on earthquake engineering
- 1979 May-Aug: R.K. MCGUIRE, USGS guest researcher at PWRI\*\* performing research on evaluation method of seismic risk
- 1980-81 Sep-Jul: J.K. WRIGHT, U. of Michigan guest researcher at BRI\* performing joint research on large-scale testing program on reinforced concrete structures
- 1981 Jan-May: D. REA, U. of California guest researcher at BRI performing joint large-scale testing program on reinforced concrete structures
- May-Aug: L.R.L. WANG, U. of Oklahoma guest researcher at PWRI performing research on aseismicity of life-line systems
- 1981-82 Jul-Apr: H.HIRAISHI, BRI guest researcher

- at Portland Cement Association, Chicago performing joint large-scale testing program
- Aug: M. WATABE and Y. YAMANOUCI, BRI participating in the meeting of large-scale testing at San Francisco and Honolulu
- 1982 Jun-Aug: H. KRAWINKIER, U. of Stanford guest researcher at BRI performing joint large-scale testing program on reinforced concrete structures
- Sept-Dec.: R. MARSHALL, NBS guest researcher at PWRI evaluating Japanese state-of-art of wind tunnel applications to industrial aerodynamics research as part of the joint Program on Wind Engineering. Results published as "Wind Tunnels Applied to Wind Engineering in Japan", Journal ASCE, Vol. 110, ST.6, June 1984
- 1982-83 Sep-Aug: D.A. FOUTCH, U. of Illinois guest researcher at BRI performing joint large-scale testing program on steel structures
- 1983 Feb-Sept: R. HAGIWARA from PWRI performing research on large-scale concrete columns under seismic forces
- Aug-Dec: C.W. ROEDER, U. of Washington guest researcher at BRI performing joint large-scale testing program on steel structures
- Oct-Nov: W. KOVACS from NBS, J.A. FARRAR from BUREC performing joint study in JAPAN on application of standard penetration method. Results published in Proceedings of the 8th World Conference on Earthquake Engineering
- Nov: US Delegation Observing Japanese Earthquake Prediction and Preparedness Measures on the Anticipated TOKAI Earthquake
- 1983-84 Nov-Nov: M. YOSHIMURA, BRI guest researcher at U. of California, Berkeley performing joint research on large-scale testing program on reinforced concrete structures
- 1984 Jan-Feb: S.C. GOEL, U. of Michigan guest researcher at BRI performing joint research on large-scale testing program on steel structures
- Mar-Apr: H. HIRAIISHI, BRI participating in the meeting of joint large-scale testing program on masonry structures at the U. of California, Berkeley
- Apr: Y. YAMANOUCI, BRI participating in the meeting of the joint large-scale testing at the U. of California, Berkeley and U. of Michigan
- Jun-Jul: M. L. WANG, U. of California, Berkeley guest researcher at BRI performing joint large-scale testing program on steel structures
- Sep: D. KEEFER and E. HARP from USGS performing

- joint investigation of the Naganoken-Seibu Earthquake
- 1985 Mar-Apr: T. KAMINOSONO from BRI guest researcher at U. of California, Berkeley performing joint research in large-scale testing program on masonry structures
- Mar-Apr: M. NAKAJIMA, BRI guest researcher at U. of Stanford and U. of Minnesota performing joint large-scale testing program on masonry structures
- 1985-86 May-Apr: M. MIDORIKAWA, BRI guest researcher at U. of Illinois performing research on steel structures under seismic forces
- Sep-Jan: M. TESHIGAWARA from BRI participating in joint research Program on Masonry Structures at the U. of California, Berkeley
- Nov-Nov: T. TSUCHIDA, PHRI researcher at WES performing research in soil dynamics
- 1986 Aug-Sep: O. SENBO, BRI guest researcher at U. of Colorado performing joint large-scale testing program on masonry structures
- Oct-Nov: J. FARRAR, BUREC guest researcher at PWRI performing research in liquefaction during earthquakes
- 1986-87 Sept-Jun: K. MINOSAKU, PWRI guest researcher at NBS performing research on behavior of large scale bridge pier subjected to seismic loads
- 1987 Jan-Mar: R. JIBSON, USGS guest researcher at PWRI performing research in ground motion
- 1987-88 Mar-Feb: Y. HACHIYA, PHRI guest researcher at WES performing research in pavements
- Aug-Oct: F. SEIBLE, U. of California, San Diego guest researcher at BRI performing joint large-scale testing program on masonry structures.

### 3. PANEL PUBLICATIONS

- 1978- o Proc. of 9th Joint Meeting, NBS SP 523 9/78  
 o Proc. of 10th Joint Meeting, PWRI (in Japanese)  
 o Preprint of 10th Joint Meeting
- 1980- o Proc. of 10th Joint Meeting NBS SP 560 10/80  
 o Proc. of 11th Joint Meeting, PWRI (in Japanese)  
 o Preprint of 12th Joint Meeting  
 o Proc. of 1st Seminar on Repair and Retrofit of Structures
- 1981- o Proc. of 12th Joint Meeting, PWRI (in Japanese)  
 o Proc. of 2nd Seminar on Repair and Retrofit of Structures
- 1982- o Proc. of 13th Joint Meeting, PWRI (in Japanese)  
 o Preprint of 14th Joint Meeting

- o Proc. of 3rd Seminar on Repair and Retrofit of Structures for Earthquake Resistance
- 1983- o Proc. of 14th Joint Meeting, PWRI (in Japanese)
- o Proc. of 11th Joint Meeting, NBS SP658 7/83
- o Proc. of 14th Joint Meeting, NBS SP651 4/83
- o Preprint of 15th Joint Meeting
- o Proc. of 1st Workshop on Evaluation of Performance of Existing Buildings
- o Proc. of Workshop on Storm Surge and Tsunami
- o Proc. of Workshop on In-Situ Testing Methods for Determining Soil Liquefaction Potential
- 1984- o Proc. of 15th Joint Meeting, PWRI (in Japanese)
- o Proc. of 12th Joint Meeting, NBS SP665 1/84
- o Preprint of 16th Joint Meeting
- o Proc. of 1st Workshop on Bridge Structures
- o Proc. of Workshop on US Japan Masonry Program
- o Proc. of Workshop on Life Line Systems
- o Proc. of 2nd Workshop on Evaluation of Performance of Existing Buildings
- o Proc. of Workshop on Large-Scale Testing of Multi-Story Structures
- o Proc. of Workshop on Large-Scale Testing of Steel Structures
- o Proc. of Workshop on Seismic Behavior on Buried Pipelines and Telecommunication Systems
- 1985- o Proc. of 16th Joint Meeting, PWRI (in Japanese)
- o Published report, Earthquake Effects on Reinforced Concrete Structures: US-Japan Research; ACI SP84 Series, 3/85
- o Preprint of 17th Joint Meeting
- o Proc. of 3rd Workshop on Evaluation of Performance of Existing Buildings
- o Proc. of 2nd Bridge Workshop
- 1986- o Proc. of 17th Joint Meeting, NBSIR 86-3363 5/86
- o Proc. of 17th Joint Meeting, PWRI (in Japanese)
- o Preprint of 18th Joint Meeting
- o Proceedings of the 1st, 2nd, and 3rd Workshops on Evaluation of Structural Performance for Resistance to Earthquakes, Cornell University
- o Published Seismic Performance of Existing Buildings in the Proc. of 3rd. US National Conference on Earthquake Engineering, Aug. 86
- 1987- o Proc. of 18th Joint Meeting, NBSIR 87-3540, 4/87
- o Proc. of 19th Joint Meeting, PWRI (in Japanese)
- o Preprint of 19th Joint Meeting
- o Results of US individual component tests and full-scale test of reinforced concrete structures in JAPAN; U of Illinois
- o Results of steel structures; U. of Michigan
- o Preliminary Report on Whittier Narrows Earthquake; USGS
- 1988- o Proc. of 19th Joint Meeting, NBSIR 88-3703, 1/88

o Translation by NSF of PWRI's, Manual of Repair  
Methods for Civil Engineering Structures Damaged  
by Earthquakes

- 
- \* BRI: Building Research Institute, Ministry of Construction,  
JAPAN
  - \*\* PWRI: Public Works Research Institute, Ministry of  
Construction, JAPAN
  - \*\*\* PHRI: Port and Harbor Research Institute, Ministry of  
Transport, JAPAN

# Two Decades of Accomplishments and Challenges for the Future

by

Nobuyuki Narita\*

## TABLE OF CONTENTS

1. Introduction	1
2. Two Decades of Accomplishments and Future Challenges of the Panel on Wind and Seismic Effect, UJNR	2
2.1 Progress of the Panel	2
2.2 Accomplishments by the Panel	2
2.3 U.S.-Japan Cooperative Research Program	2
2.4 Future Challenges of the Panel	3
3. Two Decades of Accomplishments and Future Challenges in Each Task Committee	4
3.1 Task Committee A "Strong-Motion Instrumentation Arrays and Data"	4
3.2 Task Committee B "Large-Scale Testing Programs"	6
3.3 Task Committee C "Repair and Retrofit of Existing Structures"	8
3.4 Task Committee D "Evaluation of Performance of Structures"	9
3.5 Task Committee E "Natural Hazard Assessment and Mitigation through Land Use Programs"	11
3.6 Task Committee F "Disaster Prevention Methods for Lifeline Systems"	12
3.7 Task Committee G "Wind Characteristics and Structural Response"	14
3.8 Task Committee H "Soil Behavior and Stability During Earthquakes"	15
3.9 Task Committee I "Storm Surge and Tsunamis"	17
3.10 Task Committee J "Wind and Earthquake Engineering for Transportation Systems"	19
4. Acknowledgements	20
Attachment	21

## Abstract

In 1967, the Panel on Wind and Seismic Effects, UJNR, was founded with the aim of technical cooperation between the U.S. and Japan in regard to technology for the mitigation of natural disasters such as extreme wind, earthquake, storm surge and tsunami. Since the 1st Joint Panel Meeting held in Tokyo in 1968, the Panel has been expanding and broadening its activity yearly, establishing ten task committees, exchanging personnel and technical information, conducting U.S.-Japan cooperative research and holding workshops.

This paper was prepared by the Japan Panel, commemorating the 20th Joint Panel Meeting to be held in Washington, D.C. in May, 1988, and sets forth the

progress and accomplishments of the Panel in the last two decades as well as its future prospects.

## 1. Introduction

On the occasion of the 1st Plenary Meeting of the 3rd U.S.-Japan Trade and Economy Joint Committee held in Tokyo on January 27, 1964, the U.S. side proposed the establishment of the U.S.-Japan Conference on Development and Utilization of Natural Resources (UJNR); the UJNR would not belong to either the U.S.-Japan Science Committee nor U.S.-Japan Trade and Economy Joint Committee, and subsequently, it was founded in the same year.

The aims of the proposal were: "The governments of the U.S. and Japan start the exchange of personnel and information in the field of technology for the benefit of both countries. Also, it is suggested to have a meeting of governmental officers from both countries as early as possible." Understanding the aims of the proposal, the Science and Technology Agency took the initiative in the activity on the Japan side.

The Panel on Wind and Seismic Effects is one of the 17 UJNR Panels. The Panel was established as a new cooperative activity on the occasion of the 3rd UJNR Plenary Meeting held in Tokyo in 1967. Principal objectives of this cooperative program are to give opportunities for the exchange of opinions, presenting the results of research on wind and seismic effects on structures, in view of the fact that both the U.S. and Japan are prone to suffer from natural disasters.

The Panel's area of activity has expanded yearly. The Panel aims at exchanging results of research related to the revision of design criteria and developing comprehensive measures and technical fields to mitigate loss of lives and properties from natural disasters such as extreme wind, earthquake, storm surge and tsunami.

The Panel has been established jointly in each country. The Japan Panel consists of 29 members from 6 organizations and is chaired by the Director-General of Public Works Research Institute, MOC. U.S. Panel is chaired by the Director of Center for Building Technology, NEL, NBS, and includes 35 members from 8 organizations.

Ten task committees were also organized to promote effectively the Panel program by exchanging technical information through the Joint Meeting of the Panel and workshops held on the relevant subjects.

\* Chairman, Japan Panel on Wind and Seismic Effects, UJNR (Director-General, Public Works Research Institute, Ministry of Construction, Japan)

It was proposed to submit special papers at the 20th Joint Panel Meeting to be held in Washington D.C. in May, 1988, commemorating the Panel activities in the last two decades. Thus, this paper was prepared by the Japan Panel, that is, drafted by the Task Committee Chairmen and Secretaries then finalized based on suggestions by the Panel members. The paper sets forth the accomplishments of the Panel and task committees during the last two decades along with future prospects.

## 2. Two Decades of Accomplishments and Future Challenges of the Panel on Wind and Seismic Effects, UJNR

### 2.1 Progress of the Panel

(1) Since the 1st Joint Panel Meeting held in Tokyo in 1969, Joint Panel Meetings have been held alternately in Japan and U.S. every year.

(2) On the occasion of the 10th Joint Panel Meeting in 1978, the Panel's field of activity was broadened to include topics on storm surge and tsunami and new members joined the Panel. Since that time, the activity in this field has been continued.

(3) The importance of research on earthquake prediction has been emphasized in the Panel. In 1978, it was decided to establish a new panel, the Panel on Earthquake Prediction, UJNR.

(4) Six Task Committees from A to F, such as Strong Motion Instrumentation Arrays and Data Program, Large Testing Program, were established in the Panel in 1975. Making an addition later, ten task committees continue their activities at present.

(5) Both the U.S. and Japan have exchanged a great amount of research data and literature, including data of earthquake strong motion.

(6) In 1977, the exchange of researchers and U.S.—Japan cooperative research were initiated. Several workshops have been held in which Panel members and researchers participated from U.S. and Japan as well as coordinating meetings for cooperative research program.

(7) The following five U.S.—Japan Cooperative Research Programs have been conducted:

- a. Research of Reinforced Concrete Structures (1979-1987)
- b. Research of Steel Structures (1982-continued)
- c. Research of Lifeline Facilities (1982-continued)
- d. Research of In-Situ Testing Methods for Liquefaction (1983-continued)
- e. Research of Masonry Structures (1984-continued)

The cooperative research program has facilitated exchange of researchers, including young researchers and design engineers, and technical information between both countries. The programs also have contributed to the advancement of earthquake engineering in the future.

(8) In 1979, Public Works Research Institute, Building Research Institute, Geographical Survey Institute and Meteorological Research Institute moved to Tsukuba Science City. On this occasion, modern and large-scale experimental facilities were equipped so that new experimental studies could be initiated. These facilities

have been utilized for U.S.—Japan Cooperative Research Programs.

(9) In 1987, a Charter was formulated to clarify the aims of the Panel activity.

### 2.2 Accomplishments of the Panel

(1) Up to now, over 1000 research papers and reports have been presented in the Joint Panel Meetings from the U.S. side and Japan side. Proceedings of the Joint Meetings were printed, distributed, and utilized to develop wind and earthquake engineering in both countries.

(2) More than 200 U.S. and Japanese researchers have been exchanged to join cooperative research programs, earthquake survey and other activities in the counterpart country.

(3) Under the auspices of the Panel, 16 workshops have been held. Researchers and engineers participated in the workshops to present and discuss their papers. Proceedings which contain the results of workshops were printed, distributed widely and utilized.

(4) Since strong motion records are precious data for research on earthquake engineering, the strong motion record exchange system was built between U.S. and Japan. That is, a strong motion records catalog is exchanged periodically, and wave records and digitized records of strong motion are distributed to the related agencies after publication.

Furthermore, records of strong wind and tsunami and data base have been exchanged as well to be utilized for developing relevant research.

(5) In regard to cooperation with developing countries, information was exchanged. Especially, the U.S. and Japanese investigation of damages due to Mexico Earthquake and Chile Earthquake and support of aid were reported at the Joint Panel Meetings.

### 2.3 U.S.—Japan Cooperative Research Program

#### (1) Research of Reinforced Concrete Structures

1. It was confirmed that the ultimate resistance and deformation characteristics of reinforced concrete building with shear walls through the conducting of full-scale 7-story building test. The base shear coefficient of test building which is nearly equal 0.24 by the usual calculation, was ascend to 0.36 by the joint effort of slabs.

The maximum angle of rotation was 1/64, at which point the test building showed ductile behavior since the shear walls the major lateral load resisting component, was damaged in a flexural mode.

2. It was made clear that the building behavior during earthquake by the development of Pseudo Dynamic Testing Method.

3. Since the study intended to achieve an economical design, the section were considerably less reinforced than those conforming with US and Japanese practices. In accordance with the US practice, we used the anchorage method of beam reinforcing to column and heavily shear reinforcing at the beam end. This result was given the good basic information for the revision of design guideline of reinforced concrete structures at Architectural Institute of Japan.

4. A series of pseudo dynamic test made much structural damage to the test building. Then the repair works and the installation of nonstructural elements were done in order to inspect the effect of repair works and relationship between the structural damage grade and the obstacles of nonstructural elements. The overall behavior of the structure after repair was in general similar to that of the before-repair structure. Therefore, we have the starting point of the research of "the development of seismic repair techniques".

5. The actual behaviour of the nonstructural elements in the full scale building was obtained by the pseudo dynamic test. The test results gave the precious materials for better aseismicity of non structural elements in future.

## (2) Research of Steel Frame Structures

1. A seismic test of actual full-scale 6-story steel frame building was conducted. This test is the first occasion of this field in the world. It was able to the more economical design by the provision of dynamic behavior during the earthquake of full size building with braced frame and moment resistance frame. Namely, it was confirmed by the test to the effect of moment resistance of braced frame.

2. It was confirmed that the concentration characteristics of damages to each floor of multi story building by the application of the pseudo dynamic testing method.

3. It was confirmed that the behavior of the joint effect between the steel beam and composite reinforced concrete slab, especially, the effective width and the stress flow in the concrete slab.

## (3) Research of In-Situ Testing Methods for Liquefaction

In-situ test for assessing the soil liquefaction must give the universal soil parameter whenever or wherever in the world it is conducted. However, it was noticed that there was some discrepancy in the standard penetration testing (SPT) method in both countries, which is widely used to investigate the soil liquefaction potential. Also, it should be clarified whether the blow counts (N) of SPT obtained by methods in both countries can be universal for the same soil condition or not.

In order to clarify this point, joint investigation by both sides was conducted to acquire the SPT data at the sites where the liquefaction apparently took place during past earthquakes. And the N values which were obtained by the popular manners both in U.S. and Japan were compared.

It was concluded by this cooperative research on the aquired field data that, although there was some difference between the energy ratio obtained by the Japanese practice and the U.S. practice, blow count by the Japanese practice is nearly equal to that by the U.S. practice when normalized for the same energy level.

## (4) Research of Lifeline Facilities

From a mutual understanding between the U.S. and Japan on extensive seismic damage of lifeline facilities in urban areas, resulting in significant losses of

lives and property, the U.S.-Japan Cooperative Research of Lifeline Facilities was initiated in 1982 for the purpose of studying seismic response, along with strength and deformation characteristics of lifeline facilities.

Since dynamic behavior of the lifeline facilities significantly depends on the type of facilities, cooperative study was proposed to be made of 1) reinforced concrete column structures, 2) embedded pipes, and 3) semiburied structures. Cooperative research has been made of reinforced concrete column structures from 1982 to 1987 between NBS and PWRI, and it is now being undertaken of embedded pipes from 1988 between Columbia University, Cornell University, Old Dominion University and NCEER of U.S. side and PWRI.

In the cooperative research of reinforced concrete structures, scale effects were studied by the U.S. side under static load reversals using large scale specimens with cross sections as large as 2m and medium size specimens. The effects of loading velocity and loading hysteresis were studied on the Japan side using high-velocity dynamic loading facilities. The results of both investigations have been compiled in the form of technical reports on the effect of scale by the U.S. side and on the effects of loading velocity, number of load reversals, loading time history, two directional loading and oblique loading by the Japan side. The exchange of technical findings and information has been performed at the Joint Meeting and the Bridge Workshop.

In the cooperative research for embedded pipes, cooperation has been initiated from strong motion observation for measuring seismic response of embedded pipes during earthquakes. Observations were undertaken at the site where the pipe crosses a fault in the U.S. and at the site with variation of ground conditions in Japan. The exchange of technical information on embedded pipes is to be promoted.

## (5) Research of Masonry Structures

The joint research program for masonry structures is active in progress in both countries. The developments of the large size block unit and the reinforcing method between the block units were successfully carried out already for the actualization of high rise masonry buildings.

### 2.4 Future Challenges of the Panel

(1) As the exchange of personnel and the exchange of technical information are the fundamental activities of the Panel, continuing the exchanges is considered essential.

(2) Under the auspices of the Panel, workshops have been held and joint researches have been conducted. These programs have contributed to the promotion of research relevant to the field of task committee activities. In order to achieve the objectives effectively, task committees are encouraged to clarify their research needs and to develop future research programs.

(3) To perform smooth and effective activities, the task committees should make efforts to achieve better communication and liaison among themselves with necessary coordination of activity programs.

(4) The proceedings of the Joint Meetings and other materials published by the Panel have been distributed to related organizations not only in Japan and the U.S. but also in other countries. The cooperative researches and workshops have been also coordinated with other organizations' activities. As the Panel has recognized the importance of these connections with other organizations, attention should be paid to coordinating the activity of the Panel and overseeing the activity of the related organizations.

(5) With urbanization and advancement of socio-economic activity in recent years, the effects of strong wind on structures and environments are increasing their importance. Accordingly, the research on wind characteristics and wind engineering including wind-resistant design, wind environment and so on should be strengthened.

(6) Since cooperative research programs facilitate excellent results, cooperative research programs should be promoted actively in the future as well. To facilitate this goal, the Panel will continue to encourage them and provide sponsorship.

(7) The International Decade for Natural Disaster Reduction (IDNDR) is considered to be closely related to the activities of the Panel. Attention should be paid to the IDNDR program so that the Panel will be able to contribute a great deal in connection with the IDNDR program.

(8) Cooperation with developing countries is an important subject which has been pointed out at the Joint Meetings. Recognizing that there are many developing countries which suffer from natural disasters, efforts are needed to conduct the research in order to provide technical information relevant to criteria for design of structures and disaster mitigation programs.

(9) To promote essential Panel activity, the selection of research subjects to work on and the development of a research program is important. Tentatively designated subjects for urgent progress are as follows:

- a. Foundation of data bank.
- b. Benchmark structure.
- c. Precise observation of response caused by strong wind and earthquake.
- d. Base isolation.
- e. Measures against liquefaction.
- f. Comparison of design criteria and test methods.

### 3. Two Decades of Accomplishments and Future Challenges in Each Task Committee

#### 3.1 Strong-Motion Instrument Arrays and Data

##### (1) Activities to Date

It was approved at the time of the 7th Joint Panel Meeting in 1975 to establish the Task Committee on Strong-Motion Instrument Arrays and Data. The program of the task committee's activities contained the following six items:

1) After an earthquake which has caused damage to structures or an earthquake during which maximum acceleration exceeding about 0.1g has been recorded, the task committee of the country where the earthquake has taken place will provide a list of the strong-motion

earthquake records for the counterpart of the task committee.

2) Every year the task committee will exchange catalogs of the strong-motion earthquake records during the previous year.

3) The Task Committee will make appropriate arrangements to provide digitizable copies of records when they are requested.

4) The Task Committees will exchange the lists of reports on strong-motion earthquake records published by the organizations participating in the Panel.

5) The Task Committees will exchange the lists of publications on strong-motion earthquake records published in both countries.

6) The Task Committees will exchange listings of the digitized strong-motion records. Exchange of the digitized records in different media other than the listing such as cards, magnetic tape, etc. will be considered.

Since then, the program has been examined on the occasions of every Joint Panel Meeting, and modifications of existing items and additions of new items were made depending on continuing development. In May 1978, the International Workshop on Strong Motion Instrument Array was held in Honolulu, Hawaii; the workshop adopted a resolution to promote array observation of strong ground motions under international cooperation. In response to this resolution, the Task Committee added the promotion of the array observation and exchange of related information to the program of activities. The original program which consisted of exchanges of strong-motion records and information on strong-motion earthquake observation was expanded to cover the observation and the analysis of strong-motion records with emphasis on earthquake hazard reduction and promotion of cooperative researches in those fields. On the other hand, item 5) which referred to the exchange of lists of publications on the strong-motion earthquake observation published in both countries was deleted after a few years of practice since the exchange of the publications by the organizations participating in the Panel seemed to be sufficient and the preparation of the list was too heavy a duty for the Task Committees.

The program for activities for 1987 consisted of 12 items. Ten items out of 12 are activities which should be performed regularly and two are non-regular activities such as holding a workshop. The following are summarized items which were added to the original program:

7) Exchange of technical information on the observation networks and the instruments.

8) Cooperation of international activities on observation of strong-motions in other seismically active areas and on recording strong ground motions close to the source of a large magnitude shock.

9) Exchange of staff and the instruments to record aftershocks after a large magnitude earthquake.

10) Collaborative studies involving strong-motion instrumentation and interpretation of resulting strong-motion data sets for purposes of earthquake hazard reduction.

In the following sections, some of the activities including non-regular ones will be described briefly.

## (2) Exchange of Catalog of Strong Motion Records

The "Strong-Motion Program Report" from the U.S. side and "Strong-Motion Earthquake Records in Japan" from the Japanese side are being distributed to the respective counterpart, regularly. For timely transferring of information on the strong-motion records from a large earthquake, the open file reports of U.S. Geological Survey (USGS), from the U.S. side, and the Prompt Report on Strong-Motion Earthquake Records, from the Japanese side, are distributed to the respective counterpart. The English explanation in the Prompt Report was included especially for the exchange program of the Task Committee A. In such a way, the members of both U.S. and Japan Task Committees are obtaining the information on the strong motion records from large earthquakes in both countries quickly and smoothly through the task committee.

## (3) Exchange of Strong-Motion Records

Publications including the reproduction of strong-motion records and digitized records have been distributed to the member organizations of the Task Committee as soon as they became available.

At present, magnetic tape is commonly used to distribute data for computer input. At the time when the Task Committee was established, computer cards were the principal media to distribute data for computer input. Magnetic tape was also used for distribution of data at that time; however, difficulties were often encountered due to the insufficient compatibility among the computer systems. Taking such circumstances into consideration for exchange of the records, publications and numerical outputs from the computer printer were selected as the major media. In parallel with them, it was decided to study more efficient media for the exchange of strong-motion records. As a result, the magnetic tape on which the records from the Imperial Valley earthquake of October 15, 1979 was forwarded to the Japanese side, and the tapes reproduced by the Port and Harbour Research Institute (PHRI) were distributed to the Japanese member organizations. Furthermore, the tape of the strong-motion records of the Middle Japan Sea earthquake recorded by the network of PHRI was forwarded to the U.S. side. These exchanges of the strong-motion records with magnetic tapes proved the compatibility of computer tapes among the computer systems of the member organizations of both sides. The exchanges also worked as a part of the actual exchange of the records. After this study, the item on the efficient media for data exchange was deleted. Since then, the exchange of records has been made with magnetic tape when necessary. As described here, the Task Committee has greatly advanced the exchange of strong-motion records.

## (4) Workshop on Strong-Motion Earthquake Observation

The Task Committee held the Workshop on Strong-Motion Earthquake Observation at USGS in Menlo Park, San Francisco, U.S.A., for five days from August 2, until August 6, 1987. The workshop program consisted of technical presentations and discussions on the strong-

motion networks, the strong-motion instruments, the processing of strong-motion records, experiment of digitization of strong-motion records and technical visits. In total, 12 researchers and engineers from U.S. and Japanese sides participated in the workshop. The technical presentations and discussions were made on 21 topics. As the experiments, typical U.S. and Japanese strong-motion records were digitized with the digitizer which USGS had been using for its routine job, and views were exchanged among the participants. This workshop was organized so as to avoid duplication of the topics with the Workshop on Processing of Seismic Strong Motion Records organized by IUGG and held in Vancouver, Canada on August 8, 1987. Therefore, it was possible for the participants in both workshops to exchange information and discuss wide areas of strong-motion earthquake observation. And in fact, many who attended the UJNR Workshop participated in both workshops.

## (5) Mutual Acceptance of Team for Aftershock Observation

It is very significant to observe aftershocks immediately after a large main shock in or near the source region. However, success of the observation highly depends upon how quickly such observation can be started. The Task Committee decided to study necessary arrangements for accepting the observation team from the counterpart country and scheme of cooperative research. The procedure for quick customs clearance and the necessary supports for visiting observation team were studied.

## (6) Study on Policy for Opening Strong-Motion Records to Large Users Community

The strong-motion record has a very large potential for various types of use. As a result, many engineers and researchers desire to utilize strong-motion records, and the operators of strong-motion records, and the operators of strong-motion network are requested to fulfill such desire. On the other hand, many strong-motion networks in the world are operated by researchers. Such researchers produce their own research reports with the strong-motion records which they recover. The records are, in some aspects, their original data for research and the unconditional opening of the records to a large users community may cause some difficulties for the researchers to do their research. Therefore, for opening the strong-motion records, a rule has to be established which balances requirements from the network operators and the users community. The Task Committee has been continuing its effort to draft an appropriate policy for opening the strong-motion records to the large users community.

## (7) Prospect for Future Program

Significant achievement has been made in information exchange on the strong-motion network and the recovered records, and in the exchange of strong-motion records. The activities in these fields should be continued and strengthened. Information exchange and discussion on new strong-motion instruments and processing

systems for strong-motion records are essential for development. Therefore, workshops should be held at an appropriate time interval and information exchange and advancement of the technology at both sides should be promoted.

The areas to be expanded and strengthened are the U.S. and Japanese Task Committees' cooperative effort to contribute to international activities on the strong-motion earthquake observation and the development of advanced technology to utilize the strong-motion records with emphasis on mitigation of seismic disaster. For the latter area, one possible approach is to establish a joint research program.

(H. Tsuchida)

### 3.2 Large-Scale Testing Program

#### (1) Background

Following the 1968 Tokachi-oki earthquake in Japan, during which numerous reinforced concrete school buildings of modern design suffered heavy damage, it was apparent that every effort should be made to improve new designs through (1) learning as much as possible from the experience of the Tokachi-oki earthquake, (2) reviewing and considering possible changes in building codes, (3) improving design and construction practices, and (4) initiating programs of needed research. Responding to this need, a first joint seminar, Sendai, 1970 was held for the purpose of (1) reviewing the causes of damage sustained by modern school buildings, (2) examining design and construction methods, and (3) identifying and defining needed programs of research which could be conducted more effectively on a cooperative basis.

A second seminar, in Berkeley, California, 1973, was held for purposes of reviewing (1) the causes of damage sustained by reinforced concrete structures during the 1971 San Fernando earthquake, (2) current research on earthquake resistant design, (3) the safety of existing structures and means of upgrading their resistance, and (4) post-earthquake damage repair. Prompted by informal discussions held at Sendai, a U.S.—Japan Cooperative Research Program on Earthquake Engineering with Emphasis on the Safety of School Buildings was established under the U.S.—Japan Cooperative Science Program for the period May, 1973 — October, 1975.

A review meeting of the cooperative research program emphasizing the safety of school buildings was held in Hawaii in 1975. With this experience in mind, a set of RECOMMENDATIONS FOR U.S.—JAPAN COOPERATION IN THE FIELD OF EARTHQUAKE ENGINEERING was drafted and signed by all official participants. Recommendations Nos. 2 and 3 read as follows:

RECOMMENDATION NO. 2 Establish a Cooperative Research Program in Earthquake Engineering with Emphasis on Large-Scale Testing of Structural Systems under the sponsorship of the U.S.—Japan Panel on Wind and Seismic Effects, U.J.N.R. Program. (The rest is omitted)

RECOMMENDATION NO. 3 Establish a Task Committee under the U.S.—Japan Panel on Wind and Seismic Effects, U.J.N.R. Program. The assignment

given to this Task Committee should be to make detailed plans and recommendations for implementing Recommendation No. 2 which will ensure an effective research program of maximum benefit to both countries within constraints of the sponsoring government agencies. (The rest is omitted)

#### (2) Activities of the Panel

Parallel with the above described cooperative activities of university researchers, government delegates on the Panel undertook positive steps toward strengthening such cooperative efforts. At the conclusion of its sixth Joint Meeting held in Washington, D.C., in 1974, the Panel adopted the following resolution:

3. that increased effort should be made in the near future to encourage joint research programs, especially in the area of mutual utilization of research facilities and the exchange of researchers.

At the seventh Joint Meeting, Tokyo, 1975, the justification of cooperative large-scale testing program was stated in a paper "Earthquake Disaster Mitigation: A Joint Research Approach" presented by C.C. Thiel and J.B. Scalzi as follows:

#### 2. Large Scale Destructive Testing of Structures

A plan to obtain the required data could be formulated by a joint U.S.—Japan program consisting of: (a) large scale testing of existing structures of various types of materials and construction, (b) pseudo-dynamic tests on full size specimens or structures constructed to obtain specific data, (c) shake table verifications were required for the pseudo-dynamic tests or for specimens which may be considered full size.

At the tenth Joint Meeting, Washington, D.C., 1978, the Panel again indicated its strong support of the program by adopting the following resolutions:

3. The Panel on Wind and Seismic Effects recognizes the importance of the U.S.—Japan Cooperative Program on Large Scale Testing and it urges early implementation of the program under the auspices of this Panel.

#### (3) Activities of the Planning Group.

In January, 1976, J.B. Scalzi of the NSF encouraged J. Penzien of the UCB to submit a specific proposal to NSF to implement RECOMMENDATION NO. 3. Promoted by this encouragement and the past recommendations for cooperative research, a proposal entitled "Planning a Cooperative Research Program in Earthquake Engineering with Emphasis on Large-Scale Testing of Structural Systems" was submitted to the Research Applied to National Needs (RANN) Directorate of NSF by the UCB. This proposal called for the planning effort to be conducted under the auspices of the U.S.—Japan Panel on Wind and Seismic Effects. NSF responded favorably to this proposal by issuing a grant with J. Penzien serving as Principal Faculty Investigator. The planning group consisted of university researchers and delegates of the Task Committee (B) of this Panel.

The first planning group meeting, U.S.—Japan Cooperative Research Program Utilizing Large-Scale Testing

Facilities, was held in Tokyo in September, 1977, to discuss future research programs in earthquake engineering utilizing large-scale testing facilities. At the conclusion of the meeting, eleven resolutions were adopted.

The second planning group meeting was held in San Francisco in May, 1978, to continue planning for future research programs in earthquake engineering utilizing large-scale testing facilities. At the conclusion of the meeting, ten resolutions were adopted.

The third planning group meeting was held in Tokyo in December, 1978. The meeting continued discussions to develop future research programs. At the conclusion of the meeting, nine resolutions were adopted.

The fourth planning group meeting was held in Berkeley in July, 1979, to finalize recommendations for a cooperative research program.

Some of the resolutions which were adopted at the meetings are shown as follows;

① The goal of the joint program is to improve seismic safety practices through studies to determine the relationship among full-scale tests, small-scale tests and analytical studies.

② This program should be initiated in 1979 jointly and cooperatively in both the U.S. and Japan.

③ Immediate plans for conducting full-scale pseudo-dynamic tests on a cooperative basis should be developed in accordance with the following priority listing of building types: No. 1 – Reinforced Concrete, No. 2 – Structural Steel, No. 3 – Prestressed/Precast Concrete, No. 4 – Mixed Steel/Reinforced Concrete, No. 5 – Masonry and No. 6 – Timber.

④ To insure successful execution of the recommended cooperative research program, full coordination of all research activities carried out in both countries is essential, therefore, the following committees are recommended;

(a) Joint Technical Coordination Committee to provide scientific and technical advice to participating institutions in the program. This committee should meet at least once a year during the program.

(b) Joint subcommittee to provide advice on the execution of research related to reinforced concrete buildings, steel buildings, pseudo-dynamic loading techniques and other major areas of activity. These committees should meet as frequently as needed.

⑤ Concerned government agencies in both countries are urged to complete arrangements for implementing the preceding resolutions. It is recommended that the U.S.–Japan Cooperative Science Program and the U.S.–Japan Panel on Wind and Seismic Effects, U.J.N.R. Program, coordinate their effort towards implementing the large-scale testing program.

(4) U.S.–Japan Joint Earthquake Research Program Utilizing Large-Scale Testing

#### 1) Research Program of Reinforced Concrete Structures

According to the recommendation and resolution of the Planning Group Meeting, the Science and Technology Agency and the Ministry of Construction for Japan and the National Science Foundation for the U.S. signed the "Implementing Arrangement of the U.S.–Japan

Joint Earthquake Engineering Research Program Utilizing Large-Scale Testing Facilities" on August 10, 1979. The Co-Chairmen of both sides of the UJNR Panel on Wind and Seismic Effects received a request for endorsement of the Joint Research Program in a letter signed jointly by the Parties (STA, MOC and NSF).

The Task Committee reviewed the program and its components, and recommended the endorsement of the program to the Panel Co-Chairmen. The Panel Co-Chairmen endorsed the program to STA, MOC and NSF in July, 1980.

The testing of a seven-story reinforced concrete structure was started on March, 1981, at the Building Research Institute. Support tests to be carried out in Japan were initiated in 1980 and completed in 1982. Support tests in U.S.A. were initiated in 1981 and completed in 1983.

The Joint Technical Coordination Committee met in Japan in July, 1982, for discussion of experimental data as well as exchanging of data.

All of the experimental and analytical studies have been completed in 1984. The results have been published in "Special Publication 1984" by the American Concrete Institute.

#### 2) Research Program of Steel Structures

The Ministry of Construction and National Science Foundation signed the Implementing Arrangement on May 18, 1981 and the Panel Co-Chairmen endorsed the program to MOC and NSF on May 22, 1981.

The Joint Technical Coordinating Committee met in Japan in July, 1982, under the auspices of UJNR for discussion of the research program (full-scale test in Japan and support tests in the U.S. and Japan). The JTCC met in Japan in June, 1983, and February, 1984. Research on steel structures were discussed.

Testing of the Full-scale steel structure was started in 1983. Testing full-scale steel structure and support tests were completed in 1986 in both countries.

The meeting of JTCC on Steel Structure Research was held in Tokyo in July, 1987, to summarize the Joint Research Project on steel structures.

#### 3) Research Program of Masonry Structures

The Workshop on Masonry Structures was held at BRI in March, 1984, for assessing the need for a priority coordination research program including component and large-scale tests of masonry structures. The Joint Planning Committee on Masonry Structures met in the U.S. in July, 1984, for discussion of research on the coordinated masonry structures.

MOC and NSF signed the Implementing Arrangement in December, 1984, and the Panel Co-Chairmen endorsed the Implementing Arrangement to MOC and NSF during the 17th Joint Meeting in Tsukuba.

The meetings of the Joint Technical Coordinating Committee of Masonry Structures were held in Tokyo in August, 1985, in Colorado in September, 1986 and in Hokkaido in November, 1987.

Testing of a full-scale five-story masonry building was began in November, 1987. The joint research program is active in progress in both countries.

### (5) Future Program

The Task Committee will facilitate continued deliberation of following topics between appropriate U.S. and Japan organizations and report its findings and recommendations to the Panel.

- a. Seismic performance of precast concrete construction.
- b. Seismic performance of composite and mixed constructions.
- c. Application of high strength construction materials, such as concrete and steel, to structures in high seismic zones.
- d. Application of base isolation and controlled damping systems to critical structures located in high seismic and wind zones.

The Task Committee will encourage the exchange of information on large-scale testing facilities and large-scale testing programs in both countries.

(K. Ohtani)

### 3.3 Repair and Retrofit of Existing Structures

#### (1) Particulars of the Task Committee

It was decided at the 7th Joint Meeting in 1975 that the Repair and Retrofit Task Committee (C) should be founded; previously existing were five other Task Committees, (A), (B), (D), (E) and (F). In accordance with this decision the 1st Task Committee met at the time of the 8th Joint Meeting; the Task Committee has since met along with each joint meeting, numbering through the twelfth in 1987.

At the Task Committee Meeting during the 11th Joint Meeting (1979) it was decided that U.S.—Japan seminars in relation to the Task Committee should be held. Thus, starting in 1980 the seminar was held each year for three consecutive years; in 1987 the 4th U.S.—Japan Seminar was held, after a five year interruption.

Results of the Task Committee (C) were evaluated at the four seminars along with the exchange of information; e.g., related standards and state-of-art reports, which were done through the joint meetings and the seminars.

The following review will summarize the outlines and general outcomes of the four seminars, analyses of presented papers and exchange of information on related standards; the review will also try to offer some proposals for the Task Committee in the future.

#### (2) General Aspects of the Four U.S.—Japan Seminars

Of the above mentioned four seminars, the first and the third were held in the U.S.A, and the remaining two were held in Japan. With each seminar in both countries, observation tours were done of actual construction sites concerning repair and retrofit, contributing greatly the understanding of actual construction fields. On the other hand when seminars are held in Country A, for instance, participants from Country B are very few (and vice versa); and except for the 4th Seminar, the durations of the seminars were only 1 – 1.5 days, a time too short for adequate discussions.

Reports on repair and retrofit presented at the seminars and joint meetings (Nos. 1–19) amount to 81 and 20, respectively. Because the number of papers presented at the joint meetings is limited, the seminars are very important in terms of exchanges of information in the field of repair and retrofit. As for the papers presented at the seminars, Prof. R.D. Hanson prepared the proceedings of Seminars 1, 2 and 3 through the NSF Research Fund and distributed them to the participants; Dr. Hirose did the same for Seminar 4 through the cooperation of BRI. Many copies were especially printed of the proceedings of Seminars 1–3 and have been distributed to researchers in countries other than the U.S. and Japan.

In addition, many of representative important standards in the related field from both the U.S. and Japan were introduced at each seminar. Notably, standards regarding seismic evaluations, as well as repair and retrofit of existing structures and damaged structures, have been established in Japan, particularly in the field of building structures; these standards have been summarized and reported at the seminars.

#### (3) Exchange of Information and Materials in the Task Committee

As mentioned above, the exchange of information has been quite useful for each country as related to the Task Committee and the U.S.—Japan Seminars were held four times. However, it is not always possible to hold this type of seminar every year, due to the limited allowances for business trips abroad and to the scarce accumulation of research papers and materials in the respective countries.

The Task Committee meeting every year together with the joint meetings has supplemented the functions of the seminar and served as its guide. One of the main roles that the Task Committees has played is the introduction of related papers in both countries and the sharing of parts of them.

There have been no other plans or executions of related joint research, etc., except for the holding of the seminars.

#### (4) Contents of Presented Papers and Analyses

The following (1 – 7) highlights the contents of the principal papers on repair and retrofit of structures which were presented at each joint meeting, along with all the papers presented at the four U.S.—Japan Seminars:

1) In general, papers on building structures are much more numerous than those on civil structure; this is true for both Japan and the U.S. One reason may be that on civil structures there are other task committee; e.g., (F) Lifeline Systems and (J) Transportation Systems, both also having seminars.

2) Except in cases of building structures in Japan, there have been more papers on existing structures than on damaged structures; there are still quite a few fields yet to be studied among those related to the present Task Committee.

3) If we compare methods of seismic evaluation with methods of repair and retrofit, there have been more papers on the latter.

4) Japan has presented more papers than the U.S. Of the Japanese papers, many concern technical guidelines. On the other hand, U.S. papers concentrate more on methodology and philosophies. This difference seems to be due to frequent Japanese projects of technical development and issues of technical guidelines on the national scale.

5) American papers mainly concern seismic retrofit of existing structures—both in civil structures and building structures. The contents are chiefly methodology; experiments, and examples of actual practice.

6) Japanese papers on civil structures are not many in number, but the subjects cover both existing and damaged structures, and the conditions of the subjects range from their evaluation to repair and retrofit. However, the structures studied are limited, with one exception, to bridges, including highway bridges.

7) Japanese papers on building structures cover many fields of repair and retrofit. Particularly, a number of papers have been presented on damaged structures and technical guidelines.

As can be seen from the above, in terms of the numbers and contents of presented papers, there are obvious differences between the U.S. and Japan, civil and building structures, which shows that we still have a good number of research topics yet to be investigated in the future.

#### (5) The Task Committee in the Future

Regarding the future of the working session, as judged from the various above-mentioned reference materials, the following is pointed out:

1) The technology of evaluation, and repair and retrofit of existing and damaged structures is still developing worldwide; in order to develop this technology efficiently, it is necessary for both the U.S. and Japan—both relatively advanced—to technically cooperate, exchanging information and technical reference materials. The outcomes of the cooperation will serve to mitigate seismic damage in the world.

2) For the purpose specified in 1) above, this task committee should continuously meet along with the Joint Meeting; moreover, for advancing the close cooperation mentioned below, it is necessary to hold U.S.—Japan technical seminars at proper intervals.

3) There is much in common between the basic ideas of Japan and those of the U.S. as regards methods of evaluation of existing and damaged structures, and their structural members (or parts), and their repair and retrofit (details and evaluation of the methods); but at present there are evident differences in details.

4) In order to resolve the condition specified in 3), it is useful and necessary for the U.S. and Japan to cooperate in the following work (a. and b); for that purpose, we need to make enough preparation beforehand and hold U.S.—Japan seminars of sufficient duration.

a. The U.S. and Japan work together at making comparisons between the technological guidelines of the respective countries on the subject of similar structures, using an example of clear benchmark structures.

b. In order to set up effective structural systems of repair and retrofit and their evaluation methods, the

U.S. and Japan should use examples of several typical structural systems, comparing and investigating them through experimental “back data” of the respective countries.

5) As a prerequisite to the above, it is necessary that both the U.S. and Japan properly rearrange and exchange typical technical guidelines and reference materials as their “back data.”

#### [References]

1) Proceedings of the First Seminar on Repair and Retrofit of Structure, Dept. of Civil Engi. The Univ. of Michigan, Ann Arbor, Michigan, May 1980.

2) Proceedings of the Second Seminar on Repair and Retrofit of Structure, Dept. of Civil Engi. The Univ. of Michigan, Ann Arbor, Michigan, May 1981.

3) Proceedings of the Third Seminar on Repair and Retrofit of Structure, Dept. of Civil Engi. The Univ. of Michigan, Ann Arbor, Michigan, May 1982.

4) Proceedings of the Seminar on Repair and Retrofit of Structure, Workshop on Repair and Retrofit of Existing Structures, U.S.—Japan Panel on Wind and Seismic Effect, UJNR Tsukuba, Ibaraki, Japan, May 1987.

(M. Hiroswa)

### 3.4 Evaluation of Performance of Structures

#### (1) Introduction

Structures designed based on modern seismic regulation, especially, reinforced concrete structures suffered severe damages by 1968 Tokachioki earthquake and 1971 San Fernando earthquake. These experiences accelerated the activities to revise earthquake design regulations and to develop evaluation methods of performance of structures against earthquake. A national technology development program on the establishment of a new seismic design code and regulations started in 1972 in Japan. A draft of evaluation standards of existing reinforced concrete buildings against earthquake was proposed from the Building Research Institute in 1977 and the evaluation standards of the seismic capacity of existing reinforced concrete buildings was published under the supervision of the Ministry of Construction.

The Task Committee D, Evaluation of the Performance of Structures, was initiated at the 8th U.S.—Japan Panel on Wind and Seismic Effect in 1976.

The Scope of the activities of the Task Committee has been established as follows:

1) Evaluation of Existing Structures  
2) Stochastic Risk Analysis and Probabilistic Hazard Determination.

3) Corroboration of Large-Scale Testing Program by Analytical Studies.

4) Nonstructural and Structural Component Interaction.

5) Post-Earthquake and Post-Storm Evaluation of Performance of Structures.

6) To compile data and bibliography on the results of analysis, repair and retrofit of existing buildings.

7) Benchmark Structures. A methodology should be developed to establish “benchmark” structures to which a proposed code and standards could be compared.

These structures should be tested and analyzed to determine their actual resistance to high wind and earthquake.

Active exchange of information on the above mentioned items has been made through joint meetings and task committee meetings. Through these activities, the need is for a better understanding of current safety evaluation methodologies and joint works of comparative studies between the U.S. and Japan methodologies by their application to existing buildings. In response to this need, three U.S.—Japan workshops have been conducted on the evaluation of the performance of existing buildings for resistance to earthquakes. The workshops, which were held in 1983, 1984, and 1985, were organized through Task Committee D.

- (2) U.S.—Japan Workshop on the evaluation of the performance of existing buildings for resistance to earthquakes.

The first workshop was held at the Building Research Institute in Tsukuba, on May 13 and 14, 1983. The meeting was preceded by a field trip to Shizuoka Prefecture on May 12, where earthquake preparedness plans were discussed and strengthening measures used in the prefecture buildings were described. Thirteen representatives from Japan and twelve representatives from U.S. participated in the technical sessions and discussions.

The technical session was intended to bring both U.S. and Japan participants to a common level of understanding of the main evaluation methods currently utilized in the two countries, and to simultaneously address the three key questions confronted in assessing evaluation methodologies:

- 1) What types of structures may be evaluated by a given method?
- 2) What is the level of safety (and reliability) implied in the method and its acceptance/rejection criterion?
- 3) How much effort is needed to conduct the evaluation?

The second workshop was held at the Berkeley Marriot Inn on July 27 and 28, 1984, immediately following the 8th World Conference on Earthquake Engineering held in San Francisco. Twelve representatives from Japan and eighteen representatives from U.S. participated in the workshop with the following primary goals: 1) Discuss new development in evaluation methodologies, 2) Present and discuss evaluations of selected benchmark structures by different evaluation methods, and critically compare the results of these evaluations, and 3) Present additional papers on degree of damage and analysis results for other structures.

The third workshop was held in Tokyo on May 17, 1985, with the primary goal of further critical discussion on results of comparative analyses of selected benchmark structures. Thirteen representatives from Japan and six representatives from U.S. participated in the workshop. New evaluation methodologies for composite steel and reinforced concrete buildings, were also presented. Some comparisons between predicted and measured response of actual buildings were provided.

- (3) Summary and conclusions of three workshops
- 1) Detailed and sophisticated analytical procedures

have been developed both in the U.S. and Japan to simulate the dynamic response of building structures. When the input earthquake motion and the properties of materials used in a structure are known, and the structure is relatively simple, these sophisticated procedures enable prediction of the dynamic response of the structure. Adequate accuracy is obtained for earthquake motion well into the elasto-plastic range as indicated in the reports related to the full-scale test structure results. However, low and medium size reinforced concrete buildings tend to have not only very complicated configuration (both in plan and elevation) but also many secondary structural elements which are not considered in the design but have considerable influence on the seismic response behaviour of existing buildings as a whole, reflecting the effect of secondary structural or non-structural elements; analysis is very limited even by using these sophisticated analytical procedures with given earthquake motion. The soil-structure interaction is another difficult problem in the precise prediction of the seismic behavior of existing buildings.

2) For the application of these sophisticated analytical procedures to the seismic safety evaluation of existing buildings, input earthquake motions and their intensities must be determined. Several procedures to generate artificial earthquake motion (with appropriate spectrum characteristics), and to determine their intensity based in the probabilistic approach and on the geotechnical survey of the construction site, have been proposed for the seismic safety evaluation of especially important structures such as nuclear power plant buildings.

However, these procedures have not yet been standardized for the application of seismic safety evaluation of existing reinforced concrete buildings.

3) Rapid evaluation methods for existing buildings subjected to seismic hazard, including a screening process for a large number of buildings, have been developed both in U.S. and Japan. The U.S. spectrum capacity method and Japanese standard method for the evaluation of the seismic capacity of existing reinforced concrete buildings are typical examples. Comparative studies were given on the application of these two methods to two benchmark structures: Holiday Inn Building and R/C full scale seven story test buildings. Some interesting aspects obtained from these studies are summarized as follows:

(a) The ratio of the seismic supply index  $I_s$  to the seismic demand index  $E_t$  obtained from the second level procedure of Japanese standard method is defined as the "Dj" index. The inelastic capacity used, as calculated by U.S. spectrum capacity method, is defined as the "Du" index.

(b) These two indices, Dj and Du, give a rough idea of the amount of damage that will occur due to the postulated earthquake. For example, objective buildings will be categorized into the following four ranks according to Dj or Du value:

Rank	Range of Dj (or Du)	Amount of Damage
1	over 1.0 (under 50)	non — slight
2	2/3 — 1.0 (50 — 90)	slight — moderate

3	1/3 – 2/3 (90 – 120)	moderate – severe
4	under 1/3 (over 120)	severe – failure

(c) The Du value is very sensitive for the spectrum characteristic of earthquake motion and the assumed ultimate deformation capacity of structures.

(d) Damage rank for the full scale test building obtained from this study has good correspondence with the damage rank evaluated from the test results.

4) Methods of seismic safety evaluation of existing buildings studied in the workshops range from rapid classifications of groups of buildings to detailed dynamic analysis of individual structures.

Methods developed in Japan and in the U.S. are “tuned” to the characteristics of typical buildings in each country. Comparative analyses of benchmark structures reflect the relatively more conservative Japanese seismic design approaches.

The comparisons reveal that the various method are suitable for the expected level of evaluation accuracy for buildings with good arrangements of lateral strength elements, and that a general idea of expected damage level can be estimated.

#### (4) Future Scope

Henceforth, U.S.–Japan coordinated research activities on the evaluation of performance of existing buildings for resistance to earthquake are expected to improve the methodologies for the evaluation accuracy of performance of various kinds of structures for resistance to different natural hazards.

1) The inventory of existing buildings in each country that have been evaluated and instrumented, and then observed after any future seismic activity should be expanded.

2) Future calibration work on the evaluation procedures developed in the U.S. and Japan through application to damaged structures due to actual earthquakes, or to the results of fullscale tests, is expected to improve the accuracy of the prediction of seismic safety. Evaluation methods, however, should remain as simple as possible for screening purposes.

3) For the future calibration work, earthquake measurements should be conducted on the typical reinforced concrete structures such as rigid frame type, coupled shear wall type, or more complicated types to investigate actual earthquake response, damping characteristics, and soil-structures interaction.

4) Research on standardizing input earthquake motions for their application to the evaluation of seismic safety of structures, including procedures to generate artificial earthquake motions with appropriate spectrum characteristics and to determine their intensity based on the probabilistic approach and on the geotechnical survey of the construction site is to be encouraged.

#### [References]

1. White, R.N. and Gergely, P., “Performance of Existing Buildings: Results of Benchmark Structure Analyses Performed in U.S.–Japan Workshop”, Proceedings of the Third Conference Organized by the Engineering Mechanics Division of ASCE, March 31 – April 2, 1986.

2. White, R.N. and Gergely, P. (Editors), “Proceedings of the Workshops on Seismic Performance of Existing Buildings (3 volumes – May 1983, July 1984 and May 1985)”, Department of Structural Engineering, Cornell University.

(S. Okamoto)

### 3.5 Land Use Program for Controlling Natural Hazard Effects

#### (1) Task Committee E

The scope and activity of the Task Committee E can be understood from the Task Committee Report at the 8th Joint Meeting. The Task Committee E was originally designated as “Task Committee for Land Use Program for Controlling Natural Hazard Effects”, and was planned in view of controlling wind and seismic effects to undertake (1) extension of cooperation for research on land use program, (2) exchange of technical information and literature on land use, and (3) exchange of experts in the field of objectives of Task Committee E. For such purpose, Task Committee E was scheduled to perform:

- Improvement of seismic risk analyses procedure.
- Application of microzonation to seismic risk analysis.
- Seismic risk map.
- Social and economical aspects of land use program.

It was also understood that the cooperative study for controlling seismic effect be undertaken during 1976 and 1980, and that initiation of the study for controlling wind effect should be considered at an appropriate time.

As the activities increased, covering broad aspects of cooperation between two countries, the name of Task Committee E was revised at the 18th Joint Meeting, May, 1986, to “Natural Hazard Assessment and Mitigation through Land Use Programs” so that it better represents the scope and objectives of Task Committee E. The main purpose of programs in Task Committee E include:

- Evaluation of seismic hazard and mapping procedures.
- Evaluation of damage potential of structures, soil liquefaction potential and tsunami hazard.
- Seismic response characteristics under various ground and topographic conditions.
- Planning methodologies for earthquake disaster mitigation in large populated cities.
- Evaluation of socio-economic losses from earthquake disasters.

#### (2) Main Accomplishments

Task Committee E has made many contributions, including the exchange of technical information and experts of both countries, endorsement of coordinated research programs, etc. The main accomplishments are the following:

- Exchange of Experts

In conjunction with activities of Task Committee E, Dr. Robin K. McGuire, U.S. Geological Survey, visited

Japan from January 18, 1977, to January 21, 1977, for the purpose of discussing land use programs.

Mr. Tadayuki Tazaki, senior research engineer of the Public Works Research Institute, made a study on the effectiveness of land use programs for controlling natural hazard effects from social and economic points of view<sup>1)</sup>. He stayed at the University of California, Los Angeles for one year from January, 1979, to January 1980.

A delegation from the U.S. visited Japan during 1983 to study countermeasure planning for the anticipated Tokai Earthquake of Japan. The visit was supported and assisted by Task Committee E, and the delegation's findings were reported to the 10th Joint Meeting by a representative of the Earthquake Engineering Research Institute.

Dr. John B. Scalzi, Dr. Kazuhiko Kawashima, and representatives of the Government of Shizuoka-ken, Messrs. Toshiroh Sugiyama and Katsunori Imado, participated at the August, 1984, U.S.—Japan Workshop on "Urban Earthquake Hazards Reduction", which had as a main theme the Tokai Earthquake Hazard Reduction Program. The workshop was sponsored by the U.S. Earthquake Engineering Research Institute. Arrangement for the participation of the panel members as well as representatives of the Government of Shizuoka-ken were made under the auspices of the U.J.N.R.

#### b) Exchange of Technical Information

Task Committee E has been exchanging technical information related to land use programs for controlling natural hazard effects through the presentation of two to four papers, on an arranged basis, at each joint meeting and also through discussions for coordinated as well as future research programs and accomplishments, including publications.

Furthermore, the following technical information has been exchanged:

- i) The report on "The Anticipated Tokai Earthquake"<sup>2)</sup>, published in June, 1984, by the U.S. Earthquake Engineering Research Institute, was distributed to Task Committee E members.
- ii) The report on "Urban Earthquake Hazards Reduction"<sup>3)</sup>, published in July 1985 by the U.S. Earthquake Engineering Research Institute, was distributed to Task Committee E members.
- iii) The Japanese chairman provided the U.S. chairman in September, 1987, twelve papers and reports on natural hazard assessment and mitigation through land use programs published by National Research Center for Disaster Prevention (NRCDP), Geographical Survey Institute (GSI), Public Works Research Institute (PWRI), Building Research Institute (BRI), and Port and Harbor Research Institute (PHRI).

#### (3) Future program

In view of the importance of technical cooperation on the subject of land use programs for controlling natural hazard effects, Task Committee E will continue its activities including exchange of relevant technical information and literature, execution of joint coordinated program and exchange of experts.

Aiming to hold a workshop on the occasion of 21st Joint Meeting of UJNR at Tsukuba in 1989, an outline of the projected workshop will be discussed at the Task Committee meeting of the 20th Joint Meeting in 1988.

#### [Reference]

- 1) T. Tazaki: The Current State of Research on Earthquake Disaster Mitigation in U.S.A., Civil Engineering Journal, Vol. 22-9, 1980
- 2) Earthquake Engineering Research Institute: The Anticipated Tokai Earthquake, 1984
- 3) Earthquake Engineering Research Center: Proc. of U.S.—Japan Workshop on Urban Earthquake Hazards Reduction, 1985

(K. Kawashima)

### 3.6 Disaster Prevention Methods for Lifeline Systems

#### (1) Activities of Task Committee (F) in the Past Two Decades

It is said that the word "Lifeline" was born from the severe damages to public works and utilities caused by the San Fernando Earthquake which occurred in the vicinity of Los Angeles in 1971.

"Disaster Prevention Methods for Lifeline Systems" was first adopted as a mutual interested theme at the 7th Joint Meeting of the Panel in 1975. As a matter of fact, pertinent information had been exchanged between the members before then; literature on earthquake resistant design standards, damage inspection methods and durability estimation methods for structures were exchanged through the channel of the Joint Meetings of the Panel, and papers were presented as well. For instance, papers on "Seismic Resistivity of Submerged Tunnels and Earthquake-resistant Design Standards for Underground Structures" were presented at the 4th and 5th Joint Meeting of the Panel, respectively.

#### (2) Purpose and Activity Plan

As both the U.S. and Japan have densely populated regions, traffic facilities, communication networks and other basic facilities are quite important for taking emergency measures to minimize the loss of lives and property caused by destructive earthquakes or strong wind which might affect social life seriously. Accordingly the task committee adopted the following resolutions at the 8th Joint Meeting of the Panel which set up Task Committee (F) on Disaster Prevention Methods for Lifeline Systems.

(a) Improvement of design and disaster prevention for lifeline facilities are important.

(b) "Lifeline" is defined here as important facilities in the case of taking emergency measures within 72 hours after disaster occurred, including bridges, banks, tunnels, slopes, pedestrian bridges, pipelines, water pipes, telephone lines, power sources transmission lines, water way and tidal gates, inland water for firefighting and minimum essential facilities of wharf. Excluded from the category by the Task Committee are buildings, relay facilities, electric power plants and buildings for waterworks.

The Task Committee has reached an agreement on a future program as follows at the 9th Joint Meeting:

(a) Exchange of information on design standards and guidelines shall be expanded to non-governmental authorities such as ASCE, JSCE and API, as well as by the governments.

(b) When each side makes new design standards or guidelines or revises current standard(s) on lifeline systems, the standards or the guidelines shall be exchanged promptly.

(c) Information on research programs and administrative systems concerned shall be exchanged.

At the 10th Joint Meeting in 1978, both sides agreed that co-chairmen will explore expansion of the work of the Task Committee by inviting additional agencies of their respective governments having lifeline responsibility to become involved. The Task Committee discussed coordination of the work with other task committees of the Panel and agreed that the Task Committee F will confine itself to those problems peculiar and unique to lifeline systems.

### (3) Promotion of Cooperative Research

In 1978 the lifelines of the Sendai district were heavily damaged by Miyagi-ken-oki Earthquake and research needs for safety of lifeline systems increased all the more. Thus, at the 11th Joint Meeting in 1979, coordination effort of U.S.—Japan joint research on the safety of lifeline system and its components at every level of cooperation was emphasized.

Cooperative research was initiated through the formal exchange of technical experts between U.S. and Japan sides. Many papers on the earthquake resistivity of buried pipe have begun to be presented at Joint Meetings, too.

The Task Committee discussed at the 13th Joint Meeting the establishment of a planning committee for the longer range planning of cooperative lifeline research. Both sides felt that the first priority for cooperative research should be given to bridge problems and strongly favored the need to establish a new task committee on transportation systems to further promote cooperative research. Later, a new task committee was established in 1981.

### (4) Expansion of Research Activity

Studies on the development of assessment of damage and restoration methods for seismically damaged lifeline facilities were initiated in the fiscal year of 1981 by the Japan side. Investigation of gas and oil pipeline damage caused by large ground deformations, research on seismic performance of piping systems and so on were being carried out by the U.S. side and primarily sponsored by the National Science Foundation. These activities of the Task Committee were reported at the 14th Joint Meeting in 1982.

At the 15th Joint Meeting in 1983, the Japan side reported that much data related to San-Fernando earthquake was obtained by great cooperation of U.S. members for the ongoing studies on development of assessment of damage for seismically damaged lifeline facilities. U.S.-side reported that a Federal Government

Interagency Committee on Lifelines had been established and was actively conducting a survey to determine the extent of Federal Government responsibility for lifeline; a government-private sector workshop was planned for October, 1983.

As one means of the coordinating research to promote cooperation between U.S. and Japan through the UJNR Joint Meeting of the Panel, the Public Works Research Institute initiated a 10-year research project on seismic resistivity of lifeline facilities including buried pipeline in 1983 in Japan. For the first five years (1983 — 1987), research on seismic resistivity of reinforced concrete column-like structures, which have often been damaged by earthquakes in both countries, was conducted under the close cooperation with the U.S. National Bureau of Standards. Research on seismic resistivity of buried reinforced concrete pipeline has been carried out since 1987 with Columbia University, Princeton University, Old Dominion University and others.

Workshop on Lifeline Earthquake Engineering was held on May 14, 1984, at the Road Research Center, Fairbanks, with active participation by more than 20 experts from both countries. This first workshop was so fruitful that the second one, U.S.—Japan Workshop on Seismic Behavior of Buried Pipelines and Telecommunications Systems, was held on December 5—7, 1984, at the Public Works Research Institute, Tsukuba with the participation of more than 40 experts from both countries. The workshop identified specific research areas that are most suitable for future coordinated research between the U.S. and Japan.

From the Japan side as one of the research results, an outline of the Manual of Repair Methods for Civil Engineering Structures Damaged by Earthquakes (Draft) was introduced at the 18th Joint Meeting. The Ministry of Construction and PWRI authorized NSF for translation of the Manual into English and for distribution to the U.S. professional community.

Reports of a number of research projects dealing with lifeline earthquake engineering and workshop proceedings have been exchanged through the UJNR channels. Interchange of experts in each special field to promote cooperative research studies between the U.S. side and the Japan side has become more active.

### (5) Future prospects

The Task Committee will facilitate the continued exchange for technical information and cooperation in research on specialized problems listed as follows:

- (a) Survey reports of seismic damage to lifeline systems and seismic observation results.
- (b) Seismic design procedures for lifeline systems.
- (c) Procedures and instrumentation to detect and inspect damage and the behavior of lifeline structures during earthquakes.
- (d) Repair and retrofit methodology for lifeline systems.
- (e) Estimation of reliability of lifelines.
- (f) Management and public education on the importance of lifeline systems.
- (g) Investigation of needs for large-scale testing of lifeline systems.

For the time being, it is recommended to continue U.S.-Japan coordinated research projects on field observation and analyses on seismic behavior of buried pipelines, experiments and analyses on dynamic characteristics of joint behavior, effects of soil liquefaction on buried pipes, soil-buried pipes interaction, seismic reliability of lifeline systems, and seismic design methods.

Also encouraged is an expanded effort to promote participation of experts in charge of research and development of lifeline earthquake engineering, especially by those from private companies and public utility enterprises, along with strengthening contact between all persons concerned. From this point of view, it is important to establish the planning Committee on Lifelines in each country which was agreed to at the 14th UJNR Joint Meeting and which has been postponed because of some difficulty implementing the proposal experienced by both sides.

Papers on current research presented at the Joint Meetings are a small part of the fruits of research and development by both sides. Therefore, it is also significant and beneficial to hold workshops with participation of experts to discuss lifeline earthquake engineering. Holding expanded workshops in the future with cooperation of organizations concerned under the auspices of the Panel will be discussed.

(O. Ueda)

### 3.7 Wind Characteristics and Structural Response

#### (1) Introduction

Since the establishment of the Panel, wind effect on structures has been one of major themes. A great amount of reports have been presented and technical information has been exchanged on basic wind characteristics, wind tunnel testing methods, field observation, survey of damage due to strong wind, response of structures against wind, structural design codes and so on since the 1st Joint Panel Meeting.

At the 8th Joint Panel Meeting in 1976, Task Committee G, "Strong Wind Records" was established. The Task Committee was scheduled to carry out the following items.

(a) Exchange of strong wind data, including performance characteristics of anemometers and processing methods.

(b) Exchange of information with regard to automatic observation system of wind at full-scale buildings and structures.

(c) Promotion of researches on effects of strong wind on structures.

(d) Exchange of data of wind pressure acting on low-rise buildings and structures, and data of vertical wind profile in the atmospheric boundary layer.

(e) Standardization of wind tunnel testing methods in turbulent flow.

At the 12th Joint Panel Meeting in 1980, the name of the Task Committee G was revised to "Wind Characteristics and Structural Response" and the number of the U.S. members were increased in order to broaden and expand the activity of the Task Committee. At present, the aims of the Task Committee G are as

follows:

(a) Exchange observations and records of high wind data (including remote-sensing reports, i.e., aircraft, satellite) available from the respective national meteorological services and special observation sites.

(b) Encourage the exchange of actual wind observations in appropriate format.

(c) Exchange available specialized high wind data sets and wind pressure sets. The information may include surface meteorological data sets and data sets at other levels. Documentation of instrument characteristics, exposure, and elevation above ground may be included.

(d) Encourage the establishment of standard methods for the simulation of boundary layers in wind tunnels, the promotion of data exchange of boundary layer wind observations, and the exchange of information on methods of measurement and determination of structural response. Where possible, promote exchange of meteorologists, engineers and available research facilities.

(e) Encourage the interaction between meteorologists and engineers to identify the types of wind data required for future use in establishing extreme wind distributions; in determining wind loadings on structures; in understanding the urban wind climate; and in considering structural design issues in the wind generation of energy.

#### (2) Main Accomplishments

##### 1) Exchange of Technical Information

About one hundred and twenty papers have been presented at the Joint Meetings in relation to strong wind and structural response since the 1st Joint Meeting.

The contents of the papers are classified into structure and characteristics of strong wind, wind-induced response of buildings and structures, survey of damage and the others.

Since design wind speed is one of fundamental subjects in wind engineering, studies have been carried out on estimation of expected value of strong wind speed and multi-regressive analysis of strong wind taking into account of local topographical conditions. These studies resulted in wind speed maps which are convenient for structural design.

Strong wind are mostly caused by typhoons, hurricanes and tornados. The characteristics of the strong wind and damages due to these phenomena were reported. Especially, a lot of reports have been presented by the U.S. side on the detailed characteristics of hurricanes which attacked the U.S. In Japan, severe typhoons attacked Hachijo Is. in October, 1975 and Okinoerabu Is. in September, 1977. Surveys of damage were conducted by the Japanese Panel organizations and the results were presented.

Field observation has been conducted to study spatial structure of wind and vertical wind profile. The Meteorological Research Institute set an observation tower in Tsukuba and an observation station near seashore in Kashima. The National Research Center for Disaster Prevention also set an observation station at sea in Hiratsuka. The wind data observed at these stations were analysed and reported at the Joint Panel Meetings. Recently, the characteristics of turbulence of natural

wind have been studied by many researchers in relation to wind-resistant design.

Regarding wind effects on buildings, wind-resistant design codes for buildings in both countries were introduced at the 1st Joint Meeting, and information on state of the art were exchanged in the early stage. The papers presented at the Joint Meetings have dealt with various topics, such as observation of wind pressure acting on wall of full-scale buildings, wind loads on cladding of buildings, similarity law of wind tunnel testing on wind force on buildings, wind characteristics near the ground surface around high-rise buildings, local wind pressure on buildings, prediction method of wind-induced response of high-rise buildings, wind-induced damages, wind-induced response of high-rise steel towers, wind forces on solar heater, structure of tornados and prediction method of damages caused by tornados, wind-resistant design method of window glass, wind-resistant design method of cladding of houses, and so on.

Activities on wind effects on bridges, which are described in details in 3.10, are outlined here. In Japan, researches regarding the Honshu-Shikoku Bridges Project started in 1960's. Study on the wind-resistant design of bridges has been one of the important researches. In the U.S., study on wind effects on bridges has been also important in view points of construction of cable-stayed bridges and maintenance of existing suspension bridges. Under these circumstances, wind tunnel testing, theoretical study and field observation concerning wind-induced vibrations of cable-stayed and suspension bridges have been reported in the Joint Meetings. Recently, wind tunnel tests in the simulated turbulent flow have been conducted in many institutes. The method of flow simulation and the comparison among wind tunnel testing, field observation and theoretical prediction have been discussed in the Joint Meetings.

## 2) Exchange of Strong Wind Records

Strong wind records as well as strong earthquake records are important data in engineering point of view. The exchange of the data between Japan and the U.S. was proposed in the early stage of the activities in Joint Meeting. So far, wind data at the observation tower of the Meteorological Research Institute in Tsukuba, Japan and hurricane data in the U.S. have been exchanged through the Task Committee.

## 3) Exchange of Personnel

Dr. R.D. Marshall of the NBS stayed in the PWRI from September to December, 1982 to make a cooperative research on wind-induced vibrations using the wind tunnel of the PWRI. The results were presented in the Joint Meeting. During his stay in Japan, he examined wind tunnel facilities in Japan with assistance of the Japanese members. The results were reported in *J. of Structural Engineering, A.S.C.E.*<sup>1)</sup>

## (3) Future Activities

So far, main activities of the Task Committee have been exchanges of information and literature, which were beneficial to both countries and shall be continued. There still remains, however, many and important subjects to be studied. The Task Committee G recognizes that the following subjects are important

in view points of social needs relevant to the Task Committee G.

a. Comparison of wind resistant design methods of structures between both countries.

b. Comparative wind tunnel testing between both countries using a common model to establish rational wind tunnel testing method.

c. Comparison of codes and practices of wind resistant design of bridges between both countries.

d. Study on indoor pressure of buildings with large indoor space.

e. Development of control techniques of wind-induced responses of high-rise buildings.

f. Evaluation of effects of material deterioration on wind-induced responses.

g. Accumulation of strong wind data in coastal area.

Therefore, the Task Committee G shall carry out the following items as the future activities.

(a) Exchange observation reports of high winds.

(b) Encourage interaction between meteorologists and engineers to identify the types of wind data required for future use in establishing extreme wind distributions; in determining wind loading on buildings and structures; in understanding the urban wind climate; and in considering design issues involved with the wind generation of energy.

(c) Encourage the establishment of minimum requirements for the simulation of atmospheric boundary layers in wind tunnels and the exchange of boundary layer wind tunnel test results, including comparisons with corresponding full-scale situations.

(d) Exchange information on criteria, techniques and instrumentation for structural modeling in boundary layer wind tunnels. Also encourage the exchange of information of measurements made on actual structures and on comparisons with predictions from wind tunnel studies of these structures.

(e) Expand the exchange of engineers and meteorologists, and encourage the mutual use of available research facilities in the two countries.

(f) Encourage the development of work plans for the pursuit of the research subjects listed above.

(g) Plan a workshop in the coming year, with details to be worked out between the respective U.S. and Japanese Task Committee chairmen.

## [Reference]

1. R.D. Marshall: Wind Tunnel Applied to Wind Engineering in Japan, *J. Structural Engineering*, Vol.110, No.6, June, 1984.

## 3.8 Soil Behavior and Stability during Earthquakes

### (1) Accomplishment in the Past Two Decades

#### 1) Introduction (K. Kurashige, T. Murota)

It was adopted to establish Task Committee (H) which is to deal with the soil liquefaction, slope failure and ground subsidence during earthquakes, at the 8th Joint Meeting of the Panel, held in May, 1976.

Although the above mentioned phenomena are parts of main causes of destructive seismic damage, the study on soil behavior and stability during earthquakes is the

field which has a comparatively young history in earthquake engineering. As both of the U.S. and Japan are interested in this field, information including seismic design standards for embankment and foundations for structures have been exchanged actively since the first Joint Meeting of this Panel.

This chapter describes briefly the accomplishments by the Panel during the past two decades along with the objectives of Task Committee (H).

## 2) Exchanged Materials

Over one hundred submitted papers for the Joint Meetings which have accumulated concern the technical field of Task Committee (H) since the 1st to 19th Joint Meeting of the Panel.

Dynamic soil property, interesting from practical engineering view point, may be classified into following three categories: [1] dynamic deformation characteristics of soils, the non-linear stress-strain relationships of soils under dynamic loading conditions; [2] dynamic strength characteristics, represented by the soil liquefaction; and [3] permanent deformation of soils induced by earthquakes.

Twenty years ago when the Panel began to take the first step, the dynamic deformation characteristics were seldom compiled into the design chart for practical purpose; papers on above mentioned [1] appeared in the past Joint Meetings for rationalizing the ground response analysis during earthquakes. As for [2] mentioned above, active studies in both countries have been conducted, especially since the establishment of Task Committee (H), and contributed to the progress of this field, as shown by an example of the rationalization of data base for the soil liquefaction evaluation based on the U.S.—Japan joint research. Recently, papers on [3] mentioned above have begun to be submitted to the Joint Meeting along with progress of the analytical technique and the advance in the soil dynamics.

In order to grasp the accomplishments of the Panel in the field of soil behavior and stability during earthquakes through the exchanged materials: submitted papers during these twenty years may be classified as follows if arranged by their main subjects:

- 1) introduction of seismic design standards on embankment, foundation ground and foundations.
- 2) introduction of dynamic soil testing equipment.
- 3) introduction of soil liquefaction test and evaluation technique.
- 4) introduction of dynamic analysis technique of embankment, foundation ground and foundations.
- 5) description on the actual behavior and damage of embankment, foundation ground and foundations during earthquakes.
- 6) introduction about the countermeasures against soil liquefaction.

Most of the introduction information is gathered from the research and practical experience gained individually in both countries. It is essential for mutual understanding that over one hundred papers covering above mentioned subjects have been exchanged. Adding to the submitted papers, related documents and ma-

terials in this field published from member organizations in both countries have been exchanged through the channel of the Panel.

## 3) Personnel Exchange

In these two decades, there occurred several damaging earthquakes in both countries such as San Fernando Earthquake of 1971, Izu-Ohshima Kinkai Earthquake of 1978, Miyagiken-Oki Earthquake of 1978, Nihonkai-Chubu Earthquake of 1983, and the Naganoken-Seibu Earthquake of 1984; many important lessons have been learned from these earthquakes. During field study of the damage induced by these earthquakes, each side gave assistance and/or cooperation for the dispatched mission from the other side under the auspices of the Panel. This kind of support is considered to be indispensable to conduct the efficient study in the confused field just after the earthquakes.

Researchers, engineers and scientists of both sides have stayed on the counter part side for periods from one month to one year as visiting researchers. By joining the on-going projects of the counterpart side, mutual understandings between both side engineers and scientist have been promoted in depth.

Furthermore, it should be noted that the cooperative joint research activities on soil liquefaction were conducted and joint workshops on soil liquefaction were held. Fourteen researchers and engineers from U.S. side and ten researchers and engineers from Japan participated in the U.S.—Japan Workshop on In-Situ Soil Testing for Evaluation of the Soil Liquefaction Susceptibility which was held in San Francisco, California in August, 1985. And in conjunction with the 20th Joint Meeting in May, 1988, the U.S.—Japan Workshop on Remedial Measures for the Liquefiable Ground was just held in Jackson, Wyoming.

## 4) U.S.—Japan Joint Research on In-Situ Testing for Soil Liquefaction Assessment.

Soil liquefaction, paid careful attention to by engineers after the Niigata Earthquake and the Alaska Earthquake of 1964, may cause destructive damage to structures and large scale slope failure or land slide during earthquakes. That is why it is urgent to develop effective countermeasures against soil liquefaction.

Obviously, in order to mitigate the damage due to the soil liquefaction, it is exclusively important to establish the evaluation technique of ground liquefaction susceptibility and to pursue the rationality in practical application of this evaluating method. Case studies of past damage caused by the soil liquefaction may play an important role in judging whether the proposed method of soil liquefaction estimation is rational or not. Therefore, the soil condition at the sites must be expressed in a universal way obtained by the method which can give the universal soil parameter whenever or wherever in the world it is conducted. However, some discrepancy in the standard penetration testing (SPT) method, which is widely used in both countries to investigate the soil liquefaction potential, was noticed. And it was pointed out that it should be clarified whether the blow counts (N) of SPT obtained by methods in both countries can be universal for the same soil condition or not.

The task committee agreed at the 10th Joint Meeting of the Panel held in May, 1978 to attempt to exchange boring data, field crew and equipment in order to establish uniformity of SPT as conducted in Japan and the U.S. Since then comparative research works have been continued through exchanging technical reports between the concerned Panel members of both sides.

In 1983, the National Bureau of Standards and the Bureau of Reclamation finally funded this cooperative research, and Dr. W.D. Kovacs (NBS) and Mr. J.A. Farrar (BR) visited Japan with field crew and equipment in order to perform The SPT jointly with engineers of The Public Works Research Institute at the sites where the liquefaction apparently took place during past earthquakes. The N values which were obtained by the popular manners of both the U.S. and Japan were compared.

The objective of this cooperative research is to better define the data base linking in-situ measurements with the evaluation of liquefaction, including the acquisition of calibrated SPT data by energy measurement and reevaluation of the data base for the SPT design curves.

It was concluded by this cooperative research that;

- 1) energy ratio is independent of blow count as found by Schmertman and Robertson, et al.
- 2) energy ratio by the Japanese practice is less scattered than data from the U.S. practice.
- 3) blow count for JIS sampler is larger than that for ASTM sampler when normalized for the same energy.
- 4) from the fact stated above it is concluded that blow count by the Japanese practice is nearly equal to that by the U.S. practice when normalized for the same energy level.

These findings obtained by the cooperative research have contributed to promote the better understanding of the in-situ test results for liquefaction analysis in both countries.

## (2) Future Challenges

Although considerable accomplishment on the subject of liquefaction evaluation has been achieved, however, as for other subjects such as slope failure and ground subsidence during earthquakes, which were designated when the task committee was established, not enough is considered to have been achieved.

It is necessary to promote actively the technology to mitigate slope failure, embankment instability and ground subsidence during earthquakes in the future.

The urgent problems to be solved concerning the soil behavior and stability during earthquakes include: 1) seismic stability of the ground on which structures (including buried structures) are founded, 2) seismic stability and/or permanent deformation of embankment and natural slopes, and 3) interaction between ground and substructures of bridges or buildings.

Following are examples to be solved commonly in both countries relating to soil behavior and stability during earthquakes:

- 1) Developing a universal in-situ testing method for evaluation of liquefaction susceptibility, including for gravelly soils and soils with abundant fines content.
- 2) Developing a design standard for remedial meas-

ures of the ground which is susceptible to liquefy.

3) Developing a prediction method of stability and permanent deformation of embankment and natural slopes during earthquakes and its countermeasures.

4) Developing a prediction method of ground and foundation subsidence during earthquakes.

5) Elucidation of the seismic effect on the retaining wall and semi-buried concrete structures and development of measures for their seismic stability.

6) Developing remedial measures for the existing embankment and foundations to gain their seismic stability.

7) Acquiring the actual response data of embankment dams during earthquakes.

8) Progress on the centrifuge testing technique and shaking table testing technique.

(Y. Sasaki)

## 3.9 Storm Surge and Tsunami

### (1) Introduction

Storm surge and tsunami are natural phenomena caused by wind and earthquake, respectively. Many lives have been lost and many facilities located along the shoreline damaged due to these phenomena. Some reports on storm surge and tsunami have been presented intermittently at an initial stage of the Joint Meeting. However, in order to strengthen this part of study, "Storm Surge and Tsunami" was adopted as one of the activities of the Panel. At the 11th Joint Meeting in September, 1979, the Task Committee on "Storm Surge and Tsunami", named by Task Committee (I), was officially initiated, and the first task committee was held at the 12th Joint Meeting. At the early stage of the activities on storm surge and tsunami, information on their forecasting method, countermeasures and warning system were mutually exchanged. In 1983, a U.S.-Japan Tsunami Workshop was held, including university researchers, and extensive discussions were conducted on fundamental study, numerical simulation method and countermeasures.

### (2) Activities of Task Committee

This Task Committee was initiated in September, 1979. The first meeting was held in May, 1980, and in this meeting, future plans were adopted.

Storm surge and tsunami have caused severe injury and damaged properties in the U.S. and Japan, as well as in other areas where such geophysical phenomena have occurred. It is apparent that storm surge and tsunami are caused by wind and earthquake, respectively, and therefore the adoption of these themes for the study topic in the Joint Meeting is considered to be suitable.

The Task Committee should be engaged in exchange of the information with respect to publications, data of damages and protection method regarding storm surge and tsunami.

The Task Committee should consider the following study plans:

- 1) The information on storm surge models for forecasting, planning and warning system will be exchanged. This information includes type of

models, programs, actual data for verification and actual value of coefficients in the model. Contacts between researchers are considered as a part of the exchanges of information.

- 2) The development of a storm surge forecasting model will be promoted. The generation of storm surge mainly depends on the effect of atmospheric pressure, so that a storm surge model should be connected with the atmospheric pressure model.

The activities up to the present have been conducted based on the above mentioned guiding principles. However, at the task committee in 1981 the differences in the objectives of the study between Japan and U.S. sides was pointed out.

Publications of U.S. National Hurricane Center, Miami, have been circulated among the Japanese members. Differences in the major objectives of research activities in the U.S. and Japan are noted: the former works emphasize the field of real-time forecasting of storm surges, whereas the latter emphasizes the planning and execution of coastal protection works against storm surges and tsunamis.

In 1982 the Task Committee recommended that a U.S.-Japan tsunami workshop should be organized to:

- 1) describe current research in each country,
- 2) discuss problems tractable with today's knowledge and technology including observations and verification of theory,
- 3) explore ways and means of increasing U.S.-Japan cooperation in tsunami research and technology transfer, and
- 4) explore ways of exchanging tsunami data between the U.S., Japan and other disaster prone areas.

The U.S.-Japan Tsunami Workshop was held on May 12 and 13, 1983 at the Public Works Research Institute, Tsukuba, with 13 U.S. participants and 19 Japanese participants. The workshop was held in conjunction with the 15th Joint Meeting. A total of 25 presentations and subsequent discussions were made on broad topics of:

- ① Tsunami behavior in coastal water and on land,
- ② Nonlinear problems of tsunami,
- ③ Mesh consideration in numerical work,
- ④ Finite difference vs. finite element methods,
- ⑤ Tsunami protective measures in Japan and U.S.

Following the Tsunami Workshop, a study tour to a tsunami protection facility in Kamaishi Port and tsunami research facility of Tohoku University was arranged for U.S. participants. Discussions with both research engineers and civil authorities provided the workshop participants with a unique and valuable insight into the immediate nature of the tsunami problems. As one of the results of the U.S.-Japan Joint Tsunami Workshop (1983), the National Science Foundation (U.S.) has funded an exchange program between Tohoku University and Texas A&M University. In May 1984, Dr. Goto from Tohoku University began a six-week visit to Texas A&M University. Exchange of information on tsunami was also enhanced by the Joint Tsunami Workshop. For instance, Japanese scientists sent U.S. members a package of 42 photographs of Japanese tsunami effects.

A few days after the 15th Joint Meeting in 1983, the Nihonkai-Chubu Earthquake occurred, and a tsunami

caused by this earthquake occurred along the coastline in Tohoku district along the Japan Sea side. Lives of around 100 people were lost and many properties were damaged due to this tsunami. After this tsunami, Japanese members of the Task Committee extensively investigated the features of this tsunami and damages due to this tsunami. The results of these investigations were disclosed to U.S. members in 1984. At this time, the U.S. side proposed to send some reports on storm surge prediction to the Japan side.

At the task committee meeting in 1985, various studies on the Nihonkai-Chubu Earthquake Tsunami were presented and information about storm surge and the tsunami was exchanged. The U.S. side (NOAA) supplied the Japan side (MRI) with digital records of Tsunami affecting Japan. MRI examined the records and indentified the differences with their data. The U.S. side (NOAA) made the necessary adjustments to conform with the Japanese information. Furthermore, the U.S. side (NOAA) provided the Japan side (MRI) with the Pacific Ocean Bathymetry Data Base. The data base was used in modeling tsunami and in producing tsunami propagation charts. Japan side (MRI) reported the result at 19th Joint Meeting in 1987.

There are many practical problems to be solved on forecasting, warning system and countermeasures, although the studies on the dynamics and numerical method have been advanced considerably in the basic study. Particularly, it is important to collect and exchange information on storm surge and tsunami in order to develop a practical forecasting system; the Task Committee has extensively conducted the exchange of information between U.S. and Japan sides.

### (3) Presentation

Thirty-three papers have been presented at the joint meetings in 10 years. These are divided into eight categories as shown in Table 1 according to the subject of research.

TABLE I SUBJECTS IN PRESENTATIONS

SUBJECT	NUMBER OF REPORTS
STATE OF ART	5
CASE STUDY	8
DATA BASE	3
WARNING SYSTEM	4
FORECASTING METHOD	7
COUNTERMEASURE	3
DISASTER	3
BASIC STUDY	5

All subjects included in a presentation are counted. The most frequently presented subject is the investigation of storm surges and tsunamis. The next most frequent is on forecasting method. As for the difference between U.S. and Japan, many reports of Japan side are on the investigation of actual phenomena, damage and countermeasure, whereas those of U.S. side are on the forecasting method, warning system and data base.

#### (4) Future prospects

The Task Committee on Storm Surge and Tsunami as main themes will continue to support the arrangement and development of accurate storm surge and tsunami data base using exchanged data between the U.S. and Japan, along with supporting communication among researchers. These works will contribute to following two subjects:

##### 1 Establishment of forecasting and warning systems for storm surges and tsunamis

The first purpose of this subject is to develop a method and to solve the problem of forecasting the occurrence and propagation of the storm surges and tsunamis. The second purpose is to establish available forecasting and warning systems.

##### 2 Planning of countermeasures

Effective and available countermeasures to prevent disasters due to the storm surges and tsunamis will be investigated considering the warning system.

(T. Uda)

### 3.10 Wind and Earthquake Engineering for Transportation Systems

#### (1) Introduction

The 13th Joint Meeting, held from May 19 to 22, 1981, at the Public Works Research Institute, Tsukuba, agreed that a new task committee should be created to take up the subject of wind and earthquake engineering for transportation systems, which would further promote research cooperation in this area between the United States and Japan.

In view of the wide range of wind-and-earthquake engineering technology for transportation facilities, the Task Committee was to initially confine its research to problems in earthquake engineering, and in the future expand its studies to include research on the effects of wind and earthquakes on transportation facilities.

The principal aims of the Task Committee have been to conduct cooperative research on subjects of common concern to the two countries and to periodically exchange data.

The Committee has met annually since 1982 to exchange information and conduct successive discussions on bridge workshops, U.S.—Japanese cooperative programs, and its own future plans.

Studies on wind and earthquake engineering for transportation systems during the past 20 years have primarily dealt with wind-and-earthquake-resistant designs for highway bridges.

#### (2) Exchange of research data

During the past two decades, 57 reports were given at joint meetings, while the number of people involved in preparations totaled about 200.

At the first joint meeting (1969) a report was made on "wind-resistant and earthquake-resistant design specifications for highway bridges in Japan", which described the present state of Japanese highway bridges and design standards, including those for wind-and-earthquake

resistance.

At that time, Honshu-Shikoku Bridges, one of the largest-scale projects in Japan, were still under consideration in a comparative study of five possible bridge routes. But at the first meeting in 1969 a report was presented on the "guidelines for wind-and-earthquake design for the Honshu-Shikoku Bridges", prepared in 1967 by the Japan Society of Civil Engineers.

These guidelines, however, were repeatedly revised in subsequent years in accordance with the results of research and the progress of work. At the joint meetings, basic concepts for the revision were introduced and outlines of Volume 5 (Earthquake-Resistant Design) of the Specifications for Highway Bridges, and final versions of wind-resistant design specifications and earthquake-resistant design specifications for the Honshu-Shikoku Bridges, were reported.

Research reports on the wind-resistant designs of long-span suspension bridges were presented. Kanmon Bridge, for which construction began in 1968, is the second full-scale, long-span suspension bridge in Japan after Wakato Bridge. The wind-resistant design of Kanmon Bridge and the observation system for the bridge's response to strong winds were reported. Research on the aerodynamic characteristics of long-span suspension bridges focused on gust response and aerodynamic instability of suspended structures with stiffening trusses and stiffening box girders in relation to design.

It is said that the first cable-stayed bridge ever constructed in Japan is Katsuse Bridge (180 meters), built in 1959. Full-length of bridges of this type that are over 200 meters in length, such as Onomichi Bridge (1968) and Toyosato Bridge (1970), have also been built. Cable-stayed bridges and their aerodynamic wind-resistant design were reported, including the present status of plans to build cable-stayed bridges, problems in their wind-resistant design, aeolian vibrations and examples of ways to suppress them, and plans for aerodynamic tests. Also presented was the wind-resistant design of Suehiro Bridge.

The aerodynamic stability of multi-and long-span bridges with steel box girders, that had previously received little attention was presented with a report on the aerodynamic design of the Tozaki Viaduct and a report on the aerodynamic characteristics of box-girder bridges in turbulent flow.

The first report on Substructures was made at the 3rd meeting (1971), specifically on the vibrational characteristics of the foundation of Kanmon Bridge, followed by a reports on structural characteristics of pile and sheet pile foundation against horizontal forces, seismic stability of the multi-pillar foundation used in the Honshu-Shikoku Bridge and the lateral resistance of piles in a sloped foundation.

Reports were presented on the response of reinforced-concrete piers to earthquakes at the 16th through the 19th Joint Meetings on model experiments on the dynamic behavior of reinforced-concrete bridge pier columns with repeated loads. Reports on research concerning the load endurance of concrete-filled steel tubes, originally developed as a type of bridge pier with high ductility, were presented, too.

A report on the Miyagi Offshore Earthquake (June 12, 1978) that devastated highway bridges was sub-

mitted to the 11th meeting (1979).

### (3) Bridge workshops

At the 1983 Task Committee meeting, it was decided to organize a U.S.—Japanese bridge workshop. The first workshop was subsequently held from February 20 to 22, 1984, at the Public Works Research Institute, Tsukuba. Its focus concentrated on such earthquake-related highway bridge topics as design standards, design earthquake motion, and bridge response. Fourteen Americans and 31 Japanese participated, with the latter presenting 20 papers.

The second workshop was held from August 19 to 22, 1985, in San Francisco. Twelve Japanese and 13 Americans attended. Reports presented detailed research on the safety of suspension and suspended-span bridges against wind, laboratory experiments on the behavior of reinforced concrete bridge tower legs during earthquakes, repair of bridge structures affected by earthquakes, etc.

The third bridge workshop, held on May 8 and 9, 1987 in Tsukuba, was attended by 33 Japanese and 14 Americans. They exchanged data on such subjects as the dynamic analysis of cable-stayed bridges, the reliability of bridge designs, seismic design of highway bridges and design earthquake motion, repair and retrofitting of existing bridges, the safety of suspension and cable-stayed bridges against wind, seismic design of highway bridges, seismic characteristics of reinforced-concrete bridge piers, and diaphragm wall foundations. In addition, they discussed programs for which cooperation was believed possible.

### (4) Exchange of researchers

Dr. Eiichi Kuribayashi visited the United States in 1981 to discuss future cooperation in research on the response and behavior of bridges during earthquakes. Ryoji Hagiwara of Public Works Research Institute, MOC was in the United States for six months from February 1983 to participate in joint research work for a large-scale experimental project on reinforced concrete bridge piers to be conducted by the National Bureau of Standards.

In 1985, Dr. Hirohiko Tada, the Japanese co-chairman of the task committee, spent about one month in the United States, visiting a number of U.S. institutions. In 1986, Kouichi Minosaku of Public Works Research Institute, MOC was assigned to the Center for Building Technology (NBS), participating in a joint study concerning the seismic capabilities of bridge piers and towers.

### (5) U.S.—Japan cooperative research program

This program began in 1983 with studies on the seismic capabilities of bridge piers and towers. The research has included dynamic repeated loading experiments on reinforced concrete bridge piers, model experiments on damage to reinforced concrete bridge piers, experiments on concrete bridge piers and small-scale models, and studies into the behaviour of concrete-filled steel pipes.

### (6) Future plan

As for future projects, it is hoped that the joint study program concerning the seismic capabilities of bridge piers and towers, underway since 1983, will be continued under even closer cooperation. In particular, we will promote research through cooperative experiments, with the interim exchange of views on their results.

Another project will be joint research on suspension and suspended-span bridge responses to earthquake and wind. We will conduct joint wind-tunnel experiments at related facilities to compare or evaluate methods involved and at the same time to carry out exchange of researchers.

Also, we will conduct joint research to compare seismic design standards in use by our two countries. This will involve first selecting a number of bridges designed and built in each that the other can then conduct earthquake tests on, applying its own standards. This comparison of our respective seismic design standards for the same bridges will bring to light similarities and differences between them and also identify other areas of mutual interest, thus contributing to even greater research interchange. Furthermore, we hope to stimulate joint study programs on a broad range of issues including means of reducing and preventing wind and earthquake damage to existing bridges as well as promote cooperative research efforts on ways to retrofit and strengthen them.

As we have seen, research on numerous issues in wind and earthquake engineering technology will benefit from the exchange of research data, researchers and joint studies. All such activities will require enhanced efforts under close cooperation between the United States and Japan.

(H. Shinohara)

## 4. Acknowledgements

This U.S.—Japan Panel on Wind and Seismic Effects, UJNR has continued to function well as long as two decades. The Panel has exchanged technical information and personnel, conducted U.S.—Japan cooperative researches and held workshops and seminars during that time. A great amount of accomplishments have been produced through the Panel activity, and they have contributed to develop the technology for mitigating natural disasters in both countries.

The Panel has been highly evaluated at the UJNR Plenary Meetings as one of the most active Panels in 17 UJNR Panels. The accomplishments depend upon not only understandings and aids of International Affairs Division of the Agency of Science and Technology, which is in charge of UJNR in Japan, enthusiasm and leaderships of chairmen of the U.S. Panel, Dr. E. Pfrang and Dr. R. N. Wright and of the Japan Panel, Drs. M. Fukuoka, S. Ibukiyama, M. Nagao, K. Kawakami, K. Ichihara, K. Nakazawa, Y. Sakagami, T. Okubo, R. Iida, M. Tominaga, S. Kamiyo but also efforts made by all members of the Panel. The efforts and co-operation of these people during the two decades are gratefully acknowledged.

Finally, thanks are also extended to the Task Committee chairmen and the secretaries who supported Preparing this paper.

Attachment: Activities (Since May 1978 To October 1987)

## 1. Joint Research Activities

- 1978 May: 2nd Committee for the Joint Research Program on Large-scale Testing of Structures, San Francisco  
Dec: 3rd Committee for the Joint Research Program on Large-scale Testing of Structures, Tokyo
- 1979 Jul: 4th Committee for the Joint Research Program on Large-scale Testing of Structures, San Francisco
- 1980 May: 1st Seminar on Repair and Retrofit of Structures, Los Angeles
- 1981 May: 2nd Seminar on Repair and Retrofit of Structures, Tsukuba
- 1982 May: 3rd Seminar on Repair and Retrofit of Structures for Earthquake Resistance, San Francisco  
Sep-Dec: Joint Program on Evaluation of Japanese state-of-art of wind tunnel applications to industrial aerodynamics research
- 1983 May: 1st U.S. Japan Joint Workshop on Evaluation of Performance of Existing Buildings, Tsukuba  
May: 1st Joint Workshop on Storm Surge and Tsunami, Tsukuba  
Nov: Joint Research Program on In-Situ Testing Methods for Determining Soil Liquefaction Potential
- 1984 Feb: 1st Workshop on Bridge Structures, Tsukuba  
Mar: 1st Workshop on U.S. Japan Masonry Program, Tsukuba  
May: 1st Workshop on Life Line Systems, Washington  
Jul: 2nd Workshop on Evaluation of Performance of Existing Buildings, San Francisco  
Aug: Joint Research Program on Large-Scale Testing of Multi-Story Structures. Results presented at the 8th World Conference on Earthquake Engineering  
Aug: Joint Research Program on Large-Scale Testing of Steel Structures  
Dec: 2nd Joint Workshop on Seismic Behavior on Buried Pipelines and Telecommunication Systems, Tsukuba
- 1985 May: 3rd Workshop on Evaluation of Performance of Existing Buildings, Tokyo  
Aug: Joint Research Program on Large-Scale Testing of Masonry Structures; 1st Joint Technical Coordinating Committee, Tokyo  
Aug: 2nd Joint Workshop on Bridge Structures, San Francisco  
Aug: Joint Workshop on In-Situ Test Methods for Determination of Soil Liquefaction Potential, San Francisco
- 1986 Aug: Planning Conference on Disaster Prevention for Lifeline Systems held in conjunction with 3rd US National Conference on Earthquake Engineering, Charleston, South Carolina
- 1987 May: Workshop on Repair and Retrofit of Existing Structures, Tsukuba

- May: 3rd Workshop on Performance and Strengthening of Bridge Structures, Tsukuba  
Jul: Planning Conference on Evaluation of Seismic Resistance of Existing Buildings, Tokyo  
Aug: Workshop on Strong Motion Earthquake Recording, San Francisco  
Oct: 3rd Meeting of the Joint Technical Coordinating Committee on Masonry Structures Hokkaido

## 2. Researcher Exchanges

- 1978 Jun: B.R. Ellingwood, NBS, A.G. Brady, E.L. Harp, D.K. Keefer and C.M. Wentworth, USGS, C. Arnold, J.A. Blume, J.D. Cooper, H.H. Fowler and P.I. Yanev joint investigation of the Miyagiken-Oki Earthquake  
-79 Jul-Jul: T. Uwabe, PHRI\*\*\* guest researcher at WES performing research on earthquake engineering
- 1979 May-Aug: R.K. McGuire, USGS guest researcher at PWRI\*\* performing research on the evaluation method of seismic risk
- 1980-81 Sep-Jul: J.K. Wight, U. of Michigan, guest researcher at BRI\* performing joint large-scale testing program on reinforced concrete structures
- 1981 Jan-May: D. Rea, U. of California, guest researcher at BRI performing joint large-scale testing program on reinforced concrete structures  
May-Aug: L.R.L. Wang, U. of Oklahoma, guest researcher at PWRI performing research on aseismicity of Life-line System  
-82 Jul-Apr: H. Hiraishi, BRI, guest researcher at Portland Cement Association, Chicago performing joint large-scale testing program  
Aug: M. Watabe and Y. Yamanouchi, BRI, participating in the meeting of large-scale testing at San Francisco and Honolulu
- 1982 Jun-Aug: H. Krawinkler, U. of Stanford, guest researcher at BRI performing joint large-scale testing program on reinforced concrete structures  
Sep-Dec: R. Marshall, NBS, guest researcher at PWRI evaluating Japanese state-of-art wind tunnel applications to industrial aerodynamics research as part of the Joint Program on Wind Engineering, published "Wind Tunnels Applied to Wind Engineering in Japan" Journal ASCE Vol. 110, ST. 6, June 1984  
-83 Sep-Aug: D.A. Foutch, U. of Illinois, guest researcher at BRI performing joint large-scale testing program on steel structures
- 1983 Aug-Sep: R. Hagiwara, PWRI, performing research on large-scale concrete columns under seismic forces  
Aug-Dec: C.W. Roeder, U. of Washington, guest researcher at BRI performing joint large-scale testing program on steel structures  
Oct-Nov: W. Kovacs, NBS, J.A. Farrar, BUREC, performing joint study in Japan on application of standard penetration method. Results published in Proceedings of the 8th World Conference on Earthquake Engineering

- Nov: US Delegation Observing Japanese Earthquake Prediction and Preparedness Measures on the Anticipated Tokai Earthquake
- 84 Nov-Nov: M. Yoshimura, BRI, guest researcher at U. of California, Berkeley, performing joint large-scale testing program on reinforced concrete structures
- 1984 Jan-Feb: S.C. Goel, U. of Michigan, guest researcher at BRI performing joint large-scale testing program on steel structures
- Mar-Apr: H. Hiraishi, BRI, participating in the meeting of joint large-scale testing program on masonry structures at U. of California, Berkeley
- Apr: Y. Yamanouchi, BRI, participating in the meeting of joint large scale testing at the U. of California, Berkeley, and U. of Michigan
- Jun-Jul: M.L. Wang, U. of California, Berkeley guest researcher at BRI performing joint large-scale testing program on steel structures
- Sep: D. Keefer and E. Harp, USGS, joint investigation of the Naganoken-Seibu Earthquake
- 1985 Mar-Apr: T. Kaminosono, BRI, guest researcher at U. of California, Berkeley, performing joint large-scale testing program on masonry structures
- Mar-Apr: M. Nakajima, BRI, guest researcher at U. of Stanford and U. of Minnesota, performing joint large-scale testing program on masonry structures
- 86 May-Apr: M. Midorikawa, BRI, guest researcher at U. of Illinois performing research on steel structures under seismic forces
- 86 Sep-Jan: M. Teshigawara, BRI, participating in Joint Research Program on Masonry Structures at the U. of California, Berkeley
- 86 Nov-Nov: T. Tsuchida, PHRI, researcher at WES performing research in soil dynamics
- 1986 Aug-Sep: O. Senbo, BRI, guest researcher at U. of Colorado, performing joint large-scale testing program on masonry structures
- Oct-Nov: J. Farrar, BUREC, guest researcher at PWRI performing research in liquefaction during earthquakes
- 87 Sep-Jun: K. Minosaku, PWRI, guest researcher at NBS performing research on the behavior of large-scale bridge pier subjected to seismic loads
- 1987 Jan-Mar: R. Jibson, USGS, guest researcher at PWRI performing research in ground motion
- 88 Mar-Feb: Y. Hachiya, PHRI, guest researcher at WES performing research on seismic soil stability
- Aug-Oct: F. Seible, U. of California, San Diego, guest researcher at BRI performing joint large-scale testing programs on masonry structures
- 88 Aug-Aug: O. Matsuo, PWRI, guest researcher at University of California performing research on seismic design of embankments
- \* BRI: Building Research Institute, Ministry of Construction, Japan
- \*\* PWRI: Public Works Research Institute, Ministry of Construction, Japan
- \*\*\* PHRI: Port and Harbour Research Institute, Ministry of Transport, Japan

### 3. Panel Meeting

- 1978 May: 10th Joint Meeting; Washington, D.C.
- 1979 Sep: 11th Joint Meeting; Tsukuba, JAPAN
- 1980 May: 12th Joint Meeting; Washington, D.C.
- 1981 May: 13th Joint Meeting; Tsukuba, JAPAN
- 1982 May: 14th Joint Meeting; Washington, D.C.
- 1983 May: 15th Joint Meeting; Tsukuba, JAPAN
- 1984 May: 16th Joint Meeting; Washington, D.C.
- 1985 May: 17th Joint Meeting; Tsukuba, JAPAN
- 1986 May: 18th Joint Meeting; Washington, D.C.
- 1987 May: 19th Joint Meeting; Tsukuba, JAPAN

---

**Manuscripts Authored  
for Panel Meeting but  
Not Presented Orally**



# Seismic Loading Test of 15 Story Frame-Wall Reinforced Concrete Building

by

Masaya Hirose<sup>\*1</sup>, Shinsuke Nakata<sup>\*2</sup>, Hisahiro Hiraishi<sup>\*3</sup>  
Tetsuro Goto<sup>\*4</sup> and Manabu Yoshimura<sup>\*5</sup>

## Summary

A series of organized test project on the half scale models of high-rise framed wall building (HFW) has already established. Through these test series, the seismic performance of HFW were discussed. This full scale test was executed to be testified the guide line of design criteria for high-rise framed wall system. It is clarified that the safety margin after hinge-mechanism of total structure. And the effect of infilled wall to the main frame is also checked by this test.

### 1. Design of Test Building

Basic concept of the design of test building is based on the actual design of 15 story building. As shown in Fig. 1, the plan of this test building is two span and has two planar frames. Considering larger ratio of D/b (Depth-width ratio) becomes serious condition, the value of columns D/b was decided to be 4.7 as larger as possible. (its maximum value is 5.0 as guided in the design criteria.) It was discussed on the number of the building stories aiming to adjust moment diagram at the hinge mechanism as that in prototype building. Fig. 2 shows the outline of the elevation of test specimen and seismic loading system. Seismic force which is distributed based upon Japanese code: Ai distribution, should be usually applied to each floor level of 15 story building. After the discussion of loading system, the 3 story test building with fourth floor concentrated loading showed almost same moment diagram at hinge mechanism as those in the lower 3 stories part of 15 story building.

In Fig. 2, center hole oil jacks are set on the fourth floor of the test specimen in order to apply permanent permanent axial forces of upper 12 story and temporary axial forces to exterior columns which are transferred from the shear forces of upper story beams corresponding to applied horizontal forces. By the limitation of the capacity of such jacks, finally the scale of test specimen was decided to be two - third model.

### 2. Arrangement of Reinforcement and Materials

Table 1 shows the list of arrangement of column reinforcement. The amount of longitudinal reinforcement along each story beam is uniform in the prototype building. However the lower story beams of test specimen has larger amount of longitudinal reinforcement in order to survey their behaviour in case of high reinforcement. Table 2 shows the list of beams reinforcement. Their longitudinal reinforcement along each story is uniformly same. In these two tables, the

values of  $Q_{su}/Q_{mu}$  mean safety margin factors for shear failure.  $Q_{su}$  is shear failure strength of members calculated from empirical equation recommended by AIJ code.  $Q_{mu}$  is shear force at hinge mechanism of total structure. Such  $Q_{su}/Q_{mu}$  is main parameter in this test building. The values of  $Q_{su}/Q_{mu}$  values in the members are changing from 0.9-1.36.

New design criteria recommended that  $Q_{su}/Q_{mu}$  should be larger than 1.2. However the empirical equation on  $Q_{su}$  is rather conservative i.e. actual shear failure strength of members is larger than the value of  $Q_{su}$ . Therefore the aim of this reduction of  $Q_{su}/Q_{u}$  values is to be surveyed actual relationship of the strength between shear failure and flexural failure. The reduction of such  $Q_{su}/Q_{u}$  has another meaning from the viewpoint of the effect on the multifling factor based upon the higher mode dynamic response.

An average compressive strength of concrete was 260 kg/cm<sup>2</sup>. The longitudinal reinforcing bars, D19 showed 4.1 ton/cm<sup>2</sup>, tensile yielding stress. Other average yielding stresses of D13, D10, D8 and D6 are respectively 3.9 ton/cm<sup>2</sup>, 3.98 ton/cm<sup>2</sup>, 4.2 ton/cm<sup>2</sup> and 3.55 ton/cm<sup>2</sup>.

### 3. Test Procedure

Applied horizontal force is controlled by the measured top-floor horizontal displacement angle ( $R = \delta/h$ ,  $h$ ; top-floor height from first floor.). Such displacement angle  $R$  is planned to be controlled as shown in Fig. 3.

Fig. 4 shows the relationship of applied axial force of exterior columns (Y-axis) to the horizontal force (X-axis). After exceeding the calculated hinge-mechanism force (460.5 ton, -468.1 ton), the axial force of exterior columns were assumed to be constant.

Through this loading, following instrumentation were used and were automatically stored in the computer system.

Horizontal & Vertical Displacement: 168 points  
Strain: 764 points  
Slope angle: 12 points

### 4. Test Results

#### 4.1 Crack Patterns

Hysteresis loops of horizontal shear force

\*1 Director, IISEE, Building Research Institute

\*2 Head, IISEE, Building Research Institute

\*3 Head, Structural Department, Building Research Institute

\*4 Senior Staff, Production Department, Building Research Institute

\*5 Associate Professor, Tokyo Metropolitan University

and top floor lateral displacement is shown in Fig. 5. Fig. 6 is the distribution of horizontal drift in each floor.

The hysteresis loops were very stable until top displacement angle;  $R = 1/65$ . The total shear resistance decreased at  $R = 1/50$  because of shear failure in the center columns. In Fig. 6, the distribution of horizontal displacement is almost linear relationship along each story until the stage of hinge mechanism, however the story drift was concentrated at first story after above mentioned shear failure of center columns first floor.

Fig. 7 a), b), c) and d) show the crack pattern of frames and slab at the final stage;  $R = 1/50$ . Crack development is described as below  
 $R = 1/1600$ ; at beams end, flexural cracks were appeared. at corner of opening in infilled wall diagonal cracks showed.

$R = 1/800$ ; developing above mentioned cracks, appeared diagonal cracks at infilled walls. Transverse walls; lateral cracks at first story.

$R = 1/200$ ; shear cracks at center column first story, infilled wall; shear failure, many flexural cracks on floor slab.

$R = 1/100$ ; compressive failure at bottom end of beams

Finally, shear failure occurred at the center column first story then the bottom of exterior columns subjecting compressive axial forces also showed flexural-compressive failure because of transferring beared shear force to exterior columns from exterior columns.

Fig. 8 shows the progress of crack pattern and failure mode of infilled walls. Diagonal cracks of infilled wall were observed at  $R=1/800$ . Cracks along slit part between columns and infilled wall were appeared at  $R=1/400$ . Then the diagonal cracks developed in their width at  $R=1/200$  and finally shear failure of infilled walls occurred at  $R=1/100$ . Fig. 9 shows crack patterns in B frame infilled wall. It is observed that this type of infilled wall showed typical flexural failure mode until final stage of the test procedure.

#### 4.2 Behaviour of Measured

##### Strains in Reinforcements

Fig. 10 a) and b) show the progress of tensile yielding in longitudinal reinforcements at member ends. Yield hinges were observed at all beams and column base as was expected in the design criteria. The longitudinal reinforcements at joints of beams to infilled walls didn't yield because of shear failure in such infilled walls at earlier stage. The flexural yield at column base, beam bottoms and beam tops were observed respectively at  $R=1/200$ ,  $1/400$  and  $1/200$ .

Fig. 11 shows the yielding progress of anchor reinforcements in infilled walls. The yielding of all anchor reinforcements occurred until  $R=1/400$ .

Fig. 12 is the measured strain distribution of slab top reinforcements. From this tendency, it is estimated that the slab reinforcements are much effective as the top longitudinal reinforcements of T-shaped beams.

Fig. 13 a) and b) are the strain

distributions of first floor's longitudinal reinforcements in flange wall and orthogonal wall respectively. All of longitudinal reinforcements at the flange wall were effective as tensile reinforcements of exterior columns. In the orthogonal wall, the reinforcements within 1/5 of full flange width were effective as tensile reinforcements in center columns.

#### 5. Discussion of Ultimate Shear Capacity

##### 5.1 Assumptions and Conditions for the Calculation of Ultimate Shear Capacity.

It was assumed that yield hinges are occurred at beam and column base then the shear capacity was calculated by virtual work method. General calculation procedure is based upon the "Design Criteria of HFW Building" which was published by Japan Building Center in 1987. It was selected two cases of width on slab and transverse walls for the calculation of ultimate moments considering the test results of strain distribution of longitudinal reinforcements in the transverse members. Furthermore, the axial forces of top floor beams were also taken into account which was occurred only in case of this type of loading system. Input data on materials; strength of concrete and reinforcement for the calculation are used the test values. Table 3 summarizes such calculation conditions for ultimate shear capacity. Fig. 14 shows the moment diagrams at hinge mechanism in four cases of calculation conditions as introduced in Table 3.

##### 5.2 Comparison of Ultimate Strength between Calculation and Test Results

Table 4 shows calculated value and test value of ultimate shear capacity of test specimen. The test value of maximum strength is 578 ton at  $R=1/65$ . Considering horizontal vector of applying axial force at this stage, such maximum value can be reduced to 560 ton and -556 ton. Comparing the test value and the calculated values in Table 4, CASE-2' shows much the same as the test value. The calculated values have two values in positive and negative loading direction. This dues to unsymmetric arrangements of reinforcements in columns C1 and C4. As a characteristics of this specimen, it is unique that the design margin factors for shear failure ( $Q_{su}/Q_u$ ) in some members were smaller than those which is recommended in the new design code. The value,  $Q_{su}/Q_u$  of center columns at the first floor was less than 1.0, whose value is recommended as more than 1.2 in the new code. However these columns did not show shear failure at the hinge mechanism  $R=1/100$ . Such shear failure occurred at  $R=65$ . Table 5 shows the margin factor  $Q_{su}/Q_{mu}$  in which the calculation of  $Q_u$  is not based on the nominal values but also the test values. In any case, the value of  $Q_{su}/Q_{mu}$  is less than 1.0. The reason why shear failure does not occur, although  $Q_{su}/Q_{mu}$  is less than 1.0, is that the empirical equation of  $Q_{su}$ (shear failure strength) is conservative for the test results.

6. Conclusion

- 1) Using 3 story test building it became possible to simulate the hinge mechanism of lower stories of 15 story building due to earthquake loads after the discussion of test plan. By scaling down to 67% of test specimen, observation of the behaviors of beam and slab bottom was so easy.
- 2) The shape of hysteresis loops on the top floor drift was very stable until  $R=1/100$ . The hinge mechanism was also as same as expected design criteria.
- 3) The effect of reducing the margin factor  $Q_{su}/Q_{mu}$  for shear failure was appeared after hinge mechanism;  $R=1/65$ . The center columns ( $Q_{su}/Q_{mu} < 1.0$ ) showed shear failure.
- 4) The infilled walls crushed at  $R=1/200 \sim 1/100$ . Therefore they never gave the drastic change of hinge mechanism of total structure.
- 5) The total hinge mechanism was observed at  $R=1/100$  by yield hinges of all of beam ends and column base.
- 6) From the measurement of strain distribution of longitudinal reinforcements in the transverse members (slabs and flange and orthogonal walls), it was evident that such reinforcement are effective to the calculation of ultimate strength of members.
- 7) Considering that full width of transverse members are effective, the calculated ultimate shear capacity showed exactly as same as that of measured capacity. And it was recognized that the margin factor for shear failure in the design of each member is very important for the safety margin until it's collapse.

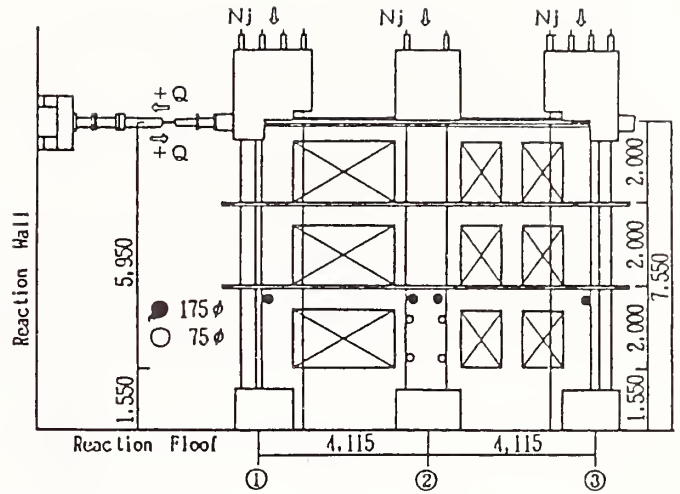
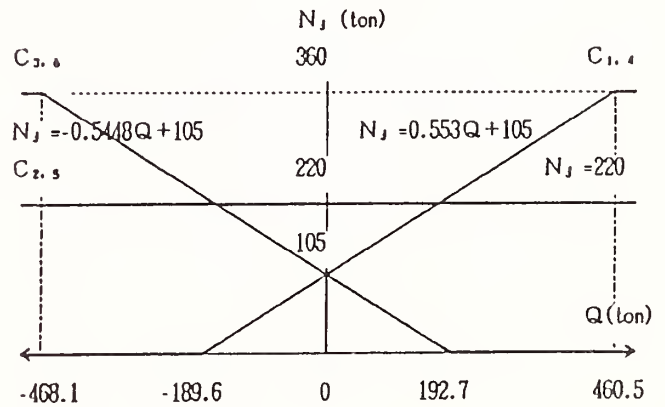


Fig. 2 Elevation of B-frame



$N_j$  : applying axial force/one column  
 $Q$  : horizontal force

Fig. 3 Plan of Load Control

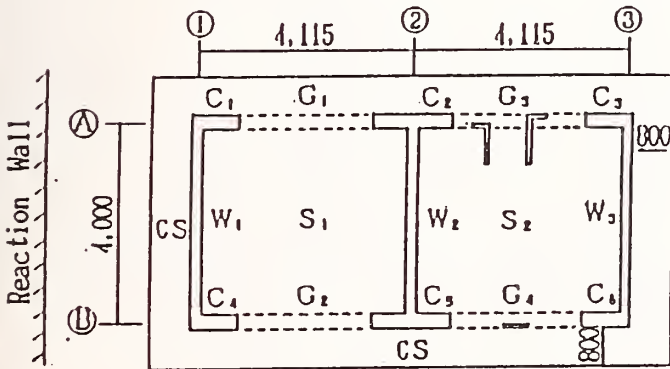


Fig. 1 1 ~3 story plan

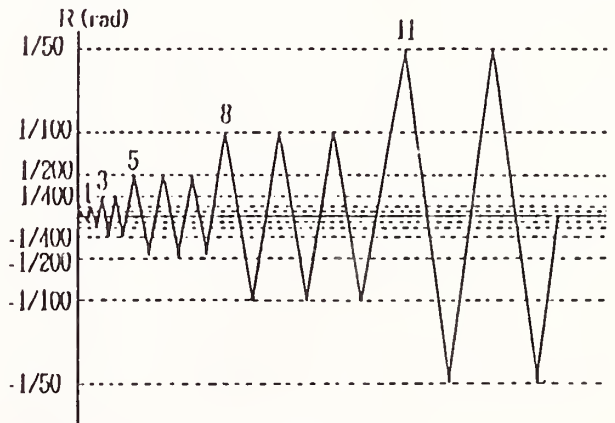


Fig. 4 Relationship of Applied Axial Forces to Applied Horizontal Forces

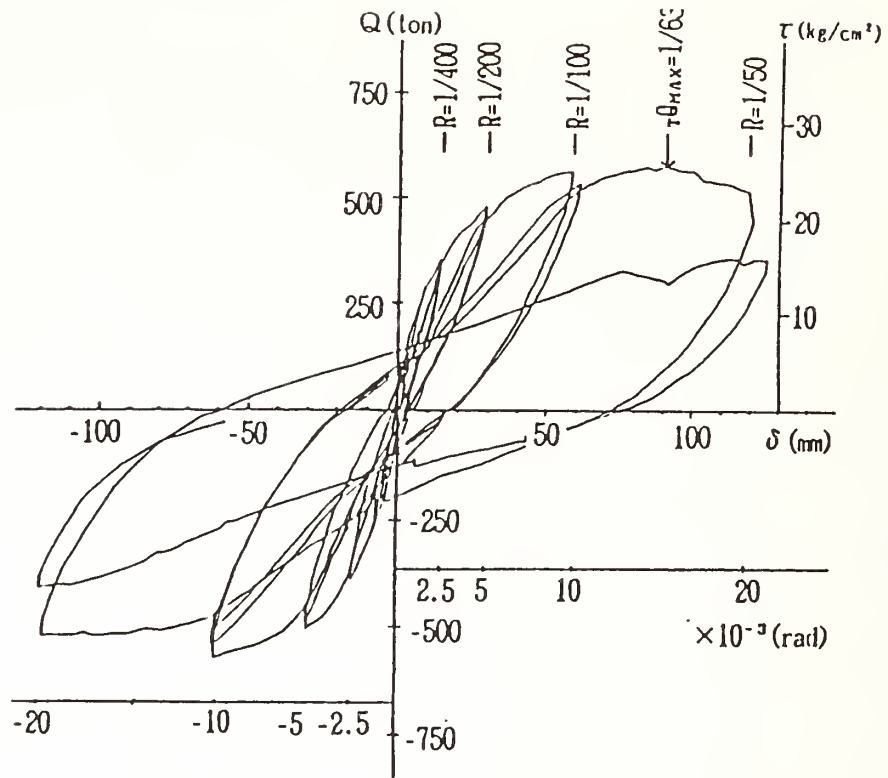


Fig. 5 Hysteresis Loops (Top floor displacement vs total shear force)

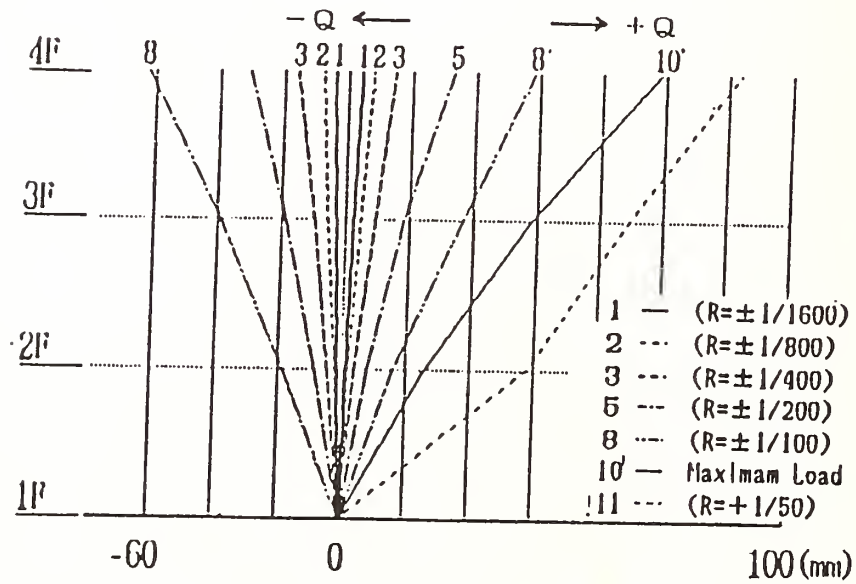
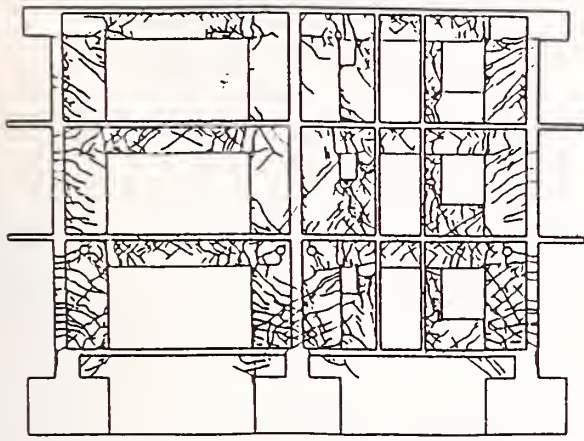
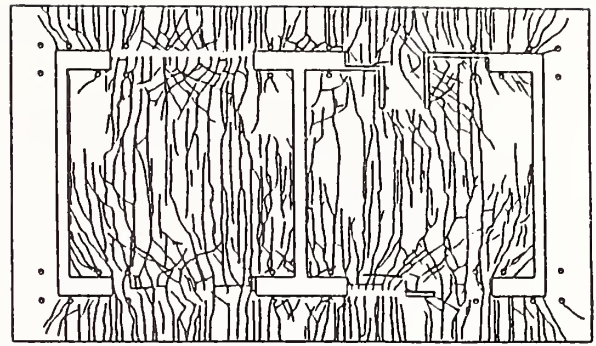


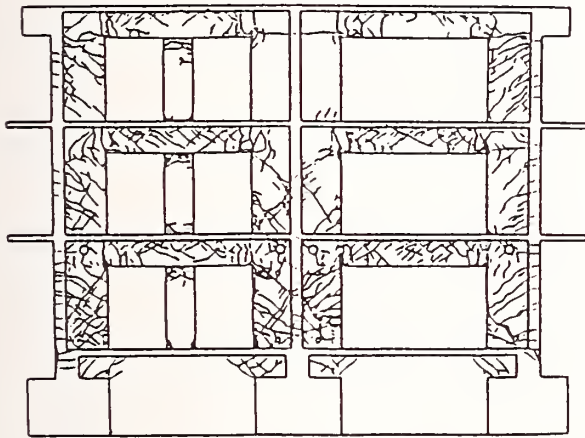
Fig. 6 Absolute Displacement of each story



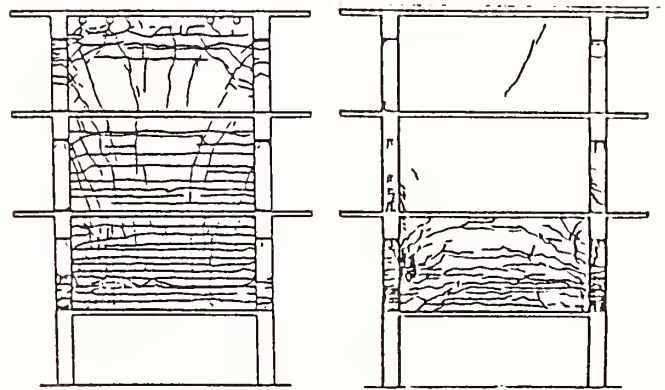
a) A-Frame



c) slab (2 F)

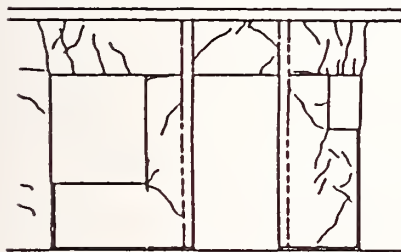


b) B-Frame



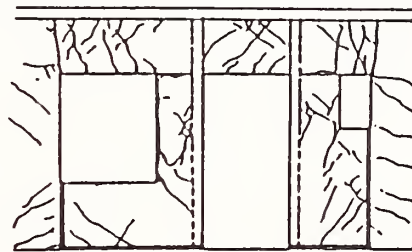
d) Flanre Wall and Orthogonal Wall

Fig. 7 Crack Pattern at Final Stage



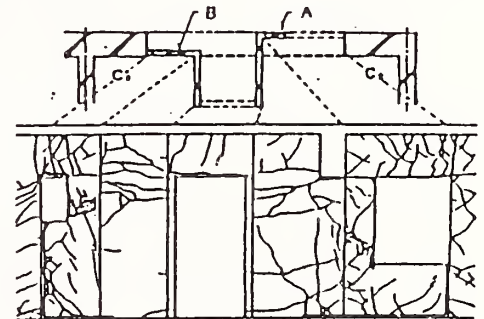
R=1/400

a)

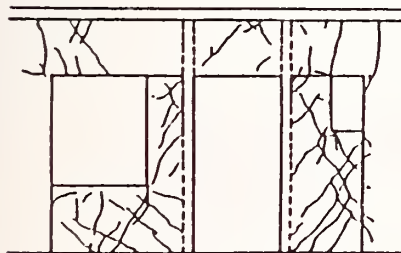


R=1/200

1 F

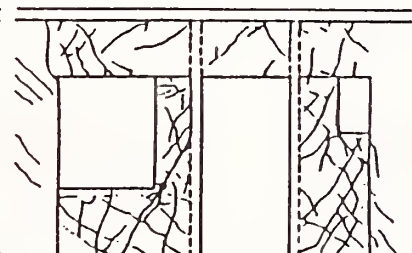


(1 F)



R=1/400

b)



R=1/200

2 F



(2 F)

c)

R=1/50

Fig. 8 Crack Pattern of Infilled Wall (A Frame)

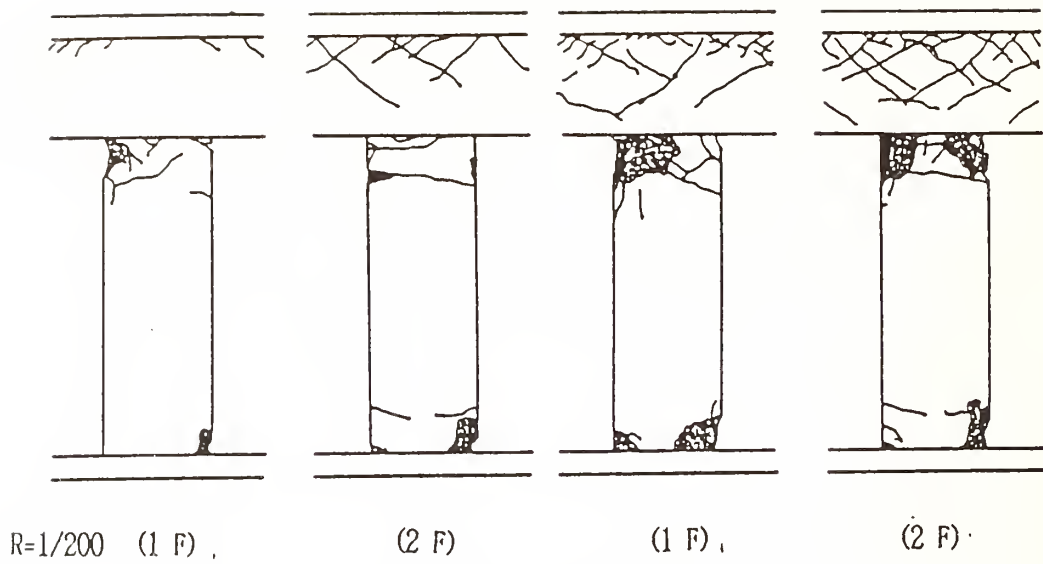


Fig. 9 Crack Pattern of Infilled Wall (B Frame)

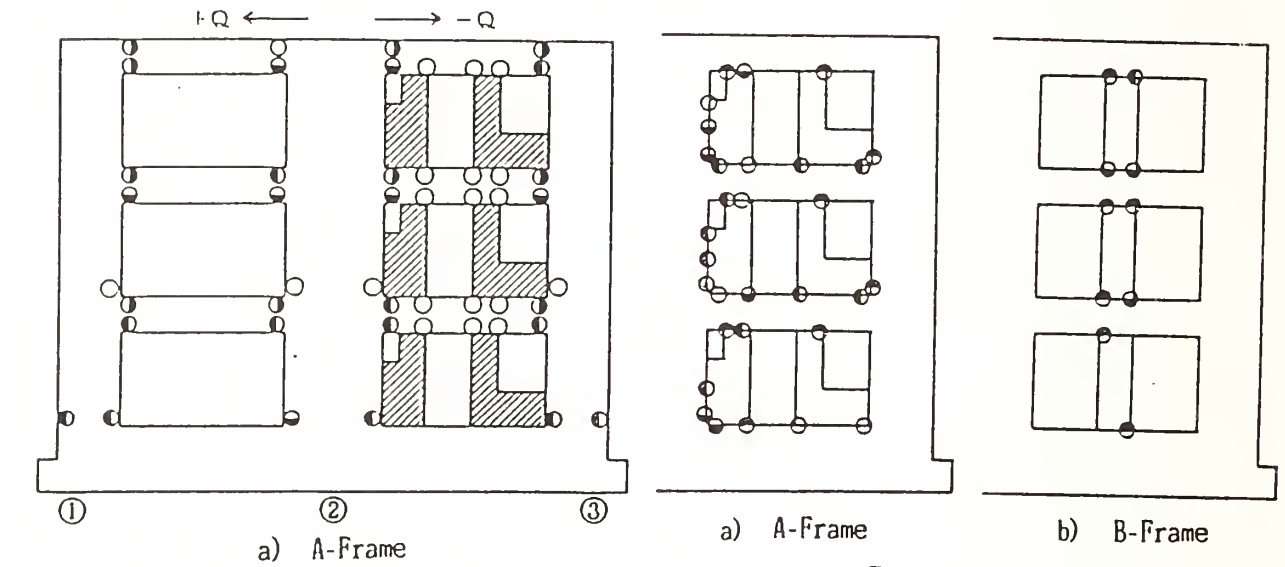


Fig. 11 Ilige Mechanism Procedure (2)

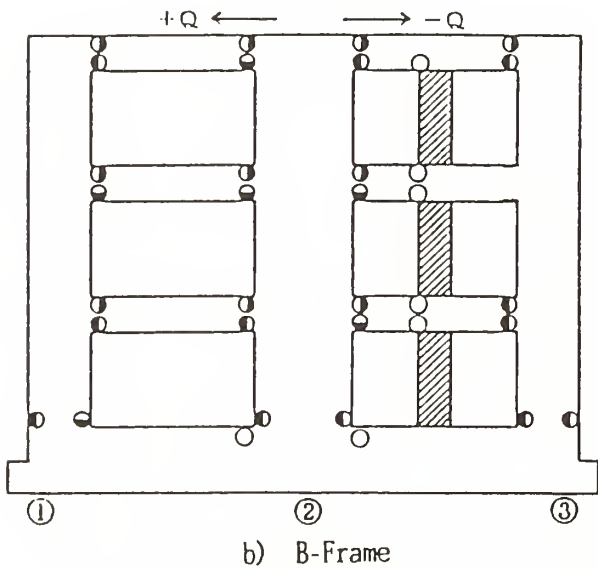


Fig. 10 Ilige Mechanism Procedure (1)

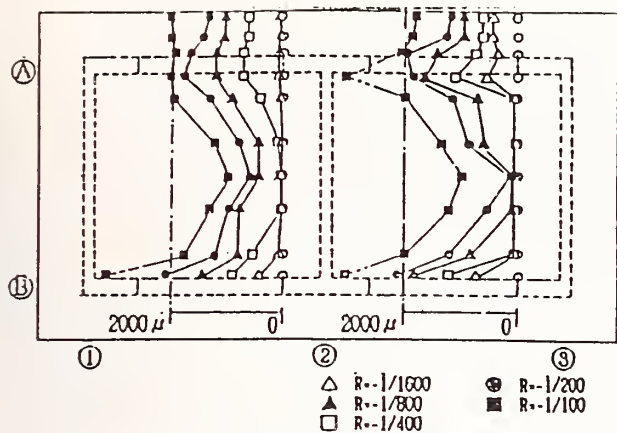
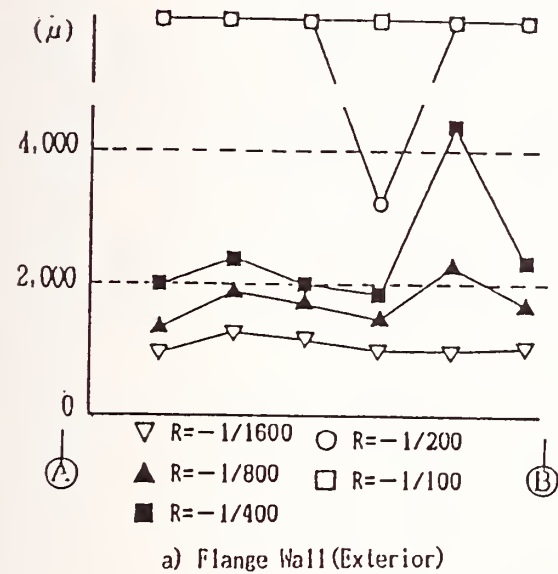
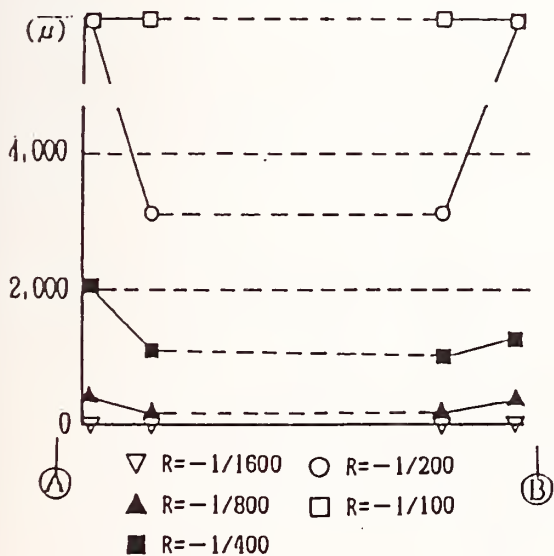


Fig. 12 Strain Distribution of Slab Top Reinforcement (2 F)

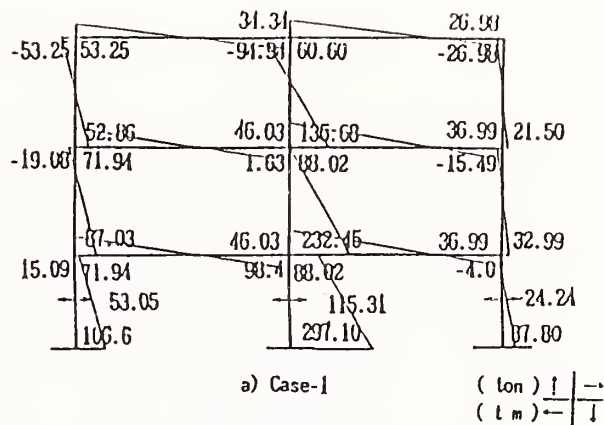


a) Flange Wall (Exterior)

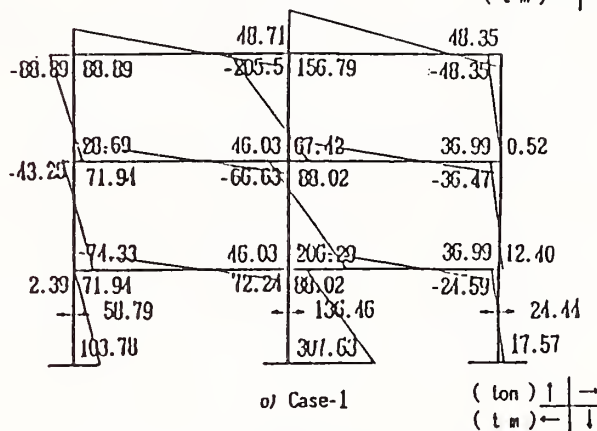


b) Orthogonal Wall (Inner)

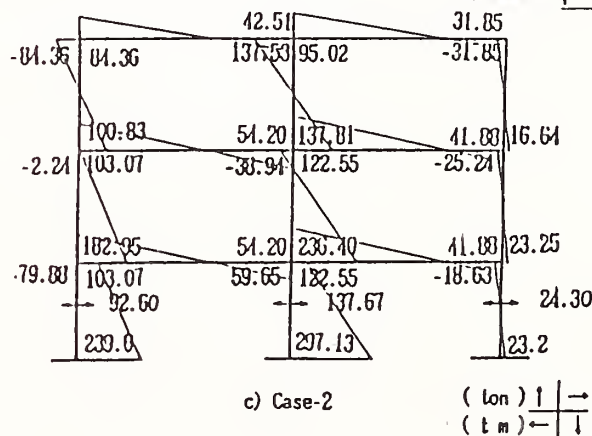
Fig. 13 Strain Distribution of Longitudinal Reinforcement at Transverse Walls



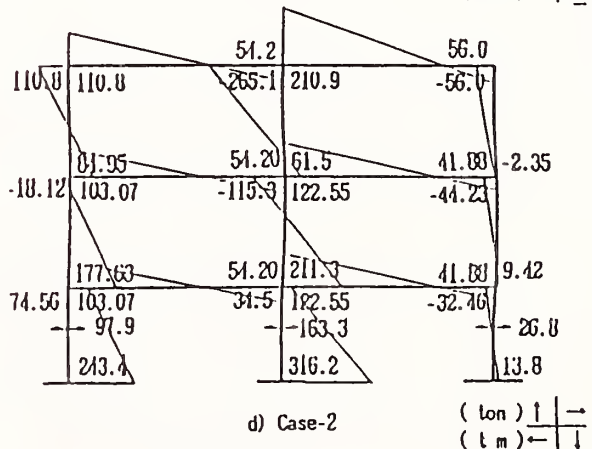
a) Case-1 (lon) ↑ ↓ (tm) ← →



b) Case-1 (lon) ↑ ↓ (tm) ← →



c) Case-2 (lon) ↑ ↓ (tm) ← →



d) Case-2 (lon) ↑ ↓ (tm) ← →

Fig. 14 Moment Diagram at Hinge Mechanism

Table 1 List of Beams

FL	Position	G <sub>1</sub>			G <sub>2</sub>			G <sub>3</sub> , G <sub>4</sub>		
		E.E.	Center	I.E.	E.E.	Center	I.E.	E.E.	Center	I.E.
4	Top	3- D19	3- D19	3- D19	3- D19	3- D19	3- D19	3- D19	3- D19	3- D19
	Bottom	3- D19	3- D19	3- D19	3- D19	3- D19	3- D19	3- D19	3- D19	3- D19
	Stirrup	3-D13@50			3-D13@50			3-D13@50		
	Q <sub>su</sub> /Q <sub>mu</sub>	1.36			1.36			1.36		
	Pt(%)	0.52		0.52	0.52		0.52	0.52		0.52
	Pw(%)	2.31		2.31	2.31		2.31	2.31		2.31
3	Top	6- D19	3- D19	6- D19	6- D19	3- D19	6- D19	6- D19	3- D19	6- D19
	Bottom	4- D19	3- D19	4- D19	4- D19	3- D19	4- D19	4- D19	3- D19	4- D19
	Stirrup	2-D8@80			E.2-D8@40 C.2-D8@80			2-D8@80		
	Q <sub>su</sub> /Q <sub>mu</sub>	0.95			1.15			1.15		
	Pt(%)	1.04		1.22	1.04		1.22	1.04		1.22
	Pw(%)	0.38		0.38	0.76	0.38	0.76	0.76		0.76
2	Top	6- D19	3- D19	6- D19	6- D19	3- D19	6- D19	6- D19	3- D19	6- D19
	Bottom	4- D19	3- D19	4- D19	4- D19	3- D19	4- D19	4- D19	3- D19	4- D19
	Stirrup	2-D8@40			2-D8@60			2-D8@40		
	Q <sub>su</sub> /Q <sub>mu</sub>	1.15			1.02			1.15		
	Pt(%)	1.04		1.22	1.04		1.22	1.04		1.22
	Pw(%)	0.76		0.76	0.51		0.51	0.76		0.76

\*B330×D550 (mm)

Table 2 List of Columns

	C <sub>1</sub>	C <sub>2</sub>	C <sub>3</sub>	C <sub>4</sub>	C <sub>5</sub>	C <sub>6</sub>
B × D	330 × 930	330 × 1560	330 × 930	330 × 930	330 × 1560	330 × 930
Main Reinforcement	6-D19	10-D19	8-D19	6-D19	10-D19	8-D19
	8-D10	18-D10	8-D10	8-D10	18-D10	8-D10
Hoop	D8- □@65	D8- □@65	D8- □@65	D6- □@65	D6- □@65	D6- □@65
Pt (%)	0.37 0.19	0.28	0.37	0.37 0.19	0.28	0.37
Pg (%)	0.75	0.81	0.93	0.75	0.81	0.93
Pw (%)	0.46	0.46	0.46	0.30	0.30	0.30
Q <sub>su</sub> /Q <sub>mu</sub>	1.36	1.00	1.24	1.27	0.91	1.16

\* sub-tie : same size, pitch as hoops

Table 3 Condition for calculation of Ultimate Capacity

	Beam Axial Force	effective width		
		slab	bay Wall	
Case-1	ignor	guide*1	guide*2	be = 1.2b
Case-1	consider	guide*1	guide*2	
Case-2	ignor	full width	full width	be = b + λ
Case-2	consider	full width	full width	be = b

\*1 ; 67cm

b; width of column

\*2 ; 92cm

λ; effective width

$$N_{max} = be D f_c + \Sigma a_g \sigma_y$$

$$N_b = 0.22 (1 + R_1) be D f_c$$

$$N_{min} = -\Sigma a_g \sigma_y$$

$$N_{max} \geq N > N_b$$

$$M_u = (0.5 \Sigma (a_g \sigma_y) R_1 D + 0.024 (1 + R_1) (3.6 - R_1) be D^2 f_c) \frac{N_{max} - N}{N_{max} - N_b}$$

$$N_b \geq N \geq 0$$

$$M_u = 0.5 \Sigma (a_g \sigma_y) R_1 D + 0.5 N D (1 - N / be D f_c)$$

$$0 > N > N_{min}$$

$$M_u = 0.5 \Sigma (a_g \sigma_y) R_1 D + 0.5 N R_1 D$$

Table 4 Comparison of Ultimate Shear Capacity

(+) / (-)	Calculation				Test (Q <sub>T</sub> )
	Case-1	Case-1'	Case-2	Case-2'	
Q <sub>c</sub>	385 t	439 t	509 t	576 t	560 t
Q <sub>T</sub> /Q <sub>c</sub>	1.45	1.28	1.10	0.97	
(-)	Calculation				Test (Q <sub>T</sub> )
	Case-1	Case-1'	Case-2	Case-2'	
Q <sub>c</sub>	391 t	446 t	510 t	579 t	556 t
Q <sub>T</sub> /Q <sub>c</sub>	1.42	1.25	1.09	0.96	

Table 5 Safety Margin for Shear Failure of Inner Columns (1 FL)

Q <sub>SU</sub> /Q <sub>MU</sub>	Case-1'		Case-2'	
	(+)	(-)	(+)	(-)
1 C <sub>2</sub>	0.98	0.97	0.87	0.87
1 C <sub>5</sub>	0.87	0.87	0.78	0.78

# Safety Analysis on the Vertical Bearing Capacity of Piles

BY

Hiroshi Shinohara<sup>1</sup>, Michio Okahara<sup>2</sup>  
Shouichi Nakatani<sup>3</sup>, Keiji Taguchi<sup>4</sup>

## ABSTRACT

Many formulas in predicting vertical bearing capacities of piles have been developed and used for practical designs. As for pile foundations of bridges, practical formulas for bearing capacities are prescribed in the Japanese Specifications for Highway Bridges published in 1980. It is known, however, that the values predicted by these formulas may at times give poor approximations. Thus in-situ loading tests have been made to determine bearing capacities since the values obtained from these tests are more reliable than those given by some formulas. However, it is not feasible to perform full scale loading tests of piles prior to construction for every case of foundations.

For the purpose of developing more reliable methods to evaluate vertical bearing capacities of piles a large number of data from full scale load tests conducted in the sites to public works are collected by the P.W.R.I. (Public Works Research Institute, Ministry of Construction, Japan) and data analysis has been done using the safety index  $\beta$ . Also referred is to the safety of the pile bearing capacities based on practical formulas in this study.

KEY WORDS: Vertical bearing capacity of piles, In-situ loading tests, Reliability analysis

## 1. INTRODUCTION

The design of bridge foundations has been done through the Specifications for substructures of Highway Bridges. The revised edition of these Specifications has supposed to be published in 1988. Since the current design method, allowable stress design method, is going to proceed to the ultimate state design method in 1995, the reliability analysis should be applied to all over the practical design field.

From this view point, the first probability approach to identify the safety of piles constructed by various kinds of piling methods is being taken into consideration in the coming Specifications.

This paper says on the characteristics of bearing capacity on the basis of the analysis through a large number of

vertical loading tests which were collected by the P.W.R.I. Also this paper refers to some correction coefficients which are derived to identify the safety against each piling method by making reliability analysis. The paper focusses on the followings:

- 1) Load-settlement characteristics of actual piles and the vertical spring constant at the pile head,  $K_v$ .
- 2) The rate of allotment between end bearing capacity and skin friction force for different piling methods.
- 3) The comparison of safety of each pile using probabilistic models.

## 2. ESTIMATION OF BEARING CAPACITY BASED ON THE RESULTS FROM IN-SITU LOADING TESTS

520 in-situ loading tests on piles are compiled from all over Japan. From among them, 157 examples are picked up corresponding to bearing piles and 52 examples corresponding to friction piles, respectively. Fig. 2.1 and Fig. 2.2 show the relations between diameter,  $D$  and length,  $L$  in piles for both bearing and friction piles. Any auger piles used as friction piles are not found among the above mentioned data.

The results from in-situ loading tests are divided into two kinds: one case that vertical loads are applied up to the ultimate bearing capacity  $R_u$ , (labeled by  $R_u$ -data) and the other case that loads are up to the yield bearing capacity  $R_y$ , (labeled by  $R_y$ -data). The ultimate bearing capacity is estimated as vertical loads corresponding to settlement at the pile head which is equal to 10% of the

1. Director, Structure & Bridge Department, Public Works Research Institute, Ministry of Construction, Japan.

2. Head, Foundation Engineering Division, Structure & Bridge Department, Public Works Research Institute, Ministry of Construction, Japan.

3. Research Engineer, Foundation Engineering Division, structure & Bridge Department, Public Works Research Institute, Ministry of Construction, Japan.

4. Foundation Engineering Division, Structure & Bridge Department, Public Works Research Institute, Ministry of Construction, Japan.

diameter of piles .

Since there are some errors in determination of  $R_y$ , the observed relation between  $R_{u10}/R_y$  and  $S_y/D$  ( $S_y$ : the settlement at pile heads corresponding to  $R_y$ ) is compared with the theoretical curve through the Weibull distribution curve, which was proposed by K. Uto et al., for theoretically estimating the value of  $R_y$ . According to the Weibull distribution curve, load  $R$  - settlement  $S$  curve is expressed by Eq(2.1).

$$R = Ru(1 - \exp(-(S/S_y)^m)) \text{ ----- (2.1)}$$

The comparison is shown in Fig. 2.3 where the theoretical curves are plotted as a parameter,  $m$  defined as the displacement index. Fig. 2.3 indicates many observers give some bigger amount of estimation against  $R_{y2}$  determined through the Weibull distribution curve. A lot of values of  $R_{u10}$ 's are required to compute the reliability of bearing capacity.  $R_{u10}$ 's could, however, be inferred from  $R_{y1}$ 's given by observers. For this purpose, the ratio of  $R_{u10}$  to  $R_{y1}$ ,  $\alpha$  is detected from the ratio of  $R_{y2}$  determined through the Weibull distribution curve to  $R_{y1}$  for SPP (Steel pipe pile) as shown in Fig. 2.4 and the theoretical ratio between  $R_{u10}$  and  $R_{y2}$ . Consequently, we obtain  $\alpha = 1.50$  as the average value for most of the piles except auger piles and  $\alpha = 1.35$  for auger piles.

### 3. SETTLEMENT CHARACTERISTICS OF PILES

#### 3.1 Load-settlement curves of piles

If experimental data are simulated by the Weibull distribution curve, the normalized settlement  $S / D$  versus the normalized resistance  $R / R_u$  relation can be classified into five kinds of curves as shown in Fig. 3.1. The values of  $S / D$  or  $S_y / D$  at  $R / R_u = 0.63$  are 2, 1.5 and 4.5% for bearing (except for auger piles), friction and auger piles respectively and the normalized settlement of friction piles is relatively less than that of bearing piles. Fig. 3.1 also indicates that as for auger piles the large value of  $S / D$  is required to arrive at ultimate bearing capacity in comparison with the other piling methods.

#### 3.2 Vertical spring constant, $K_v$

The vertical spring constant,  $K_v$  in conventional use has before been obtained as the secant gradient (modulus) in the  $R$  versus  $S$  curve corresponding to  $S = 1$  cm. In a word  $K_v$  is defined in the elastic range. As known by Fig. 3.1, however, the value of  $S = 1$  cm should have different meanings for different diameters of piles. From this point of view, three kinds of  $K_v$ 's at  $S=1$  cm,  $S=1\%$  of  $D$  and  $S=S_y$  are considered. Through the above data analysis

$K_v$  obtained by  $R_y/S_y$  is concluded to have the best rationality in practical design compared with other  $K_v$ 's. The coefficients,  $\alpha$ 's obtained by Eq (3.1) are listed Table 3.1.

$$\alpha = \frac{K_v \cdot L}{A_p \cdot E_p} \text{ --- (3.1)}$$

where  $A_p$  : Net cross section of a pile

$E_p$  : Elastic modulus of pile body

The relation between  $\alpha$  and  $L/D$  in case of SPP is illustrated in Fig. 3.2. There is no difference in this analysis between bearing and friction piles. Fig. 3.3 shows the correlation between measured and calculated values of  $K_v$ 's for all the kinds of piles as shown in Table 3.1.

### 4. CHARACTERISTICS OF BEARING CAPACITY IN PILES

#### 4.1 Relation between skin friction and end bearing capacity

$\lambda$  is defined here as the ratio of end bearing capacity to total bearing capacity. The measured  $\lambda$  is compared with the calculated  $\lambda$  at  $R_{u10}$  for both SPP and CCP (Cast in-situ Concrete pile) in Fig. 4.1. The value of  $\lambda$  depends upon the diameter and length of piles and characteristics of grounds around and beneath piles. In case of CCP,  $\lambda$  broadly distributes from 20% to 60% but both  $\lambda$ 's could be in good agreement with each other. On the other hand, the calculated values for SPP are not always fitting with the measured values though almost all of calculated values are in nearly 50% to 60%. In Fig. 4.2 is shown the comparison between both  $\lambda$ 's for auger piles. As for auger piles, both  $\lambda$ 's seem to be fitting with each other. Judging from the fact that the values of  $\lambda$ 's for auger piles ranges from 40 to 80%, it is concluded that the bearing capacity of auger piles largely relies upon the end bearing capacity. As for skin friction,  $R_f$  and end bearing capacity,  $R_p$ , on Fig. 4.3 are plotted the measured to calculated value ratios of  $R_{f1}/R_{fn}$  and  $R_{p1}/R_{pn}$  for each piling method based on  $R_u$ -data. This result endorses the above-mentioned consideration. In other words, in some cases of SPP, the measured end bearing capacity is less than the calculated. On the contrary, in case of CCP there is good consistency between measured and calculated bearing capacities at pile heads.

#### 4.2 Characteristics of bearing capacity in friction pile

According to the current Specifications of Highway Bridges, any piles which are penetrated into good bearing layers (sand and gravel layers with  $N$ -value of approximately more than 30 and clay layer

with N value approximately more than 20) are classified into bearing piles and the rest are into friction piles.

Fig. 4.4 shows the bearing capacity ratio  $R_1/R_n$  for each piling method with regard to N-values at the pile-end stratum. In calculations, end bearing capacity is neglected but observed bearing capacity includes it. In Fig. 4.5 are compared the relations between the length of piles and the ratio of  $\lambda_1$  for both bearing piles and friction piles each other. The value of  $\lambda_1$  for friction piles is smaller than one of bearing piles and decreases with the increasing length of piles while the value of  $\lambda_1$  for bearing piles remains constant and it seems to have nothing to do with the pile length in the region of  $\lambda_1=30\%$ .

##### 5. RELIABILITY OF BEARING CAPACITY FOR EACH PILING METHOD

In general, the estimation of ultimate bearing capacity of piles is done by the bearing capacity formulas prescribed to each piling method. Unfortunately, however, the quantitative evaluation has not been made on whether or not each corresponding formula would give the identical safety to piles by different piling methods. Through the reliability analysis the authors propose the correction coefficient  $\gamma$ , in order that each formula has the identical safety in estimation of the bearing capacity of piles. This coefficient is given by Eq (5.1).

$$r = \frac{3\bar{P}}{\exp(\beta_T \sqrt{V_R^2 + V_S^2})} \quad \text{--- (5.1)}$$

- where  $\bar{P}$  : mean value of bearing capacity ratio  $P$ , ( $=R_1/R_n$ )  
 $\beta_T$  : safety index  $\beta$ (driving pile)  
 $V_R$  : coefficient of variation of bearing capacity,  $R$   
 ( $= \sqrt{V_p^2 + 2 \times 0.15^2}$ )  
 $V_P$  : coefficient of variation of bearing capacity ratio  $P$ , ( $=R_1/R_n$ )  
 $V_S$  : coefficient of variation of load ( $= 0.10$ )

In addition, ultimate bearing capacity is evaluated by the model proposed by M. Okahara(1979). The results from analysis through these equations are shown in Table 5.1 and Fig. 5.1 with indication that the correction coefficient,  $\gamma$ , increases with the increasing value of  $P$  and the decreasing value of  $V_P$ . It is assumed here that the value of  $\gamma$  for driving pile (bearing pile) is unity.

##### 6. CONCLUSIONS

The following conclusions have been drawn from the study using a large

number of in-situ tests with every type of piles and every piling method.

1) The ultimate and yield bearing capacities of tests vary widely depending upon observers .

2) The ultimate bearing capacity is defined to be the pile head load corresponding to the settlement at 10% of a pile diameter. This definition has already been adopted in a few design standards or specifications in Japan.

3) The  $R/R_u$  versus  $S/D$  curves are approximately classified into 5 kinds for each piling method and each supporting type of piles.

4) The  $K_v$  value which is used for stability analysis of pile foundations should be determined from the secant modulus at yielding rather than the one corresponding to  $S = 1$  cm.

5) The method which has currently been adopted in the Japanese specification for Highway Bridges in evaluating bearing capacity, is likely to underestimate the skin friction and overestimate end bearing capacity for SSP. On the contrary, estimates seem to be proper in cases of CCP and auger piles.

6) There is no problem to use the conventional design method for friction piles. In this case ,however, end bearing capacity should be neglected.

7) The length of piles should be more than 20 to 30m if those piles are used as friction piles in order to prevent excess settlements.

8) Regarding to the proposed correction coefficient  $\gamma$ , this coefficient  $\gamma$  of cast in place and auger piles is 10 to 20% higher than of driving end-bearing piles. The coefficient  $\gamma$  of friction piles is 1.4 to 2.0 times as higher as that of driving end-bearing piles.

##### REFERENCES

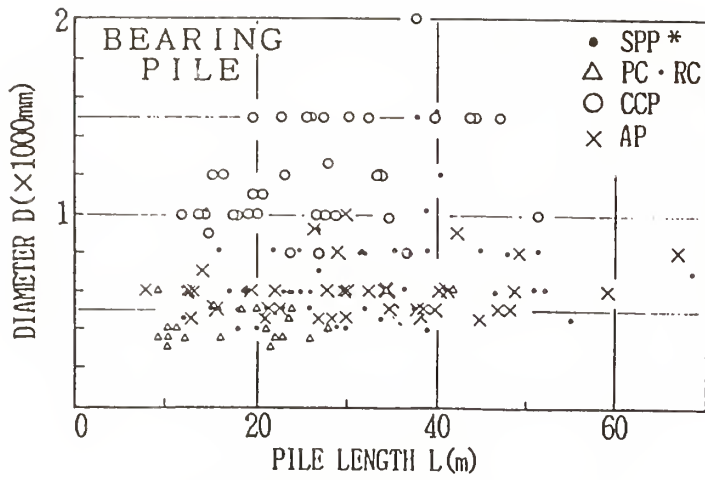
- 1) Shioi, Y, Okahara, M (1979) : Safety Evaluation for Bearing Capacity of Piles in load and Resistance Factor Design Criteria, Journal of Research, vol 20.

Table 3.1 Relation between coefficient  $a$  and  $L/D$

KINDS OF PILES	COEFFICIENT $a$
SPP	$0.016(L/D) + 0.99$
PC·RC	$0.012(L/D) + 0.51$
CCP	$0.041(L/D) - 0.36$
AUGER(PC)	$0.009(L/D) + 0.31$
AUGER(SPP)	$0.009(L/D) + 0.49$

Table 5.1 Summary of bearing capacity ratio, coefficient of variation and correction coefficient for each piling methods

	BEARING PILE			FRICTION PILE	
	DRIVEN	CAST IN-SITE	AUGER	DRIVEN	CAST IN-SITE
NUMBER OF SAMPLE $n$	76	38	43	36	16
BEARING CAPACITY RATIO $R_1/R_n$	0.914	1.051	1.216	1.836	1.079
COEFFICIENT OF VARIATION $V_p$	44%	40%	46%	42%	36%
CORRECTION COEFFICIENT $\gamma$	$\bar{\beta} \approx 2.0$	1.24	1.32	2.08	1.37



\* SPP: STEEL PIPE PILE  
 PC·RC: (PRESTRESSED) CONCRETE PILE  
 CCP: CAST IN-SITU PILE  
 AP: AUGER PILE

Fig. 2.1 Relation between diameter and length

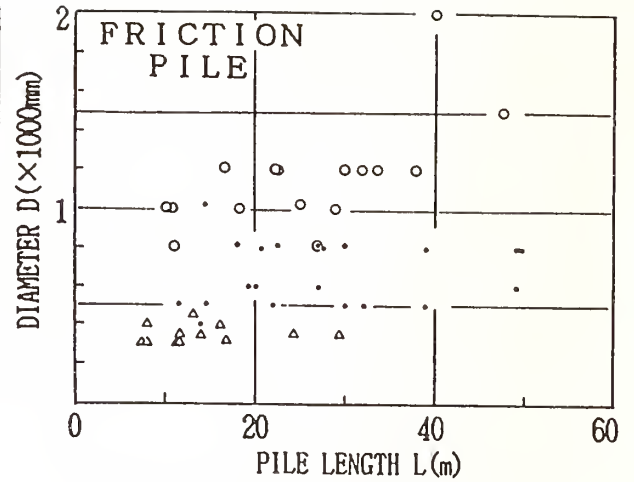


Fig. 2.2 Relation between diameter and length

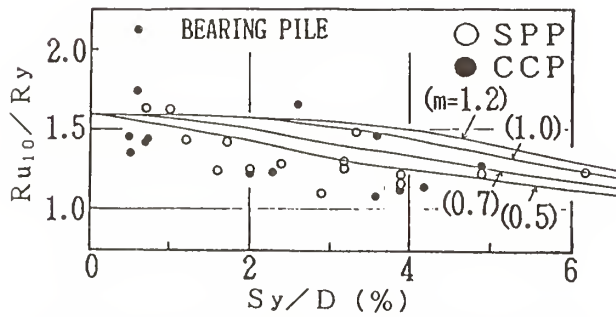


Fig. 2.3 Comparison of  $R_{u10}/R_y$  versus  $S_y/D$  curves and measured values.

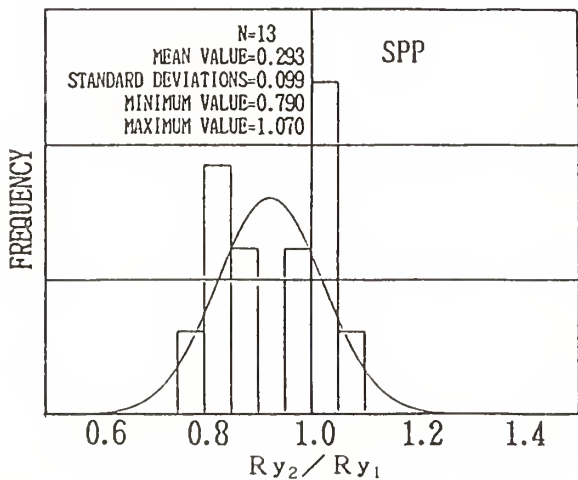


Fig. 2.4 Frequency of the ratio of  $R_{y2}/R_{y1}$

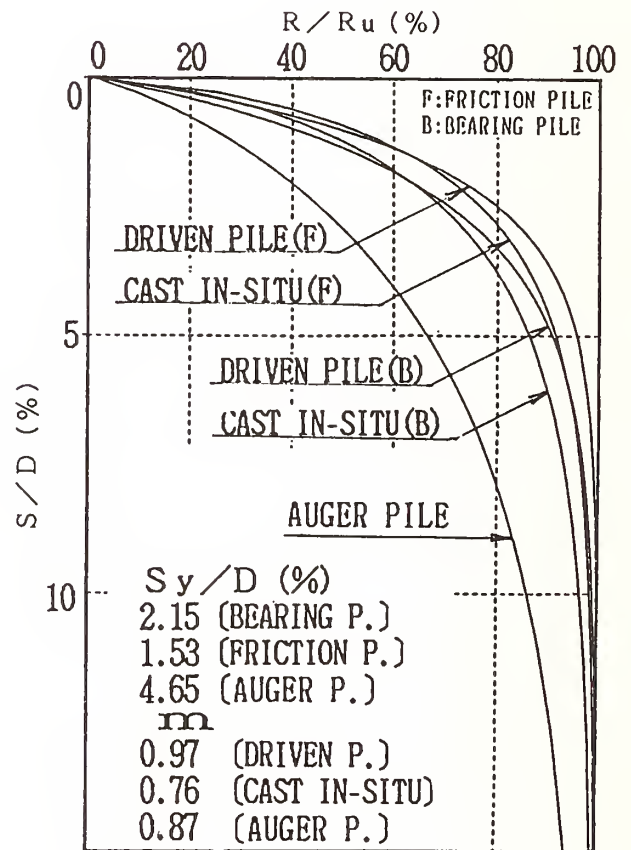


Fig. 3.1  $R/R_u$  versus  $S/D$  curves for each piling methods.

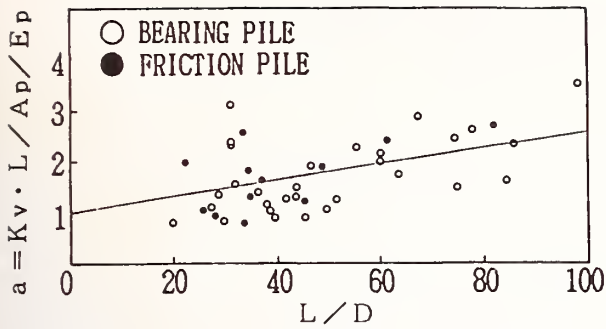


Fig. 3.2 Relation between coefficient,  $a$  and piles penetration ratio  $L/D$ .

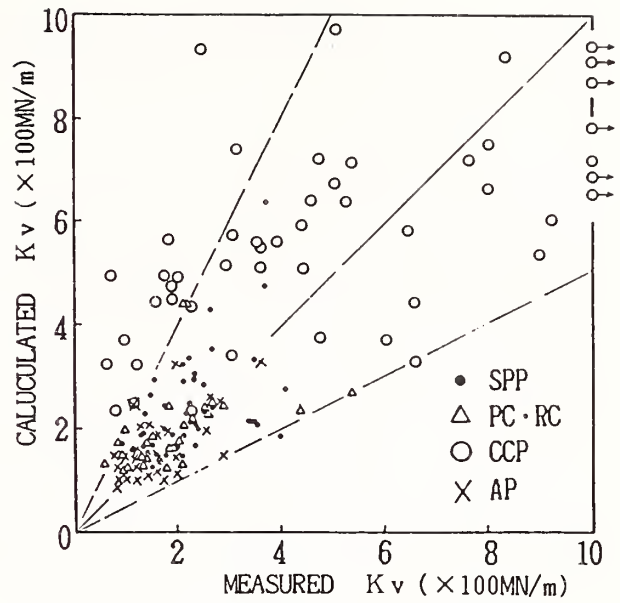


Fig. 3.3 Comparison of measured and calculated values of  $K_v$ .

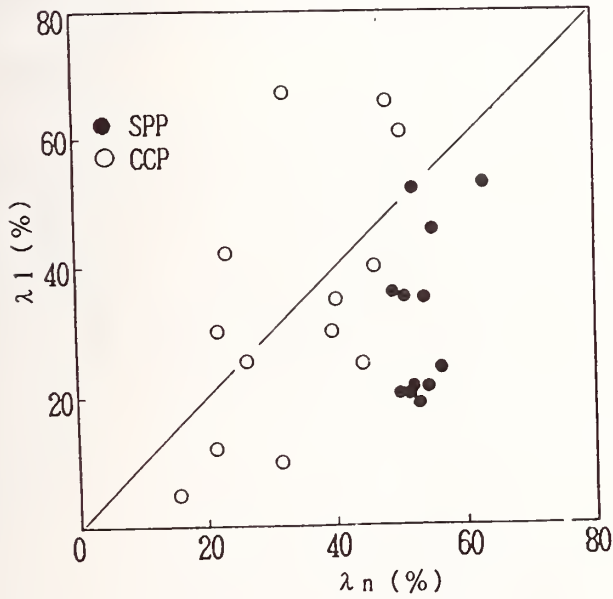


Fig. 4.1 Comparison of measured  $\lambda_1$  and calculated  $\lambda_n$  for SPP and CCP.

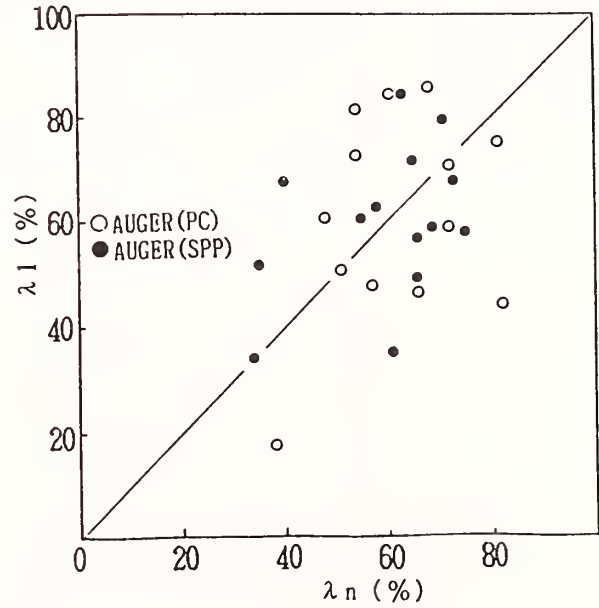


Fig. 4.2 Comparison of measured  $\lambda_1$  and calculated  $\lambda_n$  for Auger piles.

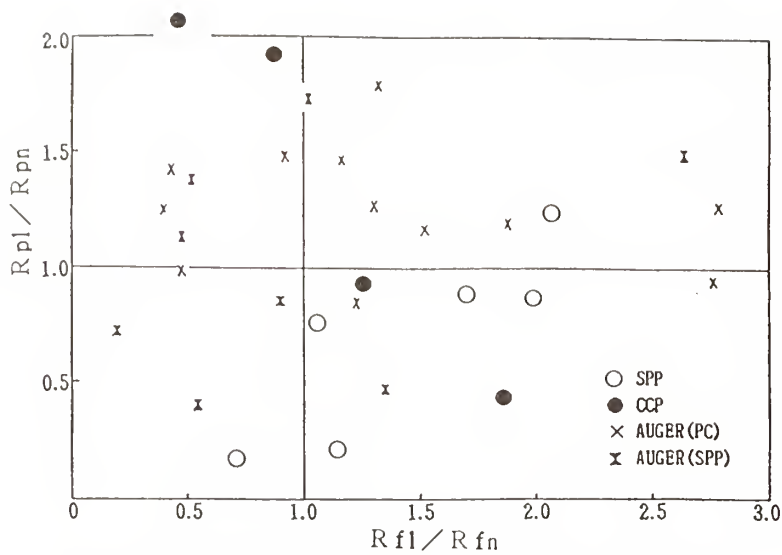


Fig. 4.3 Relation between  $R_{pl}/R_{pn}$  and  $R_{fl}/R_{fn}$

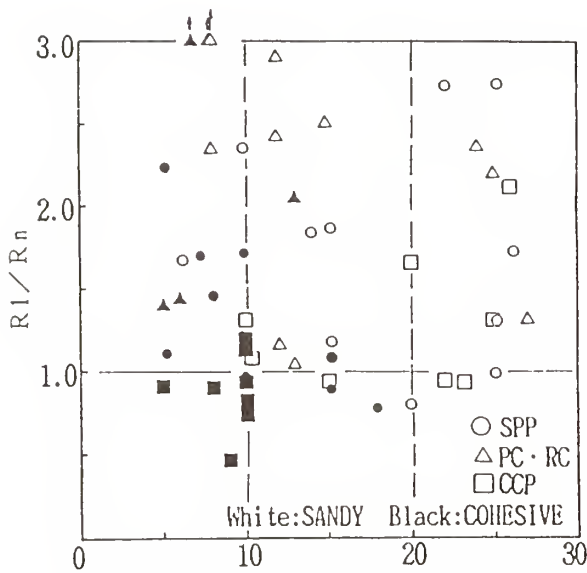


Fig. 4.4 Relation between  $R_I/R_n$  and N-value at pile-end stratum.

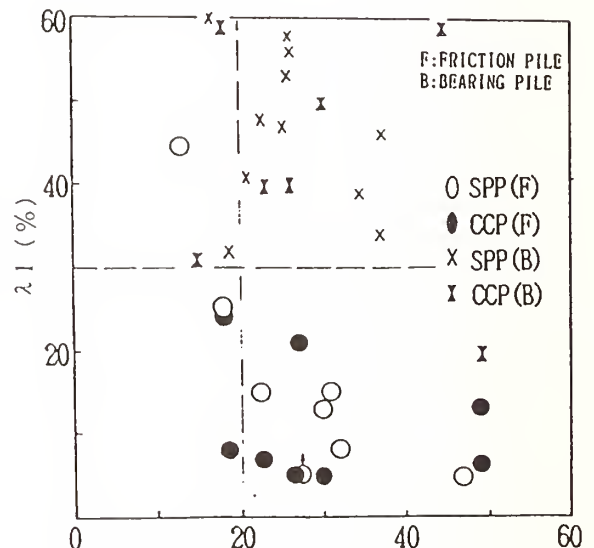


Fig. 4.5 Relation between measured  $\lambda_1$  and pile length.

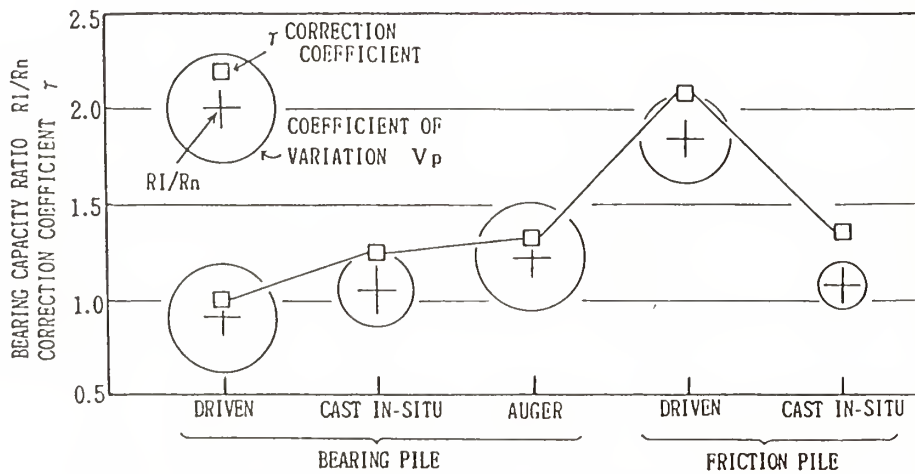


Fig. 5.1 Comparison of bearing capacity ratio and correction coefficient for each piling methods.

# Model Shaking Table Tests on Seismic Resistance of Reinforced Embankment (Part 2)

BY

Yasuyuki Koga<sup>1)</sup>, Yoshihiro Ito<sup>2)</sup>, Shuzo Washida<sup>3)</sup> and Takao Shimazu<sup>3)</sup>

## ABSTRACT

This paper presents a series of model shaking table tests on the seismic resistance of embankments on inclined ground reinforced with a few kinds of reinforcing element and their seismic stability analyses.

It was shown from 14 cases of model shaking table tests of embankments reinforced with nonwoven fabrics, plastic nets and steel bars, that the seismic resistance of an embankment is increased if a reinforcing element of high tensile stiffness is used to anchor the embankment to the bed slope. The local failure of the fill slope surface must also be prevented by an appropriate protection work. Moreover, the damage degree of embankments agreed well with calculation results by a circular slip surface method which considers the effect of the tensile force of reinforcing element.

## KEY WORDS:

Embankment, Seismic resistance, Reinforcement, Geotextile, Shaking table test

## 1. INTRODUCTION

The seismic resistance of embankments is greatly influenced by the characteristics of the fill proper and foundation. The resistance of the fill proper can be improved by reducing the slope gradient or protecting the slope with retaining wall, etc. Besides, embankments reinforced with geotextile or steel plates, etc. have recently attracted wide interest. PWRI has been performing a comprehensive research program of the utilization of geotextiles for earthworks.

The evaluation of the effect of geotextile or other reinforcing elements on the seismic resistance of embankments is an important issue in such a country with high seismicity as Japan. The effect of the geotextile on the seismic resistance of embankments has been investigated by model shaking table tests and the first report was presented in the 18th UJNR meeting (1). This paper presents a seismic effect of reinforcement with geotextile and steel bar on the embankments constructed on an inclined ground by a series of model shaking table tests and their stability analyses.

## 2. MODEL SHAKING TABLE TEST(2)

### 2.1 Shaking table

One of the shaking tables in PWRI, with the size of 4 m long and 4 m wide and the maximum capacity of 40 t·G, was used.

### 2.2 Models

Fig. 1 shows an example of cross section of test models. The model was made in a steel box of 8 m long, 2 m high and 1 m wide. Both side slopes of one model were made in different conditions and two cases were simultaneously tested using one model. As summarized in Table 1, 7 models with 14 cases were so far tested.

Following conditions were varied in each case : slope surface gradient, existence of benches on a bed slope, kind of reinforcing element, reinforcement spacing, slope protection, etc.

The bed slope was made of wet sandy silt (ML,  $w = 19\%$ ) sufficiently compacted by wooden block so as to be stable against vibration. The fill part was made of air dried sand (SP,  $w = 6-12\%$ ) which was compacted to a relative density of about 50% by human foot. Reinforcing elements were nonwoven fabrics, plastic nets and steel bars. These properties are described in Table 2. Nails, 15 cm long, were used to fix nonwoven fabrics and plastic nets to the bed slopes. Steel bars were penetrated by 30 cm to the bed slope. The overlapped length of nonwoven fabrics and plastic nets were 30 cm irrespective of the spacing. A following scaling law was adopted; the reinforcement ratio  $R$  defined by the following equation is same for prototype and model assuming the Poisson's ratio  $\nu = 0$  for reinforcing elements (1,3).

$$R = \frac{-\epsilon_{3R} \cdot E \cdot t}{\sigma_{30} \cdot \Delta l} \quad (1)$$

where  $\epsilon_{3R}$  = average horizontal tensile strain of the reinforced soil ( $\epsilon_{3R} < 0$ );  $E$  = Young's modulus of the reinforcing element;  $t$  = thickness of the reinforcing element;  $\sigma_{30}$  = horizontal confining pressure;  $\Delta l$  = spacing of the reinforcing element.

This reinforcement ratio represents the ratio of strength increase of a reinforced soil to an unreinforced one at a specified reference strain. The reinforcing element was chosen so that the model scale was to be 1/7 to the prototype.

### 2.3 Excitation conditions and measurement

Experiments were conducted under the excitation conditions in Table 3. Excitation acceleration was

1) Head, Soil Dynamics Division, Construction Method and Equipment Department, Public Works Research Institute, Ministry of Construction, Japan

2) Research Engineer, Soil Dynamics Division, Public Works Research Institute, Japan

3) Research Assistant, Soil Dynamics Division, Public Works Research Institute, Japan

increased step by step starting from a low level. The shaking table was stopped for each excitation level and the damage degree was observed and horizontal and vertical displacements of the observation marks were measured. The acceleration, settlement and tensile force of nonwoven fabrics and steel bars were measured during the excitation. Moreover the overall deformation of the model was observed by taking photos of drawn meshes with coloured sands in the front surface of the model.

#### 2.4 Test results

Fig.2 shows the overall deformation of the model 4 after the excitation of 700 gal and the model 6 after 600 gal excitation as examples of test results. When a model embankment was excited under such a large acceleration, it slid along a slip surface and its crest settled. Such figures show the damage mode and feature of each embankment model.

Fig.3. shows a relationship of a cumulative crest settlement and an excitation acceleration. The damage features of reinforced embankments are summarized as follows.

- 1) Unreinforced embankments slipped near the boundary to the bed slope. Reinforced ones with slope surface gradients of 1:1.5 and 1:1.0 also deformed relatively largely near the above boundary. The deformed region was in a shallower part for the reinforced one with gradients of 1:0.5 and 1:0.
- 2) The deformation of reinforced embankments were less than unreinforced ones for the same slope gradient(Fig.3(a)).
- 3) As the spacing of nonwoven fabrics becomes smaller, the crest settled less(Fig.3(a)).
- 4) An embankment reinforced with plastic nets, whose tensile stiffness is larger, deformed less than one reinforced with nonwoven fabrics in the same spacing (Fig.3(a)).
- 5) Embankments deformed less when the nonwoven fabrics were fixed to the bed slope (Fig.3(b)).
- 6) Embankments deformed less when nonwoven fabrics or plastic nets were overlapped to their slope surface(Fig.3(b)), however, the overlapped geotextiles were pulled out during a large vibration at the upper layer where the overburden pressure was small.
- 7) As the slope got steeper, the deformation of the reinforced and unreinforced embankments became larger, however, the tendency of deformation increase of the reinforced ones was assumed rather smaller(Fig.3(c)).
- 8) Penetrated steel bars showed an effect to decrease the settlement of the embankment. However, its effect was not enough because the shallow part of the slope was removed when the slope protection was not effective. It suggests that steel bars must be connected to the slope protection works so that the embankment be effectively reinforced.

### 3. STABILITY ANALYSIS (2)

#### 3.1 Stability analysis method

A stability of a reinforced embankment must be investigated from various viewpoints because it can possibly fail in various modes. A stability of an unreinforced embankment is generally examined for its overall stability by a slip surface method. In

the case of a reinforced embankment, not only the stability of an overall reinforced region, but such a local stability as a pulling out or a breakage of a reinforcing element and a bulging of soil of a slope surface must be examined.

The main failure mode of the embankment in these tests was that the fill slipped near the boundary to the bed slope and not that reinforcing elements were pulled out or broken apart. Therefore it was presumed that not a small strain occurred in the reinforcing element. Consequently it was considered important to examine the overall failure of the embankment which was observed in the tests.

There is not yet an established method as a seismic stability analysis method of a reinforced embankment. A circular slip surface method with a seismic coefficient was extended as follows to include the effect of reinforcing element.

$$F_s = \frac{\sum [c \ell + \{W \cdot \cos \alpha - k_h W \cdot \sin \alpha + T_r \cdot \sin(\alpha + \theta)\} \cdot \tan \phi]}{\sum [R \cdot W \cdot \sin \alpha + y \cdot k_h W \cdot \cos \alpha - R \cdot T \cdot \cos(\alpha + \theta)]} \quad (2)$$

where R = radius of a slip circle; c = cohesion of soil;  $\phi$  = friction angle of soil; W = self weight of a slice;  $\ell$  = length of an arc of a slice; b = width of a slice;  $k_h$  = horizontal seismic coefficient; y = vertical distance between the center of a circular arc and the center of gravity of a slice;  $T_r$  = tensile force of reinforcing element when the reinforced earth reaches a failure state; T = tensile force of reinforcing element acting on the sliding earth mass in equilibrium;  $\alpha, \theta$  = angles shown in Fig.4.

This equation considers the effect of the tensile force of the reinforcing element to bind and to hold the sliding earth mass. The tensile force of reinforcing element is determined from its tensile strain caused by the deformation of the surrounding soil, which was obtained so that the strain is compatible with shear strain of the soil along a failure surface (band) based on the following assumptions (see Fig.5).

- 1) A slip surface consists of a slip band with a constant thickness of a constant shear strain.
  - 2) Reinforcing element deforms in a body with the surrounding soil therefore it cannot be separated from the soil.
  - 3) The shear strain of the slip band generates a tensile strain of a reinforcing element intersecting the slip band.
  - 4) The tensile strength of the reinforcing element is large enough to hold the slip of the earth mass.
- As a consequence of these assumptions, the tensile strain of the reinforcing element  $\epsilon_g$  is given as below.

$$\epsilon_g = \frac{c d - b d}{b d} = \frac{\cos i - \cos(i + \gamma')}{\cos(i + \gamma')} \quad (3)$$

where i = angle between the reinforcing element and normal line to a slip surface;  $\gamma'$  = corrected shear strain of a soil, generally not equal to that of the slip band.

The tensile force of the reinforcing element acting

on the sliding mass in equilibrium is calculated by assuming the linear relationship between all the mobilized forces on the mass and the deformation of the mass.

### 3.2 Stability analysis conditions

Stability analyses were conducted on some of the test models changing the excitation accelerations. The analyzed models were unreinforced embankments and reinforced ones whose reinforcing elements were fixed to the bed slope.

The soil parameters of the embankment used for the calculation are shown in Table 4. It was assumed that the shear strength of the bed slope was large enough and no slip surface to cut the bed slope was considered. The friction angle and cohesion of the fill were respectively obtained from a triaxial test and a critical height of a vertical cut of a ground made in the same manner as that of shaking tests. The tensile stiffness of the reinforcing element to calculate a tensile force is shown in Table 2. The seismic coefficient was given based on the measured acceleration during shaking table tests.

### 3.3 Stability analysis results

Fig.6 shows a relationship between safety factors calculated from Eq.(2) and excitation acceleration. The shear strain of 8% is taken as a failure criterion of an embankment on the basis of a triaxial compression test result, and the tensile force of the reinforcing element  $T_r$  was calculated to correspond with the above strain. Obviously no tensile force of the reinforcing element was considered for unreinforced embankments.

1) Fig.6(a) indicates the followings.

Among the embankments of a slope gradient of 1:1, the least factor of safety was obtained for an unreinforced embankment. A little larger factors were obtained for the cases of 5 and 10 of sheets nonwoven fabrics. The largest factor was obtained for that of 5 sheets of plastic nets. The differences of safety factors among the unreinforced and 2 nonwoven fabrics-reinforced embankments were slight, which indicates that the reinforcement effect by such a reinforcing element with a small tensile stiffness is small. Besides the plastic nets with a larger tensile stiffness gave fairly larger factors of safety.

2) Fig.6(b) shows that the safety factor of the unreinforced and reinforced embankments remarkably decreases as the slope gets steeper.

Fig.7 shows a relationship between a calculated safety factor and a cumulative settlement of a fill crest. In general, a fairly unique relationship with little scatter exists in Fig.7 except the case of slope gradient of 1:0.5 and 1:0 irrespective of the existence of reinforcing elements and reinforcement spacing. The deformation of the soil and reinforcing elements may not be identical in the case of plastic nets with a large tensile stiffness, which leads an overestimation of calculated safety factors.

Moreover the settlement rapidly increases when  $F_s$  is less than from 0.95 to 1.0 in the case of nonwoven fabrics and a slope gradient of 1:1 and 1:1.5, which

suggests the calculation method by Eq. (2) is useful for the assessment of a failure or deformation of a reinforced embankment whose slope gradient is not so steep.

The reason that the calculated factor of safety is so small for the embankment of steep slope against a same amount of crest settlement is because the Eq.(2) neglects the resistant effect of the overlapped geotextile slope facing and the crest settlement of a steep slope becomes small against a certain strain of slip surface as the slip surface gets shallower as the slope gets steeper.

Followings are summarized from the above analysis results.

- 1) The calculation results by a circular slip surface method with a seismic coefficient method, which considers the binding and holding effect by a tensile force of reinforcing elements intersecting the slip surface, agreed well with the experimental results except the case of a fairly steep slope.
- 2) It proved useful to calculate a tensile strain of a reinforcing element that is compatible with a shear deformation along a slip surface of an embankment to obtain a tensile force of a reinforcing element.

## 4. CONCLUSION

- 1) Model shaking table tests of reinforced embankments with nonwoven fabrics, plastic nets and steel bars showed that a reinforced embankment has a fairly large seismic resistance if a reinforcing element with a large tensile stiffness is effectively fixed to a bed slope. Besides the slope protection to prevent a local slope surface failure is also critical.
- 2) The degree of deformation of the embankment corresponded well to the calculation results by a circular slip surface method which considers the effect of tensile force of reinforcing element intersecting the slip surface except the case of steep slope.
- 3) The selection of an appropriate slope protection works and the evaluation of its effect on the stability need a further research.

## REFERENCES

- (1) Koga, Y., et al. : Model Shaking Table Tests on Seismic Resistance of Reinforced Embankment, 18th UJNR, 1986.5.
- (2) Koga, Y., et al. : Experimental Study on Seismic Resistance of Reinforced Embankment (in Japanese), Technical Data of PWRI, 1988.3.
- (3) Tatsuoka, F., et al. : Reinforcing of Cohesive-Soil-Embankment with Unwoven Fabric (in Japanese), Tsuchi-To-Kiso, JSSMFE, Vol.33, No.5, 1985.5.

Table 1 Test Model

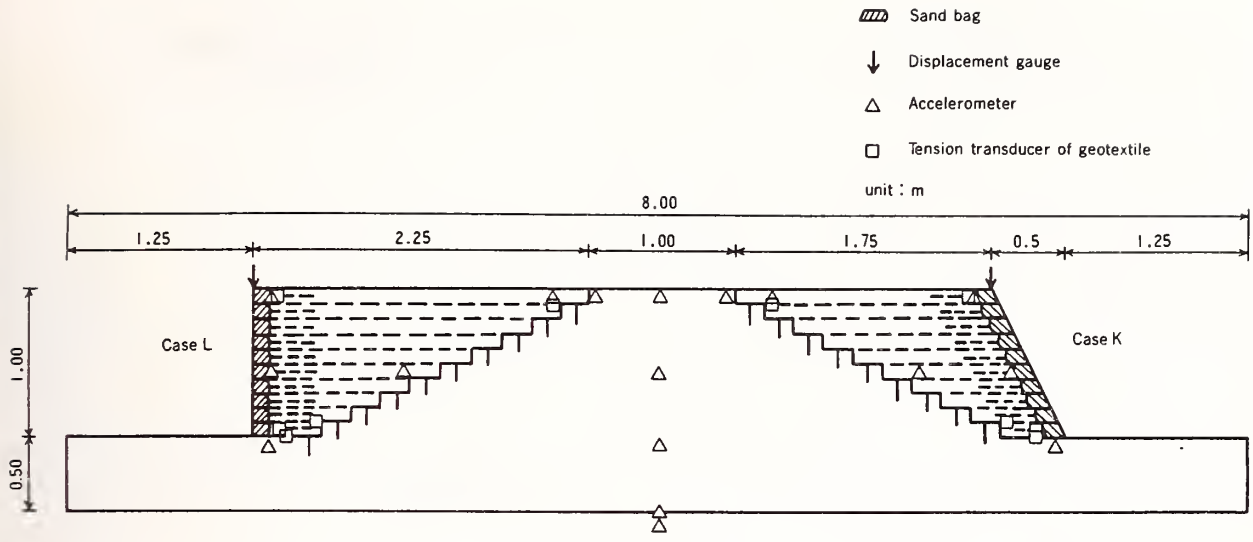
Name of embankments (case)	Model	Kinds of reinforcing elements	Reinforcement spacing	Anchorage to bed slope	Overlapping	Slope gradient	Sand bag on slope surface	Water content (%)	
A	1	R	None	—	—	1 : 1.5	—	11.5	
B		L	Nonwoven fabrics	10cm	No	No	1 : 1.5	No	11.3
C	2	R	None	—	—	1 : 1.5	—	9.3	
D		L	Nonwoven fabrics	10cm	Yes	No	1 : 1.5	No	10.1
E	3	R	None	—	—	1 : 1	—	8.1	
F		L	Nonwoven fabrics	10cm	No	Yes	1 : 1	Yes	7.8
G	4	R	do	10cm	Yes	Yes	1 : 1	Yes	6.3
H		L	do	20cm	Yes	Yes	1 : 1	Yes	6.5
I	5	R	Reinforcing bar	Horizontally 10cm Vertically 20cm	Penetrated by 30cm	—	1 : 1	—	6.3
J		L	Plastic nets	20cm	Yes	Yes	1 : 1	Yes	6.5
K	6	R	Nonwoven fabrics	10cm	Yes	Yes	1 : 0.5	Yes	8.3
L		L	do	10cm	Yes	Yes	1 : 0	Yes	8.4
M	7	R	None	—	—	1 : 1	—	15.2	
N		L	Nonwoven fabrics	10cm	Yes	Yes	1 : 1	Yes	15.4

Table 2 Properties of Reinforcing Elements

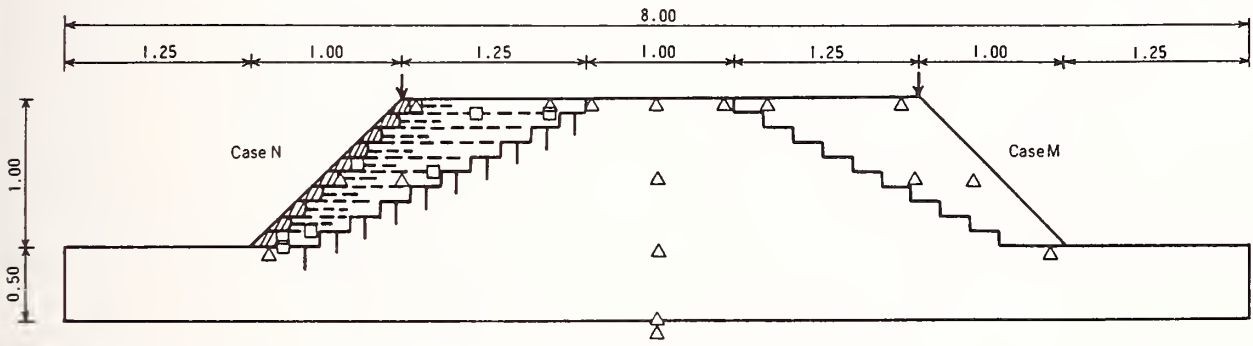
Kinds	Properties
Nonwoven fabrics	Nylon 70%, Polyester 30%, Thickness 0.2mm
Plastic net	Polyethylene 100%, Grid 2.5 × 2.5mm
Steel bar	Pianowire, diameter 3.5mm

Table 3 Excitation Conditions

Frequency	4 Hz							
Excitation Period	10 sec							
No of Models	1	2	3	4	5	6	7	
Name of Embankment (Case)	A, B	C, D	E, F	G, H	I, J	K, L	M, N	
Excitation Acceleration	123	122	90	91	92	94	105	
	248	245	189	198	198	204	204	
	395	400	242	310	285	291	294	
	580	850	590	355	373	380	391	412
			700	490	495	493	535	495
			840	610	518	610	602	670
			720	625	703			
		813	820	815				

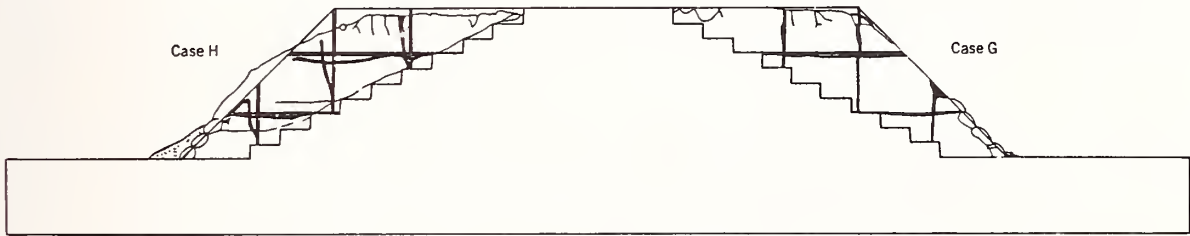


(a) Model 6 (Case K, L)

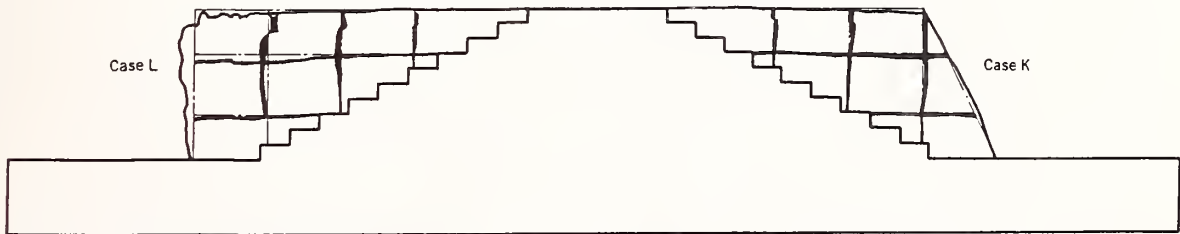


(b) Model 7 (Case M, N)

Fig.1 Examples of Test Models

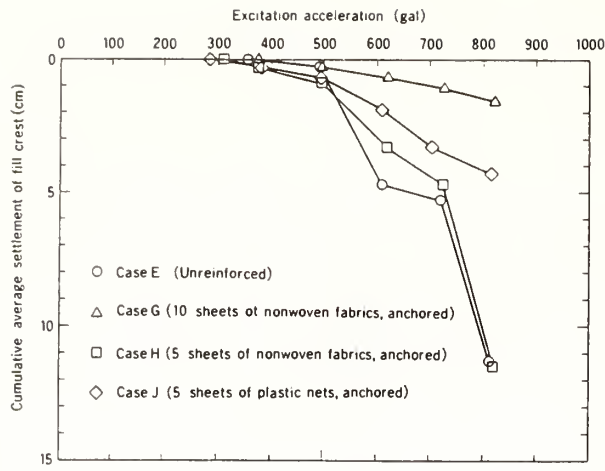


(a) Model 4 (Case G, H) after 700gal excitation

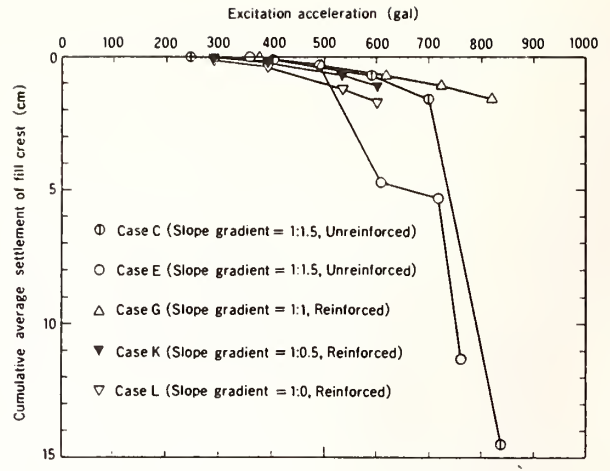


(b) Model 6 (Case K, L) after 600gal excitation

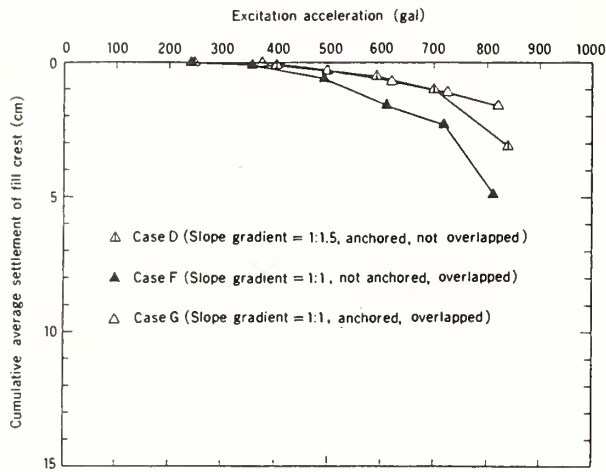
Fig.2 Deformation after Excitation



(a) Effect of Reinforcement, Spacing and Material (Slope gradient = 1 : 1)



(c) Effect of Slope Gradient (Unreinforced and reinforced with anchored 10 sheets of nonwoven fabrics)



(b) Effect of Anchorage and Overlapping (10 sheets of nonwoven fabrics)

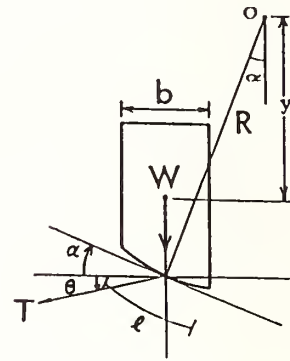


Fig.4 Slice for a Circular Slip Surface Analysis

Fig.3 Relationship between Excitation Acceleration and Cumulative Settlement of Fill Crest

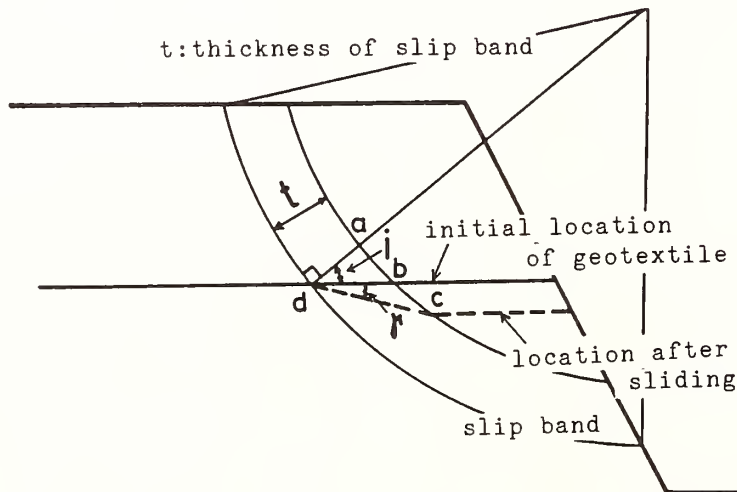
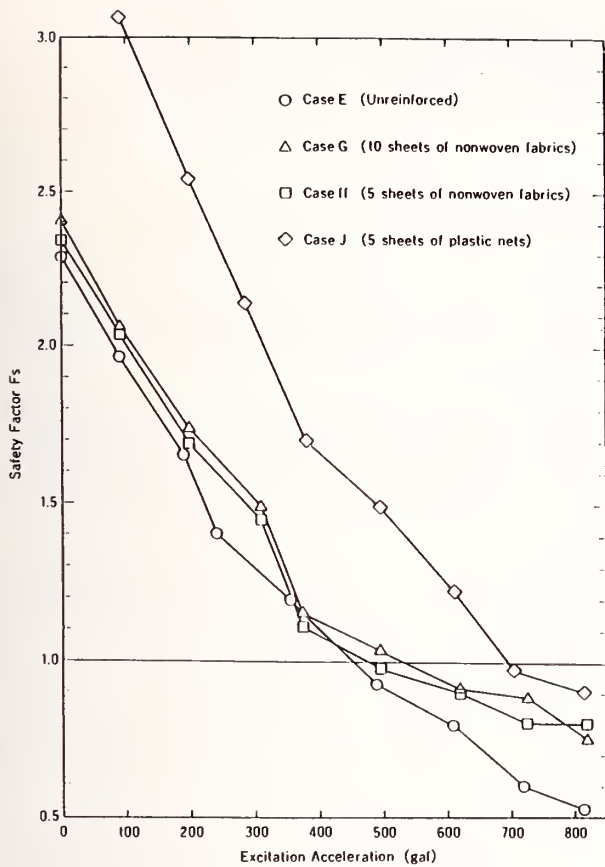
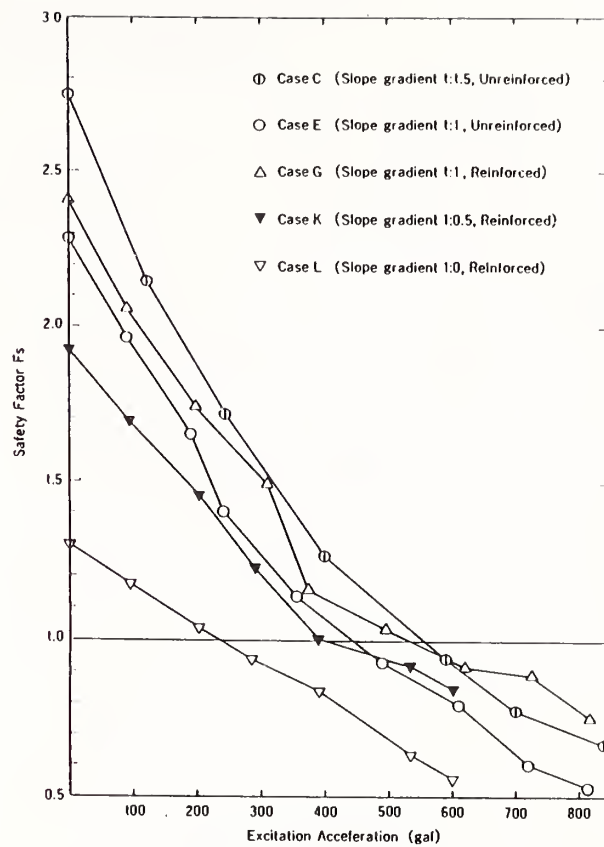


Fig.5 Calculation of Tension of Geotextile



(a) Effect of Reinforcement (Slope gradient = 1 : 1)



(b) Effect of Slope Gradient (Unreinforced and reinforced with anchored 10 sheets of nonwoven fabrics)

Fig.6 Relationship between Excitation Acceleration and Safety Factor

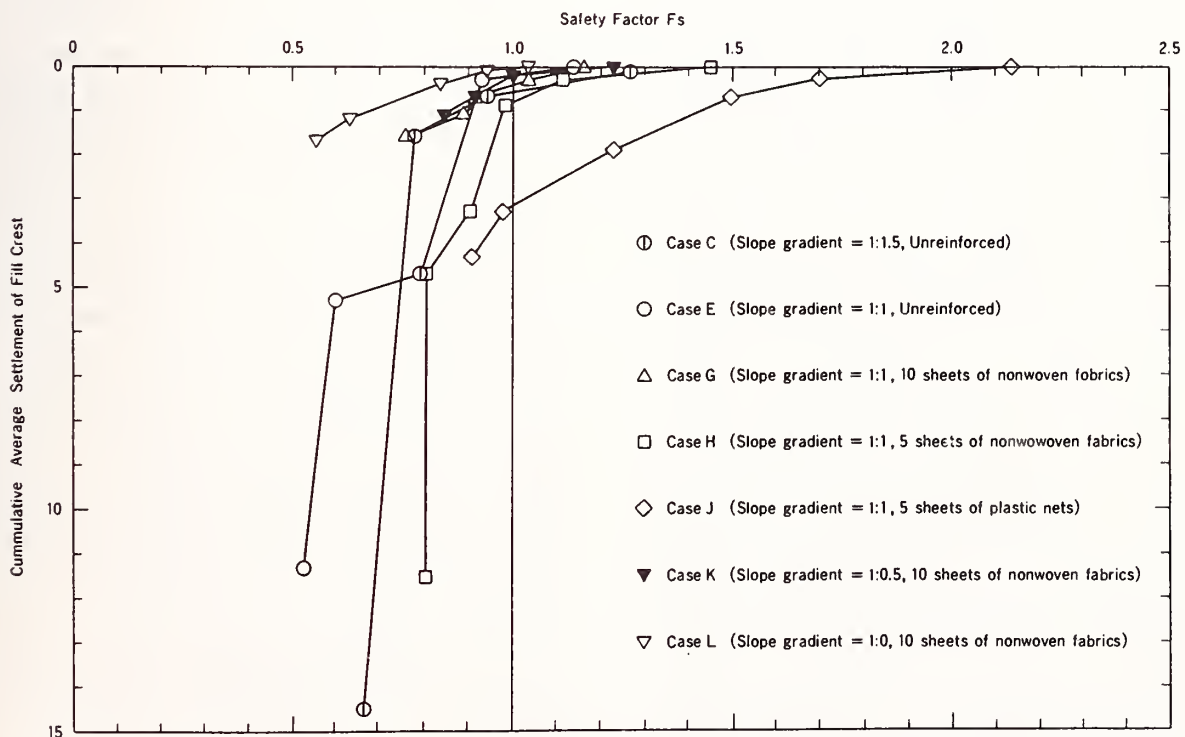


Fig.7 Relationship between Safety Factor and Measured Settlement

# Seismic and Tsunami Disaster Prevention Surveys and Preparing Geographical Information in Geographical Survey Institute, Japan

by

Masatoshi NAGAOKA <sup>1</sup>

## ABSTRACT

The Geographical Survey Institute (GSI) has been playing a leading part in surveying and mapping works of Japan as the central agency and therefore providing survey results which reveal the actual condition of the national land and contribute to its development and conservation. In particular, various kinds of maps, covering entire country, made by GSI are used extensively among the people.

On the other hand, the GSI is engaged in various geographic works including thematic maps making of major areas in Japan, such as Land Condition Map centering on landform classification and Land Use Map centering on land use and urban function. These works are also expected to contribute to prediction of earthquake damages.

Among the above-mentioned maps, the Land Condition Map is of the characteristic of a disaster prevention map other than that of ordinary maps. Besides, a wide range of geographic informations are at present digitalized to facilitate computer processing.

In addition, the GSI carried out surveys on major earthquakes and tsunami in the past to reveal the correlation between their disasters and landform conditions. Seismic disaster is closely connected with landform type according to the landform classification on the basis of the survey results. Disasters caused by earthquake movement and liquefaction are not directly affected by landform condition but underground condition. The ground condition of surface layer, not deeper than several meters, is closely related to micro-landform type. In the case of slopes, the knickline was pointed out to be in connection with the slope failure. In addition to that, the viewpoint of historical evolution (development) of landforms is adopted to explain the increase of slope instability after investigating Naganoken-seibu earthquake of 1984. These survey results have been all reflected on the above-mentioned geographical survey works.

This paper introduces some of such case studies and discloses common tendencies resulted from the researches into seismic disasters on the plains and mountain slopes and tsunami disasters on the

coastal areas and their underlying landform conditions.

**KEY WORD** : Geographical Survey, Seismic and Earthquake Disaster Prevention, Hazard Map, Digital Geographic Information

## 1. INTRODUCTION

The ongoing works of GSI are categorized as follows :

- ① Survey administration based on Survey Law
- ② Survey work with Fundamental Survey as its major business :
  - o Establishment and maintenance of geodetic control points
  - o Preparation and maintenance of base map
  - o Geographical surveys and thematic mapping
  - o Map information management, and the reproduction and publication of maps
- ③ Research on survey techniques and their development
- ④ International cooperation in relation to surveying and mapping

Survey works are incorporated as the core part into the GSI businesses. The mainstay ( Basic Survey ) includes the establishment of geodetic control points and map making such as base map.

On the other hand, as its survey works, the GSI surveys the actual conditions of land, lakes, rivers, coastal areas and land uses and consequently compiles the survey results into thematic maps.

Major ones among these works have been continued for 100 years. On the advent of today's information-oriented society, it is required to facilitate more highly accurate and various informations in more usable forms. Both surveying and mapping methods changed greatly as well. The GSI employs computer systems to enhance the automated and manpower-saving map making, and is positively

---

This report is a "State-of-the-Art Paper" of GSI's geographical work.

A part of the contents of this paper was made as an oral presentation on 18th Joint Meeting US-Japan Panel

1 : Head, Second Geographic Division,  
Geographical Survey Institute, Japan

pushing forward construction of systems covering from the digitalization of geographic information to its supply in order for users to be able to obtain various forms of expression and treatment they need.

Now the author refer to the establishment of geographical informations to help contribute to predictions of seismic and tsunami disaster.

Earthquakes occurred in Japan are known in the world to be of distinguished characteristics both in frequency and intensity. To take any effective countermeasures against earthquakes, it is necessary to predict the location of disaster-stricken area, type of disasters and its intensity.

In Japan, many surveys have been done to know the relation between natural conditions of land and degree of seismic disasters. The GSI, too, has carried out investigations on every occasion of major earthquakes since 1948 (Fukui earthquake), and the survey results were compiled into various survey maps (thematic maps) by the GSI. These are very important in that extraordinary geographic phenomena and actual disasters are recorded as maps. It is an already known fact that the damages of earthquakes greatly vary with both local landforms and ground conditions. The type of occurrence of earthquake damage varies sharply with landform and ground condition on the basis of these investigations. It is effective to recognize ground condition in the plain by landform type based on landform classification, because classified landform type is closely related to the historical evolution of landforms and is related to underground condition. This is one of the reasons why topography and Quaternary research are required in the fields of geology and engineering geology.

With tsunami disasters, the possibility of tsunami occurrence cannot be averted at any part of the coastal areas as obvious from the historical view. Because, in Japan, many large cities are situated in plains facing the sea and important productive functions are centered on the coastal areas. The frequency and types of tsunami however vary with regions. Furthermore, the magnitude of tsunami-attack varies with natural conditions such as the submarine topography of coastal areas, the shapes of coastal areas and the landform and elevation of onshore areas. The damage of tsunami greatly depends upon ways of land use as well as social conditions. It can be therefore thought that the amount of the hazard of tsunami-attack on the coastal areas consider-

ably varies with the landform and ways of land use on the coastal areas.

This paper outlines the past survey results on the magnitude of seismic or tsunami disaster and landform conditions, and summarizes what was studied so far. Besides, of among geographic informations such as landform necessary for the evaluation of the amount of hazard by earthquake and tsunami and also socio-geographic informations including land use, this paper refers to those which were so far established by GSI.

## 2. Investigations on Seismic and Tsunami Disaster Carried by the Geographical Survey Institute

The GSI investigated the damages caused by the major earthquakes after World War II and the relation between the damages and land conditions, and made thematic maps as records of seismic or tsunami disasters and investigative results. The followings are the outline of the investigative results by the GSI.

The outline of earthquakes, disasters and contents of investigative maps are presented in Table 1.

### 2.1 Fukui Earthquake of 1948

An organized survey on earthquake damages and landform conditions was carried out on the occasion of this earthquake for the first time in Japan. The following are the obtained conclusions (Ogasawara, 1949).

- o Collapsed ratio of wooden houses was found to be related to the thickness of underground soft materials.
- o Most of the diastrophisms can be explained by the slippages of deep fault and accompanying earth movements.
- o Location of earthquake fault and deformation of earth's surface were found to be able to estimate to some degree if tectonic landforms in alluvial low lands were researched.

### 2.2 Chilean Earthquake Tsunami of 1960

The tsunami propagated to all the part of the Pacific Ocean and it hit many parts of coastal areas on the Pacific Ocean side and gave severe damages. In Japan, the most severe damage (the maximum 5 ~ 6 m of wave height) occurred on the limited coastal areas including Shizukawa, Onagawa, Kesenuma, Ōfunato and Rikuzen-Takada in Sanriku region, while within another inlets water level was less than 1 m and almost no disasters occurred there. At the time of Sanriku earthquake tsunami

of 1933 (the seismic epicenter was located around the Japan trough), on the contrary, the latter area was hit by huge tsunamis.

In general, there is a big difference in the nature and damage of tsunami between that occurred at a distant place and that occurred in the neighborhood. In the case of this tsunami, the cycle of tsunami wave was as slow as 30~40 minutes (that of Sanriku earthquake tsunami of 1933 was about 20 minutes) and its velocity was as slow as man's running speed (that of Sanriku earthquake tsunami was very fast). The wave height was low at the mouth of the inlets became higher as the tsunami propagated toward the interior (opposite in the case of Sanriku earthquake tsunami). The velocity varied with places; it became fast and gave big damages at some places while almost no damages at some places such as Joban coastal area. Thus the forms of damage varied with the shapes of coasts.

Until then, most of the studies on tsunami researched into the mechanism of occurrence and types of propagation. Therefore systematic studies were very rarely done on how tsunami changes its form corresponding to landforms after it reaches coastal areas, where and how far tsunami intrudes and where tsunami causes erosion or sedimentation. Assuming that once surveys are done on the correlation between coastal landforms and tsunami, it becomes possible to some degree to predict the hazard of tsunami in each area and possible to establish the primary countermeasures against tsunami, the GSI for the first time in Japan carried out systematic survey on tsunami disasters and tsunami-stricken landforms.

This survey was done by aerial photo-interpretation and field survey. The survey results were compiled as ① a tsunami condition map which depicts the direction in which tsunami attacks, the maximum reach of tsunami, the erosion and sedimentation caused by tsunami disasters and ② a coastal landform classification map.

By the comparison of these maps, the relation between tsunami damages and landforms were studied. As a result, it was known that large regional differences in the disasters of tsunami attack are caused by the differences in coastal landforms as follows (Ohya, 1962):

- o Even along the rias coast, the intensity of damage by tsunami was found to differ from place to place. It varies with submarine topography and coastal landform. The type of tsunami varies very much with shape of bay such as V-shaped bay which is a submergence valley of a

- small river in the past, W-shaped valley which is a complex of V-shape bays, U-shaped bay which is a submergence bay of a big river in the past.
- o Routes of intrusion, maximum reach from the shore and a length of inundated period are deeply related with the landform of coastal plains.
- o By classifying shoreline and landform of coastal plain on the basis of the above-mentioned, regionally different type of tsunami and its risk can be estimated to some degree. In this sense, a survey on the coastal forms gives the basis of countermeasures against tsunami.

### 2.3 Niigata Earthquake of 1964

There occurred a unique damage due to the liquefaction at alluvial soft ground which was caused by this earthquake. With this as a momentum, studies on the liquefaction of ground came to be done very hard in respective fields. Since then, the prediction of liquefaction became indispensable for the prediction of seismic disasters. The GSI carried out surveys over a wide area to understand the result of this seismic disaster and its distribution by correlating them with the distribution of landforms which well facilitates to estimate the nature of land, by using aerial photo-interpretation of landforms and field survey. The following conclusions (GSI, 1965; Kobayashi-Magome, 1965; Takasaki et al., 1966) were obtained.

- o Damages were outstandingly serious along the former river beds. At inter-dune lowlands, back marshes and banked up lands which were former lowlands or backmarshes, too, serious damages were found.

- o Landform on ground surface is classified by characteristics such as geomorphic agent, formative age, shape and relief, structure, component material, etc. The classified landform unit by this shows not only characteristics of landform itself but also the relation with surface geology, soil and drainage condition. Such detailed classification of landform, therefore, explains the reason of occurrence of regional difference in damage.

- o Consequently, the earthquake damage potential at other places with similar characteristics can be predicted to some degree by a micro landform classification map.

- o From the above-mentioned viewpoint, it was proved that a Land Condition Map made by the GSI with regard to flood damage was effective for the prediction of earthquake damage, too.

#### 2.4 Izu-Hantō-oki Earthquake(Off Izu Peninsula) Earthquake of 1974 and Izu-Ōshima Kinkai (Adjoining Sea of Izu-Ōshima Island) Earth- quake of 1978

After the investigation into the relationship between frequent landslides and micro landform conditions, the following conclusions were obtained (GSI,1979;etc.) :

- o Landslides occurred frequently around the knick line in mountain slopes.
- o In the relationship between landslide and dip division, it was revealed that the occurrence of landslide increased rapidly at 45° or more, according to landslide occurrence ratio by every dip unit. At slopes overlain by tuff and/or pumice layer, however, landslides occurred even at about 25°.

#### 2.5 Miyagiken-oki(Off the Coast of Miyagi Pref.) Earthquake of 1978

The damages were centered at newly developed residential quarters on hills and valleys. With the correlation to landforms, the following facts (Kobayashi,1980) were revealed :

- o The correlation between the type of banked-up layer and the amount of disaster : compared with sites with valley-filled type of banked-up layers, a more amount of damage was found at sites in which the periphery of hilly land slope of former landform was banked-up and a terrace-like banked-up slope was open on one side.
- o The damage was more serious at sites in which the steep slopes of former landforms were banked-up, the specific catchment area was large or the groundwater level was high.
- o As above-mentioned, the ground disaster at the banked-up layers of hilly lands are greatly affected by the ground condition of former landform before development. It facilitates to some degree the prediction of ground damages in the future in large-scale developed areas such as newly prepared housing sites to make and read detailed maps of former landforms and understand the deformation.

#### 2.6 Nihonkai-Chūbu(Central Japan Sea) Earthquake of 1983

Immediately after this earthquake, a wide area on the Japan Sea side was attacked by a tsunami. Unlike the days when the Chilean earthquake tsunami, many research institutes carried out, owing to today's highly advanced computer technology, sets of digital simulation on the generation and propagation of the tsunami, its arrival at the coasts

and its attacks. Elaborate surveys and studies on the wave height and damages were done by many national institutes.

The River Bureau, Ministry of Construction(1986), informed on the actual damages and their characteristics, carried out a comprehensive research about countermeasures against tsunami disasters. This Bureau proposed the preparation of "Tsunami Disaster Prevention Map" with the following objectives to be used as fundamental data for tsunami disaster prevention measures and prepared trial ones of the model area :

- ① to clarify the actual amount of inundation caused by tsunami attacked in the past and disclose the locations of dangerous areas
- ② to clarify the existing disaster prevention facilities, land use at present and the present disaster prevention measures.

On the other hand, the following facts in regard to the seismic disaster on land, similar to preceding cases, were revealed (Tsurumi et al., 1984).

- o The percentage of damage of wooden houses was highest at the banked up former marsh.
- o The percentage was relatively high at cut and leveled higher sand dune, lower sand dune ( These two look safe, but groundwater level is high. The latter, in most of the cases, only thinly overlies backmarsh.), inter-sand dune, lowlands, banked up flood plains and former river beds.
- o Damage percentage at a terrace and a upland was lower than that of other type of landform.

#### 2.7 Naganoen-seibu(West Nagano Pref.) Earthquake of 1984

About 400 slope failures and landslides were caused by the earthquake. Among them, specially mentioned is a large-scale landslide (Ontake landslide) which is the largest after the World War II in Japan. It was caused on the south slope of the Ontake volcano, central Japan ;  $3.4 \times 10^7 \text{m}^3$  of mountain mass suddenly began sliding. The main mass slid along underlying pumice layer, and resulted reappearance of buried V-shaped valley.

From a viewpoint of the Quaternary historical evolution of landforms, the geomorphological process from the slope formation to the occurrence of the landslide is explained as follows ( Nagaoka et al.,1985 ; Nagaoka,1987) ;

- o The collapsed slope is characterized as buried former valley.
- o The lava and scoria layers which had kept burying the foot part of this time collapsed

mountain flank just like a retaining banked up layer was removed by the deepening and extending of the erosion-dissected area occurred in Post-glacial period.

o As a result, the deterioration of the slope of the natural ground (buried valley sediments; lava and pyroclastics) was enhanced (the necessary condition to cause slope failures was met.).

o After this, both earthquake and rain attacked the slope in question in a short geological time. In such a process, this landslide was assumed to have occurred.

In this case, it is true that the direct factors—an earthquake and preceding rainfall of 160 mm—played a decisive role for the occurrence of this landslide. But they alone did not cause it. It is rather important to realize that the level of the valley bottom had been already lowered and the slope had been already deteriorated.

Only from this viewpoint, the reasons (a) why, only at this site, a large-scale landslide occurred although the other areas had the same factors, and (b) why, for the first time, the landslide occurred at this site, can be explained rationally.

In addition, the viewpoint of the historical evolution of slope landforms makes it possible to predict landslide site potential and explain the mechanism of occurrence of a landslide reasonably.

### 3. Geographic Survey Works of the Geographical Survey Institute

#### 3.1 Seismic Disaster and Land Condition

As the above mentioned cases, seismic disasters are closely related to landform conditions.

Disasters caused by earthquake movement and liquefaction are not directly affected by landform conditions but underground conditions. Reconstructing paleogeography by a geomorphological method and researching into historical evolution of landform is a good way to know underground condition, because the underground condition is determined by geomorphological place at the time of sedimentation (= landform formation). Especially, the ground condition of surface layer, not deeper than several meters, is closely related to micro landform (Ikeda, 1964; Kadomura, 1968; Tsurumi et al., 1982; etc.). It is, therefore, possible to know the ground condition by reading micro landform.

Fig.1 shows a model of the relation between geographic place and sedimentary environment • ground condition. Fig.2 shows a sea level change since the last glacial age which had a great influence on the sedimentary environment of coast-

al plain.

In general, it is necessary to use boring data which exists as point data in order for us to know ground conditions directly. To extend the information from these data into aerial and three-dimensional informations, landform classification on the basis of geomorphological knowledge is necessary. For this purpose, it is very useful to interpret and analyse micro landforms by using aerial photographs.

On the other hand, since it is possible to read ground conditions and the development of landforms from landform classification map, this map is recommended to use. Also recommended from the view point of earthquake prevention. In the preparation of landform classification map, it is recommended to take these aspects into consideration.

The GSI has been engaged in making a Land Condition Map centering on landform classification as its major content, including the above-mentioned viewpoints. Since it is possible to know about ground conditions, such as evaluation of underground by reading a landform classification, this map is highly recommended also from the viewpoint of seismic disaster prevention. The outline of this map is explained in 3.3.3.

Earthquake damage, on the other hand, includes not only direct damage in material and life but also overall damage to living and productive activity. It is necessary to collect various kinds of geographic data in order to foresee such socio-economical damages. For this purpose, GSI's Land Use Map and digital geographic information (Digital National Land Information, etc) are available. These are explained in 3.3.2 and 3.3.5.

#### 3.2 Tsunami Disaster and Land Condition

As the above-mentioned, the magnitude of tsunami attack varies with the natural conditions such as the submarine topography of nearshore areas, the shapes of coasts, the landform and elevation of onshore areas, etc. The magnitude of damages is determined unequivocally by the height of tsunami, but the landform conditions, land use conditions and other social conditions greatly affect on the forms of damages, too.

To estimate the hazard of tsunami at each area by calculation, (1) the landform information of the coastal sea is necessary to know the wave height of tsunamis which strike the coastal areas and their velocity. (2) Information on the elevation of an onshore area above sea level and landform classification are necessary to know the maximum

height that the tsunami reached after landing, submerged area and inundating time. As mentioned in 3.1, it is necessary to know geographical informations to predict the amount and magnitude of tsunami damage.

### 3.3 Geographic Survey Works by Geographical Survey Institute

The GSI has been trying to establish of various geographic informations to utilize them for the development, conservation and disaster prevention of the national land, including the aforementioned aspects. These informations include Land Use Map, Land Condition Map, Topographical and Land Condition Map of Coastal Area and Lake Chart. Furthermore, recently the GSI has been conducting the establishment of digital geographic data across the nation to meet administrative and social demands in the highly information-oriented society and demands for geographic data which can be used in computer processing.

"Digital National Land Information" by GSI is one of digital geographic informations pertaining to natural and social conditions.

These informations are outlined as follows.

#### 3.3.1 Large-scale Map

A large-scale topographic map is indispensable to know about detailed elevation of plains. The GSI is making this type of maps of plains and their marginal parts with uniform standards. So far the GSI has made "1:5,000 National Large-scale Map" covering 40,000 km<sup>2</sup> (Fig.1) out of the planned area of 190,000 km<sup>2</sup> (about 1/2 of the national land), and 1:2,500 scale covering 10,000 km<sup>2</sup> (collaborative works with related local public bodies).

Besides, local public bodies covered themselves have made 1:2,500 City Planning Map. These are now in use.

#### 3.3.2 Land Use Map

The GSI continuously published the "1:50,000 Land Use Map" from 1967. In 1975, GSI began publishing the 1:25,000 scale of the kind, thereby up to 100,000 km<sup>2</sup> of major plains were completed and up to 1/3 area of the national land was covered by this map so far (Fig.2).

Urban land uses are regarded as of major importance in the contents of the Land Use Map in order to be used for the preparation of national land plans, city plans, etc. The items of this map are categorized first into three major divisions, that is, urban area, agricultural land

and forest. The urban area is subdivided into intermediate divisions and/or small divisions. Here, regional planning division for use of the Town Planning and Zoning Act are fully taken into consideration, and urban function is paid special attention, too. The agricultural land and forest are subdivided into intermediate and/or small divisions, paying attention to the vegetations. Six different kinds of colors are used for printing of the map. By combining the shades of colors and patterns, this map differentiates 35 land use divisions.

At the time of map making, interpretation for land use division was done mainly by an interpretation of aerial photographs and also by survey and other data.

#### 3.3.3 Land Condition Map

The GSI has been preparing and publishing the "1:25,000 Land Condition Map" since 1965 to provide basic data regarding natural conditions of land necessary for planning of disaster preventive measures, land use and regional development. Starting with mapping major areas of the plains, some 40,000 km<sup>2</sup> of plains have so far been completed (Fig.3).

Before and after Typhoon 5919 (Isewan Typhoon, 1959), surveys on landform and flood disaster were carried out in the Nōbi Plain. These surveys revealed that it was possible to predict the location and intensity of flood and upland damages by characteristics and historical evolution of landforms, altitude, history of reclamation. This experience accelerated making of Land Condition Map centering on landform classification in lowland. After this, as mentioned before, investigations were carried out on the occasion of earthquakes and this proved the correlation between micro landform - ground condition and seismic disaster. Therefore, this kind of landform classification map was recognized to be useful for predicting the seismic disaster in lowland.

After that, topographical classification and dip division of mountain slopes were added to this map to understand the slope disasters potentials. Since 1980', the information on underground has been reinforced at the large plains in Japan. That is, contour lines of the basement of Alluvium deposits (= ground surface at Last glacial stage) or isopach maps of soft layers were laid down as well as topographical classification.

The contents of the Land Condition Map consist of ① landform classification, ② accurate ground elevation, and ③ various organizations and public

facilities pertaining to land disaster or development. The map was made mainly on the basis of the interpretation of aerial photographs and field survey. Units of the landform classification are classified into homogenous morphological units, morphogenesis(natural processes such as erosion by running water, sedimentation, volcanism, crustal movement,etc.), and formative age. That is, mountain and hill slope are divided by slope angle and subdivided by shape of slope. Terrace and upland are subdivided by its formative age and relative elevation. Lowland is divided into general surface, relatively higher land and well drained landform, and furthermore, subdivided by microtopograph. Artificially deformed areas, with bad condition for seismic disaster, are expressed so that the former units of landform classification before artificial deformation can be known. In addition to the above-mentioned landform classification, plain is contoured every one meter to express subtle undulation on the ground surface and to contribute to estimate flood or up tide disaster.

Table 2 indicates the units and their characteristics classified as those of low lands closely linked with seismic disaster and tsunami attack and flood among the landforms composing the major elements of the above-mentioned map. Fig.4 is an example of the map.

Besides, the GSI carried out surveys equivalent to land condition surveys on the plains of 104 main river systems across the nation. Based on them, GSI made "1:25,000 Landform Classification Map for Flood Prevention" which expresses micro landforms closely linked with flood disaster and expresses so as to enable to estimate the nature of sediments. The map is only for internal use within the Ministry of Construction. Major plains have been covered by them. They meet the above-mentioned objectives.

#### 3.3.4 Topographical Map and Land Condition Map of Coastal Area

The GSI has continuously been making maps of both onshore and nearshore areas (coastal area) since 1972 to improve basic informations to be used for the administration, development, conservation and disaster prevention of the coastal area.

In the sea area, bathymetric, seismic and sub-bottom surveys were conducted, whereas in the onshore area, landform classification was conducted. The survey results were compiled into "1:25,000 Topographical Map of Coastal Area" and

"1:25,000 Land Condition Map of Coastal Area", that incorporate the natural conditions of onshore and nearshore area(Fig.5). The expression of submarine topography depends on isobathymetric line at 1 m interval, landform classification. Fig.6 is an example of this Map.

#### 3.3.5 Digital Geographic Informations

Conventionally, geographic informations on the national land were provided mainly from maps such as the above-mentioned topographical and thematic maps and images such as aerial photographs. Informations obtained through images are advantageous because they can easily express much information and facilitate intuitive recognition and qualitative judgement.

but informations from maps such as the Land Condition Map and the Land Use Map is not always convenient in the case of obtaining or measuring large-volume quantitative data from these.

To make up for such inconvenience, the GSI initiated supplying various digital geographic informations(Table 3,4,5) accurately corresponding to 1:25,000 topographical map. It used to require a great deal of efforts for users to obtain such data from maps. Now these data have come to be able to be obtained easily as digital data.

The data are stored on magnetic tapes. A large quantity of data can be processed and analyzed very fast by an electric computer. These data are stored as line(vector) data such as data about shoreline, river channel, administrative sector, road, railway, etc., and other areal data as mesh (mainly about 1 km square) data. In the case of ②(Table 3), there are 10 m square meshed detailed land use data.

These digital informations are at present available for governmental agencies, local public bodies and other public organizations at the Japan Map Center (for its duplication cost).

The ① is most populer and used widely. The ④, whose covering area is the administrative area of local public bodies along coastal lines, and areas with the depth up to 50 m, include many important data linked with the prediction of tsunami hazard.

#### 4. Summary and Future View

Ground disaster is a primary disaster following an earthquake. It is affected by the characteristic of ground to great degree. The ongoing land condition survey of GSI is intended to pay much attention to where earthquake disaster potential lies as well. The above-mentioned Land

Condition Map contains much of such information and other geographic informations also contribute to estimate socio-economic damage caused by seismic disaster.

It was reported at the former UJNR meetings on the acquisition of the response of the dynamic properties of ground to earthquakes with the assistance of computer analysis and the possibility of liquefaction by liquefaction judging methods and a trial mapping of such information. Examples of such cartographic representation over a wide area are maps which were prepared by the Tokyo Metropolitan Government(1985) to estimate the amount of liquefaction to be occurred in case an earthquake with magnitude equivalent to that of the Great Kanto earthquake of 1923 strikes the lowland of Tokyo. Furthermore the Tokyo Metropolitan Government (1987) researched the liquefaction potential again and prepared the liquefaction prediction map (mesh map) to know the possibility of liquefaction over the entire lowland and the liquefaction prediction map by mean of region judging method to make primary data for the construction and maintenance of structures.

These mapping methods, however, are premised on that a number of bore hole data can be obtained at urban areas in Japan. It is not always applicable to places where no direct data on underground is available such as in developing countries. Much more occasions to make this kind of landform classification map at such places will be increased in the future. It is also estimated necessary to study on the landform classification in tropical humid climate or arid climate.

Futhermore, to inform map readers of the data of maps more accurately, it is necessary to make not only general landform classification maps but also maps to meet specific purposes such as seismic disaster hazard map or flood hazard map, etc. In that case, comprehensive applied geomorphological evaluation is needed. That is, on one hand, it is necessary to evaluate new characteristics of combined units, in addition to the characteristic of each landform classification unit. On the other hand, it is necessary to assume even changes of the original characteristic when natural and social(artificial)conditions are added to landform condition. Expression of the landform classification map must be simplified to help map readers to understand easily similarity and contrast in the units of landform classification by using colors and patterns. That is, very important is that the map is easy to understand.

The GSI further intends to prepare its various

thematic maps and geographic digital informations on the national land to contribute to the objectives mentioned in this paper and improve their quality.

[ REFERENCE ]

- Ikeda,T.(1964) : Study on the Alluvial deposits on Tokaido Region. Contribution Inst.Geol.Paleontol.Tohoku Univ., No.60, p.1-85. (J+E)
- Geographical Survey Institute (1965) : Report on the Niigata earthquake. 60p. (J)
- Geographical Survey Institute (1979) : Report on the Izu-Oshima-kinkai earthquake of 1978. 56p. (J)
- Kadomura,H.(1968) : Systematic aerial photo analysis of soft ground condition. Geogr.Rev.Japan, Vol.41, p.19-38. (J+E)
- Kobayashi,M.(1980) : Disastrous ground failure in a residential area of large-scale cut-and-fill in the Sendai region caused by the earthquake of 1978. Bull.Geogr.Surv.Inst., No.24, p.15-25. (E)
- Kobayashi,M.and Magome,H.(1965) : Disaster of Niigata earthquake of 1964 and land condition survey. Jour.GSI, No.30, p.1-7. (J)
- Nagaoka,M., Hoshino,Y., Takei,Y., Ichikawa,S. and Saitoh,H.(1985) : Geomorphological characteristics and factors of the large-scale landslide and detritus flow on the south slope of Ontake volcano caused by Naganoken-seibu earthquake,1984. —reported at 17th joint meeting (UJNR). (J,E)
- Nagaoka,M.(1987) : Geomorphological characteristics and causal factors of the 1984 Ontake landslide caused by the Naganoken-seibu earthquake. Bull.GSI, 31, 72-89. (E)
- Ogasawara,Y.(1949) : Earthquake damage and disastrophism. Jour.GSI-special ser.2, 13p. (J)
- Ohya,M.(1962) : Chilean Earthquake Tsunami and coastal landform (II). Jour.GSI, No.27, p.12-19. (J)
- Public Work Resurch Institute of Tokyo Metropolis (1987) : Liquefaction prediction of Tokyo lowland. 198p.2maps. (J)
- River Bureau, Ministry of Construction (1986) : Report on countermeasure of Nihonkai-chubu earthquake. 303p. (J)
- Takasaki,M., Kanakubo,M., Minobe,M., Magome,H. and Ogino,K. (1966) : The relation of the damages caused by the Niigata earthquake and the topographical conditions in Niigata Plain. Rep.Cooperative Res.Disaster Prevention, No.11, p.13-18. (J)
- Tokyo Metropolis (1985) : Report on the prevention of earthquake damages in the Tama-region. 576p.7maps, Tokyo Met.Gov. (J)
- Tsurumi,E., Sunaga,H. and Kumaki,Y. (1982) : Seismic disasters and land conditions of lowland. ---reported at 14th joint meeting (UJNR). (J,E)
- Tsurumi,E., Horino,M. and Ohta,M.(1984) : Relationship between seismic disaster and ground condition in Noshiro Area, Akita Prefecture. —reported at 16th joint meeting (UJNR). (J,E)

note : (J) Written in Japanese only

(J+E) Written in Japanese with English abstract

(E) Written in English only

(J,E) Written in English and Japanese

Table 1 Investigative maps of earthquake disastrous situation and land condition surveyed by GSI

Earthquake/Outline of disaster #1	Investigative map by GSI/scale, size, etc. #2	Contents of map
Fukui earthquake of 1948 Epicenter: Fukui Plain, M 7.3 Annihilated damages in Fukui City Loss of 3,895 lives 35,420 houses collapsed ( collapsed ratio > 90% in plain ) Earthquake fault of N-S direction	"Fukui earthquake-damages and ground failure" 1:50,000, B1, 6 colors, 1 sheet	Damages (Jet of sand, fissure, depression, burnt district, etc.) Isopack of collapsed houses ratio Surface geology
Chilean earthquake tsunami of 1960 Epicenter: Off the Chilean coast, M8.5 Tsunami, height of max. 5 ~ 6m, at the some bays of Sanriku district along the Pacific Ocean Loss of 139 lives 2,830 houses collapsed or washed away	"Investigative map on disaster and landform classification on Chilean earthquake tsunami" Inundation map of Kesennuma district 1:10,000, A2, 6 colors, 1 sheet Landform classification map of Kesennuma district 1:10,000, A2, 8 colors, 1 sheet Tsunami disaster and landform classification map of Shizugawa district 1:10,000, A2, 9 colors, 1 sheet	Direction of intrusion or outflow of the tsunami Erosion or sedimentation area caused by the tsunami Inundation area Landform classification
Niigata earthquake of 1964 Epicenter: Adjoining sea of the Awashima Island, off the coast of Niigata Pref. M7.5 Damages in Niigata, Yamagata and Akita pref. Heavy disaster caused by liquefaction in Niigata City Tsunami, height of max. 5m, along the Japan Sea Loss of 28 lives 1,960 houses collapsed	"Niigata earthquake-damages and land condition" 1:50,000, B1, 8 colors, 2 sheets ( Niigata Plain )  1:10,000, A0, 6 colors, 2 sheets ( Niigata City )	Disastrous situation ( damages of various facilities, inundation, depression, fissure, jet of sand, burnt district, etc.) Landform classification Disastrous situation ( ditto ), Deformation of earth's surface and landform classification Important geologic columnar sections 7 Disastrous distribution maps ( 1:200,000 ) in annexed paper (60p.)
Izu-Mantō-oki earthquake of 1974 Epicenter: Off the Izu Peninsula, M8.9 Damages in southern coast area of the Izu Peninsula Loss of 29 lives, 46 houses collapsed	"Disastrous situation and land condition map on Izu-Mantō-oki earthquake" 1:50,000, A0, 8 colors, 1 sheet	Distribution of damages ( houses, roads, landslides ) Landform classification Annexed paper ( many photographs, 56p.)
Izu-Oshima-kinkai earthquake of 1978 Epicenter: Adjoining sea of the Izu-Oshima Island, M7.0 Damages in southern area of the Izu Peninsula Loss of 25 lives, 94 houses collapsed	"Disastrous situation and land condition map on Izu-Oshima-kinkai earthquake of 1978" 1:50,000, A0, 6 colors, 1 sheet	Distribution of damages ( ditto ) Landform classification, Earthquake fault whole area; 1:50,000 Mochikoshi and Washimoto district; 1:10,000 Inatori district; 1:25,000 Annexed paper ( 56p.)
Miyagiken-oki earthquake of 1978 Epicenter: Off the coast of Miyagi Pref. M7.4 Damages in Miyagi Pref., especially heavy damages in the newly developed residential quarters Loss of 27 lives, 651 houses collapsed	( Pre- and post-disaster 1:2,500 topographic maps of newly developed residential quarters: For investigation )	
Nihonkai-chūbu earthquake of 1983 Epicenter: Off the coast of Akita Pref., Central Japan Sea, M7.7 Damages in Akita, Aomori Pref. and Hokkaidō Tsunami along the Japan Sea, just after the earthquake Loss of 104 lives, 886 houses collapsed ( containing washed houses )	"Investigative maps of Nihonkai-chūbu earthquake" 1:10,000, B1, 7 colors, 1 sheet	Distribution of damages ( houses, roads, fissure ) and land condition map of Noshiro district Landform change ( fissure, jet of sand, horizontal and vertical deformation of earth's surface ) of Gomyō district
Haganoken-seibu earthquake of 1984 Epicenter: Ōtaki Mura, Nagano Pref. M6.8 Damages in Ōtaki Mura Large-scale landslide (Onkake landslide) Loss of 29 lives, 14 houses collapsed	"Landform change caused by Haganoken-seibu earthquake" 1:10,000 ~ 1:25,000, A0, 1 ~ 4 colors, 6 sheets  "Investigative map of Haganoken-seibu earthquake" 1:25,000, A0, 6 colors, 1 sheet	Topographic maps of pre- and post-landslide 1:5,000 for Ontake landslide 1:2,500 for Matsukoshi and Takikoshi landslide Isopack map of landform change amount between pre- and post-landslide, 1:10,000 Profiles of landform changes, 1:10,000 Landform classification map of denudated and deposited area, 1:10,000 Successive change of denudated area (1959, 69, 79, 84) around Ontake volcano, 1:25,000 Distribution of landslides of pre- and post-earthquake Division of slope inclination Knickline

#1: Outline of disasters is based on "Rika nenpyo (Chronological Scientific Tables), 1986, Maruzen Co., Ltd."

#2: GSI's maps have particular size and its name: "Hana"; 46×58cm ≒ A2, "Kiku"; 64×94cm ≒ B1, "46"; 79×109cm ≒ A0

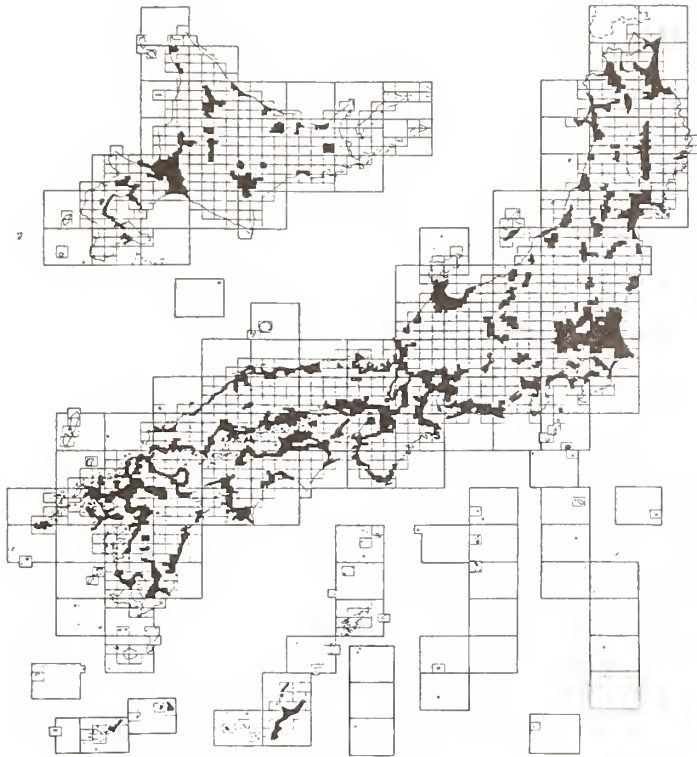


Fig. 1 Covered area of National Large-scale Map

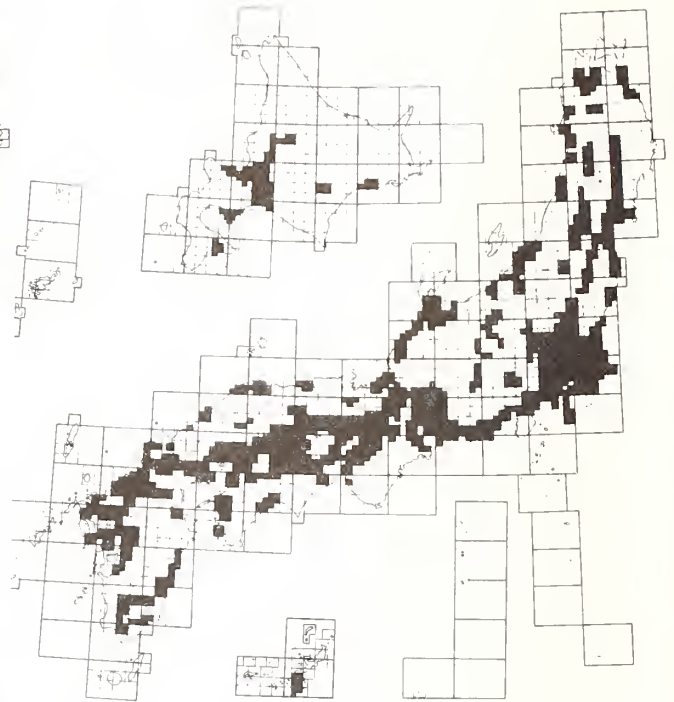


Fig. 2 Covered area of 1:25,000 Land Use Map

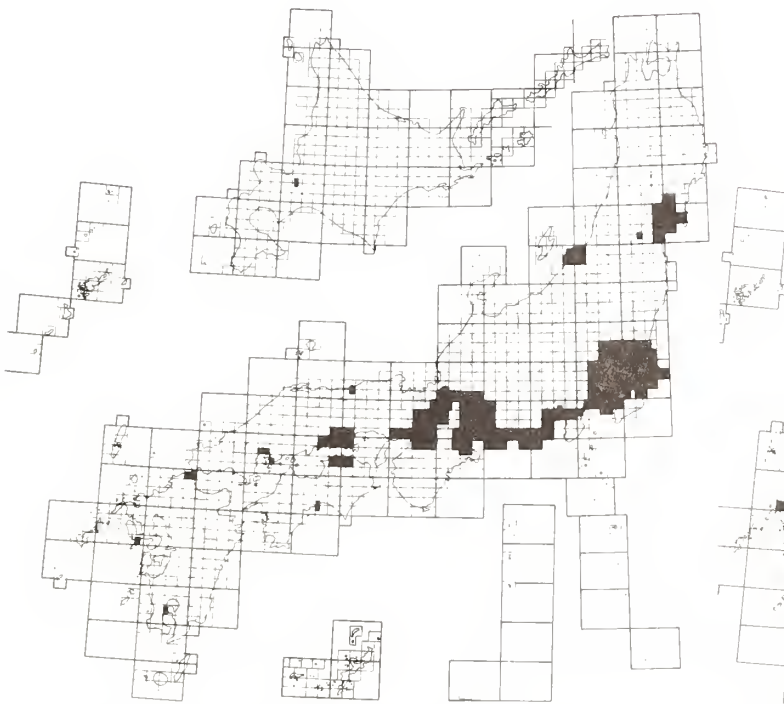


Fig. 3 Covered area of 1:25,000 Land Condition Map

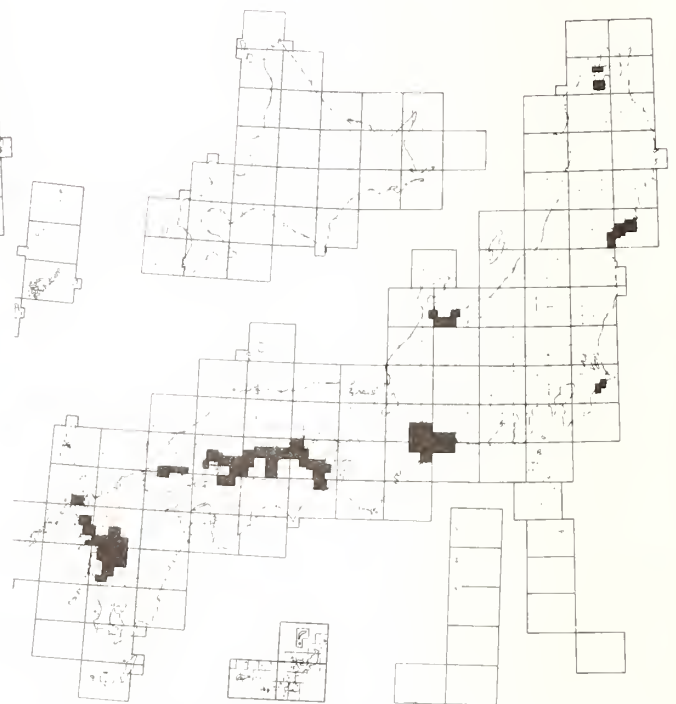


Fig. 5 Covered area of 1:25,000 Topographic Map of Coastal Area and 1:25,000 Land Condition Map of Coastal Area

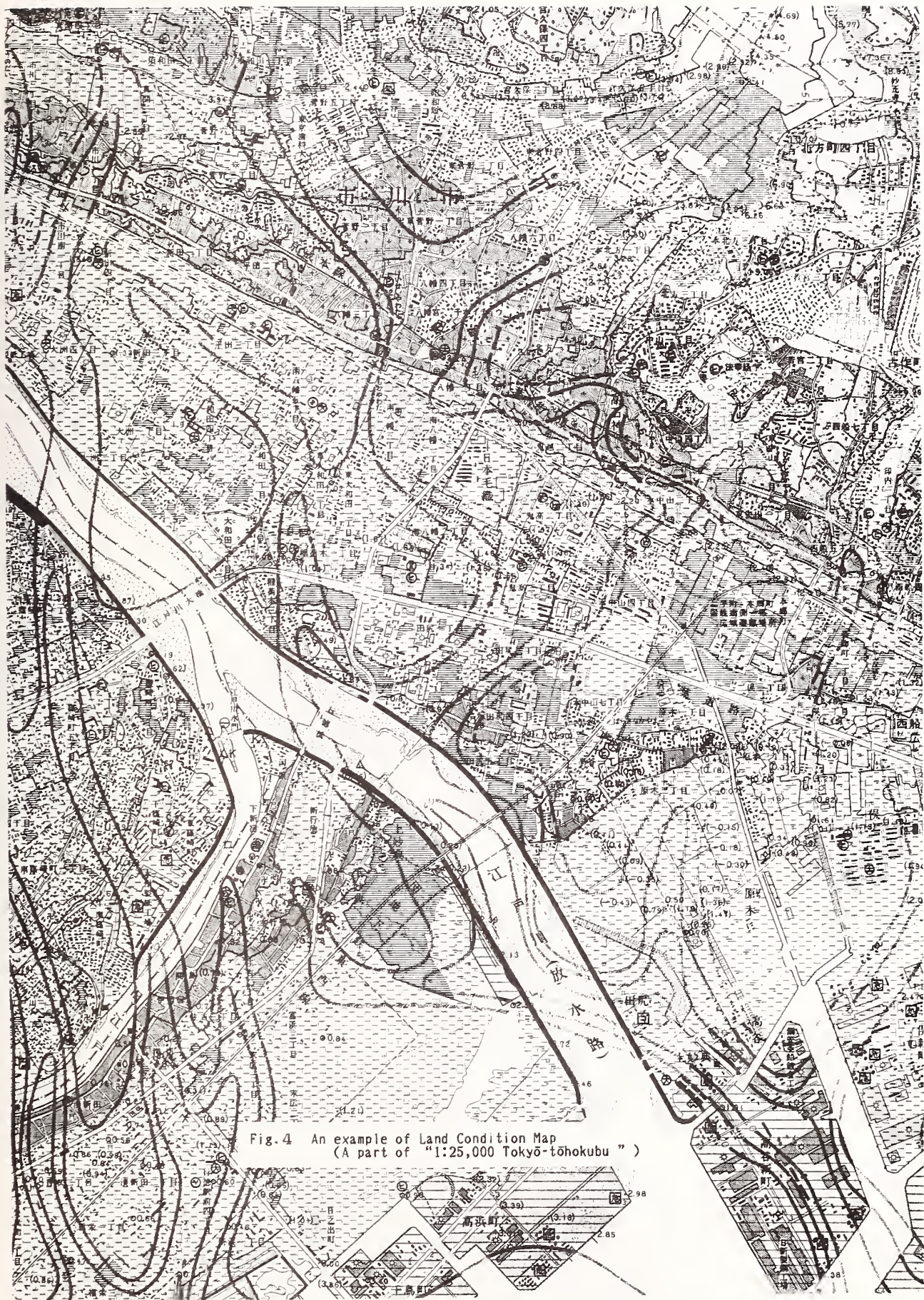


Fig.4 An example of Land Condition Map  
(A part of "1:25,000 Tokyo-tōhokubu" )

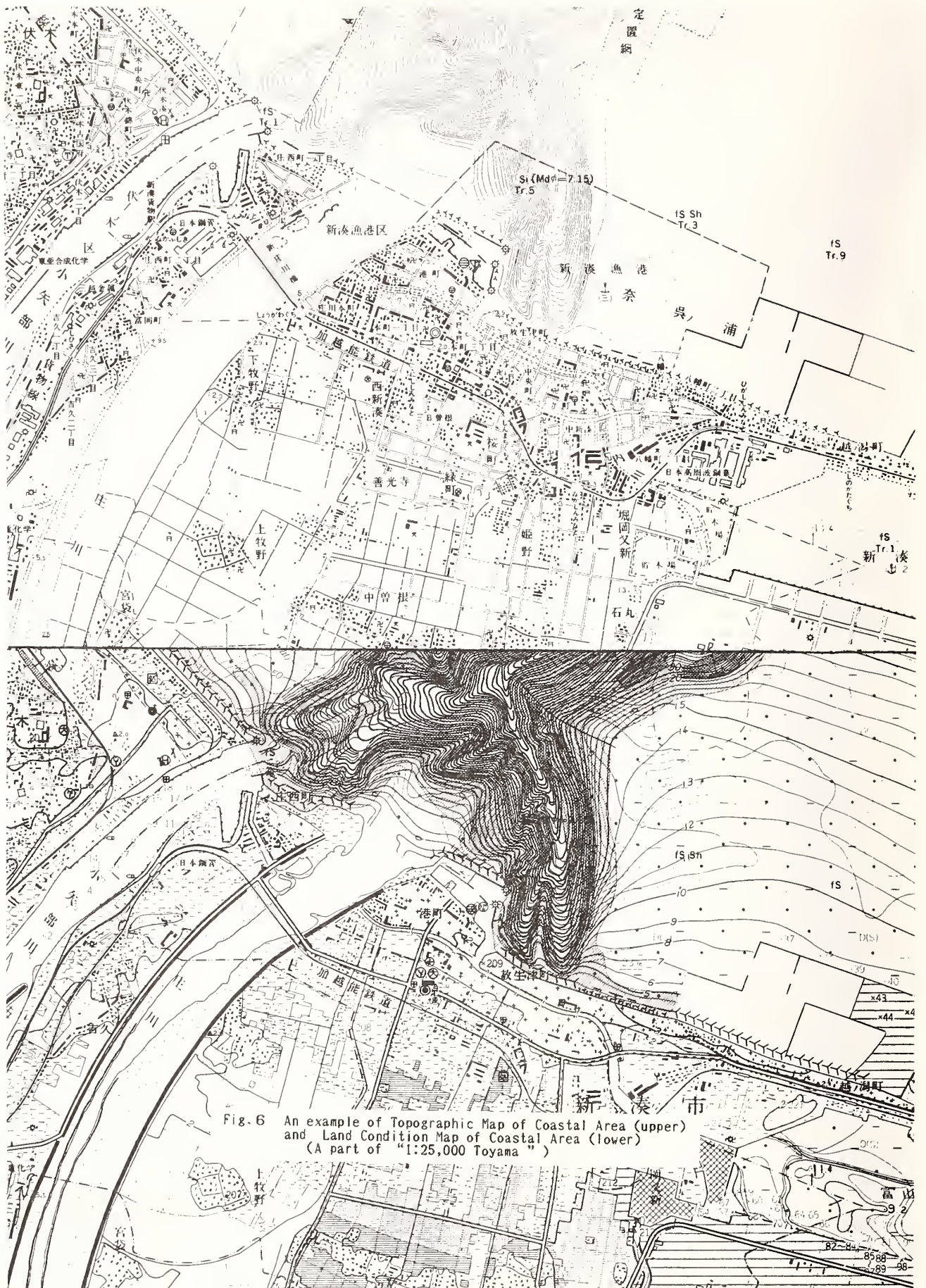


Fig. 6 An example of Topographic Map of Coastal Area (upper) and Land Condition Map of Coastal Area (lower) (A part of "1:25,000 Toyama")

Table 2 Landform classification of lowland on Land Condition Map and its characteristics  
(Miscellaneous units are omitted in this table)

(GSI's data)

	Landform unit	Underground condition	Ground high	Possibility of disaster	Desirable land use	Undesirable land use
Lowland, relatively higher and well drained	Alluvial fan	good, for the most area	high, in some degree	mud flow, flood	residential district plowed field	paddy field
	Natural levee	fairly good		great flood (unusual)		
	Sand dune Sand bank or Sand bar	good				
Lowland, general surface	Valley plain or Flood plain	slightly bad	low	flood innundation by inland water flood tide seismic disaster ground subsidence	paddy field park and green zone etc.	residential district industrial district
	Coastal plain or Delta	bad	extremely low			
	Back marsh or Interlevee lowland Former river bed	extremely bad				
Submersible land surface	High water river bed or Low water river bed				park and green zone etc.	
	Marsh or Area poorly drained					

Table 3. Series of digital geographic informations in GSI

(GSI's data)

No.	Name	Purpose (main)	Area to be covered	Information items (main)	Information sources
①	Digital National Land Information	Development planning for national and regional level	Entire country	Coast line • Lake Elevation Administrative boundary Land use River / Drainage basin Road • Railway Legally desingnated area	Topographic maps (1:25,000 ~1:200,000) Thematic maps Aerial photos Registers Statistics
②	Detailed Digital Land Use Information	Policy making for urban houseing land problems	Metropolitan and Osaka, Nagoya area	Land use (classified from viewpoint of houseing problem) Administrative boundary Regulation on land use	Topographic maps (1:10,000) Aerial photos Housing maps
③	Digital Cartographic Data of 1:25,000 Topographic Map	Creation of digital cartographic data base	Entire country	Contour (other items are being planed)	Topographic maps (1:25,000)
④	Digital Coastal Land Information	Development planning of coastal area for national and regional level	Coastal land area and sea zone	Same as ① and others	Same as ① and others

Table 4 Main items of Digital National Land Information

(GSI's data)

Items	Location expression	Remarks
Coast line	Shore line	Coordinate — Municipality code, Administration
	Length	Mesh
Lake	Shore line	Coordinate — Lake code, Depth
	Area	Mesh
River	Center line	Coordinate — River code
	Catchment	Mesh(subdiv.)
Topography	Mesh(subdiv.)	Ground elevation, Slope-gradient, Relief
Land classification	Mesh	Surface geology, Soil, Topography
Land use	Pattern	Mesh(subdiv.) — Land use classification (Paddy field, Dry field, Forest, Settlement orchard, Road, Railway, Water, etc.)
	Area	Mesh
Municipality	Boundary	Coordinate — Municipality code
	Area	Mesh
Legally designated zone	Mesh	City planning, National park, Land slide, Sand floor, etc.
Road	Coordinate	Route code, Road rank, Attachment
Rail way	Coordinate	Route code, Administration
Public facility	Coordinate	Classification, Name, Adress
Cultural property	Position	Coordinate — Historical remains, Monuments
	Distribution	Mesh
Land price	Coordinate	Official land price

Table 5 Main items of Detailed land Use Information

(GSI's data)

Item	Location expression	Remarks
Detailed land use	Mesh (10m)	Forest/Waste land, Paddy field, Dry field, Under construction, Open space, Industrial area, Residential area (Ordinary houses, Crowded houses, Higher storied houses), Commercial/Bussiness areas, Roads, Parks, Public facilities, Water surfaces, Others
Municipality		Municipality code
Large-scale development		Area for large-scale development of residential lots
Regulation on land use		National forest, Land slide prevention area, Green consavation area, Historic landscape prevention area, Agriculture promotion area
DID	Mesh (100m)	Densely Inhabited district
Use zone		Use zone prescribed by City Planning Act
Bulk ratio		Ratio of the total floor area of building to that of the lot prescribed by City Planning Act

# Dynamic Shear Moduli of Rockfill Materials

by

Norihisa MATSUMOTO<sup>1)</sup>, Nario YASUDA<sup>2)</sup>  
Masahiko OHKUBO<sup>3)</sup>

## ABSTRACT

In this paper dynamic shear moduli of two types of rockfill materials under saturated and air-dried conditions have been investigated by using the large-scale cyclic triaxial testing equipment.

Materials used in these tests are gabbro and dolerite.

The tests are performed to study the effects of confining pressure, shear strain and principal stress ratio, etc. on the dynamic shear moduli.

The following results are obtained on the dynamic deformation characteristics of rockfill materials.

- 1) Shear moduli  $G$  of saturated specimen depend on and are proportional to mean principal stress  $\sigma_m$  like on an air-dried specimen.
- 2) Shear moduli  $G$  decreases according to the increase of shear strain  $\gamma$ , but the proportion of the decrease of  $G$  is independent of  $\sigma_m$ . However it is recognized that the proportion of decrement relates to the types of rockfill materials.
- 3) The harder material from the point load tests give the greater shear moduli.
- 4) Shear moduli  $G$  of saturated specimens are around 90 percent of those of air-dried ones, but saturated specimens have the same damping ratio as air-dried ones.

KEY WORDS; Dynamic deformation characteristic, Cyclic triaxial test, Coarse-grained granular materials

## 1. INTRODUCTION

The authors presented the paper which described the dynamic deformation characteristic of coarse-grained granular materials under air-dried condition in the sixteenth joint meeting of UJNR at Washington D.C. in 1984.

Input properties of materials for dynamic analysis of rockfill dams are determined at laboratory tests with air-dried specimens. However input properties of upstream saturated zone of dam body are estimated from test results with air-dried rockfill materials.

Strength and deformation characteristics of saturated materials seem to be different from downstream dry materials from geophysical explorations of rockfill dams.

The need to clarify the deformation characteristics of saturated rockfill is recognized in the aseismatic design of rockfill dams.

Dynamic deformation characteristic is seemed to be greatly affected by the quality of rockfill, so two types of rock are prepared for tests. One type is very hard gabbro and another is slightly hard dolerite.

## 2. GENERAL DESCRIPTION OF TEST

### 2.1 Preparation of saturated specimen

The size of saturated columnar specimen is 30-cm in diameter and 60-cm in length.

The materials were placed in six layers, and each layer was compacted with 33 kgf weight electric vibratory rammer which has 950 compaction blows per minute.

The test density was determined from the compaction tests so that relative density of the materials should be 85 percent. The confining pressure of 0.2 kgf/cm<sup>2</sup> is applied to the specimen and the vacuum pressure inside the specimen is released. After carbon dioxide (CO<sub>2</sub>) is supplied to the specimen for 12 to 24 hours, de-aired water of 10 liters is also provided gradually to the specimen from the bottom for 24 hours.

Saturation degree of the specimen is investigated by Skempton's B-value (the ratio of the increment of pore water pressure to that of confining pressure) and test is carried out about the specimen which B-value is more than 0.96. The specimen is subjected to back pressure of 2.0 kgf/cm<sup>2</sup>.

### 2.2 Test method

The specimen was at first uniformly or anisotropically consolidated with a certain confining pressure, and then cyclic deviatoric axial stress of 0.2 Hz is applied to axial stress. The four levels of confining pressure were

- 
- 1) Dr. of Eng., Head, Filltype Dam Division, Dam Department Public Works Research Institute, Ministry of Construction, Japan
  - 2) Research Engineer, Filltype Dam Division, Dam Department Public Works Research Institute, Japan
  - 3) Engineer, Filltype Dam Division, Dam Department Public Works Research Institute, Japan

taken for a specimen as 1,2,3 and 4 kgf/cm<sup>2</sup>. The deviatoric stress (stress of 20 steps was provided) was increased gradually at the same confining pressure, and the specimen was subjected to next confining pressure, when the strain reached to around  $5 \times 10^{-4}$ . The test was carried out under drain condition.

### 2.3 Test material

Test materials are gabbro (material A) and dolerite (material B), and rockfill materials of dams under construction by the Ministry of Construction.

The physical properties of materials are shown in Table-1, and Figure-1 illustrates the gradation curve of the samples.

The maximum particle size of the sample  $D_{max}$  is 63.5 mm, which is less than 1/5 of the specimen size. Uniformity coefficient  $U_c$  is 6.1 for gabbro and 12.0 for dolerite.

### 2.4 Arrangement of test results

The test results are digitized and recorded by automatic data acquisition system with a personal computer.

The tenth stress-strain loop of the cyclic loading was used for obtaining dynamic deformation properties at each stress level. Poisson's ratio is calculated from axial strain and volumetric strain at the same stress level, and shear moduli and shear strains are given by dynamic elastic moduli and axial strain through Poisson's ratio at each level.

### 2.5 Point load test

Point load test was carried out in order to investigate the difference of quality of rock materials.

Two types of materials as shown in Table-1 are used under air-dried and wet condition. The particle size of rock ranges from 63.5 mm to 50.8 mm, the number of sample is about 30 in each type.

## 3. TEST RESULTS

### 3.1 The effect of confining pressure

Figure-2 indicates the relation between shear modulus  $G$  and mean principal stress  $\sigma_m$  through the parameter  $\gamma$  (shear strain) under principal stress ratio  $\sigma_1/\sigma_3$  of 1.0. Shear moduli  $G$  of both types of materials are in linear proportion to mean principal stress  $\sigma_m$  at semi-log scale like the test results of air-dried specimens, therefore it is recognized that the effect of  $\sigma_m$  to  $G$  is obvious.

The decrease of  $G$  has a tendency to become distinguished like air-dried materials with the increase of shear strain, meanwhile the slope of experimental line is not changeable to  $\sigma_m$ .

Damping ratio as shown in Figure-3 has a tendency to become smaller with increasing confining pressure, and

is slightly scattering about material A (gabbro). However, damping ratio of material B (dolerite) is independent of  $\sigma_m$ . Consequently it is concluded that damping ratio  $h$  is not affected by confining pressure  $\sigma_m$ , but affected by the quality of saturated rockfill material. The damping ratio of material A is smaller than that of material B. The damping ratio  $h$  of air-dried specimen is scattering and not appeared to depend on confining pressure.

Poisson's ratio of saturated specimen is influenced by confining pressure  $\sigma_m$  and decreasing with increasing of  $\sigma_m$  as shown in Figure-4.

### 3.2 Dependency of shear strain

The relation between shear moduli and shear strain is indicated in Figure-5 (material A,  $\sigma_1/\sigma_3 = 1.0$ ), and scattering at shear strain less than  $5 \times 10^{-6}$ . This range of shear strain is lower limit of measurement. Shear modulus  $G$  at this shear strain seems to get near initial shear modulus. Shear modulus  $G$  decreases with the increase of shear strain  $\gamma$ . Figure-6 illustrates the relation between shear strain and shear modulus which is divided by shear modulus  $G_0$  at small shear strain. The rate of decrease of shear moduli at both materials becomes smaller with the increase of confining pressure, but is not greatly affected by the amount of pressure.

The decrement of  $G/G_0$  of saturated specimen is slightly smaller than that of air-dried one.

The decrement of  $G/G_0$  of material B concerning the increment of shear strain is appeared to be faster than material A for crushing of material B due to cyclic load.

### 3.3 The effect of principal stress ratio

Figure-7 shows the relation between shear modulus  $G_0$  at very small shear strain and principal stress ratio  $\sigma_1/\sigma_3$ . However,  $G_0$  is divided by  $F(e) = (2.17 - e)^2 / (1 + e)$  to eliminate the effect of void ratio  $e$ .

Shear modulus  $G$  of material A under air-dried condition is increasing with the increase of principal stress ratio.

As for saturated material, maximum value of shear moduli is obtained in the range of the principal stress ratio of 1.0 to 1.4, but shear modulus does not depend clearly on principal stress ratio.

The dependency of principal stress ratio is not noticeable in shear modulus of material B under air-dried condition.

After the report of simple shear test by using the hollow cylindrical specimen of Toyoura standard sand<sup>3)</sup>, shear modulus is independent of principal stress ratio in the range of 1.0 to 1.4 at shear strain less than  $1 \times 10^{-4}$  when mean principal stress is constant.

The shear moduli of coarse-grained materials are not seemed to have a dependency of principal stress ratio like those of standard sand.

### 3.4 The difference of material

It is concluded that material A (gabbro) is harder than material B (dolerite) from specific gravity, absorption and the amount of grain breakage as shown in Table-1 (physical properties of materials).

Point load test was carried out to investigate the hardness of both materials quantitatively. Figure-8 shows the histogram of point load strength at an interval of 50 kgf/cm<sup>2</sup>. Point load strength of rock is calculated by the following equation<sup>4)</sup>.

$$\sigma_t = 0.891 \times F/d^2$$

where  $\sigma_t$  ; point load strength (kgf/cm<sup>2</sup>)  
F ; ultimate load (kgf)  
d ; a space between two points

The point load strength of material A is stronger than that of material B according to the histogram. The strength of both saturated materials decreases as shown in the figure.

The strength of each material with arithmetic mean is as shown in the followings.

Material A (air-dried) = 146.3 kgf/cm<sup>2</sup>  
(saturated) = 133.9 kgf/cm<sup>2</sup>  
Material B (air-dried) = 95.1 kgf/cm<sup>2</sup>  
(saturated) = 81.9 kgf/cm<sup>2</sup>

The ratio of the decrease of strength by saturation is 8.5% and 13.9% at each material.

The relation of shear moduli  $G_0$  at very small shear strain with confining pressure under saturated and air-dried conditions is illustrated in Figure-9, which shows the decrease of shear moduli due to the effect of saturation of both materials. Infiltrating fluid into the contact plane of rocks in saturated material is seemed to decrease the friction of contact plane and deform the specimen easily.

Figure-10 shows the same damping ratios of specimens under saturated and air-dried conditions.

The decrease of shear modulus at saturated material becomes smaller with increasing of confining pressure. The increase of contact pressure according to the increase of confining pressure and the diminish of fluid infiltration are appeared to restrain the deformation of specimen.

The decrement of shear modulus of saturated specimen is 12.4 percent for material A and 16.7 percent for material B concerning mean principal stress of 1.0 kgf/cm<sup>2</sup>. The shear moduli of saturated specimen are 90 percent of those of air-dried specimen for two types of material.

The shear modulus and point load strength of material B under air-dried condition are 0.6 to 0.7 as compared to those of material A, so it is concluded that the strength of rock greatly effects the shear moduli of triaxial specimens.

### 4. CONCLUSIONS

- 1) Shear moduli  $G$  of saturated specimen depend on and are proportional to mean principal stress  $\sigma_m$  like on an air-dried specimen.
- 2) Shear moduli  $G$  decreases according to the increase of shear strain  $\gamma$ , but the proportion of the decrease of  $G$  is independent of  $\sigma_m$ . However it is recognized that the proportion of decrement relates to the types of rockfill materials.
- 3) The harder material from the point load tests give the greater shear moduli.
- 4) Shear moduli  $G$  of saturated specimens are around 90 percent of those of air-dried ones, but saturated specimens have the same damping ratio as air-dried ones.

The geophysical explorations of several rockfill dams will be carried out in order to investigate above-mentioned test results.

### REFERENCE

- 1) N. Sakaino, N. Yasuda, N. Matsumoto – Dynamic deformation characteristics of coarse-grained granular materials. The 18th conference on engineering, 1985 (in Japanese).
- 2) N. Yasuda, M. Ohkubo, S. Arakawa, N. Matsumoto – Dynamic deformation characteristics of saturated coarse-grained granular materials, the 22th Japan national conference on soil mechanics and foundation engineering, 1987 (in Japanese)
- 3) F. Tatsuoka, N. Adachi – Soil mechanics (III) (Consolidation, Shearing and Dynamic analysis), Gihodo (PP. 223 ~ 224), 1979 (in Japanese)
- 4) Y. Hiramatsu, Y. Oka, H. Kiyama – Rapid determination of the tensile strength of rocks with irregular test piece, journal of the mining and metallurgical institute Japan. Vol.81, No.932, 1965 (in Japanese)

Table-1 Physical properties of materials

Material	Material A	Material B
Rock	Gabbro	Dolerite
Specific gravity	2.951	2.509
Absorption	0.875%	5.214%
Grain breakage <sup>1</sup>	2.0%	5.0%
Max. void ratio	0.691	0.744
Min. void ratio	0.349	0.319
Max. particle size	63.5 mm	63.5 mm
Min. particle size	0.84 mm	0.42 mm
Uniformity coefficient	6.1	12.0
Relative density	85%	85%

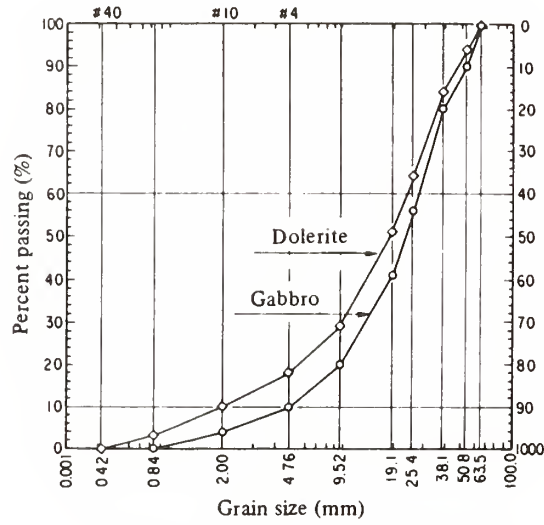


Figure-1 Grain size distribution curve

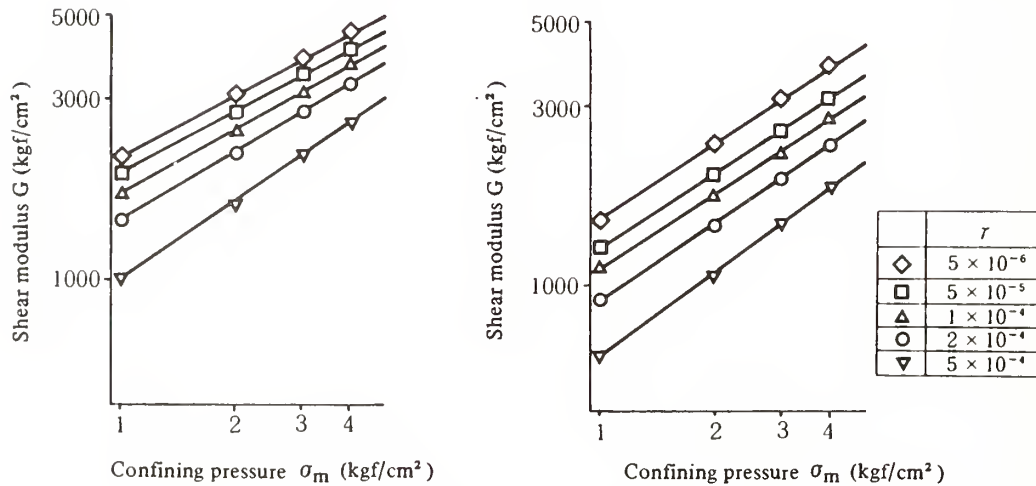


Figure-2 The relation between G and  $\sigma_m$

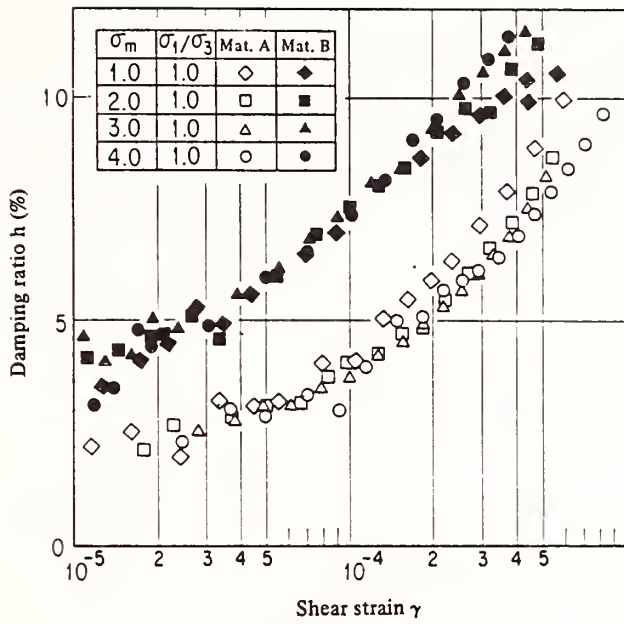


Figure-3 The relation between  $h$  and  $\gamma$

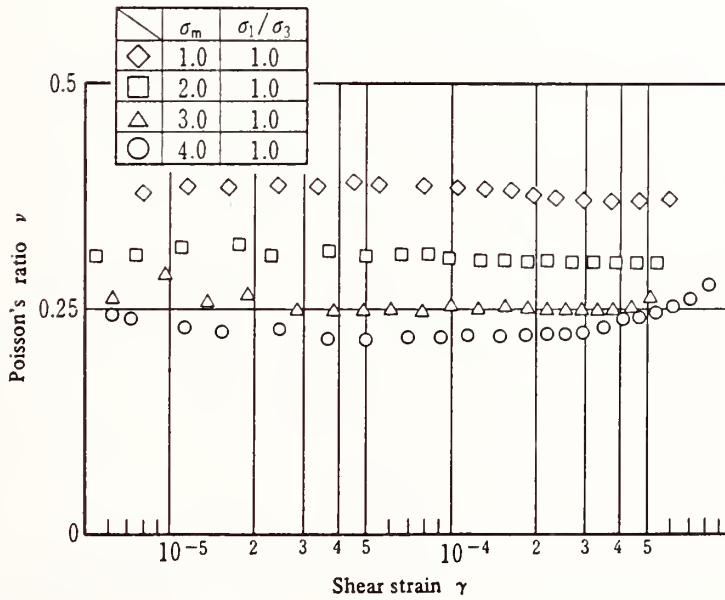


Figure-4 The relation between  $\nu$  and  $\gamma$

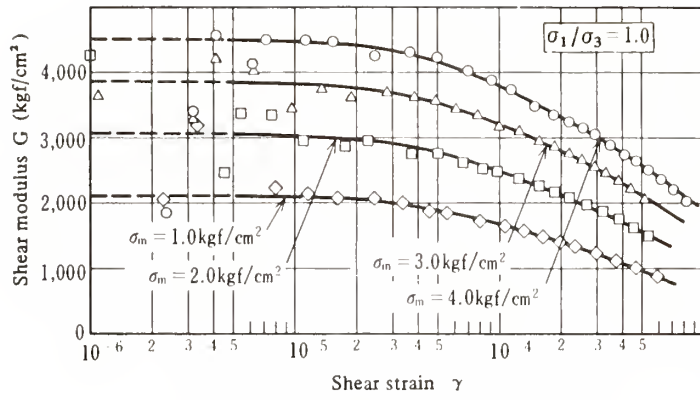


Figure-5 The relation between G and  $\gamma$

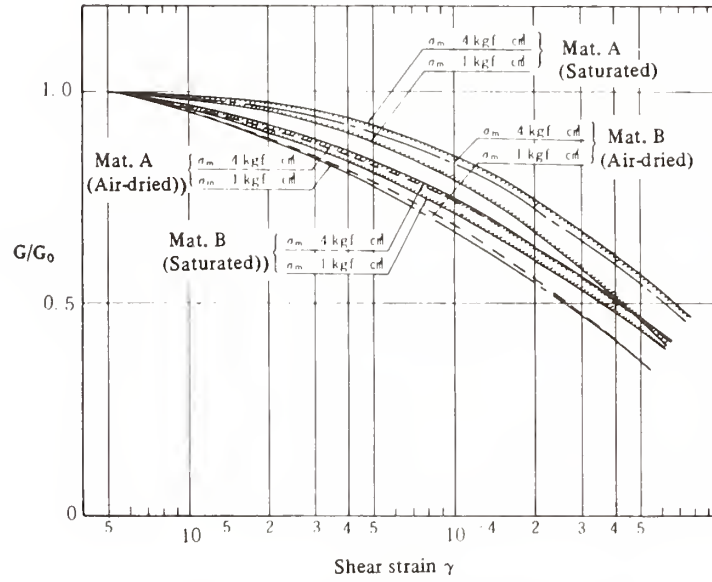


Figure-6 The relation between  $G/G_0$  and  $\gamma$

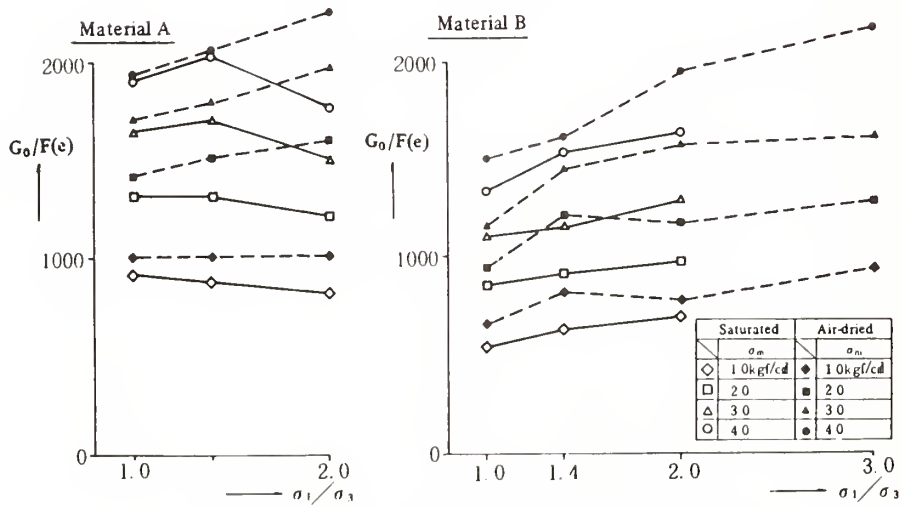


Figure-7 The relation between  $G_0/F(e)$  and  $\sigma_1/\sigma_3$

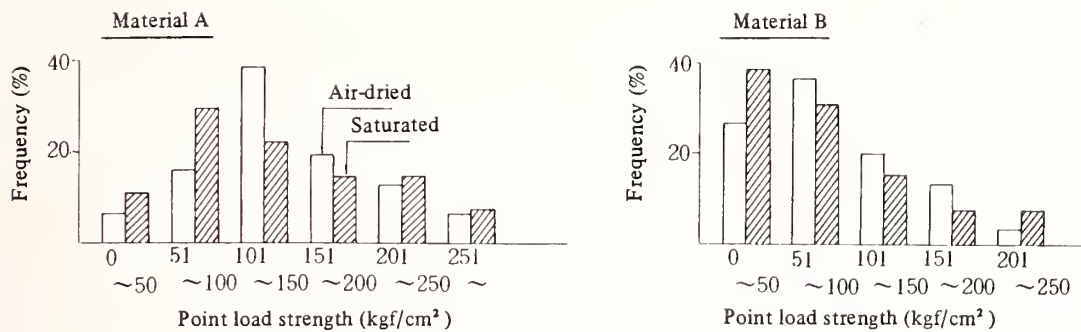


Figure-8 Frequency distribution of point load strength of rocks

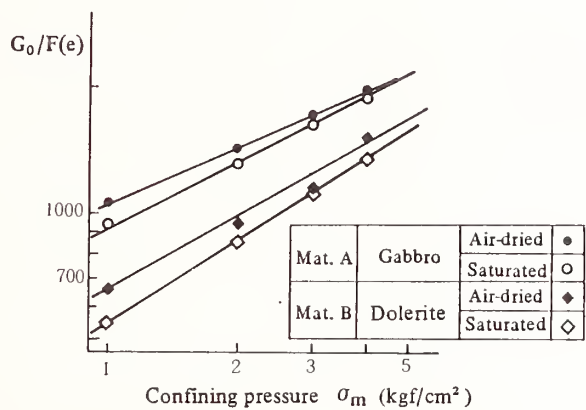


Figure-9 The relation between  $G_0/F(e)$  and  $\sigma_m$

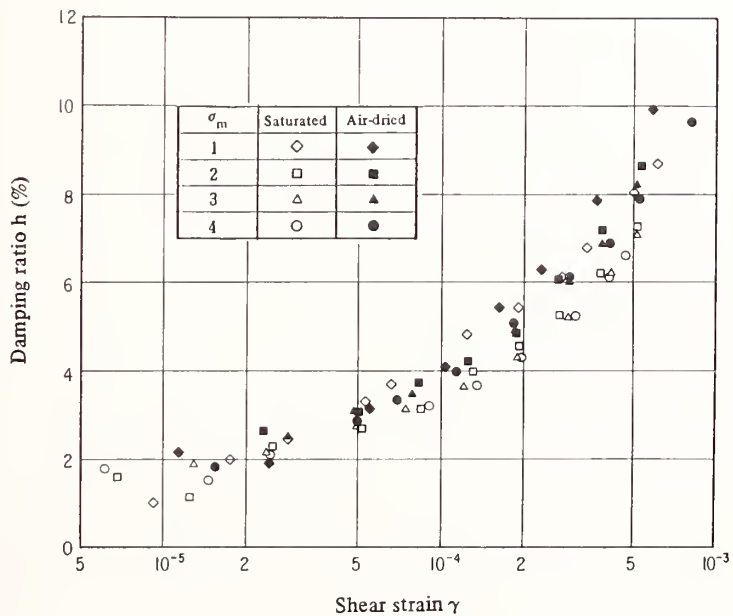


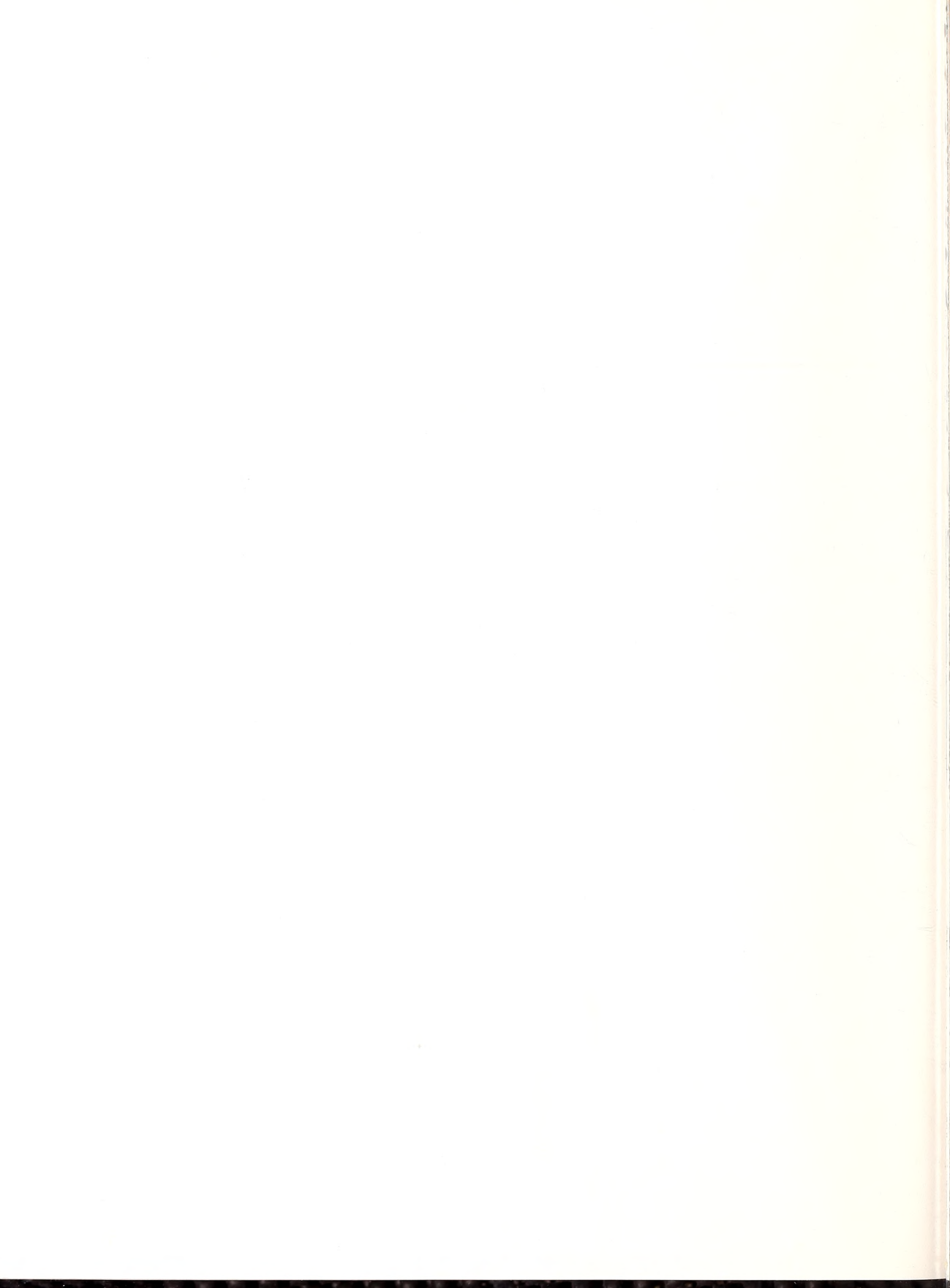
Figure-10 The relation between  $h$  and  $\gamma$



## **Appendix:**

---

### **Task Committees A–J Reports**



Report of Task Committee on

(A) STRONG-MOTION INSTRUMENT ARRAYS AND DATA

Date: May 18, 1988

Place: National Bureau of Standards  
Gaithersburg, MD 20899

Attendees: Japan Side - S. Noda (Actg. Chairman) (PHRI)  
Y. Yamazaki (BRI)  
K. Ohtani (NRCDP)

U.S. Side - H. Meyers (Actg. Chairman) (NOAA)  
W. Hayes (USGS)  
T. Holzer (USGS)

I. Activities and Principal Accomplishments to Date

1. Catalogs of strong-motion earthquake records observed both in the United States and Japan are being exchanged. U.S. data are published in the "Seismic Engineering Program Report," and the Japanese data are published in "Strong-Motion Earthquake Records in Japan." Many other publications were also exchanged.
2. A workshop on strong-motion earthquake observation was held at the USGS in Menlo Park, CA, in August 1987.
3. The U.S.-side provided to the Japanese-side information on the Whittier Narrows earthquake of 1 October 1987 and the Superstition Hills earthquake of 24 November 1987. The Japanese-side provided to the U.S.-side information on the Eastern Chiba Offshore Earthquake of 17 December 1987 and the earthquake of 18 March 1988. In all cases the information was exchanged soon after the events.
4. An effort was continued to establish a policy for international dissemination of strong-motion earthquake records. This will be an important contribution to the International Decade of Natural Disaster Reduction (IDNDR).
5. The U.S.-side presented the Japanese-side with a floppy diskette containing a preliminary global strong motion data catalog and an access program prepared by NOAA's National Geophysical Data Center. Comments were invited.

## II. Future Programs

1. After an earthquake which has caused damage to structures or an earthquake during which maximum acceleration exceeding about 0.1g has been recorded, the Task Committee of the country where the earthquake has taken place will provide a list of the strong-motion earthquake records for its counterpart Task Committee. The list will contain maximum component accelerations of each record. If such a list is compiled by others, the list mentioned above may be replaced by it.
2. Every year the Task Committee will exchange catalogs of the strong-motion earthquake records during the previous year. The catalog contains maximum component accelerations and wave forms of major records. If there is such a catalog compiled by any organization, the catalog mentioned above may be replaced by it.
3. The Task Committee makes appropriate arrangements to provide digitizable copies of records when they are requested. In addition, arrangements will be made to provide information on the characteristics of the site, instrumentation, and structures at the locations where such records are obtained.
4. When the organizations taking part in the Panel publish reports on strong-motion earthquake records, these organizations will distribute copies of the reports to the other organizations of the Panel interested in them. The Task Committee exchanges lists of the organizations and their Panel representatives who wish to receive the reports.
5. The Task Committee will continue to exchange digitized data on all the major strong-motion earthquake records recovered in both countries, under the conditions mutually acceptable to the agencies involved in acquiring the data.
6. The Task Committee will exchange technical information on development of seismometers and accelerometers, on the deployment and installation of instruments with emphasis on bore-hole instruments, and on the design of seismic arrays.
7. The Task Committee plans to assist and cooperate, where possible, in the following areas:
  - a. with governmental organizations in other seismic areas, to promote high quality strong earthquake motion observations in all seismically active areas of the world.
  - b. with any international effort to record strong ground motion close to the source of a large magnitude shock.

- c. with exchange of scientists, engineers, and appropriate equipment in a timely fashion for observations following large earthquakes in either country. As the largest and most interesting aftershocks occur immediately following the main earthquake, recovery of the most useful aftershock data requires that the response to major earthquakes be initiated as rapidly as logistics permit.
8. The Task Committee feels the UJNR Panel on Wind and Seismic Effects should play a major cooperative role in the implementation of relevant parts of the Resolution of the International Workshop on Strong-Motion Earthquake Instrument Arrays held May 1978, in Honolulu, Hawaii. Another meeting having similar goals is being discussed in conjunction with the 9th WCEE in August 1988. The exchange of complete information on all aspects of the program, as it develops particularly in Japan and the United States, will be carried out in the manner of our standard exchange, as appropriate. Task Committee Chairmen will retain the responsibility of relaying information on the existence of unique data from arrays or deep bore-hole instruments in the U.S. and Japan, and subsequently of transferring the digital data from such institutions as the USGS, CDMG, USC, and UCSD in the U.S.; and PWRI, BRI, PHRI, MRI, and NRCDP in Japan.
9. The Task Committee recommends collaborative studies involving strong-motion instrumentation and interpretation of resulting strong-motion data sets for purposes of earthquake hazard reduction.
10. The Task Committee will attempt to complete within the next year at least items 1 through 4 of the proposed table of contents of the 19th Joint Meeting Task Committee Report on Policy for International Dissemination of Strong Motion Earthquake Records (policy is attached).
11. The Task Committee recommends that one of the themes of the Panel's next meeting should be related to the results of analyses of strong motion records from subduction earthquakes, e.g. Chile, Mexico, etc.
12. The Task Committee recommends that workshops should be held approximately every two years to keep abreast of the state-of-the-art relating to strong motion seismology with special emphasis on data acquisition and analysis.

Report of Task Committee on

(B) LARGE-SCALE TESTING PROGRAM

Date: May 18, 1988

Place: National Bureau of Standards  
Gaithersburg, MD 20899

Attendees: Japan Side - K. Ohtani (Chairman) (NRCDP)  
T. Murota (BRI)  
Y. Yamazaki (BRI)

U.S. Side - H. S. Lew (Chairman) (NBS)  
J. Z. Mirski (VA)  
A. J. Eggenberger (NSF)  
D. H. Oh (DOS)  
L. G. Guthrie (USAC)  
J. B. Scalzi (T/C "C") (NSF)  
G. R. Fuller (T/C "D") (HUD)  
J. Jirsa (Temp. Member) (University of Texas)

I. Activities and Principal Accomplishments to Date

The main activities related to this task committee during the past year are as follows:

1. Based on the results of the Reinforced Concrete Structures Program, a report on seismic design implications for reinforced concrete structures has been prepared by Professor Mete Sozen and submitted for publication in the ASCE Structural Journal. This report will be made available to the Japanese-side.
2. A summary report on the Steel Structures Program conducted by Japan has been prepared by Prof. Benjamin Kato. It will be available in the near future.
3. Testing of a full-scale 5-story masonry building was carried out at the Building Research Institute during November 1987-January 1988. Supporting component tests were also carried out by university members under TCCMAR/Japan coordination.
4. The Joint Technical Coordinating Committee (JTCC) meeting was held in Tokyo, in July 1987. A summary of the joint research on reinforced concrete structures and steel structures was conducted.
5. The 3rd Joint Technical Coordinating Committee on Masonry Research (JTCCMAR) was held in Hokkaido, in November, 1987. Coordinated research projects on masonry structures were discussed.

6. Active exchanges of U.S and Japanese researchers have taken place under the Joint Research Programs and have been useful.
7. In the U.S., the phase I of the Masonry Program which included the evaluation of materials and component behavior has been completed. The Phase II was initiated in October 1987 and will be completed in January 1992. This phase includes large subassemblage evaluation and a 5-story full-scale experimental test.
8. The U.S. side (NSF) proposed that Precast Seismic Structural Systems be the fourth topic for work under the Joint Large Scale Testing Program. The proposal was reviewed by the Japan-side and accepted.
9. NBS has initiated a multi-year project on seismic behavior of precast concrete frame structures in October 1987. This project will be coordinated closely with the work in item 8 above.

## II. Future Programs

The Task Committee adopted the following work as a result of discussion:

1. The Japanese-side will prepare "Design Guidelines for Medium Rise Reinforced Masonry Buildings" for publication.
2. The Japanese-side will continue analysis of full-scale and component experiments of masonry structures in support of developing the design guidelines stated in 1.
3. The U.S.-side will prepare a tentative coordinated research proposal on the precast seismic structural systems and will communicate with Mr. T. Murota of BRI who represents the Japanese-side.
4. The 4th meeting of JTCCMAR is scheduled in October, 1988 in San Diego, CA.
5. The Task Committee members discussed topics for future joint research projects. The Task Committee will facilitate continued deliberation of the following topics between appropriate U.S. and Japan organizations.
  - a. Seismic performance of composite and mixed construction
  - b. Application of high strength construction materials, such as concrete and steel, to structures in high seismic zones
  - c. Application of base isolation and controlled damping systems to critical structures located in high seismic and wind zones.

- d. Testings of full-scale structures other than buildings and bridges.
- 6. Task Committee (B), on Large-Scale Testing Program and Task Committee (D), on Evaluation of Performance of Structures should maintain closer liaison to facilitate the planning of instrumentation and analysis for full-scale test structures.
- 7. Exchange of information on large-scale testing facilities and large-scale testing programs should be encouraged.

Report of Task Committee on

(C) REPAIR AND RETROFIT OF EXISTING STRUCTURES

Date: May 18, 1988

Place: National Bureau of Standards  
Gaithersburg, MD 20899

Attendees: Japan Side - T. Murota (Acting Chairman) (BRI)  
K. Ohtani (NRCDP)  
Y. Yamazaki (BRI)

U.S. Side - J. B. Scalzi (Chairman) (NSF)  
H. S. Lew (NBS)  
J. Z. Mirski (VA)  
A. J. Eggenberger (NSF)  
D. H. Oh (DOS)  
L. G. Guthrie (USAC)  
G. R. Fuller (T/C "D") (HUD)  
J. Jirsa (Temp. Member) (University of Texas)

I. Activities and Principal Accomplishments to Date

1. A workshop was held in September 1987 in Los Angeles to develop a research agenda for repair and retrofit of various types of buildings in the United States. A report of the workshop was prepared.
2. The Japanese Manual on Repair and Retrofit of Existing Buildings has been translated into English.
3. A compilation of data on the cost of strengthening buildings of various types is being completed.
4. A contract has been awarded to URS/John Blume (by FEMA) to develop cost data for various methods to repair and retrofit buildings.

II. Future Programs

1. Continue and expand the activity on exchanging reports, books, and special publications for the repair and retrofit of existing structures.
2. There is great interest from both sides on the repair and retrofit of buildings of various types. It has been noted that the techniques being used in both countries are similar and cooperative efforts in these areas will be useful and beneficial.
3. A workshop is planned for 1989 on the design and construction process of buildings undergoing repair and retrofit. It is scheduled to be held in southern California prior to the 21st UJNR meeting.

4. The development of non-destructive evaluation equipment to determine in-situ material properties and global structural behavior will be given more attention and emphasis.

Report of Task Committee on

(D) EVALUATION OF STRUCTURAL PERFORMANCE

Date: May 18 & 19, 1988

Place: National Bureau of Standards  
Gaithersburg, MD 20899

Attendees: Japan Side - Y. Yamazaki (Chairman) (BRI)  
T. Murota (BRI)  
K. Yokoyama (T/C "G") (PWRI)

U.S. Side - G. R. Fuller (Chairman) (HUD)  
A. J. Eggenberger (NSF)  
J. B. Scalzi (NSF)  
R. McConnell (VA)  
L. G. Guthrie (USAC)  
R. D. Marshall (T/C "G") (NBS)  
J. L. Noland (Temp. Member) (Atkinson-Noland)  
J. Jirsa (Temp. Member) (University of Texas)

I. Activities and Principal Accomplishments to Date

1. At the Task Committee meeting, members discussed several reports on evaluating seismic resistance of buildings. Copies of the following reports were given to the Japanese side:
  - a. Whittier Narrows Earthquake, October 1, 1987: NBS Reconnaissance Report by H. S. Lew, and several reports submitted to the House of Representatives Committee on Science, Space, and Technology on November 10, 1987
  - b. ATC-14 "Evaluation Methodologies for Seismic Resistance of Existing Buildings"
  - c. EERI Report on Performance of Buildings in Mexican Earthquake, Sept. 1985
2. Also discussed were the following technical reports presented at the 20th UJNR Joint Meeting:
  - a. II-11, "Seismic Performance of Reinforced Concrete High-Rise Frame Structure" by Hirosawa, et al.
  - b. II-13, "Base Isolated Building Structures in Japan" by Kitagawa and Hirosawa.
  - c. II-16, "Investigation of Two Buildings Shaken During the 19 September 1985 Mexico Earthquake" by Foutch, et al.

- d. II-17, "Recorded Behavior of Structures, Whittier Narrows Earthquake, October 1987" by Brady, USGS.
3. Members of T/C "G" met with T/C "D" to discuss a proposal for combining the two Task Committees to evaluate structural performance of buildings subjected to earthquakes and high winds. A proposal was developed for submittal by T/C "G" to the Joint Panel on Wind and Seismic Effects. T/C "D" concurs with this proposal.
4. General discussions also took place on coordination of other activities of Task Committees B, C, and D. Several proposed projects and activities were presented.

## II. Future Programs

1. Buildings with base isolation or response control systems will be added to the catalog of "Benchmark Structures." The Japan-side will furnish to the U.S.-side copies of the MOC State-of-the-Art Report and the Catalog of Base Isolation Buildings. Data will be collected on analysis and instrumentation of these buildings and evaluation of performance will be reported after future seismic events. Wind response also will be investigated. The Japan-side will furnish to the U.S. engineering community, the MOC criteria used to evaluate structural performance of buildings when it is completed.
2. A workshop on "Sensor Technology Applied to Large Engineering Systems" is being planned by T/C "G" for the Fall of 1988 in Boulder, CO. This will be coordinated with T/C "C" and T/C "D".
3. A project on Nondestructive Evaluation of Existing Masonry Buildings will be conducted on June 23-24, 1988 in Williamsburg, VA by James Noland, under the UJNR TCCMAR Program.
4. T/C "D" will participate with T/C "C" in their proposed fifth workshop on "Design and Construction Technology" for repair and retrofit of existing structures. The workshop is being scheduled in Southern California prior to 21st UJNR Joint Meeting.
5. Copies of the following reports will be forwarded to the Japan side upon completion:
  - a. "Survey of Masonry Buildings after Whittier Narrows Earthquake" by Dr. Gary Hart.
  - b. "Evaluation and Strengthening of Existing Buildings in Italy", by James Noland for NSF under US-Italy Program.

- c. ATC-20 "Development of Procedures for Post-Earthquake Safety Evaluation of Buildings", ATC-21 "Screening Methodologies", and ATC-22 "Evaluation of ATC-14 Provisions", FEMA projects.
6. Analysis, instrumentation, and post-earthquake evaluation of masonry buildings and mixed construction will be included in the scope of T/C "D".

Report of Task Committee on

(E) NATURAL HAZARD ASSESSMENT AND MITIGATION THROUGH LAND USE PROGRAMS

Date: May 19, 1988

Place: National Bureau of Standards  
Gaithersburg, MD 20899

Attendees: Japan Side - K. Hasegawa (Temp. Chairman) (PWRI)  
O. Matsuo (PWRI)  
U.S. Side - S. T. Algermissen (Chairman) (USGS)  
W. Hays (USGS)

I. Activities and Principal Accomplishments to Date

1. The Geographical Survey Institute (GSI) of Japan has been developing mapping procedures for natural hazard prediction.

The Public Works Research Institute (PWRI) of Japan has revised a procedure for assessing direct and indirect losses from earthquake disasters, and the direct and indirect losses were evaluated for the Miyagi-ken-oki earthquake of 1978 and the Nihon-kai chubu earthquake of 1983.

The Building Research Institute (BRI) of Japan is developing automatic computer programs for analyzing the expected ground intensity at an arbitrary site and has made analyses on ground response characteristics.

The National Research Center for Disaster Prevention (NRCDP) of Japan has been developing a seismic microzoning method using an urban ground database, and applying satellite remote sensing technology to natural disaster prevention.

2. The U.S. Geological Survey (USGS) conducts a broad based program in natural hazards reduction. This program includes assessment of: (1) earthquake ground motion; (2) soil liquefaction potential; (3) landslide potential; and (4) earthquake economic losses.
3. During the past year technical papers were exchanged by the two co-chairmen. Twenty-three papers were sent from the United States to Japan and twelve were sent from Japan to the United States.
4. A number of papers pertaining to Task Committee (E) were included in the proceedings of the 20th Joint Panel Meeting.

Future Programs

1. Both sides will continue to exchange technical information on the following subjects:
  - a. Evaluation of seismic hazard and mapping procedures.
  - b. Evaluation of damage potential of structures, soil liquefaction potential and tsunami hazard.
  - c. Seismic response characteristics under various ground and topographic conditions.
  - d. Planning methodologies for earthquake disaster mitigation in large populated cities.
  - e. Evaluation of social-economic losses from earthquake disasters.
2. Both sides will continue to promote coordinated research and exchange of specialists in natural hazard assessment and mitigation through land use program.
3. The U.S. chairman will furnish to task committee members future reports on natural hazard assessment and mitigation through land use programs being coordinated or sponsored by the Federal Emergency Management Agency (FEMA), the Interagency Coordinating Committee of the National Earthquake Hazards Reduction Program (ICC/NEHRP), the U.S. Geological Survey (USGS), the National Science Foundation (NSF), and the National Academy of Sciences and the National Academy of Engineering (NAS/NAE).

The Japanese chairman will perform similar responsibilities for reports from the National Research Center for Disaster Prevention (NRCDP), Geographical Survey Institute (GSI), Public Works Research Institute (PWRI), Building Research Institute (BRI), and Port and Harbor Research Institute (PHRI).

4. Both sides have agreed to hold a workshop at the Public Works Research Institute in 1989. The following workshop details were discussed:
  - a. The US-side suggested the title: "Earthquake Hazard and Risk Assessment--Research and Progress.
  - b. The following technical areas should, if possible, be included in the workshop:
    1. Probabilistic earthquake hazard assessment
    2. Delineation of seismotectonic elements
    3. Attenuation of seismic waves
    4. Site response

5. Earthquake losses
  6. Application of hazard assessment to seismic provisions of building codes
- 
- c. If possible, abstracts of presentations will be exchanged by the co-chairmen by the end of September 1988.
  - d. The number of speakers are estimated to be six from the US-side and ten from the Japan-side.
  - e. The workshop will be held for two days, probably on Thursday and Friday preceding the 21st US-Japan Joint Meeting.
  - f. Discussions will address ways to cooperate within the framework of the International Decade for Natural Disaster Reduction.

Report of Task Committee on

(F) DISASTER PREVENTION METHODS FOR LIFELINE SYSTEMS

Date: May 19, 1988

Place: National Bureau of Standards  
Gaithersburg, MD 20899

Attendees: Japan Side - S. Noda (Temp. Chairman) (PHRI)  
Y. Sasaki (PWRI)

U.S. Side - S. C. Liu (Chairman) (NSF)  
R. Eguchi (Dames & Moore)  
J. Isenberg (Paul Weidlinger Assoc.)  
T. C. Liu (USAC)  
K. Thirumalai (FEMA)

I. Activities and Principal Accomplishments to Date

1. A technical report by PWRI entitled, "The Manual of Repair Methods for Civil Engineering Structures Damaged by Earthquakes" (in Japanese) was made available to NSF. In the Manual procedures of damage surveys and repair works for civil engineering structures including buried sewer pipelines are described. An outline of the results of this research project was introduced at the 18th UJNR Joint Meeting of the Panel on Wind and Seismic Effects. The MOC and PWRI authorized NSF to translate it into English and to distribute it to the U.S. professional community. The translation of the document has been completed by the National Center for Earthquake Engineering Research at Buffalo and is being printed for public distribution.

Seminars on "The Manual of Repair Methods for Civil Engineering Structures Damaged by Earthquakes" (in Japanese) were held in 9 major Japanese cities including Tokyo, Osaka and Nagoya between April and November 1987. Approximately 2000 practitioners participated in these seminars.

2. New task committee members have been recruited to expand the technical activities of the committee. Current new additions are: Mr. James Cooper of U.S. Federal Highway Administration, Mr. Jack Spencer of U.S. Coast Guard, Dr. Spencer Wu of U.S. Air Force Scientific Research Office, Dr. Tony Liu of U.S. Army Corp. of Engineers, and Dr. K. Thirumalai of FEMA.
3. A field experimental research project is currently being conducted by Dr. Jerry Isenberg of Weidlinger Associates of Los Altos, California. The experiment placed eight segments of ductile iron pipes to the local strike of the San Andreas fault. These pipes have been instrumented with transducers and connected to a centralized data acquisition and recording

system. Two additional longer segments of welded steel pipeline are placed to the strike. These have been instrumented with strain gauges.

The objective of the experiment is to gather data to investigate the behavior of pipelines subject to lateral offset and to wave propagation effects. Discussions have been underway between Dr. Isenberg and PWRI researchers to expand the experiment by installing additional measurement devices or monitoring instruments such as soil strain gauges and to exchange results and data of such similar studies.

4. Dr. O'Rourke of Cornell University visited PWRI in June, 1987 to review the possibilities of US-Japan joint research on the effect of large-scale ground deformation on buried pipelines. He also led discussions with approximately 10 researchers on seismic resistance of lifelines.

## II. Future Program

1. The members of the Task Committee will continue to facilitate the exchange of technical information and to cooperate in the following research areas.
  - a. Field investigation reports of seismic damage to lifeline systems and seismic observation results
  - b. Seismic design procedures for lifeline systems
  - c. Procedures and instrumentation to detect and inspect damage and the behavior of lifeline structures during earthquakes
  - d. Repair and retrofit methodology and post event service restoration strategies for lifeline systems
  - e. Estimation of reliability of lifelines
  - f. Vulnerability models for lifeline components, systems, and networks, and models for damage and loss estimates
  - g. Management and public educations on importance of lifeline systems
  - h. Investigation of needs for large-scale testing of lifeline systems and laboratory studies using multiple shaking tables.
2. The U.S.-side is interested in developing a cooperative program to investigate the modeling of complicated lifeline components, e.g., treatment plants and electric power substations to the effects of earthquakes.
3. It is recommended to continue U.S.-Japan coordinated research

projects on field observations and analyses on seismic behavior of buried pipelines, experiments and analyses on dynamic characteristics of joint behavior, effects of soil liquefaction on buried pipes, soil-buried pipes interaction, seismic reliability of lifeline systems, and seismic design methods. As for field observation, the Japan-side will concentrate on seismic behavior of pipelines buried in soft soils and in boundary layers between hard and soft soils, whereas the U.S.-side will focus on dynamic behavior of pipelines buried in and near active faults.

4. To promote U.S.-Japan coordinated research programs in the earthquake resistance of lifeline facilities, it is recommended to hold a U.S.-Japan Workshop on Lifeline Earthquake Engineering in 1989. The workshop will be held in Tsukuba, Japan in 1989 in conjunction with the 21st UJNR panel meeting. Mr. Ronald Eguchi, of Dames and Moore and Dr. Ueda of PWRI will be responsible to develop the workshop program.
5. The English translation of the "Manual of Repair Methods for Civil Engineering Structures Damaged by Earthquakes" (Draft) (in Japanese) prepared by PWRI shall be printed soon and made available for wide distribution.
6. Drs. T. Iwasaki and K. Kawashima of PWRI and Dr. L. Wang of Old Dominion University are proposing a joint research project on seismic component design, analysis, and experimental observation of buried pipelines including the effects of pipe-structure interaction, and seismically induced soil liquefaction. Joint research projects shall be developed to extend the current pipeline research at Parkfield or elsewhere and to exchange data and results.

Report of Task Committee on

(G) WIND CHARACTERISTICS AND STRUCTURAL RESPONSE

Date: May 19, 1988

Place: National Bureau of Standards  
Gaithersburg, MD 20899

Attendees: Japan Side - T. Murota (Chairman) (BRI)  
K. Yokoyama (PWRI)  
U.S. Side - R. D. Marshall (Chairman) (NBS)

I. Activities and Principal Accomplishments to Date

Noting that:

- a) The scope of activities of the Task Committee (G) on Wind Characteristics and Structural Response is relatively narrow,
- b) Participation in committee activities has exhibited a steady decline in recent years, and
- c) Task Committees "D" and "G" share a common interest in response characteristics and structural performance,

It is jointly proposed by the Chairmen of Task Committees "D" and "G" that these two Task Committees be combined as a unified Task Committee to address issues related to the performance of buildings exposed to wind and seismic events, and the newly combined Task Committee be designated as Task Committee on Evaluation of Structural Performance.

The Task Committee carried out the following activities:

1. Exchanged the Proceedings of Symposium on High Winds and Building Codes, Kansas City, MO, November 2-4, 1987.
2. Obtained wind data from a National Science Foundation funded study of surface pressures and internal pressures acting on a full-scale low-rise building situated in open terrain near Lubbock, Texas.

II. Future Program

1. Exchange observation reports of high winds and wind damage.
2. Exchange information on criteria, techniques, and instrumentation for structural modeling in boundary layer wind tunnels. Encourage the exchange of information on measurements made on actual structures and on comparisons with predictions from wind tunnel studies of these structures.

3. Expand the exchange of engineers and meteorologists, and encourage the mutual use of available research facilities in the two countries.
4. Organize a workshop on "Sensor Technology Applied to Large Engineering Systems." The Workshop is tentatively scheduled for September, 1988, at the NBS Laboratories in Boulder, CO.
5. Encourage the joint development of new research topics such as:
  - a. Active and passive control of building response
  - b. Wind forces on membrane structures
  - c. Natural ventilation
  - d. Instrumentation and techniques for monitoring structural response
6. Task Committee "G" proposes to combine the work of Task Committees "D" and "G" into one Task Committee at the conclusion of 20th Joint Meeting. Task Committee "G" has the concurrence of T/C "D" to propose this action.

Report of Task Committee on

(H) SOIL BEHAVIOR AND STABILITY DURING EARTHQUAKES

Date: May 18, 1988

Place: National Bureau of Standards  
Gaithersburg, MD 20899

Attendees: Japan Side - Y. Sasaki (Chairman) (PWRI)  
O. Matsuo (PWRI)  
U.S. Side - A. G. Franklin (Chairman) (WES)  
F. G. McLean (USBR)

I. Activities and Principal Accomplishments to Date

1. Exchange of relevant documents on soil behavior during earthquakes was made throughout the year. During the 20th Joint Meeting of the Panel, six papers were submitted from the Japanese-side and three papers were submitted from the U.S.-side.
2. Under the auspices of the UJNR, the following researchers were exchanged between the U.S.-and Japanese- sides:
  - a. Mr. Yoshitaka Hachiya of the PHRI was hosted by the WES from March 1987 to March 1988.
  - b. Mr. Osamu Matsuo is performing research at the University of Southern California on liquefaction of soils.
3. A workshop on Remedial Treatment of Liquefiable Soils was held at Jackson Hole, Wyoming, from May 11 through May 14, 1988. There were 13 participants from the U.S. side and 6 from the Japan side. Eight papers were presented by the U.S. participants and six by the Japanese participants. Needs for future research were clarified by this workshop. The results of the workshop were reported to the 20th Joint Panel meeting.

## II. Goals

1. In response to the challenge from the secretariats, the Task Committee reviewed accomplishments and objectives and agrees that Task Committee "H" should continue active investigations, staff exchanges, cooperative research and information exchange into earthquake effects on soil foundations and soil structures. Its goals are:

### 1-3 Year Goal

- a. Define and initiate cooperative research into remedial methods and techniques for embankment structures and slopes.
- b. Continue cooperative investigations into in-situ investigation methods including a review of SPT procedures.
- c. Pursue the development of procedures and exchange of information on using centrifuges to investigate response of soils and prototype earth structures to earthquakes, including soil-structure interaction.
- d. Validate analytical and predictive methods for soil response to earthquakes.

### 3-5 Year Goal

- a. Complete early phases of cooperative research and develop useful remedial methods and techniques for earth structures.
- b. Plan and initiate cooperative research using centrifuges to evaluate prototype response.
- c. Plan for, instrument, and obtain actual data for the response of soils, earth structures, and foundations to earthquakes.

## III. Future Programs

1. Publish Proceedings of the 1985 workshop on In-Situ Testing for Evaluation of Soil Liquefaction Susceptibility.
2. Publish Proceedings of the 1988 workshop.
3. Arrangements are being made for a one-year visit from October 1988 by Mr. Nario Yasuda, of PWRI, to the WES, to work on Seismic Stability of Embankment Dams.
4. The Task Committee proposes a planning meeting on Cooperative Research in Remedial Treatment of Liquefiable Soils to be held in conjunction with the 21st Joint Panel Meeting. The purposes of the meeting are to identify potential areas of Joint U.S.-Japanese Research that are most feasible, most

appropriate, and most likely to produce significant benefits; and to develop a specific proposal for joint research.

5. When requested, the Task Committee will assist in arranging visits to earth embankments including fill dams and foundations which have been subjected to significant ground motions.
6. The Task Committee encourages the maximum exchange of information in the following areas of earthquake engineering (are of interest to U.S. and Japanese engineers):
  - a. Prediction of liquefaction susceptibility of soils
  - b. In-Situ testing methods for evaluation of soil liquefaction potential
  - c. Evaluation of seismic stability of embankment structures and natural slopes
  - d. Remedial treatment of embankments and foundations to improve seismic stability
  - e. Prediction of seismically induced permanent displacements in earth structures
  - f. Prediction of seismically induced settlement of soils and foundations
  - g. Earthquake effects on semi-buried concrete structures
  - h. Earthquake effects on retaining walls
  - i. Centrifuge testing facilities and methods
  - j. Laboratory testing of models of geotechnical structures
  - k. Field performance data showing full-scale seismic response of earth dams and foundations

Report of Task Committee on

(I) STORM SURGE AND TSUNAMI

Date: May 19, 1988

Place: National Bureau of Standards  
Gaithersburg, MD 20899

Attendees: Japan Side - N. Narita (Temp. Chairman) (PWRI)  
K. Ohtani (NRCDP)

U.S. Side - C. Barrientos (Chairman) (NOAA)  
H. Meyers (NOAA)  
P. Farrar (WES)

I. Activities and Principal Accomplishments to Date

1. The U.S.-side has given to the Japan-side the NGDC/NOAA tsunami database. This includes the printout, two diskettes (ASCII and DBS3+ format), documentation, and references.

II. Future Programs

1. The Task Committee supports the continuation of exchange of data and information on Tsunami and Storm Surge. The Committee also supports exchanges of researches whenever possible.
2. The Task Committee Chairmen will continue to plan and will coordinate holding the second Tsunami and Storm Surge Workshop. The workshop planning will explore scheduling it in coordination with other conferences and inviting participants from academia, local government officials, and industry. The details of the workshop, such as the focus and the venue, will be determined by the two Chairmen.
3. The membership of the Task Committee will be expanded to include persons with strong interest in the engineering aspects of storm surge and tsunamis.
4. Task Committee long-range plans will be defined more definitely during the 21st Joint Panel Meeting.
5. NGDC will test Mr. Okada's model on tsunami propagation and compare the results with actual observations.
6. The U.S.-side (NOAA) will provide to the Japan-side the report and documentation of the storm surge model, SLOSH (Sea, Land and Overland Surges from Hurricanes) when published.

Report of Task Committee on

(J) WIND AND EARTHQUAKE ENGINEERING FOR TRANSPORTATION SYSTEMS

Date: May 18, 1988

Place: National Bureau of Standards  
Gaithersburg, MD 20899

Attendees: Japan Side - K. Yokoyama (Chairman) (PWRI)  
K. Hasegawa (PWRI)

U.S. Side - C. F. Galambos (Chairman) (FHWA)  
R. D. Marshall (NBS)  
J. B. Scalzi (NSF)

I. Activities and Principal Accomplishments to Date

The major accomplishments of Task Committee (J) during the past year were as follows.

1. Summaries of wind and earthquake research on bridges, conducted by both countries, were presented to the 20th Joint Meeting, and exchange of information was made.
2. The coordinated research study on the seismic performance of bridge piers and columns was begun in 1983 and the following experiments were continued.
  - a. Performance of reinforced concrete piers and columns subjected to dynamic cyclic loading
  - b. Model tests on the failure of reinforced concrete piers
  - c. Testing full-scale concrete columns and associated small-scale model tests
  - d. Behavior of concrete filled steel tubes
3. Mr. Koichi Minosaku, researcher of the Bridge Division, PWRI, MOC, was a guest worker at the Center for Building Technology, NBS, for 10 months (September 1986 - July 1987) and performed cooperative experimental research on the seismic performance of bridge piers and columns. This assignment was a part of the personnel exchange program of the UJNR Panel.
4. The Proceedings of the third Bridge Workshop held in Tsukuba in May 1987 was published and distributed to the participants and related organizations.
5. The 4th U.S.-Japan Bridge Workshop was held in San Diego, California on May 11 & 12, 1988. The theme of the workshop was

Bridge Performance, Strengthening, and Innovation. Thirteen Japanese engineers and 21 U.S. and Canadian engineers participated. Some of the subjects discussed were:

- a. Aeroelasticity and aerodynamics of bridges
  - b. Wind engineering and full-scale dynamic testing of long span bridges.
  - c. Seismic evaluation, retrofitting, and bridge isolation
  - d. Bridge maintenance, inspection, and strengthening
  - e. Seismic and non-seismic analysis and design
  - f. Experimental investigation of bridges and components
6. Cooperative studies on comparative wind tunnel tests between Japan and Canada have been coordinated under UJNR technical guidance.

## II. Future Programs

As a result of comprehensive discussions, the Task Committee (J) hereby resolves to carry forth the following programs:

1. Continue with the coordinated experimental research study on the seismic performance of bridge piers and columns, and review the progress of the study at the intermediate stage.
2. Develop a coordinated research study, both theoretical and experimental, on the seismic, aeroelastic, and aerodynamic response of cable-supported bridges with special emphasis on cable vibration and corrosion protection.
3. Encourage the continued exchange of information and research personnel through the Panel on Wind and Seismic Effects of UJNR.
4. The Task Committee endorses the initiation of a coordinated and expanded program of research on remedial measures to mitigate or prevent damage to existing bridges by the natural hazards of earthquakes and strong winds.
5. The Task Committee recommends a fifth bridge workshop on the subject of Wind and Seismic Effects on Bridge Management, Diagnostics, and Capacity Evaluation. It is proposed to hold the workshop in Japan, in conjunction with the 21st UJNR joint panel meeting. Details of the workshop are to be worked out mutually between the respective Task Committee Chairmen.
6. Develop a coordinated research study to evaluate and compare the seismic design criteria for bridges used in Japan and the United States. Several bridges should be identified by each

group. Bridges identified by one group should be redesigned for seismic loads only by other groups using their particular seismic criteria. The study should identify the differences and similarities between the two seismic criteria and attempt to identify common areas of interest. It is recommended that one researcher from the California Department of Transportation be invited in the fall of 1988 to spend one month at PWRI for the purpose of preparing a detailed research plan.

7. A cooperative study is proposed to mutually work out the methodology for prioritization of repair and retrofiting of structures and the calibration of LRFD specifications with respect to wind and earthquake loadings.
8. It is proposed to promote coordination of field measurements, instrumentation, and design theories related to long span cable supported bridges.
9. It is proposed to continue emphasis on base isolation technology of bridges.

U.S. DEPT. OF COMM. <b>BIBLIOGRAPHIC DATA SHEET</b> (See instructions)	<b>1. PUBLICATION OR REPORT NO.</b> NIST/SP-760	<b>2. Performing Organ. Report No.</b>	<b>3. Publication Date</b> January 1988
<b>4. TITLE AND SUBTITLE</b> <p>Wind and Seismic Effects--Proceedings of the 20th Joint Meeting of the U.S.-Japan Cooperative Program in Natural Resources Panel on Wind and Seismic Effects</p>			
<b>5. AUTHOR(S)</b> Noel J. Raufaste, Editor			
<b>6. PERFORMING ORGANIZATION</b> (If joint or other than NBS, see instructions) NATIONAL INSTITUTE OF STANDARDS AND TECHNOLOGY (formerly NATIONAL BUREAU OF STANDARDS) U.S. DEPARTMENT OF COMMERCE GAITHERSBURG, MD 20899		<b>7. Contract/Grant No.</b>	<b>8. Type of Report &amp; Period Covered</b> Final
<b>9. SPONSORING ORGANIZATION NAME AND COMPLETE ADDRESS</b> (Street, City, State, ZIP) <p>Same as item #6 above.</p>			
<b>10. SUPPLEMENTARY NOTES</b> <input type="checkbox"/> Document describes a computer program; SF-185, FIPS Software Summary, is attached.			
<b>11. ABSTRACT</b> (A 200-word or less factual summary of most significant information. If document includes a significant bibliography or literature survey, mention it here) <p>The 20th Joint Meeting of the U.S.-Japan Panel on Wind and Seismic Effects was held at the National Bureau of Standards, Gaithersburg, MD, from May 17-20, 1988. This publication, the proceedings of the Joint Meeting, includes the program, list of members, panel resolutions, task committee reports, and technical papers.</p> <p>The papers covered five themes: (I) Wind Engineering, (II) Earthquake Engineering, (III) Storm Surge and Tsunamis, (IV) Summary of U.S.-Japan Cooperative Research Program, and (V) Two Decades of Accomplishments and Challenges for the Future.</p>			
<b>12. KEY WORDS</b> (Six to twelve entries; alphabetical order; capitalize only proper names; and separate key words by semicolons) accelerograph; codes; design criteria; disaster; earthquakes; earthquake hazards; geotechnical engineering; ground failure; liquefaction; pipeline; risk analysis; seismicity; standards; structural engineering; structural response; tsunami; wind loads; winds			<b>14. NO. OF PRINTED PAGES</b> 481
<b>13. AVAILABILITY</b> <input checked="" type="checkbox"/> Unlimited <input type="checkbox"/> For Official Distribution. Do Not Release to NTIS <input type="checkbox"/> Order From Superintendent of Documents, U.S. Government Printing Office, Washington, D.C. 20402. <input checked="" type="checkbox"/> Order From National Technical Information Service (NTIS), Springfield, VA. 22161		<b>15. Price</b>	









**U.S. Department of Commerce**  
National Institute of Standards and Technology  
(formerly National Bureau of Standards)  
Gaithersburg, MD 20899

Official Business  
Penalty for Private Use \$300